NIST
PUBLICATIONS

REFERENCE

A11102 953225
NAT'L INST OF STANDARDS & TECH R.I.C.
A11102953225
Wineland, David J/Trapped Ions and laser
QC100 .U5753 NO.1324 1988 V198 C.1 NIST-

NIST TECHNICAL NOTE 1324

U.S. DEPARTMENT OF COMMERCE / National Institute of Standards and Technology

Trapped Ions and Laser Cooling II

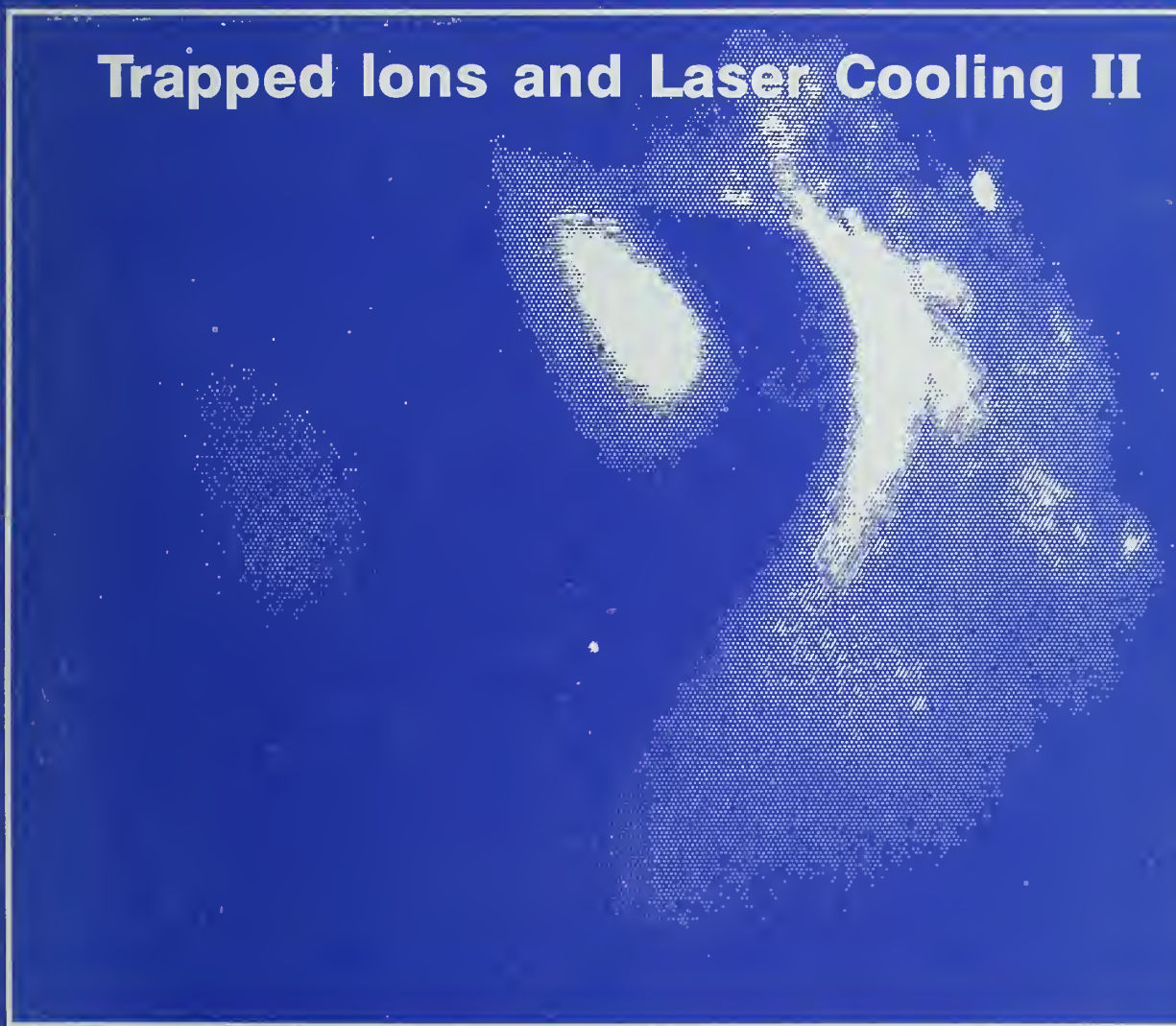

Selected publications of the
n Storage Group
me and Frequency Division
ST, Boulder, Colorado

Edited by: David J. Wineland
Wayne M. Itano
James C. Bergquist
John J. Bollinger

QC
100
.U5753
#1324
1988

NISTR QC 100 .U5753 no. 1324 1988

Trapped Ions and Laser Cooling II

Selected publications of the Ion Storage Group of the Time and Frequency Division, NIST, Boulder, Colorado

Edited by
David J. Wineland
Wayne M. Itano
James C. Bergquist
John J. Bollinger

Time and Frequency Division
Center for Basic Standards
National Measurement Laboratory
National Institute of Standards and Technology
(formerly National Bureau of Standards)
Boulder, Colorado 80303-3328

Supported in part by
U.S. Office of Naval Research
800 North Quincy
Arlington, VA 22217
and
U.S. Air Force Office of Scientific Research
Bolling Air Force Base, DC 20332

U.S. DEPARTMENT OF COMMERCE, C. William Verity, Secretary

NATIONAL INSTITUTE OF STANDARDS AND TECHNOLOGY, Ernest Ambler, Director

Research Information Center
National Institute of Standards
and Technology
Gaithersburg, Maryland 20899

Issued October 1988

National Institute of Standards and Technology Technical Note 1324
Natl. Inst. Stand. Technol., Tech Note 1324, 200 pages (Oct. 1988)
CODEN:NTNOEF

U.S. GOVERNMENT PRINTING OFFICE
WASHINGTON: 1988

For sale by the Superintendent of Documents, U.S. Government Printing Office, Washington, DC 20402

PREFACE

This collection of papers represents the work on laser cooled, stored atomic ions by the Time and Frequency Division of the National Institute of Standards and Technology (formerly the National Bureau of Standards) from July, 1985 to September, 1988. It follows the collection of papers, contained in NBS Technical Note 1086, "Trapped Ions and Laser Cooling" (June 1985). Although the primary goal of this research has been the development of techniques necessary for achieving high resolution spectroscopy, we have also been able to investigate related areas of research.

Papers listed with the prefix A are not included here but can be obtained on request. We intend to update this publication periodically to include new work not contained here. We hope this collection of papers will be useful to our colleagues in this and related fields.

We gratefully acknowledge the important contributions of several colleagues, post-doctoral and guest researchers, and students, including Charles Manney, Earl Beaty, Larry Brewer, Sarah Gilbert, Hamid Hemmati, Randy Hulet, John Prestage, Ule Daniel, Frank Diedrich, Dan Larson, Gerd Leuchs, Shao Zhong Xing, and Franklin Ascarrunz. We also acknowledge the continued support of the U.S. Office of Naval Research and the U.S. Air Force Office of Scientific Research.

David J. Wineland
Wayne M. Itano
James C. Bergquist
John J. Bollinger

Boulder, Colorado
September, 1988

CONTENTS

Page

Contents of previous NBS Technical Note 1086..... ix
List of Additional Publications..... xi

SPECTROSCOPY AND FREQUENCY STANDARDS

1. "Energy and Radiative Lifetime of the $5d^9\ 6s^2\ {}^2D_{5/2}$ State in HgII by Doppler-Free Two-Photon Laser Spectroscopy,"
J.C. Bergquist, D.J. Wineland, Wayne M. Itano, Hamid Hemmati, H.-U. Daniel, and G. Leuchs.....TN-1

2. "Measurements of the g_J - Factors of the $6s\ {}^2S_{\frac{1}{2}}$ and $6p\ {}^2P_{\frac{1}{2}}$ States in $^{198}Hg^+$,"
"W.M. Itano, J.C. Bergquist, and D.J. Wineland.....TN-5

3. "Absorption Spectroscopy at the Limit: Detection of a Single Atom,"
D.J. Wineland, W.M. Itano, and J.C. Bergquist.....TN-8.

4. "Laser-Cooling Limits and Single-Ion Spectroscopy,"
D.J. Wineland, W.M. Itano, J.C. Bergquist and R.G. Hulet.....TN-11

5. "Recoilless Optical Absorption and Doppler Sidebands of a Single Trapped Ion," TN-24
J.C. Bergquist, W.M. Itano, and D.J. Wineland.

6. "Hg^+ Single Ion Spectroscopy,"
J.C. Bergquist, F. Diedrich, W.M. Itano, and D.J. Wineland.....TN-27

7. "High Accuracy Spectroscopy of Stored ions,"
D.J. Wineland, W.M. Itano, J.C. Bergquist, J.J. Bollinger, F. Diedrich, and S.L. Gilbert.....TN-33

8. "Frequency Standards Utilizing Penning Traps,"
J.J. Bollinger, S.L. Gilbert, W.M. Itano, and D.J. Wineland.....TN-39

QUANTUM JUMPS

1. "Observation of Quantum Jumps in a Single Atom,"
J.C. Bergquist, R.G. Hulet, W.M. Itano, and D.J. Wineland.....TN-46

2. "Quantum Jumps via Spontaneous Raman Scattering,"
R.G. Hulet and D.J. Wineland.....TN-50

3. "Precise Test of Quantum Jump Theory,"
R.G. Hulet, D.J. Wineland, J.C. Bergquist, and W.M. Itano.....TN-55

4. "Radiative Decay Rates in Hg^+ from Observations of Quantum Jumps in a Single Ion,"
W.M. Itano, J.C. Bergquist, R.G. Hulet, and D.J. Wineland.....TN-59

5. "Photon Antibunching and Sub-Poissonian Statistics from Quantum Jumps in One and Two Atoms,"
W.M. Itano, J.C. Bergquist, and D.J. Wineland.....TN-63

NONNEUTRAL PLASMA STUDIES

1. "Angular Momentum of Trapped Atomic Particles,"
D.J. Wineland, J.J. Bollinger, W.M. Itano, and J.D. Prestage.....TN-67

2. "Sympathetic Cooling of Trapped Ions: A Laser-Cooled Two-Species Nonneutral Ion Plasma,"
D.J. Larson, J.C. Bergquist, J.J. Bollinger, W.M. Itano, and D.J. Wineland.....TN-76

3. "Ion Trapping Techniques: Laser Cooling and Sympathetic Cooling,"
J.J. Bollinger, L.R. Brewer, J.C. Bergquist, W.M. Itano, D.J. Larson, S.L. Gilbert, and D.J. Wineland.....TN-80

4. "Static Properties of a Nonneutral $^{9}Be^{+}$ Ion Plasma,"
L.R. Brewer, J.D. Prestage, J.J. Bollinger, W.M. Itano, D.J. Larson, and D.J. Wineland.....TN-91

5. "Atomic Ion Coulomb Clusters in an Ion Trap,"
D.J. Wineland, J.C. Bergquist, W.M. Itano, J.J. Bollinger and C.H. Manney.....TN-106

6. "Shell-Structure Phase of Magnetically Confined Strongly Coupled Plasmas,"
S.L. Gilbert, J.J. Bollinger, and D.J. Wineland.....TN-110

7. "Liquid and Solid Ion Plasmas,"
D.J. Wineland, W.M. Itano, J.C. Bergquist, S.L. Gilbert, J.J. Bollinger, and F. Ascarrunz.....TN-114

8. "Quantitative Study of Laser Cooling in a Penning Trap,"
W.M. Itano, L.R. Brewer, D.J. Larson, J.J. Bollinger, S.L. Gilbert, and D.J. Wineland.....TN-130

GENERAL ARTICLES

1. "Optical Pumping of Stored Atomic Ions,"
D.J. Wineland, W.M. Itano, J.C. Bergquist, J.J. Bollinger, and J.D. Prestage.....TN-132

2. "Laser Spectroscopy of Trapped Atomic Ions,"
W.M. Itano, J.C. Bergquist, and D.J. Wineland.....TN-144

3. "Precise Optical Spectroscopy with Ion Traps,"
W.M. Itano, J.C. Bergquist, R.G. Hulet, and D.J. Wineland.....TN-150

4. "Laser Cooling,"
D.J. Wineland and W.M. Itano.....TN-156

APPARATUS

1. "Simple Electrodes for Quadrupole Ion Traps,"
E.C. Beaty.....TN-163

2. "Ion Traps for Large Storage Capacity,"
D.J. Wineland.....TN-168

3. "Thermal Shifts of the Spectral Lines in the $^4F_{3/2}$ to $^4I_{11/2}$ Manifold of an Nd: YAG Laser,"
Shao Zhong Xing and J.C. Bergquist.....TN-182

CONTENTS OF NBS TECHNICAL NOTE 1086

"Trapped Ions and Laser Cooling,"

(Issued June 1985)

		Page
1.	"Radiation-Pressure Cooling of Bound Resonant Absorbers," D. J. Wineland, R. E. Drullinger, and F. L. Walls.....	TN-1
2.	"Laser Cooling of Atoms," D. J. Wineland and W. M. Itano.....	TN-5
3.	"Laser-to-Microwave Frequency Division Using Synchrotron Radiation," D. J. Wineland.....	TN-25
4.	"Laser to Microwave Frequency Division Using Synchrotron Radiation II," J. C. Bergquist and D. J. Wineland.....	TN-30
5.	"Frequency and Time Standards Utilizing Laser Cooled Ions," W. M. Itano and D. J. Wineland.....	TN-34
6.	"Laser Induced Magnetron Compression (Expansion) of Ions Stored in a Penning Trap," D.J. Wineland, R.E. Drullinger, J.C. Bergquist, and W.M. Itano..	TN-35
7.	"High-Resolution Optical Spectra of Laser Cooled Ions," R. E. Drullinger, D. J. Wineland, and J. C. Bergquist.....	TN-36
8.	"Double-Resonance and Optical-Pumping Experiments on Electromagnetically Confined, Laser Cooled Ions," D.J. Wineland, J.C. Bergquist, W.M. Itano, and R.E. Drullinger..	TN-40
9.	"Spectroscopy of a Single Mg^+ Ion," D. J. Wineland and W. M. Itano.....	TN-43
10.	"Proposed Stored $^{201}Hg^+$ Ion Frequency Standards," D. J. Wineland, W. M. Itano, J. C. Bergquist, and F. L. Walls...	TN-47
11.	"Precision Measurement of the Ground-State Hyperfine Constant of $^{25}Mg^+$," W. M. Itano and D. J. Wineland.....	TN-57
12.	"Laser Cooling of Ions Stored in Harmonic and Penning Traps," W. M. Itano and D. J. Wineland.....	TN-67
13.	"Shift of $^2S_{1/2}$ Hyperfine Splittings Due to Blackbody Radiation," W. M. Itano, L. L. Lewis, and D. J. Wineland.....	TN-87
14.	"Laser Cooled, Stored Ion Experiments at NBS and Possible Applications to Microwave and Optical Frequency Standards," D. J. Wineland, J. C. Bergquist, R. E. Drullinger, H. Hemmati, W. M. Itano, and F. L. Walls.....	TN-90

Page

15. "Spectroscopy of Stored Ions,"
D. J. Wineland..... TN-97

16. "Magnetic Field Dependence of (s,ℓ) Electron Configurations,"
D. J. Wineland and W. M. Itano..... TN-107

17. "Laser Cooling and Double Resonance Spectroscopy of Stored Ions,"
W. M. Itano and D. J. Wineland..... TN-108

18. "Generation of Continuous-Wave 194-nm Radiation by Sum-Frequency Mixing in an External Ring Cavity,"
H. Hemmati, J. C. Bergquist, and W. M. Itano..... TN-117

19. "Laser Fluorescence Mass Spectroscopy,"
D. J. Wineland, J. J. Bollinger, and W. M. Itano..... TN-120

20. "Time and Frequency Standards Based on Charged Particle Trapping,"
W. M. Itano, D. J. Wineland, H. Hemmati, J. C. Bergquist, and J. J. Bollinger..... TN-125

21. "Frequency Standard Research Using Stored Ions,"
D. J. Wineland, W. M. Itano, J. C. Bergquist, J. J. Bollinger, and H. Hemmati..... TN-128

22. "Precision Measurements of Laser Cooled $^{9}Be^{+}$ Ions,"
J. J. Bollinger, D. J. Wineland, W. M. Itano, and J. S. Wells... TN-132

23. "Hyperfine Structure of the $2p\,^{2}P_{1/2}$ State in $^{9}Be^{+}$,"
J. J. Bollinger, J. S. Wells, D. J. Wineland, and W. M. Itano... TN-137

24. "Trapped Ions, Laser Cooling, and Better Clocks,"
D. J. Wineland..... TN-141

25. "Spectroscopy of Stored Atomic Ions,"
D. J. Wineland, W. M. Itano, J. C. Bergquist, J. J. Bollinger, and J. D. Prestage..... TN-147

26. "Strongly Coupled Nonneutral Ion Plasma,"
J. J. Bollinger and D. J. Wineland..... TN-172

27. "Laser-Cooled-Atomic Frequency Standard,"
J. J. Bollinger, J. D. Prestage, W. M. Itano, and D. J. Wineland..... TN-176

28. "Limits for Spatial Anisotropy by Use of Nuclear-Spin-Polarized $^{9}Be^{+}$ Ions,"
J. D. Prestage, J. J. Bollinger, W. M. Itano, and D. J. Wineland..... TN-180

Additional publications of the Time and Frequency Division Ion Storage Group not included in this technical note or NBS Technical Note 1086

A1. "New Possibilities for Frequency Standards Using Laser Cooling and Detection of Stored Ions," F.L. Walls, D.J. Wineland, and R.E. Drullinger. Proc. 32nd Annual Symp. on Frequency Control, June 1978, p. 453-459. (Copies available from: Annual Frequency Control Symposium, c/o Electronic Industries Assoc., 2001 Eye St., Washington, DC, 20006).

A2. "Laser Cooling of Ions Bound to a Penning Trap," R.E. Dullinger and D.J. Wineland, in: Laser Spectroscopy IV, Eds. H. Walther and K.W. Rothe, (Springer, Berlin, 1979) p. 66-72. Same title by D.J. Wineland and R.E. Drullinger, Proc. 6th Vavilov Conf. on Non-Linear Optics, Novosibirsk, Springer, June 1979.

A3. "The Isolated Electron," Philip Ekstrom and David Wineland, Sci. American 243, no. 2, p. 105-121, August 1980.

A4. "Shift of $^2S_{\frac{1}{2}}$ Hyperfine Splittings Due to Blackbody Radiation and Its Influence on Frequency Standards," Wayne M. Itano, L.L. Lewis, and D.J. Wineland, J. de Physique, Colloque C8, suppl. to no. 12, vol. 42, Dec. 1981, p. C8-283-287.

A5. "Prospects for Stored Ion Frequency Standards," D.J. Wineland, Proc. 13th Annual Precise Time and Time Interval (PTTI) Applications and Planning Meeting, Naval Research Laboratory, Washington, DC, Dec. 1981. NASA Conf. Publ. 2220., p. 579-592.

A6. "Prospects Toward a Stored Ion Frequency Standard at NBS," Wayne M. Itano, D.J. Wineland, J.C. Bergquist, and F.L. Walls. Proc. Conf. on Precision Measurements and Fundamental Constants; Gaithersburg, MD June 1981; Precision Measurement and Fundamental Constants II, B.N. Taylor and W.D. Phillips, eds. National Bureau of Standards (US) Spec. Publ. 617 (1984), p. 93-97.

A7. "High Power Second Harmonic Generation of 257 nm Radiation in an External Ring Cavity," J.C. Bergquist, H. Hemmati, and W.M. Itano, Opt. Commun. 43, 437-442 (1982).

A8. "High Resolution Spectroscopy of Stored Ions," D.J. Wineland, Wayne M. Itano and R.S. Van Dyck Jr., in Advances in Atomic and Molecular Physics, Vol. 19, ed. by Bederson & Bates, (Academic Press, Aug. 1983), p. 135-186.

A9. "Laser Cooled $^9Be^+$ Accurate Clock," J.J. Bollinger, Wayne. M. Itano, and D.J. Wineland, Proc. 37th Annual Symp. Freq. Control, 1983, p. 37-41 (copies available from Systematics General Corp., Brinley Plaza, Rt. 38, Wall Township, NJ 07719.)

A10. "Spectroscopy of Stored Ions Using Fluorescence Techniques," D.J. Wineland, Wayne M. Itano, J.C. Bergquist, and H. Hemmati, S.P.I.E., Vol. 426-Laser Based Ultrasensitive Spectroscopy and Detection V, Society of Photo-Optical Instrumentation Engineers, 1983, p. 65-70.

A11. "Frequency and Time Standards Based on Stored Ions," J.J. Bollinger, D.J. Wineland, W.M. Itano, J.C. Bergquist, and J.D. Prestage, Proc. 16th Ann. Precise Time and Time Interval (PTTI) Applications and Planning Meeting, Naval Research Laboratory, Washington, D.C., Dec. 1984, p. 48.

A12. "Doppler-Free Two-Photon Laser Spectroscopy of HgII," J.C. Bergquist, D.J. Wineland, Wayne M. Itano, Hamid Hemmati, H.-U. Daniel, and G. Leuchs, Proc. 39th Ann. Symp. on Frequency Control, 1985.

A13. "Two-Photon Optical Spectroscopy of Trapped HgII," J.C. Bergquist, D.J. Wineland, W.M. Itano, H. Hemmati, H.-U. Daniel, G. Leuchs, Laser Spectroscopy VII, T.W. Hänsch and Y.R. Shen eds., (Springer Verlag, Berlin, Heidleberg, 1985). p. 6-9.

A14. "Frequency Standards Based on Stored Ions," D.J. Wineland, IEEE Special Issue on Radio Measurements & Standards: Proc. IEEE 74, 147 (1986).

A15. "A High-Γ, Strongly-Coupled, Non-neutral Ion Plasma," L.R. Brewer, J.D. Prestage, J.J. Bollinger and D.J. Wineland, In Strongly Coupled Plasma Physics, F.J. Rogers and H.E. Dewitt, Eds., (Plenum, New York, 1986), p. 53.

A16. "The Observation of Quantum Jumps in Hg^+," W.M. Itano, J.C. Bergquist, R.G. Hulet, and D.J. Wineland, Laser Spectroscopy VIII, W. Persson and S. Svanberg eds., (Springer Verlag, Berlin, Heidelberg, 1987) p. 117.

A17. "Cooling in Traps," R. Blatt, G. Lafyatis, W.D. Phillips, S. Stenholm, and D.J. Wineland, Physica Scripta T22, 216 (1988).

A18. "Frequency Standards in the Optical Spectrum," D.J. Wineland, J.C. Bergquist, W.M. Itano, F. Diedrich and C.S. Weimer, in The Hydrogen Atom, Ed. by F. Bassani, T.W. Hänsch, and M. Inguscio, (Springer Verlag, Heidelberg, 1988) to be published.

A19. "The Digitized Atom and Optical Pumping," D.J. Wineland, W.M. Itano, J.C. Bergquist and R.G. Hulet, in Atomic Physics 11, ed by S. Haroche, J.C. Gay, G. Grynberg, (World Scientific Press, Singapore, 1988) to be published.

A20. "Liquid and Solid Phases of Laser Cooled Ions," S.L. Gilbert, J.C. Bergquist, J.J. Bollinger, W.M. Itano, and D.J. Wineland, ibid.

A21. "Laser Cooling to the Zero Point Energy of Motion," F. Diedrich, J.C. Bergquist, W.M. Itano, and D.J. Wineland, submitted for publication.

A22. "Perpendicular Laser Cooling of Ion Plasmas in a Penning Trap," Wayne M. Itano, L.R. Brewer, D.J. Larson, and D.J. Wineland, Phys. Rev. A., to be published.

Energy and Radiative Lifetime of the $5d^9 6s^2\,{}^2D_{5/2}$ State in Hg II by Doppler-Free Two-Photon Laser Spectroscopy

J. C. Bergquist, D. J. Wineland, Wayne M. Itano, Hamid Hemmati,[a] H.-U. Daniel,[b] and G. Leuchs[c]

Time and Frequency Division, National Bureau of Standards, Boulder, Colorado 80303

(Received 22 July 1985)

The Doppler-free, two-photon $5d^{10}6s\,{}^2S_{1/2} - 5d^9 6s^2\,{}^2D_{5/2}$ transition in singly ionized Hg, attractive as an optical-frequency standard, has been observed for the first time on a small number of $^{198}Hg^+$ ions confined in a radio-frequency trap. The radiative lifetime of the $^2D_{5/2}$ state and the absolute wave number of the two-photon transition were measured to be 0.090(15) s and 17757.152(3) cm^{-1}, respectively. Optical amplitude-modulation sidebands, induced by the secular (thermal) motion of the harmonically bound ions, were observed also for the first time.

PACS numbers: 32.70.Fw, 32.30.Jc

Microwave or optical transitions of laser-cooled ions that are confined in electromagnetic traps offer the basis for frequency standards of high stability and accuracy.[1-5] The advantages of such devices are numerous: Very long interrogation times and, therefore, high transition-line Q's can be achieved; fractional frequency perturbations that are due to the trapping fields can be held below 10^{-15}; collisions with background gas and cell walls can be largely avoided; Doppler shifts are directly reduced by trapping and cooling; and finally, nearly unit detection efficiency of transitions to metastable states is possible so that the signal-to-noise ratio need be limited only by the statistical fluctuations in the number of ions that make the transition.[5] Details of ion traps and laser cooling have been published elsewhere.[1-3] A particularly attractive candidate for an optical-frequency standard is the $5d^{10}6s\,{}^2S_{1/2}$–$5d^9 6s^2\,{}^2D_{5/2}Hg^+$ transition driven either by two photons with a wavelength near 563 nm[4] or by one photon at half this wavelength.[5] The lifetime of the $^2D_{5/2}$ state, which decays by the emission of electric quadrupole radiation at 281.5 nm, is calculated to be of order 0.1 s.[6] This gives a potential optical-line Q of about 7×10^{14}. In this Letter we describe the first results of our investigation of the two-photon transition in $^{198}Hg^+$ (which is free of hyperfine structure) stored in a miniature rf trap.

Our trap is similar to the small radio-frequency traps used in the ion-cooling experiments that were conducted at Heidelberg University on Ba^+,[7] and at the University of Washington on Mg^+ and Ba^+.[8] A cross section of the trap electrodes is shown in Fig. 1. It is interesting to note that, although the inner surfaces of our trap electrodes were machined with simple conical cuts, the trap dimensions were chosen to make the fourth- and sixth-order anharmonic contributions to the potential vanish.[9] The rf drive frequency was 21 MHz with a voltage amplitude $V_0 \leq 1$ kV. The partial pressure of the background gas, with the exception of deliberately added mercury and helium, was $\leq 10^{-7}$ Pa (133 Pa $\cong$ 1 Torr). After loading of 50–200 mercury ions the mercury vapor was frozen out in a liquid-nitrogen cold trap and the vacuum vessel was backfilled with He to the order of 10^{-3}–10^{-2} Pa. This was sufficient to cool the trapped Hg^+ collisionally to near room temperature as verified by the Doppler width of the $^2S_{1/2}$-$^2P_{1/2}$ resonance line near 194 nm.

Optical double resonance[10,11] was used to detect the two-photon transition. About 5 μW of narrow-band cw sum-frequency–generated radiation near 194 nm[12] was tuned to the $6s\,{}^2S_{1/2}$ to $6p\,{}^2P_{1/2}$ first-resonance transition and was directed diagonally through the trap (between the ring electrode and the end caps). The fluorescence light scattered by the ions was detected at right angles to the 194-nm beam with an overall detection efficiency of about 10^{-4}. Our signal level depended on the ion number and temperature and, typically, was $(2–10)\times10^3$ counts/s. The signal-to-background ratio was better than 10/1. When the ions

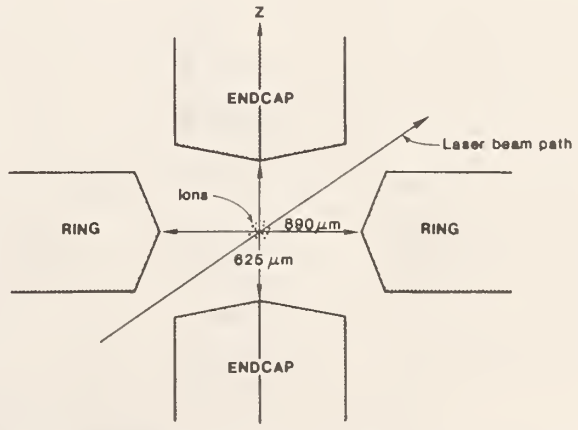

FIG. 1. Schematic showing a cross-section view of the trap electrodes. The electrodes are figures of revolution about the z axis and are made from molybdenum.

Work of the U. S. Government
Not subject to U. S. copyright

were driven by the radiation from a 563-nm cw ring dye laser out of the $^2S_{1/2}$ ground state into the $^2D_{5/2}$ metastable state, there was a decrease in the 194-nm fluorescence corresponding to the number of ions in the D state.

The dye-laser beam was also directed diagonally through the trap; the axes of the dye-laser beam, the 194-nm beam, and the collection optics were mutually perpendicular. A near-concentric standing-wave cavity was placed around the trap in order to enhance the power of the 563-nm radiation and better to ensure a nearly equal intensity of the counterpropagating beams. The cavity was positioned so that its waist ($w_0 \cong 25$–$30\ \mu$m) was located near the center of the cloud of trapped ions. The power-buildup factor was approximately 50, giving nearly 5 W of circulating power for typical input power levels of 100 mW. The frequency of the laser was offset locked and precisely scanned with respect to a second dye laser locked to a hyperfine component in the Doppler-free, saturated-absorption spectrum of $^{127}I_2$. The linewidth of the swept laser was determined to be of the order of 300 kHz by spectrum analysis of the beat note between the two lasers.

A typical resonance curve and simplified energy-level diagram is shown in Fig. 2. The full scan width is 4 MHz. The electric field vector of the 563-nm laser radiation is nearly parallel to a small applied magnetic field of approximately 11.6×10^{-4} T (11.6 G) which differentially Zeeman splits the ground and excited states. The selection rule for the two-photon transition for this polarization is $\Delta m_J = 0$, and, thus, only two components are observed, separated by approximately 13 MHz (approximately 6.5 MHz at the dye-laser frequency). In Fig. 2, we scan over only one of these Zeeman components ($m_J = -\frac{1}{2} \leftrightarrow m_J = -\frac{1}{2}$) but see sideband structure. This structure is due to amplitude modulation of the 563-nm laser intensity due to the secular motion of the ions in the rf trap. Any frequency modulation of the laser caused by the motion of the ions[13] is strongly suppressed if the cavity is well aligned so that the k vectors of the counterrunning beams are antiparallel. By a change in the well depth of the trap the harmonic frequency of the secular motion is changed, thereby shifting the sideband components of the two-photon signal. To our knowledge, this is the first observation of secular-motion sidebands at optical frequencies. In principle, the ion temperature could be derived from the relative amplitude of the sidebands.[13] The depth of the central feature in Fig. 2 is nearly 25% of full scale, implying that we have nearly saturated the two-photon transition. For the data of Fig. 2, the 194-nm laser irradiates the ions continuously, and, since the Zeeman splitting is unresolved for the first resonance transition, it mixes the ground state, maintaining equal populations in the two electron spin states. The linewidth of the two-photon resonance is about 420 kHz, and is determined in nearly equal parts by the 563-nm laser linewidth of about 320 kHz and by the nearly 270-kHz excitation rate of the $^2S_{1/2}$ state by the 194-nm radiation. When the 194-nm radiation is chopped, the two-photon linewidth drops to approximately 320 kHz, consistent with the dye-laser linewidth. The pressure broadening of the resonance in Fig. 2 was estimated to be less than 50 kHz by observation of the resonance at 5 times higher He pressure.

We have experimentally measured the radiative lifetime of the $5d^96s^2\,^2D_{5/2}$ state to be 0.090(15) s (one standard deviation) in agreement with the calculated lifetime of 0.105 s.[6] Again, in this measurement the ground-state population was monitored by measure-

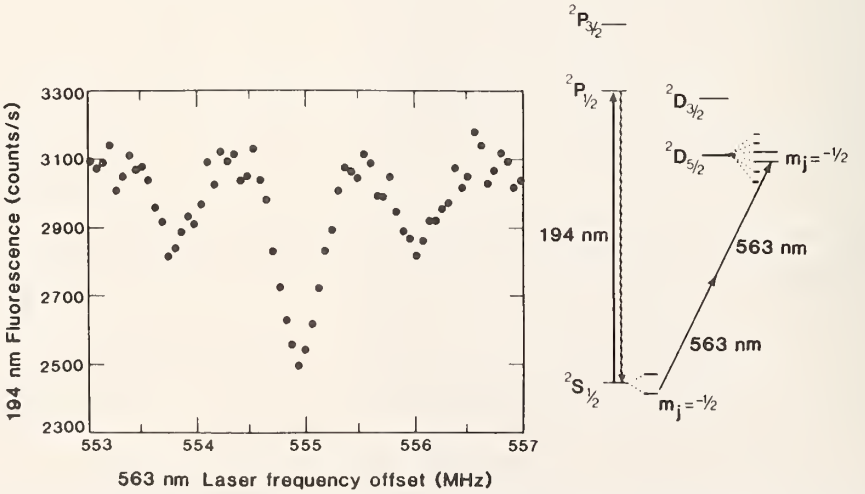

FIG. 2. Two-photon $^2S_{1/2}$ -$^2D_{5/2}$ transition in $^{198}Hg^+$. Amplitude modulation by the harmonic secular motion of the ions is visible in this scan. The frequency scan is 4 MHz at the fundamental laser frequency ($\lambda \cong 563$ nm). The depth of the central component is about 25% of full scale. The integration time is 2 s/point. In the inset is a simplified energy-level diagram of $^{198}Hg^+$, depicting the levels of interest.

ment of the laser-induced fluorescence of the 194-nm transition. The radiation from the dye laser near 563 nm was tuned to resonance with the two-photon transition and chopped on and off. During the time that the laser radiation was on, it drove (10–20)% of the ion population into the D state. The time constant for the atomic system to relax during the radiation-off period could be determined from the exponential return of the 194-nm fluorescence to steady state. An example is shown in Fig. 3. The relaxation rate was measured over a range of He pressures differing by a factor of 4. The reported radiative lifetime is the result of an extrapolation to zero pressure of a linear least-squares fit to the data. The pressure-induced decay rate was determined poorly, but amounted to only about 25% of the radiative decay rate at the highest pressure (about 6×10^{-2} Pa).

We have also measured the absolute wave number of the $^2S_{1/2}$ -$^2D_{5/2}$ two-photon transition by measuring the frequency difference between the two-photon resonance and the t hyperfine component of the nearby $R(33)$ line of the 21-1 band in $^{127}I_2$ (line No. 1220 in the iodine atlas).[14] At zero magnetic field, the two-photon transition in $^{198}Hg^+$ lies 551(2) MHz to the red of this component. To a fairly good approximation, the center of gravity for the $R(33)$ line is situated at a point $\frac{5}{9}$ the distance between the t and b hyperfine components.[15] From this approximation, we find that the two-photon signal is 998(5) MHz to the red of the center of gravity of this iodine line. Thus, the measured wave number is 17 757.1522(20) cm^{-1} as determined relative to the Gerstenkorn and Luc value of 17 757.1855(20) cm^{-1} for the center of gravity of the $R(33)$ 21-1 line in iodine.[14,15] Tellinghuisen finds a consistent discrepancy of the order of 0.002–0.003 cm^{-1} between his predictions for the line center of gravity and those of Gerstenkorn and Luc for lines with odd J values in this spectral region (there is good agreement for lines with even J values).[16] Tellinghuisen calculates a value for the line center of gravity of 17 757.182(2) cm^{-1}. Using this value, we find the two-photon transition to be at 17 757.149(2) cm^{-1}. These values are in good agreement with the direct wavelength measurement of the electric quadrupole emission of the $^2D_{5/2}$-$^2S_{1/2}$ transition obtained from a mild electrodeless discharge in a ^{198}Hg cell backfilled with about 700 Pa of neon and from a standard ^{198}Hg cell backfilled with 33 Pa of argon.[17] The wavelength measured in standard air is 2814.9389(5) Å, which corresponds to a vacuum wave number of 17 757.146(3) cm^{-1} for the two-photon transition. In this Letter, we report the wave number of the two-photon transition to be 17 757.152(3) cm^{-1}. The quoted uncertainty allows for the discrepancy in the determinations of the iodine-line center of gravity.

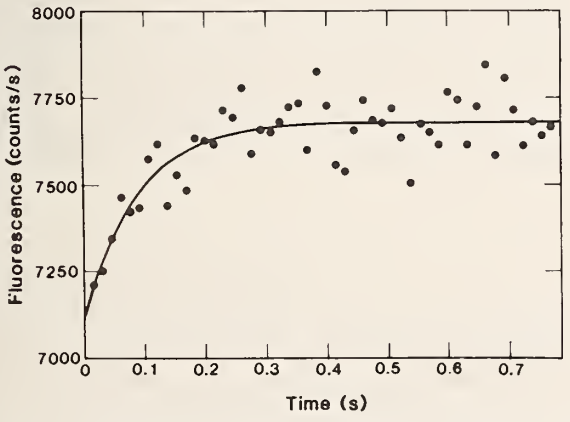

FIG. 3. Measurement of the radiative lifetime of the $5d^96s^2\,^2D_{5/2}$ state in Hg^+. The dots are the experimental points indicating the return of the atomic system to steady state after chopping off of the radiation from the 563-nm dye laser that drives the ions from the ground state to the metastable D state by two-photon absorption. The solid line is a least-squares fit of an exponential to the experimental data. The vertical axis is the counts per second obtained by measurement of the laser-induced fluorescence from the continuously driven $^2P_{1/2}$-$^2S_{1/2}$ transition. The horizontal axis shows time after the turning off of the 563-nm laser radiation.

In the near future, we anticipate narrowing the 563-nm laser linewidth to the order of a few kilohertz and studying various systematic effects including pressure broadening and shifts, power broadening, and light shifts. Ultimately, we would like to narrow the laser linewidth to a value near that imposed by the natural lifetime of the D state, and to drive this two-photon, or single-photon, electric quadrupole transition on a single, laser-cooled ion. Single-photon excitation of the $^2D_{5/2}$ state is particularly attractive because light shifts are eliminated. Light shifts are expected to contribute the largest uncertainty to the resonance frequency for two-photon excitation.[5]

We gratefully acknowledge the support of the U. S. Air Force Office of Scientific Research and the U. S. Office of Naval Research. We wish to thank R. Blatt (University of Hamburg) for technical assistance in the construction of the rf trap and H. Layer (National Bureau of Standards) for supplying the ^{198}Hg. We take particular pleasure in acknowledging the help of W. Martin, J. Reader, and C. Sansonetti (National Bureau of Standards) who provided the correct wavelength for the $^2D_{5/2}$ -$^2S_{1/2}$ transition. We also wish to thank D. Huestis (SRI) and our colleague R. Drullinger for many useful conversations and insights. One of us (G. L.) is a Heisenberg Fellow of the Deutsche Forschungsgemeinschaft.

[a]Present address: Allied Bendix Aerospace Corporation,

Columbia, Md.

[b]Present address: Springer-Verlag, Heidelberg, West Germany.

[c]Present address: Max-Planck-Institute für Quantenoptik, Garching, West Germany.

[1]H. G. Dehmelt, Adv. At. Mol. Phys. **3**, 53 (1967), and **5**, 109 (1969), and IEEE Trans. Instrum. Meas. **31**, 83 (1982).

[2]D. J. Wineland, W. M. Itano, and R. S. Van Dyck, Jr., Adv. At. Mol. Phys. **19**, 135 (1983).

[3]D. J. Wineland, W. M. Itano, J. C. Bergquist, J. J. Bollinger, and J. D. Prestage, in *Atomic Physics 9,* edited by R. S. Van Dyck, Jr. and E. N. Fortson (World Scientific, Singapore, 1984), p. 3.

[4]P. L. Bender, J. L. Hall, R. H. Garstang, F. M. Pichanick, W. W. Smith, R. L. Barger, and J. B. West, Bull. Am. Phys. Soc. **21**, 599 (1976).

[5]D. J. Wineland, J. C. Bergquist, R. E. Drullinger, H. Hemmati, W. M. Itano, and F. L. Walls, J. Phys. (Paris), Colloq. **42**, C8-307 (1981); D. J. Wineland, W. M. Itano, J. C. Bergquist, and F. L. Walls, in Proceedings of the Thirty-Fifth Annual Symposium on Frequency Control, 1981 (unpublished), p. 602 (copies available from Electronic Industries Assoc., Washington, D.C.).

[6]R. H. Garstang, J. Res. Nat. Bur. Stand. Sect. A **68**, 61 (1964).

[7]W. Neuhauser, M. Hohenstatt, P. Toschek, and H. G. Dehmelt, Phys. Rev. Lett. **41**, 233 (1978).

[8]W. Nagourney, G. Janik, and H. G. Dehmelt, Proc. Nat. Acad. Sci. U. S. A. **80**, 643 (1983); G. Janik, W. Nagourney, and H. Dehmelt, J. Opt. Soc. Am. 2, 1251 (1985).

[9]E. C. Beaty, to be published.

[10]D. J. Wineland, J. C. Bergquist, W. M. Itano, and R. E. Drullinger, Opt. Lett. **5**, 245 (1980).

[11]H. G. Dehmelt, in *Advances in Laser Spectroscopy,* edited by F. T. Arecchi, F. Strumia, and H. Walther (Plenum, New York, 1983), p. 153.

[12]H. Hemmati, J. C. Bergquist, and W. M. Itano, Opt. Lett. **8**, 73 (1983).

[13]H. A. Schuessler, Appl. Phys. Lett. **18**, 117 (1971); F. G. Major and J. L. Duchene, J. Phys. (Paris) **36**, 953 (1975); H. S. Lakkaraju and H. A. Schuessler, J. Appl. Phys. **53**, 3967 (1982); M. Jardino, F. Plumelle, and M. Desaintfuscien, in *Laser Spectroscopy VI* , edited by H. P. Weber and W. Lüthy (Springer-Verlag, Berlin, 1983), p. 173; L. S. Cutler, R. P. Giffard, and M. D. McGuire, Appl. Phys. **36**, 137 (1985).

[14]S. Gerstenkorn and P. Luc, *Atlas du Spectre d'Absorption de la Molecule de l'Iode Entre 14 800–20 000 cm*$^{-1}$ (Editions du C. N. R. S., Paris, 1978).

[15]S. Gerstenkorn and P. Luc, Rev. Phys. Appl. **14**, 791 (1979).

[16]J. Tellinghuisen, private communication.

[17]J. Reader and C. J. Sansonetti, to be published.

Reprinted from Journal of the Optical Society of America B, Vol. 2, page 1392, September, 1985
Copyright © 1985 by the Optical Society of America and reprinted by permission of the copyright owner.

Measurements of the g_J factors of the $6s\ ^2S_{1/2}$ and $6p\ ^2P_{1/2}$ states in $^{198}Hg^+$

Wayne M. Itano, J. C. Bergquist, and D. J. Wineland

Time and Frequency Division, National Bureau of Standards, Boulder, Colorado 80303

Received February 22, 1985; accepted April 19, 1985

Measurements of $^{198}Hg^+$ g_J factors by two methods are reported. The first method was based on optical wavelength measurements of the Zeeman components of the $6s\ ^2S_{1/2}$ (ground state) to $6p\ ^2P_{1/2}$ transition at 194 nm. The lines were observed by the absorption of tunable 194-nm radiation by Hg^+ ions created in a rf discharge. The results were $g_J(6s\ ^2S_{1/2}) = 2.0036(20)$ and $g_J(6p\ ^2P_{1/2}) = 0.6652(20)$. The second method was based on microwave-optical double resonance of ions confined in a Penning trap. They were optically pumped by the 194-nm source, which was tuned to a particular Zeeman component. An increase in the resonance-fluorescence intensity was observed when the microwave frequency was tuned to the ground-state Zeeman resonance. The result is $g_J(6s\ ^2S_{1/2}) = 2.003\ 174\ 5(74)$.

INTRODUCTION

Few measurements of g_J factors in Hg^+ have been made. Measurements made with optical precision (typically a few parts in 10^3) are useful for determining the purity of the configurations and coupling schemes. Van Kleef and Fred[1] measured the g_J factors of the $7s\ ^2S_{1/2}$, $6p\ ^2P_{3/2}$, and $5d^96s^2\ ^2D_{5/2}$ states by optical spectroscopy. The values agree with those calculated for LS coupling to within the accuracy of the measurements. No measurements of the $6p\ ^2P_{1/2}$ state have been published previously. The present results for this state agree with the LS coupling value.

Measurements made with higher precision, usually by microwave-resonance techniques, are sensitive to relativistic and many-body effects and test calculational methods. Schuessler and Hoverson[2] observed a ground-state magnetic resonance in $^{199}Hg^+$ by spin exchange with optically pumped Rb and derived a value for the ground-state g_J factor. The results of the present study are in considerable disagreement with this value but are in agreement with a recent calculation by Dzuba *et al.*[3]

EXPERIMENTAL METHOD

Two different methods of measuring g_J factors were used in this study. The first relied on optical wavelength measurements of the Zeeman components of an absorption line. The ions in this case were created in a rf discharge. The second method used microwave-optical double resonance. This method had much higher resolution than the first but could be applied only to the ground state. The ions in this case were contained in a Penning ion trap.[4]

A narrow-band, tunable, cw 194-nm radiation source was used in both methods. This source was described previously.[5] The 194-nm radiation was generated by sum-frequency mixing 257- and 792-nm radiation in a potassium pentaborate crystal. The 257-nm radiation was generated by frequency doubling the output of a single-mode cw 514.5-nm Ar^+ laser in an ammonium dihydrogen phosphate crystal. The 792-nm radiation was generated by a single-mode cw dye laser, which provided the tunability. Ring cavities were used to increase the circulating powers at the input frequencies at both the frequency-doubling and frequency-mixing stages. The linewidth of the 194-nm radiation was about 2 MHz, and the output power was a few microwatts. The Ar^+ laser was frequency stabilized to a saturated-absorption feature of known wavelength in the $^{127}I_2$ spectrum. The wavelength of the dye laser was measured with an interferometric wavemeter of the lambdameter type.[6]

For the optical g_J factor measurements, the Hg^+ ions were created in a cell with fused-silica windows containing Ne at a pressure of about 800 Pa (6 Torr) and a droplet of ^{198}Hg. A discharge was excited by applying a few watts of power at a frequency of approximately 150 MHz to a coil surrounding the cell. The cell was placed in the gap of an electromagnet. The magnetic field of approximately 1.3 T was measured with a nuclear magnetic resonance (NMR) probe.

The intensity (after attenuation) of the 194-nm radiation transmitted through the discharge was measured as a function of the dye-laser frequency with a photomultiplier tube (PMT). The detected signal was normalized to the incident power in order to reduce noise and to eliminate sloping baselines owing to variations of the power as a function of frequency or time. The results of a typical laser scan are shown in Fig. 1. The width of the scan, approximately 6.5 GHz, was calibrated with a Fabry–Perot interferometer of 250-MHz free-spectral range. The wavelength of the dye laser was measured at a point near the resonance center with the lambdameter.

For the microwave-optical double-resonance measurements, the Hg^+ ions were confined in a Penning trap. The trap apparatus and the optics for introducing the light and detecting the fluorescence were similar to those described previously for use with Mg^+ ions[7] except that the trap electrodes were made from Mo rather than Cu. The characteristic inner dimensions were $r_0 = 0.417$ cm and $z_0 = 0.254$ cm. The magnetic field was approximately 1.3 T, and the potential between the ring electrode and the end-cap electrodes was approximately 1 V for trapping Hg^+ and about 6 V for trapping electrons. Ions were created inside the trap by ionization of neutral ^{198}Hg, introduced through a leak valve,

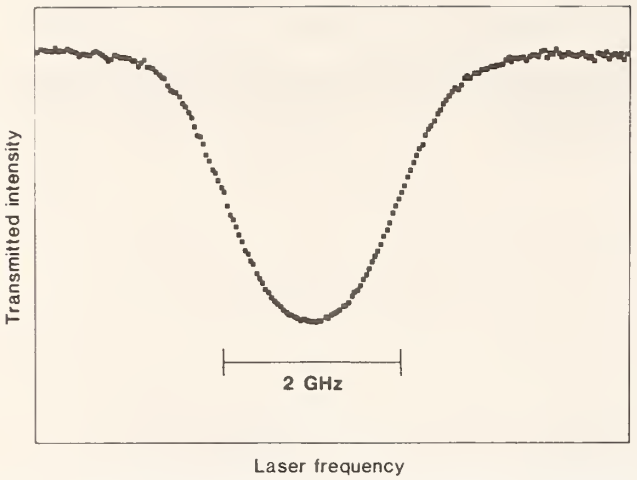

Fig. 1. Graph of the intensity of the 194-nm radiation transmitted through the rf discharge as a function of laser frequency, showing the absorption that is due to the $M_J = -1/2$ to $M_J = +1/2$ component of the $^{198}Hg^+$ $6s\ ^2S_{1/2}$ to $6p\ ^2P_{1/2}$ transition.

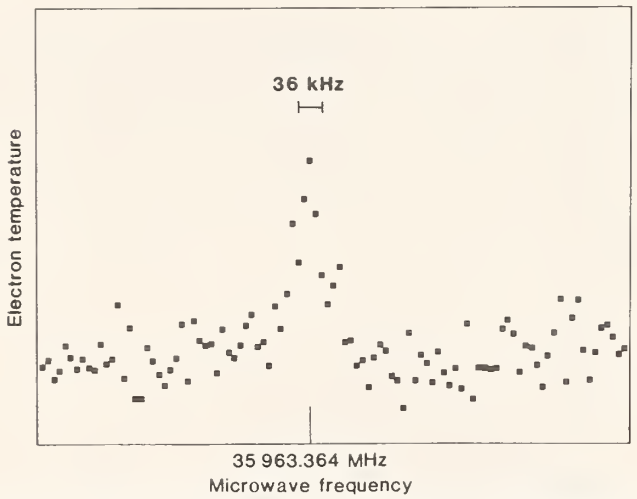

Fig. 2. Graph of the temperature of electrons in the Penning trap as a function of the applied microwave frequency, showing the cyclotron resonance.

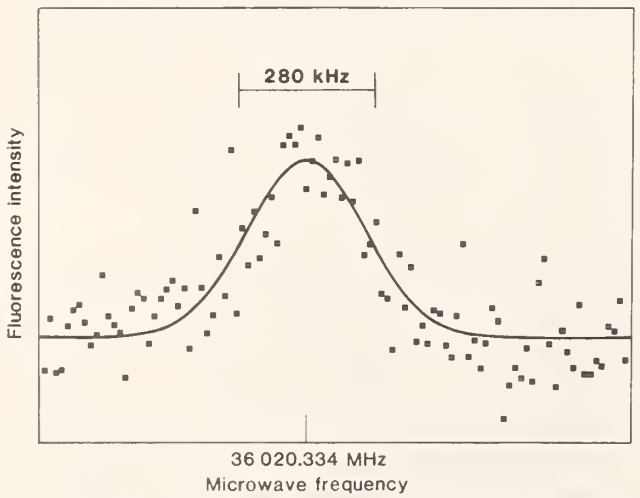

Fig. 3. Graph of the 194-nm resonance-fluorescence intensity of $^{198}Hg^+$ ions in the Penning trap as a function of the applied microwave frequency, showing the ground-state Zeeman resonance. The curve is a least-squares fit to a Gaussian.

with an electron beam directed along the trap axis. The storage time was typically a few minutes, limited by neutral ^{198}Hg pressure. The 194-nm radiation was introduced through a hole in the ring electrode along a direction perpendicular to the trap axis. Photons scattered by the ions back through the hole in the ring electrode were counted by a PMT. The net detection efficiency (number of photoelectrons counted per photon emitted by the ions) was of the order of 0.5×10^{-4}. Microwave radiation was transmitted through a window in the vacuum envelope using a pair of horns (one as a transmitter outside the vacuum apparatus and one as a receiver inside the vacuum apparatus) and introduced into the trap through the gap between the ring and one of the end caps. The number of ions trapped was estimated by driving the axial motion of the ion cloud in the wings of the resonance with a rf electric field and measuring the induced currents. The maximum number was about 8×10^4. The magnetic field was stabilized by means of a NMR probe. The magnetic field inside the trap was calibrated by detecting the cyclotron resonance of a cloud of electrons, using the bolometric method.[8] In this method the translational motions of the electrons are detected by the currents induced in an external circuit coupled to the trap electrodes. The microwave source for the electron-cyclotron excitation was a frequency tripler driven by a frequency synthesizer. A typical cyclotron-resonance curve is shown in Fig. 2.

To observe the Hg^+ ground-state Zeeman resonance, the 194-nm source was tuned to the $6s\ ^2S_{1/2}(M_J = -1/2)$ to $6p\ ^2P_{1/2}(M_J = +1/2)$ transition. The ions were pumped to the $M_J = +1/2$ ground-state sublevel and ceased scattering photons, since they were no longer in resonance. When the frequency of the applied microwave radiation matched the ground-state Zeeman resonance, the $M_J = -1/2$ sublevel was repopulated, and an increase in the resonance fluorescence was detected. Here, the microwave source was a klystron, phase-locked to a harmonic of a frequency synthesizer. Up to 100 mW of power was available at the end of the horn. A typical resonance curve is shown in Fig. 3. The linewidth was larger than for the electron-cyclotron resonance. This was probably due to magnetic-field inhomogeneities and a larger spatial extent of the Hg^+-ion cloud compared with that of the electron cloud.

RESULTS

Two or three optical measurements were made of each of the four Zeeman components. The centers of the absorption curves were determined by least-squares fitting to a function of the form, transmitted intensity $= C_1 + C_2 \exp(-C_3 \exp\{-[(\upsilon - C_4)/C_5]^2\})$, where υ was the dye-laser frequency and C_1–C_5 were constants. This line shape included the effect of saturation on the Gaussian Doppler profile, which tended to broaden the lines. All the line shapes were fitted with a Doppler-width parameter (C_5) corresponding to a temperature of approximately 400 K. The temperature of the rf discharge was not measured directly. The reproducibility of the line centers was ±20 MHz. The uncertainties in absolute frequencies of up to several hundred megahertz, which were due mostly to the uncertainty of the frequency of the reference laser of the lambdameter, were unimportant since only frequency differences were needed to determine the g_J factors. Similarly, perturbations that shifted all magnetic sublevels

of a state equally, such as pressure shifts, could be neglected. From the four frequency measurements, there were two independent ways to obtain the S-state Zeeman splitting and two independent ways to obtain the P-state splitting. The average values were 36 033(30) MHz for the S state and 11 964(30) for the P state. The measured-proton NMR frequency in a mineral-oil sample was 54.708 MHz, corresponding to a magnetic field of 1.284 95 T. The resulting values for the g_J factor were 2.0036(20) for the S state and 0.6652(20) for the P state.

The g_J factor of the ground S state was obtained from the Hg^+ microwave-resonance frequency $\upsilon(Hg^+)$ and the unperturbed electron cyclotron frequency υ_c by the equation $g_J = 2\upsilon(Hg^+)/\upsilon_c$. The measured cyclotron frequency υ_c' differed from υ_c because of the electric fields of the Penning trap.[4] The correction was calculated from the axial resonance frequency υ_z, measured by the bolometric method, according to $\upsilon_c \cong \upsilon_c' + \upsilon_z^2/2\upsilon_c'$. At a particular value of the magnetic field, $\upsilon(Hg^+)$ was measured to be 36 020.477(48) MHz, whereas υ_c' was measured to be 35 963.345(24) MHz. The line centers were determined by least-squares fitting to Gaussians. The value of υ_z was 59.25 MHz. The result was $g_J(6s\ ^2S_{1/2}) = 2.003\ 174\ 5(74)$. The statistical error was only 1.5 parts in 10^6 (ppm), but a possible systematic error may have arisen because the Hg^+ ions and the electrons may not have sampled the same average magnetic field. We estimated this error to be no more than the half-width of the Hg^+ resonance (3.4 ppm).

DISCUSSION

The measured g_J factor of the $6p\ ^2P_{1/2}$ state is equal to the value calculated for LS coupling (0.665 89) within the experimental error. This is the first reported measurement of this quantity.

The values of the ground-state g_J factor measured by the two methods are in agreement. They are both in serious disagreement with the measurement of Schuessler and Hoverson.[2] The present measurement is, however, in good agreement with a recent calculation based on the relativistic Hartree–Fock equations and many-body perturbation theory.[3] It is probably more instructive to express these results in terms of the small deviation, $\Delta g = g_J(6s\ ^2S_{1/2}) - g_e$, of the g_J factor from the free-electron g factor ($g_e = 2.002\ 319\ 30$) than in terms of the g_J factor itself. The present experimental result is $\Delta g = 0.8552(74) \times 10^{-3}$, the experimental result of Schuessler and Hoverson[2] is $\Delta g = 14.7(1.0) \times 10^{-3}$, and the theoretical result is $\Delta g = 1.02 \times 10^{-3}$. An empirically corrected result of 0.85×10^{-3} is also given in Ref. 3. The correction is based on the difference between the experimental and theoretical values for isoelectronic Au.

In light atoms, deviations of the g_J factor of a $^2S_{1/2}$ state are due to the relativistic and diamagnetic interactions given by Abragam and Van Vleck.[9] For the alkali atoms up to K, calculations based on these interactions are in good agreement with experiment.[10] For these atoms Δg is negative. However, for the heavier alkali atoms and for Au and Hg^+, which also have $^2S_{1/2}$ ground states, Δg is positive. This is primarily due to a perturbation that is of the second order in the spin–orbit interaction and of the first order in the residual Coulomb interaction. Calculations that take this effect into account agree well with experiment.[3,11,12]

ACKNOWLEDGMENTS

We gratefully acknowledge the support of the U.S. Air Force Office of Scientific Research and the U.S. Office of Naval Research. We wish to thank Howard Layer (National Bureau of Standards) for supplying the ^{198}Hg and the authors of Ref. 3 for making their results available to us before publication.

REFERENCES

1. T. A. M. Van Kleef and M. Fred, "Zeeman effect measurements in neutral and singly ionized mercury," Physica (Utrecht) **29**, 389–404 (1963).
2. H. A. Schuessler and S. J. Hoverson, "Measurement of the hyperfine structure Zeeman splitting of the Hg^+ ion," Phys. Lett. **43A**, 25–26 (1973); S. J. Hoverson, "Measurement of the hyperfine structure Zeeman splitting of the ground state of the mercury ion," Ph.D. dissertation (Texas A&M University, College Station, Tex., 1974).
3. V. A. Dzuba, V. V. Flambaum, P. G. Silvestrov, and O. P. Sushkov, "Anomalies of g-factor in heavy atoms," Phys. Scr. **31**, 275–280 (1985).
4. H. G. Dehmelt, "Radio frequency spectroscopy of stored ions. I: Storage," Adv. At. Mol. Phys. **3**, 53–72 (1967).
5. J. C. Bergquist, H. Hemmati, and W. M. Itano, "High power second harmonic generation of 257 nm radiation in an external ring cavity," Opt. Commun. **43**, 437–442 (1982); H. Hemmati, J. C. Bergquist, and W. M. Itano, "Generation of continuous-wave 194-nm radiation by sum-frequency mixing in an external ring cavity," Opt. Lett. **8**, 73–75 (1983); D. J. Wineland, W. M. Itano, J. C. Bergquist, J. J. Bollinger, and J. D. Prestage, "Spectroscopoy of stored atomic ions," in *Atomic Physics 9*, R. S. Van Dyck, Jr., and E. N. Fortson, eds. (World Scientific, Singapore, 1984), pp. 8–9.
6. J. L. Hall and S. A. Lee, "Interferometric real-time display of cw dye laser wavelength with sub-Doppler accuracy," Appl. Phys. Lett. **29**, 367–369 (1976).
7. D. J. Wineland, R. E. Drullinger, and F. L. Walls, "Radiation-pressure cooling of bound resonant absorbers," Phys. Rev. Lett. **40**, 1639–1642 (1978).
8. H. G. Dehmelt and F. L. Walls, "Bolometric technique for the rf spectroscopy of stored ions," Phys. Rev. Lett. **21**, 127–131 (1968).
9. A. Abragam and J. H. Van Vleck, "Theory of the microwave Zeeman effect in atomic oxygen," Phys. Rev. **92**, 1448–1455 (1953).
10. L. Veseth, "Many-body calculations of atomic properties: I. g_J-factors," J. Phys. B **16**, 2891–2912 (1983).
11. O. P. Sushkov, V. V. Flambaum, and I. B. Khriplovich, "The nature of the strongly forbidden $M1$ transitions and the g-factor anomalies in heavy atoms," Zh. Eksp. Teor. Fiz. **75**, 75–81 (1978) [Sov. Phys. JETP 48, 37–40 (1978)].
12. G. V. Anikin and I. L. Zhogin, "Calculation of corrections to g factors of alkali-metal atoms," Opt. Spectrosk. **51**, 549–550 (1981) [Opt. Spectrosc. (USSR) **51**, 303–304 (1981)].

Reprinted from Optics Letters, Vol. *12*, page 389, June 1987.
Copyright © 1987 by the Optical Society of America and reprinted by permission of the copyright owner.

Absorption spectroscopy at the limit: detection of a single atom

D. J. Wineland, Wayne M. Itano, and J. C. Bergquist

Time and Frequency Division, National Bureau of Standards, Boulder, Colorado 80303

Received January 21, 1987; accepted February 26, 1987

We investigate the sensitivity limit of absorption spectroscopy. An experiment is described in which the decrease in transmitted light intensity that is due to absorption by a single, electromagnetically confined atomic ion is observed.

Absorption spectroscopy dates back to the early 19th century when Fraunhofer observed characteristic lines in the solar spectrum (Fraunhofer lines) and to the mid-19th century when Kirchhoff and Bunsen identified specific absorption lines with certain elements.[1] Since that time, absorption spectroscopy has played an important role in the development of atomic and molecular theory and continues to be an important analytical tool in several fields of science. As with most experimental measurements, signal-to-noise ratio and resolution are of primary concern, and various advances have led to increased sensitivity. The laser led to a renewed interest in spectroscopic measurements. Not only can source brightness and resolution be greatly increased but the high spectral intensities have made it possible to observe a host of nonlinear effects that have greatly improved sensitivity and resolution.[2] It is always interesting to ask what the ultimate limits to a technique are. In this Letter we investigate the sensitivity limit of absorption spectroscopy when absorption is detected as a decrease in the radiation transmitted through the absorber.

There are many different kinds of sensitivity limits that could be established given the constraints of a particular experimental configuration. Here we investigate one such limit by asking the question, "What is the smallest number of atoms or molecules that one can detect by using absorption spectroscopy?" The fundamental limit is one atom or molecule, and in this Letter we describe a particular realization of this limit. Previously, the lower limit on number sensitivity was found to be about 65 atoms[3] when a four-wave mixing technique[4] was used.

We can estimate the signal-to-noise ratio in an absorption experiment in the following way. We assume that we have a collimated radiation source of power P incident upon a collection of N atoms or molecules. For simplicity, we assume that the intensity of the source at the position of the atoms is uniform with cross section A. We write the fraction of power absorbed by the atoms as ηP and assume that $\eta \ll 1$. We further assume that the detector converts the incident photons into electric current with quantum efficiency β. Therefore the total detected current is given by $I_D = P(1-\eta)e\beta/(h\nu)$, where e is the electron charge, h is Planck's constant, and ν is the frequency of the incident photons. We define the signal I_s as the change in detector current due to absorption. Therefore we have

$$I_s = \eta P e\beta/(h\nu). \tag{1}$$

The rms noise current can be written as

$$i_n = (i_D^2 + i_T^2 + i_{sh}^2)^{1/2}. \tag{2}$$

In Eq. (2), we have separated the statistically independent contributions from the detector noise i_D (e.g., Johnson noise), radiation-source technical noise i_T (e.g., intensity fluctuations in the radiation from a laser source), and shot noise in the detection process i_{sh}. The shot-noise contribution is simply written as $i_{sh}^2 = 2eI_D\Delta\nu$, where $\Delta\nu$ is the detection bandwidth. The contributions from i_D and i_T will depend on the specific experimental configuration, but we desire i_D, $i_T \ll i_{sh}$ for maximum signal-to-noise ratio.

If absorption is due to a particular atomic transition with resonance frequency ν_0, then, below saturation, the absorption coefficient η is given by the expression $\eta P = N\sigma P/A$, where $\sigma = \sigma_0 K$. σ_0 is the resonant cross section for the particular transition observed. σ_0 is of the order of $\lambda^2/(2\pi)$, where λ is the wavelength at resonance.[5] K is a factor ($K \le 1$) that expresses the reduction of the cross section from the resonant value by (1) radiative decay into atomic states other than the lower state of the transition under investigation, (2) Doppler broadening, (3) collisional broadening, (4) detuning of the source away from ν_0, or (5) finite bandwidth of the radiation source. We can write the signal-to-noise ratio, S/N, as

$$\mathrm{S/N} = I_s/i_n = \frac{N\sigma_0 K e\beta P/(Ah\nu_0)}{[i_D^2 + i_T^2 + 2e^2\beta P\Delta\nu/(h\nu_0)]^{1/2}}. \tag{2}$$

Our experimental configuration is shown in Fig. 1. Since we are interested in the case when $N = 1$, a single, laser-cooled $^{198}Hg^+$ ion was confined in a miniature rf trap[6] with inside endcap-to-endcap spacing $2z_0 = 0.064$ cm and inner ring diameter $2r_0 = 0.091$ cm. With a ring-to-endcap voltage $V_T \simeq (10 + 400 \cos \Omega t)V$, where $\Omega/2\pi = 21.07$ MHz, the ion was confined to a space with linear dimensions <0.25 μm.[6] A narrow-band (width < 5 MHz) radiation source at 194

 © 1987, Optical Society of America

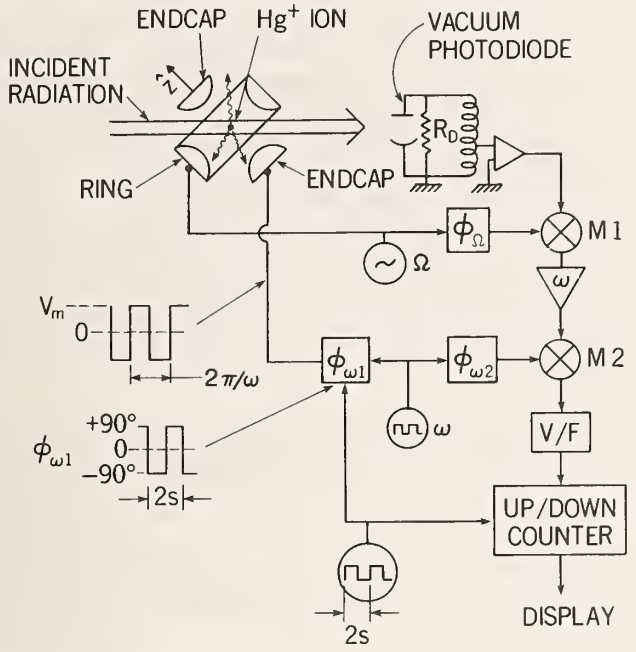

Fig. 1. Schematic diagram of the apparatus. Absorption from a single $^{198}Hg^+$ ion is detected as a change in current in the vacuum photodiode. This absorption is modulated at frequency Ω by applying a voltage V_m to one endcap electrode of the trap. To avoid a false signal from stray radiation picked up by the detector, the sign of V_m is alternated at frequency ω. To avoid drifts at the output of mixer M2, a third modulation at 0.5 Hz of the phase of ω and the sign of the signal at M2 is converted to dc by the up/down counter. V_m, ϕ_Ω, and $\phi_{\omega 2}$ are adjusted to maximize the display output.

nm ($P \simeq 3\ \mu$W) was tuned near the $6s\ ^2S_{1/2} \rightarrow 6p\ ^2P_{1/2}$ first resonance transition in $^{198}Hg^+$ and focused through the trap and onto the ion. This radiation source was derived from sum-frequency mixing a dye laser (790 nm) and a frequency-doubled Ar^+ laser (257 nm).[7] The detector was a vacuum photodiode with a Cs–Te photocathode. We had $\beta \simeq 0.055$ (10% tube efficiency; 55% transmission from trap to detector). In order to suppress i_T from the 194-nm source, it is desirable to modulate the absorption at a high frequency.[8] This was accomplished by applying a voltage V_m to one trap endcap. This displaced the ion from its equilibrium position in the rf trap and caused its velocity, which has a component along the direction of the 194-nm beam, to be modulated at the trap rf Ω. That is, the static electric force was compensated for by the pseudopotential force that gave rise to ion micromotion at frequency Ω.[9] Owing to the first-order Doppler shift, the resonance frequency of the ion was modulated at Ω. Such frequency-modulation schemes were first used in nuclear magnetic resonance[10] and microwave spectroscopy.[11] This scheme of velocity modulation is essentially identical with that developed by Saykally and co-workers.[12] As is indicated in Fig. 1, the modulated-absorption signal current was detected by a tuned circuit whose equivalent parallel resistance, $R_D \simeq 300$ kΩ, was derived from the measured resonance Q and parallel capacitance ($\simeq$3 pF owing to tube and stray capacitance). Unfortunately, the detector also picked up radiation from the unshielded trap electrodes, which gave a false signal that was unstable. To avoid this problem, we switched the phase of the absorption signal by 180° by switching the sign of the voltage V_m applied to the endcap at the frequency $\omega/2\pi = 2$ kHz. Therefore, after the first mixer (M1), the absorption signal appeared at frequency ω, which we then converted to a dc voltage in M2. To avoid drifts at the output of M2, we switched the phase, $\phi_{\omega 1}$, of V_m by 180° every second and used a voltage-to-frequency converter (V/F) followed by an up/down counter to display the signal. The values of V_m and the phases ϕ_Ω and $\phi_{\omega 2}$ were adjusted to give maximum absorption signal.

From Eq. (3), in order to maximize S/N, we want to make P as large as possible until saturation is reached. When the incident radiation exceeds saturation intensity, the numerator of Eq. (3) reaches a constant value given by $\sigma_0 KP/(Ah\nu_0) \simeq \gamma/2$, where γ^{-1} is the radiative lifetime of the upper state. Increasing P further only increases i_{sh}, thereby reducing S/N. If we assume that the incident radiation is just at saturation intensity, and if we neglect i_T in Eq. (3), Eq. (3) becomes (for $N = 1$)

$$\mathrm{S/N} = (\pi\sqrt{2})^{-1} \frac{e\beta\gamma/(2\Delta\nu^{1/2})}{[4k_BT/R_D + e^2\beta\gamma A/(\sigma_0 K)]^{1/2}}. \qquad (4)$$

The factor $(\pi\sqrt{2})^{-1}$ accounts for the modulation scheme used but makes the simplifying assumption that the atomic absorption changes linearly between zero and its maximum value as the atomic-resonance frequency is modulated through its full extent. We have made the identification $i_D^2 = 4k_BT\Delta\nu/R_D$, where k_B is Boltzmann's constant and T is the effective temperature of the input circuit. For the first resonance transition in Hg^+, $\gamma^{-1} = 2.3$ nsec, and $\sigma_0 = 6.0 \times 10^{-11}$ cm^2. The ion was at the center of our focused Gaussian laser beam ($w_0 \simeq 5\ \mu$m). $K \simeq 1$, which was the key to this experiment. Therefore, we calculate that the second term in the denominator of Eq. (4) is negligible. This was verified by a direct measurement of i_{sh}/i_D. We determined that the detector-noise temperature was $T \simeq 600$ K ($\simeq$3-dB noise figure) by measuring photon shot noise on the detector and assuming that $i_T \ll i_D$ at 21.07 MHz. Making the identification $\Delta\nu = (2\tau)^{-1}$, where τ is the integration time per point out of the up/down counter, we calculate that S/N ≈ 12.6 ($\eta \approx 2.5 \times 10^{-5}$) for $\tau = 50$ sec from Eq. (4). This compares reasonably well with the data of Fig. 2, where we measured S/N $\simeq 5.7$. For the maximum signal, the laser is tuned halfway down the resonance line and the absorption of the single ion is modulated between a few percent and nearly 100% of the maximum absorption at frequency Ω. The disagreement between theory and experiment may be due to two causes. First, the simple theory assumes that the absorption signal occurs only at frequency Ω and neglects signal content at harmonics of Ω. Second, we have neglected loss of signal due to radiative decay from the $^2P_{1/2}$ state to the metastable $^2D_{3/2}$ level. Data similar to those of Ref. 6 indicate this may account for reduction in signal by a factor of about 2 in the present experiment.

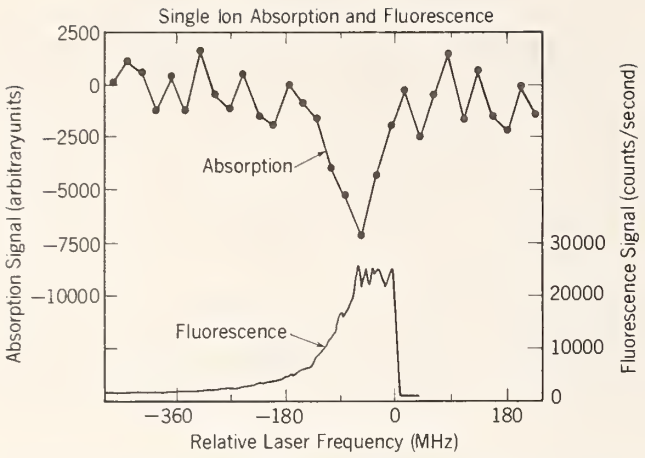

Fig. 2. Absorption signal observed as the 194-nm source is tuned through ν_0. Lower trace shows the simultaneously observed fluorescence scattering; the flat-topped appearance of this curve is due to the frequency modulation of the ion resonance. Integration times per point are 50 and 10 sec in the upper and lower traces, respectively.

We expect the signal to show a dispersion shape as the frequency of the 194-nm source is tuned through the resonance frequency ν_0. Only half of the dispersion feature (Fig. 2) was observed because the ion rapidly heated when the frequency of the 194-nm source was tuned above the resonance frequency ν_0.[13] This caused a significant decrease in scattering owing to increased Doppler broadening and decreased spatial overlap of the laser beam with the ion; i.e., K became very small. If we simultaneously observed the fluorescence scattering (lower trace in Fig. 2), the absorption signal first reached its maximum amplitude (minimum of upper curve in Fig. 2) and then returned to zero at the resonance frequency, as indicated by the sudden drop in fluorescence in the lower trace. This verified that the signal was mostly due to frequency modulation rather than to amplitude modulation (achieved by moving the ion in and out of the laser beam) since the maximum signal for amplitude modulation would be achieved at ν_0. The frequency modulation also accounts for the flat-topped shape of the fluorescence curve in Fig. 2. The optimum value of V_m was independently verified by observing the intensity modulation of the fluorescence signal at 21.07 MHz by measuring time correlations of the photons scattered by the single ion.

S/N in the present experiment could be increased by a factor of about 4 if i_D could be reduced so that the noise was dominated by i_{sh}. When i_{sh} dominates, Eq. (4) tells us that we can improve S/N by decreasing the laser spot size A. Stronger focusing in this experiment was prevented by the size of the input windows to the trap. In order just to maintain saturation we must reduce P accordingly. In the limit where A approaches σ_0, the absorption of the input beam by the ion would approach several percent. In this limit, the detector could be a photomultiplier tube operated in the photon-counting mode. i_D would be replaced by tube dark counts, and S/N would approach the square root of the number of detected counts. If we can neglect i_D and i_T, the choice of absorption or fluorescence detection is straightforward. If the fraction ϵ of fluorescence photons striking the detector is greater than η, fluorescence detection gives the greater S/N. The reverse is true for $\eta > \epsilon$. We have assumed that β is the same for the absorption and fluorescence detectors.

We gratefully acknowledge the support of the U.S. Office of Naval Research and the U.S. Air Force Office of Scientific Research. We thank R. G. Hulet for assistance in several experiments that led to the experiment reported here. We also thank R. G. Hulet, A. De Marchi, L. Hollberg, C. Wieman, C. Howard, and P. Hammer for helpful suggestions on the manuscript.

References

1. A concise historical review is given by R. A. Sawyer, *Experimental Spectroscopy*, 3rd ed. (Dover, New York, 1963), pp. 1–17.
2. See, for example, K. Shimoda, ed., *High Resolution Laser Spectroscopy* (Springer-Verlag, Berlin, 1976); R. A. Keller, ed., *Laser-based Ultrasensitive Spectroscopy and Detection V*, Proc. Soc. Photo-Opt. Instrum. Eng. **426** (1983); M. D. Levenson, *Nonlinear Laser Spectroscopy* (Academic, New York, 1982).
3. J. Bialas, R. Blatt, W. Neuhauser, and P. E. Toschek, Opt. Commun. **59**, 27 (1986).
4. S. Le Boiteux, D. Bloch, M. Ducloy, A. Pesnelle, S. Runge, and M. Perdrix, Opt. Commun. **52**, 274 (1984).
5. See, for example, R. Loudon, *The Quantum Theory of Light* (Oxford U. Press, London, 1973), p. 287.
6. J. C. Bergquist, R. G. Hulet, W. M. Itano, and D. J. Wineland, Phys. Rev. Lett. **57**, 1699 (1986).
7. H. Hemmati, J. C. Bergquist, and W. M. Itano, Opt. Lett. **8**, 73 (1983).
8. J. J. Snyder, R. K. Raj, D. Bloch, and M. Ducloy, Opt. Lett. **5**, 163 (1980); L. Hollberg, Ma Long-Sheng, M. Hohenstatt, and J. L. Hall, Proc. Soc. Photo-Opt. Instrum. Eng. **426**, 91 (1983); E. A. Whittaker and G. C. Bjorklund, Proc. Soc. Photo-Opt. Instrum. Eng. **426**, 81 (1983); M. Ducloy and J. J. Synder, Proc. Soc. Photo-Opt. Instrum. Eng. **426**, 87 (1983).
9 H. G. Dehmelt, Adv. At. Mol. Phys. **3**, 53 (1967); **5**, 109 (1969); D. J. Wineland, W. M. Itano, and R. S. Van Dyck, Jr., Adv. At. Mol. Phys. **19**, 135 (1983).
10. N. Bloembergen, E. M. Purcell, and R. V. Pound, Phys. Rev. **73**, 679 (1948).
11. R. H. Hughes and E. B. Wilson, Jr., Phys. Rev. **71**, 562L (1947).
12. C. S. Gudeman, M. H. Begemann, J. Pfaff, and R. J. Saykally, Phys. Rev. Lett. **50**, 727 (1983).
13. R. E. Drullinger, D. J. Wineland, and J. C. Bergquist, Appl. Phys. **22**, 365 (1980).

Laser-cooling limits and single-ion spectroscopy

D. J. Wineland, Wayne M. Itano, J. C. Bergquist, and Randall G. Hulet
Time and Frequency Division, National Bureau of Standards, Boulder, Colorado 80803
(Received 9 January 1987)

The limitations to the achievement of low kinetic energies for laser cooling of single ions confined in electromagnetic traps are discussed. Sideband cooling of an ion in an rf (Paul) trap is reexamined including the effects of finite laser bandwidth and the energy of the rf micromotion. The micromotion is the oscillatory motion of the ion at the same frequency as the rf voltage applied to the trap electrodes. Sideband cooling of ions in a Penning trap is examined for the first time. In both cases, cooling to the zero-point energy of the ion in the trap should be possible and a method for verifying this condition is suggested. The implications for high-resolution, high-accuracy spectroscopy are investigated. Under certain conditions, the uncertainty in the second-order Doppler shift may be significantly less than 1 part in 10^{18}.

I. INTRODUCTION

Over the past few years, the number of experimental and theoretical investigations of laser cooling has increased dramatically.[1–4] Much of this initial work has concentrated on characterizing the cooling process and understanding the lower limits to cooling. This is partly because the attainment of very low velocities will be important in applications such as high-resolution spectroscopy (reduction of Doppler shifts) and low-energy studies of atom-atom and atom-surface interactions. Minimum kinetic energies have often been expressed in terms of temperature. For free or weakly bound atomic particles, we make the identification $m\langle v_i^2\rangle/2 = k_B T_i/2$ where $m\langle v_i^2\rangle/2$ is the kinetic energy in the ith degree of freedom, T_i is the temperature for that degree of freedom, and k_B is Boltzmann's constant. For atomic particles bound in a harmonic well, T_x defined by the above relationship is therefore a measure of the average kinetic energy in the x direction.

When the above relationship between kinetic energy and temperature holds, and when laser cooling is accomplished by driving a single photon transition, the minimum achievable temperature is given by the "Doppler" cooling limit (or "heavy particle" limit[4]),

$$T_D = \hbar\gamma/2k_B \ . \tag{1}$$

In Eq. (1), γ^{-1} is the radiative lifetime of the laser-cooling transition, $2\pi\hbar$ is Planck's constant, and we have assumed that the incident radiation is well below saturation intensity. For atoms bound in a harmonic well with characteristic "vibration" or oscillation frequency ω_v, the Doppler cooling limit applies when $\gamma \gg \omega_v$. The free-particle case is for the limit $\omega_v \to 0$, and thus Eq. (1) still applies. T_D is typically in the range of 1 mK for strongly allowed electric dipole transitions. For the case of stored ions, temperatures less than about 10 mK have been achieved.[5–8] The uncertainties in the measurements have often been consistent with the temperature being at the theoretical limit given by Eq. (1). The lowest measured temperatures have recently been achieved by Chu and co-workers using neutral sodium atoms.[9] They demonstrated a temperature ($T = 240^{+200}_{-60}$ μK) equal to the Doppler cooling limit using three intersecting and mutually perpendicular, standing-wave laser beams which were tuned to give maximum cooling.

For trapped ions or atoms, cooling in the "sideband" limit (when $\gamma \ll \omega_v$) is achieved by tuning the incident radiation to one of the lower motional sidebands of the atomic absorption. For example, in Fig. 1, the laser is assumed to be tuned to $\omega_0 - \omega_v$, where ω_0 is the transition frequency for the atom at rest. In this case, the minimum kinetic energy achieved is often given in terms of the mean occupation number $\langle n_v\rangle$ of the harmonic oscillator state for the atom or ion in the well. The brackets $\langle\ \rangle$ denote the average over time or the average over an en-

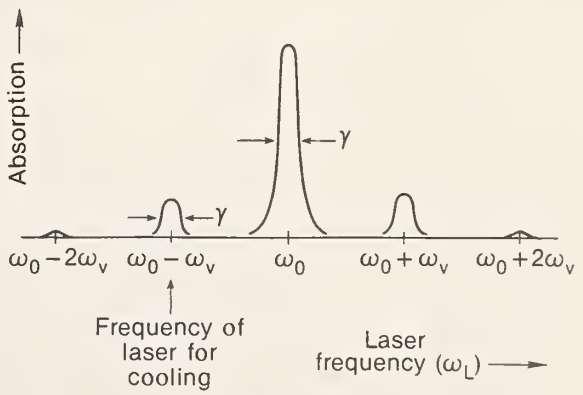

FIG. 1. Absorption spectrum of a single ion bound in a harmonic well, e.g., the absorption spectrum for the secular motion in an rf trap. It is assumed that ω_v (oscillation frequency of the ion in the harmonic well) $\gg \gamma$ (radiative linewidth of the cooling transition). The Lamb-Dicke limit is assumed, i.e., ion excursions are less than $\lambda/2\pi = c/\omega_0$. Therefore, the intensity of the sidebands is small compared to the carrier at ω_0. Maximum cooling is achieved for a narrow-band laser (bandwidth less than γ) tuned to $\omega_0 - \omega_v$.

ork of the U. S. Government
Not subject to U. S. copyright

semble of identically prepared systems, assumed to be the same. In the sideband limit we have[4,10,11]

$$\langle n_v \rangle_s = C_s(\gamma/\omega_v)^2 \ . \tag{2}$$

In Eq. (2), C_s is a constant on the order of 1 which depends on the atomic selection rules for the absorption and reemission. We have assumed that the incident radiation is well below saturation intensity. So far, sideband cooling has not been accomplished for trapped atoms or atomic ions. It has been realized in the special case of cooling the magnetron motion of trapped electrons,[12] but in this case, the minimum achievable temperature is limited by thermal excitation.[11,13]

Since laser cooling gives rise to a thermal distribution of occupation numbers,[4] we can write

$$\langle n_v \rangle = [\exp(\hbar\omega_v/k_B T) - 1]^{-1} \ . \tag{3}$$

Combining Eqs. (2) and (3), we achieve the minimum temperature in the sideband cooling limit,

$$T_s \simeq \hbar\omega_v/[k_B \ln(\langle n_v \rangle^{-1})]$$
$$= \hbar\omega_v/[k_B \ln(\omega_v^2/C_s\gamma^2)] \ . \tag{4}$$

When $\hbar\omega_v \ll k_B T$, Eq. (3) reduces to the expression $m\langle v_i^2 \rangle/2 = k_B T_i/2$, which applies to the Doppler cooling limit of Eq. (1).

Equations (1) and (4) show that lower temperatures could be achieved by using weakly allowed transitions (smaller values of γ). In addition, lower temperatures could be achieved by using combinations of evaporative and adiabatic cooling and/or novel cooling schemes using more than one atomic transition or nonadiabatic manipulation of trap parameters.[14–18] For example, several recent papers[19–23] have considered cooling by using stimulated Raman transitions. Here the cooling limits of Eqs. (1) and (4) apply but γ is now the linewidth of the stimulated Raman transition, which can be quite narrow. Other authors speculate about schemes to achieve temperatures as low as 10^{-10} K for free atoms.[16]

In this paper, we investigate the limits of laser cooling for single trapped ions. We also consider the implications of this cooling for accuracy in high-resolution spectroscopy. Some of the conclusions will also apply to the case of trapped neutral atoms but here we concentrate on the case of trapped ions. As we will try to demonstrate, describing the cooling limits in terms of temperature may not be particularly relevant for spectroscopic purposes. This may also be true for free neutral atoms. For example, if a single atom [mass of 100 u (atomic mass units)] starts from rest, the time it takes it to reach a velocity v corresponding to an effective temperature $T_e = 10^{-10}$ K (via the relationship $\frac{1}{2}mv^2 = \frac{1}{2}k_B T_e$) in the earth's gravitational field is about 10 μs. If we desired to maintain an effective temperature below 10^{-10} K, the interrogation time between applications of cooling radiation would be quite short. For trapped ions or atoms, gravity need not play an important role; it merely shifts the origin of the trap. Therefore, barring other heating effects, interrogation times can be extremely long. Shifts in spectra caused by velocity-changing effects due to recoil can be made negligible. For example, the maximum of the recoil-free "carrier" (at frequency ω_0 in Fig. 1) is shifted slightly due to the overlapping effects of the sidebands at $\omega_0 - \omega_v$ and $\omega_0 + \omega_v$ which are different in amplitude.[11] (See Sec. V.) These pulling effects can be made extremely small.

Perhaps the most interesting case is when the ion or atom is cooled to near the zeroth quantum level, $\langle n_v \rangle \ll 1$. Independently of the method used, if $\langle n_v \rangle \ll 1$ can be achieved, the accuracies for high-resolution spectroscopy need not be limited by motional effects. Since this condition can be achieved using laser cooling on single photon transitions, we investigate only this relatively simple case here. At the outset, unless specifically stated, we consider only a single ion in an rf or Penning trap.[24,25] The reason is simply that for two or more ions in the trap, the limiting kinetic energies are considerably higher than those given by Eqs. (1)–(4). For example, for more than one ion in an rf trap, in order to overcome the Coulomb repulsion between ions, there must be a force on each ion from the trapping potential towards the center of the trap. This implies a certain kinetic energy of micromotion for each ion which can far exceed the kinetic energy of the secular motion. The micromotion[24,25] in an rf trap is the oscillatory motion of the ion(s) at the frequency of the imposed rf voltage applied to the electrodes. The secular motion is the additional, lower-frequency motion of the ion(s) due to the resulting pseudopotential well established by the spatially inhomogenous rf fields. It is this secular motion, at frequency ω_v, which is cooled by laser cooling. The kinetic energy in the micromotion is directly related to the kinetic energy in the secular motion (Refs. 24 and 25 and Sec. II B) but is not directly cooled by the laser. For more than one ion in the trap, even though very low temperatures of the secular motion can be achieved through laser cooling, the kinetic energy would be dominated by the rf motion.[24] For a single ion (Sec. II), this effect is considerably reduced. Similarly, for more than one ion in the Penning trap, the velocity in the rotation of the ion sample[8,24] gives rise to a kinetic energy which can be greater than the limits of Eqs. (1)–(4). For a single ion this effect can be very small (Sec. III).

In Sec. II we reexamine the sideband cooling limit for ions in an rf trap where we include the effects of finite laser bandwidth and the importance of micromotion. In Sec. III, we examine sideband cooling in a Penning trap; this has not been done previously. In Sec. IV, we suggest a possible practical scheme for achieving $\langle n_v \rangle \ll 1$, and in Sec. V, we discuss a method for verifying that the zeroth quantum level is achieved. In Sec. VI we discuss the implications of these results for spectroscopy.

II. SIDEBAND COOLING FOR A SINGLE ION IN AN rf (PAUL) TRAP

A. Laser cooling of secular motion in an rf trap

We assume that the secular motion of the ion in the rf trap is harmonic and characterized by the frequencies ω_x, ω_y, and ω_z for the x, y, and z directions, respectively.

This case, or more generally the cooling of atoms trapped in a harmonic potential well, has been treated extensively in the literature. The most complete treatment appears to be that of Lindberg, Javanainen, and Stenholm, who include the effects of saturation.[4,26] However, lowest minimum temperatures are achieved with laser intensities below saturation, and simple perturbation methods[10,11] can be used to find the minimum kinetic energies. Here, we use the formalism of Refs. 11 and 27, which treats each photon absorption and subsequent reemission as a scattering event—spontaneous Raman scattering. This process is spontaneous scattering because we assume low intensity and therefore the ion returns to its ground state via spontaneous emission. It is Raman scattering because when the internal atomic states and vibration states (oscillation states in the trap) are treated together, the ion can change the vibration quantum number n_v in a scattering event. Let n_{lx} denote the nth vibration state of the ion in the x direction. The subscript l means that this is the initial (l, lower) vibration state of the ion before scattering. Let $P(n_{lx})$ be the probability that the ion is in the initial state with quantum number n_{lx}, where $\sum_{n_{lx}} P(n_{lx})=1$. Assume that the ion is irradiated with a narrow-band laser (bandwidth $\Delta\omega_L \ll \gamma$) directed along the x direction. The average rate of energy change in the ith direction due to this laser in the x direction is given by

$$\langle \dot{E}_{ix} \rangle = \dot{N}_x \sum_{n_{lx},n_{jx}} P(n_{lx})\{Rf_{si}+\delta_{ix}[E(n_{jx})-E(n_{lx})]\} \frac{|\langle n_{jx}|e^{ik_x x}|n_{lx}\rangle|^2}{1+\left[\frac{2}{\gamma}\{\omega_0-\omega_{Lx}+[E(n_{jx})-E(n_{lx})]/\hbar\}\right]^2} . \quad (5)$$

This is a straightforward generalization of Eq. (48) of Ref. 11. $\dot{N}_x = I_x\sigma_{0x}/\hbar\omega_0$ is the scattering rate for the laser tuned to resonance with the ion at rest, ω_0 is the rest frequency of the ion, $R=(\hbar k)^2/2m$ is the recoil energy where k is the photon wave vector ($k=k_x\simeq k_y\simeq k_z$), m is the ion mass, $\hbar k\sqrt{f_{si}}$ is the rms value of reemitted photon momentum along the ith direction,[27] $E(n_{lx}) = \hbar\omega_x(n_{lx}+\frac{1}{2})$ where ω_x is the harmonic well frequency in the x direction, δ_{ix} is the Kronecker δ, and ω_{Lx} is the laser frequency. The sum is over all possible initial vibrational states (with quantum numbers n_{lx}) and intermediate vibrational states j. The intermediate states are the states with the ion in the excited electronic state and with vibrational quantum number n_{jx}. Similar expressions hold for laser beams directed along the y and z directions.

Equation (5) holds for arbitrary ion kinetic energy (neglecting relativistic corrections). The most interesting case, however, is that for maximum laser cooling; that is, when the laser is tuned to the first lower sideband frequency $\omega_0-\omega_x$. For the final stages of cooling, we anticipate that the ion will be in the Lamb-Dicke regime.[28] This condition is given by the relationship $(k^2\langle x^2\rangle)^{1/2} = kx_0\langle 2n_x+1\rangle^{1/2} \ll 1$ where $\langle n_x\rangle = \sum_{n_{lx}} P(n_{lx})n_{lx}$. Qualitatively, the Lamb-Dicke regime implies that the amplitude of the ion's motion is less than $\lambda/2\pi$. $x_0=(\hbar/2m\omega_x)^{1/2}$ is the zero-point amplitude so that $kx_0=(R/\hbar\omega_x)^{1/2}\equiv\beta_x^{1/2}$. Hence, for the Lamb-Dicke limit to apply we must have $R\ll\hbar\omega_x$, or equivalently, $\omega_x \gg \omega_R$ where $\omega_R=R/\hbar$ is the recoil frequency. For $\lambda=300$ nm and $m=100$ u, $\omega_R/2\pi\simeq 22$ kHz. For these conditions and for $\omega_x/2\pi=1$ MHz, then $x_0\simeq 0.007$ μm and $\beta_x=0.022$. If the Lamb-Dicke limit applies, then $e^{ikx}\simeq 1+ikx$, and only three excited states j contribute to the sum in Eq. (5). Therefore (see Fig. 1),

$$\langle \dot{E}_{ix} \rangle \simeq \dot{N}_x[\langle n_x\rangle\beta_x(Rf_{si}-\delta_{ix}\hbar\omega_x)F_x + Rf_{si}\gamma^2/(4\omega_x^2) + (Rf_{si}+\delta_{ix}\hbar\omega_x)(\langle n_x\rangle+1)\beta_x\gamma^2/(16\omega_x^2)] . \quad (6)$$

In Eq. (6), we have now included the factor

$$F_x = \int_0^\infty I_x'(\omega)\frac{d\omega}{1+\left[\frac{2}{\gamma}(\omega_0-\omega_x-\omega)\right]^2} , \quad (7)$$

which allows for the fact that the laser spectral width may be larger than γ. In practice, it may be desirable to make the laser bandwidth much greater than γ to allow for anharmonic contributions to or instabilities in ω_x. For simplicity, we assume that this width is still much less than ω_x. $I_x'(\omega)$ is a normalized intensity such that $\int I_x'(\omega)d\omega=1$. Therefore, the laser spectral intensity is given by $I_xI_x'(\omega)$ where I_x is the total intensity. The average scatter (or absorption) rate $\langle \dot{N}_s \rangle$ is related to Eq. (6) as

$$\langle \dot{N}_{sx} \rangle = \dot{N}_x[\langle n_x\rangle\beta_xF_x+\gamma^2/(4\omega_x^2) + (\langle n_x\rangle+1)\beta_x\gamma^2/(16\omega_x^2)] . \quad (8)$$

If we also have laser beams directed along the y and z axes, equations analogous to Eqs. (5)–(8) hold for $\langle \dot{E}_{iy} \rangle$, $\langle \dot{N}_{sy} \rangle$, $\langle \dot{E}_{iz} \rangle$, and $\langle \dot{N}_{sz} \rangle$.

Case 1. Suppose we have only one laser beam (say, along the x axis) but that the x, y, and z degrees of freedom are thermalized to the same temperature. This would correspond to the case of more than one ion in the trap where Coulomb coupling provides the thermalization, but where we must assume that the individual ion oscillation frequencies are not significantly perturbed. That is, we neglect the effects of space-charge repulsion. The total rate of energy change is given by Eq. (6) as

$$\langle \dot{E} \rangle = \sum_{i(=x,y,z)} \langle \dot{E}_{ix} \rangle \simeq \dot{N}_x\{\langle n_x\rangle[-RF_x+R\gamma^2/(16\omega_x^2)]+5R\gamma^2/(16\omega_x^2)\} , \quad (9)$$

where terms of higher order in β_x have been neglected.

In steady state ($\langle \dot{E} \rangle = 0$), we have

$$\langle n_x \rangle = 5\gamma^2 \{ 16\omega_x^2 [F_x - \gamma^2/(16\omega_x^2)] \}^{-1} .$$

We will assume throughout that the spectral density of the laser is fairly uniform with width $\Delta\omega_L$. If the spectral width of the laser is larger than γ, we can get an estimate of F by assuming that the laser spectrum is flat with width $\Delta\omega_L$, that is, $I_x' = 1/\Delta\omega_L$. For $\Delta\omega_L \gg \gamma$, Eq. (7) gives $F_x = \pi\gamma/2\Delta\omega_L$. Since we have assumed $\Delta\omega_L \ll \omega_x$, then $F \gg \gamma^2/\omega_x^2$ and we can neglect the $\gamma^2/(16\omega_x^2)$ term in the previous expression and obtain

$$\langle n_x \rangle = 5\gamma^2/(16\omega_x^2 F_x) . \tag{10}$$

If the laser linewidth is much less than γ, $F_x = 1$ yielding $\langle n_x \rangle = 5\gamma^2/16\omega_x^2$, which is the result of Ref. 11.

Equation (10) is valid in the Lamb-Dicke limit, $R/\hbar\omega_x \ll 1$. To find corrections to this expression which are first order in $\beta_x = R/\hbar\omega_x$ we must include matrix elements $\langle n_x - 2 \mid e^{ikx} \mid n_x \rangle$ and $\langle n_x + 2 \mid e^{ikx} \mid n_x \rangle$ in Eq. (5) and take $e^{ikx} = 1 + ikx - k^2x^2/2$. In this case we obtain

$$\langle n_x \rangle = \frac{5}{16}\frac{\gamma^2}{\omega_x^2}(1 + \tfrac{22}{45}\beta_x)/F_x . \tag{11}$$

Case 2. Suppose we have three laser beams directed along the x, y, and z axes which are tuned to the appropriate first lower sidebands for each direction. We must write an equation for $\langle \dot{E}_x \rangle$, the rate of energy change in the x direction, using Eq. (6), and the analogous equations which give contributions to $\langle \dot{E}_x \rangle$ from the y and z beams. Similarly, we must write equations for $\langle \dot{E}_y \rangle$ and $\langle \dot{E}_z \rangle$. In steady state we can solve these three equations for $\langle n_x \rangle$, $\langle n_y \rangle$, and $\langle n_z \rangle$. These expressions are somewhat complicated but reflect the basic idea that if one of the scatter rates is large, say $\dot{N}_x \gg \dot{N}_y, \dot{N}_z$, and if $f_{sx} \simeq f_{sy} \simeq f_{sz}$ and $\omega_x \simeq \omega_y \simeq \omega_z$, then $\langle n_y \rangle, \langle n_z \rangle \gg \langle n_x \rangle$ due to the recoil heating in the y and z directions from the laser directed along the x direction. If, however, we examine the special case where $\dot{N}_i \simeq \dot{N}_j$, $\omega_i \simeq \omega_j$, $F_i \simeq F_j$, and $f_{si} \simeq f_{sj} \simeq \frac{1}{3}$ $(i,j = x,y,z)$, then $\langle n_x \rangle \simeq \langle n_y \rangle \simeq \langle n_z \rangle$ where $\langle n_x \rangle$ is given by Eq. (10). In this case, laser cooling and recoil heating are approximately equal in the x, y, and z directions.

Case 3. Suppose we have one laser beam (intensity I) at some oblique angle with respect to the x, y, and z axes. If $f_{sx} \simeq f_{sy} \simeq f_{sz}$, then it is natural to choose $\mathbf{k}$ parallel to $\hat{\mathbf{x}} + \hat{\mathbf{y}} + \hat{\mathbf{z}}$ in order to avoid excessive recoil heating along any axis. This is also a natural choice for a typical ion trap where the inner ring diameter is equal to $\sqrt{2}$ times the endcap-to-endcap separation. Here, the $\hat{\mathbf{x}} + \hat{\mathbf{y}} + \hat{\mathbf{z}}$ direction splits the gap between ring and endcaps. Thus the $\hat{\mathbf{x}} + \hat{\mathbf{y}} + \hat{\mathbf{z}}$ direction is a practical choice for introducing laser beams into the trap. In this case, $\dot{N}_x$ from Eqs. (5) and (6) is equal to $\dot{N}/3$ where $\dot{N} = I\sigma_0/\hbar\omega_0$ is equal to the scatter rate for a narrow-band ($\Delta\omega_L \ll \gamma$) laser tuned to resonance ($\omega_L = \omega_0$) for the ion at rest. Assume that $\omega_x \simeq \omega_y \simeq \omega_z \simeq \omega_v$ and that the laser bandwidth is broad enough to cover all three of the first lower sidebands, i.e., $F_x \simeq F_y \simeq F_z = F$. To achieve the best laser cooling, we must have $|\omega_i - \omega_j| \gtrsim R\dot{N}F/\hbar\omega_v$ $(i \neq j)$. The reason for this can be seen by first assuming $\omega_x = \omega_y$. In this case the choice of the x and y axes is arbitrary. If we chose new axes where $\hat{\mathbf{y}}' = (\hat{\mathbf{x}} - \hat{\mathbf{y}})/\sqrt{2}$ so that $\hat{\mathbf{y}}' \cdot \mathbf{k} = 0$; this implies recoil heating without bound in the $\hat{\mathbf{y}}'$ direction.[11] For $\omega_x \neq \omega_y$, again assume $\mathbf{k}$ is parallel to $\hat{\mathbf{x}} + \hat{\mathbf{y}} + \hat{\mathbf{z}}$, and choose $f_{sx} \simeq f_{sy} \simeq f_{sz} = f \simeq \frac{1}{3}$ (condition for isotropic scattering). Recoil heating occurs at a rate $Rf\dot{N}_s$ in the $\hat{\mathbf{y}}'$ direction (i.e., perpendicular to the laser beam) where $\dot{N}_s$ is the total scattering rate from the ion. For kinetic energies near the sideband cooling limit, the dominant scattering occurs in the wings of the carrier (at frequency ω_0) of the ion absorption spectrum so that $\dot{N}_s \simeq \dot{N}\gamma^2/4\omega_v^2$ [see Eq. (8)]. The closer ω_x is to ω_y, the higher is the energy in the $\hat{\mathbf{y}}'$ direction. To estimate this energy, we consider the following. In the absence of laser scattering, if at some time $t = 0$ all of the ion's energy (above the zero-point energy) is in the $\hat{\mathbf{y}}'$ direction, then after a time τ such that $|\omega_x - \omega_y|\tau = \pi$, all of the energy is in the $\hat{\mathbf{x}}' = (\hat{\mathbf{x}} + \hat{\mathbf{y}})/\sqrt{2}$ direction. This situation is like the case of two coupled oscillators (here, in the $\hat{\mathbf{x}}'$ and $\hat{\mathbf{y}}'$ directions) which exchange energy in time τ. Therefore, the decay of energy from the $\hat{\mathbf{y}}'$ direction [denoted $E(\hat{\mathbf{y}}')$] is approximately equal to $E(\hat{\mathbf{y}}')/\tau$. In steady state, we have $Rf\dot{N}_s \simeq [E(\hat{\mathbf{y}}') - E(\hat{\mathbf{x}}')]/\tau$. If we desire to keep $[E(\hat{\mathbf{y}}') - E(\hat{\mathbf{x}}')] < \langle n_x \rangle \hbar\omega_v$ due to the recoil heating in the $\hat{\mathbf{y}}'$ direction, then we require $Rf\dot{N}_s\tau < \langle n_x \rangle \hbar\omega_v$ or approximately

$$|\omega_x - \omega_y| \gtrsim \dot{N}RF/\hbar\omega_v . \tag{12}$$

From the above arguments, it is clear that we must also make the same restriction on $|\omega_x - \omega_z|$ and $|\omega_y - \omega_z|$. The condition in Eq. (12) can also be obtained by assuming that we want $|\omega_i - \omega_j|$ to be larger than the inverse of the time constant for laser cooling.[5] In an axially symmetric rf trap, $\omega_x = \omega_y$. Therefore, in order to achieve the condition given by Eq. (12), the axial symmetry must intentionally be destroyed.[5] Thus, if the condition of Eq. (12) holds, Eq. (6) and the analogous equations for $\langle \dot{E}_{iy} \rangle$ and $\langle \dot{E}_{iz} \rangle$ in steady state give

$$\langle n_i \rangle = \left[\frac{12 f_{si} + 1}{16F} \right] (\gamma/\omega_v)^2 . \tag{13}$$

Equation (13) reduces to Eq. (10) for $f_{si} = \frac{1}{3}$. If the laser spectrum is uniform with bandwidth $\Delta\omega_L (I' = 1/\Delta\omega_L)$, and $\Delta\omega_L \gg \gamma$,

$$\langle n_i \rangle = \left[\frac{12 f_{si} + 1}{8\pi} \right] \gamma \Delta\omega_L / \omega_v^2 . \tag{14}$$

The right-hand side of Eq. (14) is larger than Eq. (2) by a factor of approximately $\Delta\omega_L/\gamma$. As an example, assume $\omega_v/2\pi = 1$ MHz, $\Delta\omega_L/2\pi \simeq 100$ kHz, $\gamma/2\pi = 1$ kHz, and $f_{si} = \frac{1}{3}$. Then $\langle n_i \rangle \simeq 2 \times 10^{-5}$.

The meaning of $\langle n_i \rangle \ll 1$ is the following. After most photon scattering events, the ion's energy in the well is equal to $3\hbar\omega_v/2$, the zero-point energy. That is, most of the time the ion scatters a photon without recoil energy being imparted to the oscillation in the well. Infrequently, after some scattering events, the ion's energy in the well is equal to $(3/2 + 1)\hbar\omega_v$, that is, the ion recoils into the first harmonic oscillator state, for some direction.

Once in the first harmonic oscillator state, it is pumped by the sideband cooling mechanism back to the zero-point-energy state. That the ion does not assume some intermediate energy state in the well is reflected in the discrete spectrum of fluorescence.[11] We also note that when the ion spontaneously emits a photon, its energy, when averaged over many scattering events, increases by R per emission event,[11] even though after any given scattering event, the vibrational energy can only change by zero or some multiple of $\hbar\omega_v$. Therefore, on the average, approximately $\hbar\omega_v/R$ scattering events occur before the ion recoils into the first harmonic oscillator state. With very high probability, the next scattering event returns the ion to the zero-point energy state.

Therefore, most of the time, the ion is in the zero-point energy state and photons are being scattered at a rate $\dot{N}_s=\dot{N}\gamma^2/4\omega_v^2$ (scattering in the wings of the carrier). In order to minimize the relative time the ion spends in the $n_v=1$ state and therefore minimize the ion's kinetic energy [i.e., make Eq. (14) valid], we must avoid saturation of the first lower sideband when the ion is in the $n_v=1$ state. From Eq. (8), we require $\dot{N}\beta F/3<\gamma$. This implies that the scattering in the wings of the carrier $\dot{N}_s$ is less than $3\gamma^3/4F\omega_v\omega_R$. For the conditions of our previous example ($\omega_v/2\pi=1$ MHz, $\gamma/2\pi=1$ kHz, $\omega_R/2\pi=22$ kHz), $\dot{N}_s\lesssim 0.2/F$, which is small for F near 1.

B. Limits of micromotion energy

In Sec. II A, we have discussed the limits to laser cooling for an ion or atom in a purely harmonic well, e.g., for the secular motion of an ion in an rf trap. When an ion is confined in an rf trap, one must also consider the energy in the micromotion.[24,25] If we treat the motion classically, one can show that the average kinetic energy in the micromotion is equal to the average kinetic energy in the secular motion for two trap configurations of practical interest:[24,25] (1) when there is no static potential applied between the ring and end caps ($\omega_x=\omega_y=\omega_z/2$) or (2) when the appropriate static potential is applied between ring and end caps to give a nominally spherical trap ($\omega_x=\omega_y\simeq\omega_z$). For other cases, this equality of micromotion and secular energies does not strictly hold, but the key point is that they are of the same order.

Since the very low kinetic energies predicted by Eqs. (2), (10), and (13) require a quantum-mechanical treatment of the ion motion, it is useful to address the question of micromotion energy again, but now treating the ion motion in an rf trap quantum mechanically. Here, we examine only the case of zero static potential applied to the trap electrodes. For the quantum treatment, Cook *et al.*[29] have examined the solution to Schrödinger's equation for the rf trap in the form

$$i\hbar\frac{\partial}{\partial t}\psi=-\frac{\hbar^2}{2m}\nabla^2\psi+v(\mathbf{x})\cos(\Omega t)\psi\ , \tag{15}$$

where $v(\mathbf{x})\cos(\Omega t)$ is the potential inside the trap. By writing the wave function in the form

$$\psi(\mathbf{x},t)=g(\mathbf{x},t)u(\mathbf{x},t)\ , \tag{16}$$

where

$$u(\mathbf{x},t)=\exp[-iv(\mathbf{x})\sin(\Omega t)/\hbar\Omega]\ , \tag{17}$$

Cook *et al.*[29] show that we can identify g with the secular motion. If we take the expectation value of the kinetic energy, $E_K=-\hbar^2\nabla^2/2m$, and average over one period of the drive frequency, we obtain

$$\langle\psi\,|\,E_K\,|\,\psi\rangle_{\rm av}=\frac{1}{4m\Omega^2}\int d^3x\nabla v\cdot\nabla v g^*g+\int d^3xE_Kg^*g\ . \tag{18}$$

The first term on the right-hand side of Eq. (18) is the expectation value of the effective potential (pseudopotential), calculated with the wave function g. The second term is the expectation value of the kinetic energy calculated with the wave function g. The net result is the same as in the classical case. That is, the average value of the effective potential energy $\langle(\nabla v)^2\rangle/4m\Omega^2$ (pseudopotential energy) is equal to the kinetic energy of the micromotion. In the simple case of a quadratic pseudopotential, this contribution is equal to the kinetic energy of the secular motion.

In an experimental situation, the kinetic energy in the micromotion is typically larger than indicated above. Sometimes there can be contact potential differences, or differences in stray charge buildup, between the electrodes. In the experiments using Ba^+, Mg^+, or Be^+, contact potential differences on the electrodes might result from nonuniform deposition on the trap electrodes from the source of these atoms.[30] For example, suppose one endcap has a surface which has a higher contact potential than the other two electrodes. This implies that in addition to the usual rf trapping forces, there is an additional steady force along the z axis which shifts the center of the trap. The new center of the trap is given by the condition that the total average force on the ion is zero. Thus, the steady force due to the contact potential must be balanced by the pseudopotential force; hence, there is a resultant micromotion at the new center of the trap where the secular motion amplitude is zero (i.e., the position of the ion when it is cold). To estimate classically the size of this effect, we write the potential inside the trap due to applied voltages in the form[24,25]

$$\phi(r,z)=\frac{U_0+V_0\cos(\Omega t)}{r_0^2+2z_0^2}(r^2-2z^2)\ , \tag{19}$$

where U_0 and V_0 are the static and time-varying voltages applied between the ring and end caps and where $2r_0$ and $2z_0$ are the internal ring diameter and endcap-to-endcap spacing as indicated in Fig. 2. (Effects of truncating the electrodes are neglected.) This gives rise to a pseudopotential of the form[25]

$$\begin{aligned}\phi_p(\bar{r},\bar{z})&=\left[\frac{qV_0^2}{m\Omega^2(r_0^2+2z_0^2)^2}+\frac{U_0}{r_0^2+2z_0^2}\right]\bar{r}^2\\&\quad+\left[\frac{4qV_0^2}{m\Omega^2(r_0^2+2z_0^2)^2}-\frac{2U_0}{r_0^2+2z_0^2}\right]\bar{z}^2\\&=\frac{m\omega_r^2}{2q}\bar{r}^2+\frac{m\omega_z^2}{2q}\bar{z}^2\ ,\end{aligned} \tag{20}$$

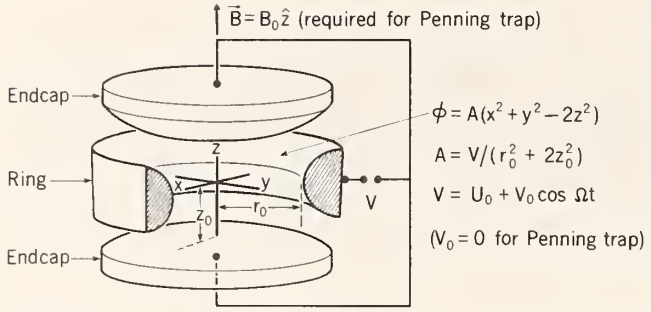

FIG. 2. Electrode configuration for an rf (Paul) or Penning trap. The inner surfaces of the electrodes are assumed to be equipotenitals of ϕ, and the effect of truncating the electrodes is neglected. r_0 is the inner radius of the ring electrode and $2z_0$ is the endcap-to-endcap spacing.

where $\omega_r=\omega_x=\omega_y$ and $\bar{r}$ and $\bar{z}$ are the radial and axial positions of the ion averaged over one cycle of the rf drive, that is, over a time $2\pi/\Omega$. The z force towards the center of the trap due to the pseudopotential is given by $F_z=-q\partial\phi_p/\partial\bar{z}$. The force away from the center of the trap due to a contact potential on one endcap is given by the following argument. Suppose we have a voltage ΔV on one endcap. This can be written as the sum of symmetric and antisymmetric terms as indicated in Fig. 3(a). The z electric field due to the antisymmetric term can be approximated[31] by a parallel-plate capacitor of separation $2z_0/\alpha$ as shown in Fig. 3(b). The factor α has been numerically estimated[32,33] to be about 0.8 for a trap where $r_0^2=2z_0^2$. If we assume the case of an rf trap with zero intentionally applied voltage U_0, then the center of the trap is given by the condition $F_z=-q\partial\phi_p/\partial\bar{z}-q\alpha\Delta V/2z_0=0$, or

$$\bar{z}=-\frac{q\alpha\Delta V}{2m\omega_z^2 z_0}\ . \tag{21}$$

From this expression, we can find the kinetic energy in

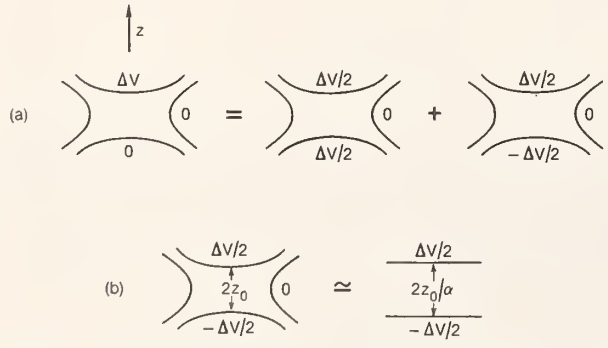

FIG. 3. Part (a) indicates how a potential ΔV applied to one endcap electrode can be viewed as the sum of voltages applied symmetrically and antisymmetrically to the electrodes. For ions near the center of the trap, the lowest-order contribution to the electric field from the antisymmetric part can be viewed as arising from a voltage ΔV applied between a parallel plate capacitor of separation $2z_0/\alpha$. This is indicated in part (b) of the figure. From Refs. 32 and 33, $\alpha\simeq 0.8$.

the micromotion $E_{K\mu}$ by recalling that it is equal to the pseudopotential energy, that is, $E_{K\mu}=q\phi_p$. Therefore, for the z motion we have

$$E_{K\mu}(z)=\left[\frac{q\alpha\Delta V}{\omega z_0}\right]^2\Big/8m\ . \tag{22}$$

To get an idea of the size of this effect, we examine the conditions of the miniature rf trap used to store single Hg^+ ions.[7] There, $\omega_z/2\pi\simeq 1.5$ MHz, $z_0\simeq 320$ μm, $r_0\simeq 450$ μm. If $\Delta V=1$ V, $E_{K\mu}(z)\simeq 7\times 10^5\hbar\omega_z$. Thus, offsets due to contact potential variations or similar effects are extremely important if it is desired to reach kinetic energies approaching those given by Eqs. (2), (10), and (13). Such problems can be alleviated by applying external voltages to the electrodes to compensate for any of the above type of asymmetries. This is easily accomplished along the z axis by applying different static voltages to the two endcaps. In the x and y directions, separate compensating electrodes could be added or, for example, the ring could be split into quadrants.[34] Different static voltages could then be applied to the quadrants in order to compensate for any asymmetric contact potential difference on the ring.

Next, we consider the effects of rf voltages which may be asymmetrically applied to the electrodes. This situation might occur, for example, because of different impedances from either endcap to ground. If the amplitude of the rf voltage on the two endcaps is different, this amounts to shifting the origin of the coordinate system for the rf voltage. In this new coordinate system, a voltage U_0 applied symmetrically to the endcap electrodes or to the ring electrode causes a static force which displaces the ion from the origin for the rf fields and yields a resultant micromotion which can be deduced from the previous arguments. A new problem to consider, however, is that the phase of the rf voltages on the electrodes might be different. To estimate the effects of this, assume that the voltage $V_0\cos(\Omega t+\theta/2)$ is applied to one endcap and the voltage $V_0\cos(\Omega t-\theta/2)$ is applied to the other endcap. The ring electrode is assumed to be grounded. If $\theta\ll 1$, we can consider the ion motion to be the sum of a solution for the condition when $V_0\cos(\Omega t)$ is applied to both endcaps and a perturbation to this solution for the additional voltages $(V_0\theta/2)\sin(\Omega t)$ and $-(V_0\theta/2)\sin(\Omega t)$ applied to the two endcaps, respectively. Classically, we can easily solve for the kinetic energy $E_{K\theta}$ due to the perturbed motion (averaged over $2\pi/\Omega$). We have

$$E_{K\theta}=\frac{m}{2}\left[\frac{\omega_z(r_0^2+2z_0^2)\alpha\theta}{8z_0}\right]^2 \tag{23}$$

For our example of the $^{198}Hg^+$ ion,[7] we obtain $E_{K\theta}\simeq 2.4\times 10^8\theta^2\hbar\omega_z$. Thus, very precise control of the phase of the rf voltage is required to reach micromotion kinetic energies near the zero-point energy of the secular motion. This can be accomplished by injecting a portion of the drive signal (with the proper phase) onto one endcap.

Because of the relatively strong effect of asymmetrically applied potentials, it is natural to ask whether imperfections in the electrode shapes can lead to residual rf motion

even when the ion reaches the position given by $\langle F \rangle = 0$. To estimate the effects of electrode distortion, we must modify Eq. (19). About a suitable origin we can write

$$\phi(r,z) = [U_0 + V_0 \cos(\Omega t)] \left[\frac{r^2 - 2z^2}{r_0^2 + 2z_0^2} + A_2(x^2 - y^2) + A_3 x^3 + B_3 x^2 y + C_3 x^2 z + D_3 x y^2 + \cdots + D_4 x^4 + \cdots \right] \tag{24}$$

where Laplace's equation is satisfied for each order. To estimate the effects of the higher-order terms, we examine the term $U_0 C_3 x^2 z = U_0 C_3' x^2 z / z_0^3$ in Eq. (24). Unless the electrodes are severely distorted, we have $C_3' \ll 1$. Near the origin, this term gives rise to a z component of electric field $E_z' = -(U_0/z_0) C_3' \langle x^2 \rangle / z_0^2$. If we can cool to near the zero-point energy ($\langle n_x \rangle < 1$), then $\langle x^2 \rangle \simeq x_0^2$. For the conditions of a Hg^+ ion in a miniature rf trap,[7] $\omega_x/2\pi = 1.5$ MHz, $z_0 = 320$ μm, $x_0 \simeq 4.1 \times 10^{-3}$ μm, $U_0 \simeq 10$ V (conditions for an approximately spherical trap). For $C_3' \simeq 0.1$, the resulting field E_z' would be equivalent to applying a voltage $\Delta V \simeq 4 \times 10^{-10}$ V to one endcap. From Eq. (22), $E_{K\mu}(z) \simeq 1 \times 10^{-13} \hbar \omega_z$ for this value of ΔV which is negligible. Therefore, this effect by itself can be small. However, electrode distortion may give rise to unbalanced rf phases on the endcaps. Other terms in Eq. (24) appear to be of this order or smaller.

III. SIDEBAND COOLING FOR A SINGLE ION IN A PENNING TRAP

Sideband cooling for a single ion in a Penning trap requires special attention because of the peculiar properties of the magnetron motion.[27] Cooling for the cyclotron and axial degrees of freedom is essentially the same as for the secular motion in the rf trap. However, for the magnetron motion, we will define cooling to be the reduction of the kinetic energy in this degree of freedom. This implies that the total energy of this degree of freedom increases, since most of the energy in the magnetron motion degree of freedom is due to electrical potential energy from the radially outward trap force. For positive charges, this potential energy is given by Eq. (19) with $V_0 = 0$ and $U_0 < 0$. In the axial direction, the ion is bound in a harmonic well, and in the radial direction the ion sits on a potential hill whose maximum is at the center of the trap where we choose $\phi = 0$. First, consider the Doppler cooling limit ($\gamma \gg \omega_m, \omega_c', \omega_z$ where ω_m, ω_c', and ω_z are the magnetron, cyclotron, and axial oscillation frequencies in the Penning trap[25,27]). To achieve cooling, we require that the ion preferentially absorb photons when it moves toward the laser due to cyclotron motion and simultaneously preferentially absorb photons when it moves away from the laser due to the magnetron motion. Since the cyclotron and magnetron motions are both in the x-y plane, the only way this can be done is to use a spatially inhomogeneous laser beam. This case has been treated previously.[27]

In the sideband cooling limit ($\gamma \ll \omega_m, \omega_c', \omega_z$), we are able to use spatially homogeneous, plane-wave laser beams for the following reason. In Fig. 4, we show the absorption spectrum in the x-y direction averaged over many scattering events for an ion that has been cooled within the Lamb-Dicke limit $\langle k^2 x^2 \rangle = k^2 r_0^2 (n_c + n_m + 1)/2 \ll 1$, where[27] $r_0 = [2\hbar/m(\omega_c' - \omega_m)]^{1/2}$. In this limit, only the first-order sidebands are of appreciable size. The schematic representation of Fig. 4 may not be to scale, but the expressions for the relative intensities above the indicated sidebands should be valid. For this figure, we have assumed $\omega_c' = 5\omega_m/2$ in order to simplify the drawing. This diagram and the remarks above show that simultaneous sideband cooling of the magnetron and cyclotron degrees of freedom can be achieved by having two plane-wave laser beams directed normal to the z axis. One laser beam can be tuned to $\omega_0 - \omega_c'$ and the other beam tuned to $\omega_0 + \omega_m$. In principle, it should be possible to achieve cooling by having one laser tuned to the sideband at frequency $\omega_0 - \omega_c' + \omega_m$, but, in the Lamb-Dicke limit, the absorption intensity of this sideband is considerably reduced. Below, we examine the limits to sideband cooling for the Penning trap. However, we first note that sideband cooling will work only at relatively low temperatures in the Penning trap where particular sidebands are well resolved as shown in Fig. 4. At much higher temper-

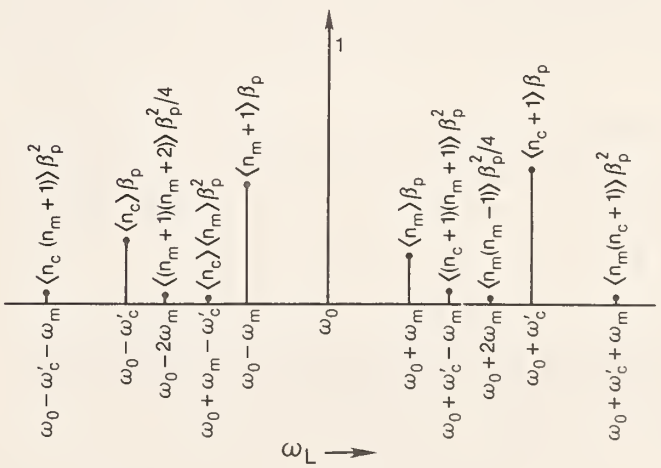

FIG. 4. Amplitudes of the lowest-order sidebands in the absorption spectrum for a single ion confined to the Lamb-Dicke region in a Penning trap. ($\omega_c' = 5\omega_m/2$ is assumed.) The radiation source (laser) is assumed to be directed normal to the z axis. The carrier amplitude (at frequency ω_0) is normalized to 1. $k = \omega_0/c$, $r_0 = [2\hbar/m(\omega_c' - \omega_m)]^{1/2}$, $\beta_p = (kr_0)^2/4$ and n_c and n_m are the cyclotron and magnetron quantum numbers, respectively. Simultaneous cooling of the magneton and cyclotron degrees of freedom will occur for two laser beams tuned to $\omega_0 + \omega_m$ and $\omega_0 - \omega_c'$, respectively.

atures, the magnetron and cyclotron sideband distributions become nearly continuous, and it is impossible to simultaneously cool the kinetic energies for both degrees of freedom using plane waves. This implies the necessity of some form of precooling as discussed in Sec. IV.

The basic formalism for cooling of ions in Penning traps has already been established.[27] In the quantum treatment of the ion motion, the total energies of the axial, cyclotron, and magnetron degrees of freedom can be written as $E_z=(n_z+\frac{1}{2})\hbar\omega_z$, $E_c=(n_c+\frac{1}{2})\hbar\omega_c'$, and $E_m=-(n_m+\frac{1}{2})\hbar\omega_m$, respectively. The mean amplitudes of the motion we desire to reduce are given by $\langle z^2\rangle=z_0^2\langle 2n_z+1\rangle$, $\langle r_c^2\rangle=r_0^2\langle n_c+\frac{1}{2}\rangle$, and $\langle r_m^2\rangle=r_0^2\langle n_m+\frac{1}{2}\rangle$, where $z_0=(\hbar/2m\omega_z)^{1/2}$ as in Sec. II. The axial cooling is identical to that described for the secular motion in the rf trap in Sec. II. Now, however, we are entirely free of the energy in the micromotion since the fields are static in the Penning trap. From Ref. 27 we can write a general expression for the average rate of change of the axial, cyclotron, and magnetron motion quantum numbers for the ξth laser beam (total intensity I_ξ) as

$$\frac{d\langle n_i\rangle}{dt}=\sum_{\{n^l\},\{n^f\}}P(\{n^l\})\Gamma(\{n^l\}\rightarrow\{n^f\})(n_i^f-n_i^l)\ . \tag{25}$$

In Eq. (25), $\{n^l\}=\{n_z^l,n_c^l,n_m^l\}$ is the set of initial (l=lower) quantum numbers, $\{n^f\}$ is the set of final (f=final) quantum numbers, and $i=z$, c, or m. P is the initial probability distribution for quantum numbers $\{n^l\}$ [$P\{n^l\}$ takes the role of $P(n_{li})$ from Sec. II]. Γ is the transition rate given by

$$\Gamma(\{n^l\}\rightarrow\{n^f\})=(I_\xi/\hbar\omega_0)\sigma^*(\{n^l\}\rightarrow\{n^f\})\ . \tag{26}$$

In Eq. (26), σ^* is the cross section given by

$$\sigma^*(\{n^l\}\rightarrow\{n^f\})=\sigma_0(\gamma/2)^2\int\left|\sum_{\{n^j\}}\frac{\langle\{n^f\}\,|\,e^{-i\mathbf{k}_s\cdot\mathbf{r}}\,|\,\{n^j\}\rangle\langle\{n^j\}\,|\,e^{i\mathbf{k}\cdot\mathbf{r}}\,|\,\{n^l\}\rangle}{\omega_0-\omega-i\gamma/2+\omega(\{n^j\})-\omega(\{n^l\})}\right|^2 P_s(\hat{\mathbf{k}}_s)d\Omega\ . \tag{27}$$

In Eq. (27), $\mathbf{k}$ and $\mathbf{k}_s$ are the wave vectors of the incident and scattered light. $P_s(\hat{\mathbf{k}}_s)d\Omega$ is the probability that a photon is emitted into a solid angle $d\Omega$ in the $\hat{\mathbf{k}}_s$ direction ($\hat{\mathbf{k}}_s=\mathbf{k}_s/|\,\mathbf{k}_s\,|$), and $\hbar[\omega(\{n^j\})-\omega(\{n^l\})]$ is the difference in motional energy between the initial (l) and intermediate (j) states. We have

$$f_{si}=\int P_s(\hat{\mathbf{k}}_s)(\hat{\mathbf{k}}_{si})^2d\Omega\ .$$

where $\hat{\mathbf{k}}_{si}$ is the component of $\hat{\mathbf{k}}_s$ in the ith direction. In Eq. (27), we have assumed $\Delta\omega_L\ll\gamma$. Equations (25)–(27) reduce to Eq. (5) for the case of harmonic oscillator cooling or cooling the secular motion in an rf trap.

If we use Eqs. (25)–(27) and the operator relations[11,27] for $[N_i,e^{i\mathbf{k}\cdot\mathbf{r}}]$, where $N_i=a_i^\dagger a_i$ is the operator whose eigenvalue is n_i, we obtain the following relationship for the cooling due to the ξth laser beam:

$$\frac{d\langle n_i\rangle}{dt}=\dot{N}_\xi\int I_\xi'd\omega\sum_{\{n^l\},\{n^j\}}P(\{n^l\})\frac{\{\beta_i f_{si}+[n_i(j)-n_i(l)]\}\,|\,\langle\{n^j\}\,|\,e^{i\mathbf{k}_\xi\cdot\mathbf{r}}\,|\,\{n^l\}\rangle\,|^2}{1+\left[\frac{2}{\gamma}[\omega_0-\omega+\omega(\{n^j\})-\omega(\{n^l\})]\right]^2}\ . \tag{28}$$

In this expression, $\dot{N}_\xi=I_\xi\sigma_{0\xi}/\hbar\omega_0$ and we have now allowed the laser spectral distribution to have some width as in Sec. II, such that $\int I_\xi'(\omega)d\omega=1$. Also,

$$\beta_i=\begin{cases}(kr_0)^2/4 & (i=c\text{ or }m)\\ (kz_0)^2 & (i=z)\ ,\end{cases}$$
$$f_{si}=\begin{cases}f_{sx}+f_{sy} & (i=c\text{ or }m)\\ f_{sz} & (i=z)\ .\end{cases} \tag{29}$$

Equation (28) looks very similar to Eq. (5) except that the recoil energy ($\beta_i f_{si}$ term) divides between the cyclotron and magnetron degrees of freedom in such a way that the average change of $\langle n_m\rangle$ or $\langle n_c\rangle$ is the same upon photon reemission (i.e., the incremental changes in r_c and r_m are the same).

In the Lamb-Dicke limit, Eq. (28) simplifies considerably because $e^{i\mathbf{k}_\xi\cdot\mathbf{r}}\simeq 1+\mathbf{k}_\xi\cdot\mathbf{r}$ and only matrix elements for transitions where $\Delta n_i=0,\pm1$ need be considered. This is the same situation as for the harmonic oscillator case of Sec. II. However, for the Penning-trap case, both the cyclotron and magnetron cooling beams are assumed to be incident in the x-y plane. Therefore, both beams cause transitions where $\Delta n_m=0,\pm1$ and $\Delta n_c=0,\pm1$, and some extra terms are encountered. For example, the contribution of $d\langle n_i\rangle/dt$ due to the cyclotron cooling beam (tuned to $\omega_0-\omega_c'$ and assumed to be directed along the y axis) is given by

$$\frac{d\langle n_i\rangle}{dt}\simeq\dot{N}_c\sum_{\{n'\}}P(\{n'\})\left\{(\beta_i f_{si}-\delta_{ic})\,|\langle n_c-1\,|\,e^{iky}\,|\,n_c\rangle|^2F_c+\beta_i f_{si}\frac{|\langle n_c\,|\,e^{iky}\,|\,n_c\rangle|^2}{(2\omega_c'/\gamma)^2}\right.$$
$$+(\beta_i f_{si}+\delta_{ic})\frac{|\langle n_c+1\,|\,e^{iky}\,|\,n_c\rangle|^2}{(4\omega_c'/\gamma)^2}+(\beta_i f_{si}-\delta_{im})\frac{|\langle n_m-1\,|\,e^{iky}\,|\,n_m\rangle|^2}{[2(\omega_c'+\omega_m)/\gamma]^2}$$
$$\left.+(\beta_i f_{si}+\delta_{im})\frac{|\langle n_m+1\,|\,e^{iky}\,|\,n_m\rangle|^2}{[2(\omega_c'-\omega_m)/\gamma]^2}\right\} \tag{30}$$

As in Sec. II, $F_c=\int I_c'(\omega)\{1+[2(\omega_0-\omega_c'-\omega)/\gamma]^2\}^{-1}d\omega$, and we have assumed $\Delta\omega_L\ll\omega_m,\omega_z,\omega_c'$ for simplicity.

We can find the other two equations which are analogous to Eq. (30) for the magnetron cooling beam and axial cooling beam. By summing these equations, we arrive at expressions for the total rates of change of average quantum numbers for the three degrees of freedom $d\langle n_i\rangle/dt$ ($i=c$, m, or z). These expressions take the form

$$d\langle n_i\rangle/dt=C_{ic}\langle n_c\rangle+C_{im}\langle n_m\rangle+C_{iz}\langle n_z\rangle+d_i \qquad (i=c,\ m,\ \text{or}\ z)\ , \tag{31}$$

where the coefficients C_{ij} and d_i come directly from Eq. (30) and the analogs for the cyclotron and magnetron beams. For steady state, ($d\langle n_i\rangle/dt=0$) and we find that the $\langle n_i\rangle$ reach certain minimum values for given $\dot{N}_\xi$ and F_ξ ($\xi=c,m,z$). These solutions can in general be quite complicated. To get some estimate for the minimum values for $\langle n_i\rangle$, we have solved these equations for the following simple conditions. We assume $f_{sx}=f_{sy}=f_{sz}=\frac{1}{3}$, $\omega_m\ll\omega_z\ll\omega_c'$, and require a solution where $\langle n_c\rangle=\langle n_m\rangle=\langle n_z\rangle=\langle n\rangle$. For $F_c=F_m=F_z=F$, this implies the condition $\dot{N}_c=2\dot{N}_z=8\dot{N}_m/11$ on the laser beam intensities and we obtain

$$\langle n\rangle=(11/48F)(\gamma/\omega_m)^2\ . \tag{32}$$

This has the same form as Eqs. (2), (10), and (13). For these solutions to hold, we have required $\beta\ll1$ or $\omega_R\ll\omega_m$ and $\omega_m\ll\omega_z\ll\omega_c'<\omega_c$. These conditions may only be approximated in an experiment. To see this, we note that we can write $\omega_R/\omega_c=1.3\ (\lambda/100\ \text{nm})^{-2}B^{-1}Z^{-1}$, where B is in tesla, Z is the ion charge (in units of the proton charge), ω_c is the unshifted cyclotron frequency, $\omega_c=qB/mc$, and λ is the wavelength of the cooling laser radiation. To satisfy the above conditions, we require a large magnetic field and a relatively long wavelength cooling transition. A possible case might be B^+ [$\lambda(^1S_0\rightarrow{}^3P_1)=268$ nm] at 15 T. Here, $\omega_R/\omega_c=0.012$, and ω_m and ω_z can be adjusted so that Eq. (32) should be reasonably accurate.

In practice, it is usually easier to make ω_x, ω_y, and ω_z in the rf trap be much larger than ω_m can be made in the Penning trap. Therefore, the conditions for sideband cooling are more easily satisfied in the rf trap than in the Penning trap. The limit on how high we can make ω_m is a limit on how large a magnetic field we can achieve, since we must always have[25] $\omega_m<\omega_z/\sqrt{2}<\omega_c'<\omega_c=qB/mc$ (conditions for stable trapping). From a comparison of Eqs. (10) or (13) and Eq. (32), we might conclude that much lower values of the kinetic energy (above the zero-point energy) can be obtained with the rf trap than with the Penning trap. This may indeed be the case for the secular motion of the rf trap, but, as we have seen at the end of Sec. II, the kinetic energy in the micromotion of the rf trap may be much more difficult to suppress. For the Penning trap, there is not an analogous problem to the micromotion since the imposed fields are static. Therefore, it may, in practice, be possible to obtain smaller values of the kinetic energy in the Penning trap.

IV. TWO-STAGE LASER COOLING

To reach the cooling limits provided by sideband cooling [Eqs. (10), (13), or (32)], some sort of two-stage cooling may be necessary. This has already been referred to in Sec. III for the Penning trap, where simultaneous sideband cooling of the magnetron and cyclotron motions can only be effective at low enough temperatures where the Lamb-Dicke limit is approached. Therefore, to approach the Lamb-Dicke limit, it may first be necessary to reach a kinetic energy provided by the Doppler cooling limit on a strongly allowed electric dipole transition. For the Penning trap, this also implies the use of a spatially inhomogeneous cooling beam.[27]

The same restriction does not apply for the rf trap. In principle, it should be possible to tune to the first lower sideband (for $\gamma\ll\omega_v$) and wait a sufficient time to reach the steady state given by Eq. (10) or (13). Initial cooling could be enhanced by tuning to the lth lower sideband where $l\omega_v$ is approximately equal to one-half of the Doppler linewidth at the initial temperature.[11] The maximum cooling rate is given by $dE/dt\simeq-l\hbar\omega_v\gamma/2$. To get an idea of the initial cooling rate, we can estimate the time Δt it takes to reduce the ion temperature from $T_1=300$ K to $T_1/2$. We have $\Delta t\simeq3k_BT_1/(\hbar l\omega_v\gamma)\simeq3.8\times10^4/\gamma$, where we assume $l\omega_v=2\pi(0.5)$ GHz. If the cooling transition is very weak (e.g., $\gamma\simeq100\ \text{s}^{-1}$), then $\Delta t\simeq380$ s. Even under ideal conditions, this time is very long. Moreover, spurious heating mechanisms, such as collisional heating, may prevent any initial cooling at all. Thus, in the case of the rf trap as well as the Penning trap, there may be some motivation for using a precooling stage [e.g., cooling to the Doppler limit of Eq. (1) where γ is due to a strongly allowed electric dipole transition].

To get some idea of how such two-stage cooling might work, we examine the case of cooling in the rf (or harmonic) trap. Assume that the initial cooling is performed

TABLE I. Examples of $k(\langle x^2\rangle)^{1/2}$, $\langle n_v\rangle$, and ϵ_{D2} for a few ions of recent experimental interest. We have assumed that the ions are confined in a harmonic well with oscillation frequency $\omega_v/2\pi$ and are cooled to the Doppler cooling limit [Eq. (1)]. $\gamma/2\pi$ and λ are the radiative linewidth and wavelength corresponding to the cooling transition, M is the ion mass in atomic mass units, $k=2\pi/\lambda$, $\langle n_v\rangle$ is the mean occupation number of the ion in the harmonic well [from Eq. (33)], and $\beta=(kx_0)^2=R/(\hbar\omega_v)$. $3\epsilon_{D2}$ is the magnitude of the fractional second-order Doppler shift for the x, y, and z directions combined [three times the value in Eq. (35)]. If the ions are confined in an rf trap, the magnitude of the second-order Doppler shift is valid only for the secular motion contribution.

Ion	$\gamma/2\pi$ (MHz)	λ (nm)	$M(u)$	$\omega_v/2\pi$ (MHz)	$k(\langle x^2\rangle)^{1/2}$	$\langle n_v\rangle$	β	$3\epsilon_{D2}$
$^{24}Mg^+$ $(3s\ ^2S_{1/2}\rightarrow 3p\ ^2P_{1/2})$	43	280	24	1	2.14	21	0.106	6×10^{-18}
$^{24}Mg^+$ $(3s\ ^2S_{1/2}\rightarrow 3p\ ^2P_{1/2})$	43	280	24	5	0.43	3.8	0.021	6×10^{-18}
$^{198}Hg^+$ $(6s\ ^2S_{1/2}\rightarrow 6p\ ^2P_{1/2})$	70	194	198	1.5	0.91	22.8	0.018	1.2×10^{-18}
$^{198}Hg^+$ $(6s\ ^2S_{1/2}\rightarrow 6p\ ^2P_{1/2})$	70	194	198	15	0.091	1.8	0.0018	1.2×10^{-18}
$^{138}Ba^+$ $(6s\ ^2S_{1/2}\rightarrow 6p\ ^2P_{1/2})$	21	493	138	1.5	0.24	6.5	0.004	5.1×10^{-19}
$^{113}In^+$ $(5s^2\ ^1S_0\rightarrow 5s5p\ ^3P_1)$	0.3	231	113	0.1	1.0	1	0.33	9.0×10^{-21}

on a strong transition (transition 1) where $\gamma_1 \gg \omega_v$. In the Doppler cooling limit, the mean oscillation quantum number can be derived from $(\langle n_v\rangle+\frac{1}{2})\hbar\omega_v=\hbar\gamma_1/2$ or

$$\langle n_v\rangle=(\gamma_1/\omega_v-1)/2\ . \tag{33}$$

In the Doppler cooling limit, we can also write

$$k(\langle x^2\rangle)^{1/2}=2\pi(\hbar\gamma_1/2m)^{1/2}/(\lambda_1\omega_v)\ . \tag{34}$$

In Table I, we have calculated $\langle n_v\rangle$ and $k(\langle x^2\rangle)^{1/2}$ from Eqs. (33) and (34) for some of the favored ions in recent experiments. This table shows that the Lamb-Dicke limit $[k(\langle x^2\rangle)^{1/2}\ll 1]$ is closely approached in the Doppler cooling limit.

If the Doppler cooling limit is first reached, the next step might be to drive a much weaker transition in the same ion (linewidth $\gamma_2 \ll \omega_v$) where the sideband cooling limit applies. As an example, consider the case of $^{198}Hg^+$ whose relevant electronic structure is shown in Fig. 5. Initial laser cooling can be achieved[7] by cooling on the $^2S_{1/2}\rightarrow{}^2P_{1/2}$ transition at $\lambda=194$ nm. Sideband cooling could be achieved by driving the $^2S_{1/2}\rightarrow{}^2D_{3/2}$ quadrupole transition at $\lambda=198$ nm or the $^2S_{1/2}\rightarrow{}^2D_{5/2}$ quadrupole transition at $\lambda=281$ nm. We could also drive the two-photon transition to accomplish this; in this case the effective $\mathbf{k}$ vector of the transition is $\mathbf{k}'=\mathbf{k}_1+\mathbf{k}_2$, where $\mathbf{k}_1$ and $\mathbf{k}_2$ are the wave vectors of the two photons required for the transition, so that if $\mathbf{k}'\|\hat{\mathbf{x}}$, then $\beta_x=(|\mathbf{k}_1+\mathbf{k}_2|x_0)^{1/2}$.

Suppose we tune the second cooling laser to the first lower sideband at frequency $(\omega_{02}-\omega_v)$. Equation (8) shows that the ion scatter rate on this sideband is equal to $\dot{N}n_v\beta F/3$, where we assume the geometry of Sec. II A (case 3). For the minimum time to reach the sideband cooling limit, we require $\dot{N}n_v\beta F/3\simeq\gamma_2/2$ for $n_v=1$. If much higher power is used, the scattering in the wings of the carrier increases while the cooling rate saturates. This would give a higher limit than that of Eq. (10) or (13). Since each scattering event removes an energy $\hbar\omega_v$ from the harmonic oscillator state, a minimum time $\sim 2\gamma_2^{-1}\langle n_v\rangle$ is required to reach the sideband cooling limit. Here, $\langle n_v\rangle$ is the value obtained from precooling. For the conditions of the second $^{198}Hg^+$ example in Table I, we estimate a minimum time of approximately 80 ms for the $^2S_{1/2}\rightarrow{}^2D_{3/2}$ transition and 400 ms for the $^2S_{1/2}\rightarrow{}^2D_{5/2}$ transition. If the goal is to perform very-high-resolution spectroscopy on the $^2S_{1/2}\rightarrow{}^2D_{5/2}$ "clock" transition, we would like to perform the sideband cooling using the $^2S_{1/2}\rightarrow{}^2D_{3/2}$ transition because of the shorter cooling time required. (We designate the $^2S_{1/2}\rightarrow{}^2D_{5/2}$ transition as the clock transition because its narrow linewidth suggests that it could be used as a frequency standard or clock.) This still is not an optimum

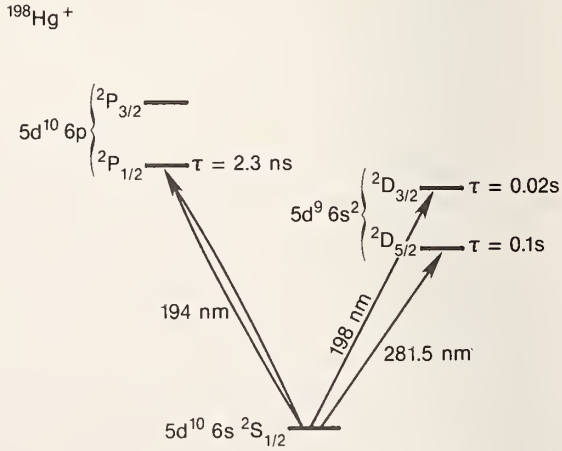

FIG. 5. Simplified energy-level diagram for $^{198}Hg^+$. The 281.5-nm quadrupole "clock" transition can be observed by monitoring the 194-nm fluorescence. If the ion has made a transition from the $^2S_{1/2}$ to the $^2D_{5/2}$ level the 194-nm fluorescence disappears. From Ref. 7.

situation because we would like the cooling time to be much less than the interrogation time ($\sim\gamma_2^{-1}$) for the clock transition in order to achieve maximum data rate and therefore best signal-to-noise ratio.

V. MEASURING THE ZEROTH QUANTUM LEVEL

We can verify that the sideband cooling limit given by Eqs. (10), (13), or (32) has been realized by measuring the spectrum of the sideband cooling transition. This corresponds to either the $^2S_{1/2}\rightarrow{}^2D_{3/2}$ or $^2S_{1/2}\rightarrow{}^2D_{5/2}$ transition in the Hg^+ example. To measure this spectrum (after cooling) we can use a simple double-resonance scheme.[7,35,36] For the Hg^+ example, we can measure absorption on the $^2S_{1/2}\rightarrow{}^2D_{5/2}$ clock transition by monitoring the changes in fluorescence from the 194-nm cooling transition.[7] In general, it will be necessary to drive the clock transition with the 194-nm laser switched off in order to avoid ac Stark shifts of the clock-transition spectrum. After the clock radiation is turned off, the fluorescence from the 194-nm cooling radiation will be absent if the clock transition has been made. If the ion remains in the $^2S_{1/2}$ state after application of the 281-nm radiation, then the fluorescence will immediately appear after admitting the 194-nm radiation. After each such detection cycle, the ion must be recooled by sideband cooling.

First, assume we measure the absorption spectrum along one of the principal axes (x, y, or z) while staying below saturation intensity on the carrier. In the Lamb-Dicke limit, the strength of the lower sideband (assuming the carrier strength is equal to 1) is $\langle n_v\rangle\beta$ and that of the upper sideband is $(\langle n_v\rangle+1)\beta$. Here we assume that $n_v=n_i$ and $\beta=\beta_i$ for $i=x$, y, or z. If $\langle n_v\rangle\ll 1$, the lower sideband will be very small and the upper sideband will have amplitude β, as indicated qualitatively in Fig. 6(a). For the $^{198}Hg^+$ examples of Table I, β is so small that the upper sideband may not be discernable above the background. If, however, we increase the power so that we are just saturating the upper sideband, then the carrier and upper sideband have amplitude ~ 1 and the lower sideband has amplitude $\langle n_v\rangle$, as indicated qualitatively in Fig. 6(b). If we further increase the laser power by a factor of K, the carrier and upper sideband maintain an amplitude ~ 1 and the lower sideband has amplitude $K\langle n_v\rangle$. By proper choice of K [e.g., $K\simeq 1/(2\langle n_v\rangle)$], we have a way to measure or put an upper limit on $\langle n_v\rangle$. Similar methods could be used to measure the amplitude of the micromotion of an ion in an rf trap.

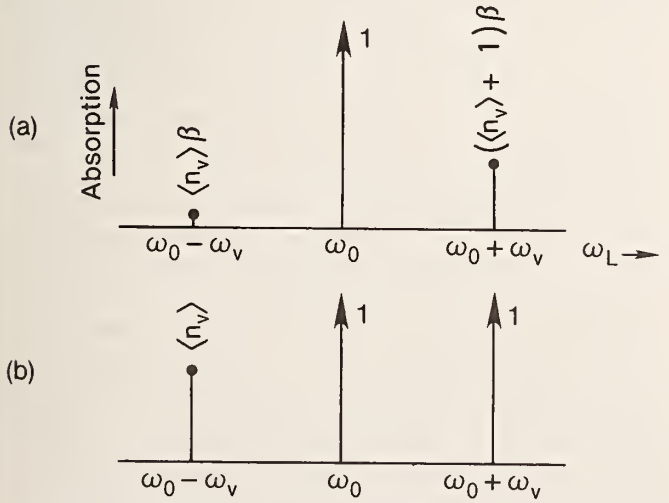

FIG. 6. Absorption spectrum of an ion in a harmonic potential for $\langle n_v\rangle\ll 1$ and $\beta=R/\hbar\omega_v\ll 1$. In (a) relative amplitudes are given for the unsaturated spectrum. In (b) the radiation intensity is adjusted so that the upper sideband is just saturated. The amplitude of the weak lower sideband is a direct measure of $\langle n_v\rangle$.

VI. IMPLICATIONS FOR SPECTROSCOPY

One of the original motivations for laser cooling was the reduction of Doppler shifts and broadening in very-high-resolution spectroscopy.[37–39] Achieving the Lamb-Dicke limit essentially eliminates first-order Doppler broadening effects since the intensity in the sidebands is very small. This result is independent of temperature, but is easier to achieve at low temperatures. Historically, the uncertainty in the second-order Doppler frequency shift has been the primary limiting systematic effect in high-resolution experiments on stored ions. This was true in the first high-resolution experiments on $^3He^+$ ions[40] (accuracy approximately equal to 1 part in 10^9) and the most accurate experiments on ions to date, those on $^9Be^+$ ions[41] (accuracy approximately equal to 1 part in 10^{13}). If the limits provided by sideband cooling can be realized, the second-order Doppler shift may no longer be the limiting systematic effect.

First, we note that even in the Doppler cooling limit for an allowed transition, the second-order Doppler shift would be extremely small. From Eq. (1), the limiting mean kinetic energy is given by $\hbar\gamma/4$ for each degree of freedom. The Penning trap has one axial degree of freedom and two cyclotron degrees of freedom which contribute; therefore, the limiting kinetic energy is $3\hbar\gamma/4$. For the rf trap, the kinetic energy is at least twice this value due to the micromotion contribution (Sec. II B). The magnitude of the resulting minimum second-order Doppler shift per kinetic-energy degree of freedom ϵ_{D2} is given by

$$\epsilon_{D2}=-\frac{\Delta\nu_{D2}}{\nu_0}=\frac{\hbar\gamma}{4mc^2}\simeq\frac{1.1\times10^{-18}[\gamma/2\pi(\mathrm{MHz})]}{M}\ , \tag{35}$$

where the right-hand side denotes the Doppler cooling limit. In Eq. (35), $\gamma/2\pi$ is expressed in MHz and M is the ion mass in u (atomic mass units). Values of ϵ_{D2} for a few kinds of ions confined in a harmonic trap are given in Table I. ϵ_{D2} gives the mean value of the second-order Doppler shift. The uncertainty in ϵ_{D2} can be less depending on actual experimental conditions. In spite of the smallness of these numbers, it may be desirable to suppress the second-order Doppler shift further since other systematic effects may be controllable[42] to levels below one part in 10^{18}.

In the sideband cooling limit, since $\langle n_v\rangle\ll 1$, the second-order Doppler shift is simply due to the kinetic energy in the zero-point oscillations $\hbar\omega_v/4$ for each degree

of freedom. Therefore,

$$\epsilon_{D2} = -\frac{\Delta\nu_{D2}}{\nu_0} = (2\langle n_v\rangle + 1)\frac{\hbar\omega_v}{4mc^2} = \frac{1.1\times 10^{-18}[\omega_v/2\pi(\mathrm{MHz})]}{M}, \quad (36)$$

where the right-hand side denotes the sideband cooling limit. ϵ_{D2} is at least twice this value for the rf trap due to micromotion. Although these values of ϵ_{D2} can be very small, the uncertainty in these values can be even lower.[11] For example, the uncertainty in ϵ_{D2} given by Eq. (36) might likely be due to the uncertainty of fluctuations in ω_v. As an example, assume we perform sideband cooling of $^{198}Hg^+$ ions in an rf trap where $\omega_v/2\pi = 10$ MHz. If the uncertainty in this oscillation frequency is 100 Hz and $\langle n_v\rangle \ll 10^{-5}$, the uncertainty in the second-order Doppler shift is 3.4×10^{-24}! It is not difficult to think about even much lower limits. If we go back to the expression for the ion temperature [Eq. (4)], we see that for fixed ω_v, the temperature for the sideband cooling limit is not a strong function of γ as it is for the Doppler cooling limit [due to the $\ln(\langle n_v\rangle^{-1})$ factor]. In fact, for fixed γ, the Doppler cooling limit gives a lower temperature than the sideband cooling limit. However, as in the example above, the uncertainty in ϵ_{D2} may be due to the uncertainty in ω_v and not directly a function of temperature. Thus, it would appear that temperature may not be a very useful parameter to describe the limits to high-resolution spectroscopy on bound atoms or ions.

With the potentially very low values of uncertainty in the second-order Doppler-shift correction, it continues to be an open question as to what will be the ultimate limit on accuracy in single-ion spectroscopy. The various effects of multipole electric and magnetic field interactions have to be considered;[42] in principle, these effects could be measured and controlled to much less than 1 part in 10^{18}. Certainly, practical issues now play an important role. At present, the required tunable narrow-band lasers do not exist, but recent experimental advances[43] may provide a solution. If we assume that the spectral purity and amplitude stability of the lasers will not be a problem, we must still consider the fundamental limits to the signal-to-noise ratio. The high quantum multiplications achievable in double-resonance spectroscopy allow 100% detection efficiency.[37] This has been demonstrated in recent experiments on single ions.[7,44,45] In this case, the noise in the experiments is dominated by the shot noise in the clock-transition measurement. That is, the noise in the measurement process is governed by the fluctuations in whether or not the ion has undergone the clock transition after application of the clock radiation. If we assume 100% detection efficiency in the double-resonance experiment described in Sec. V (Fig. 6), the maximum signal-to-noise ratio for determining line center of the clock transition is given by measuring the transition probability at the half-power points on both sides of the clock resonance and forcing the average frequency of the interrogating radiation to line center. If we make the assumption that the time-domain Ramsey method is used to interrogate the clock transition, then the frequency stability (two-sample Allan variance[46]) is given as[37]

$$\sigma_y(\tau) \equiv [\langle(\langle\omega_k\rangle_\tau - \langle\omega_{k+1}\rangle_\tau)^2\rangle_k/2\omega_0^2]^{1/2} = (2\omega_0^2 T_R\tau)^{-1/2}. \quad (37)$$

In this expression, $\langle\omega_k\rangle_\tau$ is the kth measurement of the frequency of the locked oscillator averaged over time τ, $\langle\ \rangle_k$ denotes an average over many measurements, ω_0 is the nominal frequency of the clock transition, and T_R is the interrogation time between pulses in the Ramsey method. Thus $\sigma_y(\tau)$ is a measurement of the rms fluctuations of the frequency for measurement times τ. Equation (37) assumes that optical state preparation (cooling and optical pumping) and double-resonance detection (from the 194-nm fluorescence signal in the example of Fig. 6) takes a time much less than T_R.

The accuracy of the measurement is limited to the value $\sigma_y(\tau)$ for a measurement time τ. If, for example, $T_R = 0.5$ s [linewidth approximately equal to $(2T_R)^{-1} = 1$ Hz] and $\omega_0/2\pi = 10^{15}$ Hz ($\lambda_2 = 300$ nm), then $\tau \simeq 2.5\times 10^4$ s is required to make a measurement with an imprecision $\sigma_y(\tau)$ of 1 part in 10^{18}. To reach a precision of about 10^{-25} would require a time equal to the age of the universe. Therefore, even though the intrinsic accuracy may be quite high, it may take a long averaging time to reach a comparable measurement precision. In other words, measurement precisions beyond 1 part in 10^{18} may require even higher Q transitions (through smaller values of γ) and narrower linewidth lasers.

VII. CONCLUSIONS

If the theoretical limits to laser cooling can be reached on a single trapped ion, the ion will nearly be held in the zeroth quantum level of its bound motion. This would be the closest possible realization of the ideal of a single isolated atom at rest. When cooling to near the zeroth quantum level is achieved, the temperatures achieved appear to lose their relevance; rather, we might be interested in the fluctuations of the zero-point energy due, for example, to fluctuations in the well depth of the trap.

In addition to the intellectual interest of achieving confinement to the zero-point energy state, the implications for accuracy in high-resolution spectroscopy are remarkable. For example, uncertainties in the second-order Doppler-shift correction might be 10^{-24} or lower. The possibility of these extremely low numbers clearly emphasizes the importance of many practical problems. For the rf trap, minimizing the kinetic energy in the micromotion may be a very difficult problem (Sec. II). For the Penning trap, no analog for the micromotion is apparent although it will be more difficult to obtain conditions where the sideband cooling limit applies (Sec. III). In addition, there is the fundamental problem of the limiting signal-to-noise ratio on a single ion; that is, we must ask, "Can we reach the required measurement precision in a reasonable length of time (Sec. VI)?" We must also consider the problems of laser spectral purity and the measurement of laser frequencies. Equally important, we

must address the problems of controlling the various perturbations to the internal structure of the ions produced by external electric and magnetic fields. Nevertheless, in the end, it does not seem unreasonable to think that accuracies and measurement precisions at or beyond 1 part in 10^{18} will be achieved.

ACKNOWLEDGMENTS

We gratefully acknowledge the support of the U.S. Air Force Office of Scientific Research (AFOSR) and the Office of Naval Research (ONR). We also thank J. Cooper and L. Hollberg for helpful comments on the paper.

[1]The Mechanical Effects of Light, edited by P. Meystre and S. Stenholm [J. Opt. Soc. Am. **B2**, No. 11 (1985)].

[2]*Atomic Physics 9,* edited by R. S. Van Dyck, Jr., and E. N. Fortson (World Scientific, Singapore, 1985).

[3]Symposium Alfred Kastler, [Ann. Phys. (Paris) **10**, No. 6 (1985)].

[4]S. Stenholm, Rev. Mod. Phys. **58**, 699 (1986).

[5]W. Neuhauser, M. Hohenstatt, P. E. Toschek, and H. Dehmelt, Phys. Rev. A **22**, 1137 (1980).

[6]W. Nagourney, G. Janik, and H. Dehmelt, Proc. Nat. Acad. Sci. (USA) **80**, 643 (1983).

[7]J. C. Bergquist, R. G. Hulet, W. M. Itano, and D. J. Wineland, Phys. Rev. Lett. **57**, 1699 (1986); J. C. Bergquist, W. M. Itano, and D. J. Wineland, Phys. Rev. A **36**, 428 (1987).

[8]L. R. Brewer, J. D. Prestage, J. J. Bollinger, and D. J. Wineland, in *Strongly Coupled Plasma Physics,* NATO Advanced Study Institute, Series B: Physics, edited by J. Rogers and H. Dewitt (Plenum, New York, 1987), p. 53.

[9]S. Chu, L. Hollberg, J. E. Bjorkholm, A. Cable, and A. Ashkin, Phys. Rev. Lett. **55**, 48 (1985).

[10]W. Neuhauser, M. Hohenstatt, P. Toschek, and H. Dehmelt, Phys. Rev. Lett. **41**, 233 (1978).

[11]D. J. Wineland and W. M. Itano, Phys. Rev. A **20**, 1521 (1979).

[12]R. S. Van Dyck, Jr., P. B. Schwinberg, and H. G. Dehmelt, in *New Frontiers in High-Energy Physics,* edited by B. M. Kursunoglu, A. Perlmutter, and L. F. Scott, (Plenum, New York, 1978), p. 159.

[13]S. P. Vyatchanin, Dokl. Akad. Nauk. SSSR **234**, 1295 (1977); [Sov. Phys.—Dokl. **22**, 321 (1977)]; L. S. Brown and G. Gabrielse, Rev. Mod. Phys. **58**, 233 (1986).

[14]D. E. Pritchard, Phys. Rev. Lett. **51**, 1336 (1983).

[15]S. Chu, J. E. Bjorkholm, A. Ashkin, J. P. Gordon, and L. Hollberg, Opt. Lett. **11**, 73 (1986).

[16]S. Chu, J. E. Bjorkholm, A. Ashkin, L. Hollberg, and A. Cable, in *Methods of Laser Spectroscopy,* edited by Y. Prior, A. Ben-Reuven, and M. Rosenbluh (Plenum, New York, 1986), p. 41.

[17]H. F. Hess, Bull Am. Phys. Soc. **30**, 854 (1985).

[18]R. V. E. Lovelace, C. Mehanian, J. J. Tommila, and D. M. Lee, Nature **318**, 30 (1985).

[19]H. Dehmelt, G. Janik, and W. Nagourney, Bull. Am. Phys. Soc. **30**, 111 (1985).

[20]T. Sauter, W. Neuhauser, and P. E. Toschek, in *Fundamentals of Laser Interactions,* Vol. 299 of *Lecture Notes in Physics,* edited by F. Ehlotzky (Springer, Heidelberg, 1985).

[21]J. Javanainen, in *Fundamentals of Laser Interactions,* Vol. 299 of *Lecture Notes in Physics,* edited by F. Ehlotzky (Springer, Heidelberg, 1985) p. 249.

[22]V. G. Minogin and Yu. V. Rozhdestvensky, Appl. Phys. B **34**, 161 (1984).

[23]M. Lindberg and J. Javanainen, J. Opt. Soc. Am. B **3**, 1008 (1986).

[24]D. J. Wineland, in *Precision Measurement and Fundamental Constants II,* Natl. Bur. Stand. (U.S.) Special Publ. No. 617, edited by B. N. Taylor and W. D. Phillips, (U.S. GPO, Washington, D.C., 1984), p. 83.

[25]The basic concepts of ion trapping can be found in many references. See, for example, H. G. Dehmelt, Adv. At. Mol. Phys. **3**, 53 (1967) and **5**, 109 (1969); D. J. Wineland, W. M. Itano, and R. S. Van Dyck, Jr., *ibid.* **19**, 135 (1983).

[26]M. Lindberg, J. Phys. B **17**, 2129 (1984); J. Javanainen, M. Lindberg, and S. Stenholm, J. Opt. Soc. Am. B **1**, 111 (1984).

[27]W. M. Itano and D. J. Wineland, Phys. Rev. A **25**, 35 (1982).

[28]R. H. Dicke, Phys. Rev. **89**, 472 (1953).

[29]R. J. Cook, D. G. Shankland, and A. L. Wells, Phys. Rev. A **31**, 564 (1985).

[30]G. Janik, W. Nagourney, and H. Dehmelt, J. Opt. Soc. Am. B **2**, 1251 (1985).

[31]D. J. Wineland and H. Dehmelt, J. Appl. Phys. **46**, 919 (1975).

[32]G. Gabrielse, Phys. Rev. A **29**, 462 (1984).

[33]E. C. Beaty, Phys. Rev. A **33**, 3645 (1986).

[34]R. S. Van Dyck, Jr. and P. B. Schwinberg, Phys. Rev. Lett. **47**, 395 (1981).

[35]H. G. Dehmelt, Bull. Am. Phys. Soc. **20**, 60 (1975).

[36]D. J. Wineland and W. M. Itano, Phys. Lett. **82A**, 75 (1981).

[37]D. J. Wineland, W. M. Itano, J. C. Bergquist, and F. L. Walls, in Proceedings of the Thirty-fifth Annual Symposium on Frequency Control (1981), p. 602 (copies available from Electronics Industry Assn., 2001 "Eye" St., N.W. Washington, D.C. 20006).

[38]T. W. Hänsch and A. L. Schawlow, Opt. Commun. **13**, 68 (1975).

[39]D. J. Wineland and H. Dehmelt, Bull. Am. Phys. Soc. **20**, 637 (1975).

[40]E. N. Fortson, F. G. Major, and H. Dehmelt, Phys. Rev. Lett. **16**, 221 (1966); F. G. Major and H. G. Dehmelt, Phys. Rev. **170**, 91 (1968); H. A. Schuessler, E. N. Fortson, and H. G. Dehmelt, *ibid.* **187**, 5 (1969).

[41]J. J. Bollinger, J. D. Prestage, W. M. Itano, and D. J. Wineland, Phys. Rev. Lett. **54**, 1000 (1985).

[42]See, for example, H. G. Dehmelt, IEEE Trans. Instrum. Meas. **IM-31**, 83 (1982); D. J. Wineland, Science **226**, 395 (1984), and references therein.

[43]J. Hall, C. Salomon, and D. Hils, in *Proceedings of the Fourteenth International Conference on Quantum Electronics,* Technical Digest (Optical Society of America, Washington, D.C., 1986), p. 80.

[44]W. Nagourney, J. Sandberg, and H. Dehmelt, Phys. Rev. Lett. **56**, 2797 (1986).

[45]Th. Sauter, W. Neuhauser, R. Blatt, and P. E. Toschek, Phys. Rev. Lett. **57**, 1696 (1986).

[46]J. A. Barnes, A. R. Chi, L. S. Cutler, D. J. Healey, D. B. Leeson, T. E. McGunigal, J. A. Mullen, Jr., W. L. Smith, R. L. Sydnor, R. F. C. Vessot, and G. M. R. Winkler, IEEE Trans. Instrum. Meas. **IM-20**, 105 (1971).

PHYSICAL REVIEW A VOLUME 36, NUMBER 1 JULY 1, 1987

Recoilless optical absorption and Doppler sidebands of a single trapped ion

J. C. Bergquist, Wayne M. Itano, and D. J. Wineland
Time and Frequency Division, National Bureau of Standards, Boulder, Colorado 80303
(Received 13 April 1987)

Spectroscopic measurements of the electric-quadrupole-allowed $5d^{10}6s\,^2S_{1/2}$ to $5d^96s^2\,^2D_{5/2}$ transition near 282 nm on a single, laser-cooled Hg^+ ion give a recoil-free absorption line (carrier) and well-resolved motional sidebands. From the intensity ratio of the sidebands to the carrier, the effective temperature of the Hg^+ ion was determined to be near the theoretical minimum of 1.7 mK. A fractional resolution of better than 3×10^{-11} for this ultraviolet transition is achieved.

Following the success of recent experiments on single, laser-cooled ions, most notably those experiments showing quantum jumps,[1-3] photon antibunching,[2,4] and absorption by a single ion,[5] several groups are now at the threshold of atomic spectroscopy that promises fractional resolution and accuracy exceeding 1 part in 10^{15}. In the work reported here, we experimentally demonstrate the spectroscopic resolution and signal-to-noise ratio that are attainable with a single atom nearly at rest in space. We have resolved the recoilless optical resonance[6,7] and motional sidebands of the $5d^{10}6s\,^2S_{1/2}$ to $5d^96s^2\,^2D_{5/2}$ transition ($\lambda=282$ nm) on a laser cooled $^{198}Hg^+$ ion confined in an rf trap. Since we can detect each transition to the metastable $^2D_{5/2}$ state with nearly 100% efficiency,[2] there is essentially no instrumental noise. The noise results only from the quantum statistical fluctuations in the transition probability of the single ion.[8] The unshifted resonance and sidebands shown in Fig. 1 are a convincing demonstration in the optical region of Dicke's original prediction of the spectral features of an atom whose spatial excursions are constrained to the order of λ.[6] From the sideband structure we are able to make a determination of the amplitude of the motion of the ion and its effective temperature.[9,10] We anticipate that by further cooling with narrowband laser radiation that is tuned to the first lower sideband of the $^2S_{1/2}$-$^2D_{5/2}$ transition, the Hg^+ ion can be made to reside at the zero-point energy of the trap's harmonic well most of the time.[9,11,12]

The experimental setup is essentially the same as that described in our earlier studies on the two-photon spectroscopy of Hg^+,[13] quantum jumps,[2] and single-ion absorption.[5] A mercury atom that is ionized by a weak electron beam is captured in a miniature rf (Paul) trap that has internal dimensions of $r_0\simeq455$ μm and $z_0\simeq320$ μm. The rf trapping frequency was 21.07 MHz with a peak voltage amplitude of about 730 V. The ion is laser cooled by a few microwatts of cw laser radiation that is frequency tuned below the $6s\,^2S_{1/2}$-$6p\,^2P_{1/2}$ first resonance line near 194 nm.[2,14] When the Hg^+ ion is cold and the 194-nm radiation has sufficient intensity to saturate the strongly allowed S-P transition, 2×10^8 photons/s are scattered. With our collection efficiency, this corresponds to an observed peak count rate of about 10^5 s^{-1} against a background of less than 50 s^{-1}.

The 282-nm radiation that drives the $^2S_{1/2}$-$^2D_{5/2}$ transition is obtained by frequency doubling the radiation from a cw ring dye laser that has been spectrally narrowed and stabilized in long term to less than 15 kHz. For this experiment, the dye laser is stabilized to a high-finesse optical cavity[15] to give good short-term stability. In long term, the laser is stabilized by FM optical heterodyne spectroscopy to a saturated-absorption hyperfine component in $^{129}I_2$.[16] The pressure in the iodine cell is not controlled against temperature variations, and this gave rise to pressure-induced frequency fluctuations that dominated the stability of the laser for times greater than about 10 s. The frequency of the laser is scanned by tuning the frequency applied to an acousto-optic modulator through which the laser beam is passed. We eliminated angle variation in the beam that was frequency shifted

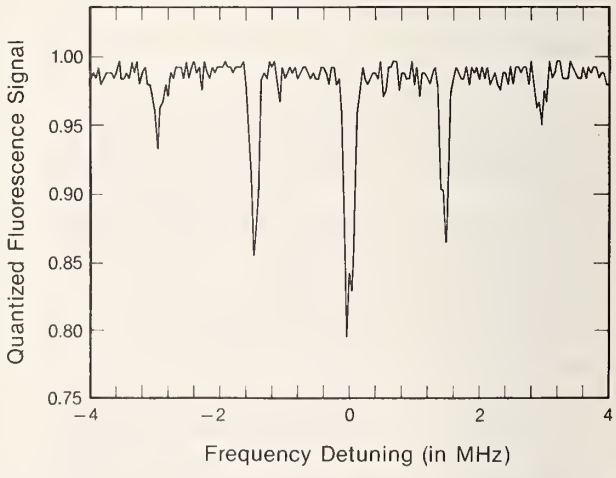

FIG. 1. Quantized signal showing the electric-quadrupole-allowed $5d^{10}6s\,^2S_{1/2}(m_J=-\frac{1}{2})$-$5d^96s^2\,^2D_{5/2}(m_J=\frac{1}{2})$ transition in a single, laser-cooled $^{198}Hg^+$ ion. On the horizontal axis is plotted the relative detuning from line center in frequency units at 282 nm. On the vertical axis is plotted the probability that the fluorescence from the $6s\,^2S_{1/2}$-$6p\,^2P_{1/2}$ first resonance transition, excited by laser radiation at 194 nm, is on. The electric-quadrupole-allowed S-D transition and the first-resonance S-P transition are probed sequentially in order to avoid light shifts and broadening of the narrow S-D transition. Clearly resolved are the recoilless absorption resonance (carrier) and the Doppler sidebands due to the residual secular motion of the laser-cooled ion. The integration time per point is about 16 s (230 measurement cycles).

Work of the U.S. Government
Not Subject to U.S. Copyright

and scanned by using the twice-frequency-shifted beam obtained by retroreflecting the first-order frequency-shifted beam back through the crystal. A computer controls the frequency and amplitude of the synthesizer that drives the acousto-optic modulator. Up to a few microwatts of 282-nm radiation could be focused onto the ion in a direction either orthogonal to, or counterpropagating with the 194-nm light beam. A magnetic field of approximately 1.2 mT (12 G) was applied parallel to the electric field vector of the linearly polarized 282-nm radiation to give well-resolved Zeeman components. This configuration gives a selection rule of $|\Delta m_J| = 1$ for the electric-quadrupole-allowed transitions to the various Zeeman states.

Optical-optical double-resonance utilizing quantum amplification[13,17-19] was used to detect transitions driven by the 282-nm laser to the metastable $^2D_{5/2}$ state. Our version of this method makes use of the fact that the 194-nm fluorescence intensity level is bistable; high when the ion is cycling between the S and P states (the "on" state) and nearly zero when it is in a metastable D state (the "off" state).[1-3] The fluorescence intensity in the on state is high enough that the state of the atom can be determined in a few milliseconds with nearly 100% efficiency. The full measurement cycle was as follows: A series of measurements of the 194-nm fluorescence was made, using a counter with a 10-ms integration period. As soon as the counter reading per measurement period was high enough to indicate that the ion was in the on state, the 194-nm radiation was shut off and the 282-nm radiation was pulsed on for 20 ms. Then, the 194-nm radiation was turned on again, and the counter was read. If the reading was low enough to indicate that the ion had made a transition to the $^2D_{5/2}$ state (the off state), the signal was defined to be 0. Otherwise, it was defined to be 1. The 282-nm laser frequency was then stepped, and the cycle was repeated. As the laser frequency is swept back and forth through the resonance, the quantized measurement of the fluorescence signal at each frequency step is averaged with the previous measurements made at that same frequency. Since we could detect the state of the ion with nearly 100% efficiency, there was essentially no instrumental noise in the measurement process. Occasionally, while the 194-nm radiation was on, the ion decayed from the $^2P_{1/2}$ state to the metastable $^2D_{3/2}$ state rather than directly to the ground state.[2] This process led to a background rate of false transitions which was minimized by the quantized data-collecting method described above and by decreasing the 194-nm fluorescence level (thereby decreasing the $^2P_{1/2}$-$^2D_{3/2}$ decay rate) until it was just high enough for the quantized detection method to work. The quantized measurement scheme also removes any contribution to the signal base line due to intensity variations in the 194-nm source. The 282- and 194-nm radiation were chopped so that they were never on at the same time. This eliminated shifts and broadening of the narrow 282-nm resonance due to the 194-nm radiation.[18,20,21]

Figure 1 shows the fluorescence signal obtained from an 8-MHz scan of the 282-nm laser through the

$$5d^{10}6s\,^2S_{1/2}(m_J=-\tfrac{1}{2}) \rightarrow 5d^9 6s^2\,^2D_{5/2}(m_J=\tfrac{1}{2})$$

Zeeman component of the laser-cooled Hg^+ ion. The recoilless absorption resonance (carrier)[6,7] and the motional sidebands due to the secular motion of the ion in the harmonic well of the rf trap are completely resolved. The inhomogeneous rf electric field produces a pseudopotential harmonic well with a radial frequency of approximately 1.46 MHz and an axial frequency of approximately twice the radial frequency, or about 2.9 MHz. An ion trapped in this pseudopotential well will execute nearly independent harmonic motions in the radial and axial directions. These harmonic motions frequency modulate the laser radiation, as seen by the trapped ion and produce sidebands on the carrier frequency at the radial and axial frequencies and their harmonics.[9] Thus, the number and amplitude of sidebands are a direct measure of the amplitude of the ion's motion and its effective temperature. In Fig. 1, only two pairs of sidebands are obtained. In this figure the 282-nm intensity is adjusted to be close to saturation on the carrier in order to enhance the relative strength of the sidebands to the carrier. Also, the laser linewidth was broadened to about 80 kHz (at 563 nm) by modulating the frequency of the acousto-optic modulator in order to reduce the number of data points required for the sweep. A careful comparison of the sideband intensities [Ref. 9, Eq. (44)], including the effects of saturation, gives an ion temperature for the secular motion of about 5.8 mK. This is near the theoretical laser-cooling limit for $^{198}Hg^+$ on the first resonance line at 194 nm given by[9] $T_{\min} = \hbar\gamma/2k_B \simeq 1.7$ mK.

The spectrum in Fig. 1 was taken with the 194-nm beam counterpropagating to the 282-nm beam. This arrangement gives optimum cooling to the ion motion in the direction that is probed by the 282-nm beam. We have also probed in a direction perpendicular to the propagation direction of the 194-nm beam. In this case, if there is perfect symmetry in the radial plane of the trap, then the ion will heat without bound in the radial direction perpendicular to the cooling beam.[9,11] Trap asymmetry in the radial plane permits cooling in all directions provided the **k** vector of the cooling beam is not in the radial plane nor collinear with the trap axis.[9,11,18] Even though cooling in all directions is possible, the limiting temperature will be higher in the direction perpendicular to the cooling beam due to recoil heating in that direction. From our data, we find this temperature to be only a few mK higher, indicating a fairly rapid energy transfer between the ion's motional degrees of freedom.

Stray static electric fields in the trap can produce residual micromotion at the rf drive frequency of 21.07 MHz. This happens because the static field shifts the ion's equilibrium point to a region where the force from the static field is compensated for by the force from the pseudopotential. In this case, there is residual micromotion at the bottom of the well even for a cold ion. The micromotion will produce sidebands on the carrier at harmonics of the micromotion frequency analogous to the secular motion sidebands. The appearance of rf sidebands in our initial scans indicated the presence of a small stray static field perhaps caused by contact potential variations on one or more of the electrodes. It was possible to null out the rf sidebands by applying a compensating dc voltage of about

0.3 V to one of the end caps. To null the rf sidebands in all directions would likely require extra compensation electrodes.

In Fig. 2, we show high-resolution scans through the Doppler-free resonance at line center and across the first upper sideband. The average integration time per point is about 10 s (160 measurement cycles). The linewidth at half maximum is approximately 30 kHz at 282 nm (or 15 kHz at 563 nm), giving a fractional resolution of about 3×10^{-11}. If we can obtain a resolution that approaches the natural linewidth limit of 1.6 Hz, the required integration time per point for the same signal-to-noise ratio of Fig. 2 will increase by a factor of less than 2. For the data of Fig. 2, an effective temperature of 1.6 ± 0.5 mK and an rms amplitude of 28 ± 5 nm for the secular motion was obtained. However, over several sets of data similar to that of Fig. 2, we obtained temperatures that ranged from 1.6 to 6.7 mK. The discrepancies between the measured temperatures and the theoretical minimum might be due to the uncertainty in the tuning of the 194-nm cooling laser to the half-power point on the S-P transition. If the frequency of the laser were detuned to a longer wavelength by a natural linewidth, the temperature obtained would be about twice the minimum. Also, some heating may have been caused by collisions with the background gas. Finally, if the frequency of the 282-nm laser is tuned to the first lower secular sideband, it would be possible to cool the ion until it occupied the zero point or $\langle n_i\rangle=0$ $(i=x,y,z)$ energy state of the harmonic well most of the time.[9,11,12,18]

In summary, we have laser cooled a single ion and probed with high resolution the $^2S_{1/2}$-$^2D_{5/2}$ quadrupole resonance at 282 nm. The ability to detect each transition with almost no ambiguity eliminated nearly all instrumental noise. We have resolved the recoilless resonance line and the Doppler-generated motional sidebands. From the relative strength of the sidebands, a direct measurement of the ion temperature and its spatial excursion was made.

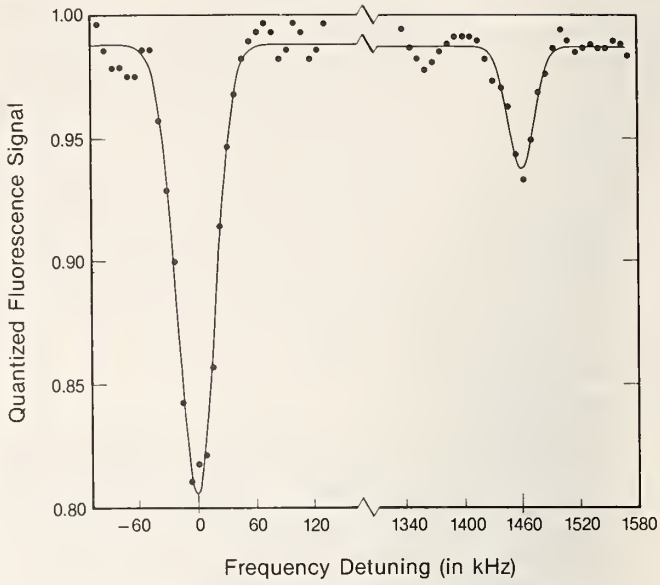

FIG. 2. High-resolution scan through the recoilless absorption resonance and first (upper) sideband of the $^2S_{1/2}$-$^2D_{5/2}$ $(m_J=-\frac{1}{2}-m_J=\frac{1}{2})$ transition in a single laser-cooled $^{198}Hg^+$ ion. The full width at half maximum of the recoilless absorption resonance and of the upper sideband is about 30 kHz at $\lambda=282$ nm (15 kHz at $\lambda=563$ nm). A comparison of the carrier-to-sideband intensity gives a temperature of 1.6 ± 0.5 mK, in agreement with the theoretical minimum of 1.7 mK. The integration time per point is about 10 s (160 measurement cycles).

We anticipate improved spectral purity of the probe laser and better magnetic shielding of the Hg^+ ion in the future to give increased spectral resolution.

We acknowledge the support of the Air Force Office of Scientific Research and the Office of Naval Research. We thank L. Hollberg, R. Hulet, and M. Young for suggestions and comments on the manuscript.

[1]W. Nagourney, J. Sandberg, and H. Dehmelt, Phys. Rev. Lett. **56**, 2797 (1986).

[2]J. C. Bergquist, R. G. Hulet, W. M. Itano, and D. J. Wineland, Phys. Rev. Lett. **57**, 1699 (1986).

[3]T. Sauter, W. Neuhauser, R. Blatt, and P. E. Toschek, Phys. Rev. Lett. **57**, 1696 (1986).

[4]F. Diedrich and H. Walther, Phys. Rev. Lett. **58**, 203 (1987).

[5]D. J. Wineland, W. M. Itano, and J. C. Bergquist, Opt. Lett. **12**, 389 (1987).

[6]R. H. Dicke, Phys. Rev. **89**, 472 (1953).

[7]See, for example, Hans Frauenfelder, *The Mössbauer Effect* (Benjamin, New York, 1962).

[8]D. J. Wineland, W. M. Itano, J. C. Bergquist, and F. L. Walls, in Proceedings of the 35th Annual Symposium Frequency Control, 1981, p. 602 (copies available from Electronic Industries Association, 2001 Eye Street, N.W., Washington, DC 20006).

[9]D. J. Wineland and W. M. Itano, Phys. Rev. A **20**, 1521 (1979).

[10]G. Janik, W. Nagourney, and H. Dehmelt, J. Opt. Soc. Am. B **2**, 1251 (1985).

[11]D. J. Wineland, W. M. Itano, J. C. Bergquist, and R. G. Hulet, Phys. Rev. A (to be published).

[12]W. Neuhauser, M. Hohenstatt, P. Toschek, and H. Dehmelt, Phys. Rev. Lett. **41**, 233 (1978).

[13]J. C. Bergquist, D. J. Wineland, W. M. Itano, H. Hemmati, H.-U. Daniel, and G. Leuchs, Phys. Rev. Lett. **55**, 1567 (1985).

[14]H. Hemmati, J. C. Bergquist, and W. M. Itano, Opt. Lett. **8**, 73 (1983).

[15]J. C. Bergquist, R. L. Barger, and D. J. Glaze, in *Laser Spectroscopy IV*, edited by H. Walther and K. W. Rothe, Springer Series in Optical Science, Vol. 30 (Springer-Verlag, New York, 1979), p. 120.

[16]J. L. Hall, L. Hollberg, T. Baer, and H. G. Robinson, Appl. Phys. Lett. **39**, 680 (1981).

[17]D. J. Wineland, J. C. Bergquist, W. M. Itano, and R. E. Drullinger, Opt. Lett. **5**, 245 (1980); D. J. Wineland and W. M. Itano, Phys. Lett. **82A**, 75 (1981).

[18]H. Dehmelt, J. Phys. (Paris) Colloq. **42**, C8-299 (1981).

[19]H. G. Dehmelt, Bull. Am. Phys. Soc. **20**, 60 (1975).

[20]W. M. Itano and D. J. Wineland, Phys. Rev. A **24**, 1364 (1981).

[21]W. Happer, Rev. Mod. Phys. **44**, 169 (1972).

From: Proc. 4th Symposium on Frequency Standards and Metrology, Ancona, Italy, Sept. 1988; A. Demarchi, ed. (Springer Verlag, Heidelberg).

Hg^+ Single Ion Spectroscopy*

J.C. Bergquist, F. Diedrich,† Wayne M. Itano, and D.J. Wineland
Time and Frequency Div., National Institute of Standards and Technology
(formerly the National Bureau of Standards)
Boulder, CO 80303

Abstract

A single Hg^+ ion that is confined in an rf (Paul) trap can be laser cooled so that the amplitude of its motion is much less than a wavelength (the Dicke limit) for optical transitions. Recently, we have used the technique of optical sideband cooling to reach the zero point of motion. This realizes for the first time the fundamental limit of laser cooling for a bound atom and the ideal of an isolated atomic particle at rest in space to within the quantum mechanical limits imposed by the surrounding apparatus. In both limits, Doppler effects become negligible to all orders, the interrogation time is long and the fundamental shot noise detection limit of a single atom is readily attained.

Introduction

Laser cooling of a single atom has led to a number of important experiments in fundamental physics [1-5] and may allow optical spectroscopy and metrology with a resolution and accuracy that approach 1×10^{-18} [6-9]. One of the candidates for an optical frequency standard that approaches this accuracy is a single, laser-cooled $^{199}Hg^+$ ion confined in a miniature rf trap [8]. At NIST we have begun with an investigation of a single $^{198}Hg^+$ ion, laser cooled into the Dicke limit for optical transitions [8] and, in a second experiment, laser cooled in the sideband limit to the zero-point energy of motion [10,12]. The $^{198}Hg^+$ ion offers the experimental advantage of zero nuclear spin; hence, no hyperfine structure and a simpler optical configuration for cooling. However, all the narrow optical transitions have a magnetic field sensitivity of the order of 10 MHz/mT (1 MHz/G), whereas the $^{199}Hg^+$ ion has several first-order magnetic field-independent transitions.

In the work summarized here we begin to show the spectroscopic resolution and signal-to-noise ratio that are possible with a single atom nearly at rest in space. We have resolved the recoilless optical resonance and the motional sidebands of the $5d^{10}6s\ ^2S_{\frac{1}{2}}(m_J=-\frac{1}{2})$ - $5d^96s^2\ ^2D_{5/2}(m_J=\frac{1}{2})$ electric quadrupole transition ($\lambda\cong282$ nm) on a laser-cooled $^{198}Hg^+$ ion [8]. Since we can detect each transition to the

*Contribution of the NIST, not subject to copyright in the U.S.

metastable $^2D_{5/2}$ state ($\gamma/2\pi \approx 1.7$ Hz) with nearly 100% efficiency, there is essentially no technical noise. The noise results only from the quantum statistical fluctuations in the transition probability of the single ion [6]. From the sideband structure we are able to make a determination of the amplitude of the motion of the ion and its effective temperature [10,11,13]. The sidebands at $\omega_0 \pm n\omega_v$ (n an integer) are generated by the oscillatory motion at frequency ω_v of the ion in its confining harmonic well. If the ion is driven with narrowband radiation tuned to the first lower sideband, the atom will absorb photons of energy $\hbar(\omega_0-\omega_v)$ and in most cases re-emit photons of energy $\hbar\omega_0$. This reduces the atom's vibrational quantum number by 1 for each scattered photon at frequency ω_0. In this way we can obtain $\langle n_v \rangle \ll 1$, which means that the atom spends most of its time in the ground state level of its confining potential [10,12-14]. To the extent that the atom is in the ground state of its confining potential the fundamental limit of laser cooling for a confined particle has been reached [12].

Experiment

The mercury ion is confined in a miniature rf trap that has internal dimensions of $r_0 \approx 466$ μm and $z_0 \approx 330$ μm [8,15]. The amplitude of the trapping field (frequency $\Omega/2\pi \approx 21$-23 MHz) could be varied to a peak of 1.2 kV. The ion is laser cooled to a few millikelvins by a few microwatts of cw laser radiation [16] that is frequency tuned below the $^2S_{\frac{1}{2}}$ - $^2P_{\frac{1}{2}}$ first resonance line near 194 nm [2,8]. In order to cool all motional degrees of freedom to near the Doppler cooling limit ($T = \hbar\gamma/2k_B \approx 1.7$ mK) the 194 nm radiation irradiates the ion from 2 orthogonal directions, both of which are at an angle of 55° with respect to the symmetry (z) axis of the trap. The 282 nm radiation that drives the narrow $^2S_{\frac{1}{2}}$ - $^2D_{5/2}$ transition is obtained by frequency-doubling the radiation from a narrowband cw ring dye laser. In the long term, the laser is stabilized by FM optical heterodyne spectroscopy to a saturated absorption hyperfine component in $^{129}I_2$ [17]. The frequency of the laser is scanned by an acousto-optic modulator that is driven by a computer controlled synthesizer. Up to a few microwatts of 282 nm radiation could be focussed onto the ion in a direction counterpropagating with one of the 194 nm light beams.

Optical-optical double resonance (electron shelving) [1-3,8,15,18-20] with a net quantum amplification (including detection efficiency) in excess of 100 at 10 ms was used to detect transitions driven by the 282 nm laser to the metastable $^2D_{5/2}$ state. The fluorescence rate from the laser-cooled ion is high when the ion is cycling between the $^2S_{\frac{1}{2}}$ and $^2P_{\frac{1}{2}}$ states and nearly zero when it is in the metastable $^2D_{5/2}$ state [1-3,8]. Thus the $^2S_{\frac{1}{2}}$ - $^2D_{5/2}$ resonance spectrum was obtained by probing the S-D transition at a particular frequency for the 282 nm radiation for 20 ms, then turning off the 282 nm radiation and turning on the 194 nm radiation to look for the presence or absence of scattered photons at 194 nm (the two radiation fields are alternately applied to avoid light shifts and broadening of the narrow

S-D transition). If there was no fluorescence at 194 nm, a transition into the metastable D state had occurred; the presence of 194 nm fluorescence indicated that the ion was in the ground state and no transition was recorded for this frequency of the 282 nm laser. The frequency was then stepped and the measurement cycle repeated. As the frequency was stepped back and forth each new result at a particular frequency of the 282 nm radiation was averaged with the previous measurements at that frequency. Normalization (or quantization) of the signal was obtained by assigning a 1 to each measurement of high fluorescence and a 0 to each measurement of no fluorescence. The high fluorescence level made it possible to determine the state of the atom with almost no ambiguity in a few milliseconds. Thus, it is easy to reach the shot noise limit imposed by the single atomic absorber [8].

The quantized fluorescence signal obtained from an 8-MHz scan of the 282 nm laser through the $^2S_{\frac{1}{2}}(m_J=-\frac{1}{2}) \rightarrow {}^2D_{5/2}(m_J=\frac{1}{2})$ Zeeman component of the electric quadrupole transition is shown in Fig. 1 [8]. The recoilless-absorption resonance (carrier) [21,22] and the motional sidebands due to the secular motion in the harmonic well of the rf trap [10] are completely resolved. The number and amplitudes of the sidebands are a direct measure of the ion's motion and its effective temperature. A careful comparison of the intensities of the sidebands to that of the carrier [9] for several sets of data similar to that shown in Fig. 1, including the effects of saturation, gave temperatures that ranged from 1.6 to 6.7 mK. This is consistent with the theoretical laser-cooling limit for $^{198}Hg^+$ on the first resonance line at 194 nm given by $T_{min} = \hbar\gamma/2k_B \approx 1.7$ mK [10].

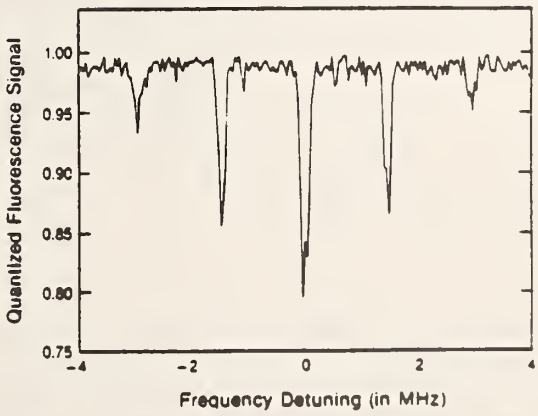

Fig. 1. Quantized signal showing the electric-quadrupole-allowed $5d^{10}6s\ ^2S_{\frac{1}{2}}(m_J=-\frac{1}{2})$-$5d^96s^2\ ^2D_{5/2}(m_J=\frac{1}{2})$ transition in a single, laser-cooled $^{198}Hg^+$ ion. On the horizontal axis is plotted the relative detuning from line center in frequency units at 282 nm. On the vertical axis is plotted the probability that the fluorescence from the $6s\ ^2S_{\frac{1}{2}}$-$6p\ ^2P_{\frac{1}{2}}$ first resonance transition, excited by laser radiation at 194 nm, is on. The electric-quadrupole-allowed S-D transition and the first-resonance S-P transition are probed sequentially in order to avoid light shifts and broadening of the narrow S-D transition. Clearly resolved are the recoilless absorption resonance (carrier) and the Doppler sidebands due to the residual secular motion of the laser-cooled ion. The integration time per point is about 16 s (230 measurement cycles).

In Fig. 2 we show a high resolution scan through the Doppler-free (recoilless) resonance at line center The full width at half maximum (FWHM) is approximately 1.7 kHz at 563 nm (3.4 kHz at 282 nm). This corresponds to a fractional resolution of about 3.4×10^{-12} ($Q\approx3\times10^{11}$). For this trace the laser was spectrally narrowed by locking to a mechanically, acoustically and thermally quiet reference cavity that had a finesse of about 60,000. The frequency of the laser fluctuates less than 1 Hz relative to this reference cavity. This is determined from the measurement of the residual noise in the error signal; the actual frequency fluctuations of the laser are then governed by the stability of the well isolated cavity [23]. The natural linewidth for the $^2S_{\frac{1}{2}}$ - $^2D_{5/2}$ transition is approximately 1.7 Hz [15]. The measured linewidth in Fig. 2 is dominated by fluctuations in the first-order magnetically-sensitive electric quadrupole transition in the $^{198}Hg^+$ ion. The field sensitivity of the $^2S_{\frac{1}{2}}(m_J=-\frac{1}{2})$ to $^2D_{5/2}(m_J=\frac{1}{2})$ transition is on the order of 22.4 MHz/mT (2.24 MHz/G). In our laboratory there are field fluctuations of a few milligausses with a frequency-noise spectrum that is dominated by 60 Hz and its harmonics. Shielding would help but is difficult in the present experiment. The better approach is to switch to the $^{199}Hg^+$ isotope. This isotope has first-order, field-independent transitions near zero magnetic field that should permit us to reach the 1.7 Hz natural linewidth. In this case, the ion will provide a good test of the spectral purity of the 282-nm laser.

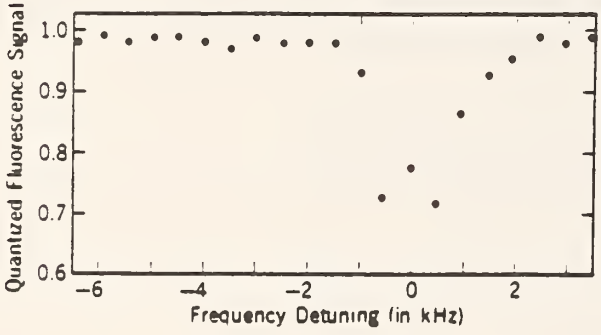

Fig. 2 High resolution scan through the recoilles absorption resonance of the $^2S_{\frac{1}{2}}(m_J=-\frac{1}{2})$-$^2D_{5/2}(m_J=1)$ transition in a single laser cooled $^{198}Hg^+$ ion. The full width at half maximum is about 1.7 kHz at λ=563 nm (3.4 kHz at λ=282 nm).

The possibility of cooling the Hg^+ ion further, to the zero point energy of motion, is intriguing for several reasons. First, cooling so that the average occupational number $\langle n_v \rangle$ for the motional energy of the bound atom is zero is a fundamental limit to laser-cooling for any bound particle [8]. This limit is imposed by the position-momentum Heisenberg uncertainty principle where the spatial confinement (Δx) is provided by the physical surroundings. Driving a single atom in a macroscopic trap to the zero point energy of motion also exploits the benign environment near the center of an rf trap - certainly a system worthy of consideration for the high resolution and accuracy in optical spectroscopy, metrology and frequency standards. Second, with an ion prepared in the lowest

vibrational state (most of the time), experiments such as squeezing the atom's position and momentum can be demonstrated.

Cooling to the zero point energy of motion is possible for a bound atom in the resolved sideband limit where the linewidth of the cooling transition ($^2S_{\frac{1}{2}}$ - $^2D_{5/2}$ in our case) is less than motional oscillation frequency of the atom [10,12,13]. When the ion is in the lowest or ground vibrational state (n_v=0) it can no longer resonantly absorb a photon at ω_0-ω_v; at this point the resonant feature at ω_0-ω_v disappears. Experimentally, a measurement of the amplitude of the resonant feature at ω_0-ω_v (for saturating intensity) is a direct measurement of $\langle n_v \rangle$ [13]. The result from ref. 12 is shown in Fig. 3.

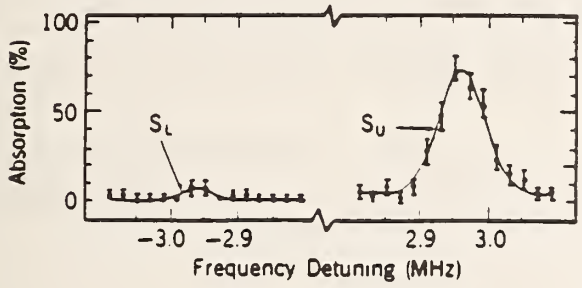

Fig. 3 First lower (S_L) and upper (S_u) motional sidebands of the $^2S_{\frac{1}{2}}$-$^2D_{5/2}$ electric quadrupole transition of a laser-sideband-cooled $^{198}Hg^+$ ion measured 10 ms after cooling. Data points are averages of 41 sweeps.

From these data we deduce that the y and z degrees of freedom are in the zero point energy state (n_v=0) 95% of the time. Because the 282 nm probe beam is nearly orthogonal to the x-axis, we were not sensitive to the x-motion. The uncertainty in the second-order Doppler shift in this example is dominated by the uncertainty in $\langle n_v \rangle$ and amounts to $\Delta\nu/\nu \approx 10^{-20}$ [13]. It could be made even lower by adiabatically lowering the potential well depth (thereby lowering ω_v) after the ion is cooled into the ground state.

With this system, the absorption of a single quantum of energy at a frequency in the megahertz range would raise n_v by one unit and this could be detected with an efficiency of nearly 100%. Also, it should be possible to produce squeezed states [24] of the atom's motion from the zero point energy state by a sudden, non-adiabatic weakening (and, in general, shifting) of the trap potential or by driving the atomic motion parametrically at 2 ω_v. If after some time the atom could then be returned to the n_v=0 state by reversing the above procedures, the zero point energy state could be unambiguously detected by the absence of the lower sideband. This would convincingly demonstrate the squeezed state of the single atom in the rf trap.

We acknowledge the support of the U.S. Air Force Office of Scientific Research, the U.S. Office of Naval Research and the continued support of the NIST. F. Diedrich thanks the Deutsche Forschungsgemeinschaft for financial support.

†Permanent address: Max Planck Institut für Quantenoptik, Garching, West Germany.

References

1. W. Nagourney, J. Sandberg, and H. Dehmelt, Phys. Rev. Lett. 56, 2797 (1986)
2. J.C. Bergquist, R.G. Hulet, W.M. Itano, and D.J. Wineland, Phys. Rev. Lett. 57, 1699 (1986)
3. T. Sauter, W. Neuhauser, R. Blatt, and P.E. Toschek, Phys. Rev. Lett. 57, 1696 (1986)
4. F. Diedrich and H. Walther, Phys. Rev. Lett. 58, 203 (1987); W.M. Itano, J.C. Bergquist, D.J. Wineland, Phys. Rev. A38, 559 (1988)
5. D.J. Wineland, W.M. Itano and J.C. Bergquist, Opt. Lett. 12, 389 (1987)
6. D.J. Wineland, W.M. Itano, J.C. Bergquist, and F.L. Walls, in Proc. of the 35th Ann. Symp. Freq. Control, 1981, p. 602 (copies available from Electronic Industries Association, 2001 Eye Street, N.W., Washington, DC 20006)
7. H. Dehmelt, IEEE Trans. Instrum. Meas. IM-31, 83 (1982); D.J. Wineland, Science 226, 395 (1984).
8. J.C. Bergquist, W.M. Itano, and D.J. Wineland, Phys. Rev. A36, 428 (1988)
9. See articles by D.J. Wineland et. al.; Dehmelt, et. al.; W. Nagourney, et. al.; R. Blatt, et al.; P. Gill et. al. in this volume
10. D.J. Wineland and W.M. Itano, Phys. Rev. A20, 1521 (1979)
11. G. Janik, W. Nagourney, and H. Dehmelt, J. Opt. Soc. Am. B2, 1251 (1985)
12. F. Diedrich, J.C. Bergquist, W.M. Itano, and D.J. Wineland, submitted for publication
13. D.J. Wineland, W.M. Itano, J.C. Bergquist, and R.G. Hulet, Phys. Rev. A36, 2220 (1987)
14. W. Neuhauser, M. Hohenstatt, P. Toschek, and H. Dehmelt, Phys. Rev. Lett. 41, 233 (1978)
15. J.C. Bergquist, D.J. Wineland, W.M. Itano, H. Hemmati, H.-U. Daniel, and G. Leuchs, Phys. Rev. Lett. 55, 1567 (1985)
16. H. Hemmati, J.C. Bergquist, and W.M. Itano, Opt. Lett. 8, 73 (1983)
17. J.L. Hall, L. Hollberg, T. Baer, and H.G. Robinson, Appl. Phys. Lett. 39, 680 (1981)
18. D.J. Wineland, J.C. Bergquist, W.M. Itano, and R.E. Drullinger, Opt. Lett. 5, 245 (1980); D.J. Wineland and W.M. Itano, Phys. Lett. 82A, 75 (1981)
19. H. Dehmelt, J. Phys. (Paris) Colloq. 42, C8-299 (1981)
20. H. Dehmelt, Bull. Am. Phys. Soc. 20, 60 (1975)
21. R.H. Dicke, Phys. Rev. 89, 472 (1953)
22. See, for example, Hans Frauenfelder, The Mössbauer Effect (Benjamin, New York, 1962)
23. J. Hough, D. Hils, M.D. Rayman, Ma L.-S., L. Hollberg, and J.L. Hall, Appl. Phys. B33, 179 (1984)
24. See for example, J. Janszky and Y.Y. Yushin, Opt. Commun. 59, 151 (1986); Fan Hong-Yi and H.R. Zaidi, Phys. Rev. A37, 2985 (1988)

From: Proc. 4th Symposium on Freq. Standards and Metrology, Ancona, Italy, Sept. 1988; A. Demarchi, ed. (Springer Verlag, Heidelberg).

High Accuracy Spectroscopy of Stored Ions*

D.J. Wineland, Wayne M. Itano, J.C. Bergquist, J.J. Bollinger,
F. Diedrich,† and S.L. Gilbert
Time and Frequency Div., National Institute of Standards and Technology
Boulder, Colorado 80303

ABSTRACT: Physical limitations to the achievement of accurate, high resolution spectroscopy on stored ions are briefly discussed. For experiments on ion clouds, a compromise between frequency stability and second order Doppler shift uncertainty must be made. Expected performance for specific examples using single ions and ion clouds is discussed.

1. Introduction

In this paper we discuss some of the basic physical limitations to the achievement of accurate, high resolution spectroscopy of electromagnetically confined ions. For brevity, we do not address many practical problems, such as local oscillator spectral purity. These problems, although important, will probably not cause the ultimate limit in accuracy and resolution.

This topic naturally divides between experiments on many ions and single trapped ions. We anticipate that for experiments using more than one stored ion, the uncertainty in the second order Doppler (time dilation) shift will be the accuracy-limiting systematic effect[1-3]. This has been the case in the past. For single ions, the uncertainty in the second order Doppler shift can be made extremely small. The limiting uncertainty for single ions may depend on the experiment[4-6], but inaccuracies should eventually be less than 1 part in 10^{18}. Use of single ions however might be precluded if the signal-to-noise ratio (S/N) is not high enough to achieve the desired measurement precision in a reasonable length of time. Therefore, we must consider a trade-off between second order Doppler shift and S/N, both of which increase as the ion number increases.

As in any spectroscopic experiment, we must account for the perturbations due to static and time varying multipole interactions for electric, magnetic, and gravitational fields. These include atom-trap field interactions, collisions, shifts due to uncontrolled electric and magnetic fields, gravitational red shifts, etc. (see refs 1-9 and other contributions in these proceedings).

2. Optical-Pumping, Double-Resonance Experiments on Stored Ions

We will assume ion spectra are observed by optical-pumping, double-resonance methods in which optical fluorescence changes are monitored. In Fig. 1, we

*Contribution of the U.S. Government, not subject to U.S. copyright.

assume that level 3 is at an optical energy above the ground state 1. The transition of interest for high resolution spectroscopy is between levels 1 and 2 (frequency ω_0) which we designate the "clock" transition. A_2 and A_3 are radiative decay rates and R is the excitation rate between levels 1 and 3. R' and R" denote pumping rates between the clock levels due to optical pumping sources (independent of the clock radiation) applied simultaneously with R.

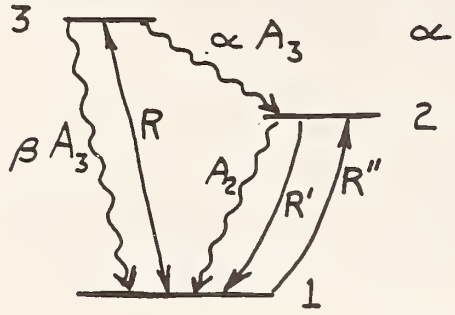

Fig. 1 Schematic diagram for optical pumping, double resonance experiments.

2.1. "Depletion" pumping. Assume A_2, R', R" « R < βA_3, and $\alpha \cong \beta$. When R is applied, atoms are pumped from level 1 to level 2 through level 3 (level 1 is depleted). If radiation (not shown in Fig. 1) is applied near the clock frequency $\omega_0 \equiv (E_2-E_1)/\hbar$, some of the atoms will be transferred back to level 1. This causes an increase in the detected fluorescence.[7,8]

2.2. "Electron Shelving."[4] We assume that the clock radiation and pumping radiation are applied sequentially to avoid light shifts on the clock transition. Assume $\alpha = 0$, R' » R", and A_3 » (A_2+R'-R"). In steady state with R, R' and R" applied, the ions spend most of the time in level 1. If ions are in level 2 after the clock radiation is applied and if $R \cong A_3$, we can observe the absence of about $N_d \cong \eta A_3(A_2+R'-R")^{-1}$ detected (3→1) photons for each photon absorbed on the clock transition (η is the net photon detection efficiency). When N_d » 1 and sources of technical noise are absent, the fluctuations in detected counts are caused not by the photon shot noise but by the fluctuations in the number of ions which have made the transition from level 1 to level 2 (Ref. 1). This is the fundamental noise limit. In Ref. 5, $\alpha \cong 10^{-7}$, R', R" = 0, $A_3 \cong 4.3\times10^8$ s^{-1}, $A_2 \cong 12$ s^{-1}, $\eta \cong 5\times10^{-4}$, $N_d \cong 20000$. In Ref. 9, $\alpha = 0$, $A_2 = 0$, $N_d \cong 1$, and R » R' » R" (R, R', and R" result from the same radiation source).

3. Frequency Stability

The signal is the response of the fluorescence detector to changes in frequency of the oscillator which drives the clock transition. As a specific example, we assume use of the Ramsey separated field method in time domain. That is, excitation of the clock transition is by two phase coherent pulses of radiation of duration ΔT_R separated by T_R.[9] For mathematical simplicity we assume ΔT_R « T_R « A_2^{-1} and R'-R" » A_2 (In Ref. 5, R', R" = 0). The electron shelving method of detection is assumed in the case where N_d » 1 in a time much less than (A_2 + R'-R")$^{-1}$ « T_R; that is, the detection time is less than the repumping time, which

is less than T_R. If we probe the clock transition on each side of the central Ramsey peak, we can develop an error signal which steers the average frequency to ω_0. Under the above assumptions, the measurement precision as characterized by the two-sample Allan variance[10] for the locked oscillator is[1,11]

$$\sigma_y(\tau) = (\tau N T_R \omega_0^2)^{-\frac{1}{2}} \qquad (1)$$

where τ is the measurement time and N is the ion number.

4. Second Order Doppler Shift in Ion Clouds

From Eq. 1, if ω_0 or T_R is too small, it may be necessary to use large N to obtain the desired measurement precision in a reasonable length of time. We anticipate that the largest systematic effect in an experiment on many stored ions will be the uncertainty in the second order Doppler shift, $\Delta\nu_{D2}$. Fractionally, this shift is equal to $\langle\Delta\nu_{D2}/\nu_0\rangle \cong -\langle v^2\rangle/2c^2$ where $\nu_0 = \omega_0/2\pi$, $\vec{v}$ is the ion velocity, c is the speed of light, and $\langle\ \rangle$ denotes an average over the N ions and over time. We would like to minimize the second order Doppler shift while simultaneously making the number of ions as large as possible to increase stability. These two requirements are contradictory and so a compromise between accuracy and stability must be made.

4.1. rf Trap

We assume that the pseudopotential approximation[12] is valid and the kinetic energy of the secular motion (the motion associated with the pseudopotential) is reduced to a value where the Debye length of the ion cloud is less than the cloud dimensions[13]. If the cloud is large enough, this can be accomplished by bringing the secular motion nearly into thermal equilibrium with a background gas (e.g., He) through ion-neutral collisions[7,14]. In principle it can also be accomplished by the method of laser cooling but so far this has been achieved with only a few ions in an rf trap because of rf heating.

Under the above conditions, the average kinetic energy per ion is dominated by the rf driven micromotion [3,14]. For a spheroidal cloud of radius r_{c1} and height $2z_{c1}$ we calculate $\langle\Delta\nu_{D2}/\nu_0\rangle = -2a(2z_{c1}^2 + r_{c1}^2)/5mc^2$ where $a \equiv q^2V_0^2/(m\Omega^2(r_0^2+2z_0^2)^2)$. Here, q and m are the ion mass and charge, V_0 and Ω are the applied rf potential and frequency and r_0 and z_0 are characteristic trap dimensions[12]. From this expression and the ion density[12,13], we have for a spherical cloud [3,14]

$$\langle\Delta\nu_{D2}/\nu_0\rangle = -3\omega_s^2 r_{c1}^2/10c^2 = -3q^2N/10r_{c1}mc^2 = -3(\omega_s Nq^2/m)^{2/3}/10c^2 \qquad (2)$$

where ω_s is the secular frequency for a single ion in the trap. From Eq. 2, we derive a relation between N and $\langle\Delta\nu_{D2}/\nu_0\rangle$,

$$N = -2.16 \times 10^{16} r_{cl} M \langle \Delta\nu_{D2}/\nu_0 \rangle / Z^2 \qquad (3)$$

where Z is the ion charge (in units of the proton charge), M is the ion mass in atomic mass units, and r_{cl} is the radius of the cloud in centimeters. Equation 3 shows that for an assumed value of $\langle \Delta\nu_{D2}/\nu_0 \rangle$, we would like to work with as large a cloud (low density) and ion mass as possible.

4.2. Penning Trap

We will assume that the internal (cyclotron and axial) temperature of the ions is reduced to a value where the second order Doppler shift is dominated by the velocity of ions due to cloud rotation at angular frequency ω[3,13,15]. This rotation is an essential part of ion storage in the Penning trap since it provides the inward Lorentz $(q(\vec{v}\times\vec{B})/c)$ force which overcomes the radially outward force due to the trapping fields and space charge. We have $\langle \Delta\nu_{D2}/\nu_0 \rangle = -(\omega r_{cl})^2/5c^2$ where the cloud is a uniformly charged spheroid of height $2z_{cl}$ and radius r_{cl}[13]. From Ref. 13, the density of ions is given by $n_0 = m\omega(\Omega_c - \omega)/2\pi q^2$ where $\Omega_c = qB_0/mc$ is the ion cyclotron frequency. From these two expressions, the total number of ions in the cloud is [3]

$$N = 3.10 \times 10^{13} B(T) \langle -\Delta\nu_{D2}/\nu_0 \rangle^{\frac{1}{2}} z_{cl}(r_{cl} - r_c')/Z \qquad (4)$$

where B is in teslas, z_{cl} and r_{cl} in centimeters and $r_c' \equiv (5 \langle -\Delta\nu_{D2}/\nu_0 \rangle)^{\frac{1}{2}} c/\Omega_c$. For a given value of $\langle \Delta\nu_{D2}/\nu_0 \rangle$, large B, z_{cl} and r_{cl} (low density) are desirable. N is independent of M (for the typical case $r_c' \ll r_{cl}$). We may choose B to make the clock transition field independent to first order[1,9].

5. Single Ions

From Eq. 1, if ω_0 and T_R are large enough, stability can be high enough for practical use, even with N = 1. For single ions, many systematic effects become negligible[1-6]. For example, from our recent experiments on single Hg^+ ions[5], we estimate uncertainties in the second order Doppler shift correction to be less than 1 part in 10^{20}. What will actually be the limiting systematic effect will depend on practical considerations and which ion is used. For the sake of definiteness we consider two cases of interest at Boulder and list what we think are the limiting systematic effects.

5.1 $^{199}Hg^+$, $5d^{10}6s\ ^2S_{\frac{1}{2}}(F=0, m_F=0) \leftrightarrow 5d^9 6s^2\ ^2D_{5/2}(F=2, m_F=0)$ optical quadrupole transition ($\nu_0 = 1.07 \times 10^{15}$ Hz).

(1) Magnetic field sensitivity. From the Breit-Rabi formula, we obtain $(\nu_0(B) - \nu_0(B=0))/\nu_0 = -1.8 \times 10^{-5} B^2$ where B is expressed in teslas. It should be possible to obtain fractional precision of better than 1 part in 10^{18}.

(2) $^2D_{5/2}$ state quadrupole interaction. The quadrupole moment of the $^2D_{5/2}$ state can couple to static electric field inhomogeneities to cause a shift of this level. In a suitable (Cartesian) coordinate system, the atomic quadrupole moment

interacts with a potential of the form $\varphi = A(x^2+y^2-2z^2) + \delta A(x^2-y^2)$. In the specific case where $\delta A = 0$ and $\vec{B}$ (quantization axis) is parallel to z, then $\Delta\nu_Q \cong -1.8$ Hz for 1 V applied to the ring electrode for the trap of Ref. 5. The presence of contact potentials on the trap electrodes makes the direction of z (in φ) uncertain but $\Delta\nu_Q$ averages to zero for three measurements of ν_0 where the directions of $\vec{B}$ are mutually orthogonal.[16]

5.2 $^{199}Hg^+$ ground state ($F=0, m_F=0$) $\leftrightarrow$ ($F=1, m_F=0$) hyperfine transition. (ν_0 = 40.5 GHz)

(1) Magnetic field sensitivity. $(\nu_0(B) - \nu_0(B=0))/\nu_0 \cong 0.24\ B^2$ where B is expressed in teslas. For single ions, magnetic field homogeneity requirements are not stringent.

Table I: Expected performance in particular systems. In rows 1 and 2, N is calculated from Eq. 4. Eq. 1 is used to determine $\sigma_y(1\ s)$. For $N > 1$, the ion cloud is assumed to be spherical (radius = r_{cl}). B is chosen to minimize field sensitivity. For $T_R > 1$ s, quoted stabilities are referred to 1 s.

SYSTEM	$\langle -\Delta\nu_{D2}/\nu_0 \rangle$	B(T)	r_{cl}(cm)	N	T_R(s)	$\sigma_y(1\ s)$
$^9Be^+$ hyperfine $\nu_0 \cong 303$ MHz (Penning trap)[9]	10^{-15}	0.819	0.5	2.0×10^5	100	1.2×10^{-13}
$^{201}Hg^+$ hyperfine $\nu_0 = 25.9$ GHz (Penning trap)[1]	10^{-16}	0.534	0.5	4.1×10^4	100	1.9×10^{-15}
$^{199}Hg^+$ hyperfine $\nu_0 = 40.5$ GHz (rf trap)	$<10^{-15}$	$\cong 0$	--	1	100	3.9×10^{-13}
$^{199}Hg^+$ optical quadrupole $\nu_0 = 1.07\times10^{15}$ Hz (rf trap)[5]	$<10^{-18}$	$\cong 0$	--	1	0.025	9.4×10^{-16}

6. Examples

Table I lists some possibilities of interest at Boulder. Implicit in the Table is the use of laser cooling. Sympathetic cooling [9,17] may be necessary for $N > 1$. Reasonable short term stability is obtained for single $^{199}Hg^+$ ions using the ground state hyperfine transition. Systematic effects should be more easily

controlled using single ions.[1-6] Fluctuations in cloud density and size (and therefore detected fluorescence) could degrade stability over that shown in the first two rows. For example, laser induced instabilities similar to those cited in Refs. 15 and 18 have been observed in all Penning traps at NBS; these instabilities must be suppressed to achieve $\sigma_y(\tau)$ given by Eq. 1.

7. Acknowledgements

We thank the U.S. Office of Naval Research and the U.S. Air Force Office of Scientific Research for support. We thank D. Heinzen and L. Hollberg for helpful comments on the manuscript.

† Present address: Max-Planck Inst. Quantenoptik, Garching.

1. D.J. Wineland, W.M.Itano, J.C. Bergquist, F.L. Walls, Proc. 35th Ann. Symp. Freq. Control (1981), p. 602 (copies available from Electronic Industries Association, 2001 Eye St., N.W., Washington, D.C. 20006)
2. D.J. Wineland, et. al., J. de Phys., Colloque C8, 42 (1981) p. C8-307
3. D.J. Wineland, in Prec. Meas. and Fundamental Constants II, B.N. Taylor and W.D. Phillips, eds., Nat. Bur. of Stand. (U.S.) Spec. Publ. 617 (1984), p. 83; D.J. Wineland, W.M. Itano, J.C. Bergquist, J.J. Bollinger and J.D. Prestage, Ann. Phys. (Fr.) 10, 737 (1985)
4. H.G. Dehmelt, IEEE Trans. Instrum. Meas. IM-31, 83 (1982); H.G. Dehmelt, in Advances in Laser Spectroscopy, ed. by F.T. Arecchi, F. Strumia, and H. Walther (Plenum, 1983) p. 153; H.G. Dehmelt, these proceedings
5. J.C. Bergquist, et. al., these proceedings; F. Diedrich et al., submitted for publication
6. D.J. Wineland, Science 226, 395 (1984) and references therein
7. L. Cutler, these proceedings
8. G. Werth, these proceedings
9. J.J. Bollinger, et. al., these proceedings
10. J.A. Barnes, et. al., IEEE Trans. Instrum. Meas. IM-20, (1971)
11. Ref. 1 is in error by a factor of $\sqrt{2}$
12. H.G. Dehmelt, Adv. At. Mol. Phys. 3, 53 (1967)
13. D.J. Wineland, J.J. Bollinger, W.M. Itano, and J.D. Prestage, J. Opt. Soc. Am. B2, 1721 (1985); L.R. Brewer, et al., Phys. Rev. A38, 859 (1988)
14. L.S. Cutler, R.P. Giffard, and M.D. McGuire, Appl. Phys. B36, 137 (1985)
15. W.M. Itano, et. al., these proceedings
16. W.M. Itano et. al., to be published
17. D.J. Larson, J.C. Bergquist, J.J. Bollinger, W.M. Itano, and D.J. Wineland, Phys. Rev. Lett. 57, 70 (1986)
18. R.C. Thompson, G.P. Barwood, and P. Gill, Opt. Acta 33, 535 (1986)

From: Proc. 4th Symposium on Freq. Standards and Metrology, Ancona, Italy, Sept. 1988; A. Demarchi, ed. (Springer Verlag, Heidelberg).

Frequency Standards Utilizing Penning Traps*

J.J. Bollinger, S.L. Gilbert, Wayne M. Itano, and D.J. Wineland
Time and Frequency Div., National Institute of Standards and Technology
Boulder, CO 80303

1. Introduction

Ion traps have a number of characteristics that make them attractive candidates for frequency standards [1]. Ion confinement times from a few hours to a few days permit long interrogation times and therefore narrow linewidths and large line Q's. In addition, ion traps typically do not suffer from the usual perturbations associated with confinement. For example, collisions of hydrogen atoms with the confining walls of a hydrogen maser can produce fractional frequency shifts greater than 1×10^{-11} on the masing transition [2]. Stark shifts due to the confining electrostatic field of a Penning trap can, in many cases, be made less than 1×10^{-15} [3,4].

The largest systematic shift and uncertainty in a frequency standard using many stored ions is typically the second order Doppler (time dilation) frequency shift $\Delta\nu_{D2}$. For a clock transition of frequency ν_0, $\Delta\nu_{D2}$ is given by

$$\langle \Delta\nu_{D2}/\nu_0 \rangle = - \langle \vec{v}^2 \rangle / (2c^2) \qquad (1)$$

where c is the speed of light, $\vec{v}$ is the ion velocity, and $\langle\ \rangle$ denotes an average over the ions in the trap. Without a means of achieving low ion temperatures, this shift can be unacceptably large. For example, a 300 K $^9Be^+$ ion has a second order Doppler shift of -4.6×10^{-12}. Laser cooling [5,6] can be used to reduce the ion temperature to much less than 1 K. For Be^+ ions, this results in second order Doppler shifts smaller than -1.5×10^{-14}. In our laboratory, up to 10^5 Be^+ ions stored in a Penning trap have been laser cooled to temperatures less than 1 K. The Penning trap is therefore a suitable candidate for a laboratory microwave frequency standard where the Dicke confinement criterion [7] is easily satisfied and where it is desirable to store many ions in a trap in order to obtain a signal-to-noise ratio that gives a useful fractional frequency stability. The number of ions used in a Penning trap frequency standard is determined from a tradeoff of signal-to-noise considerations and the second order Doppler frequency shift due to the $\vec{E}\times\vec{B}$ rotation of the ions[3,8]. We note that in an rf (Paul) trap the number of ions that can be laser cooled has been typically small (< 50)

*Contribution of the U.S. Government, not subject to U.S. copyright.

due to the problem of rf heating[9].

At the previous (Third) Symposium on Frequency Standards and Metrology, the results of an initial experiment done at the National Bureau of Standards (NBS) on $^{25}Mg^+$ ions stored in a Penning trap were reported[10]. In this experiment a 12 mHz linewidth on a 292 MHz magnetic field-independent hyperfine transition in the ground state of $^{25}Mg^+$ was obtained[11]. Below we summarize the Penning trap frequency metrology work done in our laboratory since the previous symposium. In the next section the results of a frequency standard based on up to 2000 laser cooled $^9Be^+$ ions stored in a Penning trap are discussed. The inaccuracy of this frequency standard was on the order of 1×10^{-13}[4]. It was limited by the second order Doppler shift of the ions due to the ion heating during the clock interrogation period when the cooling laser was turned off. The final section of this paper discusses our current work using sympathetic cooling[12] to maintain a cold Be^+ cloud and obtain a 0.9 mHz linewidth on the Be^+ clock transition. With sympathetic cooling we project an order of magnitude improvement in the Be^+ frequency standard. In addition to the work done at NBS discussed here, frequency metrology work with ions stored in Penning traps is being conducted by groups at Orsay, France[13] and Teddington, England[14].

2. Laser-Cooled $^9Be^+$ Frequency Standard

The Penning trap uses a uniform magnetic field to confine ions in a direction perpendicular to the magnetic field. The ions are prevented from leaving the trap along the magnetic field direction by a static electric field, typically provided by three hyperbolic electrodes[1]. Figure 1 shows the hyperfine structure of the ground state of $^9Be^+$ as a function of magnetic field. At a magnetic field of 0.8194 T the hyperfine transition ν_1 (see Fig. 1) depends only quadratically on the magnetic field deviation ΔB according to $\Delta\nu_1/\nu_1 = -0.017(\Delta B/B)^2$. In spite of its relatively low 303 MHz transition frequency, ν_1 provides the basis for a frequency standard. (We have chosen to work with Be^+, because it is easy to trap and laser cool. Heavier ions such as Hg^+ offer large microwave transition frequencies but are technically much harder to work with.) A narrow-band radiation source (power $\cong$ 20-60 μW) tuned to the low frequency side of the $2s\ ^2S_{\frac{1}{2}}(m_I = -3/2, m_J = -1/2) \rightarrow 2p\ ^2P_{3/2}(-3/2, -3/2)$ (λ = 313 nm) transition of $^9Be^+$ was used to cool and spatially compress the ions and optically pump them into the (-3/2, -1/2) ground state[11,15]. The resonance fluorescence induced by this cooling laser was used to detect the ions. The size, density, and temperature of the ion clouds were determined by use of a similar radiation source as a probe[15]. Typical clouds ranged from a few hundred to 2000 ions with cloud diameters from 300 to 500 μm and densities of about 3×10^7 ions/cm^3. Cyclotron and axial temperatures of less than 100 mK and a second order Doppler

shift due to the cloud rotation of less than 3×10^{-14} were obtained with the cooling laser applied continuously.

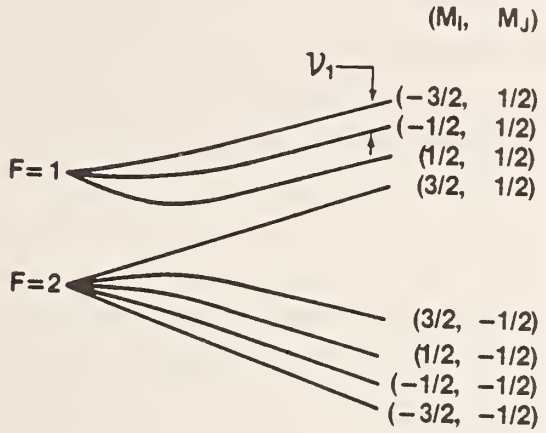

Figure 1. Hyperfine structure (not drawn to scale) of the $^9Be^+$ 2s $^2S_{\frac{1}{2}}$ ground state as a function of magnetic field. ν_1 is independent of magnetic field to first order at B = 0.8194 T.

The ν_1 transition was detected by optical-microwave-rf triple resonance. Microwave radiation tuned to the electron spin-flip resonance transferred half of the ion population from the optically pumped (-3/2, -1/2) state to the (-3/2, +1/2) state. Some of the (-3/2, +1/2) state population was transferred to the (-1/2, +1/2) state by application of rf near the 303 MHz ν_1 transition frequency. As a result of the microwave mixing this resulted in an additional decrease in the (-3/2, -1/2) state population and therefore a decrease in the observed fluorescence. The cooling laser and mixing microwaves were typically on for a period of 3 s, during which the $^9Be^+$ ions were prepared in the (-3/2, -1/2) and (-3/2, +1/2) states. The cooling laser and mixing microwaves were then turned off in order to avoid light and ac Zeeman shifts during the ν_1 interrogation period. Ramsey's method of separated oscillatory fields was used to interrogate ν_1. Typically an rf pulse of duration t = 0.5 s was applied, followed by a free precession interval of duration T = 19 s and a second rf pulse of duration t = 0.5 s coherent with the first pulse. After the interrogation period, the laser and microwaves were turned back on, and the signal was obtained from the absence of fluorescence during the first 0.3 s of this time interval. The (t,T) = (0.5 s, 19 s) interrogation resulted in a linewidth $\Delta\nu_1$ = 25 mHz and a $Q \equiv \nu_1/\Delta\nu_1$ of 1.2×10^{10} on the 303 MHz ν_1 transition frequency.

A synthesized rf source was locked to the ν_1 transition. A description of the servosystem is given in reference [4]. With about 1000 ions in the trap, a fractional frequency stability of $\sigma_y(\tau) \cong 2 \times 10^{-11} \tau^{-\frac{1}{2}}$ for measurement time τ in seconds was obtained with the (0.5 s, 19 s) Ramsey interrogation. The systematic uncertainty of 1×10^{-13} was dominated by the second order Doppler frequency shift [4]. During the 20 s interrogation period when the cooling laser was turned off,

the ion temperature increased from less than 1 K to 35 K. This heating produced a second order Doppler shift of 4×10^{-13} on the ν_1 transition and was measured with about 25% uncertainty. The rapid heating that occurred during the interrogation period was probably caused by asymmetry-induced transport [16]. With the cooling laser off, axial asymmetries of the trap can increase the total canonical angular momentum of the ions, resulting in an increase in the ion cloud radius. As the ion cloud expands, electrostatic potential energy of the ions due to the space-charge and trap electric fields is converted into thermal energy of the ions.

3. Sympathetic Cooling

An improvement in Be^+ frequency standard performance requires a reduction in the observed heating. This can possibly be done by improvement of the trap axial symmetry. With this in mind we have constructed a Penning trap with care taken to minimize axial asymmetries. Rather than the usual hyperbolic electrodes, the trap was constructed with hollow cylindrical electrodes [17]. In addition, in order to avoid asymmetric contact potentials due to plating of the trap electrodes from the Be^+ oven when ions were loaded into the trap, a second trap, mounted below the experimental trap, was used to load the ions. The ions were then transferred to the clean experimental trap. The expansion of the Be^+ ion cloud in the cylindrical Penning trap was less than in the previous Be^+ Penning trap. However, the expansion was eliminated by using a second ion species to sympathetically cool and compress [12] the Be^+ ions. Specifically, $^{26}Mg^+$ ions were loaded into the same trap with the $^9Be^+$ ions. The Mg^+ ions were continuously laser-cooled and spatially compressed by a 280 nm (power $\cong$ 50-80 μW) radiation source. Through the Coulomb interaction with the Mg^+ ions, the Be^+ ions were then cooled and compressed. Due to the ion cloud rotation, the Mg^+ ions were observed to centrifugally separate and form a doughnut surrounding the Be^+ ions.

The 313 nm source was used to optically pump and detect the Be^+ ground state. It had only a small effect on the Be^+ ion temperature and cloud size and, as in the previous experiment, was turned off during the Ramsey interrogation period. Because the 280 nm Mg^+ cooling laser beam is nonresonant with any Be^+ transitions, it was left on continuously during the Ramsey interrogation period without seriously perturbing the ν_1 transition frequency. In this way a cold, steady state cloud of Be^+ ions was obtained independently of the 313 nm radiation source, which permitted the use of very long interrogation times.

In the previous triple resonance experiment (optical-microwave-rf) only half of the stored Be^+ ions were used to measure the ν_1 transition due to the microwave mixing. The stable field of the superconducting magnet used in the present experiment permitted the following quadruple resonance procedure which

used all of the stored ions to measure the ν_1 transition. The Be^+ ions were optically pumped into the (3/2, 1/2) ground state by tuning the 313 nm source to the $2s\ ^2S_{\frac{1}{2}}(3/2,1/2) \rightarrow 2p\ ^2P_{3/2}(3/2,3/2)$ transition. The 313 nm source was turned off and the ions were transferred to the (1/2,1/2) and then the (-1/2,1/2) state by successive 0.2 s Rabi π pulses. After Ramsey's method of separated oscillatory fields was used to interrogate ν_1, the ions remaining in the (-1/2,1/2) state were transferred back to the (3/2,1/2) state by reversing the order of the previous two Rabi π pulses. The 313 nm source was turned back on, and the signal was obtained from the absence of the Be^+ fluorescence during the first few seconds after the 313 nm source was turned on. In addition to increasing the number of ions used to measure the ν_1 transition, this procedure increased the signal by a factor of 4. The long (-3/2, +1/2) $\rightarrow$ (3/2, 1/2) laser repumping time also allowed the signal counting time after the 313 nm source was turned back on to be increased. This increased the signal-to-noise ratio by increasing the change in the number of detected photons for each ion that made the clock transition.

With sympathetic cooling, long interrogation times were possible. Figure 2 shows the signal obtained with a (1 s, 550 s) Ramsey interrogation. The 0.9 mHz linewidth gives $Q = 3.3\times10^{11}$ on the ν_1 clock transition. If used to servo a local oscillator, this linewidth along with the estimated signal-to-noise ratio should result in a fractional frequency stability of $\sigma_y(\tau) = 3.8\times10^{-12}\tau^{-\frac{1}{2}}$ ($\tau > 1100$ s). This stability is consistent with the stability of our reference oscillator and is about a factor of 8 or 9 larger than the stability estimate based on the number of stored ions [8]. Shorter (1 s, 5 s) Ramsey interrogations resulted in a signal-to-noise ratio within a factor of 2 of the estimate based on the number of stored ions.

Preliminary estimates of all known systematic uncertainties for the transition frequency of Fig. 2 are less than 1×10^{-14}. With the use of an imaging tube, the cloud rotation frequency and radial distribution of the Be^+ ions were determined. The second order Doppler shift due to the cloud rotation was calculated to be -4×10^{-15}. From previous observations, we believe the sympathetic cooling provided Be^+ temperatures « 1 K and second order Doppler shifts less than 1×10^{-14}. The ac Stark shift due to the 280 nm source is estimated to be less than 1×10^{-15}. Due to the rotation of the earth, there is a systematic shift of $2.46(0.05)\times10^{-14}$ [4]. All other known systematic shifts are estimated to be less than 1×10^{-15}.

In the future we plan to evaluate the use of sympathetically cooled Be^+ ions to steer a local oscillator. With a passive hydrogen maser [2] as a source for the local oscillator, we may be able to obtain a fractional frequency stability of $\sigma_y(\tau) = 2\times10^{-12}\tau^{-\frac{1}{2}}$ ($\tau > 1000$ s), limited by the stability of the passive

hydrogen maser. An inaccuracy of less than 1×10^{-14}, limited by the second order Doppler shift, appears feasible.

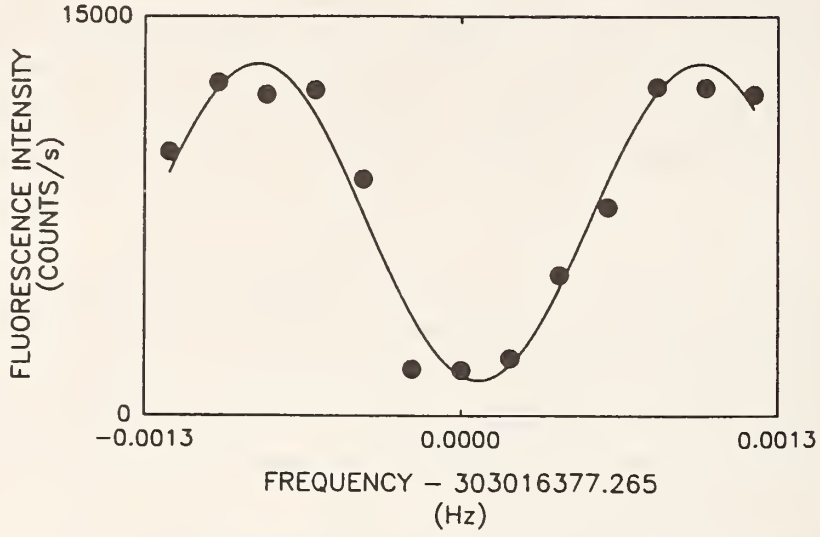

Figure 2. Signal obtained with 3200 Be^+ ions on the ν_1 field independent transition with a 550 s Ramsey free precession period. The data are the result of one sweep. The sweep width is 2.4 mHz and the frequency interval between points is 0.2 mHz. The dots are experimental and the curve is a least squares fit. A signal-to-noise ratio of 12 is estimated from the fit.

We gratefully acknowledge the support of the U.S. Air Force Office of Scientific Research and the U.S. Office of Naval Research. We thank C. Weimer and D. Heinzen for carefully reading the manuscript.

References

1. See for example D.J. Wineland, W.M. Itano, and R.S. Van Dyck, Jr.: Adv. At. Mol. Phys. 19, 135 (1983) and references therein
2. F.L. Walls: Proc. of the IEEE 74, 142 (1986)
3. D.J. Wineland, W.M. Itano, J.C. Bergquist, and F.L. Walls: in Proc. of 35th Ann. Freq. Control Symposium (USAERADCOM, Ft. Monmouth, NJ 07703) p. 602 (1981); D.J. Wineland in Precision Measurement and Fundamental Constants II, ed. by B.N. Taylor and W.D. Phillips (Natl. Bur. Stands. (U.S) Spec. Publ. 617, 1984), p. 83
4. J.J. Bollinger, J.D. Prestage, W.M Itano, and D.J. Wineland: Phys. Rev. Lett. 54, 1000 (1985)
5. S. Stenholm: Rev. Mod. Phys. 58, 699 (1986)
6. D.J. Wineland and W.M Itano: Physics Today 40, 34 (June 1987)
7. R.H. Dicke: Phys. Rev. 89, 472 (1953)
8. D.J. Wineland et al.: these proceedings

9. D.A. Church and H.G. Dehmelt: J. Appl. Phys. 40, 3421 (1969)
10. D.J. Wineland, J.C. Bergquist, R.E. Drullinger, H. Hemmati, W.M. Itano, and F.L. Walls: J. Phys. (Paris) Colloq. 42, C8-307 (1981)
11. W.M. Itano and D.J. Wineland: Phys. Rev. A24, 1364 (1981)
12. D.J. Larson, J.C. Bergquist, J.J. Bollinger, W.M. Itano, and D.J. Wineland: Phys. Rev. Lett. 57 70 (1986)
13. F. Plumelle, M. Desaintfuscien, M. Jardino, and P. Petit: Appl. Phys. B41, 183 (1986)
14. R.C. Thompson, G.P. Barwood, and P. Gill: Appl. Phys. B46, 87 (1988)
15. L.R. Brewer, J.D. Prestage, J.J. Bollinger, W.M. Itano, D.J. Larson, and D.J. Wineland: Phys. Rev. A38, 859 (1988)
16. C.F. Driscoll, K.S. Fine, and J.H. Malmberg: Phys. Fluids 29, 2015 (1986)
17. S.L. Gilbert, J.J. Bollinger, and D.J. Wineland: Phys. Rev. Lett. 60, 2022 (1988)

Observation of Quantum Jumps in a Single Atom

J. C. Bergquist, Randall G. Hulet, Wayne M. Itano, and D. J. Wineland
Time and Frequency Division, National Bureau of Standards, Boulder, Colorado 80303
(Received 23 June 1986)

We detect the radiatively driven electric quadrupole transition to the metastable $^2D_{5/2}$ state in a single, laser-cooled Hg II ion by monitoring the abrupt cessation of the fluorescence signal from the laser-excited $^2S_{1/2} \rightarrow {}^2P_{1/2}$ first resonance line. When the ion "jumps" back from the metastable D state to the ground S state, the $S \rightarrow P$ resonance fluorescence signal immediately returns. The statistical properties of the quantum jumps are investigated; for example, photon antibunching in the emission from the D state is observed with 100% efficiency.

PACS numbers: 32.80.Pj, 42.50.Dv

Recently, a few laboratories have trapped and radiatively cooled single atoms[1-4] enabling a number of unique experiments to be performed. One of the experiments now possible is to observe the "quantum jumps" to and from a metastable state in a single atom by monitoring of the resonance fluorescence of a strong transition in which at least one of the states is coupled to the metastable state. When the atomic electron moves to the metastable state, the fluorescence from the strongly driven transition disappears. When the electron drops back into the strongly driven transition, the fluorescence abruptly returns. Thus the strong transition fluorescence is a monitor of the quantum state of the atom. Several years ago, Dehmelt had proposed this optical double-resonance scheme (terming it electron shelving) as an amplification mechanism to detect a weak transition in single-atom spectroscopy.[5] This technique has been used for several years[6] in high-resolution spectroscopic studies of samples of many laser-cooled ions, achieving quantum amplifications of 10^6 and higher. In 1981, electron-shelving amplification was used to perform optical-optical double resonance in a single, laser-cooled, trapped ion.[2] While the signal-to-noise ratio in that experiment was not sufficient to see quantum jumps directly, the fact that the atomic fluorescence would be bistable was noted. More recently, the statistics of quantum switching in a single atom have been theoretically treated in some detail first by Cook and Kimble[7] and subsequently by several other authors.[8-13] In this Letter we report the clear experimental demonstration of quantum jumps in a single laser-cooled $^{198}Hg^+$ ion stored in a miniature radio-frequency trap.

The basic idea for quantum switching and the associated statistics is illustrated with the three-level system shown in Fig. 1 for the Hg II ion. In Hg II there is a "strong" resonance transition from the $5d^{10}6s\,^2S_{1/2}$ ground state to the $5d^{10}6p\,^2P_{1/2}$ state near 194 nm. The lifetime of the $^2P_{1/2}$ state has been measured elsewhere to be 2.3 ± 0.3 ns.[14] Additionally, there is a "weak" electric quadrupole transition from the $^2S_{1/2}$ ground state to the $5d^96s^2\,^2D_{5/2}$ state near 281.5 nm. The lifetime of the metastable D state has recently been measured to be about 0.1 s.[15,16] A laser tuned just below resonance on the highly allowed S-P transition will cool the ion and, in our case, scatter up to 5×10^7 photons/s. By collecting even a small fraction of the scattered photons, we can easily monitor the quantum state of the atom. If only the strong transition is radiatively driven, then for averaging times long compared to the $P_{1/2}$ state lifetime and mean $S \rightarrow P$ excitation time, a steady fluorescence level is expeced, corresponding to the atom rapidly cycling between the S and P state. If radiation to drive the weak transition is also admitted, then the atom will occasionally be driven into the metastable state and the fluorescence from the strong transition will abruptly disappear. The cessation of the scattering of many photons on the strong transition for one photon absorbed on the weak transition permits unit detection efficiency of the transition to the metastable state.[6,17] Some time later, the atom returns spontaneously or is driven out of the D state back to the ground state, which causes a sudden return of the fluorescence on the strong transition. The random on/off "telegraphic" signal provides a direct indication of the quantum state of the ion.

The experimental setup is largely the same as that

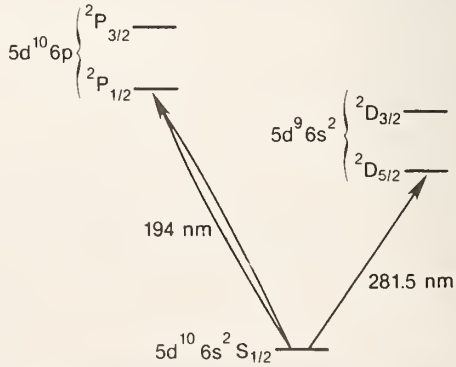

FIG. 1. Simplified optical energy-level diagram for Hg II.

Work of the U. S. Government
Not subject to U. S. copyright

used in the two-photon spectroscopic study of the $^2S_{1/2}$-$^2D_{5/2}$ transition in HgII reported earlier.[15] In the present experiment, one ion (on some occasions, two ions) was loaded[2] into the trap and cooled to below 25 mK by 2–5 μW of sum-frequency-generated radiation near 194 nm (spot size $w_0 \approx 10$ μm) tuned just below the $^2S_{1/2}$-$^2P_{1/2}$ first resonance transition. The fluorescence light scattered by the ions was detected at right angles to the 194-nm beam with an overall detection efficiency of about 5×10^{-4}. Peak signal counts exceeded 2×10^4/s against a background counting rate of 200/s. This high counting rate permitted us to monitor the fluorescence at a 10-ms sampling rate with a reasonable signal-to-noise ratio. The fast sampling rate is necessary because of the 100-ms lifetime of the $^2D_{5/2}$ state.

Radiation from a frequency-stabilized ring dye laser near[15] 563 nm was doubled to 281.5 nm in order to drive the $^2S_{1/2}$-$^2D_{5/2}$ electric-quadrupole–allowed transition directly.[18] The power of the 281.5-nm radiation could be adjusted to as much as 20 μW. The beam was focused at the center of the trap to a spot size w_0 of approximately 25 μm. A magnetic field of approximately 1 mT (10 G) was applied parallel to the electric field vector of the 281.5-nm radiation and perpendicular to its direction of propagation. The selection rule for the electric-quadrupole–allowed transitions to the various Zeeman states for this configuration is $\Delta m_J = 1$. The frequency of the 281.5-nm radiation was tuned to resonance with the $^2S_{1/2} \rightarrowtail {}^2D_{5/2}$ ($m_J = -\frac{1}{2} \rightarrowtail m_J = +\frac{1}{2}$) Zeeman component for the quantum switching results reported here. Also, the resonance signal obtained from the $P_{1/2}$ fluorescence counts during scanning of the 281.5-nm laser over this component revealed a linewidth of less than 8 MHz. If this width is due to Doppler broadening, the ion temperature (in the pseudopotential well) is less than 25 mK and the ion is estimated to be confined to a volume characterized by a linear dimension of less than 0.25 μm.

In order to observe the quantum jumps, we monitor the strong fluorescence at 194 nm while simultaneously admitting the 281.5-nm radiation. A computer strobes and displays the detected 194-nm fluorescence counts accumulated in a counter at 10-ms intervals for running times of 40 s. These data are then stored and the process repeated, but now without the 281.5-nm radiation, or, in some cases, with the 281.5-nm laser detuned from resonance. We repeat the entire sequence numerous times for different power levels of the 281.5-nm light and for different detunings of the 194-nm radiation. An example of 4 s of a sequential set of data with the 281.5-nm radiation (0.3 μW) first off and then on is shown in Figs. 2(a) and 2(b), respectively.

For the general case of coherent excitation, it is

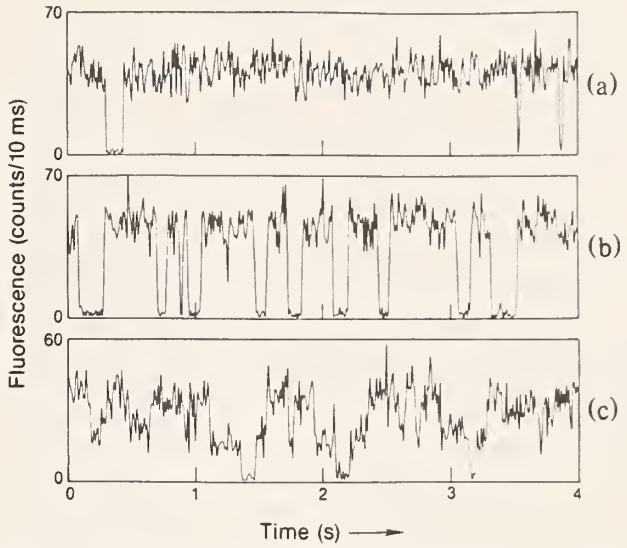

FIG. 2. Samples of the quantum-jump data. (a) The fluorescence counts detected with no resonance radiation exciting the weak $S_{1/2}$-$D_{5/2}$ transition. The few jumps observed are likely due to collisions with background Hg atoms and radiative decay to the $D_{3/2}$ state. (b) Both the 194- and 281.5-nm radiation are applied simultaneously. Compared to (a), the interruptions to the fluorescence signal are more frequent. (c) Two ions are trapped and cooled. The interruptions to the fluorescence signal show two levels corresponding to loss of fluorescence from one or both ions. The sampling rate for all the data is 10 ms per point; the length of each sample is 4 s.

necessary to examine the off-diagonal terms of the density matrix in order to include possible coherence effects.[8,13] However, for the conditions of our experiment, that is, for times longer than the inverse of the excitation and spontaneous emission rates on the strong transition, and when the excitation and emission rates on the strong transition exceed those on the weak transition, the dynamics of the quantum-jump process can be described by effective two-state rate equations for coherent or incoherent excitation.[8] As a consequence there exist simple probabilities per unit time R_+ and R_- that the electron makes an upward or downward jump on the weak transition. Using the theory of Ref. 8 adapted to arbitrary detuning, and with the additional condition relevant to our experiment that the radiation driving the strong transition is well below saturation, we find that the Einstein A coefficient for the spontaneous decay of the weak transition is related to these probabilities by

$$A(^2D_{5/2}) \approx R_- - R_+ . \quad (1)$$

From data similar to those of Fig. 2(b), we plotted the distribution of off times τ_{off} and the distribution of on times τ_{on}. Theory[7,8] predicts that the probability density for the time duration of the off (and on) intervals

is given by

$$W_{\text{off}}(\tau_{\text{off}}) = R_- \exp(-R_-\tau_{\text{off}}) \quad (2)$$

for time off, and by

$$W_{\text{on}}(\tau_{\text{on}}) = R_+ \exp(-R_+\tau_{\text{on}}) \quad (3)$$

for time on. Thus, R_+ and R_- are found from exponential least-squares fits to the data, and from these and Eq. (1) we determine the A coefficient for the metastable $^2D_{2/5}$ state. Unfortunately, the data analysis is complicated by the background events as indicated in Fig. 2(a). Although we have not unambiguously determined their origin, two contributions are collisions with background mercury atoms which temperorarily heat the ions[2] and radiative decay from the $^2P_{1/2}$ state to the $^2D_{3/2}$ state. The lifetime of the $^2D_{3/2}$ state has recently been measured to be about 20 ms.[16] According to theory[19] it decays with nearly equal probability to the lower-lying $^2D_{5/2}$ state and to the ground state. We estimate[17] the probability that a mercury ion in the $^2P_{1/2}$ state will decay to the $^2D_{3/2}$ state as 3×10^{-7}. In the present experiment there is no direct measure of the background pressure at the trap, but estimates based on ion-pump current are consistent with the observed frequency of background events. Estimated recooling rates are also consistent with the data.

If the background interruptions in the fluorescence signal were due solely to collisions, one would expect their rate of occurrence to be independent of the 194-nm scattering rate. The average duration of the off times after a collision would be a function of the 194-nm intensity and detuning, since these parameters would affect the recooling rate. If the background interruptions were due solely to radiative decay, one would expect their rate of occurrence to be proportional to the 194-nm scattering rate, but their average duration to be fixed, since this would depend only on the metastable decay rates. The present data indicate that both processes may be present in that both the rate and the average duration of off times vary with scattering rate. Even with these background events, we find the lifetime for spontaneous emission from the $^2D_{5/2}$ level given by Eq. (1) to be 90 ± 30 ms, which is in agreement with the earlier measurements.[15,16]

Also of interest is the two-time intensity-correlation function[7-13] for the 194-nm fluorescence:

$$C(\tau) = \langle I(t)I(t+\tau)\rangle. \quad (4)$$

This expression can be written as[7]

$$C(\tau) = \langle I\rangle^2 + (\langle I^2\rangle - \langle I\rangle^2)\exp[-(R_+ + R_-)\tau], \quad (5)$$

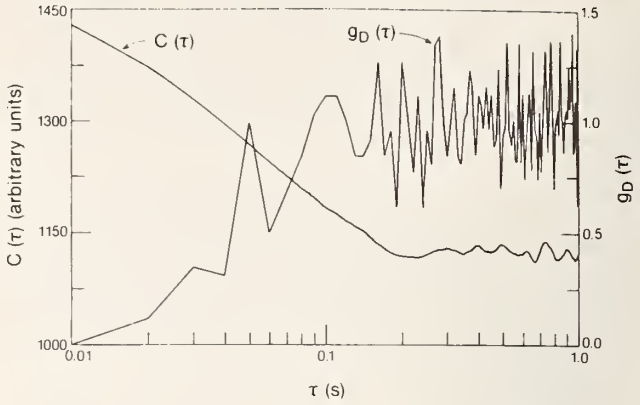

FIG. 3. Plots of the 194-nm fluorescence intensity correlation function $C(\tau)$ and the 281.5-nm emission correlation function $g_D(\tau)$. Photon antibunching in the 281.5-nm emission is inferred from the observation that $g_D(\tau)\rightarrow 0$ as $\tau\rightarrow 0$.

where

$$\langle I\rangle = I_0R_-/(R_+ + R_-), \quad (6)$$

$$\langle I^2\rangle - \langle I\rangle^2 = I_0^2R_+R_-/(R_+ + R_-)^2. \quad (7)$$

In Fig. 3 we plot the two-time intensity-correlation function for a typical run. The values of R_+ and R_- obtained from a least-squares fit agree with those derived from the distributions of off and on times.

Other statistical properties can be derived from the quantum switching data. For example, if one neglects the background interruptions to the fluorescence signal, each upward (downward) transition in the fluorescence can be assumed to mark the emission (absorption) of a $^2D_{5/2}$-$^2S_{1/2}$ photon. Let $g_D(\tau)$ denote the probability that the (assumed) emission of a 281.5-nm photon is followed by the (assumed) emission of another 281.5-nm photon at a time τ later, normalized to 1 at $\tau=\infty$. For our experimental conditions, theory predicts that $g_D(\tau) = 1-\exp[-(R_+ + R_-)\tau]$, and this is in agreement with the data. In Fig. 3 we plot $g_D(\tau)$ from some of our quantum switching data. The fact that $g_D(\tau)\rightarrow 0$ at $\tau=0$ implies the existence of photon antibunching[11,13] in the 281.5-nm radiation from the $^2D_{5/2}$ state. Because of the quantum amplification in the S-P scattering loop the photon antibunching is detected with nearly 100% efficiency.

Finally, in Fig. 2(c) we show quantum switching for the case of two laser-cooled and trapped ions (estimated separation $\approx 2.5\ \mu$m). There are three distinct levels of fluorescence corresponding to (a) a maximum when both ions are in the S-P scattering loop, (b) an intermediate level when one ion is shelved in the D state and only one ion is scattering, and (c) no fluorescence in the rare cases when both ions are shelved in the D state.

In summary, we have demonstrated quantum jumps or switching in a single atom. We have analyzed the statistics and found agreement with earlier published values for the lifetime of the $5d^9 6s^2\,{}^2D_{5/2}$ state in Hg II. It is interesting to speculate about a single atom in which the upper state on the weak transition is extremely long lived and excited by adiabatic rapid passage.[20] In this case the random nature of the excitation is eliminated and one could realize a single-atom switch or flip flop.

The authors are pleased to acknowledge the expert technical assistance of C. Manney during parts of this experiment, and the help of D. J. Larson in the earlier work to obtain single-ion cooling. We are appreciative to H. J. Kimble for helpful discussions of "quantum jumps" and to J. J. Bollinger, R. E. Drullinger, and L. Hollberg for comments on the manuscript. We gratefully acknowledge the support of the U.S. Air Force Office of Scientific Research and the U.S. Office of Naval Research. We note that a Letter by Nagourney, Sandberg, and Dehmelt[21] describing quantum jumps in a single Ba^+ atom has appeared subsequent to the submission of our Letter.

[1]W. Neuhauser, M. Hohenstatt, P. Toschek, and H. Dehmelt, Phys. Rev. A **22**, 1137 (1980).

[2]D. J. Wineland and W. M. Itano, Phys. Lett. **82A**, 75 (1981).

[3]W. Nagourney, G. Janik, and H. Dehmelt, Proc. Natl. Acad. Sci. U.S.A. **80**, 643 (1983).

[4]G. Janik, W. Nagourney, and H. Dehmelt, J. Opt. Soc. Am. B **2**, 1251 (1985).

[5]H. G. Dehmelt, Bull. Am. Phys. Soc. **20**, 60 (1975), and J. Phys. (Paris), Colloq. **42**, C8-299 (1981).

[6]D. J. Wineland, J. C. Bergquist, W. M. Itano, and R. E. Drullinger, Opt. Lett. 5, 245 (1980); D. J. Wineland, W. M. Itano, J. C. Bergquist, J. J. Bollinger, and J. D. Prestage, in *Atomic Physics,* edited by R. S. Van Dyck, Jr., and E. N. Fortson (World Scientific, Singapore, 1985), Vol. 9.

[7]R. J. Cook and H. J. Kimble, Phys. Rev. Lett. **54**, 1023 (1985).

[8]H. J. Kimble, R. J. Cook, and A. L. Wells, Phys. Rev. A **34**, 3190 (1986).

[9]T. Erber and S. Putterman, Nature **318**, 41 (1985).

[10]J. Javanainen, Phys. Rev. A **33**, 2121 (1986).

[11]A. Schenzle, R. G. DeVoe, and R. G. Brewer, Phys. Rev. A **33**, 2127 (1986).

[12]C. Cohen-Tannoudji and J. Dalibard, Europhys. Lett. 1, 441 (1986).

[13]D. T. Pegg, R. Loudon, and P. L. Knight, Phys. Rev. A **33**, 4085 (1986).

[14]P. Eriksen and O. Poulsen, J. Quant. Spectrosc. Radiat. Transfer **23**, 599 (1980).

[15]J. C. Bergquist, D. J. Wineland, W. M. Itano, H. Hemmati, H.-U. Daniel, and G. Leuchs, Phys. Rev. Lett. **55**, 1567 (1985).

[16]C. E. Johnson, Bull. Am. Phys. Soc. **31**, 957 (1986).

[17]D. J. Wineland, W. M. Itano, J. C. Bergquist, and F. L. Walls, in *Proceedings of the 35th Annual Symposium on Frequency Control, Philadelphia, 1981* (Electronic Industries Association, Washington, DC, 1981), p. 602.

[18]D. J. Wineland, J. C. Bergquist, R. E. Drullinger, H. Hemmati, W. M. Itano, and F. L. Walls, J. Phys. (Paris), Colloq. **42**, C8-307 (1981).

[19]R. H. Garstang, J. Res. Natl. Bur. Stand. Sect. A 68, 61 (1964).

[20]See, for example, A. Abragam, *Principles of Nuclear Magnetism* (Clarendon, Oxford, 1961), p. 65.

[21]W. Nagourney, J. Sandberg, and H. Dehmelt, Phys. Rev. Lett. **56**, 2727 (1986).

Quantum jumps via spontaneous Raman scattering

Randall G. Hulet and D. J. Wineland
Time and Frequency Division, National Bureau of Standards, Boulder, Colorado 80303
(Received 27 April 1987)

A single laser, which is used to induce and detect spontaneous Raman transitions, can be used to observe quantum jumps in a single atom. The population dynamics of a particular system, consisting of two $^2S_{1/2}$ ground-state levels and four $^2P_{3/2}$ excited-state levels split by a magnetic field, is analyzed for a laser tuned near a particular transition. We find that the statistics of the fluorescence emitted by this system are described by the same formalism developed for the three-level V configuration irradiated by two light sources. Over a wide range of observation times, the fluorescence intensity will be two valued, either off or on, as has been verified for the V configuration. Some surprising and elegant features of this new system are described.

The fluorescence emitted from a single atom can exhibit phenomena which are unobservable in a collection of many atomic emitters. For example, the fluorescence emitted by a driven two-level system reveals a quantum phenomenon known as "photon antibunching."[1,2] Antibunching is demonstrated by measuring the time correlation between fluorescence photons emitted by a single atom. It is found that the probability of detecting a photon instantaneously after detecting the previous one is zero, that is, they are antibunched. This is a purely quantum effect with no classical analog.

A three-level manifestation of quantum photon emission was first analyzed by Cook and Kimble[3] and is based on Dehmelt's "electron shelving" scheme.[4] Figure 1 shows a three-level system in the V configuration. The ground state (0) is strongly coupled to an excited state (1) which has a spontaneous decay rate A_1, and is weakly coupled to another excited state (2) which decays at a rate A_2 ($A_1 \gg A_2$). Two radiation sources separately drive the $0\leftrightarrow1$ and $0\leftrightarrow2$ transitions while only the fluorescence from level 1 is monitored. On a time scale which is long compared to A_1^{-1}, but less than or on the order of A_2^{-1}, the fluorescence is expected to display periods of constant intensity interrupted by periods of zero intensity while the atomic electron is "shelved" in level 2. The on-off switching of the fluorescence indicates a discontinuous jump, or "quantum jump," between level 2 and the strongly fluorescing system consisting of level 0 and level 1.[3,5–12] Recently, three groups reported the observation of this phenomenon in a single confined ion[13–15] and a fourth group is able to infer the effect from the time correlation of fluorescence from a weak atomic beam.[16]

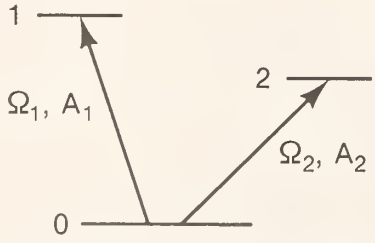

FIG. 1. The V configuration of energy levels. Two excited states are coupled to the ground state with two different lasers. The spontaneous decay rate of level i is denoted by A_i. Ω_i denotes the Rabi frequency of the $0\leftrightarrow i$ transition. It is assumed that $A_1 \gg A_2$. Quantum jumps in the intensity of the fluorescence emitted from level 1 have been observed under these conditions (Refs. 13–16).

Kimble *et al.* have shown that the excitation of the weak transition ($0\leftrightarrow2$) is a rate process for the V level configuration.[11] The population dynamics of the three levels can be reduced to those of an effective two-level system for times which are long compared to A_1^{-1}. R_+ is defined as the rate of excitation out of the strongly fluorescing level-0–level-1 system and into level 2, while R_- is the rate back out of level 2. The rate equation analysis yields the mean fluorescence on-time $\langle T_{on} \rangle$, off-time $\langle T_{off} \rangle$, and the statistical distribution of the fluorescence as a function of the two Rabi frequencies, spontaneous decay rates, and laser detunings.

In this paper we analyze the population dynamics of a single atom in a magnetic field, when a *single* laser is tuned near one of the principal transition resonances. We assume that the ground state has a $^2S_{1/2}$ configuration and the excited state is $^2P_{3/2}$. Additionally, the effects of hyperfine structure are assumed to be negligible. This configuration is realized by some singly ionized alkaline-earth atoms, $^{24}Mg^+$ or $^{26}Mg^+$, for example. We find that for the time scale of interest, the evolution of the six $^2S_{1/2}$ and $^2P_{3/2}$ levels is also described by a two-level rate equation and therefore, obeys the same statistical functions derived for the three-level V configuration. Thus this system should also exhibit quantum switching. We find that the rates R_+ and R_- for this level configuration, in contrast to the V configuration, are quite simple and, as we will show, possess a surprising and elegant feature.[17]

Figure 2 schematically shows the Zeeman levels of the $^2S_{1/2}$ and $^2P_{3/2}$ states. It is assumed that the field is sufficiently weak that the levels are well described by the LS-coupling scheme. For convenience, the levels are la-

Work of the U. S. Government
Not subject to U. S. copyright

beled from 1 to 6, starting with the lowest ground level. The energy difference between levels i and j is denoted by $\hbar\omega_{ij} \equiv \hbar(\omega_i - \omega_j)$. A laser of frequency ω is assumed tuned near ω_{31}, the $^2S_{1/2}$, $m_J = -\frac{1}{2} \leftrightarrow {}^2P_{3/2}$, $m_J = -\frac{3}{2}$ ($1 \leftrightarrow 3$) resonance frequency. If Δ denotes the detuning from resonance then $\omega = \omega_{31} + \Delta$. $\hbar\Delta$ is assumed small compared to the energy separation between Zeeman levels, which is in turn assumed to be small compared to the $^2P_{3/2}$ and $^2S_{1/2}$ energy difference. The laser light is assumed to be linearly polarized with polarization perpendicular to the magnetic field axis. The only dipole decay allowed for level 3 is back to level 1. Therefore, the fluorescence from level 3 continues until an off-resonance transition from level 1 to level 5 is induced. There is a small probability of a nonresonant excitation to this level due to the finite linewidth of the transition. If level 5 becomes populated, the atom may decay to either ground state: back to level 1 (with $\frac{1}{3}$ probability), where the $1 \leftrightarrow 3$ cycling continues, or to level 2 (with $\frac{2}{3}$ probability), where the electron remains until another transition, again far from resonance, may remove it. The dipole selection rules allow transitions from level 2 to either level 4 or to level 6. Once in level 4, the atom may decay back to level 1 (with $\frac{2}{3}$ probability) to resume the strong fluorescence cycling. From level 6, the atom may decay only to level 2. The other Zeeman ground level, level 2, is the "shelf" level which removes the electron from the strongly fluorescing system. Thus, as in the three-level V configuration, which uses two light sources, the fluorescence from this six-level, one-laser system is expected to alternate between periods of darkness and light. As opposed to other realizations of quantum jumps, the shelf level in this case "decays" via spontaneous Raman transitions since spontaneous radiative decay from level 2 to level 1 is negligible.

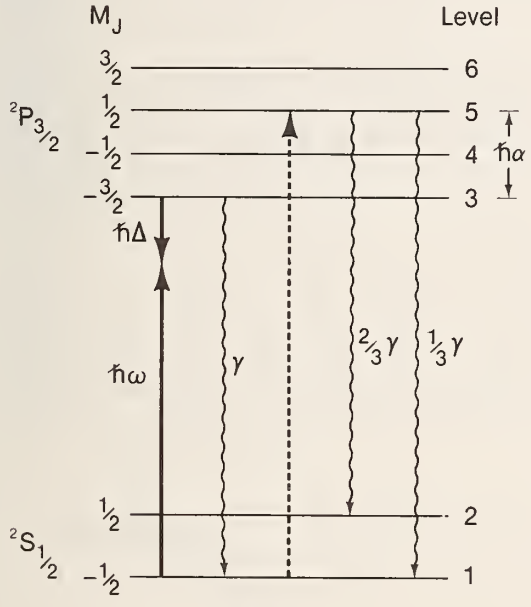

FIG. 2. The energy-level structure of the $^2S_{1/2}$ and the $^2P_{3/2}$ states of an atom in a magnetic field. A laser of frequency ω is assumed to be tuned near the level 1 to level 3 transition frequency which gives rise to a (on resonance) Rabi frequency of Ω. The laser polarization is assumed to allow only $\Delta m_J = \mp 1$ transitions. The detuning from resonance is denoted by Δ. The total spontaneous decay rate of each excited level is γ and the energy separation between excited levels is given by $\hbar\alpha/2$. The dashed arrow indicates off-resonance excitation of the $1 \rightarrow 5$ transition by the laser. The wavy arrows denote the dipole-allowed spontaneous decays from levels 3 and 5. Off-resonance excitation of the $2 \rightarrow 4$ and $2 \rightarrow 6$ transitions and spontaneous decay from levels 4 and 6 are not shown in the figure. It is assumed that $\alpha \gg \Delta, \gamma, \Omega$.

We use the density-matrix formulation to determine the steady-state level populations and to show that the two-state rate approximation is valid during the observation time of interest. In the rotating-wave approximation, the density-matrix equations are

$$
\begin{aligned}
\dot{\rho}_{11} &= \Omega(\mathrm{Im}\sigma_{13} + \mathrm{Im}\sigma_{15}/\sqrt{3}) + \gamma(\rho_{33} + 2\rho_{44}/3 + \rho_{55}/3) , \\
\dot{\rho}_{22} &= \Omega(\mathrm{Im}\sigma_{24}/\sqrt{3} + \mathrm{Im}\sigma_{26}) + \gamma(\rho_{44}/3 + 2\rho_{55}/3 + \rho_{66}) , \\
\dot{\rho}_{33} &= -\Omega\mathrm{Im}\sigma_{13} - \gamma\rho_{33} , \\
\dot{\rho}_{44} &= -\Omega\mathrm{Im}\sigma_{24}/\sqrt{3} - \gamma\rho_{44} , \\
\dot{\rho}_{55} &= -\Omega\mathrm{Im}\sigma_{15}/\sqrt{3} - \gamma\rho_{55} , \\
\dot{\rho}_{66} &= -\Omega\mathrm{Im}\sigma_{26} - \gamma\rho_{66} , \\
\dot{\sigma}_{13} &= [-i(\omega - \omega_{31}) - \tfrac{1}{2}\gamma]\sigma_{13} + \tfrac{1}{2}i\Omega(\rho_{33} - \rho_{11} + \rho_{35}^*/\sqrt{3}) , \\
\dot{\sigma}_{15} &= [-i(\omega - \omega_{51}) - \tfrac{1}{2}\gamma]\sigma_{15} + \tfrac{1}{2}i\Omega[(\rho_{55} - \rho_{11})/\sqrt{3} + \rho_{35}] , \\
\dot{\sigma}_{24} &= [-i(\omega - \omega_{42}) - \tfrac{1}{2}\gamma]\sigma_{24} + \tfrac{1}{2}i\Omega[(\rho_{44} - \rho_{22})/\sqrt{3} + \rho_{46}^*] , \\
\dot{\sigma}_{26} &= [-i(\omega - \omega_{62}) - \tfrac{1}{2}\gamma]\sigma_{26} + \tfrac{1}{2}i\Omega(\rho_{66} - \rho_{22} + \rho_{46}/\sqrt{3}) , \\
\dot{\rho}_{35} &= (i\omega_{53} - \gamma)\rho_{35} + \tfrac{1}{2}i\Omega(\sigma_{15} - \sigma_{13}^*/\sqrt{3}) , \\
\dot{\rho}_{46} &= (i\omega_{64} - \gamma)\rho_{46} + \tfrac{1}{2}i\Omega(\sigma_{26}/\sqrt{3} - \sigma_{24}^*) ,
\end{aligned}
\tag{1}
$$

where $\Omega \equiv \Omega_{13} = E_0 d_{13}/\hbar$ is the Rabi frequency of the $1 \leftrightarrow 3$ transition, γ is the total spontaneous decay rate of each excited level, $\mathrm{Im}\sigma_{ij}$ denotes the imaginary part of a coherence and the asterisk denotes complex conjugation. The other Rabi frequencies are determined by the relative size of the dipole-matrix elements for light linearly polarized perpendicular to the quantization axis: $d_{15} = d_{13}/\sqrt{3}$, $d_{24} = d_{26}/\sqrt{3}$, and $d_{26} = d_{13}$.

There are only six nonzero coherences for our choice of laser polarization. The four σ_{ij} are due to direct laser coupling of a ground and an excited level, while the two ρ_{ij} represent the stimulated Raman coherences between pairs of excited levels coupled by the laser via a ground level.

It is most compact to express the detunings, $\omega - \omega_{ij}$ in terms of Δ ($\Delta = \omega - \omega_{31}$) and the magnetic field splitting of the levels. In the LS-coupling scheme, the Lande' g factors are $g(^2S_{1/2}) = 2$ and $g(^2P_{3/2}) = \frac{4}{3}$ (we take the electron g factor equal to 2 for this calculation). The detunings become

$$\omega-\omega_{51}=\Delta-\alpha\ ,$$

$$\omega-\omega_{42}=\Delta+\alpha/4\ ,$$

$$\omega-\omega_{62}=\Delta-3\alpha/4\ .$$

In the above expressions $\omega_{53}=\omega_{64}=\alpha$, where $\hbar\alpha\equiv 8\mu_B B/3$ is twice the Zeeman energy splitting between adjacent $^2P_{3/2}$ levels due to the magnetic field B and μ_B is the Bohr magneton. We will assume hereafter that $\alpha\gg\Delta,\Omega,\gamma$.

Solving the set of algebraic equation $\dot{\rho}_{ii}=\dot{\sigma}_{ij}=\dot{\rho}_{ij}=0$, and using the conservation equation $\sum_i \rho_{ii}=1$ yields the steady-state values of the populations $\bar{\rho}_{ii}$. Thus to the first nonzero order of γ/α or Ω/α,

$$\begin{aligned}
\bar{\rho}_{11}&\approx\frac{16}{17}\frac{\gamma^2+4\Delta^2+\Omega^2}{\gamma^2+4\Delta^2+2\Omega^2}\ ,\\
\bar{\rho}_{22}&\approx\tfrac{1}{17}\ ,\\
\bar{\rho}_{33}&\approx\frac{16}{17}\frac{\Omega^2}{\gamma^2+4\Delta^2+2\Omega^2}\ ,\\
\bar{\rho}_{44}&\approx\frac{4\Omega^2}{51\alpha^2}\ ,\\
\bar{\rho}_{55}&\approx\frac{4\Omega^2}{51\alpha^2}\ ,\\
\bar{\rho}_{66}&\approx\frac{4\Omega^2}{153\alpha^2}\ .
\end{aligned}\tag{2}$$

Terms of order (Δ/α) have been neglected.

We follow Cook *et al.*[3] by defining new population variables

$$\rho_-\equiv\rho_{11}+\rho_{33}+\rho_{55}\ ,$$

$$\rho_+\equiv\rho_{22}+\rho_{44}+\rho_{66}=1-\rho_-\ .$$

Therefore, in steady state,

$$\bar{\rho}_-\approx\tfrac{16}{17}+O(\Delta/\alpha)\ ,$$

$$\bar{\rho}_+\approx\tfrac{1}{17}+O(\Delta/\alpha)\ .$$

The ratio $\bar{\rho}_-/\bar{\rho}_+=16+O(\Delta/\alpha)$ is the ratio of the mean duration of the fluorescence on periods to the off periods. A simple rate equation analysis confirms that the ratio of the ground-state level populations is 16 in the low-intensity limit ($\Omega\ll\gamma$) and for $\Delta=0$.[18] However, we find that this ratio, unlike that for the three-level V configuration, is largely independent of laser intensity and is only weakly dependent on detuning (for $\gamma,\Omega,\Delta\ll\alpha$). The surprising feature here is that this ratio is independent of saturation and power broadening effects. As Ω is increased from zero, $\bar{\rho}_{11}$ decreases as population is transferred to level 3. We might expect, therefore, that the probability of transferring population from level 1 into the shelving level should diminish. However, Eqs. (2) indicate that the population of level 5, from which the shelving level (level 2) is populated via spontaneous decay, increases as Ω^2 with no effect due to saturation of the $1\leftrightarrow 3$ transition. The apparent explanation of this phenomenon is that population is transferred from level 3 to level 5 via the Raman coherence ρ_{35}. The increase in ρ_{35} with increasing Ω exactly compensates for the effect of the decreasing population in level 1.

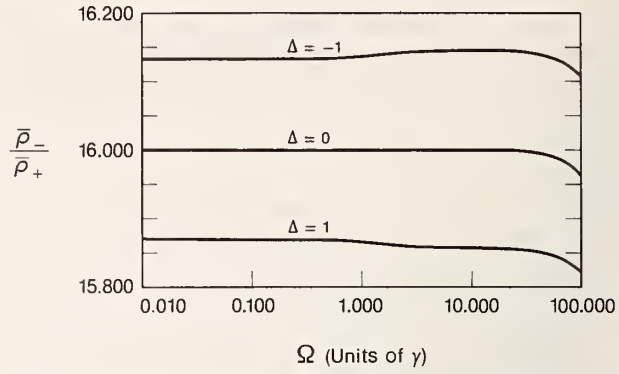

FIG. 3. The ratio of the steady-state population in levels 1, 3, and 5 (ρ_- system) to the steady population in levels 2, 4, and 6 (ρ_+ system) is plotted vs Ω for various detunings, Δ, and for $\alpha=1215$ (all in units of γ). $\bar{\rho}_-/\bar{\rho}_+$ is equal to the ratio of the mean duration of the fluorescence on periods to the off periods. There is little effect due to saturation of the $1\leftrightarrow 3$ transition and only a slight deviation from the value of 16. The downturn in $\bar{\rho}_-/\bar{\rho}_+$ for very large Ω is due to the power-broadened linewidth of the transition becoming comparable to the separation between excited levels.

We have used a computer to numerically solve Eqs. (1) for the exact steady-state solutions using various values of the parameters Δ and Ω. Figure 3 is a plot of $\bar{\rho}_-/\bar{\rho}_+$ versus Ω for several values of Δ. The ratio remains remarkably close to the value of 16 for $\Delta=0$ and $\Omega\ll\alpha$, and even for $\Omega\gg\gamma$. The ratio is offset from the value 16 when $\Delta\neq 0$ by approximately $-160(\Delta/\alpha)$.

Figure 4 demonstrates the importance of including coherence effects in the calculation. Figure 4 is a plot of $\bar{\rho}_-/\bar{\rho}_+$ versus Ω when the coherences between excited states ρ_{35} and ρ_{46} are neglected. ρ_{35} and ρ_{46} are due to stimulated, off-resonant Raman coupling. Since this

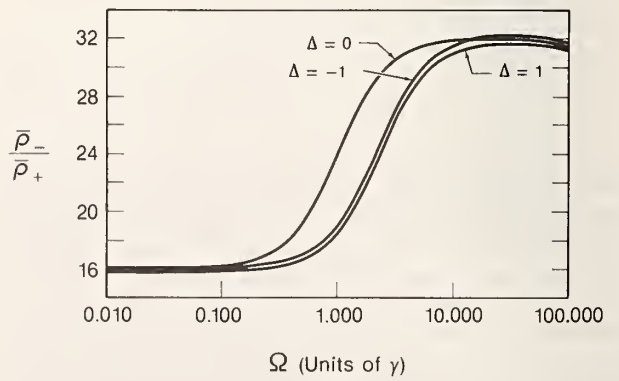

FIG. 4. Same as Fig. 3, except that the stimulated Raman coherences ρ_{35} and ρ_{46} have been neglected in the calculation. Saturation of the $1\leftrightarrow 3$ transition causes $\bar{\rho}_-/\bar{\rho}_+$ to deviate from 16 when $\Omega\gtrsim\gamma$. This demonstrates that the Raman coherences are responsible for the lack of intensity dependence of $\bar{\rho}_-/\bar{\rho}_+$.

coupling is small for $\Omega \ll \gamma$, $\bar{\rho}_-/\bar{\rho}_+$ remains close to 16 in the low-intensity regime. However, $\bar{\rho}_-/\bar{\rho}_+$ rapidly deviates from 16 when Ω is increased beyond γ, indicating the increasing role the Raman coherences assume in correctly describing the population evolution as Ω increases.

The dynamics of the population evolution is governed by rates from two widely differing time domains: (1) a "short" time of order γ^{-1} and (2) a much longer time in which population is transferred between the ρ_- and ρ_+ systems. An examination of the $\dot{\sigma}_{ij}$ equations of Eqs. (1) reveals that the short-time behavior is exponentially damped in a time γ^{-1}. Therefore, for times of interest which are greater than γ^{-1} we can ignore the short-time behavior. We would like to show that the evolution of population between the ρ_- and ρ_+ levels of this system is similar to that of the V configuration. (The population dynamics also determine the statistics of the emitted photons.) To do so, we must cast the dynamical equations in the form of a two-state rate equation. If we identify R_+ as the rate out of ρ_-, the strongly fluorescing $(-)$ system, and R_- as the rate back into it, the two-state rate equations are

$$\dot{\rho}_- = -R_+\rho_- + R_-\rho_+ ,$$

$$\dot{\rho}_+ = R_+\rho_- - R_-\rho_+ .$$

Population is transferred between the two systems via spontaneous radiative decay. To switch from the $-$ system to the $+$ system the atom must decay from level 5 to level 2. The branching ratio for this transition is $\frac{2}{3}$. Similarly, the reverse process requires a decay from level 4 to level 1, also with $\frac{2}{3}$ probability. Therefore,

$$R_+\bar{\rho}_- = (\tfrac{2}{3})\gamma\bar{\rho}_{55}$$

and

$$R_-\bar{\rho}_+ = (\tfrac{2}{3})\gamma\bar{\rho}_{44} .$$

Using the expressions [Eqs. (2)] for the $\bar{\rho}_{ii}$ gives

$$R_+ = \frac{\Omega^2\gamma}{18\alpha^2} + O(\Delta/\alpha)$$

and

$$R_- = \frac{8\Omega^2\gamma}{9\alpha^2} + O(\Delta/\alpha) .$$

The correctness of these values for R_- and R_+ has been checked by numerically integrating Eqs. (1) and verifying that the evolution towards steady state is indeed governed by these rates. The decay of the short-time behavior in a time $t \approx \gamma^{-1}$ was also verified.

The calculations which we have described assume that a laser is tuned near the $1 \leftrightarrow 3$ transition. However, we note that an entirely analogous set of equations and results are obtained by tuning the laser near the $2 \leftrightarrow 6$ transition.

The observation of quantum jumps in this system provides an excellent opportunity for comparison with theory. The very weak dependence of $\bar{\rho}_-/\bar{\rho}_+$ $(=R_-/R_+)$ on all of the parameters which can fluctuate in an experiment means that the fluorescence statistics may be very accurately measured and compared with calculation. Additionally, the switching rate can be carefully normalized by observing a portion of the laser beam transmitted through the apparatus. An experiment is now underway at the National Bureau of Standards (NBS) to observe these effects. A single $^{24}Mg^+$ ion has been confined by an electromagnetic (Penning) ion trap while a nearly resonant laser drives the $3\,^2S_{1/2}, m_J = -\frac{1}{2} \leftrightarrow 3\,^2P_{3/2}, m_J = -\frac{3}{2}$ $(1 \leftrightarrow 3)$ transition. This new apparatus has substantially better sensitivity than a previous experiment which was able to detect a single Mg^+ ion but which did not have the sensitivity to detect quantum jumps.[19] For a magnetic field of 1.4 T, the Zeeman splitting of the excited states is $\frac{1}{2}\alpha \approx \frac{1}{2}(1215\gamma) = (2\pi)26.1$ GHz for $^{24}Mg^+$, where $\gamma = (2\pi)43$ MHz. Therefore, the regime of $\alpha \gg \gamma, \Omega, \Delta$ is quite readily achieved experimentally.

The authors gratefully acknowledge the support of the U.S. Air Force Office of Scientific Research and the U.S. Office of Naval Research. One of us (R.G.H.) acknowledges the support of the National Research Council. We thank R. J. Cook and L. Hollberg for their helpful suggestions concerning the manuscript.

[1]H. J. Kimble, M. Dagenais, and L. Mandel, Phys. Rev. Lett. **39**, 691 (1977).

[2]See, for example, J. D. Cresser, J. Häger, G. Leuchs, M. Rateike, and H. Walther, in *Dissipative Systems in Quantum Optics,* Vol. 27 of *Topics in Current Physics,* edited by R. Bonifacio (Springer-Verlag, Berlin, 1982) and references therein; F. Diedrich and H. Walther, Phys. Rev. Lett. **58**, 203 (1987).

[3]R. J. Cook and H. J. Kimble, Phys. Rev. Lett. **54**, 1023 (1985).

[4]H. G. Dehmelt, J. Phys. (Paris) **42**, C8-299 (1981).

[5]T. Erber and S. Putterman, Nature (London) **318**, 41 (1985).

[6]J. Javanainen, Phys. Rev. A **33**, 2121 (1986).

[7]A. Schenzle, R. G. DeVoe, and R. G. Brewer, Phys. Rev. A **33**, 2127 (1986).

[8]C. Cohen-Tannoudji and J. Dalibard, Europhys. Lett. **1**, 441 (1986).

[9]D. T. Pegg, R. Loudon, and P. L. Knight, Phys. Rev. A **33**, 4085 (1986).

[10]A. Schenzle and R. G. Brewer, Phys. Rev. A **34**, 3127 (1986).

[11]H. J. Kimble, R. J. Cook, and A. L. Wells, Phys. Rev. A **34**, 3190 (1986).

[12]P. Zoller, M. Marte, and D. F. Walls, Phys. Rev. A **35**, 198 (1987).

[13]W. Nagourney, J. Sandberg, and H. Dehmelt, Phys. Rev. Lett. **56**, 2797 (1986).

[14]J. C. Bergquist, R. G. Hulet, W. M. Itano, and D. J. Wine-

land, Phys. Rev. Lett. **57**, 1699 (1986).
[15]Th. Sauter, W. Neuhauser, R. Blatt, and P. E. Toschek, Phys. Rev. Lett. **57**, 1696 (1986).
[16]M. A. Finn, G. W. Greenlees, and D. A. Lewis, Opt. Commun. **60**, 149 (1986).
[17]R. G. Hulet and D. J. Wineland, Bull. Am. Phys. Soc. **31**, 938 (1986).
[18]D. J. Wineland, J. C. Bergquist, W. M. Itano, and R. E. Drullinger, Opt. Lett. **5**, 245 (1980).
[19]D. J. Wineland and W. M. Itano, Phys. Lett. **82A**, 75 (1981).

PHYSICAL REVIEW A VOLUME 37, NUMBER 11 JUNE 1988

Precise test of quantum jump theory

Randall G. Hulet,* D. J. Wineland, J. C. Bergquist, and Wayne M. Itano
Time and Frequency Division, National Bureau of Standards, Boulder, Colorado 80303
(Received 16 November 1987)

Quantum jumps due solely to spontaneous Raman scattering between the Zeeman sublevels of a single $^{24}Mg^+$ ion have been observed in the fluorescence emitted by the ion. A theory of quantum jumps for this system predicts that coherences between excited levels cause the ratio of the mean duration of the "fluorescence-on periods" to the mean duration of the "fluorescence-off periods" to be independent of laser intensity. The measured value agrees with the predicted one to within the measurement precision of 2%. The distribution of the durations of the off periods also agrees with theory.

A few groups have recently observed "quantum jumps" between the energy levels of a single atomic ion as signaled by an abrupt change in the fluorescence emitted by the ion.[1-3] In another experiment,[4] quantum jumps were inferred from the statistics of the fluorescence emitted by neutral atoms in a weak beam. In these experiments, the quantum jump was a transition (either stimulated or spontaneous) into or out of a metastable excited state.

In this paper, we report the observation of quantum jumps due solely to spontaneous Raman transitions into and out of ground-state sublevels. As opposed to the earlier experiments, we quantitatively compare the predictions of the theory with the experiment. A particular realization of the process[5] is illustrated in Fig. 1. It employs just one radiation source which is tuned between a pair of Zeeman levels of an atom or ion with a $^2S_{1/2}$ ground state and an excited $^2P_{3/2}$ state (for example, an alkali atom or singly ionized alkaline earth atom). The frequency ω of the radiation is tuned near the $S_{1/2}$, $m_J=-\frac{1}{2}\leftrightarrow P_{3/2}$, $m_J=-\frac{3}{2}$ transition frequency ω_0. The atom cycles nearly continuously between these levels since the dipole selection rules allow spontaneous decay only to the original ground level. A steady stream of fluorescence photons, which are readily detected, is emitted by the atom during this period. However, if the radiation is linearly polarized with the polarization direction perpendicular to the direction of the magnetic field, the $S_{1/2}$ $m_J=-\frac{1}{2}\leftrightarrow P_{3/2}$, $m_J=\frac{1}{2}$ transition is also allowed, although it is far from resonance. This transition is indicated by the dashed arrow in Fig. 1. A spontaneous decay from the upper $m_J=\frac{1}{2}$ level can then leave the atom in the $m_J=\frac{1}{2}$ ground level. This spontaneous Raman transition into the $m_J=\frac{1}{2}$ ground level takes the atom out of the $m_J=-\frac{1}{2}\leftrightarrow m_J=-\frac{3}{2}$ cycling loop, causing the emitted fluorescence to suddenly stop. The off-resonant $S_{1/2}$, $m_J=+\frac{1}{2}\leftrightarrow P_{3/2}$, $m_J=-\frac{1}{2}\rightarrow S_{1/2}$, $m_J=-\frac{1}{2}$ spontaneous Raman transition (not shown in Fig. 1) will return the atom to the cycling loop where it will resume scattering.

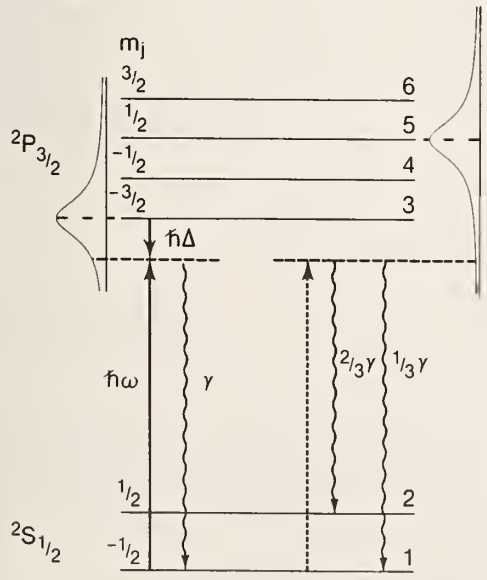

FIG. 1. The energy-level structure of the $S_{1/2}$ and $P_{3/2}$ states of an atom in a magnetic field (not to scale). A laser of frequency ω is assumed to be tuned near the $S_{1/2}$, $m_J=-\frac{1}{2}\leftrightarrow P_{3/2}$, $m_J=-\frac{3}{2}$ transition frequency ω_0. The energy separation of adjacent $P_{3/2}$ ($S_{1/2}$) sublevels is $\hbar a/2$ ($3\hbar a/4$). The indicated Lorentzian widths and detuning Δ, which are much less than a, have been exaggerated for clarity.

In a previous paper,[6] we calculated the behavior of this system when the magnetic field strength is large enough that $a\gg\gamma$, Ω, Δ, where $\hbar a/2$ is the energy separation between adjacent excited-state sublevels, $3\hbar a/4$ is the separation between the ground-state sublevels, γ is the excited-state spontaneous decay rate, Ω is the on-resonance Rabi frequency for the $S_{1/2}$, $m_J=-\frac{1}{2}\rightarrow P_{3/2}$, $m_J=-\frac{3}{2}$ transition, and $\Delta=\omega-\omega_0$ (see Fig. 1).

We have used a single $^{24}Mg^+$ ion confined by the static magnetic and electric fields of a Penning trap[7] to demonstrate this process. The magnetic field for the data presented here was 1.39 T which gives $a=(2\pi)52$ GHz$\simeq 1200\gamma$, where $\gamma=(2\pi)43$ MHz. Therefore, the condition $a\gg\gamma$, Ω, Δ is quite readily achieved in our experiment.

For the trap used in this work (Fig. 2), we achieved a large collection solid angle ($>1\%$ of 4π sr), compared to an earlier apparatus,[8] by splitting the ring electrode into two halves in the plane perpendicular to the magnetic field direction.[9] The relative trap dimensions were chosen, with the aid of a computer, to make the potential nearly quadratic at the trap center.[10] The pressure of back-

Work of the U.S. Government
Not Subject to U.S. Copyright

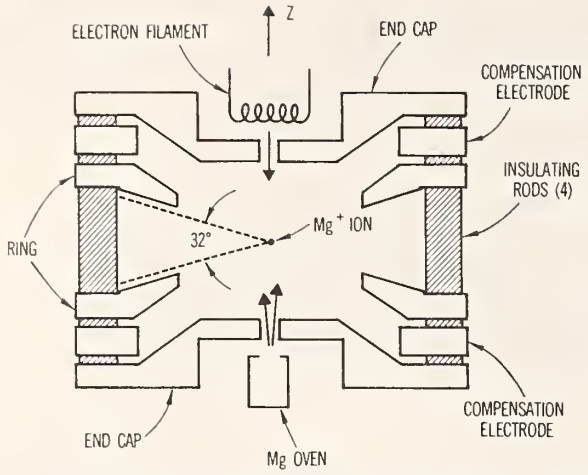

FIG. 2. Cross-sectional drawing of the Penning trap used in the experiment. The shaded regions are ceramic support rods. The end-cap separation is 1.38 cm and the inner diameter of the ring electrode is 1.63 cm. The two ring electrodes and the two compensation electrodes were grounded and the two end caps were at +12 V for this experiment.

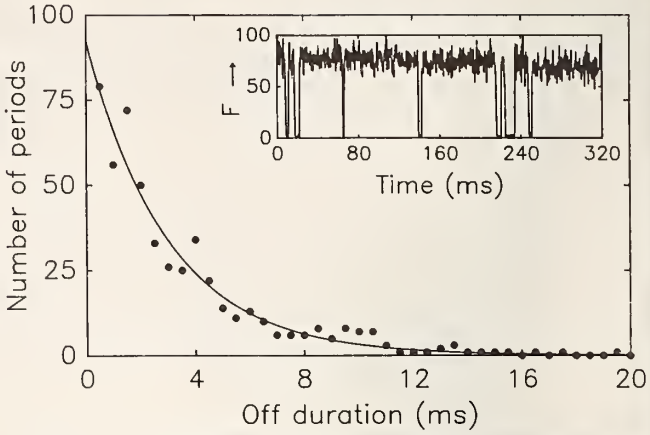

FIG. 3. A histogram of the duration of fluorescence-off periods for a data run. The number of off periods which have a particular duration are plotted vs the duration. This data run had 512 off periods in 20 s. The solid line is a fit of the data to Eq. (2). Inset: A portion of a data run showing quantum jumps in fluorescence F as a function of time.

ground gas in the apparatus was less than 10^{-8} Pa.

The $3S_{1/2}$ to $3P_{3/2}$ transition wavelength for Mg^+ is 280 nm. We generated up to 200 μW of 280-nm radiation by frequency doubling the output of a single-mode, continuous-wave dye laser in a deuterated ammonium dihydrogen-phosphate crystal. The frequency width of this radiation was much less than the natural width γ of the transition. The laser beam was focused near the center of the trap with a beam waist $w_0 \simeq 45$ μm. The ions were laser cooled when $\Delta < 0$, and since the beam was directed at an angle of 74° relative to the magnetic field axis all of the ion's degrees of motion were cooled directly. The equilibrium temperature of the ion was only a fraction of 1 K when $\Delta \simeq -\gamma/2$.[11] Under these conditions, the Doppler broadening of the transition frequency was much less than γ, as verified by a scan of the laser frequency, and the ion was confined to dimensions which were much less than w_0. In order to laser cool in a Penning trap, it is necessary to position the center of the laser beam radially outward from the trap axis.[11] With a displacement of approximately 20 μm and our value of w_0, the saturation parameter Ω^2/γ^2 was equal to 1 at the position of the ion for a laser power of approximately 50 μW. From the definitions of Ref. 6, the ion spends twice as much time in the ground $m_J = -\frac{1}{2}$ sublevel as in the excited $m_J = -\frac{3}{2}$ level when $\Omega = \gamma$ and $\Delta = 0$. The fluorescence photons were collected in a direction perpendicular to both the magnetic field and laser beam directions by focusing onto a photomultiplier tube. The maximum detected photon count rate was 2×10^5/s for a single ion.

Data exhibiting quantum jumps are displayed in the inset in Fig. 3. The horizontal axis is divided into time intervals of 0.5 ms duration. The vertical axis indicates the number of photons counted during each time interval and the points representing each interval are connected by straight lines. The sudden changes in fluorescence level are due to quantum jumps between the ground-state sublevels via spontaneous Raman transitions.

For other realizations of quantum jumps, the dynamics of the population evolution and, therefore, the statistics of the emitted fluorescence are governed by effective two-state rate equations.[12] That is, there are rates R_+ and R_- for the atom to make transitions out of or into the energy levels which comprise the strongly fluorescing or "on" system and the system of levels which comprise the "off" system. $(R_+)^{-1}$ and $(R_-)^{-1}$ are equal to the mean duration of the fluorescence on periods, $\langle T_{on} \rangle$, and off periods, $\langle T_{off} \rangle$, respectively. Although the system considered here is substantially different than those investigated before, it was shown in Ref. 6 that the dynamics of this system should also be governed by effective two-state rate equations. The expressions for the rates R_- and R_+,

$$R_+ = \langle T_{on} \rangle^{-1} = \Omega^2 \gamma/(18\alpha^2) \ , \qquad R_- = \langle T_{off} \rangle^{-1} = 8\Omega^2 \gamma/(9\alpha^2) \ , \tag{1}$$

are simple because of the off-resonance nature of the excitation, in contrast with the previously considered systems.[12]

A consequence of this type of dynamics is that the distribution of fluorescence-on and fluorescence-off times should be exponential. In Fig. 3, we plot the duration of fluorescence-off periods versus the number of periods in the data run which are off for this duration. The solid line is a fit to the equation

$$W_{off}(t) = \langle T_{off} \rangle^{-1} \exp(-t/\langle T_{off} \rangle) \ . \tag{2}$$

The data are consistent with a distribution of this form.

An important prediction of Ref. 6 is that the ratio of the mean duration of the fluorescence-on periods to the mean duration of the fluorescence-off periods should be a value which is only very weakly dependent on the variable parameters of the system, such as laser power and frequency. This is in contrast with the rather strong dependence of this ratio on system parameters in the other experi-

TABLE I. A summary of the data for seven runs with different values of the saturation parameter Ω^2/γ^2. Also shown are the calculated results when the stimulated Raman coherences between excited states are either included or neglected. Each data run contained 60000 time intervals whose length was either 0.25, 0.33, or 0.5 ms. $\langle T_{\text{off}}\rangle$ ranged from 9.5 ms for run 1 to 2.3 ms for run 7. Data runs in which the laser frequency varied excessively have been omitted from the table.

			Calculated		Measured
Run	Ω^2/γ^2	$-\Delta/\gamma$	$\frac{\langle T_{\text{on}}\rangle}{\langle T_{\text{off}}\rangle}$ (without coherence)	$\frac{\langle T_{\text{on}}\rangle}{\langle T_{\text{off}}\rangle}$ (with coherence)	$\frac{\langle T_{\text{on}}\rangle}{\langle T_{\text{off}}\rangle}$
1	0.65 ± 0.09	0.67 ± 0.03	19.1 ± 0.2	16.09	15.76 ± 0.84
2	1.82 ± 0.16	$0.22^{+0.10}_{-0.20}$	25.8 ± 0.5	16.03	16.02 ± 0.67
3	1.89 ± 0.16	$0.20^{+0.12}_{-0.20}$	26.1 ± 0.6	16.03	15.52 ± 0.58
4	2.02 ± 0.16	0.84 ± 0.05	21.7 ± 0.3	16.11	16.58 ± 0.59
5	2.45 ± 0.25	1.07 ± 0.05	21.0 ± 0.2	16.13	16.13 ± 0.70
6	2.61 ± 0.20	0.60 ± 0.05	24.4 ± 0.6	16.08	17.35 ± 0.70
7	2.64 ± 0.16	0.50 ± 0.06	25.2 ± 0.6	16.07	16.26 ± 0.69

ments.[1-4] Reference 6 shows that, for $\alpha \gg \gamma, \Omega, \Delta$,

$$\langle T_{\text{on}}\rangle/\langle T_{\text{off}}\rangle = 16 + O(\Delta/\alpha) \ . \tag{3}$$

We might intuitively expect that $\langle T_{\text{on}}\rangle/\langle T_{\text{off}}\rangle$ would increase by a factor of 2 when the $S_{1/2}$, $m_J = -\frac{1}{2} \rightarrow P_{3/2}$, $m_J = -\frac{3}{2}$ transition is saturated, since approximately half the population which was available in the $m_J = -\frac{1}{2}$ ground level to be transferred to the $m_J = \frac{1}{2}$ ground level is "stranded" in the excited state. However, the stimulated Raman coherence between the $m_J = -\frac{3}{2}$ and $m_J = \frac{1}{2}$ excited-state sublevels, through the $m_J = -\frac{1}{2}$ ground-state sublevel, compensates for the depletion of population in the ground state.[6]

We have investigated this phenomenon by measuring $\langle T_{\text{on}}\rangle/\langle T_{\text{off}}\rangle$ for various values of the saturation parameter Ω^2/γ^2. Table I shows the results of analyzing seven different data runs with saturation parameters ranging between 0.65 and 2.64. The value of the saturation parameter and its uncertainty were obtained by fitting the distribution of fluorescence-off time durations to Eq. (2) to find $\langle T_{\text{off}}\rangle$ and its uncertainty. Equation (1) then relates $\langle T_{\text{off}}\rangle$ to Ω. This procedure gives results which are consistent with estimates of the expected saturation parameter from independent measurements of the laser power and the laser beam waist w_0. The rate of fluorescence emitted by the ion during the fluorescence-on periods depends on the average population in the exited $m_J = -\frac{3}{2}$ level, which depends on the detuning Δ.[6] Therefore, if the count rate for $\Delta = 0$ is known, then Δ for each data run is determined by the mean detected count rate for the fluorescence-on periods of that run. The count rate for $\Delta = 0$ is found from the maximum detected rate when the laser is scanned through the resonance.[13,14] The uncertainty given for Δ in Table I is due to the uncertainty in the count rate for $\Delta = 0$. The fourth column gives the expected $\langle T_{\text{on}}\rangle/\langle T_{\text{off}}\rangle$ ratio if the coherences between excited states are neglected.[6] The fifth column is the expected value of the ratio when the coherences are included in the calculation. Since $\Delta \neq 0$, there is a small departure from the value of 16. The uncertainty in this calculated ratio is small compared to the uncertainty in the measured value of $\langle T_{\text{on}}\rangle/\langle T_{\text{off}}\rangle$ and is therefore not reported. Finally, the last column is our measured value for $\langle T_{\text{on}}\rangle/\langle T_{\text{off}}\rangle$ for each run. This quantity was extracted from the data by fitting the distribution of detected counts per time interval for each run to a sum of two Gaussian curves, one corresponding to the fluorescence-off periods and the other to the fluorescence-on periods. The ratio $\langle T_{\text{on}}\rangle/\langle T_{\text{off}}\rangle$ is then equal to the ratio of the areas under the Gaussian curves. The uncertainty given is estimated from the uncertainty in determining the fitting parameters. The mean for the seven runs is 16.23 and the sample standard deviation is 0.60. Combining the seven runs (weighted equally) gives $\langle T_{\text{on}}\rangle/\langle T_{\text{off}}\rangle = 16.23 \pm 0.26$. A comparison of columns 5 and 6 reveals that our data are quite consistent with the result of the coherent theory, which for the given set of values of Δ gives a mean value for the ratio of 16.08.

In this experiment, spontaneous Raman transitions induced by a single laser are responsible for quantum jumps into and out of the long-lived "shelving" level.[1] The shelving level is a ground-state sublevel rather than an electronic excited metastable state as in the previous demonstrations. The properties of this level structure have allowed the theory of quantum jumps, in which the dynamics of the jumps are described by effective two-level rate equations, to be tested with high precision. This experiment is a realization of "single-atom optical pumping." Ordinarily, the effects of optical pumping are evident only in the time-averaged values of the level populations. However, in single-atom optical pumping, the dynamical evolution of the level populations is revealed by quantum jumps in the fluorescence intensity. Finally, the existence of stimulated Raman coherences between excited states has been shown to play an important role in both the population dynamics and in the steady-state values of the level populations.

The authors thank C. Weimer for help in constructing parts of the apparatus and E. C. Beaty for performing computer calculations for the trap design. We also thank L. Hollberg and F. Diedrich for helpful comments on the manuscript. The authors gratefully acknowledge the support of the Air Force Office of Scientific Research and the Office of Naval Research. One of us (R.G.H.) thanks the National Research Council for support.

*Present address: Physics Department, Rice University, Houston, TX 77251.

[1]W. Nagourney, J. Sandberg, and H. Dehmelt, Phys. Rev. Lett. **56**, 2797 (1986).

[2]J. C. Bergquist, R. G. Hulet, W. M. Itano, and D. J. Wineland, Phys. Rev. Lett. **57**, 1699 (1986).

[3]Th. Sauter, W. Neuhauser, R. Blatt, and P. E. Toschek, Phys. Rev. Lett. **57**, 1696 (1986).

[4]M. A. Finn, G. W. Greenlees, and D. A. Lewis, Opt. Commun. **60**, 149 (1986).

[5]R. G. Hulet and D. J. Wineland, Bull. Am. Phys. Soc. **31**, 938 (1986).

[6]R. G. Hulet and D. J. Wineland, Phys. Rev. A **36**, 2758 (1987).

[7]See, for example, H. G. Dehmelt, Adv. At. Mol. Phys. **3**, 53 (1967); **5**, 109 (1969); D. J. Wineland, W. M. Itano, and R. S. Van Dyck, Jr., *ibid.* **19**, 135 (1983).

[8]D. J. Wineland and W. M. Itano, Phys. Lett. **82A**, 75 (1981).

[9]M. H. Prior and H. A. Shugart, Phys. Rev. Lett. **27**, 902 (1971).

[10]E. C. Beaty, J. Appl. Phys. **61**, 2118 (1987).

[11]W. M. Itano and D. J. Wineland, Phys. Rev. A **25**, 35 (1982).

[12]H. J. Kimble, R. J. Cook, and A. L. Wells, Phys. Rev. A **34**, 3190 (1986), and references therein.

[13]R. E. Drullinger, D. J. Wineland, and J. C. Bergquist, Appl. Phys. **22**, 365 (1980).

[14]W. Nagourney, G. Janik, and H. Dehmelt, Proc. Natl. Acad. Sci. U.S.A. **80**, 643 (1983).

Radiative Decay Rates in Hg^+ from Observations of Quantum Jumps in a Single Ion

Wayne M. Itano, J. C. Bergquist, Randall G. Hulet,[a] and D. J. Wineland
Time and Frequency Division, National Bureau of Standards, Boulder, Colorado 80303
(Received 17 September 1987)

Radiative decay rates connecting the lowest four energy levels of $^{198}Hg^+$ have been derived solely from an analysis of the fluctuations (quantum jumps) of the laser-induced fluorescence of the 194-nm first resonance transition of a single ion confined in a Paul trap. The natural linewidth of the 194-nm first resonance transition was also measured. The measured decay rates and branching ratios are in satisfactory agreement with theory.

PACS numbers: 32.70.Fw, 32.70.Cs, 32.80.Pj

Recently it has become possible to observe for extended periods the fluorescence from a single, isolated ion, kept in place by the electric fields of an ion trap. This capability has made it possible to study quantum jumps (sudden transitions between atomic energy levels)[1-3] and nonclassical photon statistics (photon antibunching).[3,4] In this Letter we report measurements of five radiative decay rates connecting the lowest four energy levels of $^{198}Hg^+$. These measurements depend on the observation of transition between the energy levels of a single ion, as exhibited by the changes in its fluorescence. This would not be possible with a sample of many ions observed simultaneously. Related methods have previously been used to measure lifetimes of metastable levels in Ba^+ (Refs. 1 and 2) and Hg^+ (Ref. 3).

An unusual feature of the techniques used in the present work is that decay branching ratios are measured without our observing the decay photons directly. It is not necessary to calibrate the detector efficiency, and it is necessary only to observe one wavelength. Instrumental noise, such as that due to changes in the laser intensity or that due to statistical fluctuations in the numbers of photons detected, is unimportant compared to the inherent quantum mechanical randomness in the behavior of a single atom. This property is shared by the quantized optical double resonance technique recently used to observe narrow resonances in a single Hg^+ ion.[5]

The lowest four energy levels of Hg^+ are shown in Fig. 1. After the ion is excited from the ground $5d^{10}6s\ ^2S_{1/2}$ level to the $5d^{10}6p\ ^2P_{1/2}$ level, it usually decays back to the ground state by electric dipole ($E1$) radiation, but has a small probability of undergoing an $E1$ decay to the metastable $5d^96s^2\ ^2D_{3/2}$ level. This probability is small because it requires configuration mixing in order to occur (the nominal configurations differ in two orbitals). In addition, the transition rate is proportional to the cube of the energy difference between the $^2P_{1/2}$ and the $^2D_{3/2}$ energy levels, which is small compared to that between the $^2P_{1/2}$ and the $^2S_{1/2}$ energy levels. From the $^2D_{3/2}$ level, the ion decays either directly to the ground state, by electric quadrupole ($E2$) radiation, or to the metastable $5d^96s^2\ ^2D_{5/2}$ level, by magnetic dipole ($M1$) and $E2$ radiation. According to calculations,[6] the $E2$ decay rate to the $^2D_{5/2}$ level is negligible compared to the $M1$ rate. The $^2D_{5/2}$ level decays to the ground state by $E2$ radiation. According to simple estimates,[7] the magnetic quadrupole ($M2$) and electric octupole ($E3$) allowed decay rate from the $^2P_{1/2}$ level to the $^2D_{5/2}$ level is much too small to observe in the present experiment.

The apparatus has been described previously.[3,8] The Hg^+ ions were confined in a radio-frequency (Paul) trap under high-vacuum conditions. The ions were loaded into the trap by ionization of Hg atoms inside the trap volume with an electron beam. A beam of narrow-band cw 194-nm radiation of about 5 μW was focused to a waist size w_0 of approximately 5 μm at the position of the ions. The frequency of the 194-nm radiation was tuned below the resonance, in order to provide laser cooling of the ions. The 194-nm fluorescence photons were collected by a system of lenses and focused on the Cs-Te photocathode of a solar-blind photomultiplier tube. The numbers of photons counted in consecutive time intervals

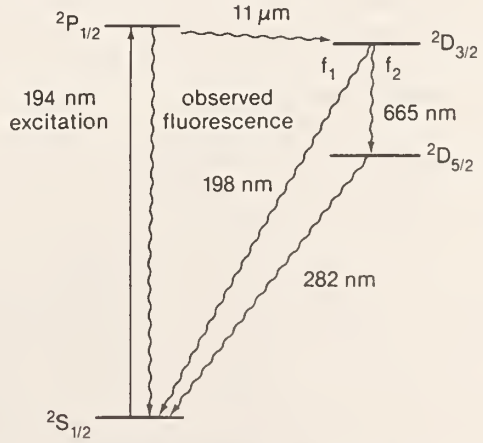

FIG. 1. Diagram of the lowest four energy levels of Hg^+. The decay rates from all three excited levels were determined by observation of only the 194-nm fluorescence.

Work of the U. S. Government
Not subject to U. S. copyright

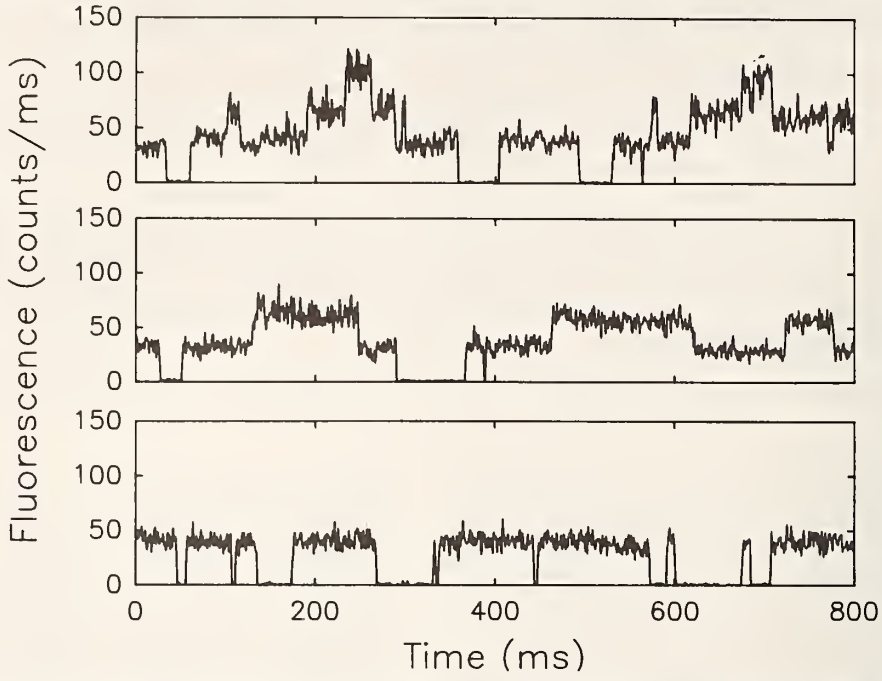

FIG. 2. Intensity of 194-nm laser-induced fluorescence as a function of time for samples of three ions (highest trace), two ions (middle trace), and one ion (lowest trace) in the trap. The integration time per point was 1 ms, and the points were connected by straight lines.

were recorded by a computer.

Figure 2 shows traces of the fluorescence intensities as functions of time when three ions, two ions, and one ion were in the trap and irradiated with radiation near the $^2S_{1/2}$-to-$^2P_{1/2}$ transition frequency. When a single ion was in the trap, as in the lowest trace in Fig. 2, the 194-nm fluorescence intensity had two observable states. When the ion was cycling between the $^2S_{1/2}$ level and the $^2P_{1/2}$ level (the "on" state), the fluorescence intensity had a constant value; when it was in either the $^2D_{3/2}$ or the $^2D_{5/2}$ metastable level (the "off" state), it was zero. When more than one ion was in the trap, as in the highest and the middle traces of Fig. 2, the fluorescence intensity at a given time was proportional to the number of ions that were in the on state at that time, so that it took one of several discrete values.

The total radiative decay rate of the $^2P_{1/2}$ level (γ_P) was determined by measurement of the width of the 194-nm transition. The decay rate γ_P, in units of inverse seconds, is equal to the natural linewidth, in units of radians per second. Only the low-frequency half of the resonance was observed, since the ion heated rapidly when the frequency of the 194-nm radiation was above the resonance center.[9,10] The frequency of the 194-nm radiation was swept slowly enough that the transitions between the on and off states were clearly resolved, and a smooth curve was interpolated through the on-state data. The effect of power broadening was removed by an extrapolation to zero intensity of the 194-nm radiation. A similar method has been used previously by Nagourney, Janik, and Dehmelt to measure the natural linewidth of the 280-nm resonance line of Mg^+.[10] The temperature was measured in a separate experiment to be a few millikelvins,[5] for the range of frequency detunings required for this line-shape analysis. This temperature was low enough that the Doppler broadening was not significant. The result was $\gamma_P = (3.8 \pm 0.6) \times 10^8\ s^{-1}$.

The radiative decay rate from the $^2P_{1/2}$ level to the $^2D_{3/2}$ level [$\gamma(P \rightarrow D)$] was determined by measurement of the rate of transitions from the on state to the off state for a single ion as a function of the 194-nm fluorescence intensity. The transition rate R_+ from the on state to the off state was obtained by division of the number of transitions in a run by the time that the ion was in the on state in that run. This rate is equal to the product of $\gamma(P \rightarrow D)$ and $P(^2P_{1/2})$, the mean population of the $^2P_{1/2}$ level when the ion is in the on state. The fluorescence intensity in the on state is also proportional to $P(^2P_{1/2})$. $P(^2P_{1/2})$ could be varied by variation of either the intensity or the frequency detuning from resonance of the 194-nm radiation. It was found experimentally that R_+ was proportional to the observed photon counting rate in the on state. A calibration of the value of $P(^2P_{1/2})$ was made by measurement of the fluorescence intensity near resonance for different intensities of the incident 194-nm radiation. The value of $P(^2P_{1/2})$ at resonance is equal to $(2+1/S)^{-1}$, where S, the saturation parameter, is a quantity proportional to the incident 194-nm intensity. Figure 3 is a plot of Y, the observed counting rate at resonance, as a function of X, the 194-

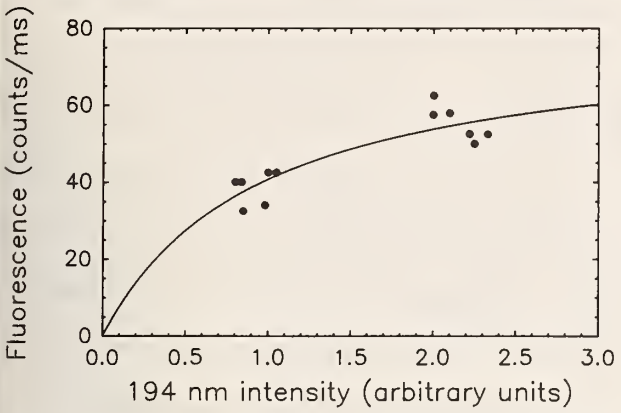

FIG. 3. Fluorescence intensity at resonance of a single Hg^+ ion as a function of the intensity of the 194-nm radiation (dots) and a least-squares fit (curve).

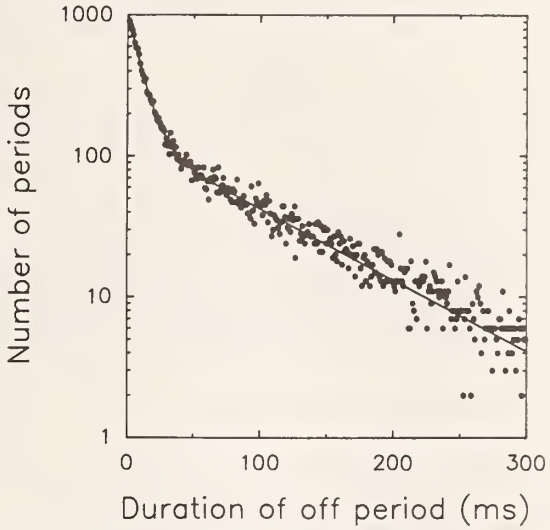

FIG. 4. Distribution of fluorescence-off periods for a single ion (dots) and a least-squares fit (curve). These data represent an analysis of approximately 40000 quantum jumps (up or down).

nm intensity in arbitrary units. The solid curve is a least-squares fit of the data by the function $Y=A(2+B/X)^{-1}$. The value of $P(^2P_{1/2})$ for a given 194-nm intensity and detuning is the observed counting rate divided by A. The value of $\gamma(P\rightarrow D)$ was determined by division of the value of R_+ for a particular run by the value of $P(^2P_{1/2})$ for the same run. The result was $\gamma(P\rightarrow D)=52\pm16\ s^{-1}$. The uncertainty in the determination of A from the least-squares fit and the uncertainty in the determination of R_+ contributed about equally to the uncertainty in $\gamma(P\rightarrow D)$.

The average behavior of the ion from the time it decays to the $^2D_{3/2}$ level until it returns to the ground state is governed by the rate equations for the probabilities P_1, P_2, and P_3 of being in the $^2D_{3/2}$ level, the $^2D_{5/2}$ level, and the $^2S_{1/2}$ level, respectively:

$$dP_1(t)/dt=-\gamma_1P_1(t), \quad (1)$$

$$dP_2(t)/dt=f_2\gamma_1P_1(t)-\gamma_2P_2(t), \quad (2)$$

$$dP_3(t)/dt=f_1\gamma_1P_1(t)+\gamma_2P_2(t). \quad (3)$$

Here γ_1 and γ_2 are the total radiative decay rates of the $^2D_{3/2}$ level and the $^2D_{5/2}$ level respectively. The probabilities for the $^2D_{3/2}$ level to decay to the $^2S_{1/2}$ level or to the $^2D_{5/2}$ level are f_1 and f_2 ($f_1+f_2=1$). The initial conditions are $P_1(0)=1$ and $P_2(0)=P_3(0)=0$. The quantity observed experimentally is the probability distribution $W_{\rm off}(\tau)$ of the duration of off periods as a function of the duration τ. This quantity is proportional to $dP_3(t)/dt$ evaluated at $t=\tau$, which is the average rate at which the ion returns to the ground state after a period τ. Solving Eqs. (1)–(3) yields the expression

$$W_{\rm off}(\tau)\propto f_2\gamma_2\exp(-\gamma_2\tau)+(f_1\gamma_1-\gamma_2)\exp(-\gamma_1\tau). \quad (4)$$

The distribution of about 20000 off periods is shown in Fig. 4, together with a least-squares fit by a sum of two decaying exponentials. The values of the parameters obtained from the fit are $\gamma_1=109\pm5\ s^{-1}$, $\gamma_2=11.6\pm0.4\ s^{-1}$, and $f_1=0.491\pm0.015$. The partial decay rates of the $^2D_{3/2}$ level are $f_1\gamma_1=53.5\pm2.0\ s^{-1}$ and $f_2\gamma_1=55.5\pm4.0\ s^{-1}$.

In order to place a limit on the effects of collisions on the measured lifetimes, data were collected at higher pressure. No shift of the decay rates of the metastable levels was observed, even when the pressure of the background gas, consisting mostly of Hg, was increased by over a factor of 10 above the normal level. The relative pressure was estimated from the time required to create an ion in the trap by electron-impact ionization and also from the decrease in the confinement time of the ion in the trap. The latter measurement was based on the observation that ions were lost from the trap when both 194-nm resonance radiation and neutral Hg atoms were present. We think that this process was caused by reactions of excited-state ions with neutral Hg atoms. The kinetic energy given to an ion by such a reaction could have been sufficient to cause it to be lost from the trap. All other perturbing effects, such as transitions out of the metastable levels induced by the 194-nm radiation or the trap electric fields, are estimated to have been negligible.

The present measurement of γ_P agrees with a previous beam-foil measurement of $(4.3\pm0.7)\times10^8\ s^{-1}$ by Eriksen and Poulsen[11] but disagrees somewhat with a previous optical-absorption measurement of $2.65\times10^8\ s^{-1}$ by Bruneteau *et al.*[12] An unpublished calculation by Al-Salameh and Silfvast[13] (AS) gives a value of $5\times10^8\ s^{-1}$, in fair agreement with the present measurement. Other theoretical values are given in Ref. 11. No previous measurements of $\gamma(P\rightarrow D)$ have been reported. The present value is in good agreement with the value of

55 s^{-1} calculated by AS.[13] No previous measurements of the partial decay rates $f_1\gamma_1$ and $f_2\gamma_1$ of the $^2D_{3/2}$ level have been reported. Johnson[14] has reported a value for the total decay rate γ_1 of 50 ± 5 s^{-1}, which disagrees with the present value. Garstang[6] has calculated the decay rate $f_1\gamma_1$ to be 54 s^{-1}, in very good agreement with the present value. The other decay rate $f_2\gamma_1$ has been calculated by Garstang[6] to be 42 s^{-1} and by AS[13] to be 75.6 s^{-1}. The present value is in fair agreement with both calculations. Two previous measurements of the $^2D_{5/2}$ level decay rate γ_2 have been reported by Bergquist *et al.*[3,8] The values obtained by the two methods were 11 ± 2 s^{-1} (Ref. 8) and 11 ± 4 s^{-1} (Ref. 3), in good agreement with the present value. A previous measurement by Johnson[14] of $\gamma_2=10.2\pm0.5$ s^{-1} disagrees slightly with the present value. The values of γ_2 calculated by Garstang[6] (9.5 s^{-1}) and by AS[13] (12.6 s^{-1}) are in fair agreement with the present value.

We acknowledge the support of the U. S. Air Force Office of Scientific Research and the U. S. Office of Naval Research.

---

[a]Present address: Physics Department, Rice University, Houston, TX 77251.

[1]W. Nagourney, J. Sandberg, and H. Dehmelt, Phys. Rev. Lett. **56**, 2797 (1986).

[2]Th. Sauter, W. Neuhauser, R. Blatt, and P. E. Toschek, Phys. Rev. Lett. **57**, 1696 (1986); Th. Sauter, R. Blatt, W. Neuhauser, and P. E. Toschek, Opt. Commun. **60**, 287 (1986).

[3]J. C. Bergquist, R. G. Hulet, W. M. Itano, and D. J. Wineland, Phys. Rev. Lett. **57**, 1699 (1986).

[4]F. Diedrich and H. Walther, Phys. Rev. Lett. **58**, 203 (1987).

[5]J. C. Bergquist, W. M. Itano, and D. J. Wineland, Phys. Rev. A **36**, 428 (1987).

[6]R. H. Garstang, J. Res. Natl. Bur. Stand. Sect. A **68**, 61 (1964).

[7]B. W. Shore and D. H. Menzel, *Principles of Atomic Spectra* (Wiley, New York, 1968), p. 440.

[8]J. C. Bergquist, D. J. Wineland, H. Hemmati, H.-U. Daniel, and G. Leuchs, Phys. Rev. Lett **55**, 1567 (1985).

[9]R. E. Drullinger, D. J. Wineland, and J. C. Bergquist, Appl. Phys. **22**, 365 (1980).

[10]W. Nagourney, G. Janik, and H. G. Dehmelt, Proc. Natl. Acad. Sci. U.S.A. **80**, 643 (1983).

[11]P. Eriksen and O. Poulsen, J. Quant. Spectrosc. Radiat. Transfer **23**, 599 (1980).

[12]A. M. Bruneteau, A. M. Icole, C. Rouillé, A. Poquérusse, and H. J. Doucet, Phys. Lett. **46A**, 309 (1974).

[13]D. Al-Salameh and W. Silfvast, unpublished calculations.

[14]C. E. Johnson, Bull. Am. Phys. Soc. **31**, 957 (1986).

PHYSICAL REVIEW A VOLUME 38, NUMBER 1 JULY 1, 1988

Photon antibunching and sub-Poissonian statistics from quantum jumps in one and two atoms

Wayne M. Itano, J. C. Bergquist, and D. J. Wineland
Time and Frequency Division, National Bureau of Standards, Boulder, Colorado 80303
(Received 22 February 1988)

Antibunching and sub-Poissonian statistics of the 11-μm photon emission from the $5d^{10}6p\,^2P_{1/2}$ to $5d^96s^2\,^2D_{3/2}$ transition in one and two trapped Hg^+ ions have been inferred from the quantum jumps of the laser-induced fluorescence of the first resonance transition at 194 nm. Each downward step in fluorescence was assumed to mark the emission of an 11-μm photon. Signals from two ions were consistent with the assumption that quantum jumps in the two ions occurred independently. Mandel's Q parameter was determined to be approximately -0.25 for one and two ions.

Studies of collections of a few atoms or of individual atoms reveal properties which are not easily observed with samples of many atoms. One such property is antibunching of the emitted photons. A closely related, though distinct, phenomenon is sub-Poissonian statistics in the number of photons emitted in a given time interval. Photon antibunching has been observed from atoms in a dilute atomic beam by Kimble, Dagenais, and Mandel[1] and by Rateike, Leuchs, and Walther,[2] and from atomic ions in a Paul trap by Diedrich and Walther.[3] Sub-Poissonian photon statistics have been observed from single atoms by Short and Mandel[4] and by Diedrich and Walther.[3] Sub-Poissonian photon statistics have also been observed in Franck-Hertz light,[5] in parametric down conversion,[6] and from squeezed-light generators.[7]

Another effect that might be observed in collections of a few atoms is the onset of cooperative atom-field processes, which are known to occur with large numbers of atoms. Sauter, Blatt, Neuhauser, and Toschek have reported observing simultaneous quantum jumps of two and more Ba^+ ions at a rate higher than that expected from random coincidences.[8] They attributed these multiple quantum jumps to a collective interaction of the atoms and the radiation field. According to a calculation by Lewenstein and Javanainen,[9] collective effects occur only if the atoms are separated by much less than the transition wavelength.

We have previously reported an indirect observation of photon antibunching.[10] Transitions from the $^2S_{1/2}$ ground state to the $^2D_{5/2}$ metastable level of a single Hg^+ ion, induced by a 282-nm radiation source, were observed by noting the sudden cessation of the 194 nm laser-induced fluorescence of the $^2S_{1/2}$ to $^2P_{1/2}$ transition (see Fig. 1). When the fluorescence suddenly reappeared, we assumed that the ion had returned to the ground state by emitting a 282 nm photon. The correlations between the times of these assumed emissions showed antibunching.

In the work reported here, the statistical properties of 11 μm photons emitted from one and two Hg^+ ions were studied. These photon emissions were inferred from the state changes of the Hg^+ ion; these state changes were indicated by the abrupt changes in the 194 nm ion fluorescence. This is similar to the way in which the state of a Rydberg atom has been used to infer properties of the photon field in a cavity.[11] This indirect method of detecting the photon emissions was the same as in Ref. 10, but a different transition was involved. Some advantages of this detection method are high efficiency (about 95%) and low background. Collisions, which can either cause or mimic state changes of the ions,[10] were previously shown to be negligible.[12] Moreover, such independent random events would tend to decrease the antibunching and sub-Poissonian statistics observed here.

The four lowest energy levels of Hg^+ are shown in Fig. 1. The radiative decay rates and branching ratios have been measured previously.[12–15] In our experiment, the ion is subjected to coherent 194 nm radiation, which drives it from the ground $5d^{10}6s\,^2S_{1/2}$ level to the $5d^{10}6p\,^2P_{1/2}$ level. Most of the time, it decays directly back to the ground state, at a rate $\gamma_4 \approx 4\times10^8\ s^{-1}$. However, about once in 10^7 times, it decays instead to the metastable $5d^96s^2\,^2D_{3/2}$ level and emits an 11 μm photon. The rate of this transition is $\gamma_3 = 52 \pm 16\ s^{-1}$. The $^2D_{3/2}$ level decays at a rate $\gamma_1 = 109 \pm 5\ s^{-1}$. The probability for the $^2D_{3/2}$ level to decay directly to the ground state is

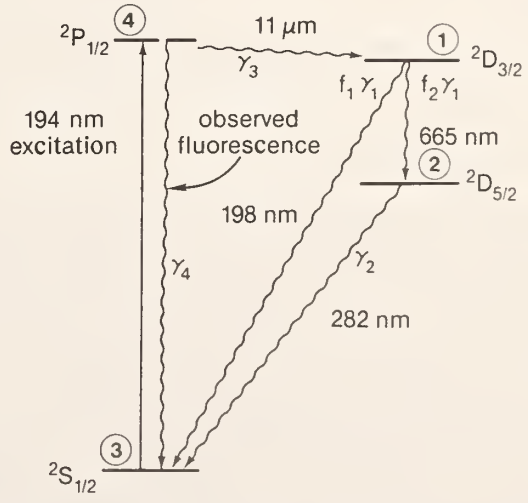

FIG. 1. Diagram of the lowest four energy levels of Hg^+. Only the 194-nm fluorescence was observed directly.

 Work of the U.S. Government

$f_1 = 0.491 \pm 0.015$. The probability for it to decay to the metastable $5d^9 6s^2\,{}^2D_{5/2}$ level is $f_2 = 1 - f_1$. The $^2D_{5/2}$ level decays to the ground state at a rate $\gamma_2 = 11.6 \pm 0.4\ s^{-1}$.

The density-matrix equations for this system are

$$d\rho_{11}/dt = -\gamma_1\rho_{11} + \gamma_3\rho_{44}\,, \tag{1a}$$

$$d\rho_{22}/dt = f_2\gamma_1\rho_{11} - \gamma_2\rho_{22}\,, \tag{1b}$$

$$d\rho_{33}/dt = f_1\gamma_1\rho_{11} + \gamma_2\rho_{22} + \gamma_4\rho_{44} - i(\rho_{34} - \rho_{43})\mu E(t)/\hbar\,, \tag{1c}$$

$$d\rho_{44}/dt = -(\gamma_3 + \gamma_4)\rho_{44} + i(\rho_{34} - \rho_{43})\mu E(t)/\hbar\,, \tag{1d}$$

$$d\rho_{34}/dt = [i\omega_{43} - \tfrac{1}{2}(\gamma_3 + \gamma_4)]\rho_{34} + i(\rho_{44} - \rho_{33})\mu E(t)/\hbar\,. \tag{1e}$$

The state labels 1, 2, 3, and 4 refer to the $^2D_{3/2}$ level, the $^2D_{5/2}$ level, the $^2S_{1/2}$ level, and the $^2P_{1/2}$ level, respectively. Here, ω_{43} is the $^2S_{1/2}$ to $^2P_{1/2}$ transition frequency, μ is the electric dipole matrix element for that transition, and the applied electric field is $E(t) = E\cos(\omega t)$. The rates γ_1, γ_2, and γ_3 are all much less than γ_4. Therefore, the $^2S_{1/2}$ and $^2P_{1/2}$ populations quickly reach a steady state with respect to each other. For times much greater than the lifetime of the $^2P_{1/2}$ level, the system is effectively a three-level system, described by rate equations for the population variables $P_1 \equiv \rho_{11}$, $P_2 \equiv \rho_{22}$, and $P_0 \equiv \rho_{33} + \rho_{44}$. We derive these equations similarly to the way Kimble, Cook, and Wells[16] reduced the density-matrix equation for a three-level system to rate equations for a two-level system. The three-level equations are

$$dP_1/dt = -\gamma_1 P_1 + \gamma_0 P_0\,, \tag{2a}$$

$$dP_2/dt = f_2\gamma_1 P_1 - \gamma_2 P_2\,, \tag{2b}$$

$$dP_0/dt = f_1\gamma_1 P_1 + \gamma_2 P_2 - \gamma_0 P_0\,, \tag{2c}$$

where

$$\gamma_0 \equiv \gamma_3\Omega^2/(4\Delta^2 + \gamma_4^2 + 2\Omega^2)\,, \tag{3a}$$

$$\Omega \equiv \mu E/\hbar\,, \tag{3b}$$

$$\Delta \equiv \omega - \omega_{43}\,. \tag{3c}$$

Let $g^{(2)}(\tau)$ be the intensity correlation function of the 11-μm field generated by the radiative decay from the $^2P_{1/2}$ level to the $^2D_{3/2}$ level, normalized such that $g^{(2)}(\infty) = 1$. Photon antibunching occurs if $g^{(2)}(0) < 1$. The function $g^{(2)}(\tau)$ is proportional to $P_0(\tau)$, where $P_0(\tau)$ is obtained from the solution of Eqs. (2a)–(2c), subject to the initial conditions $P_0(0) = 0$, $P_1(0) = 1$, and $P_2(0) = 0$. This is because the average rate at which $^2P_{1/2}$ to $^2D_{3/2}$ transitions occur is the product of γ_3 and the probability that the ion is in the $^2P_{1/2}$ level (which for given Ω and Δ is proportional to P_0). The initial conditions signify that at time $\tau = 0$, the ion has just decayed to the $^2D_{3/2}$ level. The solution of the equations yields

$$g^{(2)}(\tau) = 1 - C_+\exp(-\gamma_+\tau) - C_-\exp(-\gamma_-\tau)\,, \tag{4}$$

where

$$\gamma_\pm \equiv \tfrac{1}{2}\{(\gamma_0 + \gamma_1 + \gamma_2) \pm [(\gamma_0 + \gamma_1 + \gamma_2)^2 - 4f_2\gamma_0\gamma_1 - 4\gamma_1\gamma_2 - 4\gamma_0\gamma_2]^{1/2}\}\,, \tag{5a}$$

$$C_\pm \equiv \pm\gamma_\mp(f_1\gamma_\pm - \gamma_2)/[\gamma_2(\gamma_+ - \gamma_-)]\,. \tag{5b}$$

All of the constants required to calculate $g^{(2)}(\tau)$ are fixed by the radiative decay rates of the Hg^+ ion, except for the transition rate γ_0 from the fluorescence-on state (cycling between the $^2S_{1/2}$ and $^2P_{1/2}$ levels) to the fluorescence-off state (either the $^2D_{3/2}$ or the $^2D_{5/2}$ level). This rate was determined by dividing the number of downward quantum jumps in fluorescence by the time that the ion was in the fluorescence-on state. Since $g^{(2)}(0) = 0$, this system exhibits photon antibunching.

The apparatus has been described previously.[10,14] The Hg^+ ions were confined in a radio-frequency (Paul) trap under high-vacuum conditions. Ions were created inside the trap volume by electron impact ionization of neutral Hg atoms. A 5-μW beam of narrow-band, cw 194-nm radiation was focused to a waist w_0 of approximately 5 μm at the position of the ions. The frequency of the 194 nm radiation was tuned below the atomic resonance, so the ions were laser cooled. The 194 nm photons emitted by the ions were collected by a lens system and focused onto a photomultiplier tube. The net detection efficiency was approximately 5×10^{-4}. Peak signals were approximately 50000 counts/s per ion. The data consisted of recordings of the numbers of photons detected in a series of as many as 100000 consecutive 1-ms time intervals. An example of the data is shown in Fig. 2 of Ref. 12. Each one-ion data set was analyzed by considering the ion to be in the fluorescence-on state if the number of detected photons was above a discriminator level and in the fluorescence-off state if it was not. This discriminator level was set to minimize the number of false transitions due to noise. Each transition from the fluorescence-on state to the fluorescence-off state was assumed to indicate the emis-

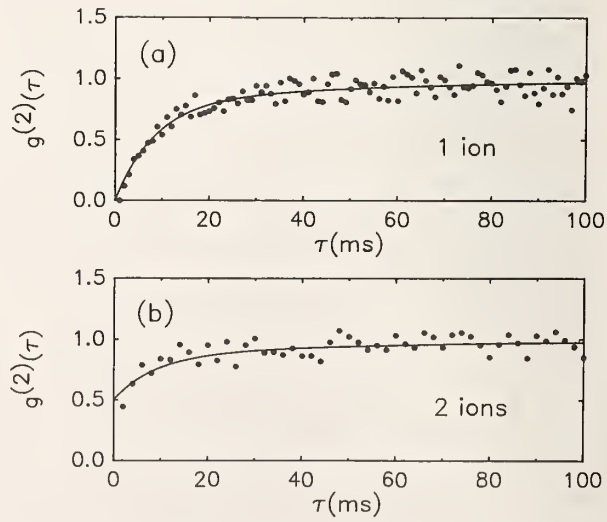

FIG. 2. Plots of $g^{(2)}(\tau)$ for (a) one Hg^+ ion and (b) two Hg^+ ions. The dots represent the experimental data. The solid lines are calculated from Eq. (4).

sion of an 11 μm photon. Analysis of simulated data, which included noise, indicated that about 5% of the transitions would have escaped detection, because they were preceded by or followed by a quantum jump in the other direction within a time interval of about 1 ms. The transitions from the fluorescence-off to the fluorescence-on state were not studied in detail, since it was not possible to tell from the 194 nm fluorescence whether a particular transition resulted from the emission of a 198 or 282 nm photon.

Data were obtained also with two Hg^+ ions, separated by approximately 3 μm. The 194 nm fluorescence switched among three distinct levels, depending on whether 0, 1, or 2 ions were in a metastable level. Discriminator levels were set to distinguish among the three different states. The time resolution was 2 ms. Each downward quantum jump was assumed to indicate the emission of an 11 μm photon from one of the ions. With an imaging photon-detector,[17] one could determine which ion had emitted the photon.

Figure 2 shows observed and calculated plots of $g^{(2)}(\tau)$ for (a) one ion and (b) two ions. The two-ion calculation was based on the assumption that photon emissions from one ion were not correlated with those from the other one. In that case, $g_2^{(2)}(\tau)=\frac{1}{2}[1+g_1^{(2)}(\tau)]$, where the subscript indicates the number of ions. The agreement of the experimental and calculated curves is an indication that the ions were independent, for time scales greater than about 2 ms. The values of γ_0 were about 15 s^{-1} for the one-ion data and about 12 s^{-1} for the two-ion data.

If the ions are independent and are subjected to the same 194 nm radiation field, then certain relationships hold among the probabilities p_0, p_1, and p_2 for zero, one, or two ions to be in the fluorescence-on state. Let p_{on} and $p_{off}=1-p_{on}$ be the probabilities for a single ion to be in the fluorescence-on or the fluorescence-off state. Then, $p_0=(p_{off})$,^{2} $p_1=2p_{on}p_{off}$, and $p_2=(p_{on})$.^{2} If the transitions of the ions were correlated in some way, then deviations from these relationships might occur. For a particular 100 s run, the measured values were $p_0=0.1836$, $p_1=0.4887$, and $p_2=0.3277$. For a value of $p_{on}=0.57224$, obtained by least-squares adjustment, the calculated values are $p_0=0.1830$, $p_1=0.4896$, and $p_2=0.3275$. Similarly good agreement was obtained for the other runs.

Another test of the independence of the two ions was a comparison of the number of apparent double quantum jumps to the number that would be expected from random coincidences, given the finite time resolution of the apparatus. In 400 s of two-ion data, 11 double quantum jumps and 5649 single quantum jumps downward in fluorescence were noted. Data generated by a Monte Carlo simulation, in which the two ions were independent, were analyzed in the same way. The simulated data had 15 double quantum jumps and 5430 single quantum jumps. Thus, the rate of double quantum jumps was consistent with independence of the two ions.

The experimental probability $P_n(\Delta t)$ of detecting n 11 μm photons in a period Δt can be derived from the quantum-jump data, where Δt is any integer multiple of the experimental time resolution. Mandel's Q parameter,[18] which measures the deviation of the distribution from Poisson statistics, is

$$Q=(\sigma^2-\langle n\rangle)/\langle n\rangle\,, \tag{6}$$

where σ^2 and $\langle n\rangle$ are the variance and the mean of the distribution. Negative values of Q indicate sub-Poissonian statistics. The theoretical value of Q is[18]

$$Q=\frac{2N}{T\Delta t}\int_0^{\Delta t}dt'\int_0^{t'}d\tau[g^{(2)}(\tau)-1]\,, \tag{7}$$

where N and T are the total number of photons emitted and the total time. Figure 3(a) shows $P_n(\Delta t)$ for one ion, with $\Delta t=200$ ms and $T=400$ s. The Poisson distribution for the same mean ($\langle n\rangle=1.45$) is also shown. For this data set, the measured value of Q, calculated from Eq. (6), is -0.253 ± 0.025; the theoretical value obtained by inserting $g^{(2)}(\tau)$ into Eq. (7) is -0.242. Figure 3(b) shows $P_n(\Delta t)$ for two ions, with $\Delta t=200$ ms, and $T=400$ s. The measured value of Q is -0.242 ± 0.025; the theoretical value is -0.243. The Poisson distribution for the same mean ($\langle n\rangle=2.84$) is also shown. Previous measurements of Q in single atoms have yielded the values -2.52×10^{-3} (Ref. 4) and -7×10^{-5} (Ref. 3). The value observed here is larger because the detection efficiency is greater.

It should be pointed out that the 11 μm photons have not been observed directly. Rather, their existence has been inferred from observations of the 194 nm fluorescence and the density-matrix equations. The 194 nm field does not itself display nonclassical properties, except on time scales of the order of the $^2P_{1/2}$ radiative lifetime, which we do not observe. Other measurements of photon antibunching[1-3] and sub-Poissonian photon statistics[3-7] require fewer assumptions about the nature of the emitter.

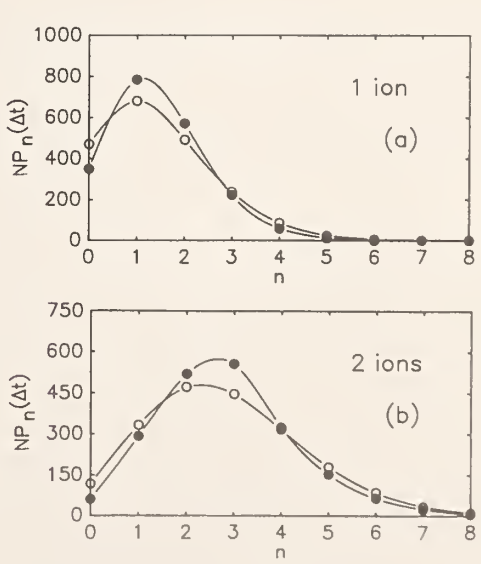

FIG. 3. Plots of the distributions of the numbers of 11-μm photons emitted in 200-ms time intervals from (a) one Hg^+ ion and (b) two Hg^+ ions. The filled circles represent experimental data. The open circles represent Poissonian distributions with the same means as the experimental distributions.

The basic elements of the density-matrix equations have, however, been confirmed by the agreement between the calculated radiative decay rates and the rates deduced from the quantum-jump data,[12] and we are confident in applying them to the present experiment.

We wish to acknowledge support from the U.S. Air Force Office of Scientific Research and the U.S. Office of Naval Research. We acknowledge helpful comments from L. Mandel. We wish to thank F. Diedrich and J. Cooper for carefully reading the manuscript.

---

[1]H. J. Kimble, M. Dagenais, and L. Mandel, Phys. Rev. Lett. **39**, 691 (1977); M. Dagenais and L. Mandel, Phys. Rev. A **18**, 2217 (1978).

[2]F.-M. Rateike, G. Leuchs, and H. Walther, results cited by J. D. Cresser, J. Häger, G. Leuchs, F.-M. Rateike, and H. Walther, in *Dissipative Systems in Quantum Optics,* edited by R. Bonifacio, Topics in Current Physics, Vol. 27 (Springer, Berlin, 1982), p. 21.

[3]F. Diedrich and H. Walther, Phys. Rev. Lett. **58**, 203 (1987).

[4]R. Short and L. Mandel, Phys. Rev. Lett. **51**, 384 (1983).

[5]M. C. Teich and B. E. A. Saleh, J. Opt. Soc. Am. B **2**, 275 (1985).

[6]J. G. Rarity, P. R. Tapster, and E. Jakeman, Opt. Commun. **62**, 201 (1987).

[7]*Squeezed States of the Electromagnetic Field,* edited by H. J. Kimble and D. F. Walls [J. Opt. Soc. Am. B **4**, No. 10 (1987)].

[8]Th. Sauter, R. Blatt, W. Neuhauser, and P. E. Toschek, Opt. Commun. **60**, 287 (1986).

[9]M. Lewenstein and J. Javanainen, Phys. Rev. Lett. **59**, 1289 (1987).

[10]J. C. Bergquist, R. G. Hulet, W. M. Itano, and D. J. Wineland, Phys. Rev. Lett. **57**, 1699 (1986).

[11]See, for example, D. Meschede, H. Walther, and G. Müller, Phys. Rev. Lett. **54**, 551 (1985); R. G. Hulet, E. S. Hilfer, and D. Kleppner, *ibid.* **55**, 2137 (1985); W. Jhe, A. Anderson, E. A. Hinds, D. Meschede, L. Moi, and S. Haroche, *ibid.* **58**, 666 (1987).

[12]W. M. Itano, J. C. Bergquist, R. G. Hulet, and D. J. Wineland, Phys. Rev. Lett. **59**, 2732 (1987).

[13]P. Eriksen and O. Poulsen, J. Quant. Spectrosc. Radiat. Transfer **23**, 599 (1980).

[14]J. C. Bergquist, D. J. Wineland, W. M. Itano, H. Hemmati, H.-U. Daniel, and G. Leuchs, Phys. Rev. Lett. **55**, 1567 (1985).

[15]C. E. Johnson, Bull. Am. Phys. Soc. **31**, 957 (1986).

[16]H. J. Kimble, R. J. Cook, and A. L. Wells, Phys. Rev. A **34**, 3190 (1986).

[17]D. J. Wineland, J. C. Bergquist, W. M. Itano, J. J. Bollinger, and C. H. Manney, Phys. Rev. Lett. **59**, 2935 (1987).

[18]L. Mandel, Opt. Lett. **4**, 205 (1979).

Reprinted from Journal of the Optical Society of America B, Vol. 2, page 1721, November 1985
Copyright © 1985 by the Optical Society of America and reprinted by permission of the copyright owner.

Angular momentum of trapped atomic particles

D. J. Wineland, J. J. Bollinger, Wayne M. Itano, and J. D. Prestage

Time and Frequency Division, National Bureau of Standards, Boulder, Colorado 80303

Received April 10, 1985; accepted July 23, 1985

In axially symmetric atomic-particle traps, the angular momentum of the particles about the symmetry axis is conserved in the absence of external torques. Changes in this angular momentum owing to laser scattering are discussed.

1. INTRODUCTION

By now, one has become fairly familiar with the idea that the momentum carried by light can be transferred to atomic (or macroscopic) particles, thereby significantly altering the velocity distribution of these particles. The status of experiment and theory will be discussed in the accompanying papers of this issue; further information can be found in other recent papers.[1–3]

In the experiments on atomic deflection and laser cooling, one is concerned primarily with the changes in linear mechanical momentum imparted to the particles by light. However, for the case of trapped particles, one must in general be concerned with the angular momentum of the trapped particles and therefore with the changes in angular momentum of the trapped particles by light. The situation discussed in this paper is illustrated in Fig. 1. If the trap (trapping fields are not shown) is symmetric about a particular axis, here assumed to be the z axis, then one would expect the z component of angular momentum of the particles, L_z, to be conserved in the absence of laser scattering. Here, L_z is the total canonical angular momentum given by

$$L_z = \sum_{i=1}^{N} l_{zi} = \sum_{i=1}^{N} (\mathbf{x}_i \times \mathbf{p}_i)_z, \tag{1a}$$

$$\mathbf{p}_i = m_i \mathbf{v}_i + q_i \mathbf{A}(\mathbf{x}_i)/c, \tag{1b}$$

where l_{zi}, $\mathbf{p}_i$, m_i, q_i, $\mathbf{x}_i$, and $\mathbf{v}_i$ are the z component of angular momentum, the linear momentum, mass, charge, position, and velocity of the ith particle, respectively; N is the number of particles; c is the speed of light; and $\mathbf{A}$ is the vector potential. From the geometry of Fig. 1, it is clear that the laser scattering can be used to increase $|L_z|$ indefinitely, *independently of the laser tuning*. This effect would be interesting to study, but of course in experiments employing laser cooling it is clearly a situation to be avoided. In practice, changes in angular momentum will also be influenced by various mechanisms, such as collisions with background gas and deviations of the trap from axial symmetry.

Assuming that the laser beam is perpendicular to $\hat{z}$, the magnitude of the average change of mechanical angular momentum per photon-scattering event is given by $\hbar d/\lambda$, where d is the distance of the laser beam from the z axis, $\hbar$ is Planck's constant, and λ is the wavelength of the photons. Changes in the internal angular momentum of atomic particles will be of order $\hbar$. Typically, $2\pi d/\lambda \gg 1$; therefore we will neglect the internal angular momentum of the particles. As in previous treatments,[4,5] for simplicity we will neglect second-order relativistic effects and saturation. We will also assume that the collision rate between trapped particles is high enough and the laser scattering rate low enough that the particles can be assumed to be in thermal equilibrium. These conditions may be violated, but the qualitative features of the problem should still apply.

To make the problem more tractable, we will discuss only angular-momentum effects in ion traps, specifically, the rf (Paul) and Penning traps.[6–11] This seems reasonable, since many experiments have been done with these traps. The qualitative features of these traps should carry over to neutral traps. The primary difference would seem to arise from the absence of long-range Coulomb repulsion between particles and the fact that the field momentum that is due to the ions' net charge [vector-potential term in Eq. (1)] is absent. Finally, in this paper angular-momentum changes are assumed to arise from laser scattering, background gas, and trap asymmetries; however, such effects may come from scattering by particle beams,[12] positive or negative feedback on the charged-particle motions,[12,13] or angular-momentum transfer from plasma waves.[14,15]

In Section 2, we will assume that ion trapping is accomplished by a combination of rf and Penning traps. For such a combined trap, single-particle trajectories have been discussed by others[9–11]; here we will use the pseudopotential approach.[6,7,9–11] Assuming that the ion cloud (or nonneutral plasma[13–15]) rotates at a frequency ω about a particular symmetry axis, we derive relations between ω and the ion cloud's density, potential, dimensions, and angular momentum. These expressions can then be applied to the rf or the Penning trap in various limits. In Section 3 we discuss torques applied to the cloud from laser scattering for a particular ion-cloud–laser-beam interaction geometry. Background-gas damping is discussed in Section 4. Changes in angular momentum owing to trap asymmetries are treated separately for the rf and the Penning traps in Sections 5 and 6, respectively. Finally, in Section 7, we make a few remarks about angular momentum in neutral-particle traps.

0740-3224/85/111721-10$02.00 © 1985 Optical Society of America

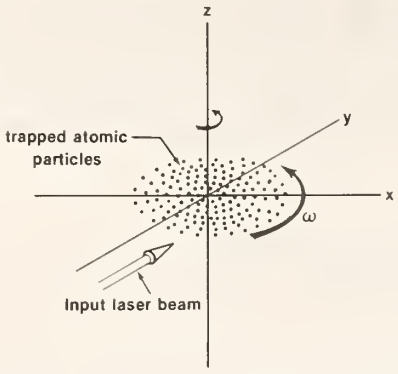

Fig. 1. Schematic representation of trapped atomic particles. The trap (not shown) is assumed to have axial symmetry about the z axis. If a laser beam is directed parallel to the y axis but does not intersect the z axis, then atomic particle–photon scattering imparts angular momentum (L_z) to the sample, which can cause it to spin about the z axis.

2. ION TRAPS

For further simplicity, we will assume idealized models for the rf and Penning traps and assume only one trapped ion species. Both traps use axially symmetric electrodes whose surfaces are figures of revolution (hyperboloids of revolution) as shown in Fig. 2. For rf trapping, when the drive (micromotion) frequency Ω is much larger than secular frequency ω_x, ω_y, or ω_z (defined in Section 5), the ions can be considered to be confined in the axially symmetric pseudopotential[6–11] of the form

$$\phi_T(r, z) = \alpha r^2 + \beta z^2, \tag{2}$$

where r and z are cylindrical coordinates and α and β are functions of the trapping parameters:

$$\alpha = qV_0^2/m\Omega^2\xi^4 - U_0/\xi^2, \tag{3a}$$

$$\beta = 4qV_0^2/m\Omega^2\xi^4 + 2U_0/\xi^2. \tag{3b}$$

V_0 is the amplitude of the rf voltage, U_0 is the amplitude of the dc voltage applied between the ring and the end caps (here, U_0 positive means that the end caps are at higher potential than the ring electrode), and $\xi^2 = r_0^2 + 2z_0^2$, where r_0 and z_0 are defined in Fig. 2. We note that the pseudopotential [the first terms in Eqs. (3a) and (3b)] always acts to give a radially inward force (independent of the sign of q) while the force that is due to the dc applied potential can be in either direction. For the rf trap we want $q\alpha$, $q\beta > 0$; the resulting potential well is equivalent to that provided by a uniform-background charge distribution whose boundary is an ellipsoid of revolution.[16] From Poisson's equation, $\nabla^2\phi = -4\pi\rho$, we see that the density inside this fictitious charge distribution is given by $\rho' = -(2\alpha + \beta)/2\pi$. The potential for the Penning trap[6,7] is usually given by Eqs. (2) and (3) with $V_0 = 0$; in this case a magnetic field $\mathbf{B} = B_0\hat{z}$ is required for trapping. For the sake of generality we will assume that $B_0 \neq 0$ and $V_0 \neq 0$ except where noted below.

The traps have symmetry about z, and, therefore, in the absence of external torques, L_z is conserved. In this case, the ion canonical angular momentum and ion energy enter the thermal-equilibrium distribution function on an equal basis. The thermal-equilibrium distribution function can be written as[17–19]

$$f = n_0\left(\frac{m}{2\pi k_B T}\right)^{3/2} \exp[-(H - \omega l_z)/k_B T], \tag{4}$$

where

$$H = mv^2/2 + q\phi(\mathbf{x}) \tag{5a}$$

is the ion energy and

$$l_z = mv_\theta r + qA_\theta(\mathbf{x})r/c \tag{5b}$$

is the ion canonical angular momentum. m, q, and $\mathbf{v}$ are the ion mass, charge, and velocity, and $v = |\mathbf{v}|$. v_θ and A_θ are the θ components of the velocity and the vector potential, and r is the radial coordinate of the ion in cylindrical coordinates. $\phi = \phi_I + \phi_T + \phi_{\text{ind}}$ is the total potential, which is written as the sum of the potential that is due to ion space charge ϕ_I, the applied trap potential ϕ_T, and the potential ϕ_{ind} that is due to the induced charges on the trap electrodes. n_0, T, and ω are determined by the total number of ions, energy, and angular momentum of the system, and k_B is Boltzmann's constant. We choose the symmetric gauge where $\mathbf{A}(\mathbf{x}) = \mathbf{B} \times \mathbf{x}/2$, so that $A_\theta = Br/2$. We can therefore write the distribution function as[19]

$$f(\mathbf{x}, \mathbf{v}) = n(\mathbf{x})\left(\frac{m}{2\pi k_B T}\right)^{3/2} \exp[-\tfrac{1}{2}m(\mathbf{v} - \omega r\hat{\theta})^2/k_B T], \tag{6a}$$

where $n(\mathbf{x})$ is the ion density given by

$$n(\mathbf{x}) = n_0 \exp\left\{-\left[q\phi(r, z) - \tfrac{1}{2}m\omega\left(\frac{q}{|q|}\Omega_c + \omega\right)r^2\right]\Big/k_B T\right\}. \tag{6b}$$

We assume that the trap potential is adjusted to make $\phi = 0$ at the origin, in which case n_0 is the ion density at the center of the trap. $\Omega_c = |qB/mc|$ is the cyclotron frequency. With the assumption that $v \ll c$, we have neglected the diamagnetic correction to the magnetic field that is due to the motion of the ions. For densities near the maximum density (discussed below) this assumption may break down for electrons.

Equations (6) have been analyzed for the case of electrons in a Penning-type geometry (axially symmetric but nonquadratic trap potential).[18,19] We can easily extend the analysis of Refs. 18 and 19 to the hyperbolic Penning and rf traps. The distribution function is a Maxwellian velocity distribu-

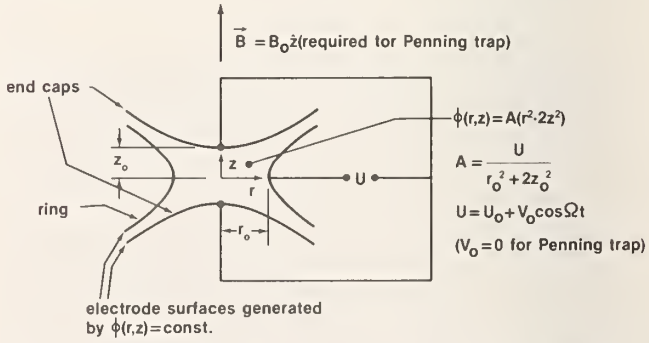

Fig. 2. Schematic representation of the electrode configuration for the Paul (rf) or Penning trap. Electrode surfaces are figures of revolution about the z axis and are equipotentials of $\phi(r, z) = A(r^2 - 2z^2)$ (cylindrical coordinates are used with the origin at the center of the trap). Typical dimensions are $\sqrt{2}z_0 = r_0 \cong 1$ cm. Typical operating parameters are the following: for the Paul trap, $V_0 = 300$ V, $\Omega/2\pi \cong 1$ MHz; for the Penning trap, $U_0 \cong 1$ V, $B \cong 1$ T.

tion superimposed upon a rigid rotation of frequency ω [positive (negative) values of ω denote rotation in the $+(-)$ θ direction]. For the Penning trap, this rotation is caused by the $\mathbf{E} \times \mathbf{B}$ drift and the pressure-gradient-induced drift [similar to $\mathbf{E} \times \mathbf{B}$ drift, where the term $(\partial n/\partial r)\hat{r}$ must be included with $E_r\hat{r}$].[20] In thermal equilibrium, these two effects in combination give rise to a rotation that is constant with radius. If the rotation is not rigid, then shear exists in the cloud; the resulting friction forces drive the cloud to thermal equilibrium. We emphasize that rigid rotation does not require a quadratic trap potential but only axial symmetry and thermal equilibrium. From the expression for the ion density, we arrive at Poisson's equation:

$$\frac{1}{r}\frac{\partial}{\partial r}\left(r\frac{\partial\phi}{\partial r}\right)+\frac{\partial^2\phi}{\partial z^2}=-4\pi q n_0$$

$$\times\exp\left\{-\left[q\phi-\tfrac{1}{2}m\omega\left(\frac{q}{|q|}\Omega_c+\omega\right)r^2\right]\Big/k_BT\right\}-4\pi\rho', \quad (7)$$

where we must include the fictitious charge density, ρ', from the pseudopotential. In Ref. 19 it was shown that the general solution to Poisson's equation leads to axially symmetric ion densities that are constant out to a certain radius and then fall to zero in a universal way in a distance approximately equal to the Debye length, λ_D, given for a nonneutral plasma by

$$\lambda_D{}^2 = k_BT/4\pi n_0q^2. \quad (8)$$

Although Ref. 19 specifically dealt with electrons in a Penning-type trap, Poisson's equation looks essentially the same for the rf trap, and therefore the general conclusion above is valid for both cases. (Recall that we are neglecting the micromotion.) Specific solutions are discussed in Ref. 19 for the Penning-type geometry and in Ref. 21 for the rf geometry.

As an example, for $T = 300$ K and $n_0 = 10^7/\text{cm}^3$, we have $\lambda_D \cong 0.38$ mm. At higher densities and lower temperatures, the general features of the density distribution noted above have been directly observed in Penning-type traps.[22,23] At higher temperatures and lower densities (where space charge becomes negligible and $\lambda_D \geqq$ ion-cloud dimensions) the density distributions become Gaussian; this has been directly observed in rf traps.[24,25]

Because of the laser-cooling experiments, it is interesting to consider the limiting case when $\lambda_D \ll$ cloud dimensions, i.e., when $T \to 0$. From the right-hand side of Eq. (6b), we can see that in the cloud interior, $q\phi - m(\Omega_cq/|q| + \omega)\omega r^2/2 \to 0$ in order for the density to be finite. Therefore, in the interior we have

$$\phi = \phi_I + \phi_T + \phi_{\text{ind}} = m\omega(\Omega_cq/|q| + \omega)r^2/2q. \quad (9)$$

The lack of z dependence in ϕ is to be expected since at low temperatures the outward z force from space charge would be expected just to cancel the restoring z force of the trap. In the case when the trap potential is quadratic [Eq. (2)], Eq. (9) can be written as

$$\phi_I = [m\omega(\Omega_cq/|q| + \omega)/2q - \alpha]r^2 - \beta z^2 - \phi_{\text{ind}} \quad (10a)$$

$$= -\tfrac{2}{3}\pi q n_0(ar^2 + bz^2) - \phi_{\text{ind}}, \quad (10b)$$

where Eq. (10b) is used to define a and b. From Poisson's equation, $2a + b = 3$. For a stable cloud of finite size, we must have $a, b > 0$; otherwise the ions are not confined. If the potential from the induced charges can be assumed constant over the ion cloud (this approximation is valid if the cloud's dimensions are small compared with r_0 and z_0), then ϕ_I is the potential distribution for a uniformly charged ellipsoid of revolution[23] of density n_0 whose spatial extent along the z axis we define as $2z_{\text{cl}}$ and whose diameter in the $z = 0$ plane we define as $2r_{\text{cl}}$. For simplicity we will therefore assume that ϕ_{ind} is constant over the ion cloud. If the dimensions and density of the ion cloud are large enough so that ϕ_{ind} is not constant over the ion cloud, then the cloud becomes elongated along z and expanded near the $z = 0$ plane.

For $a = b = 1$ the ion cloud is a sphere (i.e., $z_{\text{cl}} = r_{\text{cl}}$). For $a > 1 > b$ the cloud is a prolate ellipsoid ($z_{\text{cl}} > r_{\text{cl}}$), where[16,26]

$$a = k_p'\{1/[2(1-k_p{}^2)] - \ln[(1+k_p)/(1-k_p)]/4k_p\}, \quad (11a)$$

$$b = k_p'\{\ln[(1+k_p)/(1-k_p)]/2k_p - 1\}, \quad (11b)$$

and where $k_p = [1 - (r_{\text{cl}}/z_{\text{cl}})^2]^{1/2}$ and $k_p' = 3(1-k_p{}^2)/k_p{}^2$. For $a < 1 < b$ the cloud is an oblate ellipsoid ($r_{\text{cl}} > z_{\text{cl}}$), where

$$a = k_0'[\sin^{-1}(k_0)/2k_0 - (1-k_0{}^2)^{1/2}/2], \quad (12a)$$

$$b = k_0'[(1-k_0{}^2)^{-1/2} - \sin^{-1}(k_0)/k_0], \quad (12b)$$

and where $k_0 = [1 - (z_{\text{cl}}/r_{\text{cl}})^2]^{1/2}$ and $k_0' = 3(1-k_0{}^2)^{1/2}/k_0{}^2$.

From Eq. (10a) and Poisson's equation, we can express n_0 as a function of ω and the trapping potentials:

$$n_0(\omega,\alpha,\beta) = \frac{m}{2\pi q^2}\left[-\omega(\Omega_cq/|q| + \omega) + \frac{q}{m}(2\alpha+\beta)\right]. \quad (13)$$

For the pure Penning trap, where $V_0 = 0$ and $2\alpha + \beta = 0$, we obtain the result of Ref. 23. The usual case for the rf trap is with $\Omega_c, \omega = 0$, and we obtain the result of Refs. 6 and 7. In practice, the minimum temperature and therefore the maximum density in an rf trap might be limited by rf heating,[24,27,28] where the condition $\lambda_D \ll r_{\text{cl}}, z_{\text{cl}}$ may not be obtained. If α and β are assumed fixed we find that the density is maximum when $\omega = -\Omega_cq/2|q|$:

$$n_0(\text{max}) = \frac{m}{2\pi q^2}\left[\Omega_c{}^2/4 + \frac{q}{m}(2\alpha+\beta)\right]. \quad (14)$$

For the pure Penning trap ($2\alpha + \beta = 0$), we find[7,29] that $n_0(\text{max}) = B_0{}^2/8\pi mc^2$. Also, the parameter a of Eq. (10b) is largest (i.e., $z_{\text{cl}}/r_{\text{cl}}$ is largest) for $\omega = -\Omega_cq/2|q|$. For the pure rf trap ($\Omega_c = 0$), this implies that $\omega = 0$ as expected, since spinning in either direction causes a centrifugal distortion that tends to make the ellipsoid more oblate. Equation (13) can be used to find ω if we assume that the cloud has a certain density n_0. We find that

$$\omega = -\Omega_cq/2|q| \pm [(\Omega_c/2)^2 + q(2\alpha+\beta-2\pi qn_0)/m]^{1/2}. \quad (15)$$

In the pure Penning trap ($2\alpha + \beta = 0$), the solution for which $|\omega| < \Omega_c/2$ can be identified with the $\mathbf{E} \times \mathbf{B}$ drift magnetron motion and the solution for which $|\omega| > \Omega_c/2$ can be identified with the cyclotron frequency that is shifted by the radial electric field (see Section 6). For $n > n_0(\text{max})$ the ion orbits in the Penning trap are exponentially increasing.[7]

We note that Eq. (15) is not valid in the limit of a single ion, where one may want to substitute $n_0 \to 0$. Implicit in

Eq. (15) is the assumption that the axial force on an ion is zero. Equivalently, we assume that the cloud consists of many ions and that $\lambda_D \ll r_{cl}, z_{cl}$. In the limit of one ion in the trap, the axial force on an ion is due to the applied trapping fields (zero only at trap center). In addition, the requirement that $a > 0$ for clouds of finite size restricts the density n_0 to be greater than a minimum density given by $n_0(\min) = \beta/2\pi q$. At this minimum density, $a = 0$, and the cloud has infinite extent in the $z = 0$ plane. The requirement that $a > 0$ also restricts ω to values ranging from $\omega = -q\Omega_c/2|q| - [(\Omega_c/2)^2 + 2q\alpha/m]^{1/2}$ to $\omega = -q\Omega_c/2|q| + [(\Omega_c/2)^2 + 2q\alpha/m]^{1/2}$.

Finally, we can evaluate L_z for an ellipsoidal cloud of ions to find

$$L_z = n_0 \int_V \left[mr^2\omega + r\frac{q}{c}A_\theta(r) \right] d^3\mathbf{x}$$

$$= \frac{2}{5} Nm(\Omega_c q/2|q| + \omega) r_{cl}^2, \quad (16)$$

where $\int_V d^3\mathbf{x} = 4\pi r_{cl}^2 z_{cl}/3$ is the cloud volume.

A convenient dividing line between rf and Penning traps would seem to be when the radial electric force is absent, i.e., $\alpha = 0$. Therefore, in what follows, we will define the rf-trap mode as the case when the radial force that is due to the electric trapping fields is inward ($q\alpha > 0$) and the Penning-trap mode as the case when the radial force that is due to the electric trapping fields is outward ($q\alpha < 0$).

3. LASER SCATTERING

The problem that we wish to investigate is whether it is possible to observe angular-momentum changes induced by laser scattering in an ion cloud. For brevity, we will consider only a laser-beam/ion-cloud geometry in which these effects might be fairly strong; other interaction geometries could be similarly treated.

Consider the case of Fig. 3. We will assume that the spatial width of the laser beam is small compared with r_{cl} and z_{cl} and small enough that we can neglect the variation in first-order Doppler shift across the beam that is due to the cloud rotation. If the cloud is in thermal equilibrium, then ω is constant over the cloud; therefore the average y velocity of ions within the laser beam is $v_y = \omega r \cos\theta = \omega d$. For simplicity, we will assume that $|\omega| \ll \gamma$, where γ is the natural linewidth of the atomic transition to which the laser is nominally tuned. In this limit, photon scattering may be assumed to occur at an instant of time, and the momentum imparted to an ion is given by $\Delta\mathbf{p} = \hbar(\mathbf{k} - \mathbf{k}_s)$, where $\mathbf{k}$ and $\mathbf{k}_s$ are the photon wave vectors of the incident and scattered photons ($|\mathbf{k}| = |\mathbf{k}_s| = 2\pi/\lambda$).[4,5] Therefore the average torque from laser scattering is given by

$$T_L = \left\langle \frac{dL_z}{dt} \right\rangle_L = \int \frac{I(\mathbf{x})}{h\nu} \sigma(\mathbf{k}\cdot\mathbf{v}, T) \frac{h}{\lambda} dn(\mathbf{x}) d^3\mathbf{x}, \quad (17a)$$

where $I(\mathbf{x})$ is the intensity (power per unit area) of the laser beam, σ is the photon-scattering cross section, and $n(\mathbf{x})$ is the ion density. In the derivation of Eq. (17a), we have averaged over all angles of the reemitted photon. In general, the angular distribution of reemitted photons will not be isotropic [e.g., see Eqs. (8a) and (8b) of Ref. 5], but the torque that is due to photon reemission when averaged over angles will be zero, neglecting small relativistic corrections.[4] In the limit that the laser-beam dimensions are small compared with r_{cl}, z_{cl}, and d, and the density is nearly constant over the cloud ($\lambda_D \ll z_{cl}, r_{cl}$), then Eq. (17a) becomes

$$T_L = \left\langle \frac{dL_z}{dt} \right\rangle_L = \hbar 4\pi \dot{N}_L n_0 \sigma(v_y, T) d(r_{cl}^2 - d^2)^{1/2}/\lambda, \quad (17b)$$

where $\dot{N}_L$ is the number of incident laser photons per second and we note that σ has a line shape given in general by a Voigt profile[30] that is first-order Doppler shifted by a frequency $\omega d/\lambda$. As we noted earlier, if there is no damping, $|\langle L_z \rangle|$ will eventually increase. In principle the parameter a [Eq. (10b)] goes to zero; of course the edge of the cloud would touch the ring electrode before this condition is reached.

In practice, damping of $\langle L_z \rangle$ must be considered; it appears that this should come primarily from two sources: background neutral gas and imperfections in the trap electrodes that destroy axial symmetry and therefore prevent $\langle L_z \rangle$ conservation. Motional radiation damping should also be considered for electrons,[13,27,31] but this is expected to be a much weaker effect for ions. (In any case it would mimic background-gas damping.) Background-gas damping should occur in a similar way for the rf and Penning traps. However, since changes in L_z owing to trap asymmetries are expected to be qualitatively different for the two traps, they are treated separately.

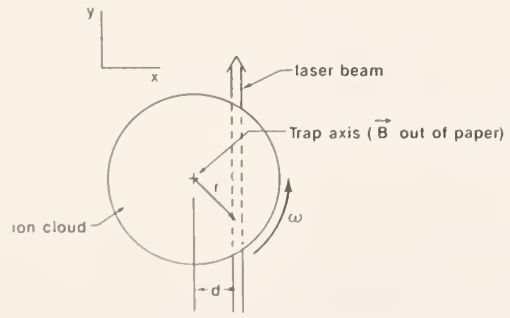

Fig. 3. Laser beam ion cloud interaction geometry. The laser beam is assumed to be in the $z = 0$ plane; the radius of the ion cloud is r. For the rf trap, laser scattering will tend to cause the cloud to spin in the direction shown. For the Penning trap, the direction of rotation shown ($\alpha > 0$) is appropriate for negative ions; for positive ions the rotation is reversed ($\alpha < 0$).

4. BACKGROUND-GAS DAMPING

An estimate of background-gas damping can be derived from measurements of ion mobility. The mobility K is defined[32] from the expression $v_d = KE$, where E is the electric field impressed on the ions in a drift experiment and v_d is the average drift velocity of the ions through some background gas. The drifting ions impart momentum to the gas at a rate

$$\frac{dp}{dt} = F = qE = qv_d/K. \quad (18)$$

Therefore, for the case of trapped ions, the torque that damps ion rotation is

$$\langle T_{bkg} \rangle = N\langle r dp/dt \rangle = -Nq\langle r^2\omega \rangle/K = -N\frac{2}{5}\frac{q}{K} r_{cl}^2 \omega, \quad (19)$$

where the last equality is valid in the low-temperature limit, $\lambda_D \ll r_{cl}, z_{cl}$.

5. rf TRAP ($q\alpha > 0$)

We can get an idea of the magnitude of the change of L_z that is due to trap asymmetries by assuming that the pseudopotential has the form

$$\phi_T(r, z) = \alpha r^2 + \beta z^2 + \epsilon(x^2 - y^2). \tag{20}$$

Assuming $\mathbf{B} = 0$, a single ion in this trap has the characteristic motions

$$x = x_1 \cos(\omega_x t + \theta_x),$$

$$y = y_1 \cos(w_y t + \theta_y), \qquad z = z_1 \cos(\omega_z t + \theta_z), \tag{21a}$$

where the frequencies ω_x, ω_y, and ω_z are given by

$$\omega_x^2 = 2q(\alpha + \epsilon)/m, \qquad \omega_y^2 = 2q(\alpha - \epsilon)/m, \qquad \omega_z^2 = 2q\beta/m. \tag{21b}$$

For $|\epsilon| \ll |\alpha|$, an ion initially in a nearly circular orbit defined by $x = \zeta \sin \omega_x t$, $y = \zeta \cos \omega_y t$ will find itself in a circular orbit of opposite sense after a time $\pi/|\omega_x - \omega_y|$. Hence, in this case, we estimate

$$T_\epsilon = \left\langle \frac{dL_z}{dt} \right\rangle_\epsilon \cong -L_z/\tau, \qquad \tau = \pi/2|\omega_x - \omega_y|. \tag{22}$$

For a cloud of ions we could expect approximately the same dephasing time if space charge could be neglected, i.e., the ions behave independently. For a "cold" cloud, where the trapping force is essentially canceled by space charge, the situation is quite different. If we neglect ion–ion collisions, then ions drift through the cloud (which is now ellipsoidal in the x–y plane) and reflect from the edge of the ion-charge distribution. However, as an estimate we will still assume the validity of Eq. (22), where ω_x and ω_y are given by the free-space values of Eqs. (21).

To determine if spinning of the cloud induced by a laser beam could be observed, we have experimentally investigated a cloud of $^{198}Hg^+$ ions confined in a small rf trap.[33] In this experiment $r_0 = 455\ \mu m$, $z_0 = 322\ \mu m$, $\Omega/2\pi = 20$ MHz, $V_0 = 400$ V, and $U_0 = -12$ V. For a single ion in this approximately spherical well ($\alpha \cong \beta$) we would expect the secular frequency $\omega_z \cong \omega_x = \omega_y = (2q\alpha/m)^{1/2} = (2\pi)1.19$ MHz. For typical conditions, where $r_{cl} = 30\ \mu m$, $d = 15\ \mu m$, laser-beam waist size $\omega_0 = 15\ \mu m$, and laser wavelength $\lambda = 194$ nm ($^2S_{1/2} \rightarrow {}^2P_{1/2}$ transition), we can ask under what conditions we would expect the cloud to spin at a frequency $\omega = (2\pi)0.5$ MHz. We choose this frequency because the corresponding first-order Doppler shift along the beam direction is about 250 MHz, which would be easily observable on the $^2S_{1/2} \rightarrow {}^2P_{1/2}$ transition. If we assume that $\lambda_D \ll r_{cl}, z_{cl}$, then we can use Eq. (13) to obtain $n_0 \cong 1.68 \times 10^{10}/cm^3$. The ions are observed[33] to be near room temperature (through the Doppler width on the $^2S_{1/2} \rightarrow {}^2P_{1/2}$ transition); hence we calculate that $\lambda_D = 9.2\ \mu m$, and thus Eq. (13) should give a reasonable estimate of the density. From Eqs. (10) and (12) we then find that $z_{cl} \cong 25.8\ \mu m$. In Eq. (17b) we write $\dot{N}_L \sigma = \dot{N}_s \pi \omega_0^2$, where $\dot{N}_s = \dot{N}_L \sigma/\pi\omega_0^2$ is the scatter rate per ion (for ions in the laser beam). We can then combine Eqs. (17b), (19), and (22) to obtain in steady state

$$\left\langle \frac{dL_z}{dt} \right\rangle_{Total} = (T_L + T_{bkg} + T_\epsilon) = 0. \tag{23}$$

For our specific example ($\omega/2\pi = 0.5$ MHz) we find that

$$\hbar[\dot{N}_s \times 3.0 \times 10^5 - n(\mathrm{He}) \times 5.3 \times 10^{-2} - \Delta\nu_{xy} \times 2.3 \times 10^{10}] = 0, \tag{24}$$

where we have assumed that the background gas is helium of density n(He) ($K = 19.6\ cm^2\ V^{-1}\ sec^{-1}$ at standard pressure[34]) and we define $\Delta\nu_{xy} = |\omega_x - \omega_y|/2\pi$. If we first assume that the pressure of helium gas is small and $\Delta\nu_{xy} \cong 1$ kHz, we require that $\dot{N}_s \cong 7.7 \times 10^7$/sec (close to saturation) in order to spin the cloud at $\omega/2\pi = 0.5$ MHz. For the more typical scatter rates in this experiment, $\dot{N}_s \lesssim 10^6$/sec, we require that $\Delta\nu_{xy} \lesssim 13$ Hz in order to see the same ω. This would require a very small trap asymmetry in order for the effect to be seen, and in fact no spinning above $|\omega| = (2\pi)50$ kHz was observed, implying that $\Delta\nu_{xy} \gtrsim 130$ Hz for $\dot{N}_s = 10^6$/sec. Note that if $\Delta\nu_{xy} = 0$ and p(He) $= 6.65 \times 10^{-3}$ Pa (5×10^{-5} Torr), we need $\dot{N}_s \cong 3.1 \times 10^5$ to obtain $|\omega| = (2\pi)0.5$ MHz. Since $\dot{N}_s \gtrsim 3 \times 10^5$/sec and the helium pressure was less than 6.7×10^{-3} Pa in these experiments, we could determine that the lack of spinning was not due to background-gas damping.

We might expect to see a smaller dephasing (i.e., $\Delta\nu_{xy}$ smaller) for traps with weaker pseudopotential wells (ω_x, ω_y smaller), but it would still be necessary to maintain the high scatter rates (more difficult now because of the reduced densities). Of course one might become sensitive to smaller values of ω by probing narrower-linewidth transitions. In the low-temperature limit where the ion cloud becomes strongly coupled,[23,35] the dephasing effects might also be expected to be smaller if conditions of laminar flow or convection exist. Addition of an axial magnetic field may also help to prevent dephasing of L_z (see Appendix A). Finally, we remark that by adjusting U_0/V_0 it is possible to make the pseudopotential of Eq. (20) axially symmetric about either the x or the y axis, and therefore it should be possible to observe spinning about either axis experimentally. This possiblity was investigated in the Hg^+ experiment above, but $\dot{N}_s$ was not large enough and U_0/V_0 was not sufficiently stable for such spinning to be observed.

Therefore it should be possible (but perhaps difficult) to observe spinning in a rf trap. It is clearly a situation that is easily avoided. It has already been noted[4,36] that it is desirable in laser-cooling experiments to avoid axial symmetry in order to avoid recoil heating of the ions in a direction perpendicular to the laser beam.

6. PENNING TRAP ($q\alpha < 0$)

Angular momentum imparted to the cloud by light may be difficult to observe in an rf trap, however. In Penning traps it plays an important role. Since the radial electric trapping force and that which is due to space charge are outward, the only way to provide trapping is from a radial inward Lorentz force that is due to a rotation of the cloud as a whole. Therefore, even in the absence of a torque applied by the laser, the cloud must rotate at a frequency ω. It is easy to see that for

the Lorentz force to be inward, ω must be negative for q positive and ω must be positive for q negative. From Eq. (16), we see that for the usual case, where $|\omega| < \Omega_c/2$, the total angular momentum is in the opposite sense to the mechanical angular momentum; that is, it is mostly angular momentum from the field [$\mathbf{x} \times \mathbf{A}$ term of Eqs. (1) or the term including Ω_c in Eq. (16)].

The case for a single trapped ion in a Penning trap interacting with a laser beam has been treated in some detail in Ref. 5. From the equation of motion

$$m\dot{\mathbf{v}} = -q\vec{\nabla}\phi + q(\mathbf{v} \times \mathbf{B})/c, \tag{25}$$

we determine that the motion in the z direction is harmonic with frequency $\omega_z = (2\beta q/m)^{1/2}$, and the motion in the x–y plane can be written in complex form:

$$x + iy = r_1 \exp(i\omega_1 t) + r_2 \exp(i\omega_2 t), \tag{26}$$

where $\omega_{1,2} = -\Omega_c q/2|q| \pm [(\Omega_c/2)^2 + 2q\alpha/m]^{1/2}$ and where r_1 and r_2 are complex. The solutions for ω_1 and ω_2 are different from Eq. (15) for the reasons noted in Section 2. Note that these solutions are valid independently of the value of Ω_c or α and thus apply for either the Penning or the rf trap (see Appendix A).

From Eq. (26), it appears that the ω_1 and ω_2 components occur in an equal way. However, making the redefinitions[5]

$$x + iy = r_m \exp(i\omega_m t) + r_c \exp(i\omega_c' t), \tag{27}$$

$$\omega_m = -\frac{q}{|q|}\{\Omega_c/2 - [(\Omega_c/2)^2 + 2q\alpha/m]^{1/2}\}, \tag{28}$$

$$\omega_c' = -\frac{q}{|q|}\{\Omega_c/2 + [(\Omega_c/2)^2 + 2q\alpha/m]^{1/2}\}, \tag{29}$$

we can make the following observations: In the limit $\alpha \to 0$ we see that $\omega_m \to 0$ and $\omega_c' \to -q\Omega_c/|q|$; therefore the x–y motion is pure cyclotron motion. We identify the first term in Eq. (27) as the $\mathbf{E} \times \mathbf{B}$ drift magnetron motion of the guiding center of the cyclotron motion. The cyclotron frequency, ω_c', is now shifted by the radial electric fields. From the expression for the total energy in the x–y plane[5]

$$E_{xy}(\text{total}) = m(q\Omega_c/2|q| + \omega_m)(\omega_m r_m^2 - \omega_c' r_c^2), \tag{30}$$

we see that the energy in the ω_c' motion is positive while that in the ω_m motion is negative (because it is mostly potential energy, $q\alpha r^2 < 0$).

As is shown in Ref. 5, momentum transfer or damping in the direction opposite the $\omega_m(\omega_c')$ motion causes r_m (r_c) to increase (decrease). As a consequence, to decrease both r_m and r_c, as is usually desired in laser-cooling experiments, we must cause momentum transfer simultaneously against the cyclotron motion and in the same direction as the magnetron motion.[5] Equivalently, we must reduce the cyclotron energy (this is similar to laser cooling of harmonically bound particles[3]) and *increase* the magnetron energy. For negative ions this can be accomplished by the laser-beam configuration shown in Fig. 3. The laser frequency ν_L should be tuned slightly below the rest frequency ν_0 ($\nu_0 = c/\lambda$), which has been first-order Doppler shifted by the magnetron rotation, i.e., $\nu_L \lesssim \nu_0(1 + |\omega|d/c)$. From the above considerations we also see why ion confinement in a Penning trap is normally a situation of unstable equilibrium. If any damping is present, then r_m increases until the ions strike the ring electrode. From similar considerations, the cyclotron motion should be damped by background-gas collisions.

We also note a qualitative difference between the Penning and the rf traps. For the Penning trap, by using the technique of laser cooling, it is experimentally possible[23] to achieve an amplitude for the cyclotron motion, r_c, much smaller than the amplitude of the magnetron motion, r_m. In this low-temperature limit the ion motion in the x–y plane is nearly circular, and L_z is conserved. If the trap potential is the distorted one given by Eq. (20), the solution for the x–y equations of motion is not a superposition of two circular motions as in Eq. (27) but a superposition of two elliptical motions (see Appendix A). Of course, in the limit that the asymmetry parameter ϵ goes to zero, these two elliptical solutions turn into the circular cyclotron and magnetron solutions of Eq. (27). In the low-temperature limit, the ion motion is elliptical (distorted magnetron motion), but fluctuations in L_z are small [expression (A10)]. This is to be contrasted with the rf trap, in which a distortion of the type in Eq. (20) causes a qualitatively different behavior for the motion and L_z can change significantly after a time τ [Eq. (22)].

The above considerations should apply when there is a cloud of ions except that $|\omega_m|$ [i.e., $|\omega| < \Omega_c/2$ in Eq. (15)] is shifted to higher values by space charge and $|\omega_c'|$ [i.e., $|\omega| > \Omega_c/2$ in Eq. (15)] is shifted to lower values. If we assume perfect axial symmetry and no damping, then it is interesting to consider the situation of Fig. 3 (appropriate for negative ions). First, if the laser beam is directed on the side of the trap axis opposite that shown, then a drag is applied to the magnetron motion that can increase the magnetron radius to large values or even expel the ions from the trap. This effect has been experimentally observed for Mg^+ (Ref. 37) and Be^+ ions. Now suppose the laser beam is directed as shown in Fig. 3. Further assume that the cyclotron motion is laser cooled ($T \to 0$) and that the cloud as a whole rotates at a frequency $|\omega_m| = |\omega| < \Omega_c/2$. As we continue to add angular momentum from the laser scattering, then we expect $|\omega|$ and the density n_0 to increase while the cloud radius, r_{cl}, decreases. This happens until $|\omega| = \Omega_c/2$ (i.e., $|\omega_m| = |\omega_c'| = \Omega_c/2$), at which point the maximum density is reached [Eq. (14)]. As more angular momentum is added by the laser, the rotation frequency $|\omega|$ becomes larger than $\Omega_c/2$ (i.e., $|\omega| = |\omega_c'|$ is now the cloud rotation frequency) and the density starts to decrease again and the cloud radius expands. In principle this continues to happen until the cloud radius reaches the ring electrode and ions are lost.

So far, the only experiment in which such effects were quantitatively studied is the one on $^9Be^+$.[23] In this experiment, small clouds of $^9Be^+$ ions were cooled and compressed, but the densities were limited to a value ($2 \times 10^7/cm^3$) that was about an order of magnitude less than the maximum density given by Eq. (14). For these densities, the mean spacing between ions, $n^{-1/3}$, was about 37 μm while at the cyclotron temperatures achieved (T_c = 10–50 mK), $r_c \cong 1$ μm. We can first ask if the experimental limit was due to background-gas damping. For steady state, Eq. (23) must still apply (assuming here that $T_c = 0$). For the particular ion cloud of the first row in Table 1 of Ref. 23, we had $\omega_0 = 60$

μm, $\lambda = 313$ nm, $r_{cl} = 160\ \mu$m, $z_{cl} = 60\ \mu$m, $d \cong 50\ \mu$m, $n_0 = 2.1 \times 10^7/\text{cm}^3$, $T_z = 144$ mK, $N \cong 142$, and $\omega_m = (2\pi)37.3$ kHz. [For a single ion in the trap, $\omega_m = (2\pi)20.5$ kHz.] From Eq. (17b), we calculate that $|T_L| = \hbar\dot{N}_s \times 7.3 \times 10^4$. From Fig. 6 of Ref. 34, we take $K_0(\text{Be}^+, \text{He}) = 25\ \text{cm}^2\ \text{V}^{-1}\ \text{sec}^{-1}$; therefore, Eq. (19) gives $|T_{bkg}| = \hbar n(\text{He}) \times 7.7 \times 10^{-3}$. From the experiment we could estimate that $\dot{N}_s = 10^6$/sec. It was very unlikely that n(He) was larger than $10^8/\text{cm}^3$ based on heating data after the laser was turned off.[38] Therefore the limit on density was not due to background-gas damping.

It seems likely that the density was limited by imperfections in the trapping fields, which might lead to angular momentum's being coupled into the system.[38,39] Experimentally this density-limiting effect appeared very nonlinear in that the densities obtained were limited at a value that was fairly independent of laser power. (In the work reported in Ref. 23, varying the laser power by a factor of 10 had no measurable effect on the ion density.) Moreover, with the laser off the ions would rapidly heat at first[38] (~20 K/sec during the first 0.1 sec), but this heating would slow down (~1 K/sec from 10 to 20 sec), and the ions would remain in the trap for many hours. A possible mechanism for the density limit and the nonlinearity of the heating can be explained by assuming that the trap-symmetry axis is slightly tilted about the x axis by an angle δ with respect to the magnetic field. If we assume that the z axis is along the magnetic field, then the potential [assuming that $V_0 = 0$ in Eqs. (3)] is

$$\phi = \frac{U_0}{\xi^2}[2z^2 - r^2 + 3(y^2 - z^2)\sin^2\delta - 3zy\sin 2\delta]. \quad (31)$$

From this expression and the corresponding equations of motion, coupling between the z and y motions is clear. The frequencies of motion can be found from the eigenvalue problem (Ref. 40 and Appendix A), and one can also solve for the eigenvectors. Here we only point out that if the tilting is considered a perturbation, then there is an oscillating electric field in the y direction owing to the z motion

$$E_y = -\frac{\partial\phi}{\partial y} = 3zU_0\sin 2\delta/\xi^2 \quad (32)$$

that can drive the x–y motion. For a single particle in a Penning trap, and $\delta \ll 1$, this driving term at frequency $\cong \omega_z$ is nonresonant with ω_m and ω_c'; therefore no energy transfer between modes will occur. However, in a cloud of ions, the ω_m and ω_c' resonances are broadened by ion–ion collisions. Moreover, as n_0 increases because of compression, ω_m increases as noted above. In addition, the ion axial frequency ω_z' (for $T \neq 0$) is reduced by space charge from the free-space value. In the $^9\text{Be}^+$ experiment discussed above,[23] an estimate of ω_z' for $T \neq 0$ can be obtained by assuming that $\omega_z'/2\pi = v_z/4z_{cl}$, where $mv_z^2/2 = k_BT_z/2$. That is, we assume that the ion drifts across the ellipsoidal cloud (in the z direction) at its thermal velocity and reflects from the edge ($z \cong z_{cl}$). Clearly this is only a crude approximation since ion–ion collisions and collective effects will play a more important role.[14,15] However, using this model, we estimate that $\omega_z'/\omega_m \cong 1.3$, and therefore we have near-resonant coupling between the axial motion and the magnetron rotation. At lower densities and higher temperatures, ω_z'/ω_m becomes larger and resonance is avoided. The apparent resonant condition causes r_m to increase rapidly, which results in an increase in the ion cloud radius. Because of the resonant nature of this expansion, the process is called resonant particle transport.[14,39] A rapid increase in the cloud radius can cause rapid heating from the decrease in electrostatic energy as the cloud expands. This may account for the rapid heating observed immediately after the laser was turned off.[38] Thus it appears that distortions in trap symmetry may also be important for the Penning traps, particularly when high densities and low temperatures are desired. For the problem discussed here, the existence of such distortions may explain why we are unable to continue adding angular momentum to the ion cloud by laser scattering.

7. NEUTRAL-PARTICLE TRAPS

The same general considerations should apply to neutral-particle traps; the problem seems qualitatively simpler in that $q = 0$. Because of the short range of interparticle collisions, the situation for axially symmetric neutral traps should be similar to the case of ions in a rf trap in the low-density limit discussed above. Dephasing of angular momentum would be expected to be similar to that described in Section 5. Hence, as noted there, a small degree of trap asymmetry is probably required in order for spinning of the trapped sample to be observed.

8. CONCLUSIONS

In this paper we have been concerned primarily with angular momentum imparted to trapped particles by light scattering. As we noted earlier, this angular momentum could come from other sources, such as background gas, trap asymmetries, particle beams,[12] positive or negative feedback on charged-particle motions[12,13] (including radiative damping), and angular-momentum transfer from plasma waves.[14,15] Such considerations may modify the results of certain experiments such as those on electron– (or ion–) atom collisions.[41–43] For the case of ions in a Penning trap, it should be possible to compress the ion cloud at the center of the trap with a neutral-particle beam, although the cyclotron and axial degrees of freedom will be heated.

Therefore, in atomic-particle traps, one must in general take into account the angular momentum of the particles about a particular axis. If the trap has symmetry about this axis then these angular-momentum considerations are important in both the rf and the Penning ion traps and in neutral traps. We emphasize that it is the axial symmetry of the trap that is important for these angular-momentum considerations, not the adherence to the quadratic electric potentials that have been assumed, for simplicity, throughout this paper. If this axial symmetry is violated then it may in fact be difficult to observe angular-momentum effects in the rf or neutral traps. In Penning traps, such deviations from trap axial symmetry owing to electric-field distortions are not so important; in fact, angular-momentum effects, including the angular momentum imparted by laser scattering, play an important role in these experiments.

APPENDIX A

In Sections 5 and 6 we noted that if the electric potential is not axially symmetric, there is a significant difference in the

behavior of L_z for the pure rf trap ($\mathbf{B} = 0$) and the Penning trap. To see how this difference might arise, we first examine the x–y motion when the trap potential is given by Eq. (20) and β and α are arbitrary. The equations of motion for a single ion are

$$\ddot{x} + 2q(\alpha + \epsilon)x/m = q\Omega_c\dot{y}/|q|, \tag{A1}$$

$$\ddot{y} + 2q(\alpha - \epsilon)y/m = -q\Omega_c\dot{x}/|q|. \tag{A2}$$

If we assume a solution $x = \mathrm{Re}[x_0 \exp(-i\omega t)]$, $y = \mathrm{Re}[y_0 \exp(-i\omega t)]$, we can write Eqs. (A1) and (A2) in matrix form:

$$M(\omega)\begin{bmatrix} x_0 \\ y_0 \end{bmatrix} = 0, \tag{A3}$$

where

$$M(\omega) = \begin{bmatrix} -\omega^2 + 2q(\alpha + \epsilon)/m & i\omega q\Omega_c/|q| \\ -i\omega q\Omega_c/|q| & -\omega^2 + 2q(\alpha - \epsilon)/m \end{bmatrix}. \tag{A4}$$

The normal mode frequencies are obtained from $\det M(\omega) = 0$, which has four roots, $\pm\omega_+$ and $\pm\omega_-$, where

$$2(\omega_\pm)^2 = \Omega_c^2 + 4q\alpha/m \pm (\Omega_c^4 + 8q\alpha\Omega_c^2/m + 16q^2\epsilon^2/m^2)^{1/2} \tag{A5}$$

or

$$2(\omega_\pm)^2 = \Omega_c^2 + 2\omega_r^2 \pm (\Omega_c^4 + 4\omega_r^2\Omega_c^2 + 4\omega_\epsilon^4)^{1/2}, \tag{A6}$$

where we have made the redefinitions $\omega_r^2 = 2q\alpha/m$ and $\omega_\epsilon^2 = 2q\epsilon/m = (\omega_x^2 - \omega_y^2)/2$. From Eq. (A3), we can find the following relationships between components of the eigenvectors:

$$\left(\frac{y_0}{x_0}\right)_{\omega=\pm\omega_+} = \mp iU_+,$$

$$U_+ = q[\Omega_c^2 - 2\omega_\epsilon^2 + (\Omega_c^4 + 4\omega_r^2\Omega_c^2 + 4\omega_\epsilon^4)^{1/2}]/2\omega_+\Omega_c|q|, \tag{A7}$$

and

$$\left(\frac{y_0}{x_0}\right)_{\omega=\pm\omega_-} = \mp iU_-,$$

$$U_- = q[\Omega_c^2 - 2\omega_\epsilon^2 - (\Omega_c^4 + 4\omega_r^2\Omega_c^2 + 4\omega_\epsilon^4)^{1/2}]/2\omega_-\Omega_c|q|. \tag{A8}$$

Therefore, the general solution is

$$x = r_+\cos(\omega_+t + \theta_+) + r_-\cos(\omega_-t + \theta_-),$$

$$y = -U_+r_+\sin(\omega_+t + \theta_+) - U_-r_-\sin(\omega_-t + \theta_-). \tag{A9}$$

In the limit $\Omega_c \to 0$, these solutions are equivalent to those of Section 5 [Eqs. (21a) and (21b)] for the pure rf trap. If $\epsilon = 0$, then $|U_\pm| \to 1$, and we obtain the solutions of Section 6, where $|\omega_-| = |\omega_m|$ and $|\omega_+| = |\omega_c|$. For $\epsilon \neq 0$, the solution [Eqs. (A9)] is a superposition of two elliptical motions at frequencies ω_+ and ω_-. For ϵ small, i.e., $\omega_\epsilon \ll \omega_r, \Omega_c$, we find that

$$\frac{q}{|q|}U_\pm \cong 1 - 2\omega_\epsilon^2/[\Omega_c^2 \pm (\Omega_c^4 + 4\Omega_c^2\omega_r^2)^{1/2}]. \tag{A10}$$

In general, L_z is a complicated function that can oscillate around zero. However, if we assume that only the (ω_+) or the (ω_-) mode is excited, then we obtain a simple expression:

$$L_{z\pm} = mr_\pm^2\frac{q}{|q|}\frac{\Omega_c}{2}\left[\mp(1 + 4\omega_r^2/\Omega_c^2 + 4\omega_\epsilon^4/\Omega_c^4)^{1/2}\right.$$

$$\left. + (U_\pm^2 - 1)\sin^2(\omega_\pm t + \theta_\pm) + 2\omega_\epsilon^2/\Omega_c^2\right]. \tag{A11}$$

If the ellipticity of the orbit is small, i.e., $||U_\pm| - 1| \ll 1$, then L_z has small fluctuations about a nonzero value. In the Penning trap, if we can assume the usual condition $|\omega_r/\Omega_c| \ll 1$, then we find that the magnetron orbit (ω_- solution) has $||U_-| - 1| \cong \omega_\epsilon^2/\omega_r^2$. In the rf trap, as $\Omega_c \to 0$, then $U_+ \to 0$ and $|U_-| \to \infty$; that is, the normal mode orbits are highly elliptical. However, if we assume that $\omega_r \gg \Omega_c \gg \omega_\epsilon$, then, from expression (A10), $||U_\pm| - 1| \cong \omega_\epsilon^2/\omega_r\Omega_c \cong |\omega_x - \omega_y|/\Omega_c$. Therefore, if we superimpose a magnetic field along the z axis so that $\Omega_c \gg |\omega_x - \omega_y|$, then the normal mode orbits would be nearly circular.

Based on the observations in Section 6 for the Penning trap, we might therefore make the following conjecture for a cloud of ions in either the Penning or the rf trap: If the x–y modes are nearly circular and if ω_+, ω_-, and the axial frequency (now shifted by space charge) are sufficiently different that mode coupling is suppressed, then the dephasing or damping of L_z might be small. Therefore in the rf trap we might expect to observe spinning more easily if we superimpose a magnetic field such that $\Omega_c \gg |\omega_x - \omega_y|$. For our $^{198}Hg^+$ example of Section 5, if $\Delta\nu_{xy} \cong 1$ kHz this would require that $B \gg 130$ G.

ACKNOWLEDGMENTS

We greatfully acknowledge the support of the U.S. Office of Naval Research and the U.S. Air Force Office of Scientific Research. We also thank J. C. Bergquist and L. R. Brewer for critical comments and helpful suggestions on the manuscript.

REFERENCES

1. A. Ashkin, "Applications of laser radiation pressure," Science **210**, 1081–1088 (1980).
2. W. D. Phillips, ed., *Laser-Cooled and Trapped Atoms*, Nat. Bur. Stand. (U.S.) Spec. Publ. **653**, (1983); Prog. Quantum Electron. **8**, 115–259 (1984).
3. D. J. Wineland, W. M. Itano, J. C. Bergquist, J. J. Bollinger, and J. D. Prestage, "Spectroscopy of stored atomic ions," in *Atomic Physics 9*, R. S. Van Dyck, Jr., and E. N. Fortson eds. (World Scientific, Singapore, 1985), pp. 3–27.
4. D. J. Wineland and W. M. Itano, "Laser cooling of atoms," Phys. Rev. A **20**, 1521–1540 (1979).
5. W. M. Itano and D. J. Wineland, "Laser cooling of ions stored in harmonic and Penning traps," Phys. Rev. A **25**, 35–54 (1982).
6. H. G. Dehmelt, "Radiofrequency spectroscopy of stored ions. I and II," Adv. At. Mol. Phys. **3**, 53–72 (1967); **5**, 109–154 (1969).
7. D. J. Wineland, W. M. Itano, and R. S. Van Dyck, Jr., "High resolution spectroscopy of stored ions," Adv. At. Mol. Phys. **19**, 135–186 (1983).
8. A quantum mechanical treatment of rf trapping is given in R. J. Cook, D. G. Shankland, and A. L. Wells, "Quantum theory of

particle motion in a rapidly oscillating field," Phys. Rev. A **31,** 564–567 (1985).
9. E. Fischer, "Die dreidimensionale Stabilisierung von Ladungsträgern in einem Vierpolfeld," Z. Phys. **156,** 1–26 (1959).
10. F. G. Major and H. G. Dehmelt, "Exchange-collision technique for the rf spectroscopy of stored ions," Phys. Rev. **170,** 91–107 (1968).
11. H. A. Schuessler, E. N. Fortson, and H. G. Dehmelt, "Hyperfine structure of the ground state of $^3He^+$ by the ion-storage exchange-collision technique," Phys. Rev. **187,** 5–38 (1969).
12. D. J. Wineland, R. E. Drullinger, J. C. Bergquist, and W. M. Itano, "Laser induced magnetron compression (expansion) of ions stored in a Penning trap," Bull. Am. Phys. Soc. **24,** 1185 (1979).
13. W. D. White, J. H. Malmberg, and C. F. Driscoll, "Resistive wall destabilization of diocotron waves," Phys. Rev. Lett. **49,** 1822–1826 (1982).
14. D. L. Eggleston, T. M. O'Neil, and J. H. Malmberg, "Collective enhancement of radial transport in a nonneutral plasma," Phys. Rev. Lett. **53,** 982–984 (1984).
15. J. D. Crawford, T. M. O'Neil, and J. H. Malmberg, "Effect of nonlinear collective processes on the confinement of a pure electron plasma," Phys. Rev. Lett. **54,** 697–700 (1985).
16. The potential for a uniformly charged ellipsoid of revolution can be found in W. D. MacMillan, *The Theory of the Potential* (Dover, New York, 1958), pp. 17 and 45; O. D. Kellog, *Foundation of Potential Theory* (Ungar, New York, 1929), p. 195.
17. L. D. Landau and E. M. Lifshitz, *Statistical Physics* (Addison-Wesley, Reading, Mass., 1974).
18. J. H. Malmberg and T. M. O'Neil, "Pure electron plasma, liquid, and crystal," Phys. Rev. Lett. **39,** 1333–1336 (1977).
19. S. A. Prasad and T. M. O'Neil, "Finite length thermal equilibria of a pure electron plasma column," Phys. Fluids **22,** 278–281 (1979).
20. T. M. O'Neil and C. F. Driscoll, "Transport to thermal equilibrium of a pure electron plasma," Phys. Fluids **22,** 266–277 (1979).
21. L. S. Cutler, R. P. Giffard, and M. D. McGuire, "Mercury-199 trapped ion frequency standard: recent theoretical progress and experimental results," in *Proceedings of the 37th Annual Symposium on Frequency Control*, 1983. (Copies available from Systematics General Corporation, Brinley Plaza, Rt. 38, Wall Township, N.J. 07719), pp. 32–36; "Thermalization of ^{199}Hg ion macromotion by a light background gas in an rf quadrupole trap," Appl. Phys. B **36,** 137–142 (1985).
22. J. S. deGrassie and J. H. Malmberg, "Waves and transport in the pure electron plasma," Phys. Fluids **23,** 63–81 (1980).
23. J. J. Bollinger and D. J. Wineland, "Strongly coupled nonneutral ion plasma," Phys. Rev. Lett. **53,** 348–351 (1984).
24. R. D. Knight and M. H. Prior, "Laser scanning measurements of the density distribution of confined $^6Li^+$ ions," J. Appl. Phys. **50,** 3044–3049 (1979).
25. H. Schaaf, V. Schmeling, and G. Werth, "Trapped ion density distribution in the presence of He-buffer gas," Appl. Phys. **25,** 249–251 (1981).
26. J. B. Jeffries, S. E. Barlow, and G. H. Dunn, "Theory of space-charge shift of ion cyclotron resonance frequencies," Int. J. Mass Spectrom. Ion Phys. **54,** 169–187 (1983).
27. D. A. Church and H. G. Dehmelt, "Radiative cooling of an electrodynamically contained proton gas," J. Appl. Phys. **40,** 3421–3424 (1969).
28. H. G. Dehmelt, "Stored ion spectroscopy," in *Advances in Laser Spectroscopy*, F. T. Arecchi, F. Strumia, and H. Walther, eds. (Plenum, New York, 1983), pp. 153–187.
29. D. J. Wineland, "Spectroscopy of stored ions," in *Precision Measurement and Fundamental Constants II*, B. N. Taylor and W. D. Phillips, eds., Natl. Bur. Stand. (U.S.) Spec. Publ. **617** (1984), p. 83–92.
30. J. T. Davies and J. M. Vaughan, "A new tabulation of the Voigt profile," Astrophys. J. **137,** 1302–1305 (1963).
31. H. G. Dehmelt and F. L. Walls, "Bolometric technique for the rf spectroscopy of stored ions," Phys. Rev. Lett. **21,** 127–131 (1968).
32. E. W. McDaniel, *Collision Phenomena in Ionized Gases* (Wiley, New York, 1964), pp. 426–482.
33. J. C. Bergquist, D. J. Wineland, W. M. Itano, H. Hemmati, H.-U. Daniel, and G. Leuchs, "Energy and radiative lifetime of the $5d^96s^2\ ^2D_{5/2}$ state in Hg II by Doppler-free two-photon laser spectroscopy," Phys. Rev. Lett. (to be published).
34. L. M. Chanin and M. A. Biondi, "Mobilities of mercury ions in helium, neon and argon," Phys. Rev. **107,** 1219–1221 (1957).
35. S. Ichimaru, "Strongly coupled plasmas: high density classical plasmas and degenerate electron liquids," Rev. Mod. Phys. **54,** 1017–1059 (1982).
36. W. Neuhauser, M. Hohenstatt, P. E. Toschek, and H. G. Dehmelt, "Localized visible Ba^+ mono-ion oscillator," Phys. Rev. A **22,** 1137–1140 (1980).
37. R. E. Drullinger, D. J. Wineland, and J. C. Bergquist, "High-resolution optical spectra of laser cooled ions," Appl. Phys. **22,** 365–368 (1980).
38. J. J. Bollinger, J. D. Prestage, W. M. Itano, and D. J. Wineland, "Laser cooled atomic frequency standard," Phys. Rev. Lett. **54,** 1000–1003 (1985).
39. C. F. Driscoll and J. H. Malmberg, "Length dependent containment of a pure electron-plasma column," Phys. Rev. Lett. **50,** 167–170 (1983).
40. L. S. Brown and G. Gabrielse, "Precision spectroscopy of a charged particle in an imperfect Penning trap," Phys. Rev. A **25,** 2423–2425 (1982).
41. M. D. McGuire and E. N. Fortson, "Penning-trap technique for studying electron-atom collisions at low energy," Phys. Rev. Lett. **33,** 737–739 (1974).
42. G. Graff, F. G. Major, R. W. H. Roeder, and G. Werth, "Method for measuring the cyclotron and spin resonance of free electrons," Phys. Rev. Lett. **21,** 340–342 (1968).
43. G. Graff and M. Holzscheiter, "Method for trapped ion polarization and polarization detection," Phys. Lett. **79A,** 380–382 (1980).

(*see overleaf*)

Sympathetic Cooling of Trapped Ions: A Laser-Cooled Two-Species Nonneutral Ion Plasma

D. J. Larson,[a] J. C. Bergquist, J. J. Bollinger, Wayne M. Itano, and D. J. Wineland
National Bureau of Standards, Time and Frequency Division, Boulder, Colorado 80303
(Received 31 March 1986)

Sympathetic cooling of trapped ions has been demonstrated in an experiment where $^{198}Hg^+$ ions were confined in a Penning ion trap with laser-cooled $^9Be^+$ ions. $^{198}Hg^+$ temperatures below 1 K were achieved. Ion plasma sizes, shapes, and rotation frequencies were measured. Dramatic changes in the $^9Be^+$ plasma were observed when the $^{198}Hg^+$ ions were introduced into the trap. These observations are consistent with the prediction of centrifugal separation for ions of different charge-to-mass ratios.

PACS numbers: 32.80.Pj, 52.25.Wz

The techniques of trapping and laser cooling have led to dramatic improvements in recent measurements and future prospects for precision spectroscopy.[1,2] However, the number of species which can be directly laser cooled is limited by the availability of tunable, narrow-band sources and by more fundamental problems such as complicated level structure (as in molecules) or the absence of optical structure (as in protons and negative atomic ions). In addition, the laser-cooling process itself strongly perturbs the levels of an atom or ion. The cooling laser must be turned off during the interrogation time to avoid light shifts (ac Stark shifts) and broadening many orders of magnitude larger than achievable linewidths. In the most accurate experiment to date,[3] the linewidth of a radio frequency transition in $^9Be^+$ was limited (≥ 0.025 Hz) by the necessity to restrict interrogation times (≤ 20 s) in order to minimize heating that occurred when the cooling laser was turned off. In principle, linewidths substantially less than 0.001 Hz should be possible on transitions in trapped ions.

Sympathetic cooling,[1,4,5] where one species is cooled by interaction with a second, directly cooled species, offers a solution to these problems. In the present experiments, spectroscopy of continuously cooled $^{198}Hg^+$ ions was made possible by confining them in a trap together with laser-cooled $^9Be^+$ ions. The 313-nm radiation used to cool the Be^+ ions did not seriously perturb the Hg^+ ions since this wavelength is far from any resonance in Hg^+. We estimate that the fractional light shift in the $^{201}Hg^+$ hyperfine separation would be less than 5×10^{-18} under conditions similar to those in the present experiment.

Although sympathetic cooling was noted previously in experiments with different isotopes of magnesium ions[1,4] we report here the first measurements of temperatures and spatial distributions for a two species, magnetically confined, nonneutral plasma. In addition, the present experiments have demonstrated that radial diffusion of the sympathetically cooled species is prevented. One interesting feature of such a plasma, that the species with higher mass-to-charge ratio moves radially to the outside of the lighter (or more highly charged) species,[6,7] was observed. The present results appear to have a direct bearing on proposed experiments to store and cool antiprotons at very low energies[8-10] and may be important in other experiments where two or more species of different charge-to-mass ratio are simultaneously present in the trap.[11] Different considerations lead to separation of species in rf traps.[12]

The experiments were carried out using a Penning ion trap[13] with hyperbolically shaped electrodes. The endcap-to-endcap spacing was 0.51 cm and the inner-ring diameter was 0.83 cm. The trap and vacuum system were at room temperature for all of the measurements except one where the trap was cooled to 77 K. A magnetic field near 1.43 T was used for all of the measurements. Be^+-ion plasmas (or "clouds") were created in the trap by use of a beam of electrons to ionize beryllium atoms which were evaporated from a tungsten filament wrapped with beryllium wire. Hg^+ ions were loaded into the trap by ionizing mercury vapor leaked into the vacuum system through a variable leak valve while the Be^+ ions were being laser cooled.

Three laser systems were used to cool and probe the ions. A frequency-doubled dye laser beam with a power of approximately 50 μW at 313 nm was directed through a hole in the ring electrode and used to cool the Be^+ ions on the $2s\,^2S_{1/2}$ to $2p\,^2P_{3/2}$, $m_J=+\frac{1}{2}$ to $m_J=+\frac{3}{2}$, transition.[1] The photons backscattered by the Be^+ ions were collected and counted. This signal was used for all of the measurements on the Be^+ ions. A second 313-nm source was directed through another hole in the ring. When tuned to the $2s\,^2S_{1/2}$ to $2p\,^2P_{3/2}$, $m_J=+\frac{1}{2}$ to $m_J=-\frac{1}{2}$, transition, this probe beam depopulated the $m_J=+\frac{1}{2}$ state and thus caused a decrease in the scattered light from the cooling beam.[1] The ion-cloud sizes and shapes were measured by observing this signal for different positions of the probe beam. The ion-cloud rotation frequencies were obtained through the Doppler shift by measuring the frequency of the probe laser which produced maximum depopulation.[14] A third laser system[15] produced

© 1986 The American Physical Society

a few microwatts of tunable power at 194 nm. The positions and velocities of the Hg^+ ions in the trap were measured by collecting and counting the 194-nm photons scattered when the frequency was tuned through the $6s\,^2S_{1/2}$ to $6p\,^2P_{1/2}$, $m_J = -\frac{1}{2}$ to $m_J = +\frac{1}{2}$ transition in the ion. Microwaves tuned to the $\Delta m_J = 1$ transition in the ground state prevented depletion of the $m_J = -\frac{1}{2}$ ground state by optical pumping.[16] For both Be^+ and Hg^+ the temperatures were determined by measuring the Doppler contribution to the frequency width of the observed signal as the appropriate laser was tuned through resonance.[14] An example of the signal from a Hg^+-ion cloud whose cyclotron temperature has been sympathetically cooled to near 1 K is shown in Fig. 1.

A cold, single-species ion cloud in a Penning trap with hyperbolic electrodes should assume a nearly spheroidal shape with constant density inside the cloud and an abrupt drop in density at the edge.[14,17,18] The eccentricity of the spheroid is determined by the trapping voltage, magnetic field, and rotation frequency. Any cloud in thermal equilibrium will exhibit uniform rotation. The rotation frequency is a measure of the density and of the angular momentum of the ions.[17–21] It can be partially controlled by varying the torque applied to the cloud by the cooling laser. Observed rotation frequencies were well below those corresponding to the maximum stable density of ions in the trap, the Brillouin density.[20] The mechanism which limits the frequency is not clearly understood, but it may depend upon trap asymmetries.[18,19,22] For precision spectroscopy, high rotation velocities and the accompanying Doppler shifts should be avoided by working at low densities.

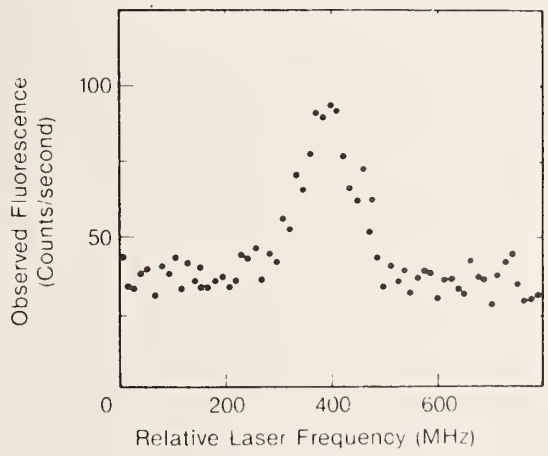

FIG. 1. Observed fluorescence from a Hg^+-ion cloud cooled to approximately 1 K by interaction with a laser-cooled Be^+ cloud. The horizontal axis is the frequency of a laser tuned through the $6s\,^2S_{1/2}$ ($m_J = -\frac{1}{2}$) to $6p\,^2P_{1/2}$ ($m_J = +\frac{1}{2}$) transition in Hg^+. The room-temperature Doppler width of this transition is about 1.4 GHz.

A dramatic change in the rotation frequency (and thus the density) and the shape (away from spheroidal) of the Be^+ cloud occurred when Hg^+ ions were introduced into the trap. With only Be^+ in the trap, rotation frequencies up to nearly 200 kHz could be achieved. The single-particle rotation (magnetron) frequency was measured to be only 9.4 kHz with −1.5 V on the ring, so the observed frequencies were due primarily to the space-charge fields. With Hg^+ and Be^+ in the trap, the largest observed rotation frequency was 21 kHz. The measured size and shape of a Be^+ cloud with and without Hg^+ is shown in Fig. 2(a). Adding the Hg^+ ions decreased the rotation frequency by a factor of 2. A larger change in density and shape of a Be^+ cloud is shown in Fig. 2(b). Figures 2(a) and 2(b) are the smallest and largest clouds examined. In all cases the Be^+ clouds were prolate spheroids without the Hg^+ and oblate and nonspheroidal with Hg^+ present. The Hg^+ clouds appeared disk shaped with diameter-to-length ratios of 6 to 1 or larger.

Clearly, the Hg^+ ions applied a substantial torque to the Be^+ ions. For all of the Hg^+ clouds measured, the axial bounce frequency (equal to twice the axial length divided by the rms axial velocity) was approximately equal to the rotation frequency. This condition is consistent with axial asymmetries of the trap and resultant resonant particle transport limiting the rotation frequency.[18,22] No definitive evidence is available, however, to exclude other mechanisms[23] from limiting the rotation frequency with the exception of drag due to background gas. Cooling of the trap electrodes to 77 K, which substantially lowered the residual mercury pressure, caused no change in measured rotation frequencies. Despite the presence of a torque on the Hg^+ ions, they remained in the trap for several hours unless the cooling was interrupted. If the cooling laser was blocked or tuned off resonance the Hg^+ ions were lost in several minutes, demonstrating that Hg^+ confinement was dependent on the torque applied to the Hg^+ ions by the laser via the coupling to the Be^+ ions.

Measured Hg^+ temperatures ranged from 0.4 to 1.8 K and Be^+ temperatures ranged from less than 0.05 to 0.2 K. The temperature difference between the two species may be a result of the thermal coupling between the directly laser-cooled Be^+ ions and the indirectly cooled Hg^+ ions being weak, due to centrifugal separation. Also, the axial temperature of the Be^+ ions should be higher than the transverse temperature because of photon recoil,[14] and this could cause the Hg^+-ion temperature to take on some intermediate value.

Given the torque due to the Hg^+ ions, the counteracting torque due to the laser on the Be^+ ions, and the temperature difference between the two clouds, it is not unreasonable to expect some shear. In a uni-

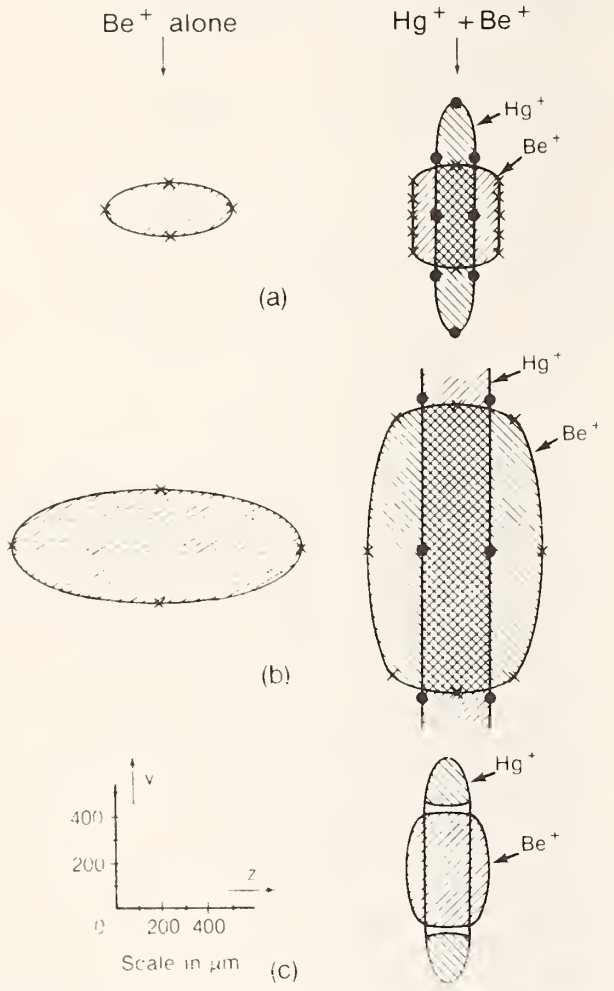

FIG. 2. (a) Measured Be^+- and Hg^+-ion-cloud shapes. The magnetic field is along the z axis. The Be^+ cloud, which contained about 800 ions, is shown with and without the Hg^+ present. The measured rotation frequencies were 41 kHz without Hg^+ [corresponding to a density, $n(Be^+) = 3.9 \times 10^7$ cm^{-3}] and 20 kHz with Hg^+ present [$n(Be^+) = 1.9 \times 10^7$ cm^{-3}, $n(Hg^+) = 1.6 \times 10^7$ cm^{-3}]. The solid lines drawn through the data points conform to the theoretically predicted and separately confirmed spheroidal shape for Be^+ alone but are drawn without consideration of theoretical shapes for Be^+ and Hg^+ together. The edges of the clouds were measured with an uncertainty of about 25 μm. (b) Measured cloud shapes for a Be^+ cloud which contained about 12 000 ions and a Hg^+ cloud which was larger in radial extent than the aperture through the ring electrode (diameter $\simeq 2100\ \mu$m). The measured rotation frequencies were 73 kHz without Hg^+ [$n(Be^+) = 7.0 \times 10^7$ cm^{-3}] and 18 kHz with Hg^+ [$n(Be^+) = 1.8 \times 10^7$ cm^{-3}, $n(Hg^+) = 1.5 \times 10^7$ cm^{-3}]. (c) Theoretically predicted shapes for cold Be^+ and Hg^+ clouds under conditions similar to those in (a).

formly rotating cloud, the Doppler shift and thus the observed optical resonance frequency should be a linear function of the radial distance from the center of the cloud. Figure 3 shows the observed resonance frequency for a Be^+ cloud, confined in the trap together

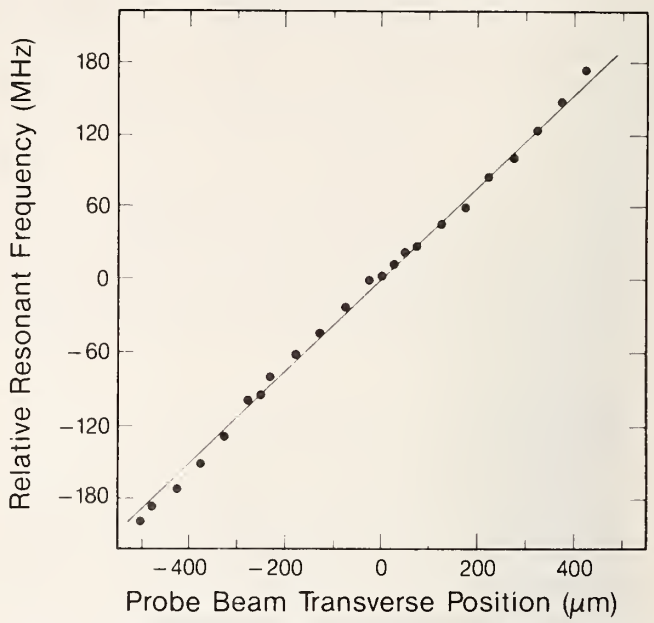

FIG. 3. Measured resonance frequency in Be^+ as a function of the transverse position (perpendicular to the trap axis) of the probe laser beam. These measurements, done with Hg^+ ions present in the trap, placed a limit on the amount of shear in the Be^+ cloud. The statistical error in the data points is smaller than the size of the points.

with a Hg^+ cloud, as a function of the transverse position of the probe laser beam. Fitting the data in Fig. 3 with a rotation frequency $\omega = \omega_r + \Delta\omega(r/r_{cl})$, where r_{cl} is the cloud radius, implies that $|\Delta\omega/\omega_r| < 0.3$. Indeed, to the extent that the data suggest that shear is present, it appears that the outer edge of the cloud is rotating faster than the middle. No evidence for shear was observed in a similar measurement on Hg^+ ions or in the comparison of the frequencies between the two species.

The measured shapes of the Be^+- and Hg^+-ion clouds were compared to numerical calculations based on a zero-temperature theory which balances magnetic, space-charge, and external electric forces.[6,17,24] The calculation used measured values for the trapping voltage, magnetic field, rotation frequency, and relative cloud diameters to predict shapes. A zero-temperature theory should be applicable when the ratio of the Debye length to the dimensions of the ion cloud is small. In the present experiments this ratio was typically less than 0.1. The theoretical prediction of complete radial separation of the ion clouds was not definitively tested since all of the probing of ion position was done in a direction perpendicular to the axis of the trap. Changes in collection efficiency for the 194-nm fluorescence as the beam position was moved prevented the use of count rate as a measure of the Hg^+ cloud thickness along the laser-beam direction. The theory[6,24] suggests that the heavier Hg^+ ions should be found in a torus around the lighter Be^+ ions

TN-78

as shown in Fig. 2(c).

These experiments have demonstrated the effectiveness of sympathetic cooling and point the way toward applications such as use in high-resolution spectroscopy and antiproton accumulation and storage. They have also allowed observation of some of the characteristics of a cold, magnetically confined, two-species nonneutral plasma. Significant features include the dramatic change in the shape of the Be^+-ion cloud when the Hg^+ ions are introduced into the trap, the temperature difference between the laser-cooled Be^+ ions and the sympathetically cooled Hg^+ ions, and the substantial torque exerted on the Be^+ cloud by the Hg^+ ions. A few features, including the source of the torque on the Hg^+ ions, are not clearly understood and may limit the number of ions that can be stored in a trap. Such techniques may be applicable to cooling neutral particles in a trap.[25]

We would like to thank J. Prestage, R. Hulet, and C. Manney for their contributions to this work. We thank T. O'Neil, C. F. Driscoll, L. Brewer, and F. Walls for helpful comments on the manuscript. We gratefully acknowledge the support of the U.S. Office of Naval Research and of the U.S. Air Force Office of Scientific Research.

---

[a]Permanent address: Department of Physics, University of Virginia, Charlottesville, VA 22901.

[1]For reviews, see D. J. Wineland, W. M. Itano, J. C. Bergquist, J. J. Bollinger, and J. D. Prestage, in *Atomic Physics 9*, edited by R. S. Van Dyck, Jr., and E. N. Fortson (World Scientific, Singapore, 1985), p. 3; W. D. Phillips, J. V. Prodan, and H. Metcalf, *ibid.*, p. 338, and references therein.

[2]The Mechanical Effects of Light, edited by P. Meystre and S. Stenholm, J. Opt. Soc. Am. B **2**, No. 11 (1985).

[3]J. J. Bollinger, J. D. Prestage, W. M. Itano, and D. J. Wineland, Phys. Rev. Lett. **54**, 1000 (1985).

[4]R. E. Drullinger, D. J. Wineland, and J. C. Bergquist, Appl. Phys. **22**, 365 (1980).

[5]D. J. Wineland, R. E. Drullinger, and F. L. Walls, Phys. Rev. Lett. **40**, 1639 (1978).

[6]T. M. O'Neil, Phys. Fluids **24**, 1447 (1981).

[7]M. Geva, M. Krishnan, and J. L. Hirshfield, J. Appl. Phys. **56**, 1398 (1984).

[8]H. G. Dehmelt *et al.*, Bull. Am. Phys. Soc. **24**, 757 (1979); G. Torelli, in *Proceedings of the Fifth European Symposium on Nucleon Anti-Nucleon Interactions, Bressanone, Italy, 23–28 June 1980*, edited by M. Cresti (Istituto Nazionale di Fisica Nucleare, Padua, Italy, 1980), p. 43.

[9]G. Gabrielse, H. Kalinowsky, and W. Kells, in *Physics with Antiprotons at LEAR in the ACOL Era*, edited by U. Gastaldi *et al.* (Editions Frontières, Gif-sur-Yvette, France, 1985), p. 665; W. Kells, IEEE Trans. Nucl. Sci. **32**, 1770 (1985).

[10]C. F. Driscoll, in *Proceedings of the Anti-Matter Facility Workshop* (Univ. of Wisconsin Press, Madison, 1985); M. H. Holzscheiter, *ibid.*

[11]D. A. Church, in Ref. 1, p. 137.

[12]C. Flory, L. Cutler, and R. Giffard, to be published.

[13]H. G. Dehmelt, Adv. At. Mol. Phys. **3**, 53 (1967), and **5**, 109 (1969); D. J. Wineland, W. M. Itano, and R. S. Van Dyck, Jr., Adv. At. Mol. Phys. **19**, 135 (1983).

[14]J. J. Bollinger and D. J. Wineland, Phys. Rev. Lett. **53**, 348 (1984).

[15]H. Hemmati, J. C. Bergquist, and W. M. Itano, Opt. Lett. **8**, 73 (1983).

[16]W. M. Itano, J. C. Bergquist, and D. J. Wineland, J. Opt. Soc. Am. B **2**, 1392 (1985).

[17]S. A. Prasad and T. M. O'Neil, Phys. Fluids **22**, 278 (1979).

[18]D. J. Wineland, J. J. Bollinger, W. M. Itano, and J. D. Prestage, J. Opt. Soc. Am. B **2**, 1721 (1985).

[19]J. H. Malmberg, C. F. Driscoll, and W. D. White, Phys. Scr. T **2**, 288 (1982).

[20]R. C. Davidson, *Theory of Nonneutral Plasmas* (Benjamin, Reading, MA, 1974), p. 4.

[21]T. M. O'Neil and C. F. Driscoll, Phys. Fluids **22**, 266 (1979).

[22]C. F. Driscoll and J. H. Malmberg, Phys. Rev. Lett. **50**, 167 (1983).

[23]D. L. Eggleston, T. M. O'Neil, and J. H. Malmberg, Phys. Rev. Lett. **53**, 982 (1984).

[24]J. J. Bollinger, C. Manney, and D. J. Wineland, to be published.

[25]W. H. Wing, Prog. Quantum Electron. **8**, 181 (1984).

This paper published in Intense Position Beams, edited by E.H. Ottewitte and W. Kells (World Scientific, Singapore, 1988), p. 63.

Ion Trapping Techniques: Laser Cooling and Sympathetic Cooling*

J.J. Bollinger, L.R. Brewer, J.C. Bergquist, Wayne M. Itano
D.J. Larson†, S.L. Gilbert and D.J. Wineland

Time and Frequency Division
National Bureau of Standards
Boulder, Colorado 80303

ABSTRACT

Radiation pressure from lasers has been used to cool and compress $^{9}Be^{+}$ ions stored in a combination of static electric and magnetic fields (Penning trap) to temperatures less than 10 mK and densities greater than 10^{7} cm^{-3} in a magnetic field of 1.4 T. A technique called sympathetic cooling can be used to transfer this cooling and compression to other ion species. An example of $^{198}Hg^{+}$ ions sympathetically cooled by laser cooled $^{9}Be^{+}$ ions is given. The possibility of making an ultracold positron source via sympathetic cooling is also discussed.

Ion traps have been used in low energy atomic physics experiments for a period of roughly 30 years.[1,2] During the past 10 years, however, the technique of laser cooling and compression has greatly increased the potential use of stored ions in a number of applications. One example is time and frequency standards. With the technique of laser cooling and compression, ion temperatures less than 10 mK, densities a factor of 10 less than the Brillouin limit (defined below), and essentially indefinite confinement times have been obtained.[3,4] Unfortunately, elementary charged particles (electrons, positrons, protons, etc.) can not be directly laser

*Work of the U.S. Government, not subject to U.S. copyright.
†Permanent address: Dept. of Phys., Univ. of Virginia, Charlottesville, VA 22901

cooled. In addition the number of atomic ion species that can be directly cooled by a laser is limited. Sympathetic cooling, [5,6] where one charged species is cooled by the Coulomb interaction with a second, directly cooled species, provides a means of transferring the desirable properties of a laser cooled ion species to a species, such as positrons, which can not be laser cooled directly.

The idea of sympathetic cooling is general and can, in principle, be used with any type of trap. In this paper, though, the idea of sympathetic cooling is examined only in the case of two different charged species in a Penning-type trap. The Penning trap[7] uses a uniform magnetic field $\vec{B} = B\hat{z}$ to confine ions in a direction perpendicular to the z axis. The ions are prevented from leaving the trap along the z axis by an electrostatic potential, φ_T, typically provided by three electrodes. In the general discussion that follows, unless explicitly stated, it is only assumed that the trap potential, φ_T, is symmetric about the z axis (i.e. $\varphi_T = \varphi_T(r,z)$ where r,z are cylindrical coordinates). This includes the Penning trap typically used in atomic physics experiments where the electrodes have hyperbolic shapes which give rise to a quadratic trap potential.[1,2] It also includes the traps of the University of California at San Diego (UCSD) group which use cylindrical tubes as the trap electrodes.[8-10]

In the next section, the technique of laser cooling and compression is described and some results of measurements on laser cooled $^9Be^+$ ions are summarized. The idea of sympathetic cooling is then described in more detail and the results of an experiment where Hg^+ ions were sympathetically cooled by laser cooled Be^+ ions are given. We conclude with a discussion of the possibilities of sympathetically cooling positrons and speculate at some possible applications of very cold positrons.

LASER COOLING AND COMPRESSION

The technique of laser cooling[11-13] utilizes the resonant scattering of laser light by atomic particles. By directing a laser beam at the ion plasma we can decrease the thermal velocity of an ion in a direction opposite to the laser beam. The laser is tuned to the red, or low frequency side of the atomic "cooling transition" (typically an electric dipole transition). Some of the ions moving in a direction opposite to the laser beam propagation will be Doppler shifted into resonance and absorb photons at a relatively high rate. Ions moving with the laser beam will be Doppler shifted away from the resonance and the absorption rate will correspondingly decrease. When an ion absorbs a photon its velocity is changed by an amount

$$\Delta\vec{v} = \hbar\vec{k}/m \qquad (1)$$

due to momentum conservation. Here $\Delta\vec{v}$ is the change in the ion's velocity, $\vec{k}$ is the photon wave vector where $|\vec{k}| = 2\pi/\lambda$, λ is the wavelength of the cooling radiation, m is the mass of the ion, and $2\pi\hbar$ is Planck's constant. The ion spontaneously re-emits the photon in a symmetric way. In particular, averaged over many scattering events, the reemission does not change the momentum of the ion. The net effect is that for each photon scattering event, the ion's average velocity is changed by an amount shown in Eq. 1. To cool an atom from 300 K to mK temperatures takes typically 10^4 scattering events. The theoretical cooling limit, due to photon recoil effects[11-13] is given by a temperature equal to $\hbar\gamma/(2k_B)$ where γ is the radiative linewidth of the atomic transition in angular frequency units and k_B is Boltzmann's constant. For a linewidth $\gamma = 2\pi \cdot 19.4$ MHz, which is the radiative linewidth of the $2s^2S_{\frac{1}{2}} \rightarrow 2p^2P_{3/2}$ transition in $^9Be^+$ (λ = 313 nm) used for cooling, the theoretical minimum temperature is 0.5 mK.

Laser scattering can also be used to change the angular momentum and compress the ion "cloud" or plasma. For simplicity, in the discussion of this paper it is assumed that particles with charge $q>0$ are trapped. In thermal equilibrium the plasma in a Penning trap undergoes a uniform rotation at an angular frequency $-\omega$.[14-16] The minus sign indicates that for positively charged particles, the rotation is in the $-\hat{\theta}$ direction. The z component of the canonical angular momentum for an individual particle is

$$l_z = mv_\theta r + \frac{qBr^2}{2c}. \qquad (2)$$

The two terms in Eq. 2 are the plasma mechanical angular momentum and the field angular momentum. The total z component of the angular momentum of the plasma is[16]

$$L_z = m(\Omega/2 - \omega)N < r^2 >. \qquad (3)$$

Here N is the total number of ions, $\Omega = qB/(mc)$ is the cyclotron frequency and $\langle r^2 \rangle$ is the mean squared radius of the plasma. For all of the work described in this paper, $\omega \ll \Omega$ and

$$L_z \cong \frac{m\Omega N}{2} \langle r^2 \rangle \ > 0 \ . \qquad (4)$$

Suppose the cooling laser beam is directed at the side of the plasma which is receding from the laser beam due to the plasma rotation. Because the rotation of the positive ions is in the $-\hat{\theta}$ direction, the torque of the laser on the ions will also be negative. Consequently angular momentum is removed from the plasma and according to Eq. 4 the radius of the plasma must decrease. As the radius decreases, the density of the plasma increases. In principle, the plasma compression continues until $\omega = \Omega/2$ where the maximum density, known as the Brillouin density occurs. The Brillouin density, n_B, is given by

$$n_B = \frac{m\Omega^2}{8\pi q^2} \ . \qquad (5)$$

In practice, the plasma is compressed until the torque due to the cooling laser is balanced by an external torque. Collisions with background gas particles and axial asymmetries of the trap are possible sources of external torques. The group at UCSD has observed that the axial asymmetry of their cylindrical traps plays an important role in the electron confinement time.[10] With the use of the plasma compression, it is possible to stop the normal processes which lead to an increase in the plasma radius and obtain a steady state plasma indefinitely. In our laboratory we routinely maintain a steady state plasma of laser cooled $^9Be^+$ ions for a period of a day.

We have used an optical double resonance technique[3,4,16] to measure the shape, density, and temperature of clouds of a few hundred to a few ten thousand laser cooled $^9Be^+$ ions stored in a Penning trap. Densities of 10^7 - 10^8 ions/cm^3 at a magnetic field of 1.4 T were obtained on both the large and small clouds. The Brillouin density for $^9Be^+$ ions in this magnetic field is 6×10^8 ions/cm^3. We believe that axial asymmetries of the trap were responsible for limiting the ion densities to about an order of magnitude less than the Brillouin density.[3,4,16] Ion temperatures less than 100 mK were routinely obtained. On smaller clouds consisting of a few hundred ions, ion temperatures less than 10 mK were measured.

SYMPATHETIC COOLING

The idea of sympathetic cooling is to use the Coulomb interaction to transfer the long term confinement, high densities, and low temperatures of a laser cooled ion species (for example, $^9Be^+$) to a charged species (for example, positrons) which can not be directly laser cooled and compressed. O'Neil has investigated the equilibrium distribution of a nonneutral multispecies ion plasma for

the case where the plasma is assumed to have infinite extent along the z axis.[17] For simplicity consider a two species ion plasma consisting of ion species with like charge q but different masses $m_2 > m_1$. Thermal equilibrium requires that both ion species undergo a uniform rotation at the same frequency, ω.[17] The uniform rotation tends to produce a centrifugal separation of the two ion species. In particular, the heavier ion species tends to reside outside the lighter species.

For the case of an infinitely long two species plasma, the lighter species forms a column of plasma centered on the z axis with outer radius b_1. The heavier species forms a cylindrical shell outside the lighter species with inner radius a_2 and outer radius b_2. In the limit of zero temperature, the edges of the plasma become sharp and the separation between the two species is complete with $b_1 < a_2 < b_2$. The separation $d = a_2 - b_1$ between the two species depends on b_1 and the density ratio n_2/n_1 of the two species and is given by the expression

$$d = b_1\{(n_2/n_1)^{-\frac{1}{2}} - 1\}. \tag{6}$$

The density ratio depends on the rotation frequency according to

$$n_2/n_1 = 1 - \frac{(m_2 - m_1)\omega^2}{2\pi q^2 n_1} \quad , \tag{7}$$

$$n_1 = \frac{m_1\omega(\Omega_1 - \omega)}{2\pi q^2} \, .$$

For a finite length plasma, the situation is similar. The heavier species tends to form a "doughnut" around the lighter species (see Fig. 1(c)). The gap, d(z), between the two species now depends on the z coordinate. Zero temperature calculations of plasma shapes for

a two component nonneutral plasma in a harmonic Penning trap [18] show that in general $d(0) \leq d(z)$ and $d(0)$ depends in a complicated way on b_1, b_2, n_2/n_1, and the voltage applied to the trap. Eq. 6 provides a lower estimate for $d(0)$. For a large range of the input parameters, this actually turns out to be a good estimate of $d(0)$.

For finite temperatures, the edge of the plasma is not perfectly sharp, but falls to zero over a distance characterized by the Debye length, $\lambda_D \equiv [k_B T/(4\pi n q^2)]^{\frac{1}{2}}$.[15] Here n is the density of the particular ion species and T is the temperature. One expects the thermal coupling between the two different ion species to be strong if the gap $d(0)$ is small compared to either of the species' Debye lengths. If $d(0)$ is large compared to the Debye lengths, the thermal coupling may be weak. The exact strength of the thermal coupling is a difficult theoretical problem to estimate.

We experimentally tested the idea of sympathetic cooling by loading $^{198}Hg^+$ in the same trap with laser cooled $^9Be^+$ ions.[6] Without the Hg^+, Be^+ rotation frequencies up to 200 kHz were observed. A dramatic change in the rotation frequency and shape of the Be^+ cloud occurred when Hg^+ ions were introduced into the trap (see Fig. 1). With Hg^+ and Be^+ in the trap, the largest observed rotation frequency was 21 kHz. Clearly the Hg^+ ions applied a substantial torque to the Be^+ ions. The source of this torque is not clearly understood. The Hg^+ ions remained in the trap for at least several hours unless the cooling was interrupted. If the cooling laser was blocked the Hg^+ ions were lost in several minutes demonstrating that the long term confinement of the Hg^+ was dependent on the torque applied to the Hg^+ ions by the cooling laser via the coupling to the Be^+ ions. Measured Hg^+ temperatures ranged from 0.4 to 1.8 K and Be^+ temperatures ranged from less than 0.05 to 0.2 K. The difference in the temperatures may result from the thermal coupling between the Be^+ and Hg^+ ions being weak. Because we were

only able to measure the plasma boundaries from a perspective along a direction perpendicular to the z axis (see Fig. 1), we were unable to experimentally verify the existence of a gap between the two ion species. Future experiments are planned which should enable us to study the two species nonneutral plasma in more detail. In particular, by viewing the plasma in a direction along the z axis, a measure of the plasma boundaries in the z = 0 plane can be obtained. This should enable us to experimentally check the presence of a gap between the two ion species. In summary, the effectiveness of sympathetic cooling and compression was demonstrated. Long confinement times, high densities, and low temperatures were achieved on the trapped Hg^+ ions.

ULTRACOLD POSITRON SOURCE

Cooling and compression of positrons by sympathetic cooling with laser cooled $^9Be^+$ ions appears to be experimentally possible. The gap between the species in this case where $m_2/m_1 >> 1$ can be quite small. For $\omega < \Omega_2 << \Omega_1$, Eq. 7 can be rewritten $n_2/n_1 \cong 1 - \omega/\Omega_2$. For a rotation frequency of $\omega \cong 0.01\Omega_2(Be^+)$ (the condition achieved in the Be^+, Hg^+ experiment), $n_2/n_1 \cong 0.99$. According to Eq. 6 this means the gap between the positrons and Be^+ ions can be quite small and the thermal coupling high. It also follows that the density of the positrons will be approximately limited to the density of the Be^+ ions. In particular, positron densities will be limited to values much less than the Brillouin density for positrons. The principal advantages of sympathetic cooling and compression of positrons, then, are long term confinement and low temperatures. Positron temperatures less than 10 mK appear possible. Two potential applications of such a source of ultracold positrons are as follows.

In a magnetic field $B \geq 6$ T, positron densities greater than 10^{10} cm^{-3} are potentially achievable by sympathetic cooling with Be^+

ions. A positron plasma with densities $n \geq 10^{10}$ cm^{-3} and temperatures $T < 10$ mK is an interesting object to study. In addition to being strongly coupled, the cyclotron and plasma frequencies are quantized,[14] making a quantum mechanical description of the plasma dynamics necessary. Another application of ultracold positrons may be in antihydrogen production. A recent proposal[19] for making antihydrogen uses the three body recombination

$$\bar{p} + e^+ + e^+ \rightarrow \bar{H} + e^+.$$

The rate of this three body process has a $T^{-9/2}$ temperature dependence. Production of antihydrogen would therefore be greatly enhanced by using ultracold positrons.

We gratefully acknowledge the support of the U.S. Office of Naval Research and of the U.S. Air Force Office of Scientific Research. We thank Carl Weimer and Jerome Helffrich for carefully reading the manuscript.

REFERENCES

1. Dehmelt, H.G., Adv. At. Mol. Phys. 3, 53 (1967) and 5, 109 (1969).
2. Wineland, D.J., Itano, W.M., and Van Dyck, Jr., R.S., Adv. At. Mol. Phys. 19, 135 (1983).
3. Bollinger, J.J. and Wineland, D.J., Phys. Rev. Lett. 53, 348 (1984).
4. Brewer, L.R., Prestage, J.D., Bollinger, J.J., and Wineland, D.J., in "Strongly Coupled Plasma Physics," edited by F.J. Rogers and H.E. DeWitt (Plenum, New York, 1987), p. 53.
5. Drullinger, R.E., Wineland, D.J., and Bergquist, J.C., Appl. Phys. 22, 365 (1980).

6. Larson, D.J., Bergquist, J.C., Bollinger, J.J., Itano, W.M., and Wineland, D.J., Phys. Rev. Lett. 57, 70 (1986).
7. Penning, F.M., Physica (Utrecht) 3, 873 (1936).
8. Malmberg, J.H. and deGrassie, J.S., Phys. Rev. Lett. 35, 577 (1975).
9. Malmberg, J.H., Driscoll, C.F., and White, W.D., Physica Scripta T2, 288 (1982).
10. Driscoll, C.F., Fine, K.S., and Malmberg, J.H., Phys. Fluids 29, 2015 (1986).
11. Wineland, D.J., and Itano, W.M., Phys. Rev. A 20, 1521 (1979).
12. Itano, W.M. and Wineland, D.J., Phys. Rev. A 25, 35 (1982).
13. Wineland, D.J. and Itano, W.M., Phys. Today 40, 34 (June 1987); Stenholm, S., Rev. Mod. Phys. 58, 699 (1986).
14. Malmberg, J.H. and O'Neil, T.M., Phys. Rev. Lett. 39, 1333 (1977).
15. Prasad, S.A. and O'Neil, T.M., Phys. Fluids 22, 278 (1979).
16. Wineland, D.J., Bollinger, J.J., Itano, W.M., and Prestage, J.D., J. Opt. Soc. Am. B2, 1721 (1985).
17. O'Neil, T.M., Phys. Fluids 24, 1447 (1981).
18. Bollinger, J.J., Manney, C., and Wineland, D.J., to be published.
19. Kells, W.P., Proceedings of this conference.

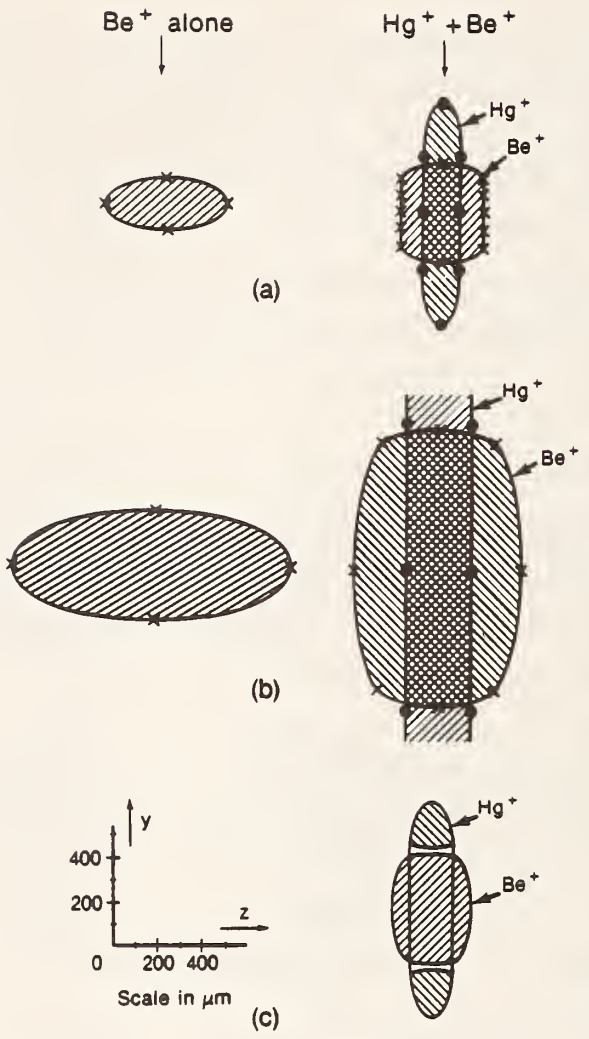

Fig. 1. (a) Measured Be^+- and Hg^+-ion-cloud shapes. The magnetic field is along the z axis. The Be^+ cloud, which contained about 800 ions, is shown with and without the Hg^+ present. The measured rotation frequencies were 41 kHz without Hg^+ [corresponding to a density, $n(Be^+)=3.9\times10^7$ cm^{-3}] and 20 kHz with Hg^+ present [$n(Be^+)=1.9\times10^7$ cm^{-3}, $n(Hg^+)=1.6\times10^7$ cm^{-3}]. The solid lines drawn through the data points conform to the theoretically predicted and separately confirmed spheroidal shape for Be^+ alone but are drawn without consideration of theoretical shapes for Be^+ and Hg^+ together. The edges of the clouds were measured with an uncertainty of about 25 μm. (b) Measured cloud shapes for a Be^+ cloud which contained about 12 000 ions and a Hg^+ cloud which was larger in radial extent than the aperture through the ring electrode (diameter ≅ 2100 μm). The measured rotation frequencies were 73 kHz without Hg^+ [$n(Be^+)=7.0\times10^7$ cm^{-3}] and 18 kHz with Hg^+ [$n(Be^+)=1.8\times10^7$ cm^{-3}, $n(Hg^+)=1.5\times10^7$ cm^{-3}]. (c) Theoretically predicted shapes for cold Be^+ and Hg^+ clouds under conditions similar to those in (a). The scale in (c) also applies to (a) and (b).

Static properties of a non-neutral $^9Be^+$-ion plasma

L. R. Brewer,* J. D. Prestage,† J. J. Bollinger, Wayne M. Itano, D. J. Larson,‡ and D. J. Wineland
Time and Frequency Division, National Bureau of Standards, Boulder, Colorado 80303
(Received 4 January 1988)

We report measurements of the static properties of laser-cooled non-neutral $^9Be^+$-ion plasmas stored in Penning traps under a variety of experimental conditions. We have measured the shape, rotation frequency, density, and temperature of the ions as functions of the Penning-trap potential and laser-cooling configuration. Two different traps were used. In one trap, we were able to measure the ion temperature in directions both perpendicular and parallel to the trap magnetic field. In the other trap, $^{198}Hg^+$ ions were stored simultaneously with the $^9Be^+$ ions and their effect on the $^9Be^+$ ions was measured. The experimental measurements are compared with theoretical predictions. Within experimental error, the ion plasmas rotate without shear and exhibit approximate thermal equilibrium. For a single stored species, a static model of the ion plasmas, based on thermal equilibrium, is formulated. When the ion-plasma dimensions are small compared to the trap dimensions, this model predicts that the ion plasmas are spheroidal and have an aspect ratio which is a function of the plasma rotation frequency, and the single-particle cyclotron and axial frequencies. This is verified by measurement. The ion densities and temperatures measured in our experiments show that the plasmas are strongly coupled and should exhibit liquid and solid properties.

I. INTRODUCTION

In this paper, we discuss some of the static properties of non-neutral $^9Be^+$-ion plasmas stored in Penning traps. In particular, we describe both experimental and theoretical investigations of the shape, rotation frequency, density, and temperature of the $^9Be^+$ ions. Some aspects of these investigations have been briefly reported in Refs. 1–3. They are interesting from the standpoint of basic plasma physics and may have other applications as well. For example, uncertainties in very-high-resolution spectroscopy of stored ions may be dominated by inaccuracies in the measurement of the second-order Doppler-frequency shift. Therefore, a precise knowledge of the velocity distribution of the ions in the plasma would be desirable.

The $^9Be^+$ ions are cooled by a laser to temperatures less than 1 K. The number of ions stored in these experiments ranges from a few hundred to about 40 000. Even with these small ion numbers, the low temperatures obtained by the laser cooling result in Debye lengths (defined below) which are small compared to the stored plasma dimensions. The $^9Be^+$ ion "clouds" can be considered plasmas in the sense that they satisfy this criterion.[4]

In Sec. II we begin by describing the Penning trap, its electrostatic potential, and the characteristic motion of ions in the trap. We examine the single-particle distribution function, which gives the probability of finding a particle with a specific position and velocity, assuming axial symmetry of the trap and thermal equilibrium of the ions. We then examine the distribution function in the limit that the temperature $T=0$ and solve for the ion density, electrostatic potential, and shape. We find a relationship between the plasmas' rotation frequency and aspect ratio. Next, we discuss laser cooling and its effect on the angular momentum of the ion plasma. Finally, we discuss the one-component plasma, a particularly well-studied theoretical model, which is relevant to our experiment. Section III presents a description of the experimental apparatus, including the two traps used in the experiments, the loading procedure for these traps, the optical excitation scheme, and the experimental layout. The experimental diagnostics for measuring the plasma shape, rotation frequency, and temperature are then discussed. In Sec. IV the experimental data are presented and compared with theoretical predictions. Data on plasma shear, shape, and rotation frequency versus aspect ratio are discussed as well as low-temperature data for small plasmas. Finally, we conclude and briefly discuss possible future experiments.

II. THEORY

A. Confinement geometry

The quadrupole Penning trap,[5–8] shown schematically in Fig. 1, is composed of two "endcap" electrodes and a "ring" electrode which are biased with respect to each other by a static electric potential. The symmetry axis of the trap is assumed to be parallel to a static magnetic field B. The magnetic field provides confinement of the ions in directions perpendicular to the magnetic field. The ions are prevented from leaving the trap along the magnetic-field lines by the applied electrostatic potential. This configuration is similar to that used by Malmberg and De Grassie.[4] In our apparatus, electrodes which are hyperboloids of revolution give rise to an applied trap potential (in cylindrical coordinates)

$$\phi_T=\frac{m\omega_z^2}{4q}(2z^2-r^2)\ , \tag{1}$$

where m and q are the ion mass and charge, and the axial

 1988 The American Physical Society

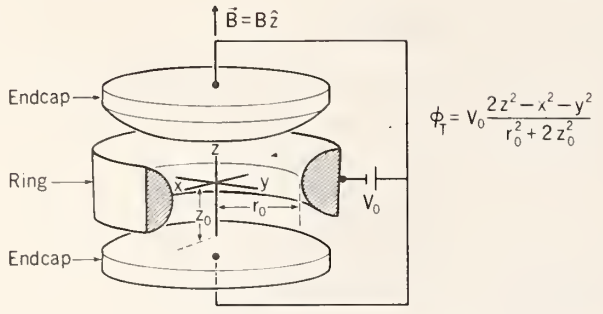

FIG. 1. Penning trap. The two endcap electrodes are biased with respect to the ring electrode by a voltage V_0. The quadratic trap potential is a consequence of the shape of the electrodes, which are hyperboloids of revolution. We neglect the distortion of the potential from the effects of truncation and holes in the electrodes. The motion of the ions in a direction perpendicular to the trap axis is constrained by the trap magnetic field. Ions are prevented from escaping along the magnetic field lines by the quadrupole electric field. Two coordinate systems are used in this paper: the Cartesian and cylindrical coordinate systems.

frequency ω_z is defined by the equation

$$\omega_z^2 = \frac{4qV_0}{m(r_0^2+2z_0^2)} \ . \tag{2}$$

Here V_0 is the electric potential applied between the ring and endcaps, and r_0 and z_0 are the characteristic trap dimensions as shown in Fig. 1. The motion of a single trapped ion is composed of a harmonic oscillation along the z axis at frequency ω_z, and two circular motions in the x-y plane. The ion undergoes a circular $\mathbf{E}\times\mathbf{B}$ drift at a frequency ω_m (this is sometimes called the magnetron frequency). In addition, the ion undergoes a circular motion at a frequency typically near the cyclotron frequency $\Omega = qB/(mc)$, where c is the speed of light. For simplicity we assume that $q>0$ throughout this paper. This frequency is shifted from the cyclotron frequency by the trap electric fields and is equal to $\Omega-\omega_m$. Typically the trap is operated with $\omega_m \ll \Omega$. For a sample of many ions, the $\mathbf{E}\times\mathbf{B}$ drift frequency ω_m is replaced by a rotation frequency for the plasma as a whole. Since the rotation frequency is partly determined by space charge, measurement of this frequency allows a determination of the ion density as discussed in the following sections.

B. Thermal equilibrium

We assume that the $^9Be^+$ ions are in thermal equilibrium due to the Coulomb interaction between ions. Because the Penning trap is axially symmetric, in thermal equilibrium the single-particle distribution function (Boltzmann distribution) can be written (in cylindrical coordinates) as[2,9–11]

$$f = n_0 \left[\frac{m}{2\pi k_B T}\right]^{3/2} \exp\left[-\frac{H+\omega l_z}{k_B T}\right] , \tag{3}$$

$$H = mv^2/2 + q\phi(r,z) \ , \tag{4}$$

$$l_z = mv_\theta r + qA_\theta r/c, \quad A_\theta = Br/2 \ . \tag{5}$$

Here H is the Hamiltonian for an ion in the plasma in the laboratory frame of reference, l_z is the canonical angular momentum about the z axis for an individual ion of the plasma, and k_B is Boltzmann's constant. The parameters ω and T, the temperature, are determined by the total angular momentum and energy of the system. In addition, v_θ is the velocity of an ion in the $\hat{\theta}$ (azimuthal) direction, A_θ is the component of the vector potential $\mathbf{A}$ in the $\hat{\theta}$ direction, and ϕ is the total electrostatic potential. If we assume $\phi=0$ at the center of the trap, then n_0 is the density of the plasma at the center of the trap. In Eq. (3), we chose to use a plus sign in front of ω because for positively charged ions this convention leads to $\omega>0$. For a more unified presentation where trapping particles of either sign is being considered, see Ref. 2. Inserting Eqs. (4) and (5) into Eq. (3), we find

$$f = n(r,z)\left[\frac{m}{2\pi k_B T}\right]^{3/2} \exp\left[-\tfrac{1}{2}m\frac{(\mathbf{v}+\omega r\hat{\theta})^2}{k_B T}\right] , \tag{6}$$

where

$$n(r,z) = n_0 \exp\{-[q\phi(r,z) + \tfrac{1}{2}m\omega(\Omega-\omega)r^2]/k_B T\} \ . \tag{7}$$

The density as a function of the coordinates r and z is given by $n(r,z)$. Bounded solutions exist for $\omega_m < \omega < \Omega-\omega_m$.[2] The velocity distribution in Eq. (6) describes a Maxwell-Boltzmann velocity distribution superimposed on a rigid-body rotation with frequency $-\omega$. The negative sign means that the rotation is in the $-\hat{\theta}$ direction. In particular, the plasma rotates without shear. This result relies only on thermal equilibrium and axial symmetry of the confinement geometry.

The single-particle distribution function of Eqs. (3)–(5) neglects any correlated behavior of the ions. For the densities and temperatures that can be achieved in our experiment, correlations in the spatial positions of the ions are expected (see Sec. II E). In general, the theory developed in the remainder of this section from Eqs. (3)–(5) will not provide a correct description for short length scales, in particular, for length scales less than the interparticle spacing. For small, correlated plasmas with dimensions of a few interparticle spacings, the theory may only give an approximate, qualitative description of the plasma state. Nevertheless, Eqs. (3)–(5) should give a correct description of the plasma state for length scales longer than the coherence length of the correlations (typically, a few interparticle separations). Since the spatial resolution obtained in the experiments reported here is larger than the interparticle spacing, the theory developed here should be adequate.

In the $T=0$ limit, for the plasma density [Eq. (7)] to remain finite in the plasma interior, the following condition must hold:

$$q\phi(r,z) + \tfrac{1}{2}m\omega(\Omega-\omega)r^2 = 0 \ . \tag{8}$$

TN-92

The potential ϕ is independent of z. This is just the statement that there can be no force along a magnetic-field line in a zero temperature plasma. If the expression for $\phi(r,z)$ obtained from Eq. (8) is substituted into Poisson's equation, we see that the density is constant and is given by[2,10,11]

$$n_0=\frac{m\omega(\Omega-\omega)}{2\pi q^2} . \tag{9}$$

In this paper we are interested in the case where the trap potential ϕ_T is given by the quadratic potential of Eq. (1). However, we note that Eq. (9) holds independently of the form of ϕ_T as long as it is axially symmetric. For finite temperatures, Eq. (7) and Poisson's equation imply that the ion density is constant up to the edge of the plasma and then drops off in a distance characterized by the Debye length,[11]

$$\lambda_D\equiv\left[\frac{k_BT}{4\pi n_0q^2}\right]^{1/2} . \tag{10}$$

The picture obtained in the limit $T=0$ of a constant density plasma with sharp boundaries is valid for temperatures low enough so that $\lambda_D \ll$ plasma dimensions. Most of the plasma temperatures measured in our experiment were of order 1 K or less. Typically, the density of the trapped $^9Be^+$ plasmas was 2×10^7 ions/cm^3. These values gave a Debye length λ_D of 15 μm or less, whereas the measured plasma dimensions were typically larger by more than an order of magnitude. Therefore the $T=0$ limit is appropriate.

The total electrostatic potential ϕ is composed of three terms:

$$\phi=\phi_T+\phi_I+\phi_{\text{ind}} . \tag{11}$$

Here ϕ_I is the potential due to the trapped ions and ϕ_{ind} is the potential due to the charges induced on the electrodes by the trapped ions. The potential ϕ_{ind} can be neglected when the trap dimensions are large compared to the plasma. This condition was achieved in the experiments and is assumed below. Solving for the ion potential using Eqs. (1), (8), and (11), we find that inside the plasma,

$$\phi_I=\phi-\phi_T , \tag{12}$$

$$\phi_I=\frac{-m}{2q}[\omega(\Omega-\omega)-\omega_z^2/2]r^2-\frac{m\omega_z^2z^2}{2q}$$

$$=-\tfrac{2}{3}\pi qn_0(ar^2+bz^2) , \tag{13}$$

where Eq. (13) serves to define a and b, and $2a+b=3$ as required by Poisson's equation. The last expression in Eq. (13) is just the potential in the interior of a uniformly charged spheroid.[2] A spheroid is the shape obtained by rotating an ellipse about one of its principal axes.

C. Aspect ratio versus rotation frequency

From the definition of b in Eq. (13) and the expression for n_0 in Eq. (9), we find that

$$b=\frac{3\omega_z^2}{2\omega(\Omega-\omega)} . \tag{14}$$

For a uniformly charged spheroid of diameter $2r_{\text{cl}}$ in the $z=0$ plane and axial extent $2z_{\text{cl}}$, the coefficient b in the potential is given in terms of the aspect ratio $z_{\text{cl}}/r_{\text{cl}}$ by the following expressions.[2,12] When the plasma or ion cloud is a prolate spheroid ($z_{\text{cl}}>r_{\text{cl}}$),

$$b=k_{p'}\{\ln[(1+k_p)/(1-k_p)]/2k_p-1\} ,$$
$$k_{p'}=3(1-k_p^2)/k_p^2 , \tag{15}$$
$$k_p=[1-(r_{\text{cl}}/z_{\text{cl}})^2]^{1/2} .$$

When the plasma is an oblate spheroid ($r_{\text{cl}}>z_{\text{cl}}$),

$$b=k_{0'}[(1-k_0^2)^{-1/2}-\sin^{-1}(k_0)/k_0] ,$$
$$k_{0'}=3(1-k_0^2)^{1/2}/k_0^2 , \tag{16}$$
$$k_0=[1-(z_{\text{cl}}/r_{\text{cl}})^2]^{1/2} .$$

Equations (14)–(16) relate the aspect ratio of the plasma to its rotation frequency ω. These equations are valid for uncorrelated plasmas with λ_D much less than the plasma dimensions which are much less than the trap dimensions. They should also give an approximate description for correlated plasmas, with the additional condition that the plasma dimensions are much larger than the coherence length of the spatial correlations.

D. Laser cooling and angular momentum

Laser cooling[13–15] uses the resonant scattering of laser light by atomic particles. The laser is tuned to the red, or low-frequency side of the atomic "cooling transition" (typically an electric dipole transition). Some of the ions with a velocity component opposite to the laser beam propagation ($\mathbf{k}\cdot\mathbf{v}<0$) will be Doppler shifted into resonance and absorb photons at a relatively high rate. Here, $\mathbf{k}$ is the photon wave vector ($|\mathbf{k}|=2\pi/\lambda$, where λ is the wavelength of the cooling radiation). For the opposite case ($\mathbf{k}\cdot\mathbf{v}>0$), the ions will be Doppler shifted away from the resonance and the absorption rate will decrease. When an ion absorbs a photon, its velocity is changed by an amount

$$\Delta\mathbf{v}=\hbar\mathbf{k}/m \tag{17}$$

due to momentum conservation. Here $\Delta\mathbf{v}$ is the change in the ion's velocity, m is the mass of the ion, and $2\pi\hbar$ is Planck's constant. The ion spontaneously reemits the photon symmetrically. In particular, averaged over many scattering events, the reemission does not change the momentum of the ion. The net effect is that for each photon scattering event, the ion's average velocity is changed by an amount shown in Eq. (17). To cool an atom from 300 K to millikelvin temperatures takes typically 10^4 scattering events. The theoretical cooling limit, due to photon recoil effects,[13–15] is given by a temperature equal to $\hbar\gamma/(2k_B)$ where γ is the radiative linewidth of the atomic transition in angular frequency units. For a linewidth $\gamma=2\pi\times19.4$ MHz, which is the radiative

linewidth of the $2s\ ^2S_{1/2} \rightleftharpoons 2p\ ^2P_{3/2}$ transition in $^9Be^+$ ($\lambda = 313$ nm), the theoretical minimum temperature is 0.5 mK.

Laser scattering can also be used to change the angular momentum of the plasma. Equation (5) shows that the z component of the canonical angular momentum for an individual ion in the plasma is

$$l_z = mv_\theta r + \frac{qBr^2}{2c} \ . \tag{18}$$

The two terms in Eq. (18) are the plasma's mechanical angular momentum and the field angular momentum. The total z component of the angular momentum of the plasma is

$$\begin{aligned} L_z &= \int dz \int 2\pi r\, dr \int d^3v\, f(r,z,v) l_z \\ &= m(\Omega/2 - \omega) N \langle r^2 \rangle \ . \end{aligned} \tag{19}$$

Here N is the total number of ions and $\langle r^2 \rangle$ is the mean-squared radius of the plasma. For all of the work described in this paper, $\omega \ll \Omega$ and

$$L_z \approx \frac{m\Omega N}{2} \langle r^2 \rangle > 0 \ . \tag{20}$$

Therefore the total angular momentum is dominated by the field angular momentum. Suppose the cooling laser is directed normal to the z axis but at the side of the plasma which is receding from the laser due to the plasma rotation. Because the rotation of the positive ions is in the $-\hat{\theta}$ direction, the torque of the laser on the ions will also be negative. Consequently, angular momentum is removed from the plasma and according to Eq. (20) the radius of the plasma must decrease. In general, the plasma is compressed until the torque due to the cooling laser is balanced by another external torque. As the radius decreases, the density of the plasma increases. Even in the absence of external torques, there is a limit to how far the plasma can be compressed. From Eq. (9), the maximum density, known as the Brillouin density, occurs when the rotation frequency $\omega = \Omega/2$. The Brillouin density is given by

$$n_{\max} = \frac{m\Omega^2}{8\pi q^2} \ . \tag{21}$$

Collisions with background gas particles produce an external torque which increases the angular momentum of the plasma. This is one of the effects that could limit the compression of the plasma. External torques due to axial asymmetries of the trap are also limiting effects. Driscoll, Fine, and Malmberg observed that the axial asymmetries of their cylindrical traps play an important role in determining the trap confinement time.[16] Axial asymmetries are also expected to be a limiting effect in the experiments reported here.[2]

E. One-component plasma

In the frame of reference rotating about the trap axis with frequency $-\omega$, the ion plasma behaves like a neutral one-component plasma. A one-component plasma[17] is composed of a single species of charge embedded in a background of neutralizing charge of uniform density. Malmberg and O'Neil[10] have shown that the static properties of magnetically confined non-neutral plasmas are the same as those for a one-component plasma. In our experiments, the identification of the neutralizing background charge can be made by writing $\phi = \phi_I + \phi_T$ [from Eq. (12)], in Eq. (7). With Eqs. (1) and (13), the terms $q\phi_T(r,z) + \frac{1}{2}m\omega(\Omega - \omega)r^2$ can be interpreted as the potential energy of the ions due to a hypothetical spheroid of uniform negative charge. The hypothetical spheroid has the same aspect ratio as the ion plasma and has a charge density equal to $-qn_0$.

The one-component plasma is characterized by a coupling constant

$$\Gamma = \frac{q^2}{a_S k_B T} \ , \tag{22}$$

which is a measure of the nearest-neighbor Coulomb energy divided by the thermal energy of a particle. The ion-sphere or Wigner-Seitz radius a_S is defined by

$$\tfrac{4}{3}\pi a_S^3 n_0 = 1 \ . \tag{23}$$

For $\Gamma > 1$, the plasma is said to be strongly coupled.[17] When $\Gamma > 2$, the plasma should exhibit liquidlike behavior characterized by short-range order. Theoretical calculations predict[18] that at $\Gamma = 178$, the plasma undergoes a phase transition to a crystal-like structure. Because the static thermodynamic properties of the one-component plasma are the same as those for a magnetically confined non-neutral plasma, the magnetically confined plasmas of a Penning trap are also characterized by the coupling Γ. In particular, at $\Gamma = 178$, a liquid-solid phase transition may take place. At a magnetic field of 10 T, the Brillouin density for $^9Be^+$ is 3×10^{10} ions/cm^3. This density and the 0.5-mK cooling temperature limit gives a theoretical limit on the coupling of $\Gamma = 1.7 \times 10^4$. Consequently, the possibility of obtaining couplings large enough to observe a liquid-solid phase transition looks promising.

Because this is a first-order phase transition, the plasma may remain in a metastable fluidlike state if it is rapidly cooled below the transition temperature. Ichimaru and Tanaka have investigated the lifetime of the metastable supercooled state.[19] For a $^9Be^+$ plasma with density of 10^{10} ions/cm^3, they estimate that at $\Gamma = 400$ the metastable state has a minimum lifetime with a value between 20 and 2×10^5 s. At larger values of Γ, the metastable-state lifetime increases rapidly and at $\Gamma \approx 1000$ the supercooled plasma may undergo a dynamic glass transition. In the absence of heating effects, the laser cooling rate for cold $^9Be^+$ ions ($T < 10$ mK) can be much larger than 100 K/s. Consequently, it appears that the laser cooling of the ions can be done rapidly compared to the $\Gamma = 400$ metastable lifetime. This would permit the investigation of the dynamic glass transition. The correspondence between the magnetically confined non-neutral plasma and the one-component plasma rigorously exists only for static properties. The possibility of a dynamic glass transition in a one-component plasma is therefore a suggestion

of what might happen in the magnetically confined non-neutral plasma.

III. EXPERIMENTAL TECHNIQUES

A. Traps

Two different Penning traps were used in this experiment. The first trap (trap I) was constructed from gold mesh (for the endcaps) and molybdenum wire (for the ring electrode) so that a large fraction of the resonance fluorescence from the ions could be collected by an ellipsoidal mirror and focused onto a phototube. Trap I was used in experiments on $^9Be^+$ ions only. Trap II was used to observe both $^{198}Hg^+$ and $^9Be^+$ ions. It was constructed of solid molybdenum with 0.25-cm-diam holes in the ring electrode to allow entrance and exit of the laser beams directed in the x-y plane and to allow the ions' fluorescence to be collected by a phototube. In addition, small holes were located in the endcap electrodes of trap II for the purpose of loading the ions into the trap. Both traps had dimensions $r_0=0.417$ cm and $z_0=0.254$ cm (see Fig. 1). In order that the vacuum region be relatively contaminant-free, both traps were baked out at temperatures between 300 and 400 °C for several days. Base pressures of about 10^{-8} Pa ($\approx 10^{-10}$ Torr) were maintained in both traps by sputter-ion pumps. This allowed the ions to be trapped for hours even without laser cooling. Typically, the trap voltages V_0 in both traps were varied between 1 and 4 V. The magnetic field B was 1.4 T for the work reported here.

B. Loading

Ions were loaded into the traps as follows. In both traps, a 75-μm-diam, coiled-tungsten electron filament was located behind one endcap. During loading, the electron filament was biased negatively with respect to the endcap. Electrons emitted from the filament spiraled along the magnetic field lines with enough kinetic energy to ionize atomic beryllium (ionization potential $=9.32$ eV) in the trap. The electron energy inside the trap near the endcap electrodes typically exceeded the ionization potential of $^9Be^+$ by only 0.5 to 1 eV. This helped prevent the creation of other ions with higher ionization potentials. The beryllium oven was located behind the ring electrode in trap I and behind an endcap electrode in trap II. Both ovens consisted of a 75-μm-diam tungsten filament around which was wrapped a 50-μm-diam beryllium wire. Beryllium atoms were evaporated by heating the tungsten filament with a current. The tungsten wire provided strength for operation of the ovens in the magnetic field. To create $^9Be^+$ ions in the trap, the beryllium oven and the electron filament were turned on for approximately a 15-s duration after the trap potential was momentarily reversed to clear any other ions out of the trap. The trapping voltage was then briefly raised to a value sufficiently high to remove any heavier ions with mass-to-charge ratio >15 (atomic mass units divided by the proton charge) that may have been formed in the trap. After this, the ions were laser cooled to temperatures less than 1 K. In practice, for the laser powers and ion numbers reported in this paper, this cooling was rapid, taking a few seconds to accomplish. The $^{198}Hg^+$ was loaded into trap II by ionizing neutral ^{198}Hg vapor which was leaked into the vacuum system.

C. Laser excitation scheme

The energy-level structure of the $^9Be^+$ ground state and lowest $^2P_{3/2}$ state are shown in Fig. 2. The cooling laser (polarization perpendicular to B) is tuned slightly to the red of the transition between the $2s\,^2S_{1/2}(m_I,m_J)=(+\frac{3}{2},+\frac{1}{2})$ and the $2p\,^2P_{3/2}(+\frac{3}{2},+\frac{3}{2})$ states. Ions are optically pumped by the cooling laser into the $2s\,^2S_{1/2}(+\frac{3}{2},+\frac{1}{2})$ state with $\frac{16}{17}\approx 94\%$ efficiency[20,21] [see Eq. (25)]. That is, for laser intensity below saturation, $\frac{16}{17}$ of the ions reside in the $2s\,^2S_{1/2}(+\frac{3}{2},+\frac{1}{2})$ state. The cooling laser had a wavelength of 313 nm and a power of up to 50 μW. The 313-nm laser light was obtained by frequency-doubling 626-nm light from a single-mode dye laser in a temperature phase-matched crystal of rubidium dihydrogen phosphate (RDP). The dye-laser frequency was locked to an iodine reference line using a Doppler-

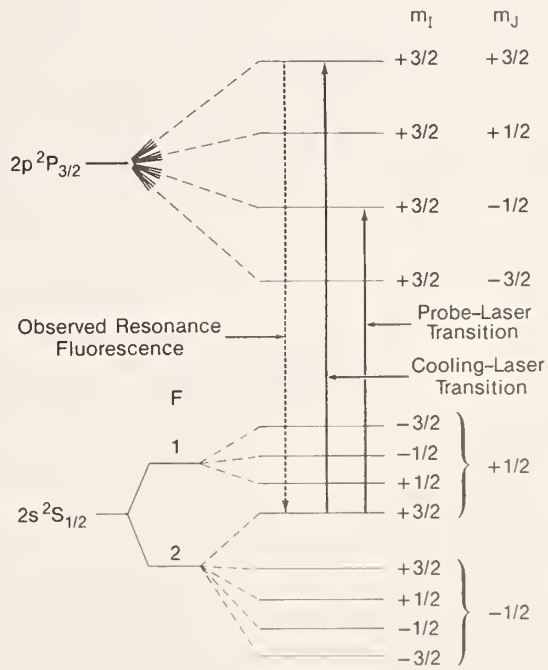

FIG. 2. Hyperfine structure of $^9Be^+$ in a magnetic field, showing the transitions pertinent to the analysis of the experiment. The cooling transition is from the $2s\,^2S_{1/2}(m_I,m_J)=(+\frac{3}{2},+\frac{1}{2})$ state to the $2p\,^2P_{3/2}(+\frac{3}{2},+\frac{3}{2})$ state. The probe depopulation transition is from the $2s\,^2S_{1/2}(+\frac{3}{2},+\frac{1}{2})$ state to the $2p\,^2P_{3/2}(+\frac{3}{2},-\frac{1}{2})$ state. The figure is not drawn to scale. The frequency splittings between the $2s\,^2S_{1/2}$ $|\Delta m_I|=1$, $|\Delta m_J|=0$ states are on the order of 300 MHz. Only the $2p\,^2P_{3/2}$, $m_I=+\frac{3}{2}$ states are shown because the frequency splittings between the $2p\,^2P_{3/2}$ $|\Delta m_I|=1$, $|\Delta m_J|=0$ states are on the order of 1 MHz.

free saturated absorption technique. The ions' resonance fluorescence (i.e., the scattered light) from the cooling transition was detected in a photomultiplier tube. The fluorescence is proportional to the number of ions in the $2s\ ^2S_{1/2}(+\frac{3}{2},+\frac{1}{2})$ state.

A second laser, called the probe laser, could be used to remove ions from the $2s\ ^2S_{1/2}(+\frac{3}{2},+\frac{1}{2})$ state by resonantly exciting them to the $2p\ ^2P_{3/2}(+\frac{3}{2},-\frac{1}{2})$ state (the "depopulation transition") from which they decayed with a probability of $\frac{2}{3}$ to the $2s\ ^2S_{1/2}(+\frac{3}{2},-\frac{1}{2})$ state. This produced a decrease in the observed resonance fluorescence. After the probe laser was turned off, the cooling laser then optically repumped[20] the ground state in about 1 s. The power of the probe laser was $\ll 1\ \mu$W and any direct fluorescence due to excitation with this laser was negligible compared to that of the cooling laser. Figure 3 shows the resonance line shape when the probe laser's frequency was scanned through the depopulation transition. The depopulation resonance was used to measure the shape of the plasma, its rotation frequency, and temperature as described below. The density and number of ions were then derived from these measurements.

D. Laser-beam configuration

The laser-beam configuration for trap I is shown in Fig. 4. The cooling laser beam passed through a 50% beam splitter. The portion of the beam transmitted by the splitter entered the ion cloud perpendicularly to **B**, and the other beam, referred to as the diagonal cooling beam, entered the trap between the ring and one endcap at an angle of $\psi=55°$ with respect to the z axis. The probe laser beam passed through a telescope which was used to translate the beam spatially. This was done by translating one of the probe telescope lenses in a plane perpendicular to the probe beam direction. The probe beam can be directed either at $\psi=90°$ or $\psi=55°$ by means of the splitter. In order to direct the laser beams along the diagonal of the trap, mirrors were mounted inside the vacuum system next to the trap. The cooling laser light scattered from these mirrors was larger than the signal count rate. Consequently the diagonal cooling light beam was chopped at 1 kHz and resonance fluorescence from the perpendicular cooling beam was detected when the diagonal cooling beam was off. In trap II, the experimental setup was similar except that there was only cooling and probing of the ion cloud in a direction perpendicular to **B**. Both the cooling and probe laser beams were focused to waists at the position of the plasma which were small compared to r_{cl} and z_{cl}.

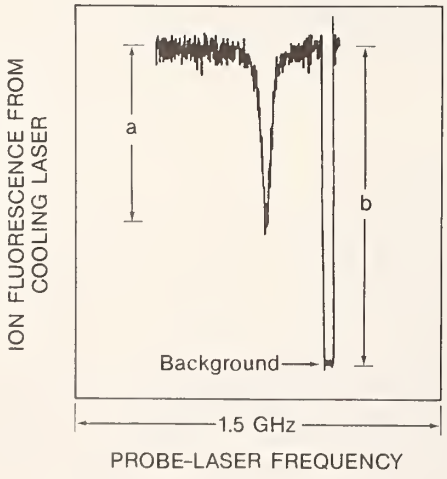

FIG. 3. Ion fluorescence from the cooling laser is plotted as a function of the probe laser frequency. The background signal, due to light scattered from the trap electrodes, not ion fluorescence, is the light the photomultiplier receives when the magnetic field is shifted so that the ions are detuned far from resonance. The quantity $\beta(0)$ [Eq. (26)] is determined experimentally from the ratio a/b.

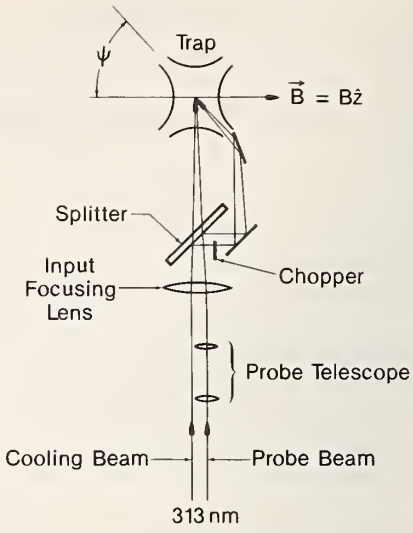

FIG. 4. A schematic diagram of the optical layout for trap I. The cooling laser beam passes through a 50% beam splitter, producing the diagonal cooling beam and a perpendicular cooling beam. The probe laser beam is translated spatially using one lens of the telescope. The diagonal cooling beam is chopped because the diagonal beam mirrors, which are mounted inside the vacuum system, scatter too much light. Resonance fluorescence light from the perpendicular cooling beam is detected only when the diagonal cooling beam is off.

E. Diagnostics

1. Saturation

The width and amplitude of the depopulation resonance (Fig. 3) were used to determine the temperature and shape of the ion cloud. It is easy to saturate the depopulation transition, that is, to remove most of the ions from the $2s\ ^2S_{1/2}(+\frac{3}{2},+\frac{1}{2})$ state and broaden the resonance. This effect must be taken into account in order to determine the true full width at half maximum of the depopulation resonance. In the following discussion it is assumed that the ions have been optically pumped into the $m_I=+\frac{3}{2}$ states. This pumping was reported in

Refs. 20 and 21. First, we note that the cooling laser nonresonantly drives ions from the $2s\,^2S_{1/2}(+\frac{3}{2},-\frac{1}{2})$ ground state to the $2p\,^2P_{3/2}(+\frac{3}{2},+\frac{1}{2})$ state where they decay with $\frac{2}{3}$ probability to the $2s\,^2S_{1/2}(+\frac{3}{2},+\frac{1}{2})$ ground state. This rate is very small compared to the $2s\,^2S_{1/2}(+\frac{3}{2},+\frac{1}{2}) \Longrightarrow 2p\,^2P_{3/2}(+\frac{3}{2},+\frac{3}{2})$ scattering rate because of the large detuning (about 13 GHz at 1.4 T). Let R_p denote the rate for this repumping process. In addition, the cooling laser depletes the $2s\,^2S_{1/2}(+\frac{3}{2},+\frac{1}{2})$ ground state by nonresonantly driving the depopulation transition. The detuning of the cooling laser in this process is approximately four times greater than its detuning in the repumping process. If a Lorentzian line shape far from resonance is assumed, this results in a depletion rate of $R_p/16$. The details of this pumping have been verified in Ref. 22. Finally, let $\alpha(\nu_p-\nu_0')$ be the depletion rate of the $2s\,^2S_{1/2}(+\frac{3}{2},+\frac{1}{2})$ state due to the probe laser. Here ν_p is the probe laser frequency and ν_0' is the center frequency of the depopulation resonance. Because of Doppler shifts, ν_0' will depend on the location of the probe laser in the plasma and the plasma rotation frequency. (See Sec. III E 3). Since the probe laser intensity is very small, we neglect optical pumping effects on other transitions driven nonresonantly by the probe laser. We use a rate equation analysis to determine the full width at half maximum of the depletion rate $\alpha(\nu_p-\nu_0')$ from the observed fluorescence signal (Fig. 3). Let N_+ be the number of ions in the $2s\,^2S_{1/2}(+\frac{3}{2},+\frac{1}{2})$ state. If the cooling laser is well below saturation, we have

$$\frac{dN_+}{dt} = -\alpha(\Delta\nu_p)N_+ + R_p(N-N_+) - \frac{R_p}{16}N_+ \ , \tag{24}$$

where $\Delta\nu_p=\nu_p-\nu_0'$. In steady state, $dN_+/dt=0$, and the number of ions in the $2s\,^2S_{1/2}(+\frac{3}{2},+\frac{1}{2})$ ground state is

$$N_+ = \frac{\frac{16}{17}N}{\frac{16\alpha(\Delta\nu_p)}{17R_p}+1} \ . \tag{25}$$

The fluorescence is proportional to the number of ions N_+. From Eq. (25) we can see that $N_+=(16/17)N$ when the probe laser is off $[\alpha(\Delta\nu_p)=0]$. We normalize this baseline fluorescence ($\propto(16/17)N$) to a value of one when the probe laser is off. The fractional decrease in fluorescence $\beta(\Delta\nu_p)$ for a given detuning of the probe laser is

$$\beta(\Delta\nu_p) = 1-\frac{1}{\frac{16\alpha(\Delta\nu_p)}{17R_p}+1} = \frac{\frac{16}{17}\frac{\alpha(\Delta\nu_p)}{R_p}}{1+\frac{16\alpha(\Delta\nu_p)}{17R_p}} \ . \tag{26}$$

From Eq. (26) we can solve for $\alpha(\Delta\nu_p)/R_p$ and obtain

$$\frac{\alpha(\Delta\nu_p)}{R_p} = \frac{\beta(\Delta\nu_p)}{\frac{16}{17}[1-\beta(\Delta\nu_p)]} \ . \tag{27}$$

This is the equation for the magnitude of the depletion rate α in terms of the magnitude of the observed resonance $\beta(\Delta\nu_p)$. We define the frequencies at half maximum of the depletion rate α to be $\nu_p(\pm)$. At these points $\alpha(\pm)\equiv\alpha[\nu_p(\pm)-\nu_0']=\frac{1}{2}\alpha(0)$. From Eq. (26), the values of β at $\nu_p(\pm)$ are

$$\beta(\pm)\equiv\beta[\nu_p(\pm)] = \frac{\frac{16}{17}\frac{\alpha(\pm)}{R_p}}{1+\frac{16\alpha(\pm)}{17R_p}} = \frac{\frac{16}{17}\frac{\alpha(0)}{2R_p}}{1+\frac{16}{17}\frac{\alpha(0)}{2R_p}} \ . \tag{28}$$

By substituting Eq. (27) into Eq. (28), we obtain

$$\beta(\pm) = \frac{\beta(0)}{2-\beta(0)} \ . \tag{29}$$

Therefore, the full width at half maximum of the depletion rate α is equal to the observed frequency difference between the points $\beta(+)$ and $\beta(-)$ determined from Eq. (29).

2. *Plasma shape*

The probe laser was used to determine the shape, rotation frequency, and temperature of the $^9Be^+$ plasma. The shape of the ion plasma was determined from the depletion rates α obtained for different spatial positions of the probe laser beam. The area under the curve given by $\alpha(\Delta\nu_p)$ is proportional to the number of ions intersected by the probe beam. This assumes that there is good spatial mixing of the ions, so that the ions which are affected by the probe laser beam then migrate to the position of the cooling laser beam in a time which is short compared to R_p^{-1}. This assumption was verified by comparing the method described here with the spatial maps obtained by observing the fluorescence from a second, low-intensity laser beam (intensity much less than the cooling laser beam), which is tuned through the cooling transition[23] (also, see Sec. IV E). Under the conditions of thermal equilibrium, the width of the $\alpha(\Delta\nu_p)$ resonance should be independent of the probe beam position, as long as the waist w_0 of the probe laser beam is small compared to the plasma dimensions. We define the waist of the probe beam in terms of the laser intensity $I=I_0e^{(-2r^2/w_0^2)}$. Typically the waist of the probe beam varied from 15 to 44 μm and was more than a factor of 10 smaller than the plasma dimensions. Consequently $\alpha(0)$, the magnitude of the $\alpha(\Delta\nu_p)$ resonance, is proportional to the number of ions intersected by the probe beam. In addition, in the $T=0$ limit, the density of the ions is constant and $\alpha(0)$ is proportional to the length of the probe beam which intersects the ion plasma. In both traps we determined the plasma shape with the probe laser beam directed perpendicularly to the y-z plane (see Fig. 5). Because of the rotational symmetry of the trap about the z axis we assume that the profiles of the plasma along the x and y axes are equal, that is, the plasma has a circular cross section in the x-y plane.

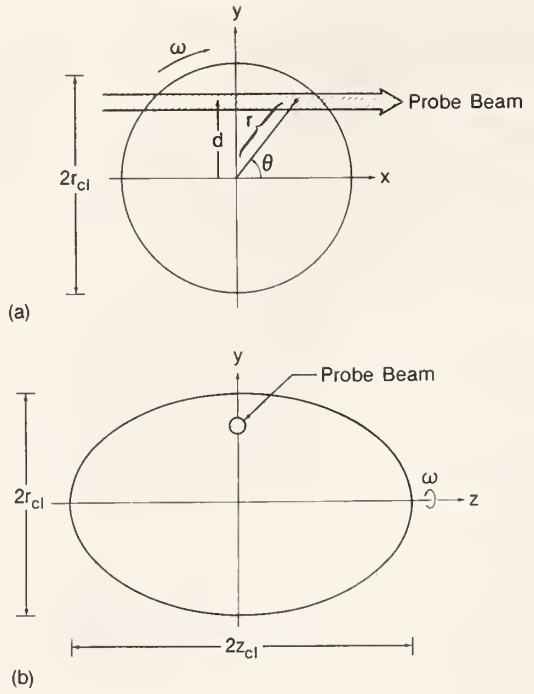

FIG. 5. Plasma with rotation frequency ω is shown in (a) the x-y and (b) the y-z planes. The probe laser beam is directed parallel to the x axis and passes a distance d from the plasma z axis. The sign of d is positive on the side of the plasma which is receding from the probe beam due to the plasma rotation. The plasma shape is mapped by determining the region of intersection of the probe beam with the ion plasma. The dimensions $2z_{cl}$ and $2r_{cl}$ of the plasma are indicated.

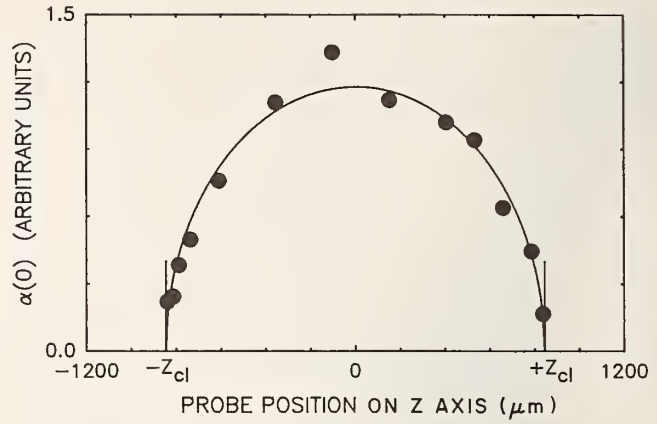

FIG. 6. Depletion rate $\alpha(0)$ is plotted as a function of the probe laser beam position along the z axis for $d=0$. The data have been fitted to an ellipse. This determines the dimension $2z_{cl}$ of the plasma along the z axis and the plasma shape in the x-z plane, to within a scale factor.

The dimensions of the plasma along the y and the z axes, $2r_{cl}$ and $2z_{cl}$, were measured as follows. The plasma dimension along the z axis was determined by scanning the probe laser frequency at various points along this axis. By plotting $\alpha(0)$ versus the probe laser-beam position we could construct, within a scalar factor, a profile of the plasma along the z axis. This profile was then fitted to an ellipse and the dimension of the plasma along the z axis was determined. An example of this is shown in Fig. 6. This process was then repeated for the y axis. The probe laser beam was also used to determine the coordinates of other boundary points of the plasma in the y-z plane by varying its position along different lines parallel to the y and z axes.

3. *Rotation frequency and density*

The rotation frequency ω was determined by measuring the center frequency of the depletion rate α as a function of the y position of the probe laser beam (see Fig. 5). For a cloud without shear, the change in the center of this resonance is expected to vary linearly with the y position of the probe laser beam because of the first order Doppler shift of the depopulation transition, as observed in the laboratory. Figure 5(a) shows the plasma rotating about the z axis. The laser beam passes through the point $x=0$, $y=d$, parallel to the x axis. The Doppler-shifted, depopulation transition frequency ν_0', in the laboratory frame, is

$$\nu_0'=\nu_0+\frac{1}{2\pi}\langle \mathbf{k}\cdot\mathbf{v}\rangle \ . \tag{30}$$

Here ν_0 is the depopulation transition frequency in the rest frame of the ion, $\mathbf{k}$ is the laser light wave vector, $\mathbf{v}$ is the velocity of an ion, and $\langle \mathbf{k}\cdot\mathbf{v}\rangle$ denotes the average value of $\mathbf{k}\cdot\mathbf{v}$ over ions in the probe laser beam. In the absence of shear, the average of $\mathbf{k}\cdot\mathbf{v}$ over the ion velocities is constant along the path of the laser beam (neglecting the finite waist of the laser beam). For any point along the probe laser beam a distance r from the plasma origin [see Fig. 5(a)], we have $\mathbf{k}\cdot\mathbf{v}=k\omega r\sin\theta=k\omega d$.

Let d_1 and d_2 be two different y positions of the probe beam and let $\nu_0'(d_1)$ and $\nu_0'(d_2)$ be the corresponding transition frequencies. The difference in the depopulation transition frequencies is

$$\Delta\nu_0'=\nu_0'(d_1)-\nu_0'(d_2)=\frac{1}{2\pi}k\omega(d_1-d_2)=\frac{1}{2\pi}k\omega\Delta d \ . \tag{31}$$

Solving for the rotation frequency of the plasma, we find that

$$\omega=\frac{\Delta\nu_0'}{\Delta d}\lambda \ . \tag{32}$$

The density is then determined from Eq. (9).

We emphasize that by measuring the rotation frequency of the ion plasma by the first-order Doppler shift of the probe laser beam, we have measured the frequency of an internal degree of freedom of the plasma. In contrast, if we try to measure the rotation frequency by applying a low-frequency, spatially uniform electric field near the frequency ω, the excitation is at the center-of-mass fre-

quency ω_m, the single-particle magnetron frequency (see discussion in Refs. 24 and 25).

4. Temperature

There are several contributions to the width of the depletion resonance α. The resonance is a Voigt profile, that is, a convolution of Gaussian and Lorentzian profiles. The Lorentzian full width at half maximum of the contribution is just the radiative linewidth $\Delta\nu_L = \gamma/2\pi = 19.4$ MHz. The full width at half maximum of the Gaussian contribution $\Delta\nu_G$ is composed of three terms

$$\Delta\nu_G = (\Delta\nu_{T_\perp}^2 + \Delta\nu_{T_\parallel}^2 + \Delta\nu_\omega^2)^{1/2} . \quad (33)$$

Here $\Delta\nu_{T_\perp}$ and $\Delta\nu_{T_\parallel}$ are the Doppler widths due to the assumed thermal distribution of velocities in the ion-cyclotron motion and the ion motion along the z axis, respectively. They are separated because the cyclotron and axial temperatures may be different. The contribution $\Delta\nu_\omega$ is the broadening of the resonance line due to the finite width of the laser-beam waist; this occurs because the Doppler shift for ions changes from one side of the probe waist to the other. We have assumed that the laser beam is Gaussian. In general, for a probe laser beam at an angle ψ with respect to **B** (see Fig. 4), the contributions due to Doppler broadening are

$$\Delta\nu_{T_\perp} = 2\left[\frac{2(ln2)k_B T_\perp \sin^2\psi}{m\lambda^2}\right]^{1/2} , \quad (34)$$

$$\Delta\nu_{T_\parallel} = 2\left[\frac{2(\ln2)k_B T_\parallel \cos^2\psi}{m\lambda^2}\right]^{1/2} . \quad (35)$$

The contribution due to the finite laser-beam waist is

$$\Delta\nu_\omega = w_0\omega(2\ln2)^{1/2}\sin\psi/\lambda . \quad (36)$$

Shear in the plasma would contribute to a further broadening, since the ion's first-order Doppler shift would vary with the ion's position along the probe beam in the plasma. We neglect the effects of shear here and in the data analysis for the temperatures presented later. If shear is present, then the calculated temperatures will be too high.

The temperature $T_\perp$ is measured with the probe laser beam directed perpendicularly to **B**. The Gaussian contribution $\Delta\nu_G$ to the resonance is determined by first deconvoluting the natural linewidth from the full width at half maximum of α. This can be done with the use of tables[26] or by computer algorithm. The term $\Delta\nu_\omega$ is subtracted in quadrature from the Gaussian width and the temperature is given by

$$T_\perp = (\Delta\nu_G^2 - \Delta\nu_\omega^2)m\lambda^2/(8k_B\ln2) . \quad (37)$$

In trap I the axial (or parallel) temperature is obtained by probing at an angle of $\psi = 55°$ and using the measured Gaussian contribution, $\Delta\nu_G(\psi = 90°)$ obtained with the probe beam directed perpendicularly to **B**. In this case

$$T_\parallel = \frac{m\lambda^2[\Delta\nu_G^2(\psi=55°) - \sin^2(55°)\Delta\nu_G^2(\psi=90°)]}{8k_B\cos^2(55°)\ln2} . \quad (38)$$

In trap II we could only cool and probe in a direction perpendicular to **B** and therefore we could only measure $T_\perp$.

IV. RESULTS

A Shear

It was important to test for shear in the plasma because its absence was a fundamental assumption of the theory presented in Sec. II and the data analysis of this paper. Earlier data taken by Larson *et al.*[3] indicated the possible presence of shear when both $^9Be^+$ and $^{198}Hg^+$ ions were loaded into trap II. We attempted to measure shear in $^9Be^+$ plasmas in trap II both with and without simultaneously loaded $^{198}Hg^+$ ions. Figure 7 shows data taken on a $^9Be^+$ plasma without $^{198}Hg^+$ ions. The depopulation resonance center frequency ν_0' is plotted versus the probe beam position d. According to Eq. (32), the

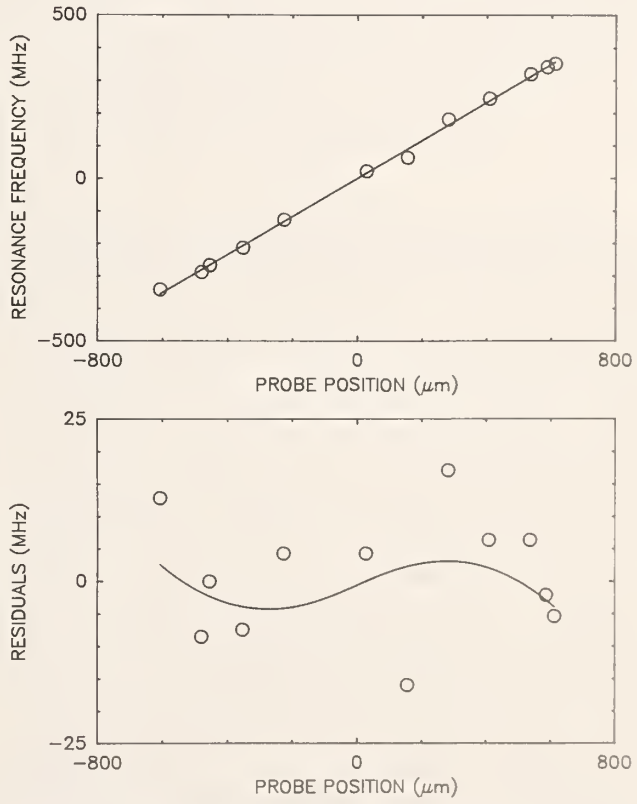

FIG. 7. Depopulation resonance center frequency ν_0' is plotted in the upper graph vs the probe beam position d for a plasma of 30000 $^9Be^+$ ions with a density of 2.8×10^7 ions/cm^3. The resonance frequency ν_0' is plotted relative to the unshifted transition frequency ν_0 in the rest frame of an ion. The solid line is a least-squares linear fit. The residuals are plotted below, along with a fit which includes shear. The result of the fit is $\xi = -0.1\pm0.1$. The data were taken at a magnetic field of 1.4 T and a trap axial frequency of $\omega_z/2\pi = 212$ kHz.

plot should be linear with a slope determined by the plasma rotation frequency. Any deviations from a linear relationship would provide evidence for shear. The data were fitted using the following treatment. We assumed that the shear, if present, was linear with radius, so that the rotation frequency as a function of radial position was given by

$$\omega' = \omega \left[1 + \frac{\xi r}{r_{\rm cl}} \right] , \tag{39}$$

where r is the cylindrical radial coordinate, $r_{\rm cl}$ is the radius of the plasma, and ξ is a coefficient providing a measure of the size of the shear. The Doppler-shifted, depopulation transition frequency ν_0' [see Eq. (30)] is then given by

$$\nu_0' = \nu_0 \left[1 + \frac{d\omega}{c} \left[1 + \xi \frac{\langle r \rangle}{r_{\rm cl}} \right] \right] , \tag{40}$$

where d is the distance (along the y axis) of the probe laser beam from the center of the plasma (see Fig. 5), and $\langle r \rangle$ is the average cylindrical radius for ions in the path of the probe beam. We have chosen d to be positive on the side of the plasma which is receding from the laser due to the plasma rotation. If we neglect the finite waist of the probe beam, $\langle r \rangle$ can be calculated analytically from a one-dimensional integral with the result

$$\frac{\langle r \rangle}{r_{\rm cl}} = \frac{1}{2} + \frac{(d/r_{\rm cl})^2}{2[1-(d/r_{\rm cl})^2]} \ln \left[\frac{[1-(d/r_{\rm cl})^2]^{1/2}+1}{|d|/r_{\rm cl}} \right] . \tag{41}$$

Equation (41) was substituted into Eq. (40) and the resulting equation was fitted to the data of Fig. 7 with the result $\xi = -0.1 \pm 0.1$. Therefore within experimental error there was no shear in this plasma. A correct treatment of the Doppler shift due to shear involves integrating the Voigt resonance profile along the path of the probe laser beam. In general this will result in an asymmetric line. The center of gravity of this line, however, will be given by Eqs. (40) and (41). This more detailed calculation was done for typical conditions obtained in the lab. For a $^9Be^+$ plasma with radius $r_{\rm cl} = 500$ μm, rotation frequency of 19 kHz, and a shear coefficient $\xi = 0.33$ (see Fig. 8), the asymmetry of the resulting resonance profile was small, producing less than a 0.5-MHz deviation in the resonance center. The broadening of the Voigt profile due to this shear was less than 5%, which would increase the apparent temperature of the plasma by a small amount.

A dramatic change in the $^9Be^+$ plasma was observed when $^{198}Hg^+$ ions were added to the trap.[3] Without $^{198}Hg^+$ ions in the trap, rotation frequencies as large as 200 kHz were measured. With $^{198}Hg^+$ ions in the trap, rotation frequencies on the order of 20 kHz were obtained. Clearly the $^{198}Hg^+$ ions applied a substantial torque to the $^9Be^+$ ions. In addition, in the $T = 0$ limit, the $^{198}Hg^+$ ions are expected to centrifugally separate and be located outside of the $^9Be^+$ ions.[27] A direct measurement of this separation was not possible in Ref. 3, due to the restricted probe laser-beam directions, although the separation was indirectly verified by the agreement between the measured plasma shapes and the shapes calculated from a $T = 0$ theory. The torque applied by the $^{198}Hg^+$ ions on the $^9Be^+$ ions opposes the torque due to the cooling laser, and, if centrifugal separation takes place, this torque is applied on the edge of the $^9Be^+$ cloud, while the cooling laser torque is applied in the interior of the $^9Be^+$ cloud. Shear, if present, may therefore be larger in a two-species plasma of $^9Be^+$ and $^{198}Hg^+$ ions and is expected to consist of $^9Be^+$ ions rotating more slowly at the plasma edge than the center. Figure 8 shows data taken by Larson *et al.*[3] of the $^9Be^+$ depopulation resonance center frequency versus the probe position with both $^9Be^+$ and $^{198}Hg^+$ ions in the trap. A least-squares fit of Eqs. (40) and (41) to the data determined $\xi = 0.33 \pm 0.12$. The condition $\xi > 0$ indicates that the $^9Be^+$ ions are rotating faster at the plasma edges than at the center, contrary to what was expected. Figure 9 shows more recent data for another $^9Be^+$ and $^{198}Hg^+$ plasma. The fit to the data resulted in $\xi = 0.06 \pm 0.1$ and shows that in the context of the model described by Eq. (39), there was no shear in this plasma greater than the limits set by the experimental error.

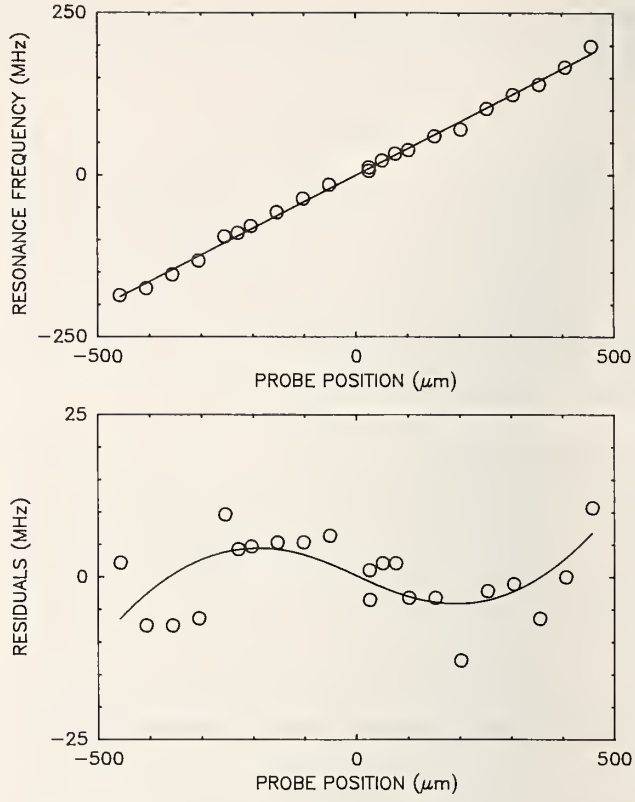

FIG. 8. A plot similar to Fig. 7 of data from Larson *et al.* (Ref. 3). The $^9Be^+$ resonance frequency ν_0' is plotted vs d for a plasma of 7000 $^9Be^+$ ions (density of 2.0×10^7 ions/cm^3) stored simultaneously with $^{198}Hg^+$ ions. The data show a well-defined departure from a linear fit, with $\xi = 0.33 \pm 0.12$. The data were taken at a magnetic field of 1.4 T and a trap axial frequency of $\omega_z/2\pi = 212$ kHz.

An effect other than shear may be responsible for the

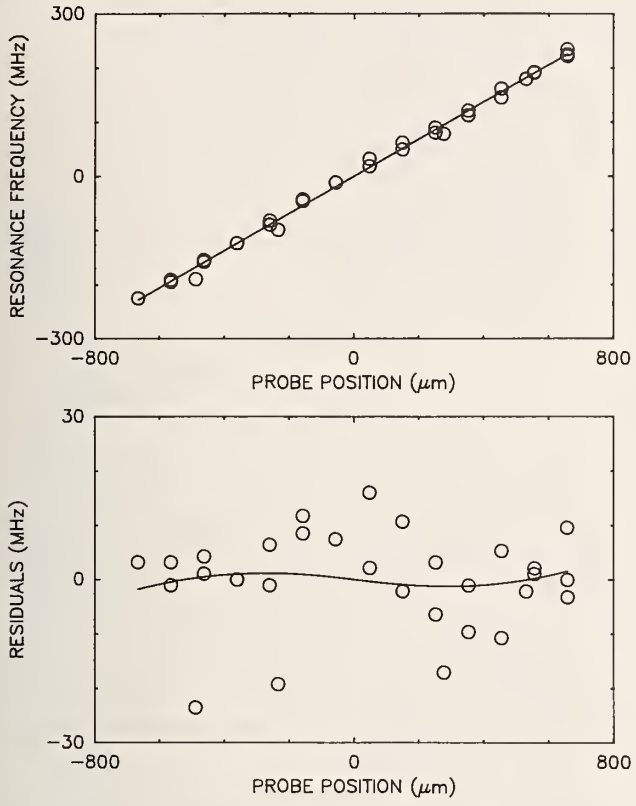

FIG. 9. A plot similar to Fig. 7. The $^9Be^+$ resonance frequency ν_0' is plotted vs d for a plasma of 25 000 $^9Be^+$ ions (density of 1.7×10^7 ions/cm^3) stored simultaneously with $^{198}Hg^+$ ions. The result of the fit is $\xi=0.06\pm0.1$. The data were taken at a magnetic field of 1.4 T and a trap axial frequency of $\omega_z/2\pi=212$ kHz.

$\xi>0$ result of Fig. 8. As the probe laser is scanned through the depopulation transition, $^9Be^+$ ions are removed from the cooling transition. Therefore, there are fewer ions available to resonantly scatter cooling laser light. The cooling laser exerts less of a torque on the plasma and the rotation frequency is expected to be lower. The probe laser removes more ions from the cooling laser transition when the probe laser beam is positioned at the center of the plasma than when the probe beam is at the edge of the plasma. According to this theory, the edge of the plasma would appear to rotate faster than the center of the plasma. To test this possibility, the probe beam was fixed spatially near the edge of the plasma and a sequence of measurements of the depopulation resonance center frequency ν_0' was taken with different probe laser powers and hence depopulation signal amplitudes $\beta(0)$ (see Sec. III E 1). For each measurement the magnitude $|\nu_0'-\nu_0|$ of the Doppler shift of the depopulation resonance was determined. The difference $\delta|\nu_0'-\nu_0|$ in the Doppler shifts between two sequential measurements was plotted as a function of the difference $\delta\beta(0)$ in the corresponding depopulation resonance amplitudes in order to eliminate contributions due to the drift of the probe laser frequency with time. Figure 10 shows the results of these measurements. The graph suggests that the rotation frequency of the plasma is decreased as the amplitude of the probe resonance is increased. This effect has the right sign to explain the "reverse shear" of Fig. 8. The measurement of Fig. 10 was done on the plasma of Fig. 9. The effect is large enough to create about a 10% change in the rotation frequency as the probe laser beam is moved from the center to the edge of the plasma, comparable to the limits of shear set by the data of Fig. 9. This measurement was unfortunately not done on the plasma of Fig. 8. Consequently we cannot say whether the size of this effect would have been large enough to fully explain the apparent shear observed there. (The dependence of the rotation frequency on the cooling laser torque may have been different for the two plasmas of Figs. 8 and 9 because the number of $^9Be^+$ ions, the ion density, and possibly the number of $^{198}Hg^+$ ions differed in the two plasmas.)

In summary, we looked for shear in the rotation of the $^9Be^+$ ions in a single-species plasma consisting of only $^9Be^+$ ions and in two-species plasmas consisting of $^9Be^+$ and $^{198}Hg^+$ ions. Shear, if present, may be larger in the two-species plasmas because of the large torque applied by the $^{198}Hg^+$ ions on the $^9Be^+$ ions. In Figs. 7 and 9 no shear was observed at the limits $|\xi|\leq0.1$. The fit to the data of Fig. 8 gave a statistically nonzero and positive value for the coefficient ξ, but we believe other effects may account for this reverse shear. While the basic experimental technique appears capable of establishing limits on any possible shear of $|\xi|\leq0.1$, systematic effects of the probe laser on the plasma rotation must be carefully studied before this limit is set. At the level of $|\xi|<0.3$ we believe we have experimentally demonstrated that the $^9Be^+$ ions are undergoing a uniform rotation, in agreement with the predictions of thermal equilibrium.

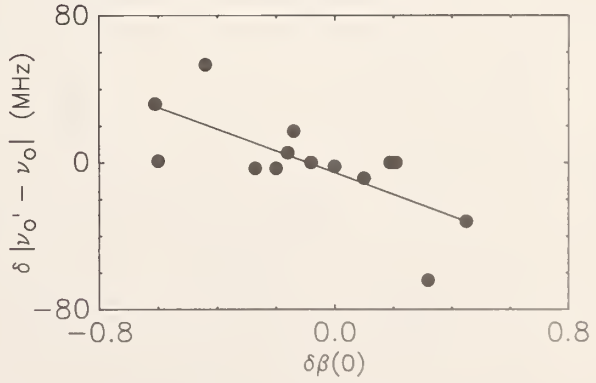

FIG. 10. Shift $\delta|\nu_0'-\nu_0|$ in the magnitude of the depopulation resonance Doppler shift as a function of the change $\delta\beta(0)$ in the depopulation resonance amplitude. The data were taken with $d\approx\pm0.9r_{el}$ on the plasma of Fig. 9. The graph indicates that the rotation frequency of the plasma decreased as the amplitude of the depopulation resonance increased

B. Plasma shape and aspect ratio

From the discussion of Sec. II B, we expect the $^9Be^+$ plasmas to have constant density (for length scales larger than the interparticle spacing) with sharp boundaries consisting of a drop in density over a short distance compared to the plasma dimensions. Figure 6 and Sec. III E 2 indicate how the plasma boundaries in the y-z plane were experimentally determined. Figure 11 shows the results of these measurements for a $^9Be^+$ plasma. According to Eq. (13), the plasma should have an elliptical shape in the y-z plane in the limit $\lambda_D \ll$ plasma dimensions $\ll$ trap dimensions. The agreement between the predicted elliptical shape and the measured boundaries in Fig. 11 is good. Because of the axial symmetry of the trap and the plasma rotation about the z axis, the cross section of the plasma in the x-y plane is expected to be circular. Our inability to direct the probe laser beam parallel to the z axis prevented us from verifying this experimentally.

For a given single-particle axial frequency ω_z [Eq. (2)] and cyclotron frequency Ω, Eqs. (14)–(16) of Sec. II C predict that there is a relationship between the plasma rotation frequency ω and the plasma aspect ratio z_{cl}/r_{cl} for plasmas of sufficiently large size. This relationship was experimentally tested by measuring the aspect ratio and rotation frequency of $^9Be^+$ plasmas with 2000 to 40 000 ions. The aspect ratio was determined from the plasma shape measurements. Plasmas with different aspect ratios and rotation frequencies were obtained with different positions (and therefore torques) of the cooling laser beam. As the cooling laser beam was moved from near the center to the edge of the plasma, the rotation frequency and the aspect ratio z_{cl}/r_{cl} increased. In Fig. 12 we show a plot of $3\omega_z^2/[2\omega(\Omega-\omega)]$ versus the plasma aspect ratio for data taken on both traps I and II and at different trap voltages. The data should lie on a single curve, independent of the trap potential and magnetic field. The theoretical prediction of Eqs. (14)–(16) is given by a solid curve in Fig. 12. The agreement between the data and theory is good and confirms a prediction of the zero-temperature theory.

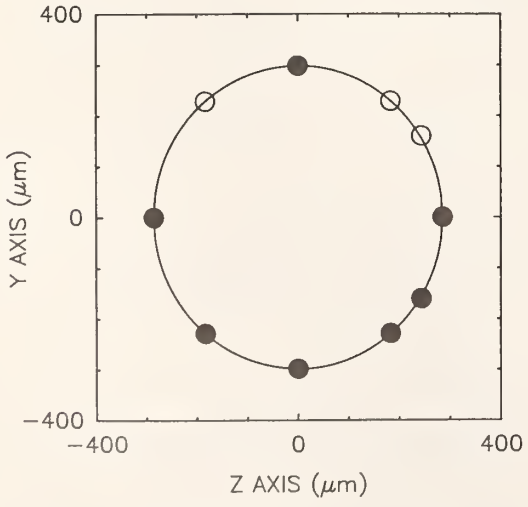

FIG. 11. Boundaries of a $^9Be^+$ plasma in the y-z plane. The ● data points were measured and the ○ data points were determined by assuming rotational symmetry about the plasma z axes. The ellipse was determined from the end points along the y and z axis. The plasma consisted of 5000 $^9Be^+$ ions (density of 4.7×10^7 ions/cm^3). The data were taken on trap I at a magnetic field of 1.4 T and axial frequency of $\omega_z/2\pi = 290$ kHz.

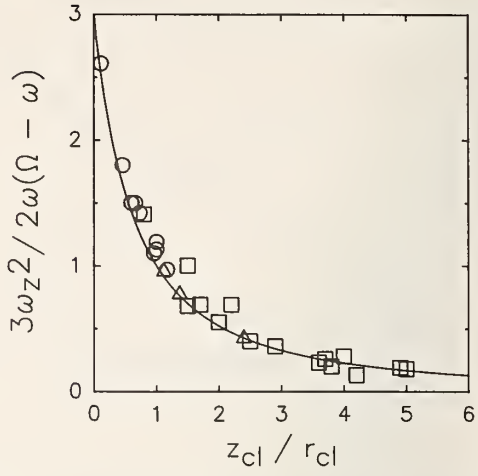

FIG. 12. Relationship between the plasma rotation frequency and the plasma aspect ratio is shown. The quantity $3\omega_z^2/[2\omega(\Omega-\omega)]$ is calculated from the measured values of ω, ω_z, and Ω and plotted vs the measured aspect ratio z_{cl}/r_{cl}. The solid, theoretical curve is determined from Eqs. (14)–(16) and is independent of the trap voltage and magnetic field. Data were obtained for $^9Be^+$ plasmas with 2000 to 40 000 $^9Be^+$ ions. Three different sets of data from two different traps are plotted. The first set (○) was taken in trap I with 2 V trap voltage ($\omega_z/2\pi = 290$ kHz). The second set (□) was taken at a trap voltage of 1.5 V ($\omega_z/2\pi = 212$ kHz) on trap II. The third set (△) was taken at trap voltages of 0.9 V ($\omega_z/2\pi = 170$ kHz) and 1.5 V on trap II. All data were taken at a magnetic field of 1.4 T.

C. Temperature

The temperature of the plasmas was determined from the width of $\alpha(\Delta\nu_p)$. Much of the data from trap I was taken using a chart recorder and analyzed manually from the recording. For each depopulation resonance, the fractional decrease in fluorescence on resonance $\beta(0)$ was obtained from the point of minimum fluorescence, as indicated in Fig. 3. The full width at half maximum points of α were then determined using Eq. (29). This width was then deconvoluted using a Voigt table to give the Gaussian contribution, as described in Sec. III E 4. Frequency calibration for the probe laser was provided using a spectrum analyzer with a free spectral range of 3 GHz. The temperatures $T_\perp$ and $T_\parallel$ were then determined from Eqs. (37) and (38) by measurements made with the probe laser beam both perpendicular and at an angle 55° with respect to the magnetic field.

Data on trap II and the rest of the data from trap I were taken with a computer. The depletion rate $\alpha(\Delta\nu_p)$

was calculated using Eq. (27). Most of these data consisted of measurements on large plasmas, where the natural linewidth of the depopulation transition was a small fraction of the Voigt resonance width. Consequently, the data were well fitted by a Gaussian curve. A graph of $\alpha(\Delta\nu_p)$ and a Gaussian fit is shown in Fig. 13. The full width at half maximum of α was obtained from the fit. This width was then deconvoluted using a computer algorithm to obtain the contribution $\Delta\nu_G$ [see Eq. (33)]. The temperature $T_\perp$ was then determined using Eq. (37).

D. Discussion

In Table I we show some examples of data taken in traps I and II with perpendicular cooling only. The first row of data was taken in trap I. The parallel temperature was measured to be an order of magnitude greater than the perpendicular temperature. The cooling laser beam, directed perpendicular to the magnetic field, only indirectly cooled the parallel (z) motion of the ions by collisional coupling of the parallel motion with the cooled perpendicular motion. The parallel motion was directly heated by the recoil of the scattered photons.[13–15] This may explain the observed temperature difference between the perpendicular and parallel motion. From Table II, it is clear that cooling at an angle of 55°, in addition to perpendicular cooling, decreases the parallel temperature. The remaining rows of data in Table I were taken on larger plasmas than in Table II. Typically there were 30 000 ions in these plasmas, as opposed to the small plasmas, which typically had a few hundred ions. The perpendicular temperatures for the larger plasmas were greater than for the smaller plasmas. The coupling parameter Γ was not calculated for the large plasmas in Table I because it was not possible to measure the parallel temperature. As suggested by the trap-I data, this temperature was probably larger than the perpendicular temperature. We were able to achieve higher rotation frequencies and therefore higher densities in trap II than in trap I. Some of the shapes of the plasmas in trap II were prolate, whereas in trap I the plasma shapes were oblate. Both of these facts may be due to the higher degree of axial symmetry present in trap II.[2]

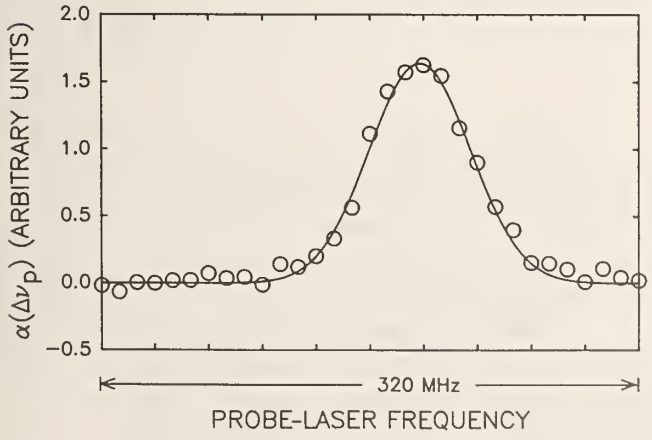

FIG. 13. Graph of $\alpha(\Delta\nu_p)$ as determined from the measured depopulation curve $\beta(\Delta\nu_p)$ along with a Gaussian fit. The full width at half maximum of this resonance is 71.3 MHz. This corresponds to a temperature of 0.11±0.05 K.

Diagonal cooling data were taken on small $^9Be^+$ plasmas to try to achieve conditions of maximum density and minimum temperature, that is, the strongly coupled regime. Using trap I we were able to cool $^9Be^+$ plasmas both in a perpendicular direction and at an angle of $\psi=55°$ with respect to the magnetic field. We were also able to probe in both directions and extract temperatures in both the perpendicular and parallel directions to the trap magnetic field. Table II shows the plasma dimensions, density, number of ions, rotation frequency, perpendicular and parallel temperatures, and coupling parameter Γ of several small plasmas. To provide a conservative estimate, Γ was calculated using the higher temperature $T_\parallel$.

The Brillouin density at a field strength of 1.4 T is 5.8×10^8 ions/cm^3. The measured densities of Table II were typically of the order 2×10^7 ions/cm^3. This is a factor of 30 less than the theoretical limit. The mechanism which limits the density is not well understood but it may have to do with axial asymmetries in the Penning trap.[2,16]

The theoretical laser cooling limit discussed in Sec. II D is 0.5 mK. While the uncertainty in the temperature measurement of Table II is large enough to include this limit in some cases, the temperatures measured were consistently higher by about an order of magnitude. The 0.5-mK limit was derived for the case of a single ion in a trap. For an ion plasma, the temperature limit for laser cooling perpendicular to the trap magnetic field depends on the distance of the cooling laser from the center of the plasma, the rotation frequency, and the saturation of the cooling transition. This can account for the larger temperatures we measured and will be discussed more thoroughly in a future publication. By changing the configuration of the laser cooling, we should be able to more closely approach the theoretical limit. For example, laser cooling along the z axis should permit a temperature limit of 0.5 mK. A laser beam with a component perpendicular to the magnetic field is required to contain the ion plasma in the radial direction, but in principle it could be fairly weak and not significantly perturb the temperature.

The largest coupling parameter measured was $\Gamma\approx340$. The uncertainty in this measurement was due largely to the uncertainty in the temperature measurement for the axial direction, which in this case was 2.4±6.0 mK. The measurement error is statistical and the lower bound on the measured temperature is more realistically given by the theoretical cooling limit of approximately 0.5 mK. This temperature uncertainty results in a range of values for Γ from 100 to a maximum of 2000. Therefore the coupling may be large enough for the plasma to be crystalline. The lowest temperatures were measured on plasmas of several hundred ions. These plasmas cannot be truly called infinite, three-dimensional plasmas. Since boundary conditions of the ion plasmas may be important in our measurements on small ion numbers, the results

TABLE I. Experimental data for perpendicular cooling only. The first row of data is for trap I. The remaining rows of data are for trap II. The error convention is as follows: 1.8(10)=1.8±1.0. Here $2z_{cl}$ and $2r_{cl}$ are the axial and the radial extent of the plasma. The coupling parameter Γ is derived from $T_{\parallel}$. For both traps I and II the magnetic field was 1.4 T, corresponding to a cyclotron frequency of $\Omega/2\pi=2.4$ MHz.

V_0 (V)	$2z_{cl}$ (μm)	$2r_{cl}$ (μm)	n_0 (10^7/cm^3)	N (10^4)	$\omega/2\pi$ (kHz)	$T_{\perp}$ (K)	$T_{\parallel}$ (K)	Γ
2.0	160(30)	290(30)	2.6(7)	0.018(9)	27(7)	0.005(2)	0.13(7)	6.1
1.5	1402(36)	1250(36)	2.85(4)	3.27(31)	29.2(4)	0.13(4)		
0.9	1692(36)	1234(36)	2.26(4)	3.05(28)	23.1(4)	0.11(5)		
1.5	1723(36)	718(36)	6.33(15)	2.94(43)	65.7(16)	1.30(10)		

are probably best compared to a theory somewhere between an infinite plasma theory and a theory for Coulomb clusters of ions (see discussion of Sec. IV E).

The temperature $T_{\perp}$ was also determined for several plasmas as a function of the probe laser beam position d. Within the signal-to-noise reported for the $T_{\perp}$ temperatures in Table I, the temperature was constant. This, together with the lack of observable shear, indicated that the plasma was approximately in global thermal equilibrium.

E. Future measurements and conclusion

Information about the spatial correlations in a plasma can be obtained by measuring the static structure factor.[17] The static structure factor is the spatial Fourier transform of the radial distribution function and is experimentally observed in the diffraction pattern resulting from the scattering of coherent light by the ions. It should be possible to directly measure the static structure factor of a correlated $^9Be^+$ plasma with Bragg scattering from a laser.[28]

It may be possibe to obtain some information about the spatial correlations of ions in the plasma by directly imaging the ion-resonance fluorescence from the cooling laser beam. Recently, several molecular dynamics simulations of a plasma of a few hundred to a few thousand stored ions have been conducted.[29] A result of these simulations is that the ions tend to reside in concentric shells. The shells exist even for couplings $\Gamma < 178$ but become more pronounced and clearly separated with larger coupling. The image of the ion-resonance fluorescence from the cooling laser beam should consist of bright areas corresponding to the intersection of the laser beam and the ion shells and dark areas where no ions are present. This assumes that the cooling laser-beam waist is small compared to the plasma dimensions. The separation between the bright and dark areas should be on the order of the interparticle spacing, approximately 20 μm for the ion densities reported here. Because of the cylindrical symmetry of the shells, the image is not destroyed by the plasma rotation.

By "tagging" ions with the probe laser used in a pulsed mode and monitoring the cooling laser fluorescence versus time,[28] we should be able to measure the ion diffusion between spatially separated probe and cooling laser beams. This may provide a technique to tell whether the plasma is a solid or liquid. If the plasma is a solid, the diffusion will not take place and a decrease in the cooling laser fluorescence will not be observed.

In conclusion, we have measured static properties of beryllium ion plasmas stored in quadratic Penning traps under a number of different experimental conditions. Within experimental error, we have found that there is no shear present in the ion plasmas; this suggests that the ions are nearly in global thermal equilibrium. Near

TABLE II. Experimental data on small $^9Be^+$ plasmas from trap I. The cooling was done at $\psi=0°$ and $\psi=55°$ simultaneously. The error convention is as follows: 1.8(10)=1.8±1.0. The coupling parameter Γ is derived from $T_{\parallel}$. The trap magnetic field was 1.4 T. This corresponds to a cyclotron frequency of $\Omega/2\pi=2.4$ MHz.

V_0 (V)	$2z_{cl}$ (μm)	$2r_{cl}$ (μm)	n_0 (10^7/cm^3)	N	$\omega/2\pi$ (kHz)	$T_{\perp}$ (mK)	$T_{\parallel}$ (mK)	Γ
2.0	130(30)	450(30)	2.4(6)	330(170)	25(6)	2.3(5)	10(5)	80
2.0	150(30)	450(30)	1.9(5)	300(150)	20(5)	1.8(10)	7.4(70)	100
2.0	130(30)	480(30)	2.2(6)	350(170)	23(6)	0.9(15)	8.9(60)	90
2.0	160(30)	450(30)	2.6(7)	450(230)	27(7)	2.4(10)	6(6)	130
2.0	160(30)	260(30)	2.8(7)	150(80)	30(7)	2.7(30)	2.4(60)	340
4.0	80(30)	390(30)	3.9(10)	250(120)	40(10)	2.9(20)	20(12)	50
1.0	190(30)	360(30)	1.2(3)	150(80)	13(3)	2.9(10)	4.7(60)	130

thermal equilibrium has also been verified by measuring $T_\perp$ as a function of position. Differences in $T_\perp$ and $T_\parallel$ are expected for perpendicular cooling due to scattered photon recoil heating. This may be reflected in the data taken with trap I. Measured plasma shapes are spheroidal, which is in agreement with a theory that assumes that the plasma is in thermal equilibrium with dimensions small compared to the Penning trap dimensions, but large compared to the coherence length of any spatial correlations. The data on the aspect ratio versus rotation frequency also agrees with this theory. The temperature, density, and rotation frequency were measured for several plasmas under varying conditions. Measured coupling parameters of 100 or greater for small plasmas of a few hundred ions indicate that these plasmas are strongly coupled and may be in a liquid and possibly solid state.

For the study reported here, the measurement of the size of the plasma and therefore the ion number and total angular momentum was quite laborious. However, for the conditions obtained here, this can be simplified in the future. The rotation frequency ω requires only two probe transition measurements as long as no shear is present. The plasma dimension $2r_{cl}$ could be easily measured by imaging the resonance fluorescence scattered by the ions onto a position sensitive detector. The frequencies Ω and ω_z, which are constant and independent of the plasma shape or size, could be measured using fluorescence detection.[24] From r_{cl} and Fig. 12, z_{cl} is then determined.

ACKNOWLEDGMENTS

We gratefully acknowledge the support of the U.S. Office of Naval Research and the U.S. Air Force Office of Scientific Research. One of us (D.J.L.) would like to acknowledge partial support of the National Science Foundation. We thank D. H. E. Dubin and S. L. Gilbert for their helpful suggestions.

---

*Present address: L250, Lawrence Livermore National Laboratory, Livermore, CA 94550.

†Present address: Jet Propulsion Laboratories, California Institute of Technology, 298-104, 4800 Oak Grove Dr., Pasadena, CA 91109.

‡Permanent address: Department of Physics, University of Virginia, Charlottesville, VA 22901.

[1]J. J. Bollinger and D. J. Wineland, Phys. Rev. Lett. **53**, 348 (1984).

[2]D. J. Wineland, J. J. Bollinger, W. M. Itano, and J. D. Prestage, J. Opt. Soc. Am. B **2**, 1721 (1985).

[3]D. J. Larson, J. C. Bergquist, J. J. Bollinger, W. M. Itano, and D. J. Wineland, Phys. Rev. Lett. **57**, 70 (1986).

[4]J. H. Malmberg and J. S. deGrassie, Phys. Rev. Lett. **35**, 577 (1975).

[5]F. M. Penning, Physica **3**, 873 (1936).

[6]H. G. Dehmelt, Adv. At. Mol. Phys. **3**, 53 (1967).

[7]H. G. Dehmelt, Adv. At. Mol. Phys. **5**, 109 (1969).

[8]D. J. Wineland, W. M. Itano, and R. S. Van Dyck, Jr., Adv. At. Mol. Phys. **19**, 135 (1983).

[9]R. C. Davidson, *Theory of Nonneutral Plasmas* (Benjamin, Reading, MA, 1974).

[10]J. H. Malmberg and T. M. O'Neil, Phys. Rev. Lett. **39**, 1333 (1977).

[11]S. A. Prasad and T. M. O'Neil, Phys. Fluids **22**, 278 (1979).

[12]J. B. Jeffries, S. E. Barlow, and G. H. Dunn, Int. J. Mass Spectrom. Ion Processes **54**, 169 (1983).

[13]D. J. Wineland and W. M. Itano, Phys. Rev. A **20**, 1521 (1979).

[14]W. M. Itano and D. J. Wineland, Phys. Rev. A **25**, 35 (1982).

[15]D. J. Wineland and W. M. Itano, Phys. Today **40** (6), 34 (1987); S. Stenholm, Rev. Mod. Phys. **58**, 699 (1986).

[16]C. F. Driscoll, K. S. Fine, and J. H. Malmberg, Phys. Fluids **29**, 2015 (1986).

[17]S. Ichimaru, Rev. Mod. Phys. **54**, 1017 (1982); S. Ichimaru, H. Iyetomi, and S. Tanaka, Phys. Rep. **149**, 91 (1987).

[18]E. Pollack and J. Hansen, Phys. Rev. A **8**, 3110 (1973); W. L. Slatterly, G. D. Doolen, and H. E. DeWitt, *ibid.* **21**, 2087 (1980); **26**, 2255 (1982).

[19]S. Ichimaru and S. Tanaka, Phys. Rev. Lett. **56**, 2815 (1986); S. Tanaka and S. Ichimaru, Phys. Rev. A **35**, 4743 (1987).

[20]D. J. Wineland, J. C. Bergquist, W. M. Itano, and R. E. Drullinger, Opt. Lett. **5**, 245 (1980).

[21]W. M. Itano and D. J. Wineland, Phys. Rev. A **24**, 1364 (1981).

[22]R. G. Hulet, D. J. Wineland, J. C. Bergquist, and W. M. Itano, Phys. Rev. A (to be published).

[23]R. E. Drullinger, D. J. Wineland, and J. C. Bergquist, Appl. Phys. **22**, 365 (1980).

[24]D. J. Wineland, J. J. Bollinger, and W. M. Itano, Phys. Rev. Lett. **50**, 628 (1983); **50**, 1333(E) (1983).

[25]D. J. Wineland, W. M. Itano, J. C. Bergquist, J. J. Bollinger, and J. D. Prestage, in *Atomic Physics 9*, edited by R. S. Van Dyck, Jr. and E. N. Fortson (World Scientific, Singapore, 1984), p. 3.

[26]J. Tudor Davies and J. M. Vaughan, Astrophys. J. **137**, 1302 (1963).

[27]T. M. O'Neil, Phys. Fluids **24**, 1447 (1981).

[28]L. R. Brewer, J. D. Prestage, J. J. Bollinger, and D. J. Wineland, in *Strongly Coupled Plasma Physics*, edited by F. J. Rogers and H. E. DeWitt (Plenum, New York, 1987), p. 53.

[29]A. Rahman and J. P. Schiffer, Phys. Rev. Lett. **57**, 1133 (1986); H. Totsuji, in *Strongly Coupled Plasma Physics*, edited by F. J. Rogers and H. E. DeWitt (Plenum, New York, 1987), p. 19; D. H. E. Dubin and T. M. O'Neil, Phys. Rev. Lett. **60**, 511 (1988).

Atomic-Ion Coulomb Clusters in an Ion Trap

D. J. Wineland, J. C. Bergquist, Wayne M. Itano, J. J. Bollinger, and C. H. Manney
Time and Frequency Division, National Bureau of Standards, Boulder, Colorado 80303
(Received 29 September 1987)

We observe small numbers of laser-cooled Hg^+ ions, which are confined in a Paul radio-frequency ion trap, to crystallize into regular arrays or clusters. We investigate the structure of these clusters by direct imaging, optical spectroscopy, and numerical calculations. The spectroscopy of such "pseudomolecules" is unique in that we can probe individual atoms of the molecule separately. The ratio of Coulomb potential energy per ion to k_BT in these clusters is observed to be as high as 120.

PACS numbers: 32.80.Pj, 35.10.−d, 36.40.+d

The success of various techniques for cooling of charged atomic and elementary particles in traps and storage rings has stimulated considerable interest in the observation of the expected spatial ordering of a collection of such particles. The study of ordering not only has a direct bearing on the dynamics of these stored particles but has applicability to the study of cluster formation, Wigner crystallization, strongly coupled plasmas, and spectroscopy.[1–8]

In this experiment, we investigated, both by direct imaging and by spectroscopic methods, the structure of small clusters or crystals of laser-cooled atomic ions which were confined in a Paul radio-frequency (rf) trap.[9] Photographic images of one, two, and three ions in a Paul trap have previously been reported,[10] but the resolution achieved did not allow investigation of possible ordering. Indirect evidence for ordered structures of trapped atomic ions was reported by Diedrich *et al.*[11] Imaging of ordered structures of macroscopic charged particles stored in a Paul trap was reported in the experiments of Wuerker, Shelton, and Langmuir.[12] The ordering observed here was similar but occurred under substantially different experimental conditions. One advantage of the present experiments is that the charge and mass of the particles were well defined. In addition, the structure of clusters of atomic ions can be spectroscopically probed. As a demonstration, we have measured the vibrational frequency of the diatomic pseudomolecule $(^{198}Hg^+)_2$ by measuring its optical spectrum. This experiment is unique in that we were able to probe a specific atom by fixing the pseudomolecule in space.

Small numbers of $^{198}Hg^+$ ions were stored in a miniature Paul trap,[13] which has properties equivalent to those of a hyperbolic trap with dimensions $r_0 \simeq 466$ μm and $z_0 \simeq 330$ μm.[14] An oscillating voltage V_{ac} with peak amplitude between 145 and 325 V at a frequency of 23.26 MHz was applied between the ring and end-cap electrodes for trapping. The ions were laser cooled by 1–2 μW of cw 194-nm radiation (bandwidth <2 MHz), whose beam waist was varied between 5 and 15 μm at the position of the ions. This radiation was tuned near the $5d^{10}6s\,^2S_{1/2} \rightarrow 5d^{10}6p\,^2P_{1/2}$ first resonance line, which has a natural linewidth of 70 MHz. Some of the 194-nm fluorescence from the ions was focused onto the photocathode of a resistive-anode photon-counting imaging tube as shown schematically in Fig. 1. The optics for this imaging was provided by a three-stage fused-quartz lens system with an aberration-compensated first stage. The first lens was apertured to give an f number of 4.5. The overall magnification of the lens system was 60×. The positions of the photons detected by the imaging tube could be displayed on an oscilloscope in real time or stored by a computer in order to make time exposures. The resolution was limited by the imaging tube to about a factor of 3 worse than the diffraction limit. In Fig.

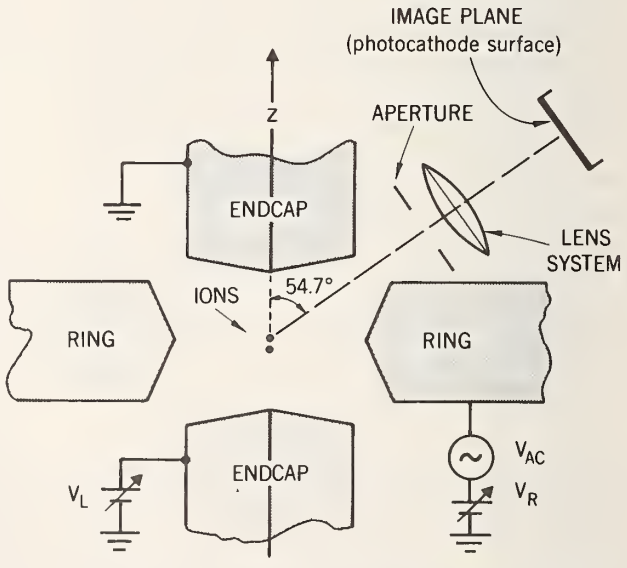

FIG. 1. Schematic drawing of the trap electrodes (to scale) and imaging system (not to scale). The end-cap to end-cap separation along the z axis is approximately 625 μm. The overall magnification of the lens system is 60×. The laser beam used to illuminate the ions also enters the trap at an angle of 54.7° with respect to the z axis and is perpendicular to the observation axis shown.

Work of the U. S. Government
Not subject to U. S. copyright

2(a) we show the trap coordinate system as viewed by the imaging tube. If we apply a positive static potential V_L to the lower end cap in Fig. 1 and hold the static ring voltage V_R at ground potential, a single ion[15] moves in the positive z direction by a known amount.[16] This determined the length scale in the images (after we accounted for viewing angle) and therefore also determined the magnification.

The harmonic pseudopotential well of the trap[9] is characterized by the single-ion resonance frequencies ν_z and ν_r for the motion in the axial and radial directions, respectively. For $V_L=0$, these frequencies take the form[9]

$$\nu_r^2=\nu_{r0}^2+BV_R, \tag{1a}$$

$$\nu_z^2=\nu_{z0}^2-2BV_R, \tag{1b}$$

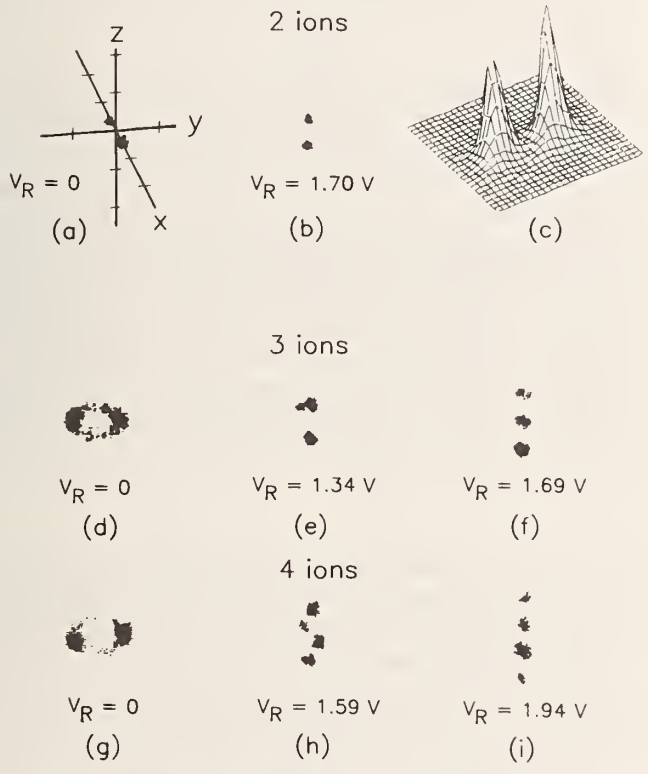

FIG. 2. Images of clusters of two, three, and four trapped and laser-cooled Hg^+ ions for the condition where $\nu_{z0}\simeq 2\nu_{r0}\simeq 500$ kHz. The coordinate system of (a) applies to the remaining pictures except for (c). The tick marks on the axes are separated by 10 μm. (c) A three-dimensional intensity plot for two ions pinned along the z axis ($V_R=1.95$ V) and separated by 7.4 μm in the plane perpendicular to the direction of observation. The variation in the intensity for different ions is due, in part, to variations in intensity of the laser beam at the sites of the different ions. Peak counting rates were about 2000 s^{-1}/ion. Transitions between the observed configurations can be induced by the variation of the ring voltage V_R, and thereby the variation of the relative strengths of the axial and radial pseudopotential wells.

where ν_{z0} and ν_{r0} ($\nu_{z0}=2\nu_{r0}$) are proportional to V_{ac}. ν_z and ν_r were measured from the sideband spectra of an optical transition[15] and by direct electric field excitation of the motional resonances.[17] From these measurements we obtained $B=0.0567(15)$ MHz^2/V. This agrees fairly well with the calculated value 0.0596 MHz^2/V based on the designed trap dimensions.

If two ions were loaded into the trap with $V_R=V_L=0$, and the 194-nm source was slowly swept into resonance, the ions were observed to first "swarm" around the center of the trap with orbit radii up to a few tens of micrometers. As the laser detuning was further reduced, thereby increasing laser cooling, the ions oriented or "pinned" themselves along a preferred direction, separated by a distance d. Here the inward pseudopotential force on each ion is balanced by their mutual Coulomb repulsion. Since $V_R=0$, the pseudopotential well in the axial direction is four times as strong as in the radial direction and the ions lie in the x-y plane. Although the trap was designed to have axial symmetry, the preferred spatial alignment of the cold ions indicates an asymmetric potential due to trap imperfections, contact-potential variations, or some other trap asymmetry. For convenience, we choose this preferred direction to be the x axis as indicated in Fig. 2(a).

If V_R is increased until $\nu_z<\nu_r$, we expect the ions to align along the z axis since this is the configuration which minimizes the potential energy. This configuration is shown in Fig. 2(b). For the conditions of Fig. 2 ($\nu_{r0}\simeq 250$ kHz), we expected this transition to occur at $V_R\simeq 1.11$ V and observed it to occur at $V_R\simeq 1.17$ V. The transition appeared to occur gradually over a range of about 30 mV rather than suddenly; this was probably related to the source of trap asymmetry in the x-y plane. For two $^{198}Hg^+$ ions pinned along a certain direction, the interparticle spacing is theoretically given by $d=3.29\nu_d^{-2/3}$ μm, where ν_d (in megahertz) is the single-ion oscillation frequency along the direction of separation. For the conditions of Fig. 2(b), we predicted $d=8.5$ μm and measured 7.5(1.1) μm.

In Figs. 2(d)–2(i), we show various configurations for three and four ions. We also observed ordered structures for five or more ions. For three or four ions, when V_R was equal to zero, the ions appeared to lie the same distance from the z axis but were not pinned, as was the case for two ions. Instead, they appeared to circulate about the z axis [see Figs. 2(d) and 2(g)]. This interpretation is supported by the observation that the size of the circular image could be made to increase by more than a factor of 2 by appropriate positioning and tuning of the 194-nm laser beam. This is not surprising since the trap asymmetry in the x-y plane was relatively weak and since it was fairly easy to position the laser to apply a radiation-pressure torque about the z axis. Three stable configurations were observed for three and four ions. For large values of V_R, the ions were aligned along the z

TN-107

axis as in Figs. 2(f) and 2(i). In the intermediate configuration for three ions [see Fig. 2(e)], one ion appeared to lie on the negative x axis and the others equidistant from the x-y plane and on a line parallel to the z axis which intersects the positive x axis. In the intermediate configuration for four ions [see Fig. 2(h)], two of the ions appeared to lie in the x-y plane pinned along the x axis, and two ions were positioned above and below the x-y plane along the z axis. We have verified the ordered structures in Figs. 2(d)–2(i) by calculating the configurations which minimize the potential energy for the specified trap parameters.

We also observed clusters where an ion apparently occupied a normal cluster position but did not fluoresce. This "phantom ion," which may have been $^{199}Hg^+$, or perhaps an impurity ion like $HgOH^+$, switched positions with $^{198}Hg^+$ ions of the cluster if the cooling was weak.

Such clusters of atomic ions can be viewed as pseudomolecules whose optical spectra would be expected to show rovibronic structure. As a demonstration, we have measured the vibrational structure of the diatomic pseudomolecule $(Hg^+)_2$ by probing its optical structure. By pinning the molecule along the z axis as in Fig. 2(b), we could probe the optical structure of one of the atoms of the molecule by detecting the fluorescence of only this atom. In particular, we measured the structure of the $5d^{10}6s\,^2S_{1/2}(m_J=\frac{1}{2})\rightarrow 5d^96s^2\,^2D_{5/2}(m_J=-\frac{1}{2})$ electric quadrupole transition ($\lambda\simeq 282$ nm) of one of these Hg^+ ions.

We first adjusted V_{ac} and V_R to make $\nu_r\simeq 2\nu_z\simeq 473$ kHz for a single ion in the trap. We than observed the quadrupole transition on this single trapped ion by the following method.[15] The 194-nm source was first tuned to give an easily detectable value of fluorescence. A radiation source near the quadrupole transition frequency was focused onto the ions and slowly swept through resonance. While being swept, the 282- and 194-nm sources were alternately chopped to avoid ac Stark shifts on the quadrupole transition from the 194-nm source. Each time the 282-nm source was shut off and the 194-nm radiation readmitted, the absence of 194 nm fluorescence from the ion indicated that it had made the transition to the $^2D_{5/2}$ level. The presence of 194-nm fluorescence indicated that the ion had remained in the $^2S_{1/2}$ state. The spectrum of the quadrupole transition could be taken by our plotting the probability of our observing 194-nm fluorescence as a function of the tuning of the 282-nm source. Figure 3(a) shows the central part of the spectrum for a single trapped $^{198}Hg^+$ ion. The carrier is identified by the invariance of its frequency upon variation of V_{ac} and V_R. The resolution achieved was limited by the 282-nm source spectral width; the natural linewidth of the quadrupole transition is about 2 Hz. The sidebands are Doppler-effect–generated FM sidebands due to the harmonic oscillations of the trapped ion at frequencies ν_z and ν_r.[15] They can also be viewed as

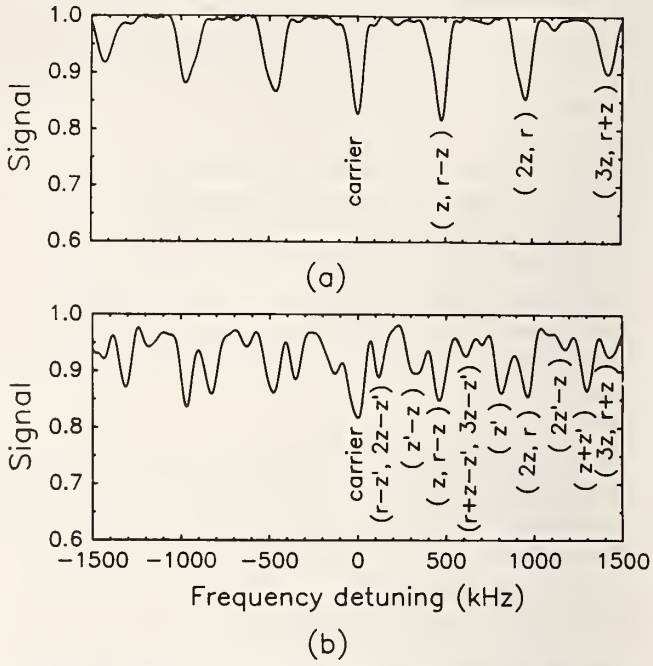

FIG. 3. Absorption spectra of the electric quadrupole transition $^2S_{1/2}(m_J=+\frac{1}{2})\rightarrow {}^2D_{5/2}(m_J=\frac{1}{2})$ for individual $^{198}Hg^+$ ions. (a) The central part of the spectrum for a single trapped ion. Adjacent to the carrier are Doppler-effect–generated sidebands due to the harmonic motion of the ion in the trap. Trapping conditions were adjusted to satisfy $\nu_r\simeq 2\nu_z\simeq 473$ kHz. The identifications below the lines show the order of the sideband. For example, the identification $(z, r-z)$ denotes absorption at the frequencies $\nu_0+\nu_z$ and $\nu_0+\nu_r-\nu_z$, where $\nu_0\simeq 1.07\times 10^{15}$ Hz is the carrier frequency. (b) The quadrupole spectrum for one of two ions, trapped in the same orientation as in Fig. 2(b). The trapping conditions were the same as for (a). The new lines are due to the stretch vibration mode of the ions at frequency $\nu_z'=\sqrt{3}\nu_z$.

the vibration modes of the pseudomolecule composed of the ion plus the trap. For optimum laser cooling, the maximum amplitude of the ion's motion for the conditions of this experiment was about 0.18 μm.[15,16]

When two ions are confined in the trap and aligned along the z axis, an additional vibrational mode is allowed; this is the stretch mode between the two ions. For small amplitudes of motion, this mode is expected to have a frequency $\nu_z'=\sqrt{3}\nu_z$. By using the double resonance method described above, we have observed the quadrupole spectrum of one of the trapped Hg^+ ions by detecting the fluorescence of only that ion. This spectrum is shown in Fig. 3(b). It is possible to attribute all of the new lines to the internal vibration mode at frequency ν_z' and its combinations with ν_z and ν_r. By fitting the observed spectra (assuming $\nu_r=2\nu_z$), we derive the frequency of this mode to be $\nu_z'=1.725(25)\nu_z$, which is in agreement with the theory. It should also be possible to observe this internal vibrational mode by direct excitation with spatially nonuniform electric

fields.[18] Finally, by measuring the width of the Doppler envelope of the quadrupole resonance,[15] we determined that the temperature of the ions was less than 8 mK. This gave a ratio of Coulomb potential energy per ion to $k_B T$ greater than 120.

The imaging and spectroscopic techniques described here should prove useful in the study of spatial ordering under various experimental conditions.[1-8] With careful control of the trap parameters, such as static field offsets, it should be possible to distinguish different cluster patterns whose minimum energies differ by small amounts[5,7] and to study the transitions between these patterns for different experimental conditions. Careful control of the balance between heating and cooling,[11] and spectroscopic measurements of the temperature, should allow the study of the transition from ordered to disordered structures. These studies may be aided by observation of the mobility of ions "tagged" by optical pumping or ions of different species in substitution as observed here. In a Paul trap, the amplitude of an ion's micromotion[9] due to the oscillating electric fields is proportional to the distance that the ion is from the center of the trap. Therefore rf heating is expected to be more of a problem for large-number clusters. This problem does not occur for particles trapped in static electric and magnetic fields.[1]

We gratefully acknowledge the support of the U.S. Office of Naval Research and the Air Force Office of Scientific Research. We thank R. Drullinger, S. Gilbert, J. Helffrich, and C. Weimer for suggestions on the manuscript. At the time of this submission, we learned by private communication that the authors of Ref. 11 had succeeded in observing images at the same time as the work reported here.

[1]J. H. Malmberg and T. M. O'Neil, Phys. Rev. Lett. **39**, 1333 (1977); J. J. Bollinger and D. J. Wineland, Phys. Rev. Lett. **53**, 348 (1984); H. Totsuji, in *Strongly Coupled Plasma Physics,* edited by F. J. Rogers and H. E. Dewitt (Plenum, New York, 1987), p. 19; D. H. E. Dubin and T. M. O'Neil, to be published.

[2]S. Ichimaru, Rev. Mod. Phys. **54**, 1017 (1982).

[3]D. Habs, in "Frontiers of Particle Beams" (Springer-Verlag, Berlin, to be published); E. N. Dement'ev, N. S. Dikanskii, A. S. Medvedko, V. V. Parkhomchuk, and D. V. Pestrikov, Zh. Tekh. Fiz. **50**, 1717 (1980) [Sov. Phys. Tech. Phys. **25**, 1001 (1980)].

[4]A. Rahman and J. P. Schiffer, Phys. Rev. Lett. **57**, 1133 (1986); J. P. Schiffer and O. Poulsen, Europhys. Lett. **1**, 55 (1986).

[5]J. Mostowski and M. Gajda, Acta Phys. Pol. A **67**, 783 (1985); E. V. Baklanov and V. P. Chebotayev, Appl. Phys. B **39**, 179 (1986).

[6]J. Javanainen, J. Opt. Soc. Am. B (to be published).

[7]R. Casdorff, R. Blatt, and P. E. Toschek, to be published.

[8]R. S. Berry, T. L. Beck, H. L. Davis, and J. Jellinek, Acc. Chem. Phys. (to be published).

[9]H. G. Dehmelt, Adv. At. Mol. Phys. **3**, 53 (1967), and **5**, 109 (1969); D. J. Wineland, W. M. Itano, and R. S. Van Dyck, Jr., Adv. At. Mol. Phys. **19**, 135 (1983).

[10]W. Neuhauser, M. Hohenstatt, P. Toschek, and H. Dehmelt, Phys. Rev. A **22**, 1137 (1980).

[11]F. Diedrich, J. Krause, G. Rempe, M. O. Scully, and H. Walther, in *Proceedings of the Fourth International Conference on Multiphoton Processes, Boulder, Colorado, 1986,* edited by S. Smith and P. L. Knight (Cambridge Univ. Press, New York, 1987).

[12]R. F. Wuerker, H. Shelton, and R. V. Langmuir, J. Appl. Phys. **30**, 342 (1959).

[13]J. C. Bergquist, D. J. Wineland, W. M. Itano, H. Hemmati, H. U. Daniel, and G. Leuchs, Phys. Rev. Lett. **55**, 1567 (1985).

[14]E. C. Beaty, J. Appl. Phys. **61**, 2118 (1987).

[15]J. C. Bergquist, W. M. Itano, and D. J. Wineland, Phys. Rev. A **36**, 428 (1987).

[16]D. J. Wineland, W. M. Itano, J. C. Bergquist, and R. G. Hulet, Phys. Rev. A **36**, 2220 (1987).

[17]F. G. Major and G. Werth, Appl. Phys. **15**, 201 (1978); W. Neuhauser, M. Hohenstatt, P. Toschek, and H. Dehmelt, Phys. Rev. Lett. **41**, 233 (1978); D. J. Wineland, J. J. Bollinger, and W. M. Itano, Phys. Rev. Lett. **50**, 628, 1333(E) (1983).

[18]D. J. Wineland and H. G. Dehmelt, Int. J. Mass Spectrom. Ion Phys. **16**, 338 (1975), and **19**, E251 (1976).

Shell-Structure Phase of Magnetically Confined Strongly Coupled Plasmas

S. L. Gilbert, J. J. Bollinger, and D. J. Wineland
Time and Frequency Division, National Bureau of Standards, Boulder, Colorado 80303
(Received 4 March 1988)

We report the observation of shell structure in $^9Be^+$ nonneutral plasmas (ion clouds) confined in a Penning trap. Clouds containing up to 15000 ions (density $\approx 10^8$ cm^{-3}) were laser cooled to temperatures of about 10 mK. Under these conditions, the ions are strongly coupled and exhibit liquidlike and solidlike behavior through the formation of concentric shells. The shells were observed by direct imaging of the laser-induced ion fluorescence for values of the Coulomb coupling constant Γ ranging from about 20 to 200. The shell structure is compared with theoretical predictions.

PACS numbers: 32.80.Pj, 52.25.Wz

The ability to cool collections of electrons or ions to temperatures where the Coulomb repulsion may produce a spatially ordered state has stimulated interest in several fields of physics. Detailed studies have been made in two-dimensional Coulomb systems[1] and in charged particles interacting through a shielded Coulomb potential.[2] In work more closely related to that described here, crystal-like structures of small numbers (<100) of macroscopic charged particles[3] and atomic ions[4] in Paul rf traps have been observed. The experiments on atomic ions appeared to be limited to small numbers because of the presence of rf heating,[5] which elevates the ion temperature in larger samples. Possibilities also exist for the observation of ordered structures of ions in storage rings.[6,7]

In Penning-type traps, where ions are confined by static electric and magnetic fields, rf heating does not take place and large collections of ions can be cooled to temperatures less than 10 mK. Several molecular-dynamics simulations on collections of a hundred to a few thousand ions confined in storage rings and traps have recently been completed.[7-10] Under conditions of strong coupling where the Coulomb potential energy between nearest neighbors is greater than the ion thermal energy, the ions are predicted to reside in concentric shells. Experimentally, strong coupling has been reported in systems of ions[11] and electrons[12] confined in Penning-type traps, but no evidence for spatial correlation was obtained. Here we report direct evidence for spatial correlation in magnetically confined ions. In clouds of laser-cooled $^9Be^+$ ions we observed structures containing from one shell (≈ 20 ions) to sixteen shells (≈ 15000 ions). The larger clouds may be approaching the infinite volume regime in which a bcc structure is predicted.[13]

The static thermodynamic properties of an ion cloud confined in a Penning trap are identical to those of a one-component plasma (OCP).[14] An OCP consists of a single species of charge embedded in a uniform-density background of opposite charge. For the system of ions in a Penning trap, the trapping fields play the role of the neutralizing background charge. An OCP is characterized by the Coulomb coupling constant,[13,14]

$$\Gamma \equiv q^2/a_s k_B T, \tag{1}$$

which is a measure of the nearest-neighbor Coulomb energy divided by the thermal energy of a particle. The quantities q and T are the ion charge and temperature. The Wigner-Seitz radius a_s is defined by $4\pi a_s^3 n_0/3 = 1$, where $-qn_0$ is the charge density of the neutralizing background. An infinite OCP is predicted[13] to exhibit liquidlike behavior (short-range order) for $\Gamma > 2$ and have a liquid-solid phase transition to a bcc lattice at $\Gamma = 178$.

For a finite plasma consisting of a hundred to a few thousand ions, the boundary conditions are predicted to have a significant effect on the plasma state. Simulations involving these numbers of ions have been done for the conditions of a spherical trap potential.[8-10] These simulations predict that the ion cloud will separate into concentric spherical shells. Instead of a sharp phase transition, the system is expected to evolve gradually from a liquid state characterized by short-range order and diffusion in all directions, to a state where there is diffusion within a shell but no diffusion between the shells (liquid within a shell, solidlike in the radial direction), and ultimately to an overall solidlike state.[10] These conclusions should apply to a nonspherical trap potential as well if the spherical shells are replaced with shells approximating spheriods. Preliminary independent investigations[15,16] of the nonspherical case support this conjecture.

We have investigated this interesting system using $^9Be^+$ ions trapped in the cylindrical Penning trap shown schematically in Fig. 1. A magnetic field $\mathbf{B} = B\hat{\mathbf{z}}$ ($B = 1.92$ T) produced by a superconducting magnet confined the ions in the direction perpendicular to the z axis. A static potential V_0 between the end and central cylinders confined the ions in the z direction to a region near the center of the trap. The dimensions of the trap electrodes were chosen so that the first anharmonic term of the trapping potential was zero. Over the region near the trap center, the potential can be expressed (in cylin-

Work of the U. S. Government
Not subject to U. S. copyright

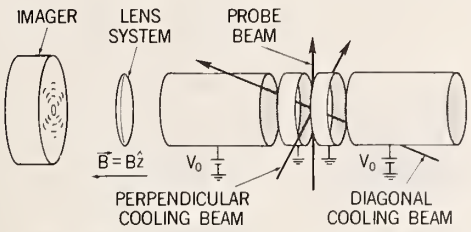

FIG. 1. Schematic drawing of the trap electrodes, laser beams, and imaging system (not to scale). The overall length of the trap is 10.2 cm. The trap consists of two end cylinders and two electrically connected central cylinders with 2.5-cm inner diameters. Ion clouds are typically less than 1 mm in both diameter and axial length. The diagonal cooling beam crosses the cloud at an angle of 51° with respect to the z axis.

drical coordinates) as $\Phi \cong AV_0(2z^2-r^2)$ where $A = 0.146\ \text{cm}^{-2}$. A background pressure of 10^{-8} Pa ($\approx 10^{-10}$ Torr) was maintained by a triode-sputter ion pump. The ions can be characterized by a thermal distribution where the "parallel" (to the z axis) temperature $T_\parallel$ is approximately equal to the "perpendicular" temperature $T_\perp$ (from the cyclotron motion). This thermal distribution is superimposed on a uniform rotation of the cloud[11,14] (frequency ω) which, at the low temperatures of this experiment, is due to the $\mathbf{E}\times\mathbf{B}$ drift, where $\mathbf{E}$ is the electric field due to the trap voltage and the space charge of the ions.

The ions were laser cooled and optically pumped into the $2s\,^2S_{1/2}(M_I=\frac{3}{2}, M_J=\frac{1}{2})$ state by our driving the $2s\,^2S_{1/2}(\frac{3}{2},\frac{1}{2}) \rightarrow 2p\,^2P_{3/2}(\frac{3}{2},\frac{3}{2})$ transition slightly below the resonant frequency.[11] The 313-nm cooling radiation ($\approx 30\ \mu$W) could be directed perpendicular to the magnetic field and/or along a diagonal as indicated in Fig. 1. In addition to cooling the ions, the laser also applied an overall torque which could either compress or expand the cloud.[11] This allowed us to control the cloud size by choosing the radial positions (and thus the torques) of the perpendicular and diagonal beams.

About 0.04% of the 313-nm fluorescence from the decay of the $^2P_{3/2}$ state was focused by $f/10$ optics onto the photocathode of a resistive-anode photon-counting imaging tube. The imager was located along the z axis, about 1 m from the ions. The imaging optics was composed of a three-stage lens system with overall magnification of 27 and a resolution (FWHM) of about 5 μm (specifically, the image of a point source when referred to the position of the ions was approximately 5 μm in diameter). Counting rates ranged from 2 to 15 kHz. Positions of the photons arriving at the imager were displayed in real time on an oscilloscope while being integrated by a computer.

A second laser (power $\approx 1\ \mu$W, beam waist $\cong 30$ μm) was used to map the shell structure of the cloud spatially. This probe laser was tuned to the same transition as the cooling laser and was directed through the

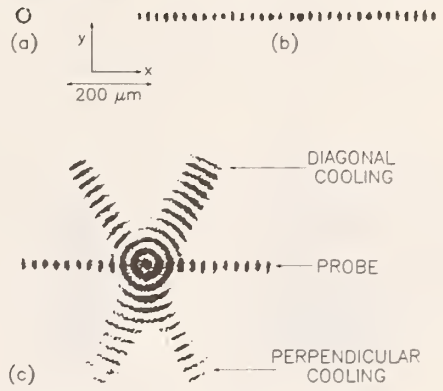

FIG. 2. Images of shell structures. (a) A single shell in a cloud containing approximately 20 ions. Trap voltage $V_0=14$ V and cloud aspect ratio a_r (axial length/diameter) $\cong 6.5$. This image was obtained from the ion fluorescence of the perpendicular and diagonal cooling beams. (b) Sixteen shells (probe-beam ion fluorescence only) in a cloud containing about 15000 ions with $v_0=100$ V and $a_r \cong 0.8$. (c) Eleven shells plus a center column in the same cloud as (b), with $V_0=28$ V and $a_r \cong 2.4$. This image shows the ion fluorescence from all three laser beams. Integration times were about 100 s for all images.

cloud perpendicularly to the magnetic field. With the probe laser on continuously, the cooling laser could be chopped at 1 kHz (50% duty cycle) and the image signal integrated only when the cooling laser was off. Different portions of the cloud could be imaged by the translation of the probe beam, in a calibrated fashion, either parallel or perpendicular to the z axis. Images were also obtained from the ion fluorescence of all three laser beams.

The probe beam was also used to measure the cloud rotation frequency ω and ion temperature.[11] For these measurements, the probe laser was tuned to the $2s\,^2S_{1/2}(\frac{3}{2},\frac{1}{2}) \rightarrow 2p\,^2P_{3/2}(\frac{3}{2},-\frac{1}{2})$ "depopulation" transition. Ions in the $2p\,^2P_{3/2}(\frac{3}{2},-\frac{1}{2})$ state can decay to the $2s\,^2S_{1/2}(\frac{3}{2},-\frac{1}{2})$ state, temporarily removing some of the ion population from the $2s\,^2S_{1/2}(\frac{3}{2},\frac{1}{2})$ state. This results in a decrease in the cooling fluorescence as the probe laser is scanned through the depopulation transition. We determined ω by measuring the change in the Doppler shift of the depopulation signal as the probe beam was translated perpendicular to the z axis. The density n_0 could then be calculated[11,14] from $n_0 = m\omega(\Omega-\omega)/2\pi q^2$, where $\Omega = qB/mc$ is the cyclotron frequency. With use of n_0 and the cloud size obtained from probe-beam images, the total number of ions was calculated. The ion temperature was derived from the Doppler broadening contribution to the width of the depopulation signal.[11] The temperature $T_\perp$ was measured with the probe beam perpendicular to the magnetic field and $T_\parallel$ was measured by our sending the probe beam along the magnetic field direction (not shown in Fig. 1). In the latter case, crossed polarizers were used to reduce the intensity of the probe beam at the imager.

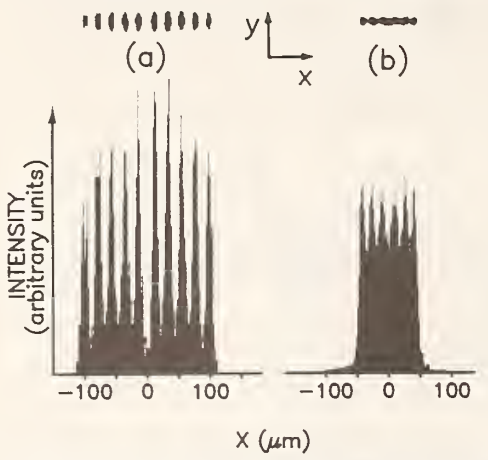

FIG. 3. Intensity plots along the imager x axis (parallel to the probe beam) through the center of the ion cloud with corresponding images (above). (a) $\Gamma = 180^{+90}_{-70}$ ($T = 6^{+4}_{-2}$ mK, $n_0 \cong 7\times10^7$ ions cm^{-3}). Cloud aspect ratio $a_r \cong 3.5$. (b) $\Gamma = 50^{+30}_{-20}$ ($T = 33^{+17}_{-13}$ mK, $n_0 = 2\times10^8$ ions cm^{-3}), $a_r \cong 5$. The clouds contained about 1000 ions in both cases.

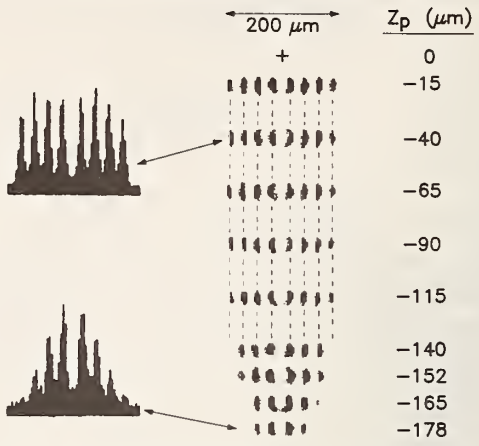

FIG. 4. Data showing evidence for concentric cylindrical shells. On the right is a series of images obtained with the probe beam for different z positions z_p of the probe beam (lower half of the cloud only). Intensity plots for $z_p = -40$ μm and $z_p = -178$ μm are shown on the left. The cloud aspect ratio a_r was about 1.9.

From the measured values of the temperature T and the density n_0, Γ was calculated with Eq. (1). In the case of $T_\perp \neq T_\parallel$, the larger temperature was used in the calculation of Γ.

We have observed shell structure in clouds containing as few as 20 ions (one shell) and in clouds containing up to about 15000 ions (sixteen shells). Images covering this range are shown in Fig. 2. We measured the coupling constant Γ for several clouds containing about 100 ions. Drift in the system parameters was checked by our verifying that the same images were obtained before and after the cloud rotation frequency and ion temperatures were measured. Figure 3 shows examples of shell structures at two different values of Γ. The first image is an example of high coupling ($\Gamma \approx 180$) showing very good shell definition in an intensity plot across the cloud. The second image is an example of lower coupling ($\Gamma \approx 50$) and was obtained with cooling only perpendicular to the magnetic field. Variations in peak intensities equidistant from the z axis are due to signal-to-noise limitations and imperfect alignment between the imager x axis and the probe beam.

We obtained three-dimensional information on the shell structure by taking probe images at different z positions. We found that there were two types of shell structure present under different circumstances. The first type showed shell curvature near the ends of the cloud, indicating that the shells may have been closed spheriods. Shell closure was difficult to verify because of a lack of sharp images near the ends of the cloud where the curvature was greatest. This may have been due to the averaging of the shells over the axial width of the probe beam. In the other type of shell structure, it was clear that the shells were concentric right circular cylinders with progressively longer cylinders near the center. An example of these data is shown in Fig. 4. Other evidence for cylindrical shells can be obtained from the fact that shells in the diagonal-beam images occur at the same cylindrical radii as those from the perpendicular beams. This can be seen in the three-beam images such as that shown in Fig. 2(c). Systematic causes of these two different shell configurations have not yet been identified.

One comparison which can be made between the theoretical calculations and our experimental results is the relationship between the number of shells and the number of ions, N_i, in a cloud. For a spherical cloud, approximately $(N_i/4)^{1/3}$ shells are predicted.[8] For the nearly spherical cloud of Fig. 2(b) ($N_i \cong 15000$) this formula predicts 15.5 shells and we measure 16. At present, it is difficult to make further quantitative comparisons between our data and the theoretical calculations. For example, there is substantial uncertainty in our measurement of Γ due to uncertainty in the temperature measurement. Our data do agree qualitatively with the simulations with the exception of the presence, in some cases, of an open-cylinder shell structure as opposed to the predicted closed spheroids. Schiffer has suggested[15] that shear (that is, different rotation frequencies) between the shells may account for this discrepancy. In our experiment, shear could be caused by differential laser torque or the presence of impurity ions.[17] For the data here, we have determined that the rotation frequency does not vary by more than 30% across the cloud. This is comparable to the limits discussed by Larson and co-workers.[17,18]

Future improvements will allow a more complete comparison of the data and the simulations, such as the rela-

tionship between shell definition and Γ for a variety of conditions. Also, we have observed that it is possible, using the probe depopulation transition, to tag ions in different parts of the cloud and see the presence (and lack) of ion diffusion. We plan to use this technique in a pulsed mode and obtain information on diffusion times within and between shells. Finally, with more laser power, even larger clouds (10^5 ions or more) can be cooled to these temperatures (10 mK). This may permit observation, by Bragg scattering,[11] of the predicted infinite volume structure.

We gratefully acknowledge the support of the U.S. Office of Naval Research and the Air Force Office of Scientific Research. We thank D. H. E. Dubin and J. P. Schiffer for useful discussions and C. Manney and W. Itano for help with image processing. We also thank G. Dunn, W. Itano, and C. Wieman for helpful suggestions on the manuscript.

[1]A. J. Dahm and W. F. Vinen, Physics Today **40**, No. 2, 43 (1987).

[2]D. J. Aastuen, N. A. Clark, and L. K. Cotter, Phys. Rev. Lett. **57**, 1733 (1986); J. M. di Meglio, D. A. Weitz, and P. M. Chaikin, Phys. Rev. Lett. **58**, 136 (1987); C. A. Murray and D. H. Van Winkle, Phys. Rev. Lett. **58**, 1200 (1987).

[3]R. F. Wuerker, H. Shelton, and R. V. Langmuir, J. Appl. Phys. **30**, 342 (1959).

[4]F. Diedrich, E. Peik, J. M. Chen, W. Quint, and H. Walther, Phys. Rev. Lett. **59**, 2931 (1987); D. J. Wineland, J. C. Bergquist, W. M. Itano, J. J. Bollinger, and C. H. Manney, Phys. Rev. Lett. **59**, 2935 (1987).

[5]D. A. Church and H. G. Dehmelt, J. Appl. Phys. **40**, 3421 (1969); H. G. Dehmelt, in *Advances in Laser Spectroscopy*, edited by F. T. Arecchi, F. Strumia, and H. Walther (Plenum, New York, 1983), p. 153.

[6]J. P. Schiffer and O. Poulsen, Europhys. Lett. **1**, 55 (1986).

[7]D. Habs, in "Frontiers of Particle Beams" (Springer-Verlag, Berlin, to be published).

[8]A. Rahman and J. P. Schiffer, Phys. Rev. Lett. **57**, 1133 (1986); J. P. Schiffer, to be published.

[9]H. Totsuji, in *Strongly Coupled Plasma Physics*, edited by F. J. Rogers and H. E. Dewitt (Plenum, New York, 1987), p. 19.

[10]D. H. E. Dubin and T. M. O'Neil, Phys. Rev. Lett. **60**, 511 (1988).

[11]J. J. Bollinger and D. J. Wineland, Phys. Rev. Lett. **53**, 348 (1984); L. R. Brewer, J. D. Prestage, J. J. Bollinger, and D. J. Wineland, in Ref. 9, p. 53.

[12]J. H. Malmberg, T. M. O'Neil, A. W. Hyatt, and C. F. Driscoll, in *Proceedings of the 1984 Sendai Symposium on Plasma Nonlinear Phenomena*, edited by N. Sato (Tohoku University, Sendai, Japan, 1984), p. 31.

[13]S. Ichimaru, H. Iyetomi, and S. Tanaka, Phys. Rep. **149**, 91 (1987), and references therein.

[14]J. H. Malmberg and T. M. O'Neil, Phys. Rev. Lett. **39**, 1333 (1977).

[15]J. P. Schiffer, private communication.

[16]D. H. E. Dubin, private communication.

[17]D. J. Larson, J. C. Bergquist, J. J. Bollinger, W. M. Itano, and D. J. Wineland, Phys. Rev. Lett. **57**, 70 (1986).

[18]L. R. Brewer, J. D. Prestage, J. J. Bollinger, W. M. Itano, D. J. Larson, and D. J. Wineland, Phys. Rev. A (to be published).

From: Proc. of the ONR Conference on Non-neutral Plasmas, National Academy of Sciences, Washington, D.C., March, 1988; Non-neutral Plasma Physics, ed by C.W. Roberson and C.F. Driscoll, A.I.P. Conf. Proc. 175, Amer. Inst. of Physics, New York, 1988, p. 93.

LIQUID AND SOLID ION PLASMAS

D.J. Wineland, Wayne M. Itano, J.C. Bergquist, S.L. Gilbert, J.J. Bollinger, and F. Ascarrunz

National Bureau of Standards, Boulder, CO 80303

ABSTRACT

Experiments on strongly-coupled nonneutral ion plasmas, performed at the National Bureau of Standards, are summarized. We first discuss strong coupling of small numbers (< 100) of macroscopic and atomic ions confined in Paul (electrodynamic) traps, in which crystalline structures are observed. We then discuss experiments in which shell structure is observed for up to 10^4 atomic ions confined in static electric and magnetic fields. In our experiments, we have progressed from working with very small numbers of ions up to an intermediate value. Future experiments are suggested, including some where infinite volume behavior might be observable.

INTRODUCTION

This paper briefly summarizes the work on strong coupling in nonneutral ion plasmas at the National Bureau of Standards at Boulder. This work has grown out of a project whose goal is very high resolution atomic spectroscopy on samples of ions contained in an "ion trap." Since spectral lines are, in general, shifted and broadened by Doppler effects associated with the motion of the ions, we desire an accurate characterization of the velocity distributions of the nonneutral plasmas (or "clouds") of ions contained in these traps.

Our interest in the strong coupling problem was in part stimulated by a 1977 paper[1] of Malmberg and O'Neil who discussed the possibility of achieving liquid and solid like behavior of a pure electron nonneutral plasma confined by static electric and magnetic fields. Their confinement device has typically been called a Penning trap[2] by atomic physicists. At about this time, we demonstrated the method of laser cooling[3] on atomic ions in a Penning trap.[4] Since the achievable temperatures are in the millikelvin range and below, we realized that strong coupling could probably be achieved in such a sample of ions. In addition, at low temperatures, the resonant light scattering cross section for atomic ions can be on the order of 10^{-10} cm^2. This is to be compared to the Thomson cross-section for electrons which is approximately 10^{-24} cm^2. Therefore, for atomic ions, the large cross sections for light scattering and long confinement times (many hours) made it possible to take pictures and "movies" of the plasmas. This sensitivity is dramatically illustrated by the pictures of single ions.[3,5,6]

The static thermodynamic properties of an ion cloud confined in a trap are identical to those of a one-component plasma (OCP).[1,7] An OCP consists of a single species of charged

particles embedded in a uniform-density background of opposite charge. For the system of ions in a trap, the trapping fields play the role of the neutralizing background charge. An OCP can be characterized by the Coulomb coupling constant,[1,7]

$$\Gamma \equiv q^2/(a_s k_B T), \qquad (1)$$

which is a measure of the nearest neighbor Coulomb energy divided by the thermal energy of a particle. The quantities q and T are the ion charge and temperature. The Wigner-Seitz radius a_s is defined by $4\pi a_s^3 n_0/3 = 1$, where $-qn_0$ is the charge density of the neutralizing background. An infinite volume OCP has been predicted[7] to exhibit liquid-like behavior (short range order) for $\Gamma > 2$ and a liquid-solid phase transition to a bcc lattice at $\Gamma \simeq 178$.

The occurrence of spatial ordering when $\Gamma > 1$ can be understood qualitatively. At low enough temperature, where $\Gamma > 1$, the ions do not have enough kinetic energy to overcome the Coulomb repulsion. Therefore they cannot approach each other very closely and become more evenly spaced. Even though this basic idea is understood, interest in this subject has continued to grow, possibly due to the richness of phenomena expected[7] and the difficulty of achieving this condition experimentally. Moreover, strong coupling has been studied or is expected in many fields besides plasma physics, for example in: 2-D configurations of electrons or ions near the surface of liquid helium,[8,9] charged particles in liquid suspension which act through a shielded Coulomb potential,[10] electrons in solids (Wigner crystallization), astrophysics (Curtis Michel, this conference) and perhaps somewhat surprisingly, in particles which are confined in high energy storage rings and cooled by electron cooling.[11]

ION TRAPS

Atomic physicists have most often used two kinds of devices in ion trapping work, the Penning trap and the Paul (radio-frequency) trap[2] whose electrodes are shown schematically in Fig. 1. The Penning trap is essentially the same device as that used in other nonneutral plasma studies.[12,13] In atomic physics experiments, the electrodes are often made to conform to equipotentials of a quadratic potential (Fig. 1). This insures that motion of single ions (or the center-of-mass motion for a single species) is harmonic. Thus the "hyperbolic" traps can be used as charge-to-mass analyzers. Ions in a Penning trap can be thought of as comprising an OCP where the static magnetic and electric fields play the role of the neutralizing background charge.[1,13]

The Paul (rf) trap typically uses the same electrode configuration as shown in Fig. 1. Trapping is provided by the ponderomotive potential or pseudopotential, resulting from the application of spatially inhomogeneous, time varying electric

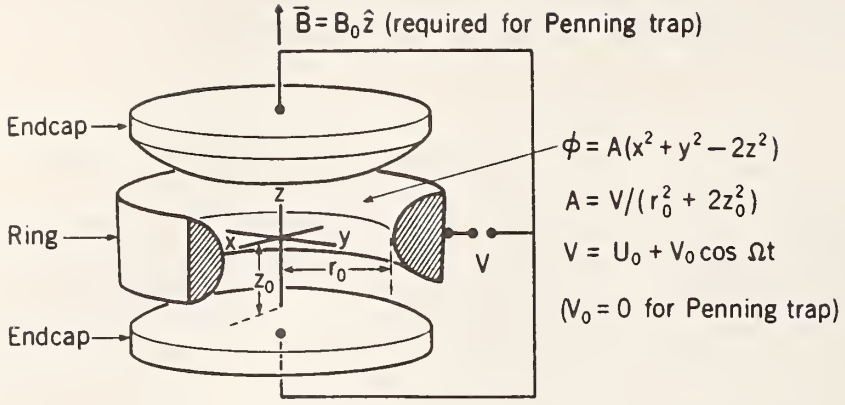

Fig. 1 Schematic representation (cutaway view) of the electrode configuration for the Paul (rf) or Penning trap. Electrode surfaces are figures of revolution about the z axis and are equipotentials of $\phi(r,z)=A(r^2-2z^2)$. For this equation, cylindrical coordinates are used with the origin at the center of the trap. Typical dimensions are $\sqrt{2}z_0 = r_0 \simeq 1$ cm. Typical operating parameters are the following: for the Paul trap, V_0=300 V, $\Omega/2\pi \simeq 1$ MHz; for the Penning trap, $U_0 \simeq 1$ V, $B \simeq 1$ T.

fields.[2] For the hyperbolic trap (Fig. 1) this ponderomotive potential takes the form[2,14]

$$\phi_p = \alpha r^2 + \beta z^2, \tag{2}$$

where

$$\alpha = qV_0^2/(m\Omega^2\xi^4) + U_0/\xi^2 \tag{3a}$$

$$\beta = 4qV_0^2/(m\Omega^2\xi^4) - 2U_0/\xi^2. \tag{3b}$$

$\xi^2 = r_0^2 + 2z_0^2$, m is the ion mass, and the other parameters are defined in Fig. 1. The center-of-mass oscillation frequencies of ions in the quadratic potential of Eq. 2 are usually called the secular frequencies.[2]

Equation 2 is equivalent to the potential inside of a uniformly charged spheroid.[14] Therefore, ions confined in a Paul trap may be thought of as comprising an OCP where the uniform neutralizing background charge density has the shape of a uniformly charged spheroid consistent with Eq. 2. This picture is valid when the micromotion of the ions at the drive frequency Ω can be neglected. For large numbers of ions this is not always justified as discussed below.

The Penning and Paul traps can be superimposed; the general solution was given by Fischer.[15] OCP properties have been discussed in Ref. 14.

MACROSCOPIC PARTICLE PAUL TRAP EXPERIMENTS

The Paul trap was experimentally demonstrated in 1959.[15] In the experiments of Wuerker, et al., macroscopic aluminum particles (diameter $\simeq$ 20 μm) were stored. The charges on these particles were quite high ($\simeq 5 \times 10^5$ electron charges) leading to $\Gamma >> 1$ and the observation of regular crystalline arrays. The key to these experiments is the high value of q. Since $\Gamma \propto q^2$, large values of Γ can be obtained even though the interparticle spacings are macroscopic (~1 mm) and temperatures were near room temperature.

Fig. 2. Cluster of alumina particles (center part of picture) in a Paul trap. Endcaps are not visible in this picture; inner diameter of ring electrode is 2.5 cm, $\Omega/2\pi$ = 60 Hz.

We have performed experiments similar to those of Ref. 15. In Fig. 2, we show a suspension of approximately 25 alumina particles (clumps of grinding powder) which have crystallized into a regular array. The inner part of the ring electrode (diameter $\simeq$ 2.5 cm) is visible but the endcap electrodes are obscured from view. For this picture, we had $V_0 \simeq 350$ V at $\Omega/2\pi$ = 60 Hz. Although the electrode surfaces were not hyperbolic, their shapes were chosen by computer calculation [16] to make the potential near the center of the trap nearly quadratic. The dimensions of an equivalent hyperbolic trap are $r_0 = 1.36$ cm $= \sqrt{2}\, z_0$. The background gas pressure for this trap was about 13 Pa (100 mTorr) of air which maintained the particle temperature near 300 K. From either the measured secular frequency along the z axis of symmetry, or from the potential applied to one endcap in order to counteract gravity (the z axis is vertical) we determined that the charge-to-mass ratio is $q/m \simeq 10^{-10} \times q/m(\text{proton})$. From the

separation of two charged particles in the x-y plane ($U_0 = 0$), we determined that the mass of the particles was approximately 10^{-9}g and therefore the particle's charge was about $q = 6 \times 10^4 \times$ q(proton). (For $U_0 = 0$, the balance of the pseudo potential (inward) force by the Coulomb repulsion (outward) is charge independent, but mass dependent). This gives a value of $\Gamma \gtrsim 10^5$. For Fig. 2, the particles were illuminated by a laser but a simple lamp would suffice.

MACROSCOPIC VS. ATOMIC PARTICLE EXPERIMENTS

Under fairly simple experimental conditions, very high values of Γ can be obtained in the macroscopic particle experiments because of the high values of charge obtained. It is therefore reasonable to ask why we would like to use atomic ions where the charge is much smaller, typically q = q(proton). One reason is that for a given size of the ion sample with respect to the trap dimensions, the number of ions N_i is proportional to q^{-1} (see Appendix A). Therefore, if we desire samples of many particles, small charge on the particles is advantageous. Perhaps more important is that in the macroscopic particle experiments, q and m are difficult to control precisely so that comparison of the observed crystals with theory is more difficult to make. Also, even though the macroscopic particles have high charge, their mass is relatively high and their charge-to-mass ratio q/m relatively small compared to atomic particles (typically about 10 orders of magnitude smaller). This consideration is important for Penning trap confinement where the maximum density given by the Brillouin density[17] is equal to $n_{max} = B^2/(8\pi mc^2)$. For the macroscopic particles of Fig. 2, we estimate $m = 10^{-9}$ g, so that even for B = 10 T, $n_{max} \simeq 4 \times 10^{-4}$ cm^{-3} which is extremely small (not to mention the problems with stray electric fields). For atomic particles, $n_{max} \simeq 10^{10}$ cm^{-3}. Thus, magnetic confinement of large numbers of particles can only be accomplished with atomic or molecular ions or electrons. Finally, atomic ions have internal structure which can be spectroscopically probed to give information on plasma dynamics.[18] Therefore, even though the macroscopic particle traps can provide interesting information on the strong coupling problem, many experiments require atomic ions or electrons.

STRONGLY COUPLED ATOMIC IONS IN PAUL TRAPS

With the practical density and charge limitations imposed on atomic ions in Penning and Paul traps, very low temperatures must be realized in order to obtain $\Gamma \gg 1$. This has been achieved by laser cooling.[3] Here we describe an experiment using Hg^+ ions at NBS.[18] A similar experiment has been performed at the Max Planck Institute for Quantum Optics in Garching.[19]

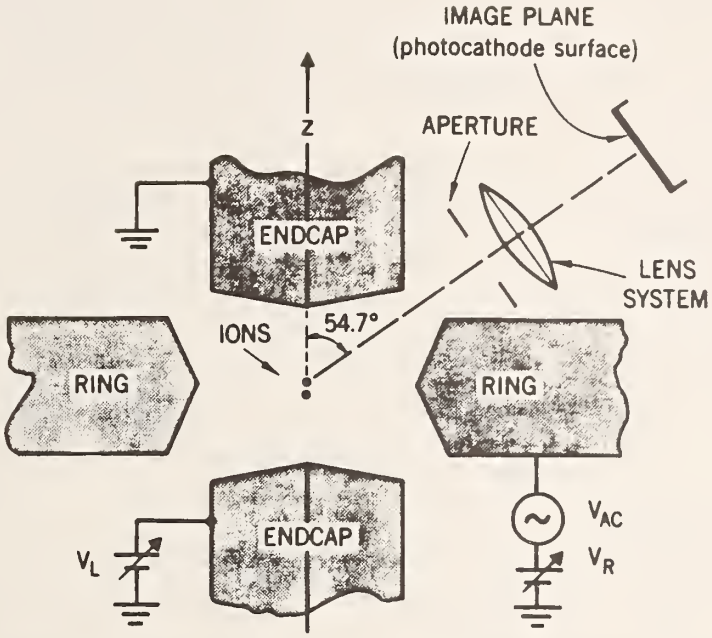

Fig. 3 Schematic drawing of the trap electrodes (to scale) and imaging system (not to scale) for Hg^+ cluster experiments. The end-cap to end-cap separation along the z axis is approximately 625 μm. The overall magnification of the lens system is 180X. The laser beam used to illuminate the ions also enters the trap at an angle of 54.7° with respect to the z axis and is perpendicular to the observation axis shown.

Small numbers of $^{198}Hg^+$ ions were stored in a miniature Paul trap, which has properties equivalent[16] to those of a hyperbolic trap with dimensions $r_0 \simeq 466$ μm and $z_0 \simeq 330$ μm. An oscillating voltage V_0 with peak amplitude between 145 and 325 V at a frequency of 23.26 MHz was applied between the ring and end-cap electrodes for trapping. The ions were laser cooled by 1-2 μW of cw 194-nm radiation[20] (bandwidth < 2 MHz), whose beam waist was varied between 5 and 15 μm at the position of the ions. This radiation was tuned near the $5d^{10}6s\ ^2S_{\frac{1}{2}} \rightarrow 5d^{10}6p\ ^2P_{\frac{1}{2}}$ first resonance line, which has a natural linewidth of 70 MHz. Some of the 194-nm fluorescence from the ions was focused onto the photocathode of a resistive-anode photon-counting imaging tube as shown schematically in Fig. 3. The optics for this imaging was provided by a three-stage fused-quartz lens system with an aberration-compensated first stage. The first lens was apertured to give an f number of 4.5. The positions of the photons detected by the imaging tube could be displayed on an oscilloscope in real time or stored by a computer in order to make time exposures.

In Fig. 4(a) we show the orientation of the trap as viewed by the imaging tube. In Fig. 4(b), two ions are made to lie in the x-y plane by making $\alpha < \beta$ in Eq. 2. Although the trap was designed to have axial symmetry, the preferred spatial alignment of the two cold ions indicates that an asymmetric potential exists which could be due to trap imperfections, contact-potential variations, or some other trap asymmetry. For convenience, we choose this preferred direction to be the x axis as indicated in Fig. 4b.

In the remainder of Fig. 4 we show images obtained for a few cases of up to 16 ions. We can characterize the ponderomotive potential as in Eqs. 2 and 3 or, equivalently, by the single ion resonance frequencies ν_z and ν_r for the motion in the axial and radial directions respectively. (In Fig. 4, we assume $\nu_x \simeq \nu_y = \nu_r$.) We chose this latter method in Ref. 18 and for Fig. 4 since the measured oscillation frequencies[21] are a more direct means of characterizing the trap than the applied potentials and trap dimensions. We find $\alpha = 2\pi^2 m\nu_r^2/q$ and $\beta = 2\pi^2 m\nu_z^2/q$ where α and β are from Eq. 2. When ν_z/ν_r is made large enough, all of the ions are forced by the strength of the potential in the z direction to lie in the x-y plane as in Figs. 4b and d. When ν_z/ν_r is small enough, the ions lie along the z axis as in Fig. 4c. This allowed us to count the ions. Below the images in Figs. 4d through 4g, we show the configurations obtained theoretically[22] for each value of the number of ions N_i obtained by minimizing the function

$$E_\phi = q \sum_{i=1}^{N_i} (\alpha r_i^2 + \beta z_i^2) + q^2 \sum_{i<j}^{N_i} |\vec{r}_i - \vec{r}_j|^{-1} \qquad (4)$$

where α and β are determined from the experimentally measured values of ν_r and ν_z.

The circular images or rings in Figs. 4e through g are due to ion circulation about the z axis. For a small asymmetry in the x,y plane, we can modify Eq. 2 to be approximately

$$\phi_p = \alpha_x x^2 + \alpha_y y^2 + \beta z^2 . \qquad (5)$$

When $\alpha_x < \alpha_y < \alpha_z$, and $N_i = 2$, the potential energy of Eq. 4 is minimized for two ions along the x axis as in Fig. 4b. The strength of this alignment is given by ΔE_ϕ, the maximum variation of E_ϕ for 2 ions constrained in the x-y plane. This is given by the difference between E_ϕ for ions on the x axis and E_ϕ for ions constrained along the y axis. For 3 or more ions in the same ring, the maximum variation in E_ϕ is considerably smaller than for two ions. Therefore, the ions more easily rotate in the azimuthal direction even though they must be nominally equally spaced in the ring. The number of ions in Fig. 4e could be

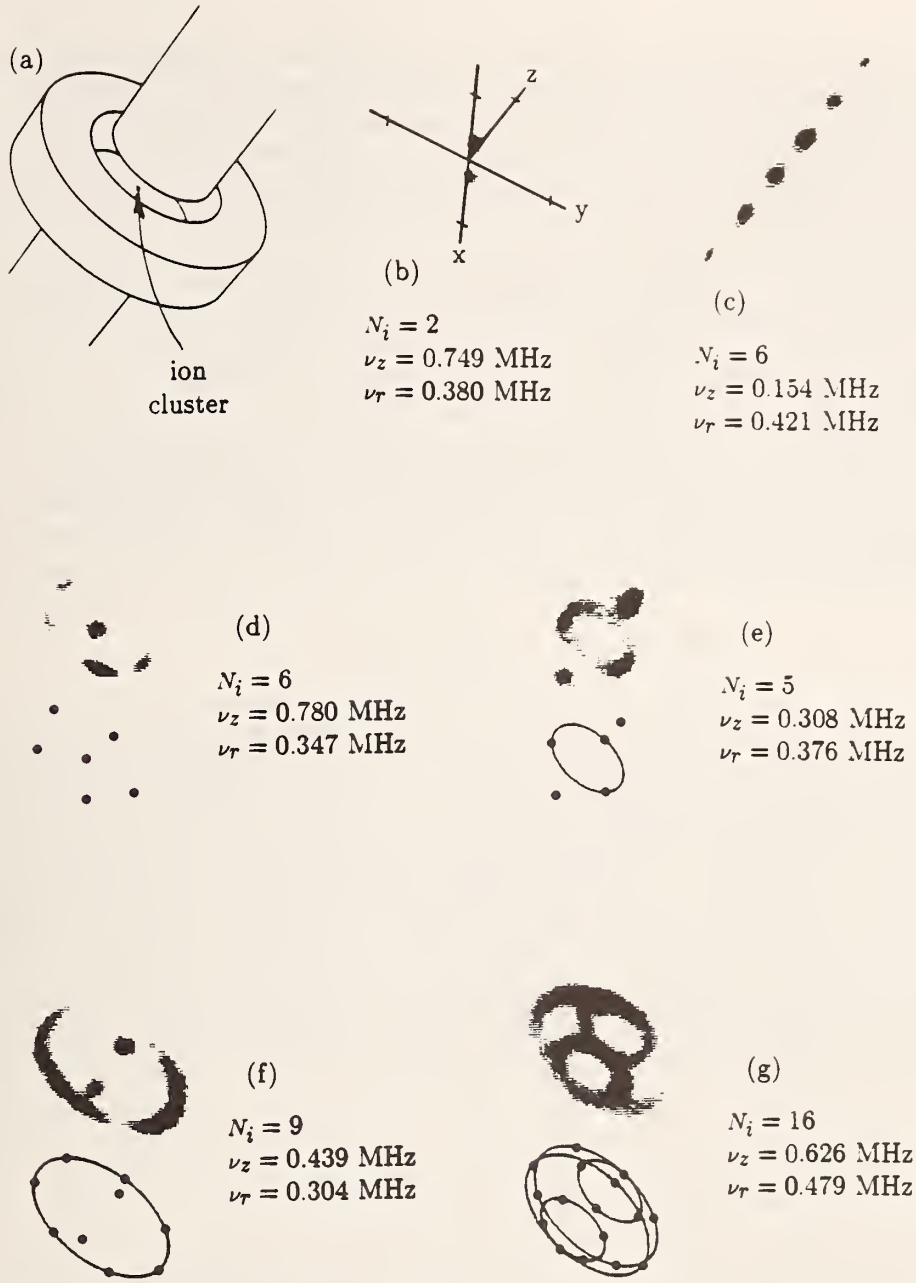

Fig. 4 Images of Hg^+ ion "clusters" in a Paul trap. In (a), the trap electrodes are shown schematically in the same orientation as for the remainder of the pictures, but at reduced magnification (inner diameter of the ring electrode is ≈ 0.9 mm). The coordinate system in (b) applies to the rest of the images. The tick marks on the axes are 10 μm from the origin. In (d) through (g), we display numerical solutions for the expected cluster shapes using the experimental values of ν_z and ν_r. The "rings" are caused by ion circulation about the trap z axis of symmetry. In (d), a non-fluorescing impurity ion occupies a particular ion site in the cluster and helps to pin the ions in the radial plane.

verified by aligning them along the z axis and counting. For Figs. 4f and g, the number of ions could be assigned by varying ν_z/ν_r and comparing the observed images (with rings) with the simulations. In principle, we could have aligned and counted 9 and 16 ions along z, but the ratio ν_z/ν_r required to do this was so low, that ions would have evaporated from the trap along the z axis.

In Fig. 4d, we see the approximate configuration expected for 6 ions but one of the ions appears to be missing. In addition, the ions are pinned in the x-y plane rather than forming a ring as in Fig. 4f. These observations are consistent with a nonfluorescing or "phantom" ion that occupies the missing cluster site. This ion may be another isotope of Hg^+. For example, fluorescence from $^{199}Hg^+$ would be extremely weak because of ground state hyperfine optical pumping. It might also be an impurity molecular ion like $HgOH^+$ formed from the exothermic reaction

$$Hg^+ + H_2O \rightarrow HgOH^+ + H. \qquad (6)$$

In any case, an impurity ion with charge-to-mass ratio different from $^{198}Hg^+$ will make ΔE_ϕ for ions in the same ring be larger than ΔE_ϕ if all the ions are $^{198}Hg^+$. This can happen because of the differences in α and β for ions of different charge-to-mass ratio. Thus we would expect pinning to be more likely with the impurity ion present. In the experiments of Ref. 19, the trap asymmetry in the x-y plane was probably larger than observed here. This apparently made ΔE_ϕ larger for ions in the same ring, resulting in pinning of like ions.

For these configurations, the agreement between data and simulations appears to be fairly good.[22] To estimate Γ, we use for the background density n_0 the expression[14]

$$n_0 = \frac{1}{2\pi q}(2\alpha+\beta) = \frac{\pi m}{q^2}(2\nu_r^2 + \nu_z^2) \qquad (7)$$

For the conditions of Fig. 4(g), Eq. 7 implies $n_0 = 3.8 \times 10^9$.

In these experiments, the temperature was extracted from the Doppler broadening of the ion's spectral lines.[23] This broadening contributes significantly to the width of $^2S_{\frac{1}{2}} \rightarrow {}^2D_{5/2}$ quadrupole transition in $^{198}Hg^+$.[18,24] From these measurements, we determined that the secular motion temperature for two ions in the trap, when $\nu_r \simeq 2\nu_z = 473$ kHz, was less than 8 mK. If we take 8 mK as a typical upper limit for the ions in fig. 4g then we obtain $\Gamma \geq 525$.

Finally, in Fig. 4g, we see that 16 ions approximately lie on 3 rings. The larger ring, containing 8 ions, lies in the x-y plane and the smaller rings, each containing 4 ions, lie in planes above and below but parallel to the x-y plane. We may also view these ions as lying on the surface of a spheroidal

shell characteristic of the structure for large numbers of ions.[11,13,26-28]

In principle, it should be possible to observe ordered structures of much larger numbers of atomic ions in Paul traps. In our trap, this was apparently prevented for $N_i \gtrsim 20$ because the small amount of laser power available for cooling was unable to overcome the rf heating.[25] In rf heating, the kinetic energy of the ion's driven motion at frequency Ω is coupled into the secular motion characteristic of the pseudopotential well.

STRONGLY COUPLED ATOMIC IONS IN PENNING TRAPS

In Penning traps,[2] where ions are confined by static electric and magnetic fields, rf heating[25] does not take place and large collections of ions can be laser-cooled to temperatures less than 10 mK. The static properties of ions in a Penning trap are identical to those of a one component plasma where the background density is given by [1,13,14]

$$n_0 = \frac{m\omega}{2\pi q^2}(\Omega_c - \omega) \quad . \tag{8}$$

Here, Ω_c is the ion cyclotron frequency and ω is the rotation frequency of the cloud. For a finite plasma consisting of a hundred to a few thousand ions, the boundary conditions are predicted to have a significant effect on the plasma state. Several molecular dynamics simulations on collections of a hundred to a few thousand ions confined in storage rings and traps have recently been completed.[11,26-28,30,31] When $\Gamma > 1$, the ions are predicted to reside in concentric shells. As the ions are cooled, instead of a sharp phase transition, the system is expected to gradually evolve from a liquid state characterized by short range order and diffusion in all directions, to a state where there is diffusion within a shell but no diffusion between the shells (like a smectic liquid crystal) and ultimately to an overall solid-like state.[28]

We have investigated[29] this interesting system using $^9Be^+$ ions trapped in the cylindrical Penning trap shown schematically in Fig. 5. A magnetic field $\vec{B} = B\hat{z}$ (B = 1.92 T) produced by a superconducting magnet confined the ions in the direction perpendicular to the z axis. A static potential U_0 between the end and central cylinders confined the ions in the z direction to a region near the center of the trap.

The $^9Be^+$ ions were laser cooled by driving the $2s\ ^2S_{\frac{1}{2}}(m_I = 3/2, m_J = 1/2) \rightarrow 2p\ ^2P_{3/2}(3/2,3/2)$ transition slightly below the resonant frequency. The 313 nm cooling radiation ($\approx 30\ \mu W$) could be directed perpendicular to the magnetic field and/or along a diagonal as indicated in Fig. 5. In addition to cooling the ions, the laser also applied an overall torque which could either compress or expand the cloud.[14,23] This allowed us to control the cloud size by choosing the radial positions (and thus the torques) of the perpendicular and diagonal beams.

About 0.04% of the 313 nm fluorescence from the decay of the $^2P_{3/2}$ state was focused by f/10 optics onto the photocathode of the same imaging tube used in the Hg^+ ion experiments. The imager was located along the z axis, about 1 m from the ions. The imaging optics was composed of a three stage lens system with overall magnification of 27 and a resolution (FWHM) of about 5 μm. Positions of the photons arriving at the imager were displayed in real time on an oscilloscope while being integrated by a computer.

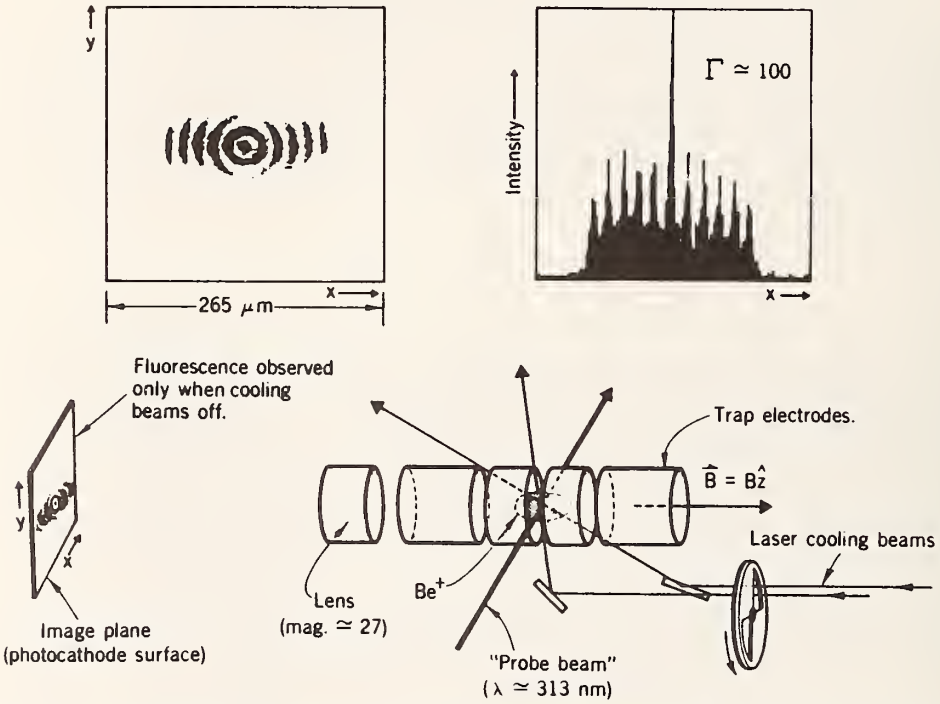

Fig. 5. Schematic representation of apparatus for observation of shell structure of strongly coupled $^9Be^+$ ions in a Penning trap. Images are made of the ions which are intersected by the probe beam. In the upper right, an intensity plot vs x for a value of y intersecting the center of the cloud is shown. Shell structure results from the boundary conditions at the edge of the cloud.

A second laser (power $\approx$ 1 μW, beam waist $\simeq$ 30 μm) was used to spatially map the shell structure of the cloud. This probe laser was tuned to the same transition as the cooling laser and was directed through the cloud perpendicularly to the magnetic field. With the probe laser on continuously, the cooling laser could be chopped at 1 kHz (50% duty cycle) and the image signal integrated only when the cooling laser was off as shown in Fig. 5. Different portions of the cloud could be imaged by translating the probe beam, in a calibrated fashion, either parallel or perpendicular to the z axis. Images were also obtained from the ion fluorescence of all three laser beams.[29]

The rotation frequency ω was determined from the first order Doppler shift of the ion's optical spectrum due to the cloud

rotation.[23,29,32] From ω and an independent measurement of Ω_c,[21] n_0 was determined from Eq. 8. From the Doppler broadening of the spectrum, T was determined.[23,29,32] From n_0 and size of the ion cloud, N_i was determined. Γ was determined from n_0 and T.

We have observed clouds containing from 1 shell ($N_i \simeq 20$) up to 16 shells ($N_i \simeq 15\ 000$). For a spherical cloud, approximately $(N_i/4)^{1/3}$ shells are predicted.[26] For the nearly spherical cloud of Ref. 29 ($N_i \simeq 15\ 000$) this formula predicts 15.5 shells and we measured 16. At present, it is difficult to make further quantitative comparisons between our data and the theoretical calculations. For example, there is substantial uncertainty in our measurement of Γ due to uncertainty in the temperature measurement. Also, the spatial resolution is partially limited by optics. Our data do agree qualitatively with the simulations with the exception of the presence, in some cases, of an open cylinder shell structure[29] as opposed to the predicted closed spheroids. Schiffer has suggested[30] that shear (that is, different rotation frequencies) between the shells may account for this discrepancy. In our experiment, shear could be caused by differential laser torque or the presence of impurity ions.[32] For the data here, we have determined that the rotation frequency does not vary by more than 30% across the cloud. This is comparable to the limits discussed in Refs. 32 and 33.

FUTURE EXPERIMENTS

A number of future experiments will allow us to better understand strong coupling in nonneutral ion plasmas. Increasing the cooling power in the experiments should allow larger ($N_i >> 10^5$) samples of ions to be cooled. This may permit, perhaps by Bragg scattering,[23] the observation of structure characteristic of the infinite volume regime in which a body-centered cubic (bcc) structure is predicted.[7] Detailed images in the Penning traps are made difficult by the rotation of the cloud which averages over azimuthal angle. In principle, it should be possible to strobe the laser (or detection) at a frequency harmonically related to ω, but this requires ω to be sufficiently stable. Fluctuations in ion density may make this difficult but perhaps an individual strongly fluorescing ion (such as Mg^+) which is locked onto the rotating lattice (of Be^+) could serve as a "beacon" and aid in determining ω. In addition, the present experiments would benefit from improved light collection optics.

At present, the rather large uncertainty in Γ in the Penning trap experiments comes from the uncertainty in our measurement of temperature. This is because the Doppler broadening contribution of the optical spectrum used is small compared to the radiative, or natural broadening. This limitation can be overcome by driving transitions whose radiative broadening is negligible as in the Hg^+ experiments.[24] For Be^+ and Mg^+ ions, two-photon stimulated Raman transitions might be used for this purpose.[3,23]

So far, our measurements have been limited to the static structure of nonneutral ion plasmas. Various other experiments may provide dynamical information. For example, ions can be

switched off by optically pumping them with an additional laser beam into states which don't fluoresce.[23,32,33] By appropriate positioning of this depopulating laser beam, certain parts of the ion cloud can be tagged allowing ion diffusion studies via the movement (or lack of movement) of the tagged ions.[29] In this way, relatively rapid diffusion within the shells of Be^+ ions in the Penning trap has been distinguished from the much slower diffusion of ions between the shells. In addition, spectrum analysis of the scattered light from strongly coupled ions can possibly be used to study mode structure of ordered ion motion. Such studies may be aided by the use of sympathetic cooling[32] whereby two ion species are confined simultaneously in the same trap. One ion species is laser cooled and by Coulomb interaction cools and maintains the second ion species at constant temperature. Dynamical studies are then performed on the second ion species.

It would be very useful to study large numbers of particles in a Paul trap. One clear advantage over a Penning trap is that ions can remain fixed without rotation. This could be insured by making the trap asymmetric in the x-y plane. For example, by splitting the ring into sectors and applying different static potentials to these sectors, the asymmetry could be easily controlled. For large numbers of ions, the mechanism of rf heating[25] must be overcome. This may be aided by working at higher laser cooling power, using smaller ratios of secular to drive frequencies (smaller q parameter, Appendix A) and making sure that impurity ions are absent.

ACKNOWLEDGEMENTS

We gratefully acknowledge support from the Office of Naval Research and the Air Force Office of Scientific Research. We thank A. Bauch for helpful suggestions on the manuscript.

APPENDIX A

In studies of strong coupling we want low temperature and high density. In addition, we may desire large numbers to more nearly approach the infinite volume regime.

Paul (rf) trap

From Eqs. 3 and 7, we can write, for a low temperature sample:

$$n_0 = 3q_r V_0/(4\pi q\xi^2) \tag{A1}$$

where the dimensionless parameter $q_r = 4qV_0/(m\Omega^2\xi^2)$ is the ion's stability parameter.[2] Typically, $q_r < 0.3$ for stable operation. If we assume for simplicity, that U_0 is adjusted to make the cloud spherical with radius r_{cl}, the total number of ions N_i is given by

$$N_i = 4\pi n_0 r_{cl}^3/3 = V_0(q_r/q)(r_{cl}^3/\xi^2) \tag{A2}$$

Assuming q_r and r_{cl}/ξ are fixed, then to make N_i large, we want V_0 and ξ big and q small.

Similarly, we can derive

$$\Gamma = (q^5 V_0 q_r/\xi^2)^{1/3}/(k_B T), \tag{A3}$$

implying that for large Γ, we want q and V_0 big and T and ξ small. For both large N_i and Γ, we want V_0 big and T small; the choice of q and ξ may depend on specific experimental constraints.

Penning trap

If we assume a fixed value K for the ratio of the achievable density to Brillouin density and assume U_0 is chosen to make a spherical cloud (radius r_{cl}), we have

$$N_i = K\, B^2 r_{cl}^3/(6mc^2), \tag{A4}$$

and

$$\Gamma = \left(\frac{K\, B^2}{6mc^2}\right)^{1/3} q^2/k_B T. \tag{A5}$$

Therefore, except for practical limitations on maximum possible values of U_0,[3,4] in the Penning trap, we can make both N_i and Γ large by making B, ξ ($\propto r_{cl}$), and q big and m and T small.

REFERENCES

1. J.H. Malmberg and T.M. O'Neil, Phys. Rev. Lett. 39, 1333 (1977).
2. See for example: H.G. Dehmelt, Adv. At. Mol. Phys. 3, 53 (1967) and 5, 109 (1969); D.J. Wineland, W.M. Itano, and R.S. Van Dyck, Jr., Adv. At. Mol. Phys. 19, 135 (1983).
3. See for example: D.J. Wineland and W.M. Itano, Physics Today 40(6), 34 (1987) and references therein.
4. D.J. Wineland, R.E. Drullinger, and F.L. Walls, Phys. Rev. Lett. 40, 1639 (1978). At the same time, laser cooling of ions confined in Paul (rf) trap was observed: W. Neuhauser, M. Hohenstatt, P. Toschek, and H. Dehmelt, Phys. Rev. Lett. 41, 233 (1978).
5. W. Neuhauser, M. Hohenstatt, P.E. Toschek, and H. Dehmelt, Phys. Rev. A22, 1137 (1980).
6. W. Nagourney, Comments on At. Mol. Phys., to be published; H.G. Dehmelt, Physica Scripta, to be published.
7. S. Ichimaru, H. Iyetomi, and S. Tanaka, Phys. Rep. 149, 91 (1987) and references therein.
8. See for example: A.J. Dahm and W.F. Vinen, Physics Today 40, 43 (Feb., 1987).
9. G. Morales, these proceedings.
10. D.J. Aastuen, N.A. Clark, and L.K. Cotter, Phys. Rev. Lett. 57, 1733 (1986); J.M. di Meglio, D.A. Weitz, and P.M. Chaikin, Phys. Rev. Lett. 58, 136 (1987); C.A. Murray and D.H. Van Winkle, Phys. Rev. Lett. 58, 1200 (1987).
11. J.P. Schiffer and O. Poulsen, Europhys. Lett. 1, 55 (1986); D. Habs, in Lecture Notes in Physics 296, M. Month and S. Turner, eds. (Springer-Verlag, Berlin) 1988, p. 310.
12. J.H. Malmberg, these proceedings.
13. T.M. O'Neil, these proceedings.
14. D.J. Wineland, J.J. Bollinger, W.M. Itano, and J.D. Prestage, J. Opt. Soc. Am. B2, 1721 (1985).
15. E. Fischer, Z. Phys. 156, 1 (1959); R.F. Wuerker, H. Shelton, and R.V. Langmuir, J. Appl. Phys. 30, 342 (1959).
16. E.C. Beaty, J. Appl. Phys. 61, 2118 (1987).
17. R.C. Davidson, Theory of Noneutral Plasmas (Benjamin, Reading, Mass., 1974), p. 7.
18. D.J. Wineland, J.C. Bergquist, W.M. Itano, J.J. Bollinger, and C.H. Manney, Phys. Rev. Lett. 59, 2935 (1987).
19. F. Diedrich, E. Peik, J.M. Chen, W. Quint, and H. Walther, Phys. Rev. Lett. 59, 2931 (1987).
20. H. Hemmati, J.C. Bergquist, and W.M. Itano, Opt. Lett. 8, 73 (1983).
21. F.G. Major and G. Werth, Appl. Phys. 15, 201 (1978); W. Neuhauser, M. Hohenstatt, P. Toschek, and H. Dehmelt, Phys. Rev. Lett. 41, 233 (1978); D.J. Wineland,J.J.

Bollinger, and W.M. Itano, Phys. Rev. Lett. 50, 628, 1333(E) (1983).
22. W.M. Itano, et al., to be published. Our simulations agree with independent ones performed by D.H.E. Dubin (performed on up to 10 ions), private communication.
23. J.J. Bollinger and D.J. Wineland, Phys. Rev. Lett. 53, 348 (1984); L.R. Brewer, J.D. Prestage, J.J. Bollinger, and D.J. Wineland, in Strongly Coupled Plasma Physics, edited by F.J. Rogers and H.E. Dewitt (Plenum, New York, 1987), p. 53.
24. J.C. Bergquist, W.M. Itano, and D.J. Wineland, Phys. Rev. A36, 428 (1987).
25. D.A. Church and H.G. Dehmelt, J. Appl. Phys. 40, 3421 (1969); H.G. Dehmelt, in Advances in Laser Spectroscopy, edited by F.T. Arecchi, F. Strumia, and H. Walther (Plenum, New York, 1983), p. 153.
26. A. Rahman and J.P. Schiffer, Phys. Rev. Lett. 57, 1133 (1986); J.P. Schiffer, submitted for publication.
27. H. Totsuji, in Strongly Coupled Plasma Physics, edited by F.J. Rogers and H.E. Dewitt (Plenum, New York, 1987), p. 19.
28. D.H.E. Dubin and T.M. O'Neil, Phys. Rev. Lett. 60, 511 (1988).
29. S.L. Gilbert, J.J. Bollinger, and D.J. Wineland, Phys. Rev. Lett., 60, 2022 (1988).
30. J.P. Schiffer, private communication.
31. D.H.E. Dubin, private communication.
32. D.J. Larson, J.C. Bergquist, J.J. Bollinger, W.M. Itano, and D.J. Wineland, Phys. Rev. Lett. 57, 70 (1986).
33. L.R. Brewer, J.D. Prestage, J.J. Bollinger, W.M. Itano, D.J. Larson, and D.J. Wineland, Phys. Rev. A., to be published.
34. C.F. Driscoll, in Low Energy Antimatter, Ed. by D.B. Cline (World Scientific, Singapore, 1986), p. 184.

From: Proc. 4th Symposium on Freq. Standards and Metrology, Ancona, Italy, Sept., 1988 (Springer Verlag).

Quantitative Study of Laser Cooling in a Penning Trap*

W.M. Itano, L.R. Brewer, D.J. Larson,
J.J. Bollinger, S.L. Gilbert, and D.J. Wineland
National Institute of Standards and Technology
Boulder, Colorado, 80303 U.S.A.

Penning traps are currently being studied at our laboratory [1,2] and elsewhere [3,4] for use in atomic frequency standards. A Penning trap confines ions by a combination of a static, uniform magnetic field and a static, nonuniform electric field. The fact that the fields are static makes it feasible to laser cool more than 10^4 ions to low temperatures [5]. In contrast, the radio-frequency (Paul) ion trap uses oscillating electric fields, which, in combination with the nonlinear Coulomb coupling between ions, cause heating and make it difficult to laser cool large numbers of ions [6]. For either trap, large numbers increase the signal-to-noise ratio; low temperatures reduce the second-order Doppler shift [7].

Several experimental groups have reported laser cooling of ions confined in Penning traps to temperatures below 1 K [1-5,8-10]. Typically, the measured temperatures were one or two orders of magnitude higher than the theoretical limit $T_{min} = \hbar\gamma_0/(2k_B)$ (about 1 mK), where γ_0 is the natural linewidth of the optical transition used for laser cooling [9]. The reason for this discrepancy is now understood [10]. The rotation of the ion plasma about the magnetic field axis, due to the presence of crossed electric and magnetic fields, has a great effect on the temperature. In order for the ion plasma to be stable, it is necessary to displace the laser beam radially so that it illuminates the side of the plasma which is receding from the laser. The radiation pressure applies a torque to the plasma which counteracts the torques induced by axially nonsymmetric, static electric and magnetic fields. This radial displacement of the beam, however, results in higher temperatures. The reason stems from the requirement that the work done by the laser on the ions be zero for a steady state. The rate at which work is done on an ion of velocity $\vec{v}$ by a force $\vec{F}$, which, in this case, is parallel to the direction of propagation of the laser beam, is $\vec{F}\cdot\vec{v}$. Because of the radial displacement of the beam and the plasma rotation, $\vec{F}\cdot\vec{v}$ tends to be positive. In order to make the average value $\langle\vec{F}\cdot\vec{v}\rangle$ be zero, the frequency of the laser must be tuned below the optical resonance. Because of the Doppler shift, this makes $\vec{F}$ stronger for ions with $\vec{F}\cdot\vec{v} < 0$ than for ions with $\vec{F}\cdot\vec{v} > 0$. The width of the velocity distribution must have a particular value in order for cancellation between negative and positive contributions to make the average value

be zero. The required width increases with the rotation frequency and with the distance of the laser beam from the axis of rotation of the plasma. This width corresponds to a temperature higher than T_{min}.

Temperatures and rotation frequencies of $^9Be^+$ plasmas were measured for a wide range of experimental parameters [10]. The measured temperatures varied from 40 mK to 2 K. These measured temperatures were in agreement with the calculation, within an rms error of about 10%. For these measurements, the cooling laser beam was in the plane perpendicular to the magnetic field. Lower temperatures have been attained by the use of laser beams whose direction of propagation were not perpendicular to the magnetic field axis, but the calculation in this case is more complicated [5].

For certain ranges of laser frequency detuning and beam position, we have observed strong oscillations in the total ion fluorescence, with periods from less than a second to over a minute. These oscillations have been observed in all Penning traps at our laboratory and are similar to those reported by others [3,11]. Sometimes, a deliberate misalignment of the magnetic field direction with respect to the trap axis was necessary in order for oscillations to occur. This was an indication that external torques were involved. An ion plasma undergoing oscillations was observed with a photon-counting imaging tube. The change in ion fluorescence was accompanied by a change in the radius (which is directly related to the total canonical angular momentum) of the plasma. For the plasma to reach a steady state, the rate of both the energy and angular momentum imparted to the plasma by external forces must be 0. Apparently, these two conditions sometimes cannot be satisfied simultaneously, and this leads to oscillations.

We wish to acknowledge support from the U.S. Office of Naval Research and the U.S. Air Force Office of Scientific Research.

* Work of the U.S. Government. Not subject to U.S. copyright.

1. J.J. Bollinger et al.: Phys. Rev. Lett. 54, 1000 (1985)
2. J.J. Bollinger et al.: these Proceedings
3. R.C. Thompson et al.: Opt. Acta 33, 535 (1986); Appl. Phys. B 46, 87 (1988)
4. F. Plumelle et al.: Appl. Phys. B 41, 183 (1986)
5. L.R. Brewer et al.: Phys. Rev. A 38, 859 (1988)
6. J. Hoffnagle et al.: Phys. Rev. Lett. 60, 2022 (1988); R. Blümel et al.: Nature, 334, 309 (1988)
7. D.J. Wineland et al.: these Proceedings
8. R.E. Drullinger, D.J. Wineland, and J.C. Bergquist: Appl. Phys. 22, 365 (1980)
9. W.M. Itano and D.J. Wineland: Phys. Rev. A 25, 35 (1982)
10. W.M. Itano et al.: Phys. Rev. A (in press)
11. J. Yu, M. Desaintfuscien, and F. Plumelle: (submitted to Appl. Phys. B)

Ann. Phys. Fr. **10** (1985) 737-748 DÉCEMBRE **1985**, PAGE 737

Optical pumping of stored atomic ions (*)

D. J. Wineland, W. M. Itano, J. C. Bergquist, J. J. Bollinger and J. D. Prestage

Time and Frequency Division, National Bureau of Standards, Boulder, Colorado 80303, U.S.A.

Résumé. — Ce texte discute les expériences de pompage optique sur des ions atomiques confinés dans des pièges électromagnétiques. Du fait de la faible relaxation et des déplacements d'énergie très petits des ions confinés, on peut obtenir une très haute résolution et une très grande précision dans les expériences de pompage optique associé à la double résonance. Dans la ligne de l'idée de Kastler de « lumino-réfrigération » (1950), l'énergie cinétique des niveaux des ions confinés peut être pompée optiquement. Cette technique, appelée refroidissement laser, réduit sensiblement les déplacements de fréquence Doppler dans les spectres.

Abstract. — Optical pumping experiments on atomic ions which are stored in electromagnetic « traps » are discussed. Weak relaxation and extremely small energy shifts of the stored ions lead to very high resolution and accuracy in optical pumping-double resonance experiments. In the same spirit of Kastler's proposal for « lumino refrigeration » (1950), the kinetic energy levels of stored ions can be optically pumped. This technique, which has been called laser cooling, significantly reduces Doppler frequency shifts in the spectra.

1. Introduction.

For more than thirty years, the technique of optical pumping, as originally proposed by Alfred Kastler [1], has provided information about atomic structure, atom-atom interactions, and the interaction of atoms with external radiation. This technique continues today as one of the primary methods used in atomic physics. Moreover, it is a tribute to Kastler's foresight that some of his ideas have only recently been realized — for example, the relatively new technique of laser cooling is essentially contained in Kastler's idea of « lumino-refrigeration » [1].

Experiments on optical pumping of ions have not been as extensive as those on neutral atoms partly due to the difficulty of producing and maintaining sufficient ion populations and partly due to the difficulty of producing the required optical radiation which for positive ions is usually in the ultraviolet region of the spectrum. The subject of optically pumped ions was reviewed by Weber [2] in 1977; most of the experiments reported there used buffer gas cells to hold the ions and gas discharges as sources of radiation.

Since that time, a number of experiments using electromagnetic ion « traps » and laser sources for optical pumping have been carried out. In this paper we will restrict our attention to the unique features of the traps for optical pumping experiments; the basic methods of trapping have been discussed elsewhere [3, 4].

(*) Work of the U.S. Government; not subject to U.S. copyright.

2. Properties of ion traps for optical pumping experiments.

2.1 Relaxation. — Often in ion trap experiments, ions are stored under ultra-high vacuum conditions ($p \lesssim 10^{-8}$ Pa [5]; neutral density $n \lesssim 2.7 \times 10^{6}/\mathrm{cm}^3$ at room temperature) for long periods of time (hours are not uncommon). As opposed to buffer gas cell experiments, this suggests that ion-neutral relaxation processes such as electron spin relaxation are extremely weak. As an example, suppose that ion-neutral relaxation proceeds at a typical Langevin rate for orbiting type collisions [6] : $k \cong 2 \times 10^{-9}$ cm^3/s. For a pressure of 10^{-8} Pa at room temperature, the relaxation time constant is given by $\tau \cong (kn)^{-1} \cong 190$ s. Using cryogenic vacuum systems, this relaxation time could be made much longer.

Of course in samples of many trapped ions, the ions « see » or interact with each other through the Coulomb interaction; this might lead to relaxation in various ways. For example, electron spin relaxation in ions with $^2S_{1/2}$ ground states could be driven by the relativistic magnetic fields $\mathbf{B}_c = \mathbf{v} \times \mathbf{E}_c/c$, produced in ion-ion collisions. To estimate this effect, assume B_c has a magnitude equal to that given by the above expression where $\mathbf{E}_c$ is the electric field at the distance of closest approach r (here assumed to be the impact parameter) and a duration given by $2\,r/v$ where v is the magnitude of the root mean square velocity between colliding ions. Then the spin precession angle for a single ion-ion collision is given by $\Delta\theta = (4\,\pi\mu_B\,B_c/h).(2\,r/v)$ where μ_B is the Bohr magneton and h is Planck's constant. For ions of mass 100 u (atomic mass units) at room temperature, the mean precession angle averaged over all distances of closest approach (from the minimum distance of closest approach, $d_0 = q^2/3\,k_B\,T$, up to the mean spacing between ions, $n^{-1/3}$, where q is the ion charge, k_B is Boltzmann's constant and n is the ion density in cm^{-3}) is $\langle \Delta\theta \rangle \cong 1 \times 10^{-12}\,n^{1/3}$. We would expect the angle to increase from multiple collisions in a random walk fashion so that $\mathrm{d}\theta^2/\mathrm{d}t \cong \langle \Delta\theta \rangle^2\,vn^{1/3} \cong 5 \times 10^{-20}\,n$. Even for ion densities of $n \cong 10^8$ cm^{-3}, such relaxation is negligible.

Relaxation might also occur in a similar way *via* electric dipole transitions — the rate would be approximately $(c/v)^2\,(qa_0/2\,\mu_B)^2$ times faster or $\mathrm{d}\theta^2/\mathrm{d}t \cong 5 \times 10^{-4}\,n$ (a_0 is the Bohr radius). However these calculations are valid only when the transition frequencies of interest are small compared to the inverse of the time of duration of the collision. If the transition frequencies are higher, then the states tend to adiabatically adjust during the collision and no relaxation occurs. Another way of saying this is that the spectrum of the **E** and **B** fields during the collision does not have components much above a frequency v/r. For room temperature ions ($M = 100$ u), even at the minimum distance of closest approach this cutoff frequency is around 20 GHz. This cutoff frequency would be expected to increase as $T^{3/2}$, therefore at elevated temperatures, such relaxation might play a rôle with molecular rotational (or perhaps vibrational) relaxation. In one way it is unfortunate that such relaxation is so weak. If electric dipole relaxation were stronger, significant rotational-translational energy exchange might be expected to occur for heteronuclear molecules. Since the temperature of ions can be sensitively monitored by the bolometric technique [7, 8], such relaxation might be a way to detect rotational/vibrational transitions in molecular ions. We note that significant rotational (vibrational)-translational energy exchange might be expected to occur between stored molecular ions and a neutral background gas (because of the shorter range of interaction); for this case, the bolometric technique might be used to detect rotational/vibrational transitions in the ions even though part of the energy released in the collision goes to the neutral.

Relaxation of atomic ions in metastable excited levels (e.g. the lowest $^2D_{5/2}$ states in Ba^+ or Hg^+) can proceed *via* ion-neutral collisions (expected to be efficient) or *via* the electric fields of ion-ion collisions. For the D states of Ba^+ or Hg^+, the collisional electric field from ion-ion collisions mixes some $^2P_{3/2}$ state into the $^2D_{5/2}$ state; therefore during the collision the ion decays at a rate given approximately by $[\langle {}^2P_{3/2} \mid q\mathbf{r}\cdot\mathbf{E} \mid {}^2D_{5/2}\rangle/(E(^2P_{3/2}) - E(^2D_{5/2}))]^2 A(^2P_{3/2})$ where E(i) and A(i) are the energy and decay rate of state i. If as before, the collision is assumed to have a duration $2\,r/v$ then when averaged over impact parameters between d_0 and $n^{-1/3}$, the probability of de-excitation per collision is given by $\langle P\rangle \cong 4\,q^4\,a_0^2\,n^{2/3}\,A(^2P_{3/2})/(\Delta E^2\,d_0\,v)$ where $\Delta E \equiv E(^2P_{3/2}) - E(^2D_{5/2})$, and we have assumed $\langle {}^2P_{3/2} \mid q\mathbf{r}\cdot\mathbf{E} \mid {}^2D_{5/2}\rangle = qa_0 \mid \mathbf{E} \mid$. Therefore the overall relaxation rate for this process is given by $\langle P\rangle . vn^{1/3}$; for Hg^+ ions at $n = 10^8/cm^3$ and $T = 300$ K, the relaxation rate from the $^2D_{5/2}$ state is about 5×10^{-9}/s which is negligible.

Therefore we see that at high vacuum, relaxation of the internal energy states of ions is expected to be extremely weak. This may be regarded as an advantage if for example, the objective of an experiment is to obtain sub-Hertz linewidths in double resonance experiments, but may be regarded as a disadvantage if the ions become « trapped » in a metastable state. In this case a buffer gas such as He or H_2 might be added to provide the necessary relaxation [9].

2.2 Energy shifts. — One of the primary advantages of the stored ion technique is that ions can be confined in a small region of space without the usual perturbations associated with confinement (e.g. shifts due to ion-neutral collisions in a buffer gas cell).

At finite vacuum one must still worry about ion-neutral collisions but the resulting shifts should be quite small. For example, the fractional shifts of the ground state hyperfine frequencies of $^{137}Ba^+$ (Ref. [10]) and $^{199}Hg^+$ (Ref. [11]) due to He collisions have been measured to be about 5×10^{-11}/Pa and 4×10^{-11}/Pa respectively. Therefore, at 10^{-8} Pa, such shifts are extremely small. Similarly, on optical transitions, frequency shifts due to ion-neutral collisions would be expected to be smaller than the collision rates; in the high vacuum case fractional shifts would therefore be very small.

One must also consider the frequency shifting effects of the electric fields of ion-ion collisions and ion-trap « collisions » [12]. The latter effect is analogous to ion-neutral collisions in a buffer gas cell however the « collisions » with the electric fields of the ion traps can be much softer. If the ions have linear shifts of energy levels with respect to electric field ($\delta v \propto \langle \mathbf{E} \rangle$), then these shifts averaged in time must vanish. We know that because if $\langle \mathbf{E} \rangle \neq 0$ the ions would leave the trap.

Energy shifts of non-spherical electronic levels (e.g. the D states in Ba^+ or Hg^+) due to the electric quadrupolar trapping fields of a Penning trap [3, 4] occur at a level of a few Hz [13]; these shifts should however be precisely controllable. For clouds of many ions in a trap, the ion cloud can also have a quadrupole moment which can interact with an atomic quadrupole moment. Such shifts might become important in very high resolution optical spectra for example. To estimate such an effect, assume that we have a « cold » ion cloud in an rf trap. Its shape will be determined by a balance between the forces from the trap pseudopotential and the space charge [3, 4]. If there is no D.C. bias on the ring electrode, the potential from the ions is then given by $\phi(\text{ions}) = -\pi qn(x^2 + y^2 + 4\,z^2)/3$. Using equations (3.6) of Kopfermann [14], the quadrupole energy shift is given by $\Delta E_Q = q[Q_{xx}\,\phi_{xx} + Q_{yy}\,\phi_{yy} + Q_{zz}\,\phi_{zz}]$ where Q_{ii} is the ith diagonal element of the atomic quadrupole

tensor [14] and $\phi_{xx} \equiv \partial^2\phi/\partial x^2$ etc. Therefore we have approximately $\Delta\nu_Q = \Delta E_Q/h \cong q^2\, nQ/h$ where Q is the usual quadrupole moment [14]. For $Q \cong (1\ \text{Å})^2$, $\Delta\nu_Q \cong 3 \times 10^{-9}\, n$ Hz. This shift is probably negligible except perhaps in small rf traps where very deep pseudo potential wells and high densities can be obtained. One must also worry about quadrupole shifts if collisions are asymmetric; this might be the case if for example, the x, y motion was hotter than the z motion. As an extreme case, assume that two cold ions are trapped in a deep pseudo potential well at a fixed separation of 1 μm along the z axis. In this case, $\Delta\nu_Q \cong qQ\phi_{zz}/h = 2\, q^2\, Q/hz^3 \cong 7$ kHz.

One is often concerned with quadratic Stark shifts ($\delta\nu \propto \langle E^2 \rangle$); the source of the electric fields may be due to the trapping fields, ion-ion interactions, optical pumping radiation or perhaps the black body radiation field which at room temperature has a value [15] $\langle E^2 \rangle \cong 70\ (\text{V/cm})^2$. The shifting effects of optical pumping radiation have been known for quite some time; due to the near resonance condition of this radiation, resulting shifts can be quite large. In high precision double resonance experiments it is usually necessary to probe the transitions with the pumping radiation off (i.e. : chop the pumping light). Electric fields due to trapping [3, 4] can be of the order of 100 V/cm but in many cases they can be significantly smaller [12]. We can estimate $\langle E^2 \rangle$ due to ion-ion collisions by assuming that the electric field is due to binary collisions ($E(r) = q/r^2$). If we average $E^2(r)$ over the volume between two spheres defined by the minimum distance of closest approach and the mean spacing between ions, we obtain $\langle E^2 \rangle = 3\, q^2\, n/d_0$. For $T = 300$ K, $n = 10^8/\text{cm}^3$, $\langle E^2 \rangle \cong 3\ (\text{V/cm})^2$.

For hyperfine structure, frequency shifts due to quadratic Stark effects can be quite small. For example, for Ba^+ ground state hyperfine structure ($\delta\nu/\nu_0$) $\cong 3.5 \times 10^{-17} \langle E^2 \rangle$ where E is expressed in V/cm [15]. For optical structure, we can for example estimate the shift of the $^2D_{5/2}$ state in Hg^+ or Ba^+ as $\delta\nu = |\langle {}^2P_{3/2} | q\mathbf{r} \cdot \mathbf{E} | {}^2D_{5/2} \rangle|^2/h(E(^2P_{3/2}) - E(^2D_{5/2})) = q^2\, a_0^2 \langle E^2 \rangle/\Delta Eh$ using the same approximation as previously. For Hg^+, $\delta\nu \cong \langle E^2\,(\text{V/cm}) \rangle .(0.002$ Hz). Therefore quadratic Stark shifts can be quite small; they can be further reduced by chopping the pumping light, cooling the kinetic temperature of the ions [12] (see below) and reducing the ambient temperature to reduce the black-body radiation fields.

For ions stored in a Penning trap, the required magnetic fields are on the order of 1 tesla. In this case, therefore, shifts of atomic ion energy levels can be quite strong. Of course the study of magnetic interactions appears to be quite interesting, and certain effects such as diamagnetic shifts to atomic hyperfine structure have been only recently measured [16]. For high resolution double resonance experiments, magnetic field dependent shifts could be regarded as a severe disadvantage because of field fluctuations, but in certain cases, transition frequencies become immune to field fluctuations to first order and extremely high resolution can be obtained [17-19].

2.3 ION NUMBER. — Typically, the numbers of ions in stored ion experiments are rather small. Densities are on the order of $10^6/\text{cm}^3$ and sample sizes are $\lesssim 1\ \text{cm}^3$. For many experiments (such as spectroscopy of molecular ions), this is a disadvantage but in some cases even single ions can be sensitively detected [20-22]. The small densities obtained are to be compared with the much larger densities in buffer gas experiments [2] where space charge neutralization is used. In rf traps, some space charge neutralization has been realized [23, 24] by storing ions of opposite charge but this technique has not been widely used perhaps because of the mechanism of rf heating [7, 25].

Although the ion numbers are typically rather small, usable samples can be confined to an extremely small region of space — down to less than $(1\ \mu m)^3$ for the case of single ions [20, 22]. This is important because in certain high resolution experiments on optical spectra, it is desirable to satisfy the Lamb-Dicke criterion (confinement to dimensions less than $\lambda/2\ \pi$) in order to suppress first order Doppler broadening [13]. Small sample sizes also reduce the requirements on magnetic field homogeneity in high resolution magnetic field dependent spectra.

3. Direct optical pumping.

The essential features of optical pumping in ion traps are not different from the experiments on neutrals or ions in buffer gas cells. Nevertheless, there are some unique features of optical pumping on trapped ions; here we give a simple example.

In the inset in figure 1, we show the 3s $^2S_{1/2}$ and 3p $^2P_{3/2}$ level structure of $^{24}Mg^+$ ions in a magnetic field. If a laser (assumed to have linear polarization perpendicular to the magnetic field) is tuned to the $(-\ 1/2) \rightarrow (-\ 3/2)$ transition (numbers in parentheses refer to the ground $^2S_{1/2}$ and excited $^2P_{3/2}$ values of M_J respectively) then we note that ions must decay to the $M_J = -\ 1/2$ ground level because of the selection rule $\Delta M_J = 0, \pm 1$. At first, one might guess that after many photon scattering events, the ions are gradually pumped from the $M_J = -1/2$ to $M_J = +1/2$ ground state level because of excitation in the wings of other allowed transitions. In fact just the opposite occurs. Although excitation in the wings of the $(-\ 1/2) \rightarrow (+\ 1/2)$ transition pumps ions out of the $(-\ 1/2)$ ground state, excitation in the

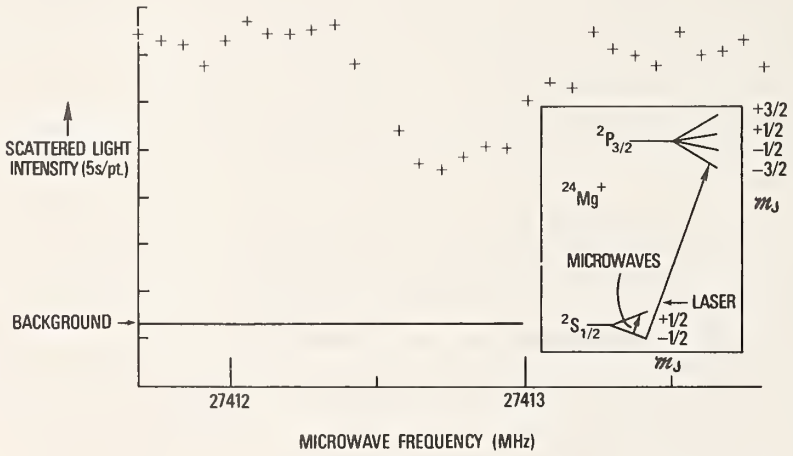

Fig. 1. — Microwave-optical double resonance spectrum of $^{24}Mg^+$. Inset shows relevant energy levels of $^{24}Mg^+$ in a magnetic field. With the laser tuned to the transition shown, 16/17 of the ions are pumped into the $^2S_{1/2}$ $(M_J = -\ 1/2)$ ground state and a quasi two level system is formed with this ground state and the excited $^2P_{3/2}$ $(M_J = -\ 3/2)$ state. When incident microwaves are tuned to the $(M_J = -\ 1/2) \leftrightarrow (M_J = +\ 1/2)$ ground state Zeeman transition, these levels are nearly equally populated which causes a decrease in fluorescence scattering from the ions. Transitions in other ions can be detected in a similar way (from Ref. [26]).

[Spectre de double résonance micro-onde-optique de $^{24}Mg^+$. L'encadré montre les niveaux d'énergie concernés de $^{24}Mg^+$ dans un champ magnétique.]

wings of the $(+ 1/2) \rightarrow (- 1/2)$ transition also occurs which tends to pump ions from the $(+ 1/2)$ to $(- 1/2)$ ground state. Since this latter transition is four times closer in frequency to the laser than the former one, the net result is that about 16/17 of the population is pumped into the $(- 1/2)$ ground state [26]. Of course, by using circularly polarized light, all of the population could be pumped to the $(- 1/2)$ ground state. This pumping is very weak (the time constant for pumping in this experiment was a few seconds) but because of the very long relaxation times of the ions in the trap it can be very efficient.

This experiment is somewhat unusual because, using linearly polarized light, the ions are pumped into the ground state energy level that the laser is tuned to. However, noting that the $(- 1/2) \rightarrow (- 3/2)$ transition takes no part in the pumping, this is just another case of depopulation pumping (out of the $(+ 1/2)$ ground state) using frequency selected light [27]. Similar optical pumping can also be observed when hyperfine structure is present; for example [18], in the case of $^{25}Mg^+$ and $^9Be^+$. Hyperfine pumping effects have also been observed [28] in the excited $^3S_1$ states of Li^+.

Depopulation pumping in the more typical sense (i.e. depopulation of the ground state level one is driving on) occurs if one excites for example the $^2S_{1/2} \rightarrow {}^2P_{1/2}$ transitions in alkali-like ions. In this case one must redistribute or mix the ground state populations in order to see additional scattering from the pumping source. In this instance one of the advantages of the traps for high resolution spectroscopy (weak relaxation) becomes a disadvantage in terms of observation. Solutions to this problem are : (1) Provide a buffer gas for relaxation. For example, Ruster *et al.* [9] observed fluorescence from single Ba^+ ions in an rf trap by relaxing the ions against an H_2 buffer gas. (2) If the number of ground (and metastable) states is not too large, artificial relaxation can be provided by auxiliary microwave or laser radiation [4, 20, 29, 30].

4. Optical pumping-double resonance.

Double resonance detection of atomic ion spectra using traps is achieved in most cases using the same techniques developed for neutrals. However, because of the weak relaxation *and* high scatter rates using lasers, some novel effects appear. For example, in the $^{24}Mg^+$ case above, if the scattered fluorescence light from the ions is monitored, the $(M_J = - 1/2)$ to $(M_J = + 1/2)$ ground state Zeeman transition (induced by microwave radiation) can be detected by observing the decrease in laser fluorescence as the microwave oscillator is swept through resonance (Fig. 1). An interesting feature of this optical pumping-double resonance detection scheme is that each microwave photon absorbed causes a change of about $\Delta N^* = 24\, B(- 1/2, - 3/2)/17\, B(- 1/2, + 1/2)$ in the number of scattered photons where $B(M_J, M_J')$ is the transition rate due to the laser from the M_J ground state to the M_J' excited state. For Mg^+ ions in a magnetic field of about 1 T, ΔN^* can be as high as 2×10^6. This technique has been called « electron shelving » because the ion's outer electron is temporarily « shelved » in a state from which the laser scattering is essentially absent [31]. It has been used in all the optical pumping double resonance experiments on Mg^+ and Be^+ ions stored in Penning traps. This photon amplification scheme was independently developed in optical pumping experiments on neutral atomic beams [32].

The overall detection sensitivity is increased by this photon number amplification effect and also by the photon energy conversion. Perhaps noteworthy is the case of

detecting absorbed 303 MHz photons in Be^+ hyperfine transitions [33] where an energy enhancement factor of $\Delta N^* \lambda(303\ \text{MHz})/\lambda(\text{laser}) > 10^{12}$ is obtained. These impressive numbers are of course not realized in practice since fluorescence collection efficiencies are typically significantly less than 100 %. However, a more important statement is that if (the absence of) enough scattered photons per ion (theoretically $\gtrsim 2$) are *observed* before repumping takes place, then the signal to noise ratio in such experiments need only be limited by the statistical fluctuations in the number of ions that make the transition [34]. This is the maximum signal to noise ratio possible.

The long relaxation times and small perturbations achieved in the traps can lead to very high resolution and accuracy. In $^{25}Mg^+$, the first derivative of the ground state ($M_I = -3/2$, $M_J = 1/2$) to ($M_I = -1/2$, $M_J = 1/2$) transition goes to zero at a value of the magnetic field near 1.24 T. Near this field, a resonance with a width of 0.012 Hz and a center frequency of 291.996251899(3) MHz was observed (Fig. 2) [18]. High resolutions have also been obtained in Yb^+ ($\Delta\nu \cong 0.06$ Hz, $Q \cong 2 \times 10^{11}$ [35]) and Hg^+ ($\Delta\nu = 0.85$ Hz, $Q \cong 5 \times 10^{10}$ [11]). Very high accuracies in stored ion spectra have also been achieved [11, 30, 33, 34]. In the case of Be^+, the (M_I, M_J) $= (-3/2, 1/2) \rightarrow (-1/2, 1/2)$ ground state hyperfine transition frequency at the magnetic field independent point has been measured with an accuracy of about one part in 10^{13} [33]. From the discussion of section 2, it should be possible to obtain much higher resolutions and accuracies.

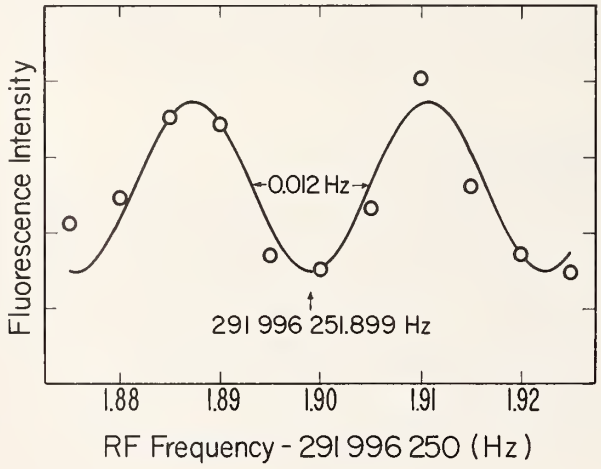

Fig. 2. — The ($M_I = -3/2$, $M_J = 1/2$) to ($M_I = -1/2$, $M_J = 1/2$) resonance in $^{25}Mg^+$ about 1.24 T. The oscillatory lineshape results from the use of the Ramsey separated oscillatory field method, implemented by applying two phase-coherent RF pulses 1.02 s long, separated by 41.4 s (from Ref. [18]).

[Résonance ($M_I = -3/2$, $M_J = 1/2$) → ($M_I = -1/2$, $M_J = 1/2$) dans $^{25}Mg^+$ à environ 1,24 T. La forme de raie oscillante résulte de l'utilisation de la méthode de Ramsey à champs oscillants séparés; on applique ici deux impulsions RF cohérentes en phase de durée 1,02 s, séparées par 41,4 s (Réf. [18]).]

5. Optical pumping of kinetic energy levels-laser cooling.

In 1950, Kastler proposed the idea of « lumino refrigeration » [1]. His idea was to cool the salts of the rare earth ions with an anti-Stokes transition of sufficient intensity. The basic principle was that perhaps ions embedded in a solid could be made to undergo anti-Stokes scattering where the energy deficit would be supplied by the energy of lattice vibrations. Partly because of different motivations (high resolution spectroscopy) and different technology available (the laser) this idea was reinvented for atoms [36] and trapped ions [37] in 1975.

Laser cooling of trapped ions can be described in various ways [29], here we briefly discuss the analogy to optical pumping and anti-Stokes scattering [38]. In figure 3 we have illustrated the energy levels of a trapped ion which we assume has an internal structure composed of two states — the ground (g) and excited (e) states. If we assume that the ion is also constrained to move along one direction in a harmonic well (frequency ν_v) then its kinetic energy levels are given by $E_K = (n+1/2)\, h\nu_v$. In this picture we can think of the ion bound to the trap as a kind of « super-molecule » whose energy level structure can be investigated [38].

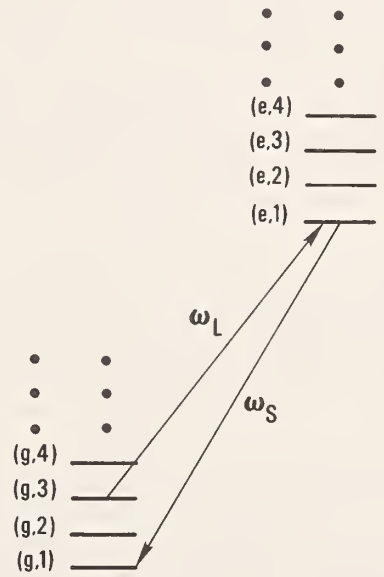

Fig. 3. — Pictorial representation of electronic [ground (g) and excited (e)] energy states and translational energy states (denoted by integers) for an atom. When the atom is very weakly bound or unbound the spacing between translational energy levels goes to zero. The cooling can be described as anti-Stokes Raman scattering or optical pumping where the frequency (ω_S) of the scattered photon is greater than the frequency (ω_L) of the « laser » photon (from Ref. [38]).

[Schéma des niveaux d'énergie électroniques (fondamental (g) et excité (e)) et de translation (repérés par des entiers) pour un atome. Quand l'atome est très faiblement lié, ou libre, la séparation entre niveaux d'énergie de translation tend vers zéro. Le refroidissement peut être décrit comme une diffusion Raman anti-Stokes, ou un pompage optique où la fréquence ω_S du photon diffusé est plus grande que la fréquence ω_L du photon « laser » (Réf. [38]).]

Assume the ion is initially in the (g, n_i) state (normally we would expect it to be in some distribution of states). Then if we excite the (g, n_i) → (e, $n_i - \Delta n$) transition with radiation, the ion can decay to a number of lower states but (neglecting terms of order $R = h^2/2\lambda^2 m$) on the average it decays to the (g, $n_i - \Delta n$) ground state. Therefore in a single scattering event, the ion's kinetic energy has been reduced by $h\nu_v \Delta n$. Laser cooling of free atoms can also be described in this picture; in this case $\nu_v \to 0$ and the ground and excited states become continuous bands. In principle, laser cooling should work for solids but inhomogeneous broadening and non radiative relaxation would appear to cause problems.

Laser cooling of trapped ions has been accomplished in experiments at the National Bureau of Standards, Heidelberg and Hamburg, University of Washington and at Orsay [4, 12, 13, 18-22, 25, 29-31, 39]. Temperatures of < 1 K are not uncommon for a small sample of ions; these low temperatures significantly reduce Doppler effects in those experiments.

6. Exchange pumping.

6.1 Exchange pumping of internal energy levels. — Although polarization or pumping of trapped ions using polarized, externally injected neutral beams has been accomplished [3, 40, 41], exchange pumping due to ion-ion collisions would ordinarily seem to be precluded. This is illustrated by the weak relaxation discussed in section 2.1 and is mainly due to the fact that the Coulomb repulsion usually prevents the ions from getting close enough for exchange to occur. For room temperature ions, $d_0 \cong 200$ Å. At elevated temperatures, exchange pumping might be expected to take place; for ions of energy 10 eV, $d_0 \lesssim 1$ Å. If it could be realized, such exchange pumping might significantly extend spectroscopic measurements on ions as it has for the case of neutral-neutral and ion-neutral collisions.

6.2 Exchange pumping of kinetic energy levels. — In the sense that an ion bound in the trap forms a supermolecule as in section 5, we can think of performing exchange pumping on the kinetic energy levels of the ions. The idea of buffer gas cooling of ions [3, 25, 29, 30, 42-51] fits within this context. Here the (bound) ions exchange their kinetic energy with a light buffer gas (e.g. He, or H_2) whose kinetic energy is thermalized (or « pumped » in the sense here) to the ambient temperature. Analogous arguments could be made for radiative damping of the ions [7, 8].

Although relaxation between the internal states of ions due to ion-ion collisions is rather weak (except at elevated temperatures) the relaxation between kinetic degrees of freedom is rather strong due to the long range of the Coulomb interaction. At temperatures near room temperature, this relaxation time is typically of order 10 ms. (See for example Refs. [3, 7, 8, 25, 52]). Such collisional coupling between different degrees of freedom can be important in the laser cooling experiments when only one or two kinetic degrees of freedom are directly cooled by the laser and the remaining degree(s) of freedom are heated by photon recoil [38, 53].

This coupling may also extend the number of ion species which can benefit from laser cooling. That is, we could simultaneously store two kinds of ions, one which is easily laser cooled and another one which is of spectroscopic interest and *via* the Coulomb collisions is also cooled [54]. This has been demonstrated in experiments on Mg^+ where $^{24}Mg^+$ was laser cooled and by collisions « sympathetically » cooled $^{25}Mg^+$ and $^{26}Mg^+$ [55]. We note that in subsequent experiments at NBS it was possible to sympathetically cool $^{24}Mg^+$ by laser cooling $^{25}Mg^+$; this result

is more definitive because the laser was tuned to the heating side of the $^{24}Mg^{+}$ transition.

It is interesting to note that at very low temperature (the case for a laser cooled cloud of ions) we can expect species of ions with different charge to mass ratio to centrifugally separate [56]. This can be seen by considering two ion species (1 and 2) of different charge to mass ratio, which are in thermal equilibrium in a Penning trap. In this case we can write the distribution function for the ions as a product [56] :

$$f = f_1 \, f_2$$

where

$$f_j = n_j(0) \left(\frac{m_j}{2 \pi k_B T} \right)^{3/2} \exp\left[- \frac{(H_j + \omega P_{\theta j})}{k_B T} \right]$$

$$= n_j(\mathbf{r}) \left(\frac{m_j}{2 \pi k_B T} \right)^{3/2} \exp\left[- \frac{m_j}{2 k_B T} (\mathbf{v} + \omega r \hat{\theta})^2 \right]$$

$$n_j(\mathbf{r}) = n_j(\mathbf{r} = 0) \, e^{-\psi_j(\mathbf{r})}$$

$$\psi_j(\mathbf{r}) = \frac{q_j}{k_B T} \left(\phi(\mathbf{r}) - \frac{m_j}{q_j} \frac{\omega^2 r^2}{2} + \frac{B \omega r^2}{2 c} \right)$$

where $$\phi(\mathbf{r}) = \phi(x, y, z) = \phi(r, z) = \phi(\text{ions}) + \phi(\text{trap}) ,$$

r and z are cylindrical coordinates, and the (conserved) angular momentum ($P_{\theta j}$) is parallel to the z axis of the trap and the magnetic field $\mathbf{B} = B\hat{z}$. The ion cloud behaves as a rigid rotor plasma [57] which rotates at frequency $-\omega$. For the distribution function to be well behaved as $T \to 0$, we must have

$$\phi(\mathbf{r}) - \frac{m_j}{q_j} \frac{\omega^2 r^2}{2} + \frac{B \omega r^2}{2 c} \to 0$$

therefore the charge density inside the cloud is given by [53]

$$\rho = - \frac{1}{4 \pi} \nabla^2 \phi(\text{ions}) = \frac{1}{2 \pi} \left(\frac{B \omega}{c} - \frac{2 m_j}{q_j} \omega^2 \right)$$

where we have used the fact that $\nabla^2 \phi(\text{trap}) = 0$. For the density to be single valued, ions with different m_j/q_j cannot overlap. For the case of a very weak axial well, the cloud breaks up into a cylinder of uniform density ρ_1 surrounded by an annulus of uniform density ρ_2 [56]. (We have assumed $m_1/q_1 < m_2/q_2$.) Solutions in the more typical case will be discussed in a future publication. A similar separation is expected to occur in an rf trap except when there is no angular momentum in the cloud. We note that in an experiment using lasers, we would, in general expect there to be angular momentum in the cloud unless the laser beam exactly overlaps the center of the cloud. Qualitatively, the separation should occur because for a given total angular momentum, a friction force exists between species of different m/q; ions of lower m/q tend to push out ions of higher m/q and *vice versa.*

As a potential application, spectroscopy could be done on $^{9}Be^{+}$ ions which are held at the center of the trap and sympathetically cooled by an outer annulus of $^{24}Mg^{+}$ ions which are laser cooled. The cooling laser could be applied so that it would not spatially overlap the $^{9}Be^{+}$ ions and therefore light shifts on the $^{9}Be^{+}$

energy levels could be avoided. In this way, extremely narrow linewidths ($\ll$ 1 mHz) and high accuracy spectra on Be^+ (or other ions) might be obtained. For ions in an rf trap, sympathetic cooling may be limited by rf heating.

Acknowledgments.

The authors greatfully acknowledge the support of the U.S. Air Force Office of Scientific Research and the U.S. Office of Naval Research. We thank P. L. Bender and F. L. Walls for reading the manuscript and for helpful comments.

References

[1] Kastler, A., *J. Phys. Rad.* **11** (1950) 255.
[2] Weber, E. W., *Phys. Rep.* **32** (1977) 123.
[3] Dehmelt, H. G., *Adv. At. Mol. Phys.* **3** (1967) 53 and *Adv. At. Mol. Phys.* **5** (1969) 109.
[4] Wineland, D. J., Itano, W. M. and Van Dyck, Jr., R. S., *Adv. At. Mol. Phys.* **19** (1983) 135 and references therein.
[5] 133 Pa (Pascals) $\cong$ 1 torr.
[6] See for example : E. W. McDaniel, *Collision Phenomenon in Ionized Gases,* Wiley, New York, 1964.
[7] Church, D. A. and Dehmelt, H. G., *J. Appl. Phys.* **40** (1969) 3421.
[8] Dehmelt, H. G. and Walls, F. L., *Phys. Rev. Lett.* **21** (1968) 127 ; Wineland, D. J. and Dehmelt, H. G., *J. Appl. Phys.* **46** (1975) 919.
[9] Ruster, W., Bonn, J., Peuser, P. and Trautmann, N., *Appl. Phys.* **B 30** (1983) 83 ; Blatt, R. and Werth, G., *Phys. Rev.* **A 25** (1982) 1476.
[10] Vetter, J., Stuke, M. and Weber, E. W., *Z. Physik* **A 273** (1975) 129.
[11] Cutler, L. S., Giffard, R. P. and McGuire, M. D., *Appl. Phys.* **B 36** (1985) 137.
[12] Wineland, D. J., in « Precision Measurement and Fundamental Constants II » (B. N. Taylor and W. D. Phillips, eds.). NBS Spec. Publ. (U.S.) **617** (1984) 83.
[13] Dehmelt, H., IEEE Trans. Instrum. Meas. IM-31, 83 (1982).
[14] Kopfermann, H., *Nuclear Moments* (Academic, New York, 1958), p. 11.
[15] Itano, W. M., Lewis, L. L., Wineland, D. J., *Phys. Rev.* **A 25** 1233 (1982).
[16] Economou, N. P., Lipson, S. J. and Larson, D. J., *Phys. Rev. Lett.* **38** (1977) 1394.
[17] Kusch, P. and Taub, H., *Phys. Rev.* **75** (1949) 1477.
[18] Itano, W. M. and Wineland, D. J., *Phys. Rev.* **A 24** (1981) 1364.
[19] Bollinger, J. J., Itano, W. M. and Wineland, D. J., *Phys. Rev. Lett.* **54** (1985) 1000.
[20] Neuhauser, W., Hohenstatt, M., Toschek, P. and Dehmelt, H. G., *Phys. Rev.* **A 22** (1980) 1137.
[21] Wineland, D. J. and Itano, W. M., *Phys. Lett.* **82A** (1981) 75.
[22] Nagourney, W., Janik, G. and Dehmelt, H., *Proc. Natl. Acad. Sci. USA* **80** (1983) 643.
[23] Major, F. G. and Schermann, J. P., *Bull. Am. Phys. Soc.* **16** (1971) 838.
[24] Audoin, C., private communication.
[25] Dehmelt, H. G., in « *Advances in Laser Spectroscopy* » (F. T. Arecchi, F. Strumia and H. Walther, Eds.). Plenum, New York (1983) p. 153.
[26] Wineland, D. J., Bergquist, J. C., Itano, W. M. and Drullinger, R. E., *Opt. Lett.* **5** (1980) 245.
[27] Happer, W., *Rev. Mod. Phys.* **44** (1972) 169.
[28] Prior, M. H. and Knight, R. D., *Opt. Commun.* **35** (1980) 54.
[29] Wineland, D. J., Itano, W. M., Bergquist, J. C., Bollinger, J. J. and Prestage, J. D., in *Atomic Physics 9,* ed. by R. S. Van Dyck, Jr. and E. N. Fortson (World Scientific Publ. Co., Singapore 1985) p. 3.

[30] WERTH, G., *ibid* p. 28.
[31] DEHMELT, H. G., *J. Physique* **42** (1981) C8-299 ;
DEHMELT, H. G., *Bull. Am. Phys. Soc.* **18** (1973) 1521.
[32] PICQUÉ, J. L., *Metrologia* **13** (1977) 115.
[33] BOLLINGER, J. J., ITANO, W. M. and WINELAND, D. J., Proc. 37th Annu. Symp. Freq. Control, 37 (1983). (Copies available from Systematics General Corp., Brinley Plaza, Rt. 38 Wall Township, NJ 07719.) J. J. Bollinger, J. D. Prestage, W. M. Itano and D. J. Wineland, *Phys. Rev. Lett.* **54** (1985) 1000.
[34] WINELAND, D. J., ITANO, W. M., BERGQUIST, J. C. and WALLS, F. L., Proc. 35th Annu. Symp. Freq. Control (1981) p. 602 (copies available from Electronic Industries Assoc., 2001 Eye St., NW, Washington, DC 20006).
[35] BLATT, R., SCHNATZ, H. and WERTH, G., *Phys. Rev. Lett.* **48** (1982) 1601.
[36] HÄNSCH, T. W. and SCHAWLOW, A. L., *Opt. Commun.* **13** (1975) 68.
[37] WINELAND, D. J. and DEHMELT, H. G., *Bull. Am. Phys. Soc.* **20** (1975) 637.
[38] WINELAND, D. J. and ITANO, W. M., *Phys. Rev.* A **20** (1979) 1521 ;
ITANO, W. M. and WINELAND, D. J., *Phys. Rev.* A **25** (1982) 35.
[39] PLUMELLE, F., Abstract for 15th EGAS Conf. Madrid, July 5-8 (1983).
[40] SCHUESSLER, H. A., in « *Physics of Atoms and Molecules, Progress in Atomic Spectroscopy* » (W. Hanle and H. Kleinpoppen, eds.), Plenum, New York, 999 (1979).
[41] GRÄFF, G., MAJOR, F. G., ROEDER, R. W. H. and WERTH, G., *Phys. Rev. Lett.* **21** (1968) 340 ;
GRÄFF, G., HUBER, K., KALINOWSKY, H. and WOLF, H., *Phys. Lett.* **41A** (1972) 277 ;
GRÄFF, G. and HOLZSCHEITER, M., *Phys. Lett.* **79A** (1980) 380.
[42] JARDINO, M., PLUMELLE, F., DESAINTFUSCIEN, M. and DUCHÊNE, J. L., Proc. 38th Annu. Symp. Freq. Control, Phil. PA (1984) to be published.
[43] VEDEL, M., *J. Physique* **37** (1976) L-336.
[44] DAWSON, P. H., *Adv. Electron. Electron Phys. Suppl.* **13B** (1980) 173.
[45] PLUMELLE, F., DESAINTFUSCIEN, M., DUCHÊNE, J. J. and AUDOIN, C., *Opt. Commun.* **34** (1980) 71.
[46] SCHAAF, H., SCHMELING, U. and WERTH, G., *Appl. Phys.* **25** (1981) 249.
[47] ANDRÉ, J. and VEDEL, F., *J. Physique* **38** (1977) 1381.
[48] ANDRÉ, J., VEDEL, F. and VEDEL, M., *J. Physique* **40** (1979) L-633.
[49] VEDEL, F., ANDRÉ, J. and VEDEL, M., *J. Physique* **42** (1981) 1611.
[50] VEDEL, F., ANDRÉ, J., VEDEL, M. and BRINCOURT, G., *Phys. Rev.* A **27** (1983) 2321.
[51] VEDEL, M., ANDRÉ, J., CHAILLAT-NEGREL, S. and VEDEL, F., *J. Physique* **42** (1981) 541.
[52] HEPPNER, R. A., WALLS, F. L., ARMSTRONG, W. T. and DUNN, G. H., *Phys. Rev.* A **13** (1976) 1000.
[53] BOLLINGER, J. J. and WINELAND, D. J., *Phys. Rev. Lett.* **53** (1984) 348.
[54] WINELAND, D. J., DRULLINGER, R. E. and WALLS, F. L., *Phys. Rev. Lett.* **40** (1978) 1639.
[55] DRULLINGER, R. E., WINELAND, D. J. and BERGQUIST, J. C., *Appl. Phys.* **22** (1980) 365.
[56] O'NEIL, T. M., *Phys. Fluids* **24** (1981) 1447.
[57] DAVIDSON, R. C., *Theory of Nonneutral Plasmas* (Benjamin, Reading MA, 1974).

Laser Spectroscopy of Trapped Atomic Ions

Wayne M. Itano, J. C. Bergquist, D. J. Wineland

Recent developments in laser spectroscopy of atomic ions stored in electromagnetic traps are reviewed with emphasis on techniques that appear to hold the greatest promise of attaining extremely high resolution. Among these techniques are laser cooling and the use of single, isolated ions as experimental samples. Doppler shifts and other perturbing influences can be largely eliminated. Atomic resonances with line widths of a few parts in 10^{11} have been observed at frequencies ranging from the radio frequency to the ultraviolet. Experimental accuracies of one part in 10^{18} appear to be attainable.

Atomic spectroscopy dates from the 19th century, when it was discovered that atomic vapors emitted and absorbed light at discrete resonance wavelengths, characteristic of each chemical element. When the quantum theory of atoms was developed in the 20th century by Niels Bohr and others, it was realized that these characteristic patterns of resonances, called spectra, were due to the quantum nature of the atom. The atom normally exists only in certain states of definite energy. Transitions between these allowed states are accompanied by the absorption or emission of quanta of light, called photons. The frequency ν of the light is related to the energy change ΔE of the atom by the formula $h\nu = |\Delta E|$, where h is Planck's constant. Accurate and detailed information about atomic spectra was crucial to the development of the modern theory of quantum mechanics.

Traditional (that is, nonlaser) optical spectroscopic methods, such as dispersing the light emitted from a gas with a diffraction grating, are limited in resolution by Doppler frequency shifts. Doppler shifts are the result of the motions of the atoms in a gas and cause the resonance absorption or emission lines to be much broader than the natural line widths (the line widths that would be observed if the atoms were motionless and isolated from perturbing influences such as collisions). Under typical laboratory conditions, the Doppler broadening results in a line width of about one millionth of the transition frequency, whereas the natural line widths are typically at least 100 times narrower. For example, the 280-nm first resonance line of Mg^+, which has a frequency of about 1.07×10^{15} Hz, has a Doppler-broadened line width at room temperature of about 3 GHz, whereas the natural line width is only 43 MHz. For a transition with a stable lower level, the natural line width (in hertz) is the inverse of the mean lifetime of the upper level (in seconds), divided by 2π.

The development of tunable lasers in the 1970s led to great advances in the resolution and accuracy with which optical atomic spectra could be observed. Laser light sources have high intensity and narrow line width. These properties make it possible to use various nonlinear spectroscopic techniques, such as saturated absorption or multiphoton absorption, that cancel the effects of first-order Doppler shifts, that is, Doppler shifts that are linear in the velocities of the atoms (*1*). The natural line width and the second-order Doppler shift, which is quadratic in the atomic velocities, still remain, however. The second-order Doppler shift is a result of relativistic time dilation. The atomic resonance is shifted like a clock, which runs at a rate that is slower for a moving atom than for an atom at rest. For typical laboratory conditions, this shift is very small, about one part in 10^{12}. Sometimes, even this shift can be troublesome. A good example is the work of Barger *et al.* on the 657-nm transition of calcium, which has a frequency of 4.57×10^{14}

The authors are with the Time and Frequency Division, National Bureau of Standards, Boulder, CO 80303.

Hz and a natural line width of 410 Hz (*2*). Resonances with line widths as small as 2 kHz were observed, but they were severely shifted and distorted by the second-order Doppler shift.

In order to reduce both the first- and second-order Doppler shifts, some method of reducing the temperature of the atoms under study is required. An atomic vapor placed in a conventional refrigeration device would quickly condense on the walls of the container. But laser cooling, a method by which laser radiation pressure is used to reduce the velocities of atoms, achieves the cooling without contact with material objects (*3–5*). The technique was proposed independently by Hänsch and Schawlow (*6*) for free atoms and by Wineland and Dehmelt (*7*) for trapped ions. Laser cooling to temperatures on the order of 1 mK has been demonstrated with some kinds of atoms and atomic ions. This reduces the second-order Doppler shifts to the level where they are not a problem. An atom or atomic ion of mass 100 u (unified atomic mass units) cooled to 1 mK has a second-order Doppler shift of 1.4 parts in 10^{18}.

Transit-time broadening is another effect that limits the resolution with which spectra can be observed. The observed resonance line width cannot be much less than the inverse of the observation time. This is a consequence of Heisenberg's uncertainty relation applied to time and energy. In the case of the work on calcium, the observation time was limited to about 0.3 msec by the time it took the atoms to pass through the 21-cm-long resonance region (*2*). One way to increase the observation time is by trapping the atoms with electromagnetic fields. In some experiments, atoms are confined with specially coated walls or by buffer gases, but collisions with the wall or buffer gas molecules shift and broaden the observed resonances. Atomic ions can be trapped for long periods by fields that do not disturb their resonance frequencies by significant amounts. Neutral atoms have been trapped by static magnetic fields (*8*) and by optical fields (*9, 10*), but the trapping fields tend to strongly perturb the resonances.

The work described in this article has the goal of achieving greatly improved spectroscopic resolution and accuracy. The experimental methods involve the use of frequency-stabilized lasers to measure the spectra of atomic ions, sometimes single ions, that are laser cooled and electromagnetically trapped. The most obvious applications of such work are frequency standards and clocks of great accuracy; this is the primary goal of the work done in our laboratories at the National Bureau of Standards (NBS). These experiments have applications to other areas of physics, however, such as atomic physics and quantum optics. One example is the recent observation of quantum jumps (sudden changes of quantum state) of an individual atomic ion (*11–13*).

Ion Traps

Ion traps confine ions by means of electric and magnetic fields (*14, 15*). Two types of ion traps are commonly used for spectroscopic experiments, the Penning trap and the Paul or rf (radio frequency) trap.

The Penning trap is based on a combination of static electric and magnetic fields. The electric fields are produced by applying an electric potential between the ring and endcap electrodes, which are shown schematically in Fig. 1. The electric forces repel the ions from the endcaps and provide confinement along the axis of the trap. A strong, uniform magnetic field is applied along the trap axis to provide radial confinement. Full three-dimensional confinement is provided by this combination of electric and magnetic fields. For a trap with inside dimensions of about 1 cm, a typical value of the electric potential difference is 1 volt and of the magnetic field, 1 tesla. The potential energy of an ion is lowered as it moves out

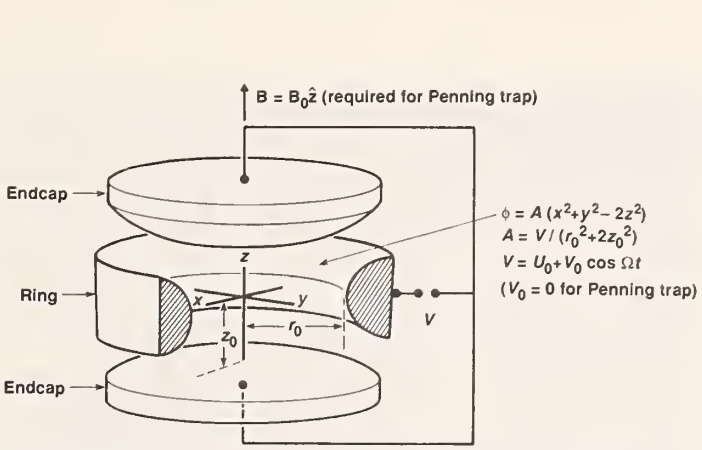

Fig. 1. Electrodes for a Penning or rf ion trap. The electric potential field ϕ is created by applying the voltage V between the endcap electrodes and the ring electrode. The uniform magnetic field **B** is required only for a Penning trap. [Adapted from (*42*) with permission from Plenum Press]

radially from the axis of the trap. Hence, even though an ion would remain trapped forever if undisturbed, collisions with neutral background gas molecules increase the radial extent of the orbit until eventually the ion collides with the ring. In practice, under conditions of high vacuum, it is not uncommon for an ion to remain confined for days.

The rf trap uses oscillating electric fields and does not require a magnetic field. The electrode structure is the same as that of a Penning trap (see Fig. 1), but the applied electric potential varies sinusoidally in time. The electric field forces an ion to oscillate in position with an amplitude proportional to the field strength. The phase of the motion with respect to the applied field is such that the average force on the ion in the spatially nonuniform field is directed toward regions of weaker field (the center of the trap in this case). The trajectory of an ion can be separated into a part that oscillates at the frequency of the applied field, called the micromotion, and a part that varies more slowly, called the secular motion. The oscillating field creates an effective potential-energy well, sometimes called a pseudopotential, for the secular motion of an ion. For a trap with electrodes like those in Fig. 1, the pseudopotential is approximately a three-dimensional harmonic well, so the secular motion is characterized by well-defined frequencies. The electrodes of an rf trap identical to those used in the NBS experiments with Hg^+ ions (*12, 16, 17*) are shown in Fig. 2. The inside radius of the trap is slightly less than 1 mm. Under typical operating conditions, an electric potential of peak amplitude 570 volts and frequency 21 MHz is applied, creating a pseudopotential well about 15 eV deep. The frequency of the secular motion is about 1.5 MHz. In some cases, an ion can be held in the trap for several days before it is lost, possibly through a chemical reaction with a residual gas molecule.

Laser Cooling

It has been known for a long time that light can exert a force on a material body. In 1873, Maxwell showed that his theory of electromagnetic fields predicted that a beam of light would exert a force on a reflecting or absorbing body. This phenomenon is commonly known as radiation pressure. Light has momentum, the momentum density being numerically equal to the energy density divided by c, the speed of light. Radiation pressure is thus a consequence of conservation of momentum. In the early 1900s, radiation pressure was observed experimentally by Nichols and Hull in the United States (*18*) and by Lebedev in Russia (*19*), and shown to be in good agreement with theory. In 1933, Frisch first observed radiation pressure on the atomic scale (*20*). In his experiment, a beam of

TN-145

sodium atoms traveling through an evacuated chamber was deflected by a lamp emitting sodium resonance light of wavelength 589 nm. The average deflection of an atom was that due to a transfer of momentum equal to that of a single photon, $h\nu/c$.

The force exerted by light on atoms is often divided into two parts. These are called the light-pressure or scattering force and the gradient or dipole force (*21*). In some simple cases, these two forces can be clearly distinguished, but in the general case, particularly for high light intensities, the simple descriptions of the forces break down, and a quantum-mechanical description is required.

The scattering force is simply radiation pressure at the atomic level, the force observed by Frisch (*20*). The average scattering force is in the direction of propagation of the light and is equal to the product of the momentum per photon and the photon scattering rate. The force reaches a maximum when the light is resonant with an atomic transition. Fluctuations in the scattering force arise because the photon scatterings take place at random times and because the direction of the reemitted photon, and hence the direction of the recoil momentum due to this reemission, is random.

The dipole force can be understood by considering the atom to be a polarizable body. The optical electric field induces an electric dipole moment in the atom; the induced dipole is acted on by the optical electric field. If the light intensity is spatially nonuniform, a force is induced parallel to the gradient of the intensity. The dipole force attracts an atom to a region of high light intensity if the frequency of the light is below the atomic resonance and repels it if it is above. Sodium atoms have been trapped, by means of the dipole force, near the focus of a laser beam tuned below the first resonance transition (*10*).

The laser cooling that has been demonstrated in ion traps is based on the use of the scattering force only. [It is also possible to cool by use of the dipole force (*22*), as has recently been demonstrated in an atomic beam experiment (*23*), but this method does not appear to have any advantage for trapped ions.] The theoretical description of the cooling depends on whether the natural line width γ of the resonance transition used for cooling is greater than or less than the frequencies of the oscillatory motion (ω_v) of the ion in the trap. The former case is called the heavy-particle or weak-binding limit; the latter is called the sideband-cooling or strong-binding limit (*3, 5, 24*). (Both γ and ω_v are expressed in angular frequency units.)

Consider first the heavy-particle limit ($\gamma >> \omega_v$, where ω_v is any of the motional frequencies). In this limit, each photon scattering event takes place in a time much less than a motional cycle, so that the scattering force can be considered to be made up of a series of impulses. Assume that a trapped ion is irradiated with a beam of light tuned lower than the resonance frequency. When the velocity of the ion is opposed to the direction of propagation of the laser beam, the frequency of the light in the frame of reference of the ion is Doppler-shifted closer to resonance than if it had zero velocity. Hence, the magnitude of the scattering force is higher when the atom moves against the laser beam, and its velocity is damped. When it moves in the same direction as the light, the light is Doppler-shifted away from resonance, and the magnitude of the scattering force is reduced. The net effect is to reduce the kinetic energy of the ion, that is, to cool it. (The ion is heated if the light is

Fig. 2. The electrodes of a small rf trap, shown on a coin for scale.

Fig. 3. False color image of a single Hg^+ ion (small isolated dot slightly below the center) stored in an rf trap. The other shapes are due to light reflected from the trap electrodes, whose orientation is the same as in Fig. 2. The largest reflection is from the front surface of the ring electrode. The two smaller reflections are from the edges of one of the endcap electrodes. Computerized imaging system developed by C. Manney and J. J. Bollinger (NBS). [Adapted from (*43*) with permission from the American Institute of Physics]

TN-146

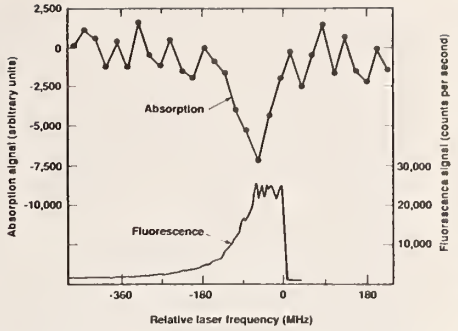

Fig. 4. The absorption signal of a single Hg^+ ion stored in an rf trap (upper trace). Radio-frequency modulation and demodulation techniques were used to reduce noise, resulting in a signal proportional to the derivative of the absorption with respect to laser frequency. The lower trace is the fluorescence signal, observed at the same time. The fluorescence drops off suddenly when the frequency is above resonance, due to laser heating. The flattened top of this curve is due to the frequency modulation. Integration times per point are 50 seconds and 10 seconds in the upper and lower traces, respectively. [Adapted from (*17*) with permission from the Optical Society of America]

higher in frequency than the resonance.) The minimum number of photon scatterings required to cool an ion substantially, starting from 300 K, is on the order of the ratio of the ion's momentum to a photon momentum, or about 10,000. Because of the inherent fluctuations of the scattering force, which cause heating, the kinetic energy is not damped to zero, but eventually reaches a steady value that depends on the degree of frequency detuning below the resonance. The detuning that gives the lowest temperature is equal to one half of the natural line width. This minimum temperature T_{min} is given by the relation $k_B T_{min} \simeq \hbar\gamma/2$, where k_B is Boltzmann's constant and $\hbar$ is Planck's constant divided by 2π. For example, T_{min} for Mg^+ ($\gamma/2\pi$ = 43 MHz) is 1 mK.

Now consider the sideband-cooling ($\gamma << \omega_v$) limit. The absorption spectrum of the ion consists of an unshifted resonance line at angular frequency ω_0, called the carrier, and a series of discrete lines on both sides of the carrier, each having (ideally) the natural line width, and separated by multiples and combinations of the motional frequencies. These extra lines, called motional sidebands, are the result of the periodic frequency modulation of the light frequency, arising from the Doppler effect, as observed by the moving ion. To cool an ion, the frequency of the laser beam is tuned to a sideband on the low-frequency side of the carrier, for example, to $\omega_0 - p\omega_v$, where p is a positive integer. The ion is induced to make transitions to the upper electronic state, with a decrease in the vibrational energy. When the ion makes a transition back to its ground electronic state, it may either increase or decrease its vibrational energy, but the average vibrational energy change is equal to $R = (\hbar\omega_0)^2/(2Mc^2)$, where M is the mass of the ion. The quantity R, sometimes called the recoil energy, is the kinetic energy that an initially motionless-free ion acquires after emitting a photon of energy $\hbar\omega_0$. If $R < p\hbar\omega_v$, the ion is cooled. If $R << \hbar\omega_v$, which is not hard to satisfy in practice, and if the frequency width of the light is much less than γ, then the ion can be cooled until it occupies the lowest quantum state of the trap potential most of the time. In this limit, the fraction of the time that the ion is not in the lowest state is on the order of $(\gamma/\omega_v)^2$ (*3, 5, 24, 25*). The sideband cooling discussion can also be applied to the $\gamma >> \omega_v$ case (*24, 26*). Recently, Lindberg, Javanainen, and Stenholm (*27*) have treated theoretically the general case of laser cooling of an ion trapped in a harmonic well, for an arbitrary ratio of γ to ω_v and also for arbitrary laser intensity. The lowest temperatures are obtained in the low-intensity limit.

The first experimental observations of laser cooling were made in 1978 at NBS by Wineland, Drullinger, and Walls (*28*) and at the University of Heidelberg by Neuhauser, Hohenstatt, Toschek, and Dehmelt (*26*). The NBS experiment used Mg^+ ions in a Penning trap, whereas the Heidelberg experiment used Ba^+ ions in an rf trap. In later experiments at these and other laboratories, cooling of trapped ions has been observed to temperatures in the range of a few millikelvin, close to the theoretical limit. So far, only strongly allowed transitions have been used for cooling, so the theory for the $\gamma >> \omega_v$ case applies.

Only a few kinds of ions have been laser-cooled. Laser cooling requires that the ion be cycled repeatedly between the ground state and an excited state. To be laser-cooled easily, an ion should have a strongly allowed resonance transition, at a wavelength where a tunable, continuous wave radiation source is available, and be free of intermediate metastable levels that would interrupt the cycling. Even Ba^+, one of the first ions to be laser-cooled, is not ideal, since it can decay into a metastable level from the upper level of the resonance transition. A second laser is required to drive the ion out of the metastable level. A way to cool a species of ion that cannot be laser-cooled directly is to store it in a trap together with a species that can be cooled directly. As one species is laser-cooled, the other species is cooled indirectly by Coulomb collisions. This technique, called sympathetic laser cooling, has been demonstrated in an experiment in which Hg^+ ions in a Penning trap were cooled to less than 1 K by Coulomb coupling with laser-cooled Be^+ ions (*29*).

Spectroscopy of Atomic Ions in Traps

A number of spectroscopic measurements have been made of non-laser-cooled ions in traps, particularly at microwave frequencies (*14, 15, 30, 31*). In the more accurate of these experiments, the uncertainty was due mainly to the second-order Doppler shift. For cases in which laser cooling can be applied, Doppler shifts are suppressed, and spectra can be observed with extremely high resolution, nearly free from perturbing influences.

Dicke showed in 1953 that the confinement of an atom to a

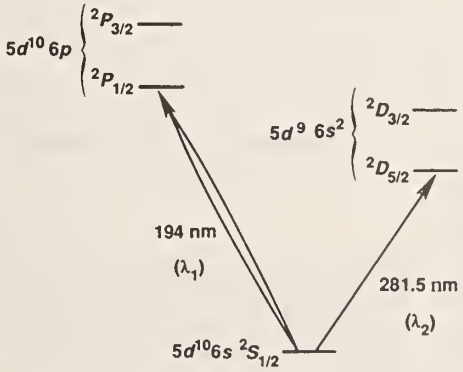

Fig. 5. Lowest energy levels of Hg^+. Absorption of a λ_2 photon is detected by the cessation of laser-induced fluorescence at λ_1. [Adapted from (*12*) with permission from the American Institute of Physics]

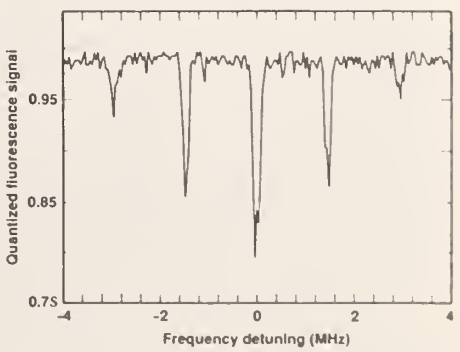

Fig. 6. The 281.5-nm transition observed in a single Hg^+ ion. The frequency detuning of the laser is plotted on the horizontal axis. The intensity ratios of the motional sidebands to the carrier (central line) indicate a temperature of about 6 mK. [Adapted from (*16*) with permission from the American Institute of Physics]

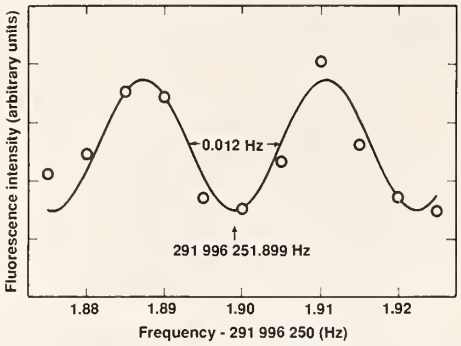

Fig. 7. Graph of a radio frequency hyperfine-structure resonance in $^{25}Mg^+$ ions stored in a Penning trap. Fluorescence intensity is plotted as a function of field frequency minus an offset of 291 996 250 Hz. Arrow indicates center of resonance. The oscillatory line shape results from the use of Ramsey's separated-oscillatory-field method. [Adapted from (*38*) with permission from the American Institute of Physics]

region of space smaller than the resonance-radiation wavelength leads to a suppression of the first-order Doppler shift broadening (*32*). It is easy to satisfy this condition, commonly called the Lamb-Dicke criterion, for a microwave resonance, since the wavelengths can be several centimeters long. Microwave frequency standards such as the atomic hydrogen maser make use of this fact. In the optical region, it can be satisfied for a single, laser-cooled ion confined in a trap. (Coulomb repulsion between ions makes it difficult to satisfy the Lamb-Dicke criterion when more than one ion is in the trap.)

The second-order Doppler shift of an ion that is laser-cooled to T_{min} is around one part in 10^{18} even for a strongly allowed transition (high γ). If more than one ion is present in the trap, then the kinetic energies per ion, and hence the second-order Doppler shifts, are necessarily higher. In the case of the rf trap, the Coulomb repulsion between ions leads to their being trapped away from the center of the trap, so the oscillating electric field, and hence the micromotion, is nonzero. In the case of the Penning trap, the presence of the other ions leads to increased velocities of rotation around the trap axis in the presence of crossed electric and magnetic fields. It appears that, for a single ion, shifts of resonance frequencies owing to electric and magnetic fields could be as small as a part in 10^{18}, since the ion is trapped in a region where the electric field approaches zero (*33, 34*).

Naturally, the signal-to-noise ratio suffers when the sample under observation consists of only a single ion. However, once an ion has been trapped and cooled, its presence can be detected easily by laser-induced fluorescence, since a strongly allowed transition can scatter as many as 10^8 photons per second. In fact, a single, trapped Ba^+ ion has been observed visually, through a microscope, by laser-induced fluorescence (*35*). Single ions have been observed in both Penning and rf traps (*11, 13, 15, 30, 35*). Figure 3 shows a false color image of the 194-nm laser-induced fluorescence of a single Hg^+ ion confined in an rf trap. This image was obtained at NBS with a position-sensing photomultiplier tube interfaced to a computer. It has even been possible to detect the resonance absorption due to a single Hg^+ ion by a decrease of the intensity of the 194-nm beam passing through the trap (*17*). The fraction of the light absorbed by the ion was around 10^{-5}. Figure 4 shows the absorption signal and the fluorescence signal, measured simultaneously as the laser was swept through the resonance.

A transition with a narrow natural line width would be difficult to detect directly by fluorescence, since the long lifetime of the upper state limits the rate at which photons are emitted. A way around this problem was suggested by Dehmelt (*36*). Consider an atom that has both a strongly allowed transition (at wavelength λ_1) and a weakly allowed transition (at wavelength λ_2) from the ground state. Figure 5 shows an example of such an atom (Hg^+). The narrow resonance at λ_2 is detected as follows: The atom is assumed to be initially in the ground state. Laser light at a wavelength near λ_2 is pulsed on, possibly driving the atom to the long-lived upper level of this transition. Then light at a wavelength near λ_1 is pulsed on. If the atom had made a transition in the previous step, no fluorescence would be observed; otherwise fluorescence will be observed at an easily detectable level. The detection of presence or absence of the λ_1 fluorescence is much easier than attempting to detect the one λ_2 photon that eventually is emitted when the long-lived state spontaneously decays. The method is called "electron shelving," since the optical electron is temporarily shelved in the long-lived level.

So far, only a few measurements of the optical spectra of trapped laser-cooled ions have been made. Some measurements have been made of strongly allowed transitions in Be^+ and Mg^+, with resolutions near the natural line widths of tens of megahertz. These measurements have yielded some values for energy level splittings, including fine-structure and hyperfine-structure splittings (*15, 30*). A two-photon transition from the ground $6^2S_{1/2}$ to the $5^2D_{3/2}$ state has been observed in a single Ba^+ ion, with a resolution, limited by the laser line width, of 3 MHz (*37*). Recently, at NBS, the $5d^{10}6s\ ^2S_{1/2}$ to $5d^96s^2\ ^2D_{5/2}$ 281.5-nm transition has been observed in a single, trapped Hg^+ ion (*16*). The ion was laser-cooled, by means of the 194-nm $6s\ ^2S_{1/2}$ to $6p\ ^2P_{1/2}$ transition, to near the theoretical limit of 1.7 mK. Figure 6 shows the spectrum obtained by tuning a laser across the narrow *S*-to-*D* transition. The electron shelving detection method was used. Immediately after the 281.5-nm radiation was shut off, the 194-nm fluorescence intensity was measured. If it was low enough to indicate that the ion had made a transition to the *D*-state, the signal was defined to be 0. Otherwise, it was defined to be 1. The average of these measurements is plotted along the vertical axis. The carrier and the two closest motional sidebands on each side are visible. The line widths were deliberately broadened to reduce the time required to sweep the resonance. On other sweeps, line widths of about 30 kHz were observed, a result mainly of laser frequency instability. The lifetime of the upper level is approximately 0.1 second, so the natural line width is about 1.6 Hz. The size of the sidebands indicates that the ion has been cooled approximately to the Lamb-Dicke regime. The root-mean-square amplitude of motion is estimated to be 50 nm.

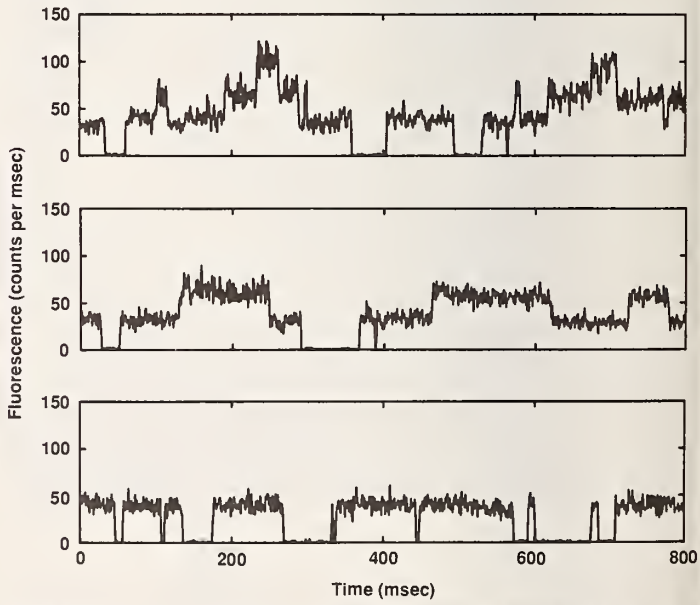

Fig. 8. Fluorescence intensity as a function of time for samples of three ions (top trace), two ions (middle trace), and one ion (bottom trace) in an rf trap. The fluorescence changes suddenly each time an Hg^+ ion either makes a transition to a metastable *D*-state (step down) or back to the ground *S*-state from a *D*-state (step up). The integration time per point is 1 msec.

TN-148

Microwave spectra of trapped ions are usually observed by some form of microwave-optical double resonance. Hyperfine splittings and g-factors of the ground states of several atomic ions have been measured (*15, 30, 31*). So far, all of these experiments involve samples of more than one ion. Figure 7 shows an example of the kind of resolution that can be obtained with trapped ions (*38*). The line width of the resonance (a hyperfine transition in $^{25}Mg^+$) is only 12 mHz. The fractional resolution is about the same as for the Hg^+ S-to-D optical transition. In another experiment at NBS, the frequency of a hyperfine transition in $^9Be^+$ has been measured with an accuracy of about one part in 10^{13}, which is comparable to the most accurate frequency standards in existence (*39*). The accuracy was limited to this value by the second-order Doppler shift, because the laser cooling had to be shut off while the microwave transition was being driven, in order not to perturb the resonance frequency, and the ions heated up during this period. Sympathetic laser cooling using Mg^+ might provide a solution to this problem.

Quantum Jumps

Recently, Cook and Kimble (*40*) theoretically investigated a three-level atom like the one considered by Dehmelt in his "shelved electron" proposal. Light at wavelengths λ_1 and λ_2 was assumed to be present at the same time. They predicted that one would observe the λ_1 fluorescence to turn off and on abruptly as the atom made transitions (quantum jumps) to and from the long-lived upper level. This paper generated a great deal of theoretical interest, and the problem was approached from various viewpoints (*41*). The novelty of this problem is that theorists are accustomed to calculating, and experimenters are accustomed to measuring, ensemble averages rather than following the development in time of a single quantum system.

The experiment that is the most similar to the one treated by Cook and Kimble was performed at NBS on a single, trapped Hg^+ ion (*12*). Light at 194 nm (λ_1) and 281.5 nm (λ_2) was present at the same time (see Fig. 5). The 194-nm fluorescence level was observed to be bistable, switching suddenly between a steady level and zero. The rate at which the switches occurred increased as the intensity of the 281.5-nm light was increased. The statistical properties of the quantum jumps were consistent with theory and with previous measurements of the lifetime of the $^2D_{5/2}$ state. If the intensity of the 194-nm light is increased, then quantum jumps are observed even without the 281.5-nm light present. [These events occurred at a low rate in the data of (*12*).] The reason for these events is that the upper level of the 194-nm transition has a small probability (about 1 in 10^7) of decaying to the $^2D_{3/2}$ level rather than back to the ground state. The $^2D_{3/2}$ state has a lifetime of about 10 msec and about an equal probability of decaying either to the $^2D_{5/2}$ level or to the ground state. The bottom trace of Fig. 8 shows the 194-nm fluorescence intensity of a single ion as a function of time, clearly showing the quantum jumps. The middle and top traces in Fig. 8 show the fluorescence when two or three ions are in the trap. When more than one ion is present in the trap, the fluorescence level jumps between several discrete levels, depending upon how many ions are in one of the D-states. Quantum jumps have been observed by other groups, using trapped Ba^+ ions (*11, 13*).

Conclusions

Spectroscopy of trapped atomic ions has already achieved impressive levels of accuracy and resolution. The ultimate limits have certainly not been reached, and no fundamental (as opposed to technical) obstacles preventing the achievement of measurement accuracies (in special cases) of one part in 10^{18} are foreseen (*33, 34*). Interesting spin-offs from the quest for improved spectroscopic methods, such as the observation of quantum jumps, will no doubt continue to appear.

REFERENCES AND NOTES

1. *High-Resolution Laser Spectroscopy*, K. Shimoda, Ed. (Springer-Verlag, Berlin, 1976); M. D. Levenson, *Introduction to Nonlinear Laser Spectroscopy* (Academic Press, New York, 1982).
2. R. L. Barger, J. C. Bergquist, T. C. English, D. J. Glaze, *Appl. Phys. Lett.* **34**, 850 (1979); R. L. Barger, *Opt. Lett.* **6**, 145 (1981).
3. S. Stenholm, *Rev. Mod. Phys.* **58**, 699 (1986).
4. W. D. Phillips and H. J. Metcalf, *Sci. Am.* **256**, 50 (March 1987).
5. D. J. Wineland and W. M. Itano, *Phys. Rev. A* **20**, 1521 (1979); W. M. Itano and D. J. Wineland, *ibid.* **25**, 35 (1982).
6. T. W. Hänsch and A. L. Schawlow, *Opt. Commun.* **13**, 68 (1975).
7. D. J. Wineland and H. Dehmelt, *Bull. Am. Phys. Soc.* **20**, 637 (1975).
8. A. L. Migdall, J. V. Prodan, W. D. Phillips, T. H. Bergeman, H. J. Metcalf, *Phys. Rev. Lett.* **54**, 2596 (1985).
9. S. Chu, L. Hollberg, J. E. Bjorkholm, A. Cable, A. Ashkin, *ibid.* **55**, 48 (1985).
10. S. Chu, J. E. Bjorkholm, A. Ashkin, A. Cable, *ibid.* **57**, 314 (1986).
11. W. Nagourney, J. Sandberg, H. Dehmelt, *ibid.* **56**, 2797 (1986).
12. J. C. Bergquist, R. G. Hulet, W. M. Itano, D. J. Wineland, *ibid.* **57**, 1699 (1986).
13. T. Sauter, W. Neuhauser, R. Blatt, P. E. Toschek, *ibid.*, p. 1696.
14. H. Dehmelt, *Adv. At. Mol. Phys.* **3**, 53 (1967); *ibid.* **5**, 109 (1969).
15. D. J. Wineland, W. M. Itano, R. S. Van Dyck, Jr., *ibid.* **19**, 135 (1983).
16. J. C. Bergquist, W. M. Itano, D. J. Wineland, *Phys. Rev. A* **36**, 428 (1987).
17. D. J. Wineland, W. M. Itano, J. C. Bergquist, *Opt. Lett.*, **12**, 389 (1987).
18. E. F. Nichols and G. F. Hull, *Phys. Rev.* **13**, 307 (1901).
19. P. Lebedev, *Ann. Phys. (Leipzig)* **6**, 433 (1901); *ibid.* **32**, 411 (1910).
20. O. Frisch, *Z. Phys.* **86**, 42 (1933).
21. A. Ashkin, *Science* **210**, 1081 (1980); V. S. Letokhov and V. G. Minogin, *Phys. Rep.* **73**, 1 (1981); A. P. Kazantsev, G. A. Ryabenko, G. I. Surdutovich, V. P. Yakovlev, *ibid.* **129**, 75 (1985).
22. A. P. Kazantsev, V. S. Smirnov, G. I. Surdutovich, D. O. Chudesnikov, V. P. Yakovlev, *J. Opt. Soc. Am. B* **2**, 1731 (1985); J. Dalibard and C. Cohen-Tannoudji, *ibid.*, p. 1707.
23. A. Aspect, J. Dalibard, A. Heidmann, C. Salomon, C. Cohen-Tannoudji, *Phys. Rev. Lett.* **57**, 1688 (1986).
24. H. Dehmelt, in *Advances in Laser Spectroscopy*, F. T. Arecchi, F. Strumia, H. Walther, Eds., vol. 95 of NATO Advanced Science Institutes Series B (Plenum, New York, 1983), pp. 153–187.
25. D. J. Wineland, W. M. Itano, J. C. Bergquist, R. G. Hulet, *Phys. Rev. A*, in press.
26. W. Neuhauser, M. Hohenstatt, P. Toschek, H. Dehmelt, *Phys. Rev. Lett.* **41**, 233 (1978).
27. M. Lindberg, *J. Phys. B* **17**, 2129 (1984); J. Javanainen, M. Lindberg, S. Stenholm, *J. Opt. Soc. Am. B* **1**, 111 (1984).
28. D. J. Wineland, R. E. Drullinger, F. L. Walls, *Phys. Rev. Lett.* 40, 1639 (1978).
29. D. J. Larson, J. C. Bergquist, J. J. Bollinger, W. M. Itano, D. J. Wineland, *ibid.* **57**, 70 (1986).
30. D. J. Wineland, W. M. Itano, J. C. Bergquist, J. J. Bollinger, J. D. Prestage, in *Atomic Physics Nine: Proceedings of the Ninth International Conference on Atomic Physics, Seattle, Washington, July 1984*, R. S. Van Dyck, Jr., and E. N. Fortson, Eds. (World Scientific, Singapore, 1984), p. 3.
31. G. Werth, in *ibid.*, p. 28.
32. R. H. Dicke, *Phys. Rev.* **89**, 472 (1953).
33. H. G. Dehmelt, *IEEE Trans. Instrum. Meas.* **IM-31**, 83 (1982).
34. D. J. Wineland, *Science* **226**, 395 (1984).
35. W. Neuhauser, M. Hohenstatt, P. E. Toschek, H. Dehmelt, *Phys. Rev. A* **22**, 1137 (1980); W. Nagourney and H. Dehmelt, personal communication.
36. H. G. Dehmelt, *Bull. Am. Phys. Soc.* 20, 60 (1975).
37. G. Janik, W. Nagourney, H. Dehmelt, *J. Opt. Soc. Am. B* **2**, 1251 (1985).
38. W. M. Itano and D. J. Wineland, *Phys. Rev. A* 24, 1364 (1981).
39. J. J. Bollinger, J. D. Prestage, W. M. Itano, D. J. Wineland, *Phys. Rev. Lett.* **54**, 1000 (1985).
40. R. J. Cook and H. J. Kimble, *ibid.*, p. 1023.
41. J. Javanainen, *Phys. Rev. A* **33**, 2121 (1986); A. Schenzle, R. G. DeVoe, R. G. Brewer, *ibid.*, p. 2127; C. Cohen-Tannoudji and J. Dalibard, *Europhys. Lett.* **1**, 441 (1986); D. T. Pegg, R. Loudon, P. L. Knight, *Phys. Rev. A* **33**, 4085 (1986); A. Schenzle and R. G. Brewer, *ibid.* **34**, 3127 (1986); H. J. Kimble, R. J. Cook, A. L. Wells, *ibid.*, p. 3190; P. Zoller, M. Marte, D. F. Walls, *ibid.* **35**, 198 (1987).
42. L. R. Brewer, J. D. Prestage, J. J. Bollinger, D. J. Wineland, in *Strongly Coupled Plasma Physics*, F. J. Rogers and H. E. De Witt, Eds. (Plenum, New York, 1987).
43. D. J. Wineland and W. M. Itano, *Phys. Today* 40, 34 (June 1987).

44. We gratefully acknowledge the support of the Air Force Office of Scientific Research and the Office of Naval Research. This article is not subject to copyright in the United States.

Physica Scripta. Vol. T22, 79–84, 1988.

Precise Optical Spectroscopy with Ion Traps*

Wayne M. Itano, J. C. Bergquist, Randall G. Hulet, and D. J. Wineland

Time and Frequency Division, National Bureau of Standards, Boulder, Colorado 80303, U.S.A.

Received September 24, 1987; accepted October 8, 1987

Abstract

We have used stored ion methods to improve resolution and sensitivity in optical spectroscopy. Single atomic ions have been confined by electric and magnetic fields, cooled by laser radiation pressure to temperatures on the order of 1 mK, and probed spectroscopically with narrowband lasers. The absorption resonance of a single Hg^+ ion has been observed by a decrease in the transmitted light intensity. An ultraviolet transition in Hg^+ has been observed with a linewidth of only 30 kHz. Quantum jumps to and from metastable levels of Hg^+ have been observed and used to determine radiative decay rates and to infer the existence of photon antibunching. Quantum jumps have also been observed in single Mg^+ ions.

1. Introduction

Ion traps have only recently been used in obtaining high resolution optical spectra, although their advantages have been realized for a long time. Microwave spectra of trapped ions, on the other hand, have been observed with high resolution since the 1960s [1, 2]. Elsewhere in these Proceedings, G. Werth discusses some recent experiments in this area [3]. A few years ago, at the Ninth International Conference on Atomic Physics, the field of optical spectroscopy of trapped ions was reviewed [4]. At that time, the highest resolution that had been achieved in the optical domain corresponded to a linewidth of about 3 MHz at an effective wavelength of 2.1 μm [5]. In a recent experiment to be discussed later in this Paper, an ultraviolet transition was observed with a fractional resolution about three orders of magnitude better than this [6].

Some general problems which tend to limit the resolution with which optical spectra are observed are Doppler shifts, perturbations due to collisions or to electric and magnetic fields, and the limited observation time. At least in a few favorable cases, these problems can be greatly alleviated for ions stored in traps, so that we are left with the natural linewidth. For a transition with a stable lower level, the natural linewidth (in hertz) is the inverse of the mean radiative lifetime (in seconds) of the upper level, divided by 2π.

The Doppler shift is usually divided into a term which is linear in the atomic velocity, called the first-order Doppler shift, and a part which is quadratic, called the second-order Doppler shift. The high intensity and narrow frequency width of laser light sources make it possible to apply various nonlinear spectroscopic techniques, such as saturated absorption or multiphoton absorption, that cancel the effects of first-order Doppler shifts [7]. However, the second-order Doppler shift, which is a result of relativistic time dilation, still remains. For typical laboratory conditions, this shift is only about one part in 10^{12}, but in some cases, it may seriously limit the resolution or accuracy of the measurement. One example is the work of Barger *et al.* on the 657 nm transition of calcium, which has a frequency of 4.57×10^{14} Hz and a natural linewidth of 410 Hz [8]. Resonances with linewidths as small as 2 kHz were observed, but they were severely shifted and distorted by the second-order Doppler shift.

If both the first- and second-order Doppler shifts are to be reduced, the atoms must be cooled. An atomic vapor placed in a conventional refrigeration device would quickly condense on the walls of the container. But laser cooling, a method by which laser radiation pressure is used to reduce the velocities of atoms, achieves the cooling without contact with material objects [9]. The technique was proposed independently by Hänsch and Schawlow for free atoms [10] and by Wineland and Dehmelt for trapped ions [11]. Laser cooling to temperatures on the order of 1 mK has been demonstrated with some kinds of atoms and atomic ions. This reduces the second-order Doppler shifts to the level where they are presently not a problem. An atom or atomic ion of mass 100 u (unified atomic mass units) cooled to 1 mK has a second-order Doppler shift of 1.4 parts in 10^{18}.

The observed resonance linewidth cannot be much less than the inverse of the observation time. In the case of the work on calcium, the observation time was limited to about 0.3 ms by the time it took the atoms to pass through the 21 cm long resonance region [8]. In some experiments, the observation times have been increased by confining the atoms with specially coated walls or by buffer gases, but collisions with the wall or buffer gas molecules shifted and broadened the observed resonances. Ions can be trapped for long periods by electric and magnetic fields. External field perturbations of carefully chosen transition frequencies can be less than a part in 10^{15} [12, 13]. Collisions are almost entirely absent in the ultra-high-vacuum environment of an ion trap. Neutral atoms have been trapped by static magnetic fields [14–16] and by optical fields [17], but these trapped atoms have not yet been studied spectroscopically. In these traps, the fields responsible for trapping would also have perturbed the resonances.

2. Sensitive detection of ions

A single atomic ion can easily be observed by the laser-induced fluorescence of an allowed transition, once it has been cooled so that the Doppler broadening of the transition is small. In this case, a single ion may scatter as many as 10^8 photons per second. Even if only a small fraction of the photons, around 10^{-4} in typical experimental cases, are collected and counted, the fluorescence can easily be observed [18].

The apparatus used at the National Bureau of Standards

* Contribution of the National Bureau of Standards. Not subject to copyright in the U.S.

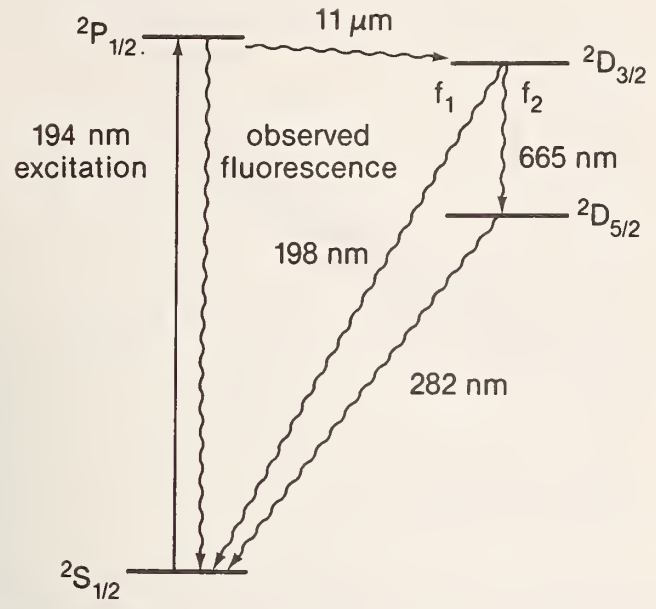

Fig. 1. The lowest energy levels of Hg^+ and the transition wavelengths. The decay rates from all three excited levels were determined by observing only the 194 nm fluorescence. (From Ref. [33]).

for experiments with Hg^+ has been described previously [19, 20]. The Hg^+ ions were confined in a radiofrequency (Paul) trap under ultra-high-vacuum conditions. In one case, a single Hg^+ ion has been kept in the trap for over a week. The lowest energy levels of Hg^+ are shown in Fig. 1. The $5d^{10}6s\ ^2S_{1/2}$ ground level is connected to the $5d^{10}6p\ ^2P_{1/2}$ level by a strong electric dipole transition. The $5d^9 6s^2\ ^2D_{3/2}$ and the $5d^9 6s^2\ ^2D_{5/2}$ levels are metastable. In order to laser cool and optically detect the ions, a few microwatts of c.w. 194 nm radiation were required. This radiation was generated by sum-frequency mixing the output of a frequency doubled 514.5 nm Ar^+ laser with the output of a 792 nm dye laser in a potassium pentaborate crystal [21]. The 194 nm fluorescence was collected by a lens system and detected by a photomultiplier tube. As many as 60 000 photons per second were detected from a single ion.

2.1. *Single-ion absorption detection*

In a recent experiment, an optical transition in a single Hg^+ ion was detected by observing the decrease in the intensity of the 194 nm beam transmitted through the trap [22]. Radio-frequency modulation techniques were used in order to avoid low frequency noise, such as that due to amplitude fluctuations of the 194 nm radiation. A maximum of about 10^{-5} of the light was absorbed. Figure 2 shows the absorption signal and the fluorescence signal, taken at the same time. The modulation and phase-sensitive detection of the absorption resulted in a signal which was approximately proportional to the frequency derivative of the fluorescence signal. Laser heating caused the fluorescence signal to drop suddenly to zero when the frequency was tuned above resonance. The integration time per point on the absorption curve was 50 s.

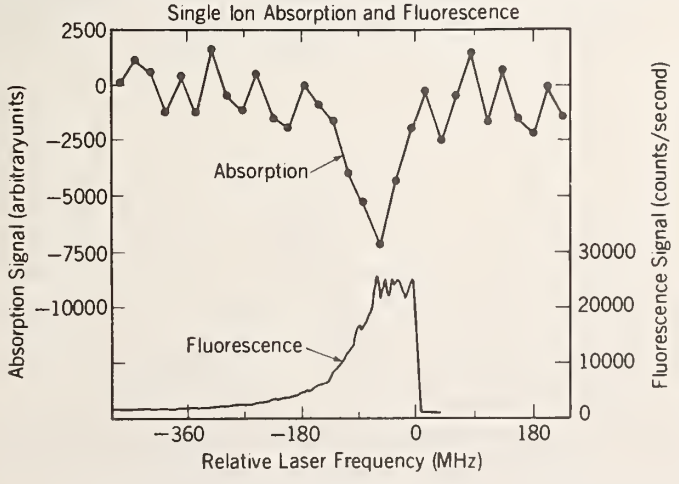

Fig. 2. The 194 nm resonance of a single Hg^+ ion due to absorption (upper trace) and fluorescence (lower trace), detected at the same time. (From Ref. [22]).

2.2. *Electron shelving*

Detecting a narrow (weakly allowed) transition by observing fluorescence from the same transition would be very difficult. A double-resonance method originally proposed by Dehmelt [23] makes it possible to detect such transitions with very high efficiency. The method can be applied to Hg^+ (see Fig. 1). The narrow, weakly-allowed, 282 nm transition is detected as follows: The ion is assumed to be initially in the ground level. Light at a wavelength near 282 nm is pulsed on, possibly driving the ion to the $^2D_{5/2}$ level. Light at a wavelength near 194 nm is then pulsed on. If the ion had made a transition in the previous step, no fluorescence would be observed; otherwise an easily detectable fluorescence signal would be observed. The method is called "electron shelving", since the optically active electron is temporarily shelved in the upper level of the weak transition.

3. Quantum jumps

The electron shelving techniques suggests a method of observing quantum jumps. If light near both resonance wavelengths is present simultaneously, then the fluorescence observed from the strong transition should turn off and on abruptly as the atom makes transitions to and from the metastable level. The dynamics of this process was investigated theoretically by Cook and Kimble [24] and later by others [25]. Quantum jumps of single ions were observed by this method in Ba^+ [26, 27], in Hg^+ [20], and recently in Mg^+ [28].

Quantum jumps have also been observed by us in Hg^+ with only the 194 nm radiation present. Once excited to the $^2P_{1/2}$ level, the ion usually decays back to the ground level, but it has a probability of about 10^{-7} to decay to the $^2D_{3/2}$ level. The probability is small because the transition frequency is low and because it requires configuration mixing to occur (the nominal configurations differ in two orbitals). From the $^2D_{3/2}$ level, the atom decays either directly to the ground level with probability f_1 or to the $^2D_{5/2}$ level with probability $f_2 = 1 - f_1$. The 194 nm fluorescence jumps between a steady level (the "on" state) when the ion is cycling between the ground level and the $^2P_{1/2}$ level and zero (the "off" state) when it is in either the $^2D_{3/2}$ level or the $^2D_{5/2}$ level.

Typical fluorescence data are shown in Fig. 3 for one, two, and three ions. The fluorescence intensity jumped from one discrete level to another and was proportional to the number of ions in the "on" state. For these data, only the 194 nm radiation was present. The intensity was high enough that quantum jumps due to the weak $^2P_{1/2}$ level to $^2D_{3/2}$ level decay occurred several times per second.

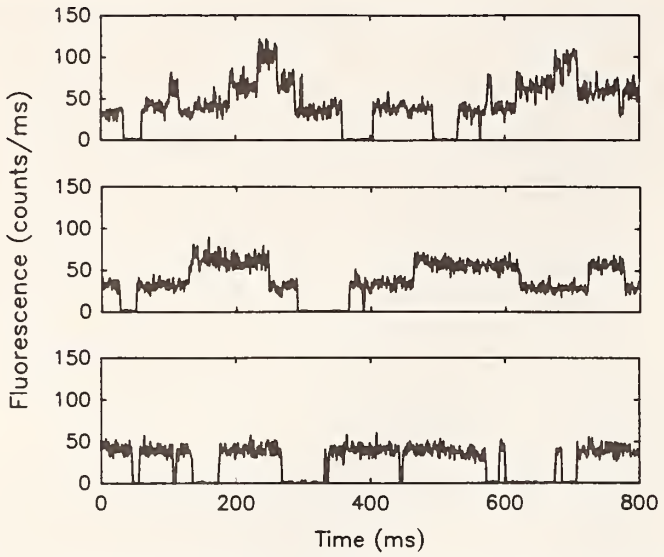

Fig. 3. Fluorescence intensities as a function of time for three Hg^+ ions (top trace), two Hg^+ ions (middle trace), and one Hg^+ ion (lowest trace). The fluorescence takes a step down when an ion makes a transition to the metastable $^2D_{3/2}$ level and takes a step up when an ion returns to the ground level from a metastable level. The integration time per point is 1 ms and the points are connected by straight lines. (From Ref. [33]).

3.1. *Quantum jumps of two and three ions*

Sauter *et al.* have reported observing multiple quantum jumps, that is, simultaneous quantum jumps of two or more ions, when several Ba^+ ions were stored in the same trap [29]. They attributed this phenomenon to a cooperative interaction between the atoms and the radiation field. We have examined our data to test the statistical independence of the quantum jumps of two or more simultaneously trapped ions.

One test was based on measuring the fractions of the time that the ions spent in each of the possible fluorescence levels. The probability distribution of fluorescence intensities was plotted for the data from one, two, and three ions. The distribution for one ion is shown in Fig. 4. The counts at low intensity (left side of plot) are due to stray scattered light when the ion is in the "off" state; the peak at high intensity (right side) is due to the fluorescence of the ion in the "on" state. The solid curve is a least-squares fit of the data to a sum of a Poisson distribution (for the left peak) and a Gaussian

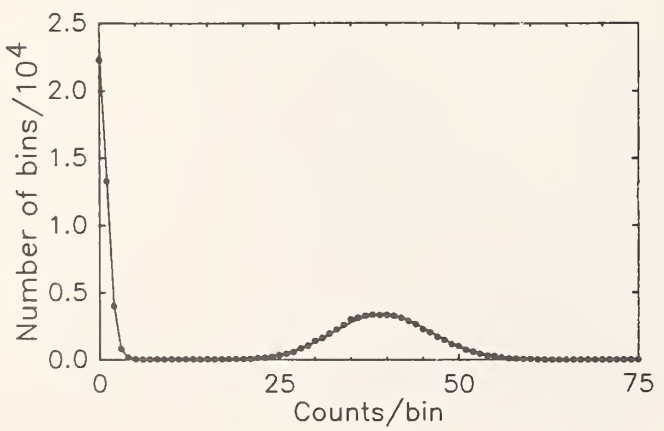

Fig. 4. Fluorescence intensity distribution for one Hg^+ ion. The numbers of 1 ms time bins in which a given number of photons was detected are plotted as dots. The solid curve is a least-squares fit to the data.

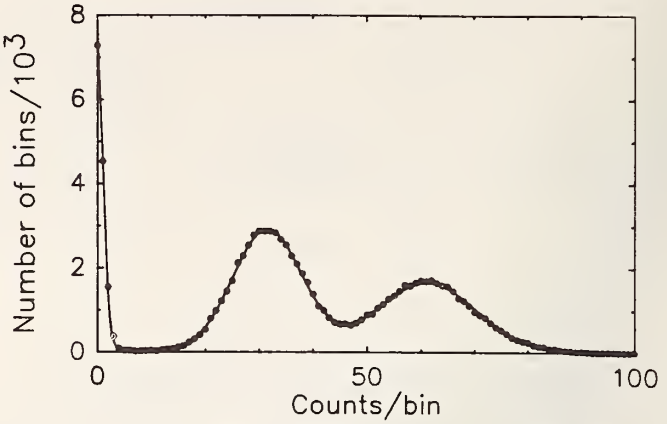

Fig. 5. Fluorescence intensity distribution for two Hg^+ ions (dots) and a least-squares fit (solid curve).

distribution (for the right peak). The standard deviation (sigma) of the fitted Gaussian is about 8% larger than the square root of the mean, which is the expected value due to statistical fluctuations. This is probably due to intensity and frequency fluctuations of the 194 nm source. The ratio of the area under the Poisson distribution to that under the Gaussian distribution is a measurement of the ratio of the time that the ion was in the "off" state to the time that it was in the "on" state (0.71 for this data set). Plots of the two-ion and three-ion intensity distributions and least-squares fits are shown in Figs. 5 and 6. The areas under the peaks of the distributions are proportional to the amounts of time that the fluorescence was at each of the various discrete levels. The curves fitted the data well, even though the peaks were not completely resolved.

Let p_{off} and p_{on} be the probabilities that a single ion is in the "off" state or the "on" state, respectively. Consider two ions subjected to the same 194 nm intensity and acting independently of each other. In this case, the probability p_0 that both are in the "off" state is equal to $(p_{\text{off}})^2$; the probability p_1 that one ion is in the "off" state and the other in in the "on" state is equal to $2p_{\text{on}}p_{\text{off}} = 2p_{\text{on}}(1 - p_{\text{on}})$; and the probability p_2 that both are in the "on" state is equal to $(p_{\text{on}})^2$. Similar relationships hold for three ions. The least-squares fit to the two-ion data yielded the values $p_0 = 0.139$, $p_1 = 0.472$, and $p_2 = 0.389$. If p_1 is (arbitrarily) chosen to calculate the value of p_{on}, then the prediction, based on the assumption of independence, is that $p_0 = 0.145$ and

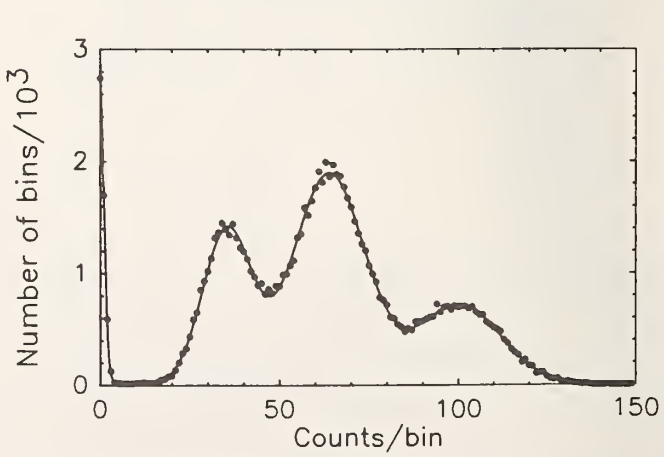

Fig. 6. Fluorescence intensity distribution for three Hg^+ ions (dots) and a least-squares fit (solid curve).

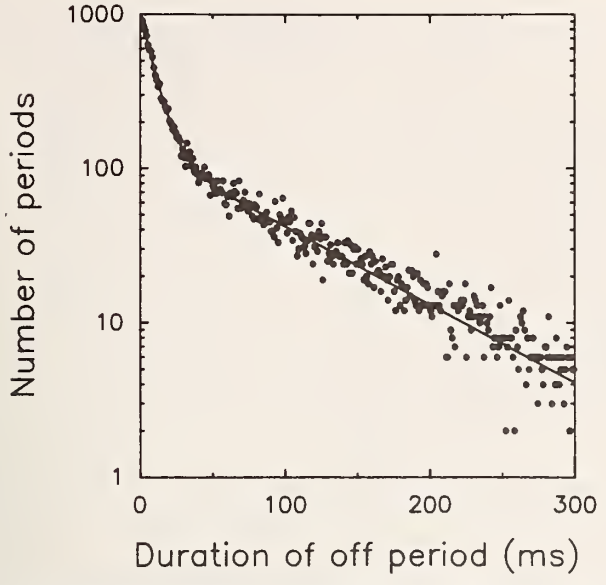

Fig. 7. Distribution of fluorescence-off periods for a single Hg^+ ion as a function of the duration of the periods (dots) and a least-squares fit. (From Ref. [33]).

$p_2 = 0.383$. For the three-ion data, let p_n ($n = 0, 1, 2, 3$) be the probability that n ions are in the "on" state. The least-squares fit yielded the values $p_0 = 0.053$, $p_1 = 0.244$, $p_2 = 0.485$, and $p_3 = 0.218$. If p_3 is used to calculate the value of p_{on}, the prediction based on independence is that $p_0 = 0.061$, $p_1 = 0.286$, and $p_2 = 0.433$. Thus, the two- and three-ion data agreed fairly well with the assumption of independence of the ions. The discrepancies from the predictions were most likely due to effects of intensity and frequency variations of the 194 nm radiation source, which are not included in the simple model used to fit the data.

In another test of independence, a search through the two-ion data was made for double quantum jumps. Over 500 consecutive jumps, which took place in a period of 20 s, were tabulated. A total of five apparent double quantum jumps were found, which is approximately the number that would be expected due to random coincidences within the finite resolving time of the instrumentation (1 ms).

3.2. *Measurements of radiative decay rates*

The radiative decay rates of the $^2D_{3/2}$ level and the $^2D_{5/2}$ level are reflected in the probability distribution W_{off} of the durations of the "off" periods for a single ion irradiated by 194 nm radiation. A calculation based on the rate equations for the probabilities of being in the various levels yields

$$W_{off}(\tau) \propto [f_2\gamma_2 \exp(-\gamma_2\tau) + (f_1\gamma_1 - \gamma_2)\exp(-\gamma_1\tau)]. \quad (1)$$

Here γ_1 and γ_2 are the total radiative decay rates of the $^2D_{3/2}$ level and the $^2D_{5/2}$ level respectively.

The experimental fluorescence-off distribution was least-squares fitted to eq. (1) to obtain values for γ_1, γ_2, and f_1. Figure 7 shows the data and the least-squares fit. The values obtained from the fit are $\gamma_1 = 109 \pm 5\,s^{-1}$, $\gamma_2 = 11.6 \pm 0.4\,s^{-1}$, and $f_1 = 0.491 \pm 0.015$. These values are in fair agreement with calculations [30, 31]. The value of γ_2 is in good agreement with previous measurements [19, 20, 32], but the value of γ_1 is about a factor of 2 higher than the only previously reported value [32]. No previous measurements of f_1 exist. The measurements will be described in more detail elsewhere [33].

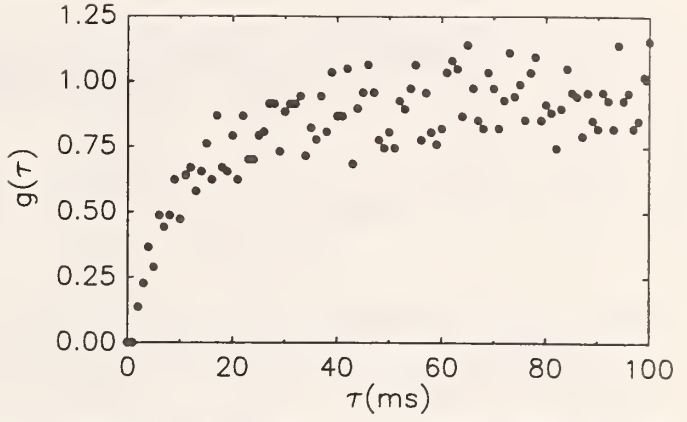

Fig. 8. Intensity correlation function of the 11 μm radiation field generated by the radiative decay from the $^2P_{1/2}$ level to the $^2D_{3/2}$ level in a single Hg^+ ion, showing the photon antibunching. The data from several runs were averaged.

3.3. *Photon antibunching*

The two-time intensity correlation function of a light field is defined by $C(\tau) = \langle I(t)I(t+\tau)\rangle$, where I is the intensity. A field is said to exhibit photon antibunching if $C(0) < C(\infty)$. No classical field can have this property, so a quantum theory is required to explain it. The quantum jumps of a single Hg^+ ion from the "on" state to the "off" state, as in the lowest trace of Fig. 3, are assumed to mark the emission of an 11 μm photon (see Fig. 1), even though these photons have not been observed directly. The probability density $g(\tau)$ that the emission of an 11 μm photon is followed a time τ later by the emission of another one is proportional to $C(\tau)$ for the 11 μm field. We expect $g(\tau)$ to go to zero for small τ, since the ion has to decay to the ground level and be excited to the $^2P_{1/2}$ level again before it can emit another 11 μm photon. The function $g(\tau)$ (normalized to 1 as $\tau \to \infty$) was calculated for several one-ion runs and averaged to obtain the graph shown in Fig. 8, which clearly shows photon antibunching. A similar graph, showing photon antibunching in the 282 nm radiation emitted when light at both 194 nm and 282 nm was applied, has been shown previously [20].

3.4. *Quantum jumps in Mg^+*

Quantum jumps of a single $^{24}Mg^+$ ion in a Penning trap were investigated recently [28]. A single 280 nm radiation source was present and was tuned close to the $m_J = -1/2$ to $m_J = -3/2$ Zeeman component of the transition from the $3s\ ^2S_{1/2}$ ground level to the $3p\ ^2P_{3/2}$ level. The fluorescence intensity dropped to zero when the ion was driven to the $m_J = +1/2$ sublevel of the ground level by a spontaneous Raman transition, and returned to its previous level when another spontaneous Raman transition drove the ion back to the $m_J = -1/2$ sublevel. A trace of the fluorescence intensity as a function of time is shown in Fig. 9. The data are in agreement with the theoretical prediction that the ratio of the time when the fluorescence is on to the time when it is off is very close to 16 [34]. This ratio is nearly independent of the 280 nm intensity because of the existence of coherences between excited levels. The experimental results provide a high precision (2%) verification of an effective two-state rate equation description of the dynamics of the quantum jumps.

TN-153

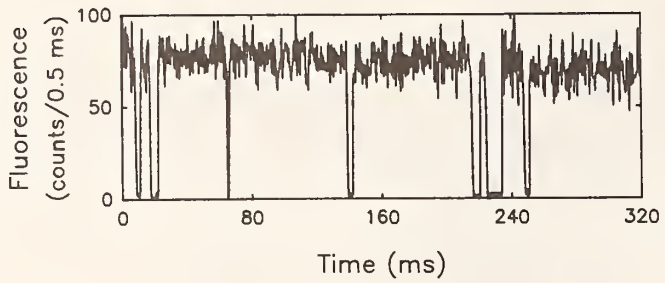

Fig. 9. Fluorescence intensity of a single Mg^+ ion as a function of time, showing the sudden changes due to quantum jumps to and from the ground-state Zeeman level which is not in resonance with the incident radiation. (Adapted from Ref. [28]).

4. Suppression of Doppler broadening by confinement

In 1953 Dicke showed that the confinement of an atom to a region smaller than the resonance-radiation wavelength leads to a suppression of the first-order Doppler shift broadening [35]. This condition is the basis for the observation of narrow Mössbauer transitions of the nuclei in solids. It is also easy to satisfy this condition, commonly called the Lamb–Dicke criterion, for a microwave resonance, since the wavelengths can be several centimeters long. Microwave frequency standards such as the atomic hydrogen maser make use of this fact. In the optical domain, it can be satisfied for a single, laser-cooled ion confined in a trap. The residual first-order Doppler broadening takes the form of discrete resonances, displaced from the unshifted central resonance (the carrier), by multiples and combinations of the frequencies of motion of the ion. These extra resonances are called motional sidebands.

4.1. *High resolution spectra of Hg^+*

We have used the shelved-electron method to detect the weak $^2S_{1/2}$ to $^2D_{5/2}$ transition of a single Hg^+ ion [6]. If the fluorescence was high enough to indicate that the ion was cycling between the $^2S_{1/2}$ and the $^2P_{1/2}$ levels, the 194 nm radiation was turned off and the 282 nm radiation was turned on for 20 ms,

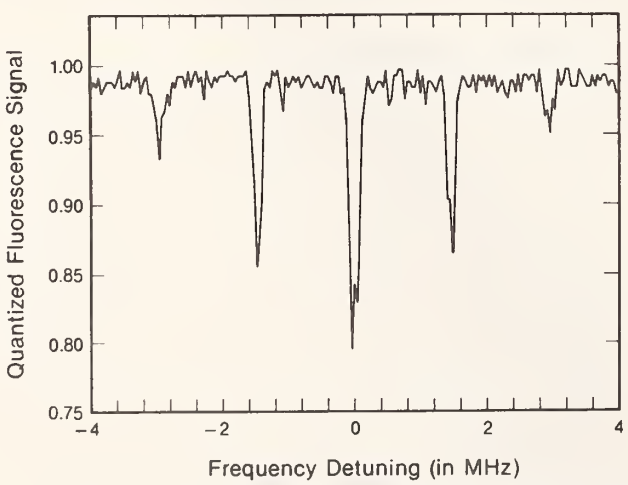

Fig. 10. The $^2S_{1/2}$ to $^2D_{5/2}$ resonance due to absorption of 282 nm radiation from a frequency-doubled dye laser by a single Hg^+ ion. The shelved electron method was used to detect this weakly allowed transition. The weaker absorption lines (motional sidebands) are separated from the central resonance by multiples of the frequencies of harmonic motion of the trapped ion and are due to the Doppler shift of the 282 nm radiation in the frame of the ion. (From Ref. [6]).

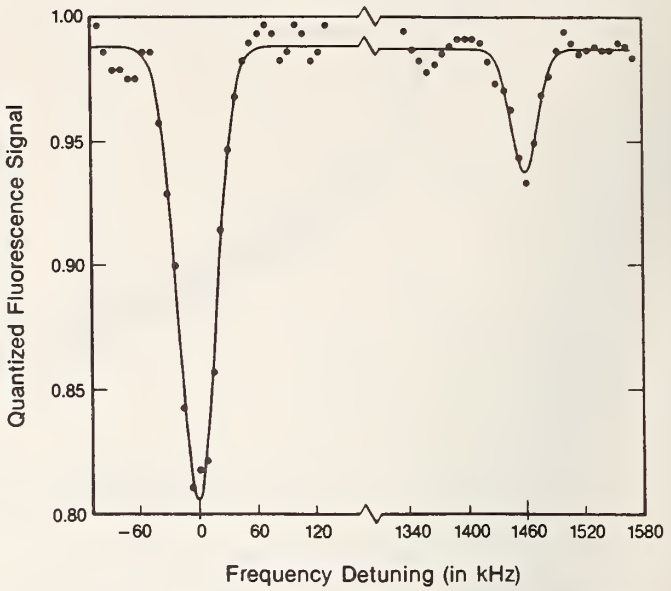

Fig. 11. High resolution frequency scan of the $^2S_{1/2}$ to $^2D_{5/2}$ resonance, showing the central resonance and the first upper motional sideband. From Ref. [6]).

which is much less than the $^2D_{5/2}$ level lifetime. The 194 nm radiation was turned on again, and the fluorescence photons were counted for 10 ms to see whether the ion had made a transition to the $^2D_{5/2}$ level. The result of the measurement was a 0 or a 1, depending on whether the number of photons detected was below or above a threshold level. This eliminated certain kinds of instrumental noise, such as intensity fluctuations of the detection laser, leaving only the inherent quantum fluctuations of the atom. Figure 10 shows a spectrum taken in the manner just described, displaying the carrier and two motional sidebands on each side. Figure 11 shows a high resolution scan of the carrier and the first upper sideband. The resonances are approximately 30 kHz wide. The ratio of intensities of the carrier and sideband indicates that the ion was cooled to near the theoretical minimum of 1.7 mK. The limit of 30 kHz resolution was due to laser frequency fluctuations. If a suitably stabilized laser were used, the resolution would approach the natural linewidth of about 2 Hz. The sensitivity of the transition frequency to fluctuations in the magnetic field could essentially be eliminated by using a suitable Zeeman component in either $^{199}Hg^+$ or $^{201}Hg^+$ [36].

Acknowledgements

We gratefully acknowledge the support of the Air Force Office of Scientific Research and the Office of Naval Research.

References

1. Dehmelt, H., Adv. At. Mol. Phys. **3**, 53 (1967); *ibid*, **5**, 109 (1969).
2. Wineland, D. J., Itano, W. M. and Van Dyck, Jr., R. S., Adv. At. Mol. Phys. **19**, 135 (1983).
3. Werth, G., these Proceedings.
4. Wineland, D. J., Itano, W. M., Bergquist, J. C., Bollinger, J. J. and Prestage, J. D., Atomic Physics 9 (Edited by R. S. Van Dyck, Jr. and E. N. Fortson), p. 3. World Scientific, Singapore, 1985.
5. Janik, G., Nagourney, W. and Dehmelt, H., J. Opt. Soc. Am. B **2**, 1251 (1985).
6. Bergquist, J. C., Itano, W. M. and Wineland, D. J., Phys. Rev. A **36**, 428 (1987).

7. High-Resolution Laser Spectroscopy (Edited by K. Shimoda). Springer Verlag, Berlin, 1976; Levenson, M. D., Introduction to Nonlinear Laser Spectroscopy. Academic Press, New York, 1982.
8. Barger, R. L., Bergquist, J. C., English, T. C. and Glaze, D. J., Appl. Phys. Lett. **34**, 850 (1979); Barger, R. L., Opt. Lett. **6**, 145 (1981).
9. Wineland, D. J. and Itano, W. M., Phys. Today **40**, 34 (June 1987).
10. Hänsch, T. W. and Schawlow, A. L., Opt. Commun. **13**, 68 (1975).
11. Wineland, D. J. and Dehmelt, H., Bull. Am. Phys. Soc. **20**, 637 (1975).
12. Dehmelt, H. G., IEEE Trans. Instrum. Meas. **IM-31**, 83 (1982).
13. Wineland, D. J., Science **226**, 395 (1984).
14. Migdall, A. L., Prodan, J. V., Phillips, W. D., Bergeman, T. H. and Metcalf, H. J., Phys. Rev. Lett. **54**, 2596 (1985).
15. Bagnato, V. S., Lafyatis, G. P., Martin, A. G., Raab, E. L., Ahmad-Bitar, R. N. and Pritchard, D. E., Phys. Rev. Lett. **58**, 2194 (1987).
16. Hess, H. F., Kochanski, G. P., Doyle, J. M., Masuhara, N., Kleppner, D. and Greytak, T. J., Phys. Rev. Lett. **59**, 672 (1987).
17. Chu, S., Bjorkholm, J. E., Ashkin, A., and Cable, A., Phys. Rev. Lett. **57**, 314 (1986).
18. Neuhauser, W., Hohenstatt, M., Toschek, P. E. and Dehmelt, H., Phys. Rev. **A22**, 1137 (1980).
19. Bergquist, J. C., Wineland, D. J., Hemmati, H., Daniel, H.-U. and Leuchs, G., Phys. Rev. Lett. **55**, 1567 (1985).
20. Bergquist, J. C., Hulet, R. G., Itano, W. M. and Wineland, D. J., Phys. Rev. Lett. **57**, 1699 (1986).
21. Hemmati, H., Bergquist, J. C. and Itano, W. M., Opt. Lett. **8**, 73 (1983).
22. Wineland, D. J., Itano, W. M. and Bergquist, J. C., Opt. Lett. **12**, 389 (1987).
23. Dehmelt, H. G., Bull. Am. Phys. Soc. **20**, 60 (1975).
24. Cook, R. J. and Kimble, H. J., Phys. Rev. Lett. **54**, 1023 (1985).
25. Javanainen, J., Phys. Rev. **A33**, 2121 (1986); Schenzle, A., DeVoe, R. G. and Brewer, R. G., Phys. Rev. **A33**, 2127 (1986); Cohen-Tannoudji, C. and Dalibard, J., Europhys. Lett. **1**, 441 (1986); Pegg, D. T., Loudon, R. and Knight, P. L., Phys. Rev. **A33**, 4085 (1986); Schenzle, A. and Brewer, R. G., Phys. Rev. **A34**, 3127 (1986); Kimble, H. J., Cook, R. J., and Wells, A. L., Phys. Rev. **A34**, 3190 (1986); Zoller, P., Marte, M. and Walls, D. F., Phys. Rev. **A35**, 198 (1987); Nienhuis, G., Phys. Rev. **A35**, 4639 (1987); Porrati, M. and Putterman, S., Phys. Rev. **A36**, 929 (1987).
26. Nagourney, W., Sandberg, J. and Dehmelt, H., Phys. Rev. Lett. **56**, 2797 (1986).
27. Sauter, Th., Neuhauser, W., Blatt, R. and Toschek, P. E., Phys. Rev. Lett. **57**, 1696 (1986).
28. Hulet, R. G., Wineland, D. J., Bergquist, J. C., and Itano, W. M., (submitted for publication)
29. Sauter, Th., Neuhauser, W., Blatt, R. and Toschek, P. E., Opt. Commun. **60**, 287 (1986).
30. Garstang, R. H., J. Res. Natl. Bur. Stand. Sect. **A68**, 61 (1964).
31. Al-Salameh, D. and Silfvast, W., AT&T Bell Laboratories, Holmdel, NJ, unpublished calculations.
32. Johnson, C. E., Bull. Am. Phys. Soc. **31**, 957 (1986).
33. Itano, W. M., Bergquist, J. C., Hulet, R. G. and Wineland, D. J., Phys. Rev. Lett. (in press).
34. Hulet, R. G. and Wineland, D. J., Phys. Rev. A **36**, 2758 (1987).
35. Dicke, R. H., Phys. Rev. **89**, 472 (1953).
36. Wineland, D. J., Itano, W. M., Bergquist, J. C. and Walls, F. L., in Proc. 35th Annual Symposium on Frequency Control, p. 602. Electronic Industries Association, Washington, D.C., 1981.

FROM: PHYSICS TODAY, JUNE 1987

Laser cooling

The mechanical forces exerted by light can dramatically lower the temperature of a sample of atoms or ions, allowing very-high-resolution spectroscopic measurements and ultralow-temperature atomic physics experiments.

David J. Wineland and Wayne M. Itano

In the photograph on the opposite page we see a single mercury ion held nearly at rest in an electromagnetic "trap." Physicists have seen individual atoms before, in arrays imaged by field ion microscopes and more recently by vacuum tunneling microscopes, but what we see here is different. It graphically demonstrates a physicist's ideal: holding a single isolated atom nearly at rest for careful examination.

A technique now commonly called laser cooling made the photograph possible by reducing the mercury ion's kinetic energy. This cooling not only limited the ion's movement, but also sharpened its spectral features by reducing Doppler broadening, enhancing the scattering of laser light tuned to one of its transitions. Several laboratories now use lasers to cool ions and neutral atoms to kinetic energies corresponding to temperatures near a millikelvin. (See PHYSICS TODAY, September 1986, page 17.)

As originally proposed in 1975 by Theodor Hänsch and Arthur Schawlow at Stanford University and independently by Wineland and Hans Dehmelt at the University of Washington, laser cooling can substantially reduce Doppler effects in high-resolution spectroscopy.[1] The technique should eventually reduce inaccuracies in spectroscopy to 1 part in 10^{18} or better for single trapped ions.[2,3] More accurate atomic clocks are an obvious prospect. Other applications include tests of gravitational interactions. Laser-cooled neutral atomic beams may finally allow realization of Jerrold Zacharias's 1953 proposal for an "atomic fountain" experiment. Here one would achieve long observation times by directing a slowed atomic beam upward and letting gravity return it to near its original position. Even with moderately slowed atomic beams, the velocity compression achieved from laser cooling will greatly reduce the uncertainty in the second-order, or time dilation, Doppler shift.

Laser cooling has a potential role in many other experiments. It may give us ways to:

- Study collisions between very cold atoms or ions. Such studies should give detailed information on interactions, with very high energy resolution.
- Study atom–surface collisions at low temperature. It may be that at sufficiently low temperature, atoms will "bounce" with minimal perturbation to their structure. This would allow the construction of nearly ideal boxes for storing atoms for use in spectroscopy and other experiments.
- Focus atomic beams. Laser beams directed transversely to an atomic beam act as lenses. These lenses are dissipative in the direction normal to the atomic beam, so beam focusing is not limited by Liouville's theorem. Laser cooling may also be used to advantage in ion storage rings.
- Manipulate antihydrogen, which, if produced, must be used efficiently.
- Obtain unique states of condensed matter. Observing liquid and solid plasmas is a possibility, as we discuss below.
- Observe Bose condensation of hydrogen or other atoms. This phenomenon may eventually be observed by cooling atoms held in a suitable "trap."

In many cases laser cooling may be the only practical way to control the velocity distribution of a sample of ions or neutral atoms.

We begin this article with an explanation of how light imparts mechanical forces on atoms. Because these forces are the same on both ions and neutral atoms, we will take the term "atom" to include both unless we specifically state otherwise. We then discuss how one can use these forces to reduce the

David Wineland and Wayne Itano are physicists in the Time and Frequency Division of the National Bureau of Standards, in Boulder, Colorado.

TN-156

Single ion of mercury. The white dot at the center of this false-color image is a laser-cooled Hg^+ ion in an electromagnetic trap. This image was made with a photon-counting imaging tube sensitive to the 194-nm fluorescence light scattered from the ion and trap electrodes. The white overlay shows the position of the electrodes of the ion trap. The circular ring electrode has an inner diameter of about 0.9 mm. To photograph such an ion requires a minimum exposure time of about 50 μsec. The effective temperature of the ion was approximately 2 mK. The computerized imaging system used here was developed by Charles Manney and John Bollinger at the National Bureau of Standards. The first photographic images of single ions were reported in reference 15.

kinetic energy of a sample. Finally, we discuss what can be achieved in the laboratory.

Early history. The study of the mechanical forces that light exerts on matter has a long history. In 1873 James Clerk Maxwell used the theory of electromagnetism to calculate the force on a solid body due to the absorption or reflection of a beam of light. In the early 1900s quantitative measurements of the force exerted by light on solid bodies and gases verified Maxwell's radiation pressure calculations.[4] In 1917 Albert Einstein used quantum theory to calculate the influence of the electromagnetic radiation field on the motion of molecules.[5] He showed that the light pressure causes molecules to come into thermal equilibrium with a radiation field if that field has the Planck spectrum. Aside from showing the consistency of quantum theory and statistical mechanics, this calculation was important in establishing the quantum nature of light, because it was necessary to assume that the molecule emits radiation as a discrete bundle with a definite energy and momentum, and not as a spherical wave.

In 1933 Otto Frisch did the first experiment to show directly the momentum transferred to an atom by the absorption of a photon.[6] In this experiment, light from a sodium resonance lamp deflected a beam of sodium atoms. When tunable lasers became available in the 1970s, experiments of this sort were repeated. Due to the much higher spectral intensities available, an atom could be made to absorb many photons one at a time, but at a high rate, resulting in larger deflections. Around this time physicists made proposals to use intense, resonant optical fields to manipulate atoms in various ways, such as accelerating them or trapping them in optical potential wells. Among those who first recognized the possible applications of resonant laser radiation pressure on atoms were Arthur Ashkin in the United States and several scientists in the Soviet Union.[7] In his 1950 paper on optical pumping, Alfred Kastler suggested some ways of using light to cool or heat atoms.[8] These ideas are related to laser cooling but are difficult to realize in practice.

Optical forces on atoms

The force that light exerts on atoms is often conceptually divided into two parts.[9] These are called the light pressure or scattering force and the gradient or dipole force. At least in some simple cases, one can distinguish these forces clearly. In the general case, and particularly for intense fields, the simple descriptions of the forces and their fluctuations break down, and a more fully quantum mechanical description is required.[9,10]

We can understand the scattering force as the momentum transferred to the atom as it scatters a photon. The average scattering force is in the direction of propagation of the light and is equal to the product of the momentum $\hbar k$ per photon and the photon scattering rate. The photon wavevector k has magnitude $2\pi/\lambda$, where λ is the wavelength of the light. The average force reaches a maximum when the light is resonant with an atomic transition. The scattering force fluctuates because the photons scatter at random times and because the direction of the re-emitted photon, and hence the direction of the recoil momentum due to this re-emission, is also random.

To see how large the scattering force can be, let us consider a specific example. Assume that the light from a single laser beam is resonant with the lowest-frequency atomic transition and that the light is intense enough to saturate the transition, that is, that the rate for stimulated emission exceeds the spontaneous decay rate. When saturated, the atom spends about half of its time in the excited state. Therefore the average force on

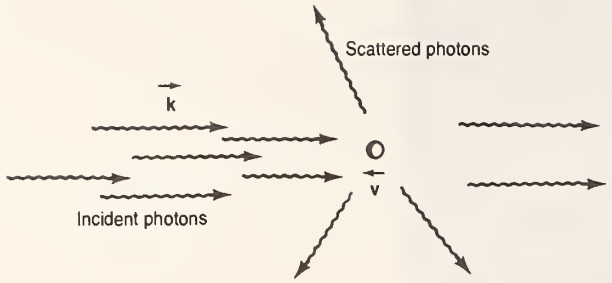

Laser cooling mechanism for free or weakly bound atoms or ions. "Weakly bound" means that the oscillation period of the trapped atom or ion is longer than the lifetime of the upper state of the cooling transition. The frequency ω_L of incident photons is assumed to be less than the rest frequency ω_0 of the atomic transition. At a velocity where the atom's transition frequency ω_0 is equal to $(1 - \mathbf{k}\cdot\mathbf{v})\omega_L$, the atom resonantly scatters photons. When the photon wavevector $\mathbf{k}$ is antiparallel to the atom's velocity $\mathbf{v}$, the average reduction in the atom's velocity is $\hbar\mathbf{k}/m$ per scattering event, where m is the atom's mass.

one atom is equal to the product of the photon momentum $\hbar k$, the rate γ of spontaneous decay from the excited state, and the probability of being in the excited state, or $\hbar k\gamma/2$. Note that absorption followed by stimulated emission imparts no net momentum to the atom because the photon resulting from stimulated emission also has momentum $\hbar k$.

If the wavelength is 500 nm and the decay rate γ is 10^8/sec, then the scattering force is about 40 000 times the force of gravity for an atom of mass 100 u, or atomic mass units. This force is the same as the electric force on a singly charged ion in a field of about 5×10^{-8} V/cm. Therefore, the scattering force can be much greater than the gravitational force, but is weak compared with typical electric forces. In practice, about 10^4 scattering events are required to change atomic velocities by as much as room temperature thermal velocities. The basic idea of laser cooling, then, is to have the atom preferentially scatter photons when its momentum and the photon momentum are antiparallel.

The origin of the gradient or dipole force is somewhat less obvious, although certain of its properties do have a classical interpretation. The atom can be thought of as a polarizable body. The optical electric field induces an electric dipole moment in the atom and then acts on that dipole moment. If the optical intensity is spatially inhomogeneous, the dipole interaction causes a force along the gradient of the intensity. Like the scattering force, the dipole force has a strongly resonant character, but unlike the scattering force, it is dispersive in nature. Its sign is such that it attracts an atom to a region of high light intensity if the frequency of the light is below the atomic resonance and repels an atom if it is above. That is, the electric polarizability is positive below resonance and negative above resonance. To this extent, the atom is like a charged harmonic oscillator—an electron bound to a positive core by a spring, in an oscillating electric field. The charge oscillates in phase with the external force if the frequency is below resonance, and 180° out of phase if the frequency is above. If the electric field is spatially inhomogeneous, then averaged over one cycle of the optical radiation a net force on the atom can result. Some proposals for trapping atoms with optical fields are based on the use of the dipole force.

Laser cooling of free atoms

Laser cooling based on the use of the scattering force can be explained as follows: Consider an atom with a strongly allowed resonance transition. For simplicity, let this be the lowest-frequency transition, so that if this transition is excited, the atom must decay to the ground state. A laser beam whose frequency is close to but lower than the atomic resonance frequency irradiates the atom. If the atom is moving against the laser beam, then the frequency of the light in the rest frame of the atom is Doppler shifted toward resonance. Hence, the scattering force is higher for an atom moving against the laser beam, and the atom's velocity is damped. In this way, the velocity of an atomic beam can be reduced substantially.

If only one laser beam is used and the atom is otherwise free, the atom will eventually turn around and move away parallel to the beam. Therefore, for a gas of atoms, if another laser beam of equal intensity and frequency but opposite direction is introduced, atoms with their velocities in the other direction also have their speeds reduced. The intensities must be equal for the average scattering force on a motionless atom to be zero; if the intensities are not equal, the atoms will have a net drift velocity. One can obtain cooling in all directions by using three orthogonal pairs of counterpropagating laser beams. However, because of the inherent fluctuations of the scattering force, the velocity is not damped to zero.

The theoretical minimum temperature that can be obtained is given by a balance between the dissipation and fluctuations.[2,11] Assume the laser intensity is below saturation, even when tuned to resonance. We also assume that the recoil energy R, given by $(\hbar k)^2/2m$, is less than $\hbar\gamma$. The recoil energy is the kinetic energy that an initially motionless atom of mass m would have due to its recoil after emitting a photon of wavevector k. The minimum temperature T_{min} is achieved when the laser frequency is tuned below the atomic resonance frequency by an amount equal to $\gamma/2$, in which case[2,11]

$$kT_{min} = \tfrac{1}{2}\hbar\gamma \qquad (1)$$

For a decay rate γ of 10^8/sec, the minimum temperature is about 0.38 mK.

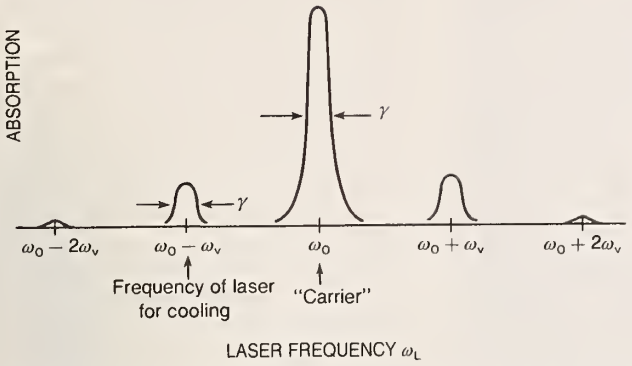

Absorption as a function of laser frequency. In the sideband cooling limit, the oscillation frequency ω_v of the atom in the trap is assumed to be larger than the radiative decay linewidth γ. Therefore the absorption spectrum consists of a "carrier," or recoilless line, at the atom's rest frequency ω_0 plus Doppler-effect sidebands separated by the frequency ω_v. If the laser is tuned to $\omega_0 - \omega_v$, the atom absorbs photons of energy $\hbar(\omega_0 - \omega_v)$ and re-emits photons of average energy $\hbar\omega_0 - R$, where the recoil energy R is $(\hbar k)^2/2m$. When R is much less than $\hbar\omega_v$ there is an energy deficit of approximately $\hbar\omega_v$ per scattering event, causing a decrease in the kinetic energy of the atom.

The laser cooling effects just described rely only on the scattering force. There is another cooling effect, called "stimulated cooling," which is due to the dipole force in a strong standing wave.[12] It is effective only for low atomic velocities and requires that the laser frequency be higher than the transition frequency. In a high-intensity, nearly resonant field, the simplest description of the atom–field system is in terms of dressed-atom states, which are coherent superpositions of the ground state atom with $n+1$ photons in the field and the excited state atom with n photons. The dressed-atom states depend on the light intensity, and hence on spatial position. The various dressed-atom states are either attracted to or repelled from regions of high light intensity. The rate of spontaneous decay, which leads to transitions between different dressed-atom states, is proportional to the admixture of excited atomic states in the dressed-atom state. It turns out that for positive laser detuning, the time-averaged dipole force opposes the velocity of the atom. It should be possible to decelerate or accelerate beams of atoms by changing the relative frequencies of two counterpropagating laser beams to create a moving standing wave. Atoms with velocities close to that of the standing wave could be swept along with the standing wave. An advantage of the dipole force is that it continues to increase as the intensity increases, while the scattering force approaches a limiting value when the scattering rate is about $\gamma/2$. However, the minimum achievable temperature using stimulated cooling is no lower than that given by equation 1.

Laser cooling of trapped atoms

For trapped atoms, the theoretical limit to cooling is the same as for free atoms when the natural linewidth γ of the atomic transition used for cooling is much greater than the motional frequency ω_v of the atom in the trap. The reason for this is that the atom is essentially free during the time required to scatter a photon. This is the usual experimental case for a strongly allowed transition. For trapped atoms it is not necessary to have opposed beams with equal intensities, because the average light pressure just displaces the equilibrium position of the atom slightly. It is possible to cool with a single laser beam as long as none of the normal modes of oscillation in the trap are perpendicular to the direction of propagation of the beam.

In the opposite limit, where the natural linewidth of the transition is much less than the motional frequencies, the cooling limit is different.[2,11] The absorption spectrum of the atom consists of an unshifted resonance line at frequency ω_0, called the carrier, and a series of discrete lines on both sides of the carrier, each having the natural linewidth and separated by multiples and combinations of the motional frequencies. These extra lines, called motional sidebands, are due to the periodic frequency modulation of the light owing to the Doppler effect as observed by the moving atom.

To cool a trapped atom, one tunes a narrow-band laser to a sideband on the low-frequency side of the unshifted resonance, for example, to a frequency $\omega_0 - p\omega_v$, where p is an integer. The atom makes transitions to the upper electronic state, decreasing its vibrational energy, by absorbing photons of energy $\hbar(\omega_0 - p\omega_v)$. When the atom makes a transition back to its ground electronic state, it may, in general, either increase or decrease its vibrational energy, but the average change in the vibrational energy is equal to the recoil energy R. When R is less than $p\hbar\omega_v$, cooling occurs.

Consider a particular case. A single ion is trapped in a nearly isotropic three-dimensional harmonic potential well, a situation that is approximated[13] by an ion in an rf trap, or Paul trap, with normal-mode vibrational frequencies all approximately equal to ω_v. A quantum state of the atom in the well is identified by its internal quantum numbers and the set of harmonic oscillator quantum numbers $\{n_x, n_y, n_z\}$ corresponding to the well. Three laser beams propagate along the x, y and z axes, and each is tuned to the corresponding first lower sideband. We assume that the recoil energy R is much less than the energy $\hbar\omega_v$, a condition that is not hard to satisfy in practice. In the steady state, the mean values of the quantum numbers are[11]

$$\begin{aligned}\langle n_x\rangle &\simeq \langle n_y\rangle \simeq \langle n_z\rangle \\ &\simeq {}^5\!/_{16}(\gamma^2/\omega_v{}^2) \\ &\ll 1\end{aligned} \qquad (2)$$

There are two reasons that the mean values do not go to zero with laser cooling. First, the average change R in the atom's vibrational energy after it

Stopping sodium atoms with light. A beam of sodium atoms approaching the camera from the upper right at speeds exceeding 1000 m/sec is brought to a virtual standstill by a laser beam aimed in the opposite direction. In this experiment at NBS, Gaithersburg, the atoms travel down the axis of a solenoid (whose opening appears as the dark circle at the center of the photograph) and spread out as they come to a virtual halt near the opening.[18]

emits a photon is positive. Second, there is some probability of driving a transition that leads to an increase in vibrational energy on absorption rather than a decrease, because the neighboring sidebands, although far from resonance, still have finite intensities. The simple theory just outlined applies when the cooling transition is not saturated. Markus Lindberg at the University of Frankfurt and Juha Javanainen and Stig Stenholm at the University of Helsinki have calculated the steady state for an arbitrary ratio of natural linewidth to motional frequency and also for arbitrary laser intensity.[14] As in the case of free atoms, the lowest temperatures are achieved in the limit of low intensity, so the simple theory is usually adequate.[2,11]

Experiments on trapped ions

It is perhaps not surprising that the first laser cooling experiments were on trapped ions, because ions can be held for long periods in high vacuum with a fairly high degree of thermal isolation.[13] Therefore, unlike in the case of neutral atoms, a long time is available to do the cooling.

The first laser cooling experiments were done in 1978. At the National Bureau of Standards in Boulder, Robert Drullinger, Fred Walls and Wineland demonstrated cooling by a direct observation of ion temperature, which they determined from the currents that ion motion induces in trap electrodes. They observed the cooling of Mg^+ ions to 40 K in a Penning trap.[11,13] At the same time in Heidelberg, Werner Neuhauser, Martin Hohenstatt, Peter Toschek and Dehmelt demonstrated cooling of Ba^+ ions in a Paul trap by observing the ions' increased storage time in the trap.[15]

In subsequent experiments at these and other laboratories, physicists have measured temperatures on the order of 10 mK or less. They have typically determined the temperatures by measuring the contribution of Doppler broadening to spectral lines. For strongly allowed electric dipole transitions, this method is not very sensitive at low temperatures because Doppler broadening contributes only a small fraction of the overall linewidth. For positive magnesium-24 ions at 1 mK, for example, the Doppler broadening of the first resonance line (at 280 nm) is only 0.5 MHz, while the natural radiative linewidth $\gamma/2\pi$ is 43 MHz. One realizes a more sensitive measurement of temperature by probing a transition with a linewidth γ that is much less than the motional oscillation frequency ω_v of an ion in the trap.[15] Here one can use the strength of the motional sidebands to determine the ion temperature.[16] So far, only cooling in the limit $\gamma \gg \omega_v$ (equation 1) has been demonstrated for ions, but if cooling in the limit $\omega_v \gg \gamma$ is used, it should be possible to reduce the kinetic energy to nearly the zero-point energy (equation 2). Laser cooling of trapped ions is now done in laboratories at NBS in Boulder, Hamburg University, the University of Washington in Seattle, the University of Paris in Orsay, the National Physical Laboratory at Teddington in England and the Max Planck Institute at Garching in West Germany. Other laboratories are setting up similar experiments.

Single ions. Single, laser-cooled, trapped ions are interesting because they provide a simple system for study. First, the oscillation frequencies of an ion in a trap are nearly harmonic, which makes spectra of single ions particularly simple. In contrast, if two or more ions are stored together in a trap, the oscillation frequencies of the individual ions are dominated by ion–ion interactions at low temperature. Second, the lowest possible kinetic energies, given by equations 1 and 2, are obtained for single ions. This is because part of the motion in the Paul trap (the rf-driven micromotion) or in the Penning trap (the magnetron or rotation motion) is nonthermal and not affected in the same way by laser cooling.[13] The kinetic energy in these nonthermal motions can be minimized for single ions. Finally, the simplicity of single trapped ions allows a straightforward comparison of laser cooling theory and experiment.

Single ions are also interesting from the standpoint of spectroscopy because the perturbations in spectral measurements can be extremely small or well controlled.[2,11] Historically, the most difficult problem in high-accuracy ion trap spectroscopy has been minimizing the second-order Doppler frequency shift, which is due to relativistic time dilation.[2,11,13] Reducing this systematic effect requires low temperatures. Experimenters have achieved temperatures of about 10 mK or less with single Ba^+ ions at Hamburg University, with single Mg^+ and Ba^+ ions at the University of Washington, with single Mg^+ and Hg^+ ions at NBS in Boulder and with single Mg^+ ions at Garching. At a temperature of 10 mK, an ion with mass 100 u has a fractional second-order Doppler shift of -1.4×10^{-17}, which is almost negligible. Single la-

ser-cooled ions have also allowed detailed studies to be made of the interaction between atoms and radiation, as seen, for example, in quantum "jumps" and in photon "antibunching," an effect in which the distribution of arrival times of fluorescence photons at a detector is nonclassical because atoms can emit only one photon at a time.

Liquid and solid plasmas. Large numbers, or "clouds," of trapped ions are more properly referred to as non-neutral ion plasmas.[17] These plasmas are interesting because, unlike fusion plasmas, they can reach a global thermal equilibrium. When these plasmas can be laser cooled, the densities are high enough—above $10^7/cm^3$—and the temperatures are low enough—less than 10 mK—that the plasmas become strongly coupled and should show liquid and solid behavior.[17] It should be possible to obtain non-neutral plasmas whose dynamics are dominated by quantum effects—for example, a positron plasma "sympathetically" cooled with laser-cooled ions of beryllium-9, as described below.

Even though single ions give the lowest temperatures, larger samples of laser-cooled trapped ions have already yielded interesting spectroscopic results. Spectroscopy[11] in the rf and microwave regions has featured linewidths of 0.01 Hz and fractional inaccuracies as small as 1 part in 10^{13}.

Sympathetic laser cooling. Unfortunately, direct laser cooling of ions and neutral atoms is relatively easy only for a very few elements. Sodium is often the practical choice for neutral atom researchers; singly ionized magnesium, which is isoelectronic with sodium, is a favorite choice for ion trappers. So far both groups have avoided working with molecules. The reason is simply that if one drives a suitably allowed transition at a convenient wavelength in a molecule, the molecule quickly becomes optically pumped into a state of different vibrational or rotational quantum number and cooling stops.

One can extend laser cooling to other species of ions by storing two ion species in the same trap. The species that is easy to laser cool will cool the second species through Coulomb collisions, making the second species available for high-resolution spectroscopic investigation or other experiments. Under typical conditions, ion–ion thermalization by Coulomb coupling takes place in less than a second. As a demonstration of this technique, Hg^+ ions have been cooled to less than 1 K by laser-cooled ions of beryllium-9 in a Penning trap.[17] It should be possible to extend sympathetic cooling in order to cool neutral atoms or molecules by ion–atom or atom–atom collisions.

'**Optical molasses**' holding approximately 2×10^5 sodium atoms at a temperature of about 240 μK. The atomic sample, which is the orange ball in the photograph, is at the intersection of six collimated laser beams that form the optical molasses. It is made visible by the light that the atoms scatter out of the laser beams. The "ball" of atoms is roughly 7 mm in diameter. The green light is from a pulsed laser used to evaporate sodium atoms from the solid.[20] (Photograph courtesy of Bell Laboratories.)

Experiments on neutral atoms

If neutral atoms could be trapped easily and held in thermal isolation from the surroundings, then laser cooling them would be similar to laser cooling ions. Unfortunately, neutral-atom traps with the required thermal isolation are not very deep. For example, magnetic traps, which convert the atom's kinetic energy into internal, Zeeman energy, at best have a depth of about 5×10^{-4} eV, or 8 K. This assumes that an atom with a magnetic moment equal to one Bohr magneton is captured in a magnetic well that is 10 T deep. Ion traps, in contrast, can be kilovolts deep.

Most neutral-atom laser cooling experiments start with an atomic beam of an alkali such as sodium and slow and cool the beam with a counterpropagating laser beam.[18] Because sodium atoms are emitted from an oven source with a velocity of about 1000 m/sec, the slowing and cooling must be done very efficiently to stop the atoms before they strike some portion of the apparatus. Even at maximum cooling efficiency, this requires about 50 cm. The first neutral-atom cooling experiments were reported by S. V. Andreev, Victor Balykin, Vladilen Letokhov and Vladimir Minogin in Moscow and by William Phillips and Harold Metcalf at NBS in Gaithersburg, Maryland. The Moscow group saw beam slowing and velocity compression due to a counterpropagating fixed-frequency laser beam. If a fixed-frequency laser beam is used, atoms with velocities that put them in resonance with the laser through the first-order Doppler frequency shift are efficiently slowed. However, these atoms are soon slowed enough that they are Doppler shifted out of resonance with the laser beam and the slowing is greatly reduced. Similarly, faster atoms are slowed only very slightly. The result is that a hole is carved out of the atoms' velocity distribution at a velocity corresponding to the Doppler-shifted laser frequency, and the affected atoms tend to bunch at slightly lower velocity.

To make the cooling more efficient, one needs a way to keep the atoms in resonance with the laser while they are slowed down. The NBS group accom-

plished this by continuously tuning the atoms' frequency. Investigators from the group directed the atomic beam down the bore of a solenoid whose magnetic field varied with position. The field varied in such a way as to keep the slowed atoms, whose Zeeman frequency shift depended on position in the magnet, continuously in resonance with the fixed-frequency laser beam. This enabled more of the atoms to be slowed to lower velocities. Recent experiments at MIT have also used this technique.

Another way to keep the atoms tuned to the frequency of the laser is to sweep, or "chirp," the frequency at an appropriate rate. The first demonstration of beam slowing by this technique was made in 1983 at NBS, Gaithersburg. Physicists at the Joint Institute for Laboratory Astrophysics later used the same technique to slow and stop atoms.[19] Subsequent experiments at Bell Laboratories,[20] Bonn University, the State University of New York at Stony Brook, the Ecole Normale Supérieure in Paris and by another group at JILA[21] have employed laser chirping for cooling. The latter experiments at JILA accomplished slowing and cooling using diode lasers, demonstrating that cooling at a relatively low cost is practical. With these techniques, atoms are now stopped (and even turned around) in several of the above laboratories. Temperatures of the stopped atoms are typically a few tens of millikelvins, and gravity starts to play a role because the slowed atoms are in the apparatus long enough to fall a significant distance.

The group at Bell Labs has demonstrated the lowest temperatures yet achieved through laser cooling.[20] Researchers there used a chirped laser to precool sodium atoms from a pulsed laser ablation source. They then subjected these atoms to three mutually orthogonal, intersecting pairs of counterpropagating laser beams of cross section about 1 cm^2, tuned to achieve minimum temperature. The region of intersection features a laser cooling damping force in all directions. The accompanying recoil heating causes the atoms to undergo Brownian motion. The diffusion time for atoms to leave this "optical molasses" can be on the order of 1 sec, which is plenty of time for many experiments. By rapidly turning the molasses off and on, the Bell Labs group was able to measure the velocities of the atoms and determine that the temperature was 240 μK (with a probable range of 180–440 μK), which is in agreement with the limit implied by equation 1.

Now that sources of slow atoms exist, they can be used as injection sources for the relatively shallow neutral-atom traps. Phillips and his coworkers were the first experimenters to capture atoms in a magnetic trap.[18] (Wolfgang Paul and his collaborators had held neutrons in a magnetic trap in 1978.) The MIT group recently used a different magnetic trap to hold atoms.[22] The Bell Labs group has used their optical molasses to inject atoms into a gradient-force or dipole-force laser trap.[20] In Moscow, Balykin and A. I. Sidorov have demonstrated cooling in two dimensions by collimating atomic beams.[23] The Paris group recently demonstrated stimulated cooling by its effect on the collimation of atomic beams.[24]

In principle, one could apply laser cooling to normal solids. For example, crystals that are doped with impurity ions could be driven on the lower phonon sidebands of certain transitions. Unfortunately, nonradiative decay from the upper level of the cooling transition, which shows up as heat, may dominate the cooling process. It is interesting to examine the economics of large-scale laser cooling. If substantial cooling requires about 10^4 scattering events per atom, then cooling one mole of material will require more than 10^9 joules of laser energy. Therefore, laser cooling may not be practical on a large scale, but in many cases it may be the only way to lower or manipulate the velocities of atomic samples. Judging by the number of laboratories now using laser cooling or setting up experiments using laser cooling, it appears likely that the technique will have many interesting applications in the future.

* * *

We acknowledge the support of the Office of Naval Research and the Air Force Office of Scientific Research.

References

1. T. W. Hänsch, A. L. Schawlow, Opt. Commun. 13, 68 (1975). D. J. Wineland, H. Dehmelt, Bull. Am. Phys. Soc. 20, 637 (1975).
2. H. Dehmelt, in *Advances in Laser Spectroscopy*, F. T. Arecchi, F. Strumia, H. Walther, eds., Plenum, New York, (1983), p. 153.
3. D. J. Wineland, W. M. Itano, J. C. Bergquist, J. J. Bollinger, J. D. Prestage, in *Atomic Physics 9*, R. S. Van Dyck Jr, E. N. Fortson, eds., World Scientific, Singapore (1984), p. 3. D. J. Wineland, Science **226**, 395 (1984).
4. E. F. Nichols, G. F. Hull, Phys. Rev. **13**, 307 (1901). P. Lebedev, Ann. Phys. (Leipzig) **6**, 433 (1901); Ann. Phys. (Leipzig) **32**, 411 (1910).
5. A. Einstein, Phys. Z. 18, 121 (1917).
6. O. Frisch, Z. Phys. **86**, 42 (1933).
7. A. Ashkin, Phys. Rev. Lett. **24**, 156 (1970). G. A. Askar'yan, Zh. Eksp. Teor. Fiz. **42**, 1567 (1962) [Sov. Phys. JETP **15**, 1088 (1962)]. A. P. Kazantsev, Zh. Eksp. Teor. Fiz. **63**, 1628 (1972) [Sov. Phys. JETP **36**, 861 (1973)]. V. S. Letokhov, Pis'ma Zh. Eksp. Teor. Fiz. **7**, 348 (1968) [JETP Lett. **7**, 272 (1968)].
8. A. Kastler, J. Phys. Radium **11**, 255 (1950).
9. The following are review articles on laser cooling and related phenomena: S. Stenholm, Rev. Mod. Phys. **58**, 699 (1986). A. Ashkin, Science **210**, 1081 (1980). V. S. Letokhov, V. G. Minogin, Phys. Rep. **73**, 1 (1981). A. P. Kazantsev, G. A. Ryabenko, G. I. Surdutovich, V. P. Yakovlev, Phys. Rep. **129**, 75 (1985).
10. J. P. Gordon, A. Ashkin, Phys. Rev. A **21**, 1606 (1980). R. J. Cook, Phys. Rev. A **22**, 1078 (1980). V. G. Minogin, Zh. Eksp. Teor. Fiz. **79**, 2044 (1980) [Sov. Phys. JETP **52**, 1032 (1980)].
11. D. J. Wineland, W. M. Itano, Phys. Rev. A **20**, 1521 (1979). W. M. Itano, D. J. Wineland, Phys. Rev. A **25**, 35 (1982).
12. A. P. Kazantsev, V. S. Smirnov, G. I. Surdutovich, D. O. Chudesnikov, V. P. Yakovlev, J. Opt. Soc. Am. B **2**, 1731 (1985). J. Dalibard, C. Cohen-Tannoudji, J. Opt. Soc. Am. B **2**, 1707 (1985).
13. H. Dehmelt, Adv. At. Mol. Phys. **3**, 53 (1967); Adv. At. Mol. Phys. **5**, 109 (1969). D. J. Wineland, W. M. Itano, R. S. Van Dyck Jr, Adv. At. Mol. Phys. **19**, 135 (1983).
14. M. Lindberg, J. Phys. B **17**, 2129 (1984). J. Javanainen, M. Lindberg, S. Stenholm, J. Opt. Soc. Am. B **1**, 111 (1984).
15. W. Neuhauser, M. Hohenstatt, P. Toschek, H. Dehmelt, Phys. Rev. Lett. **41**, 233 (1978); Phys. Rev. A **22**, 1137 (1980).
16. G. Janik, W. Nagourney, H. Dehmelt, J. Opt. Soc. Am. B **2**, 1251 (1985). J. C. Bergquist, W. M. Itano, D. J. Wineland, Phys. Rev. A (1987), to be published.
17. J. H. Malmberg, T. M. O'Neil, Phys. Rev. Lett. **39**, 1333 (1977). L. R. Brewer, J. D. Prestage, J. J. Bollinger, D. J. Wineland, in *Strongly Coupled Plasma Physics*, F. J. Rogers, H. E. DeWitt, eds., Plenum, New York (1987), to be published. D. J. Larson, J. C. Bergquist, J. J. Bollinger, W. M. Itano, D. J. Wineland, Phys. Rev. Lett. **57**, 70 (1986).
18. W. D. Phillips, H. J. Metcalf, Sci. Am., March 1987, p. 50. P. Meystre, S. Stenholm, eds., *The Mechanical Effects of Light*, J. Opt. Soc. Am. B **2**(11) (1985).
19. W. Ertmer, R. Blatt, J. L. Hall, M. Zhu, Phys. Rev. Lett. **54**, 996 (1985).
20. S. Chu, L. W. Hollberg, J. E. Bjorkholm, A. Cable, A. Ashkin, Phys. Rev. Lett. **55**, 48 (1985). S. Chu, J. E. Bjorkholm, A. Ashkin, A. Cable, Phys. Rev. Lett. **57**, 314 (1986).
21. R. N. Watts, C. E. Wieman, Opt. Lett. **11**, 291 (1986).
22. V. S. Bagnato, G. P. Lafyatis, A. G. Martin, E. L. Raab, D. E. Pritchard, Phys. Rev. Lett. (1987), to be published.
23. V. I. Balykin, A. I. Sidorov, Appl. Phys. B **42**, 51 (1987).
24. A. Aspect, J. Dalibard, A. Heidmann, C. Salomon, C. Cohen-Tannoudji, Phys. Rev. Lett. **57**, 1688 (1986). □

Simple electrodes for quadrupole ion traps

Earl C. Beaty
National Bureau of Standards, 325 Broadway, Boulder, Colorado 80303

(Received 23 September 1986; accepted for publication 19 November 1986)

Quadrupole traps for charged particles often involve electrodes with portions carefully machined to the shape of hyperboloids. It is shown here that the more important features of such traps can be achieved using electrode shapes which are much easier to fabricate. Detailed numerical calculations are reported on some sample electrodes. The numerical method can be easily extended to other shapes which accommodate specialized laboratory situations.

I. INTRODUCTION

Quadrupole ion traps are used in a wide variety of research applications. It is well known that it is not possible to construct static electric fields which will trap ions in all three dimensions. However, it is possible to build an effective trap by either adding a magnetic field[1] (Penning trap) or by making the electric field time dependent[2] (Paul trap). For many applications it is desirable to achieve a special electric-potential function which is referred to below as the "ideal." It is generally desirable for the electric-potential function to have both cylindrical and reflection symmetry. With these symmetry restrictions, a general potential can be expressed in the form,

$$V(r,z) = C_0 + C_2H_2(r,z) + C_4H_4(r,z) + C_6H_6(r,z) + C_8H_8(r,z) + \dots , \quad (1)$$

where

$$H_2(r,z) = (2z^2 - r^2)/s^2 ,$$

$$H_4(r,z) = (8z^4 - 24z^2r^2 + 3r^4)/s^4 ,$$

$$H_6(r,z) = (16z^6 - 120z^4r^2 + 90z^2r^4 - 5r^6)/s^6 ,$$

$$H_8(r,z) = (128z^8 - 1792z^6r^2 + 3360z^4r^4 - 1120z^2r^6 + 35r^8)/s^8 .$$

The H_j functions (spherical harmonics) are homogeneous polynomials in z/s, r/s with the numerical coefficients chosen so that each satisfies the Laplace equation. The C_j are constants (independent of position) with the units of potential, and s is a distance to be chosen to suit the circumstances of the problem. The ideal potential referred to above corresponds to the first two terms of this expansion. A special quality of the ideal potential is that the equations of motion of trapped particles are particularly simple. For instance, for the Paul trap, the r and z components have separate equations of motion, making it relatively easy to specify stability criteria. Also, in a Penning trap, the ideal potential yields axial, cyclotron, and magnetron frequencies which are independent of the amplitude of excitation (neglecting relativistic effects). Thus a trap with the ideal potential is sometimes described as "harmonic." Some relatively recent reviews cover both the operations and the applications.[3,4]

II. THE PROBLEM

To achieve the ideal potential represented by the first two terms of Eq. (1), three electrodes are needed, each a hyperboloid (and therefore infinite in extent). The electrodes which produce the ideal potential are referred to below as ideal electrodes. The three electrodes, each conforming to an equipotential surface of the ideal potential function, consist of a central "ring" electrode and "endcaps" on either side. Some errors are caused by making finite electrodes; however, these can be minimized by careful treatment of the truncation boundaries.[5] The hyperbolic electrodes are difficult to fabricate and for many purposes it is worth considering a much simpler shape. The purpose of this paper is to point out that it is possible to achieve a good approximation to the ideal with very simple electrodes.

The electrode structures examined below have the same general topology as the ideal electrodes. They have cylindrical and reflection symmetry, and involve a region of space substantially surrounded by a ring and two endcaps. To preserve the reflection symmetry, the two endcap electrodes must have the same potential (assuming they have the same shape). By appropriate choice of the potentials of the two free electrodes, it is possible to make C_0 and C_2 match any preset conditions. To make the other terms small with a three-electrode system, it is necessary to choose the shapes of the electrodes carefully. A more general version of Eq. (1) involves terms with odd powers of z and r, and also terms involving the angle coordinate. Such terms are not included here because it is easy to choose experimental conditions which, in principle, make them zero. If the electrodes and applied potentials have reflection symmetry, the odd-order terms will all be zero, and if the electrodes have cylindrical symmetry, the terms involving the angle coordinate all vanish. In practice, errors in fabrication or mounting (also nonuniform contact potentials) can cause these terms to be nonzero. The term of order one $[C_1H_1(r,z)]$ caused by these laboratory errors can be made small by either choosing a different origin of coordinates for the expansion, or by making the endcap potentials unequal. If the machining and mounting are precise enough to make the third-order term small, then it is appropriate to look for electrode shapes which make the fourth-order term small.

Some example calculations are reported below to show that simple electrodes are capable of adequately producing the ideal potential over a substantial volume. The basic computational method as it applies here is described in some detail in Ref. 5. The general method has previously been used by Harting and Read[6] for electron lens calculations. Only a brief summary of the method is given here. In this

TN-163

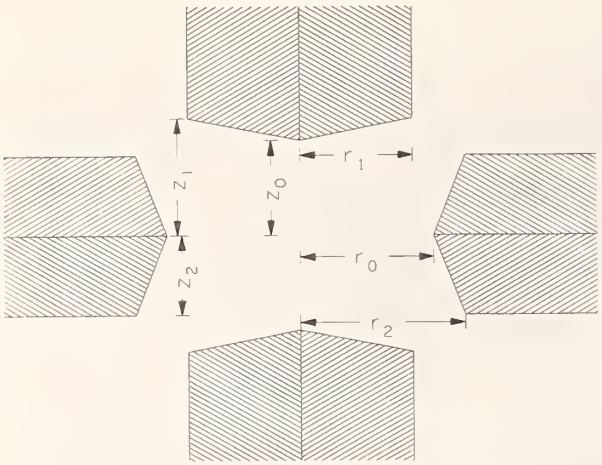

FIG. 1. A drawing of the trap geometry examined in this paper. The electrodes are cylindrically symmetric about the z axis.

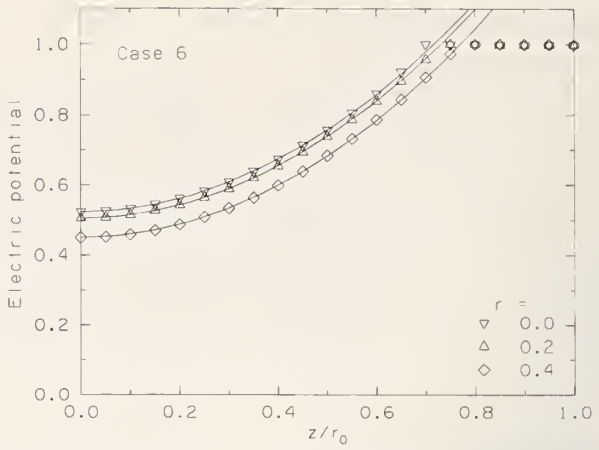

FIG. 2. Sample plot of the potential function $V(r,z)$ vs z for three values of r.

procedure the surface-charge density on all the electrode surfaces is determined numerically, using the condition that the potential is known on all the electrode surfaces. Then either the C_j or the potential can be calculated by application of Coulomb's law. The numerical representation of the surface-charge density involves the arbitrary division of the electrode surfaces into N small areas each of which has approximately uniform surface charge density across it. The surface-charge distribution is represented by giving N numbers, each of which provides the assumed constant surface-charge density on one of the surface elements. One of the principal computational chores is the solution of N linear algebraic equations. The values of N used were of the order of 100. Much larger values of N require a large amount of computation time and tend to cause digital truncation error to be a significant problem. Much smaller values of N cause unacceptable errors in the results.

III. RESULTS

A diagram of the example electrode shape examined in this paper is displayed in Fig. 1. Detailed calculations of the surface-charge densities have been carried out for a variety of the variables defined in Fig. 1. By using a simple search procedure it is easy to find values of the dimensions which yield small values of C_4. It is even reasonable to search for conditions which make C_6 small also. In the following discussion, all dimensions are given relative to r_0 and the length variables are therefore treated as dimensionless.

The C_j are each linear functions of each of the electrode potentials. The zero of potential is arbitrary and here the potential is assumed to approach zero far from the electrodes. For the purposes of this paper it is not necessary to have a completely general solution. The values of C_j were calculated for a specific set of potentials on the electrodes. These special values of C_j are called A_j. The reference set of potentials are 0 for the ring and 1 for the endcaps (as defined here the A_j have the same units as the endcap potential). Scaling the results to other values of the endcap potential is straightforward. These results cannot be generally scaled to other ring potentials; however, in most circumstances it is only the potential difference between the endcaps and the ring which is important (for a more complete discussion see Ref. 5). A general solution would involve generating a second set of C_j with other values for the electrode potentials, including a nonzero value for the ring potential. The distance s in Eq. (1) is assigned the value r_0. With these normalizations the set of A_j are functions of the shape of the electrodes and are independent of the size or the potentials which are applied to the electrodes in use.

Table I contains results for eight cases which have been found to yield $A_4 = A_6 = 0$. Figure 2 displays the potential for case six as a function of axial position. The data points in the graphs are the calculated values and the solid lines are the ideal potentials as represented by the first two terms of

TABLE I. Data for eight sets of values for the variables defined in Fig. 1. The dimensions were selected to yield $A_4 = A_6 = 0$. The dimensions specified have been scaled to the condition $r_0 = 1$. The A_j are the spherical harmonic expansion coefficients with normalized potentials on the electrodes.

	z_0	r_1	z_1	r_2	z_2	A_0	A_2	A_8
1	0.6122	0.8812	0.7952	1.1020	0.5913	0.545486	0.568051	0.002312
2	0.7000	0.6856	0.8182	1.0462	0.2678	0.497635	0.489588	0.000142
3	0.7000	0.6950	0.8197	1.1147	0.2949	0.508734	0.478829	0.000103
4	0.7000	0.7095	0.8224	1.3654	0.4438	0.524285	0.463748	0.000053
5	0.7000	0.7799	0.8518	1.1000	0.4000	0.492112	0.488948	0.000623
6	0.7071	0.8435	0.8728	1.2340	0.5956	0.493999	0.476988	0.000569
7	0.8000	0.7884	0.9356	1.2030	0.4569	0.441861	0.416657	0.000025
8	0.8000	0.8841	0.9683	1.2224	0.5573	0.435476	0.417169	0.000177

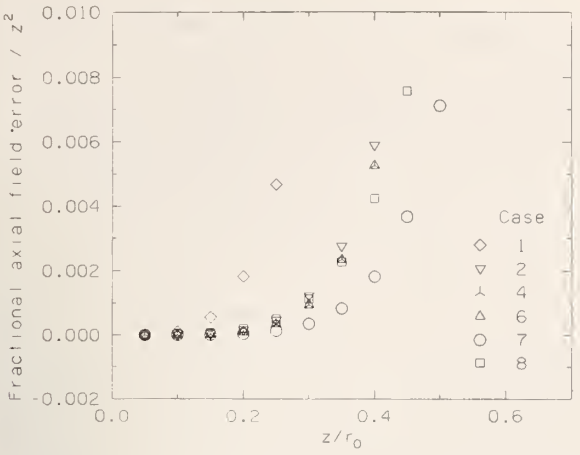

FIG. 3. Plot of E_f/z^2 vs displacement from the center of the trap. E_f is the fractional error in the electric field on the axis.

Eq. (1). Data are shown for $r = 0$, 0.2, and 0.4. Equation (1) with values of C_j derived from Table I can be used to calculate the potential near the center of the trap. Near the walls Eq. (1) is generally useless because too many terms contribute significantly to the sum. The data of Fig. 2 were calculated directly from the charge distributions without involving Eq. (1). The potential is reasonably close to the ideal all the way to the endcap.

The electric field on the z axis can be relatively easily calculated from the surface-charge distributions (the derivative of the potential can be done analytically). The electric field on the z axis corresponding to the ideal potential is $2A_2 z$. The fractional error in the electric field is given by

$$E_f = \left(\frac{\partial V}{\partial z} - 2A_2 z\right) \Big/ 2A_2 z$$

$$= 16\frac{A_4}{A_2} z^2 + 48\frac{A_6}{A_2} z^4 + 512\frac{A_8}{A_2} z^6 + \ldots .$$

Figure 3 is a plot of E_f/z^2 vs z for several of the cases of Table I. The limit of these curves as z goes to zero is $16A_4/A_2$, a quantity which is small by design. The field errors displayed in Fig. 3 are all positive because the electrode shape chosen here has a sharp point on the z axis. This point contributes particularly large fields in a small volume near the point. Away from the polar axis the electric field is not necessarily in the same direction as the ideal, making a comparison more difficult. While the departures from the ideal are more difficult to display in other regions, the data of Fig. 3 are reasonably representative. Two of the cases are not included in the plot because case 3 is similar to case 2, and case 5 is similar to case 6.

Case 7 of Table I has the best value of A_8/A_2 suggesting that it might be a particularly favorable choice. Actually, any of these cases may be difficult to implement with enough precision to make the eighth-order term the dominant error in a laboratory situation. Case 1 has a small ring-endcap gap providing good shielding from external fields. Cases 2, 3, and 4 have a relatively large ring-endcap gap allowing easy access with light beams, etc. Case 6, also relatively open, has already been used in an atomic spectroscopy application.[7] It may be helpful in visualizing the shapes to know that the diagram of Fig. 1 was drawn using the dimensions of case 6 from the table. For some purposes it would have been better to have a hole in the endcaps on the $r = 0$ axis (instead of a point), thereby reducing the electric-field anomaly and allowing a convenient access for ions, electron beams, etc. Such holes would not have greatly complicated the computations, and unless they were very large, they would not have interfered with making A_4 and A_6 small.

An investigation of the errors in the general method was reported in Ref. 5. Less extensive tests conducted in conjunction with the generation of the data of Table I confirm the general conclusion that the principal errors were due to representing the charge distribution on too coarse a grid. The grid used was kept relatively coarse to speed the calculation through the tedious search. Any small errors in the A_0 and A_2 can be easily compensated for by adjusting the potentials applied to the electrodes. Errors in the computation of A_4 and A_6 result in errors in the five length variables of Table I. The length data given in the table are estimated to have approximately four digit accuracy.

Might electrodes such as those of Fig. 1 be more sensitive to misalignments than hyperbolic electrodes? An easy and useful test is to make a small change in one of the dimensions and repeat the calculation to observe the change in the A_j. Tests made in conjunction with the work of Ref. 5 but not reported there yield the result that $\partial A_2/\partial z_0 = -0.72$ and $\partial A_4/\partial z_0 = 0.04$ for the case of ideal electrodes with $2z_0^2 = r_0^2$ (z_0 is the distance from the trap center to each of the endcaps). In changing z_0 both endcaps were displaced but their shape was not changed. Such tests were carried out both with truncated hyperbolas and with the design of Fig. 1. Some of the cases of Table I were found to have A_4 about twice as sensitive to this displacement as the ideal electrodes cited. Similar sensitivities were also found for truncated hyperbolas. A conclusion is that the electrodes examined here are not significantly more sensitive to laboratory errors than those with hyperbolic shapes.

In Fig. 1 the electrodes extend beyond the boundaries of the drawing. An assumption was made that in practice the portion off the drawing would involve wires and mounting brackets special to the particular installation. Thus, the impact of various ways of handling the remote portions was not systematically investigated. For the results of Table I electrodes were extended a short distance and simply terminated. In each case the straight boundaries parallel to the axes had a length of $1.5r_0$. To test the sensitivity to this dimension, some of the calculations were repeated with both ring and endcap extended by an additional $0.5r_0$. For cases 1, 4, and 7, the changes in A_4 were $(-1, -17, -10)\times 10^{-5}$, respectively. Generally, increasing the size of the endcap increases A_4, and expanding the ring decreases it. If the ring and endcap are close together, the region near the center of the trap is shielded from charges on the more remote parts of the electrodes. For cases where the intrinsic shielding is inadequate a reasonable step is to insert a relatively large extra electrode and empirically adjust its potential to produce optimum performance.

IV. DISCUSSION

Some general comments can be made about the use of the data of Table I in applications needing the ideal potential. In a common form of the problem the potential must approximate the ideal to some specified tolerance over a specified volume. This means that C_0 and C_2 have specified values, and limits are available for the other C_j. To meet these requirements with hyperbolic electrodes is straightforward with the condition that the minimum electrode size be large enough not to intrude on the specified volume. To meet these requirements with the electrodes of Fig. 1, it is necessary to have larger values of r_0 and z_0 (perhaps by a factor of 2 or 3) and therefore higher potentials.

An application where simple electrodes might be useful is mass spectroscopy. In one kind of mass spectrometer, the electric potentials are made time dependent in such a way that ions with small masses have unstable orbits for one reason, and ions with large masses have unstable orbits for another reason.[8] With the ideal potential the stability conditions are well defined and it is possible to create a situation in which only ions in a narrow mass range have stable orbits. Particles with unstable orbits leave the trap rather quickly. Also some of the particles in stable orbits are removed because the orbits intersect one of the electrodes. Many such traps have been built and found to give good service. It is clearly possible to arrange the electrodes of Fig. 1 (or other simple shapes) such that near the trap center the orbits of the ions and the stability conditions are not materially changed. A failing of the simple electrodes is that near the electrode surfaces the orbits are much more complex, blurring the distinction between stable and unstable orbits. Ions near the center which fail to meet the stability conditions will move out where the fringing field may produce stability or at least a long lifetime. The impact of this problem on mass resolution can't be easily evaluated. Fulford *et al.* and Mather *et al.*[9] experimentally investigated the performance of some traps that had cylindrical rings and plane endcaps. They found the mass resolution to be significantly lower than they were accustomed to finding with hyperbolic electrodes. It is not clear what the specific failing of the cylindrical traps was. The design has the endcap and ring quite close together, resulting in high electric fields in a place easily available to the trapped particles. Also, as implemented, the endcaps had large holes such that A_4 may not have been small.

In some precise atomic physics measurements the potential function must be very close to the ideal. In many of these experiments the precise fields are achieved by having a way to compress the cloud of ions into a relatively small volume near the center of the trap.[4] While the electrodes used have typically been modified hyperbolas, in some cases extra "compensation" electrodes have been added so that C_4 can be electrically adjusted to zero.[10] In many of these experiments it is important to closely approximate the ideal field near the trap center while giving little concern to irregularities near the electrodes. For this situation the design of Fig. 1 is quite appropriate. It might be desirable to add electrodes to a design such as that in Fig. 1 to allow compensation for some mounting errors. There is a significant need for the extra electrodes to have both reflection and rotation symmetry, with the penalty that it would be possible to compensate only those errors with these symmetries.

Gabrielse and MacKintosh[11] have examined the electrostatic properties of cylindrical traps where it is possible to solve the Laplace equation using series methods. They show that A_4 can be made zero by appropriate choice of the ratio of height to radius. They also consider the option of dividing the cylindrical ring electrode into three parts such that the outer two can be used as compensation electrodes. This arrangement allows the user to empirically adjust A_4 to zero after assembly is complete. This analysis is based on very small interelectrode gaps. While a practical design may require larger gaps and other holes, the adjustment should have enough latitude to cover these problems. This is a good example of how extra electrodes can be used to compensate for incomplete design information. For the case of the Penning trap the potentials normally do not vary rapidly with time and the potentials for the extra electrodes can be derived from a simple resistive divider network. In Paul traps, high-frequency potentials are needed and the divider network is not so easy to adjust. Also, in many applications the test for small A_4 is very difficult.

V. CONCLUSIONS

Normally the most effective way to generate a close approximation to the ideal potential distribution is to use hyperbolic-shaped electrodes. This is especially true if the application demands that the close approximation extend all the way to the electrodes. The only intrinsic problem with hyperbolic electrodes is the truncation. The truncation errors can be made small either by careful design[5] or by inserting compensation electrodes.[10] Practical problems with hyperbolic electrodes are that they are difficult to fabricate and, in some applications, it is necessary to make holes which spoil the ideal fields. The simple electrodes discussed above can, in some applications, be adequate and much easier to fabricate. With electrodes requiring only simple lathe cuts it is possible to be rather free with making access holes and special mounting fixtures, while preserving some of the more important features of the potential distribution. In circumstances where the dominant errors in the potential function are caused by alignment or machining errors, the simple electrodes may have a positive advantage.

ACKNOWLEDGMENTS

This work was supported in part by the U. S. Office of Naval Research and the U. S. Air Force Office of Scientific Research.

[1] F. M. Penning, Physica **3**, 873 (1936).
[2] E. Fischer, Z. Phys. **156**, 1 (1950); R. F. Wuerker, H. Shelton, and R. V. Langmuir, J. Appl. Phys. **30**, 342 (1959).
[3] H. G. Dehmelt, Adv. At. Mol. Phys. **3**, 53 (1967); **5**, 109 (1969); L. S. Brown and G. Gabrielse, Rev. Mod. Phys. **58**, 233 (1986).
[4] D. J. Wineland, Wayne M. Itano, and R. S. Van Dyck, Jr., Adv. At. Mol. Phys. **19**, 135 (1983).

[5]Earl C. Beaty, Phys. Rev. A **33**, 3645 (1986).
[6]E. Harting and F.R. Read, *Electrostatic Lenses* (Elsevier, Amsterdam, 1976).
[7]J. C. Bergquist, D. J. Wineland, Wayne M. Itano, Hamid Hemmati, H.-U. Daniel, and G. Leuchs, Phys. Rev. Lett. **55**, 1567 (1985).
[8]P. H. Dawson, *Quadrupole Mass Spectroscopy and its Applications* (Elsevier, Amsterdam, 1976).
[9]J. E. Fulford, R. E. March, R. E. Mather, J. F. J. Todd, and R. M. Waldren, Can. J. Spectros. **25**, 85 (1980); R. E. Mather, R. M. Waldren, J. F. J. Todd, and R. E. March, Int. J. Mass Spectrom. Ion Phys. **33**, 201 (1980).
[10]R. S. Van Dyck, Jr., D. J. Wineland, P. A. Ekstrom, and H. G. Dehmelt, Appl. Phys. Lett. **28**, 15 (1976); Gerald Gabrielse, Phys. Rev. A **27**, 2277 (1983); **29**, 462 (1884).
[11]G. Gabrielse and F. C. MacKintosh, Int. J. Mass Spectrom. Ion Phys. **57P**, 1 (1984).

TN-167

From: Proc. of the Cooling, Condensation, and Storage of Hydrogen Cluster Ions Workshop, SRI, Menlo Park, Ca., Jan., 1987; ed by J.T. Bahns, p. 181.

ION TRAPS FOR LARGE STORAGE CAPACITY*

D. J. Wineland
Time and Frequency Division
National Bureau of Standards
Boulder, Colorado 80303

ABSTRACT

Ion storage in Penning-type or rf (Paul)-type traps is discussed. Emphasis is given to low-energy, long-term confinement of high densities and large numbers of ions. Maximum densities and numbers are estimated using a low-temperature, static model of the ion plasmas in the traps. Destabilizing mechanisms are briefly discussed.

INTRODUCTION

The following notes are concerned with the storage of large densities and numbers of charged particles or ions in electromagnetic traps. Certainly, this is a small part of the problem concerned with the accumulation, storage, and manipulation of antimatter. However, this particular problem appears to be interesting by itself and may have interesting applications elsewhere.[1-3] Devices such as tokamaks and tandem-mirror machines for fusion plasmas are not discussed because we concentrate on long-term, low-energy confinement which is desirable for antimatter storage. For brevity, only Paul (rf) and Penning-type traps[4,5] are discussed. Maximum densities and maximum numbers of ions for one or a mixture of species with different charge to mass ratio are investigated.

GENERAL CONSIDERATIONS

We will assume that thermal equilibrium of the stored ion sample has been achieved. This condition may not always be achieved or desirable. For example, antihydrogen might best be made by passing antiprotons through positrons without thermal equilibrium between these two species being achieved. For long term storage, however, thermal equilibrium appears likely.

If we assume that the ion trap has symmetry about the z axis, the thermal equilibrium distribution function for the ith species can be written[6-9]

$$f_i = n_i \left(\frac{m_i}{2\pi k_B T}\right)^{3/2} \exp[-(H_i - \omega \ell_{z i})/k_B T]. \qquad (1)$$

*Contribution of the National Bureau of Standards; not subject to U.S. Copyright.

m_i is the ion mass, k_B is Boltzmann's constant, T is the ion temperature, and ω and n_i are constants (determined below). If a magnetic field is superimposed along the z axis ($\vec{B} = B\hat{z}$), then

$$H_i = m_i v_i^2/2 + q_i \phi(x) \tag{2}$$

is the ion energy and

$$\ell_{zi} = m_i v_{\theta i} r_i + q_i A_\theta(\vec{x}) r_i/c \tag{3}$$

is the ion canonical angular momentum. q_i and $\vec{v}_i$ are the ion charge and velocity, and $v_i = |\vec{v}_i|$. $v_{\theta i}$ and $A_{\theta i}$ are the θ components of the velocity and the vector potential, and r_i is the radial coordinate of the ion in cylindrical coordinates. $\phi = \phi_I + \phi_T + \phi_{ind}$ is the total potential, which is written as the sum of the potential that is due to ion space charge ϕ_I, the applied trap potential ϕ_T, and the potential, ϕ_{ind}, that is due to the induced charges on the trap electrodes.[9] We choose the symmetric gauge where $\vec{A}(\vec{x}) = \vec{B} \times \vec{x}/2$, so that $A_{\theta i} = Br_i/2$. We can therefore write the distribution function as

$$f_i(\vec{x},\vec{v}) = n_i(\vec{x}) \left(\frac{m_i}{2\pi k_B T}\right)^{3/2} \exp[-\tfrac{1}{2}m_i(\vec{v}_i - \omega r_i \hat{\theta})^2/k_B T], \tag{4}$$

where $n_i(\vec{x})$ is the ion density given by

$$n_i(\vec{x}) = n_i \exp\{-[q_i\phi(r,z) + \tfrac{1}{2}m_i\omega(\Omega_{ci} - \omega)r_i^2]/k_B T\}. \tag{5}$$

We assume that the trap potential is adjusted to make $\phi = 0$ at the origin, in which case n_i is the ion density at the center of the trap for a single ion species. From Eq. 4, we see that the ion cloud, or non-neutral ion plasma, rotates at frequency ω. $|\Omega_{ci}| = |q_i|B/m_i c$ is the cyclotron frequency. The signs of ω and Ω_{ci} indicate the sense of circulation where we use the right-hand rule. For example, Ω_{ci} is negative for positive ions ($q_i > 0$) and is positive for $q_i < 0$.

In the limit $T \to 0$, we must have $q_i\phi - m_i\omega(\omega - \Omega_{ci})r_i^2/2 \to 0$ for f_i to be well behaved. This condition and Poisson's equation imply that the charge density, ρ, at the position of the ions be given by

$$\rho = -\rho_i' + m_i\omega(\Omega_{ci} - \omega)/(2\pi q_i), \tag{6}$$

where ρ_i' is a fictitious charge density arising for rf traps since the pseudopotential does not satisfy Poisson's equation[9] (see below). By low temperature, we mean that the Debye length, λ_D, for the plasma given by[6-9]

$$\lambda_D^2 = k_B T/(4\pi n_i q_i^2), \tag{7}$$

is short compared to the plasma dimensions. From Eq. 7, we can write

$$\lambda_D \simeq 6.9(T/n_i)^{\frac{1}{2}}/Z \text{ cm}, \tag{8}$$

where T is expressed in kelvin, n_i is expressed in cm^{-3}, and Z is the ion charge in units of the proton charge. For T = 4 K, Z = 1, and $n_i = 10^8/cm^3$, $\lambda_D \simeq 14$ μm. Therefore, for the low temperatures desired for long term storage, the T→0 limit will usually be valid.

PENNING TYPE TRAPS

By Penning-type trap, we will mean that the trap is formed by a static magnetic field $\vec{B} = B\hat{z}$ and an axially symmetric electric trap potential, ϕ_T, of the form (in spherical coordinates)

$$\phi_T = \sum_k C_k r^k P_k(\cos\theta), \tag{9}$$

where C_k are constants and P_k is a Legendre polynomial of order k. Axial symmetry is particularly important for the Penning trap. If the trap is not axially symmetric, angular momentum can be coupled into the ions and they will diffuse out of the trap. If the trap is axially symmetric, angular momentum is a constant of the motion and stable ion clouds are maintained.[10] For spectroscopy,[4,5] particularly mass spectroscopy,[5,11,12] we desire $\phi_T \propto r^2 P_2(\cos\theta)$ as indicated in Fig. 1. This is because the ion motions (neglecting relativistic effects) will be harmonic. A fourth order trap where $\phi_T \propto r^4 P_4(\cos\theta)$ would look something like that in Fig. 2.

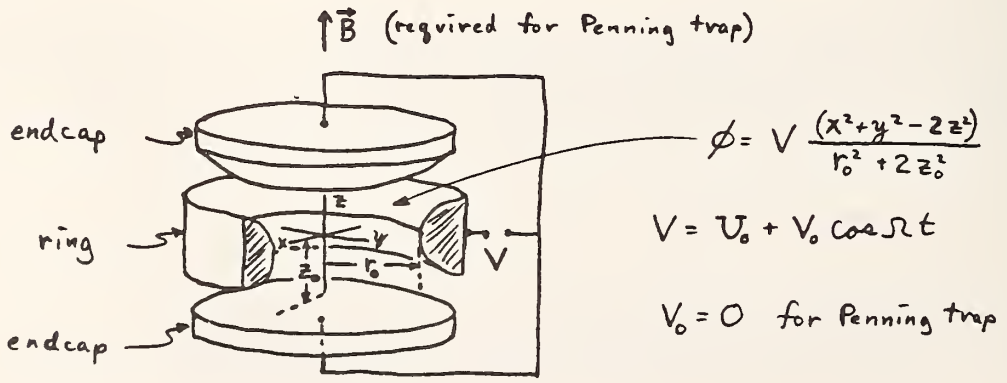

Fig. 1. Electrode configuration for the quadrupole rf (Paul) or Penning trap. Inner surfaces of electrodes are assumed to be equipotentials of ϕ, and the effect of truncating the electrodes is neglected. r_0 is the inner radius of the ring electrode and $2z_0$ is the endcap to endcap spacing.

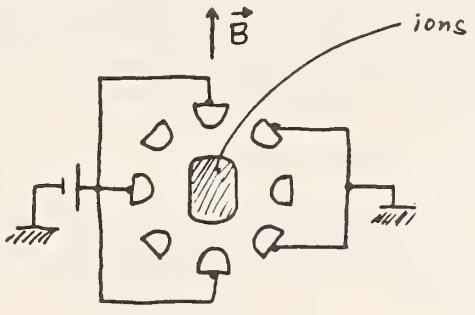

Fig. 2. Sketch of fourth order Penning-type trap for positive ions. The view shown is a cross section in the y-z plane.

An experimentally convenient geometry[1] might be a "cylinder trap" as shown in Fig. 3.

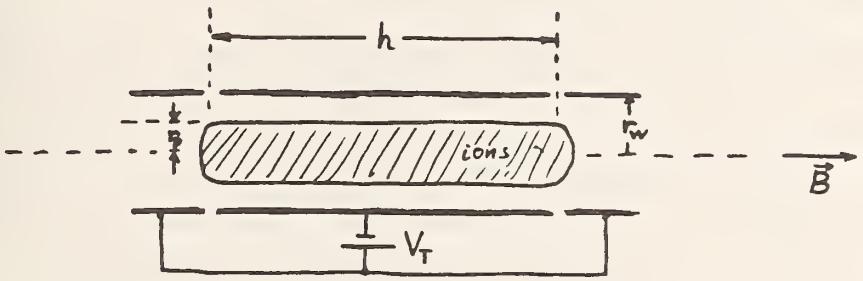

Fig. 3. Sketch of cylinder Penning-type trap for positive ions.

With $\rho_i'=0$, Eq. 6 can be written

$$n_i = m_i\omega(\Omega_{ci}-\omega)/(2\pi q_i^2). \tag{10}$$

Therefore, if we assume axial symmetry, n_i is independent of ϕ_T. Because of this, we will assume throughout that we are using the experimentally convenient geometry of the cylinder trap (Fig. 3). n_i is maximum for $\omega = \Omega_{ci}/2$, which is called the Brillouin limit.[6] ω may be determined by initial loading conditions or may be altered as discussed below. If we assume a single ion species and drop the indices,

$$n(\max) = B^2/(8\pi mc^2) \simeq 2.7 \times 10^9\ B(T)^2/M, \tag{11}$$

where B(T) is the magnetic field in tesla and M is the ion mass in u (atomic

mass units). n(max) is independent of Z. From Fig. 3 and Eq. 11, the maximum number of ions, N(max), is given by

$$N(max) \simeq 8.4 \times 10^9 \; r_p^2 h B(T)^2/M, \tag{12}$$

where r_p and h are the plasma radius and height in cm, respectively. The potential, ϕ_c, at the center of the plasma (assuming the central cylinder is grounded as in Fig. 3) is easily calculated to be[1]

$$\phi_c(V) \simeq 1.4 \times 10^{-7} \; NZ(1+2\ell n(r_w/r_p))/h, \tag{13}$$

where ϕ_c is given in volts. The magnitude of V_T must be higher than the magnitude of this potential to confine ions along the z axis. If we eliminate N from Eqs. 12 and 13, we obtain

$$r_p^2 = 8.3 \times 10^{-4} M\phi_c/(B(T)^2 Z(1+2\ell n r_w/r_p)). \tag{14}$$

For ϕ_c = 30 kV, B = 10T, r_p/r_w = 0.5, and Z = 1, we find $r_p^2 \simeq M/10$.

A few examples of n(max) and N(max) for these values of ϕ_c, B, and r_p/r_w are illustrated in table I. From the above considerations and table I, large mass storage would favor ions with large values of M.

Table I. Example parameters for a cylinder Penning-type trap. Fig. 3 applies with $V_T > \phi_c$ = 30 kV, B = 10 T, r_p/r_w = 0.5, and Z = 1.

M(u)	h(cm)	r_p(cm)	n(max)(cm^{-3})	N
1	500	0.32	2.7×10^{11}	$4.3\times10^{13} \simeq 0.7\times10^{-7}$mg
1000	500	10	2.7×10^{8}	$4.3\times10^{13} \simeq 0.7\times10^{-4}$mg
1/1836	500	0.0075	5.0×10^{14}	4.3×10^{13}

rf(PAUL) - TYPE TRAPS

Paul or rf - type traps provide trapping of charged particles in oscillating, spatially-nonuniform electric fields. It is also possible to use static electric fields to alter the trapping geometry somewhat,[4,5] but for simplicity, we assume trapping in pure oscillating fields here. If the trapping potential is given by

$$\phi_T = \phi_0(\vec{r}) \cos\Omega t, \tag{15}$$

then, for Ω sufficiently high (defined below), ions are confined in a pseudo potential, ϕ_{pi}, given by[4]

$$\phi_{pi} \simeq q_i |\vec{\nabla}\phi_0(\vec{r})|^2/(4m_i\Omega^2). \quad (16)$$

The fictitious charge density is given by $\nabla^2\phi_{pi} = -4\pi\rho_i'$. For spectroscopy, the usual choice is the quadrupole rf trap where $\phi_0 \propto r^2P_2(\cos\theta)$ (spherical coordinates).[4,5] This makes the trap pseudopotential harmonic in all directions. In this case, Ω sufficiently high means[4,5]

$$q_{zi} \equiv \frac{8|q_i|V_0}{m_i\Omega^2(r_0^2+2z_0^2)} \lesssim 1. \quad (17)$$

V_0 is the magnitude of the rf voltage applied between ring end endcaps whose dimensions are indicated in Fig. 1.

If we assume that the "secular" motion in the pseudopotential well of Eq. 16 can be cooled, and if we assume $\omega = 0$, the density of ions for a single species is determined by space charge repulsion and is given by [4,5] (dropping the subscripts)

$$n = 8.3 \times 10^8 \; q_z V_0(kV)/(Z(r_0^2+2z_0^2)). \quad (18)$$

If we neglect ϕ_{ind}, the shape of the ion plasma is a spheroid of revolution.[9] If we also assume $r_0 = 2z_0$, and assume that the dimensions of the ion cloud are equal to inner trap dimensions, the maximum number of ions is given by

$$N(max) = 2.3 \times 10^9 \; q_z \; z_0 V_0(kV)/Z. \quad (19)$$

From Eq. 17, we have

$$\Omega/2\pi(MHz) = 5.7(V_0(kV)Z/(Mq_z))^{\frac{1}{2}}/z_0. \quad (20)$$

From Eqs. 18-20, we tabulate a few example parameters in table II.

Table II. Example parameters for a quadrupole rf trap.

M	V_0(kv)	q_z	Z	r_0(cm)	n(cm^{-3})	N	$\Omega/2\pi$(MHz)
1000	10	0.5	1	1	2.8×10^9	5.8×10^9	0.81
1	"	"	"	"	"	"	25
1/1836	"	"	"	"	"	"	1100
"	"	0.005	"	"	2.8×10^7	5.8×10^7	11 GHz
M	"	0.5	"	20	6.9×10^6	1.2×10^{11}	$1.3/M^{\frac{1}{2}}$

We note the independence of n and N(max) on M. For electrons and positrons, the practical limits on n and N(max) may be due to the required large values of Ω.

For higher order rf traps, $\phi_0(\vec{r})$ might take the form given by Eq. 9. Perhaps a more useful form of ϕ_0 is given by the potential (in cylindrical coordinates)

$$\phi_0(r,\theta,z) = V_0 r^{k+1} \cos[(k+1)\theta]/r_0^{k+1}, \tag{21}$$

where θ is the azimuthal angle and k is an integer. A sketch of such a trap for k=2 is given in Fig. 4. Ideally, the electrode surfaces are equipotentials of Eq. 21; in Fig. 4, they are shown as cylindrical rods for simplicity. k=1 describes the Paul quadrupole mass filter. The ends of the trap could be closed off by bending the rods in towards the axis of the trap or using endcaps with appropriate static potentials thereby making a cylinder rf-type trap. Alternatively, the individual rods could be connected end-on-end to make a kind of race track.[13]

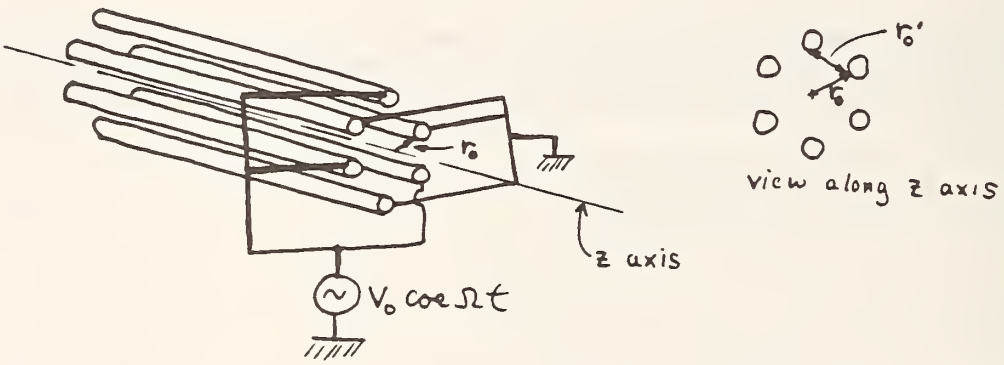

Fig. 4. Sketch of cylinder rf-type trap for k = 2.

Experimental examples of higher order traps are given in refs. 14 and 15. From Eqs. 16 and 21,

$$\phi_{pi} = C_{ki} r^{2k}, \tag{22}$$

where

$$C_{ki} = q_i V_0^2 (k+1)^2/(4m_i \Omega^2 r_0^{2(k+1)}). \tag{23}$$

ϕ_{pi} is cylindrically symmetric.

From Gauss's law, the density of stored ions is determined by space charge repulsion and is given by (if we assume $\omega = 0$)

$$n_i(r) = k^2 C_{ki} r^{2(k-1)}/(\pi q_i). \tag{24}$$

Therefore, for $k \gg 1$, the ions tend to form cylindrical shells near the inner edge of the trap electrodes where $r = r_0$. If the ions occupy the space out to $r = r_0$, integration of Eq. 24 gives

$$N(\max) = \frac{k(k+1)^2}{32} \frac{V_0 h}{q_i} \left(\frac{r_0'}{r_0}\right)^2 q_{xi}, \tag{25}$$

where q_{xi} is the stability parameter analogous to Eq. 17, and r_0' is defined in Fig. 4. We have

$$q_{xi} = 8 V_0 q_i / (m_i \Omega^2 r_0'^2). \tag{26}$$

For $k = 1$, $r_0'/r_0 = \sqrt{2}$ and $q_{xi} \sim 1$ for stability. For $k = 1$, the ratio of N(max) for the cylinder rf - trap to N(max) for the rf quadrupole trap of Eqs. 15 - 20, is equal to $3h/(4z_0)$ where h is the length of the plasma column as in Fig. 3. For $k \gg 1$, we have

$$N(\max)_k / N(\max)_{k=1} \simeq k\pi^2/8, \tag{27}$$

where we have assummed that the required value of the trap stability parameter, q_x, is independent of k. Thus, N(max) increases approximately as kh/z_0.

ION MIXTURES

For brevity, we consider only two ion species, with charge-to-mass ratios $q_1/m_1 \neq q_2/m_2$. The results are easily generalized to more species. When $q_1/q_2 > 0$, we consider only cylinder-type traps for simplicity. However the qualitative aspects of the results apply to other geometries.

Cylinder Penning-type trap, $(q_1/q_2 > 0)$

In Eq. 6, with $\rho' = 0$ for the Penning-type trap, ρ can be single valued only if the two ion species occupy different spatial regions. Qualitatively, since thermal equilibrium implies that ω is the same for all ions, if $q_1 = q_2$ and $m_2 > m_1$, species 2 is forced to larger radii than species 1 because of the larger centrifugal force acting on it. This separation has been theoretically and experimentally studied.[16,17] In the $T = 0$ limit, the separation should be complete with a gap between the species. If we look along the z axis of the trap, the spatial distributions appear as in Fig. 5.

The ion densities are still given by Eq. 10. The maximum density of the outer species is again given by $\omega = \Omega_{c2}/2$. Using this value of ω, we can find the corresponding value of n_1. The separation of the plasmas is given by solving the equation of motion for the rotation motion of species 2 at the radius a_2. We find

$$a_2/b_1 = (\rho_1/\rho_2)^{\frac{1}{2}}. \tag{28}$$

For $a_2 - b_1 > \lambda_D$, we expect the thermal contact between the two species to be reduced.[17]

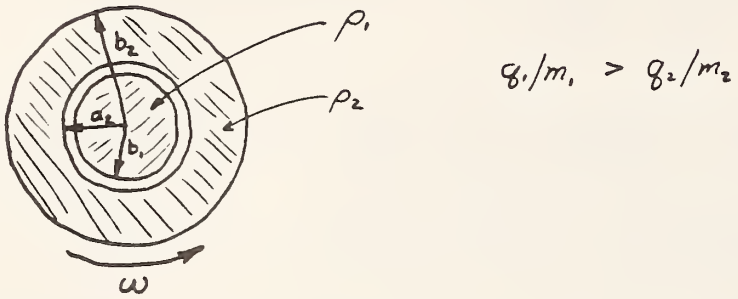

Fig. 5. Centrifugal separation of ion species in cylinder Penning or rf-type trap. The view is along the z axis, $\vec{B}$ is into the paper, and q_1, $q_2 > 0$.

A possible configuration for maintaining cold trapped positrons[3] in a Penning trap might be the following. Consider simultaneous trapping of positrons and $^9Be^+$ ions. The $^9Be^+$ ions would form a hollow cylinder around the central e^+ column. Using laser cooling, the $^9Be^+$ ions and therefore the positrons could be cooled to temperatures much less than 1 K.[17] In addition, angular momentum can be imparted to the ions in the laser cooling process to prevent radial diffusion of both species.[17] In this way, a stable, low temperature positron sample could be maintained. It is likely that ω would be limited to the value for maximum $^9Be^+$ density; that is $\omega(\max) = \Omega_c(^9Be^+)/2$. If we assume B = 10 T this would limit the maximum positron density to $n(e^+) \simeq 5.9\times10^{10}/cm^3$.

It would be nice to realize a similar scheme for antiprotons; unfortunately, negative ions suitable for laser cooling do not seem to be available. Cooling of antiprotons by thermalized electrons should work[1,18-20]. In the condition of thermal equilibrium, the antiprotons form a hollow cylinder around the electrons. In order to prevent radial diffusion, angular momentum of the appropriate sign might be imparted to the ions by particle beams,[21] positive or negative feedback on the ion motion[21,22] or angular momentum transfer from plasma waves.[23,24]

Cylinder rf-type trap ($q_1/q_2 > 0$)

For the rf-type trap, assumming $\omega = 0$, separation of the species with $q_1/m_1 \neq q_2/m_2$ occurs because the pseudopotential wells are unequal. This phenomenon has been investigated[25] for the quadrupole trap configuration. A simpler case to analyze is that of the cylinder rf-type trap where ϕ_0 is given by Eq. 21. If we assume $q_1/m_1 > q_2/m_2$, Fig. 5 again applies. Ion densities are still given by Eq. 24 and the separation of species can be easily determined by noting that at $r = a_2$, the space-charge electric field outward from species 1 is just equal to the pseudopotential field inward acting on species 2. We find

$$\frac{a_2}{b_1} = \left(\frac{Z_1 M_2}{Z_2 M_1} \right)^{\frac{1}{2k}} . \qquad (29)$$

Low order traps (e.g., k = 1 (quadrupole trap)) can give rise to a significant separation of the species.

Penning-type traps ($q_1/q_2 < 0$)

Simultaneous trapping of charges of opposite sign is particularly interesting in the context of this meeting. An important example is the simultaneous trapping of positrons and antiprotons for the production of antihydrogen by radiative recombination.

For the Penning-type trap, simultaneous trapping of charges of opposite sign is precluded because it is impossible to simultaneously trap both species along z. Therefore, to achieve a mixture of positive and negative ions, one species must be injected through the other. A possible arrangement might be to stack Penning traps for charges of opposite sign along the z axis in a "nested" arrangement as suggested in ref. 26. If positrons are stored in the central trap, antiprotons could be passed back and forth between traps adjacent to the central trap. Angular momentum transfer would tend to spread the positrons, but this might be overcome as described in the previous section.

rf - type traps ($q_1/q_2 < 0$)

In the pseudopotential approximation, it is apparent that if $N_1 q_1 = N_2 q_2$ the ions shrink to a point! The practical limit would appear to be due to rf heating which tends to keep the ions very hot. This problem is accentuated for simultaneous storage of positive and negative ions since they can come very close together due to Coulomb attraction and the rf micromotions[4,5] are 180° out of phase for the two species. Some experimental work has been reported in ref. 27, where Tl^+ and I^- ions were simultaneously stored in a quadrupole rf trap. In this work, an increase in density over the maximum value for a single stored species was observed, but overall densities were still fairly low. Clearly more work needs to be done on this interesting possibility.

Penning - rf trap combinations

An example of such a combined trap might be an rf-type trap for positrons superimposed on a Penning-type trap for antiprotons. Such a scheme appears valid for small numbers of positrons in an antiproton sample. When the number of positrons exceeds the number of antiprotons, trapping is more likely to occur because the positrons are held by the rf trap pseudopotential and antiprotons are held by the attractive space charge of the positron sample.

PROBLEMS

The analysis in this paper has considered only the static properties of nonneutral ion plasmas held in Penning-type or rf-type traps. The calculated maximum densities and numbers will be reduced by various effects which we might classify as plasma instabilities.

Penning-type traps

The most serious problem appears to be due to asymmetry induced transport. Radial transport can also occur due to ion collisions with background gas, but at very high vacuum, this process is negligible. The basic idea of asymmetry induced transport is that if the trap is not axially symmetric, angular momentum can be coupled into the ions which causes them to spread radially in the trap. Eventually, the ions will strike the electrodes and be lost. During this spreading process, the electrostatic space-charge energy will be converted to heat. In a cylinder Penning-type trap, spreading rates proportional to $(h/B)^2$ have been observed,[28] where h is the plasma length (Fig. 2). Although the spreading mechanism is not understood, one possibility might be resonant particle transport.[9,28,29] Resonant particle transport might occur if the trap geometric axis and magnetic field axis are misaligned. As the ion density increases, ω becomes larger. As the temperature becomes lower, the individual ion axial frequency, ω_z', defined as the mean axial velocity, v_z, divided by h/π, becomes smaller. When $\omega_z' \simeq \omega$, a coupling exists[9,29] which can simultaneously heat the axial motion and increase the ion radii. At the densities required for this condition, ω_z' becomes less well defined due to collisions, but the same mechanism may still apply. For $\omega = \omega_z'$, the densities may be considerably less than the maximum density given by Eq. 11. For small samples, some experimental evidence for such a resonant effect exists.[9]

Independently of the mechanism, such transport is likely caused by trap asymmetries. Conversely, if axial symmetry is preserved, angular momentum is a constant of the motion and confinement is assured.[10] Therefore, axial symmetry in the Penning-type traps appears to be at a premium.

rf-type traps

Historically, the mechanism of rf heating[30] has prevented the attainment of low temperatures and long confinement times in the rf traps. Therefore, attainable densities have typically been less than those dictated by space charge limitations (Eqs. 18 and 24). Cooling with a buffer gas allows the space-charge limited densities to be obtained, but this option seems to be precluded for antimatter storage.

The basic mechanism for ion-ion rf heating is that the rf driven micromotion can impart energy to the secular motion, that is, the motion in the pseudopotential well. In many experiments, this has limited the ion kinetic energy to a value of about 1/10 of the well depth of the trap due to evaporation.[4,5,30] This problem is often accentuated since it is desirable to operate the trap with large q_z values (Eq. 17) in order to obtain deep well depths. For the quadrupole rf trap (Eqs. 15-20), the relation $\omega_z/\Omega = q_z/(2\sqrt{2})$ holds, where ω_z is the single ion secular frequency.[4,5,30] Therefore, for

large values of q_z, ω_z approaches Ω and subharmonic excitation of the secular motion becomes more likely.

For stored ions of the same sign of charge, it would appear that rf heating could be made less by using much lower values of q_z ($q_z < 0.01$). This reduces the ion micromotion amplitude at a given distance from the center of the trap and it increases the mean spacing between ions. Both of these effects would reduce the rf heating mechanism and thereby allow the space charge density limit to be approached. Unfortunately, reducing q_z also reduces n (Eq. 18), so that a reasonable compromise would have to be met to achieve maximum stored numbers.

ACKNOWLEDGEMENTS

This work is supported by the U.S. Office of Naval Research and the U.S. Air Force Office of Scientific Research. The author thanks J. J. Bollinger for many useful discussions, and thanks C. Weimer and J. J. Bollinger for helpful comments on the manuscript.

REFERENCES

1. C.F. Driscoll, Low Energy Antimatter, Ed. by D.B. Cline, (World Scientific, Singapore, 1986), p. 184. This paper summarizes the work of J.H. Malmberg, T.M. O'Neil, Driscoll and their colleagues. It addresses some of the same issues of this paper.
2. L.R. Brewer, J.D. Prestage, J.J. Bollinger and D.J. Wineland, in Strongly Coupled Plasma Physics, ed. by F.J. Rogers and H.E. DeWitt, Plenum, 1986, to be published; J.J. Bollinger and D.J. Wineland, Phys. Rev. Lett. 53, 348 (1984).
3. C.M. Surko, M. Leventhal, W.S. Crane and A.P. Mills, Jr., H. Kugel, and J. Strachan, in Positron Studies of Solid Surfaces and Atoms, ed. by K.F. Canter, W.S. Crane and A.P. Mills, Jr. (World Scientific, Singapore, 1986), p. 221.
4. H.G. Dehmelt, Adv. At. Mol. Phys. 3, 53 (1967) and 5, 109 (1969).
5. D.J. Wineland, W.M. Itano, and R.S. Van Dyck, Jr., Adv. At. Mol. Phys. 19, 135 (1983).
6. R.C. Davidson, Theory of Nonneutral Plasmas (Benjamin, Reading, MA, 1974), p. 4.
7. T.M. O'Neil and C.F. Driscoll, Phys. Fluids 22, 266 (1979).
8. S.A. Prasad and T.M. O'Neil, Phys. Fluids 22, 278 (1979).
9. D.J. Wineland, J. J. Bollinger, W.M. Itano, and J.D. Prestage, J. Opt. Soc. Am. B2, 1721 (1985).
10. T.M. O'Neil, Phys. Fluids 23, 2216 (1980).
11. R.S. Van Dyck, Jr., F.L. Moore, D.L. Farnham, and P.B. Schwinberg, Int. J. Mass Spectrom. and Ion Processes 66, 327 (1986).
12. D.J. Wineland, W.M. Itano, J.C. Bergquist, J.J. Bollinger, and J.D. Prestage, in Atomic Physics 9, R.S. Van Dyck, Jr., and E.N. Fortson, eds., (World Scientific, Singapore, 1985), p. 3.
13. D.A. Church, J. Appl. Phys. 40, 3127 (1969).
14. E. Teloy and D. Gerlich, Chem. Phys. 4, 417 (1974); A. Sen and J.B.A. Mitchell, J. Phys. B: At. Mol. Phys. 19, L545 (1986).
15. M. Okumura, L.I. Yeh, D. Normand, and Y.T. Lee, J. Chem. Phys. 85, 1971 (1986).
16. T.M. O'Neil, Phys. Fluids 24, 1447 (1981).
17. D.J. Larson, J.C. Bergquist, J.J. Bollinger, W.M. Itano, and D.J. Wineland, Phys. Rev. Lett. 57, 70 (1986).
18. H.G. Dehmelt et al., Bull, Am. Phys. Soc. 24, 757 (1979); G. Torelli, in Proceedings of the Fifth European Symposium on Nucleon Anti-Nucleon Interactions, Bressanone, Italy, 23-28 June 1980, edited by M. Cresti (Istituto Nazionale di Fisica Nucleare, Padua, Italy, 1980), p. 43.
19. G. Gabrielse, H. Kalinowsky, and W. Kells, in Physics with Antiprotons at LEAR in the ACOL Era, edited by U. Gastaldi et al. (Editions Frontieres, Gif-sur-Yvette, France, 1985), p. 665; W. Kells, IEEE Trans. Nucl. Sci. 32, 1770 (1985).
20. M.H. Holzscheiter, in Low Energy Antimatter, Ed. by D. B. Cline, (World Scientific, Singapore, 1986).
21. D.J. Wineland, R.E. Drullinger J.C. Bergquist, and W.M. Itano, Bull. Am. Phys. Soc. 24, 1185 (1979).
22. W.D. White, J.H. Malmberg, and C.F. Driscoll, Phys. Rev. Lett. 49, 1822 (1982).
23. D.L. Eggleston, T.M. O'Neil, and J.H. Malmberg, Phys. Rev. Lett. 53, 982 (1984).

24. J.D. Crawford, T.M O'Neil, and J.H. Malmberg, Phys. Rev. Lett. 54, 697 (1985).
25. L. S. Cutler, private communication.
26. G. Gabrielse, K. Helmerson, R. Tjoelker, X. Fei, T. Trainor, W. Kells, and H. Kalinowsky, in Proc. of 1st Workshop on Antimatter Physics at Low Energy, B.E. Bonner and L.S. Pinsky eds., Fermilab, Apr. 1986, p. 211.
27. F.G. Major and J.P. Schermann, Bull. Am. Phys. Soc. 16, 838 (1971).
28. C.F. Driscoll, K.S. Fine, and J.H. Malmberg, Phys. Fluids 29, 2015 (1986).
29. C.F. Driscoll and J.H. Malmberg, Phys. Rev. Lett. 50, 167 (1983).
30. D.A. Church and H.G. Dehmelt, J. Appl. Phys. 40, 3421 (1969); H.G. Dehmelt, in Advances in Laser Spectroscopy, F.T. Arecchi, F. Strumia, and H. Walther eds., Plenum, 1983, p. 153.

Thermal Shifts of the Spectral Lines in the $^4F_{3/2}$ to $^4I_{11/2}$ Manifold of an Nd:YAG Laser

SHAO ZHONG XING AND J. C. BERGQUIST

Abstract—We report the thermal shifts of eleven of the twelve lines from the $^4F_{3/2}$ Stark energy levels to the $^4I_{11/2}$ energy levels in an Nd:YAG laser for a temperature change from 20–200°C. The thermal shift difference between the Stark sublevels R_1, R_2 in $^4F_{3/2}$ is found to be about -0.6 ± 0.6 cm^{-1}/100°C. Within our experimental uncertainty, all of the lasing lines either moved to longer wavelength or remained unchanged with increasing temperature.

Introduction

RECENT advances in high-power diode lasers have led to extremely efficient, CW operation of neodymium-doped crystal and fiber lasers [1]–[3]. There have also been important strides toward low threshold operation of miniature hybrid and monolithic neodymium-doped lasers [1], [4], [5]. These devices have inherently much better mode quality and frequency stability than the diode lasers used as the pump sources. Additionally, several new nonlinear crystals that are used to double these lasers into the visible have been developed with good optical quality and large nonlinear coefficients [6]–[8].

For these reasons, interest in these devices as ultrastable frequency sources near 1 and 0.5 μm is strong. While there are few atomic and molecular transitions near 1 μm with suitably narrow linewidths to which to lock a laser, there are many such transitions in the visible. One very attractive candidate that we are investigating is the $5d^{10}6s\ ^2S_{1/2}$–$5d^96s^2\ ^2D_{5/2}$ transition in a single laser-cooled Hg^+ ion near 281 nm (1.126 μm ÷ 4) [9], [10]. This transition has a natural linewidth of about 1.7 Hz [10], [11]. A laser that has been spectrally narrrowed to less than 1 Hz and tuned to this wavelength could be stabilized to this transition to better than 1×10^{-17}. The accuracy of such a frequency standard should also exceed 1×10^{-17} [12].

We have begun to study various neodymium-doped crystals and fibers to determine their suitability as narrowband radiation sources whose fourth harmonic could be tuned to match the transition frequency in Hg^+. Unfortunately, the neodymium-doped crystal laser and bulk glass lasers are generally not tunable by more than a few wavenumbers at any temperature. But some of the transitions do tune by as much as several wavenumbers per 100°C change in temperature (generally to lower frequencies). In this letter we report on our measurements of the thermal shifts of the spectral lines in the $^4F_{3/2}$ to $^4I_{11/2}$ manifold of a neodymium-doped, yttrium–aluminum–garnet (Nd:YAG) laser. Although the linewidths, spectral lineshapes, and thermal shifts of several lines of Nd:YAG have been studied both theoretically and experimentally [13]–[20] we were able to measure the thermal shifts of all the laser lines in this manifold with the exception of the weak R_2–Y_2 transition near 1.0551 μm. Thereby we were able to do a comprehensive study of the temperature dependence of these lines in the temperature range from 20–200°C.

Manuscript received March 9, 1988; revised April 20, 1988. This work was supported in part by the U.S. Air Force Office of Scientific Research and by the Office of Naval Research.

S. Z. Xing is with the Changchun Institute of Optics and Fine Mechanics, Changchun, China, on leave at the Time and Frequency Division, National Bureau of Standards, Boulder, CO 80303.

J. C. Bergquist is with the Time and Frequency Division, National Bureau of Standards, Boulder, CO 80303.

IEEE Log Number 882227.

Experimental Setup

The experimental setup is shown in Fig. 1. Although we used a ring laser cavity, the oscillation of the laser was bidirectional. The radius of curvature of the concave mirrors M_1 and M_2 was 10 cm, and of M_3, 15 cm. M_4 was flat. To ensure that all the lines from the $^4F_{3/2}$ manifold to the $^4I_{11/2}$ manifold would oscillate, all the mirrors were highly reflecting from 1.0–1.15 μm. The 5 mm diameter by 10 mm long Nd:YAG crystal was cut at Brewster's angle for low loss and ease of cleaning. The crystal was placed in the 80 μm beam waist between mirrors M_2 and M_3. The cavity was adjusted to nearly compensate for the astigmatism introduced by the crystal. The Nd:YAG crystal was end pumped by laser light near 750 nm that was focused through mirror M_3. M_3 was nearly 90 percent transmitting at 750 nm. The pump laser was a ring dye laser pumped by a krypton ion laser. The output radiation from the dye laser could be tuned from 735 to 800 nm with as much as 600 mW of power. The oven for the crystal was made of aluminum and was heated by a 15 W thermal plug-heater. A chromel–alumel thermocouple monitored the temperature of the oven. The birefringent filter (BF) consisted of a single quartz plate approximately 5 mm thick. The monochromator is a 0.8 m focal length scanning monochromator with a 150 lines/mm grating blazed for an 8 μm wavelength. A 40 μm slit was generally used in the entrance plane of the monochromator. In the exit plane of the monochromator, a diode array with a resolution of 25 μm was used to receive and display the spectrum signal on an oscilloscope.

Experimental Results

The twelve possible transitions from the upper $^4F_{3/2}$ manifold to the lower $^4I_{11/2}$ manifold in Nd:YAG are

0018-9197/88/0900-1829$01.00 © 1988 IEEE

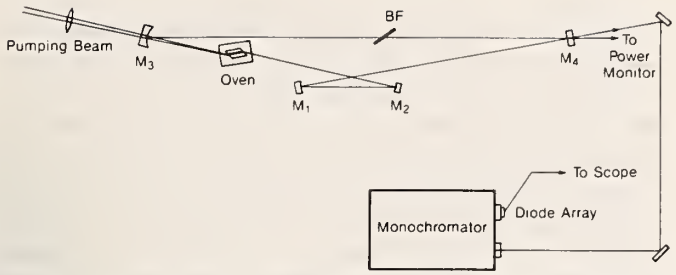

Fig. 1. The setup used to measure the thermal shifts of spectral lines in Nd:YAG laser. The ring laser consists of mirror, M_1, M_2, M_3, and M_4, a single plate birefringent filter (BF), and an Nd:YAG crystal. The Nd:YAG crystal is housed in an oven that can be heated from room temperature to $\geq 200°C$. The crystal is axially pumped by up to 600 mW of power from a ring dye laser tunable near 750 nm. A diode array in the exit plane of the 0.8 m focal length monochromator receives and displays the signal on a scope.

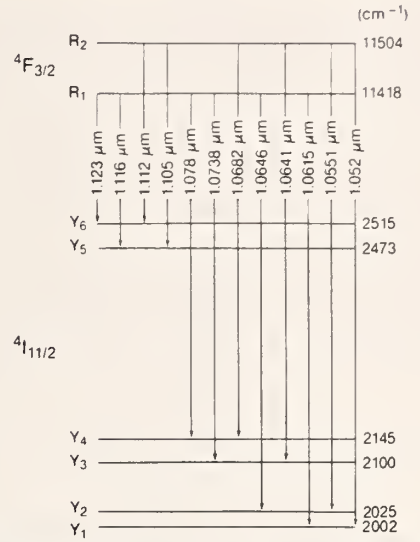

Fig. 2. A simplified optical energy level diagram showing the $^4F_{3/2}$ manifold and the $^4I_{11/2}$ manifold in Nd:YAG. The twelve possible infrared transitions from the upper two Stark sublevels (R_1, R_2) to the lower six Stark sublevels ($Y_1 \rightarrow Y_6$) are also indicated.

shown in Fig. 2. Customarily, the Stark sublevels are labeled with increasing energy as R_1 and R_2 in the $^4F_{3/2}$ manifold and as Y_1 and Y_6 in the $^4I_{11/2}$ manifold. The ring laser oscillated on all of the transitions with the exception of the R_2–Y_2 transition near 1.0551 μm. Some of the light from the Nd:YAG laser that escaped through M_4 was directed into the monochromator. The diode array in the exit plane of the monochromator made it possible to monitor the thermal shift and gain width of each transition easily. The array had 512 diodes and a resolution of 25 μm. To make a thermal shift measurement, the monochromator setting was adjusted until the signal was centered on the diode array. This setting was noted and the birefringent filter was then adjusted to allow another transition to oscillate. By tuning the birefringent filter over the line to find the maximum power, we could roughly determine line center. The monochromator setting was changed to bring the diffracted signal for the wavelength of this transition to the center of the diode array and this setting was noted. Several readings for all eleven transitions were taken at one temperature, then the oven temperature was changed, and the entire process repeated. On most lines, the line center could be measured to only a few tenths of a wavenumber. This limitation was not due to poor signal-to-noise ratio but rather due to large asymmetries in the line. Some of these asymmetries were caused by fundamental asymmetric-broadening mechanisms in the crystal [13]. But the more difficult problem, because of our inability to properly characterize it, was the fact that the different transitions competed to oscillate. Before fully tuning across any line, the laser was likely to jump to another transition. The wavelength at which the jump occurred depended on the birefringent filter position, the mirror reflectances and losses at the various wavelengths, and the gain profile of the different transitions. Because of this systematic uncertainty, the line centers could not be located to better than ± 0.5 cm^{-1}.

In Fig. 3 the thermal shifts of the eleven transitions that lased are plotted as a function of temperature from 20 to 200°C (solid lines). For all lines except the R_1–Y_4 transition at 1.0779 μm and the $R_2 \rightarrow Y_4$ transition at 1.0682

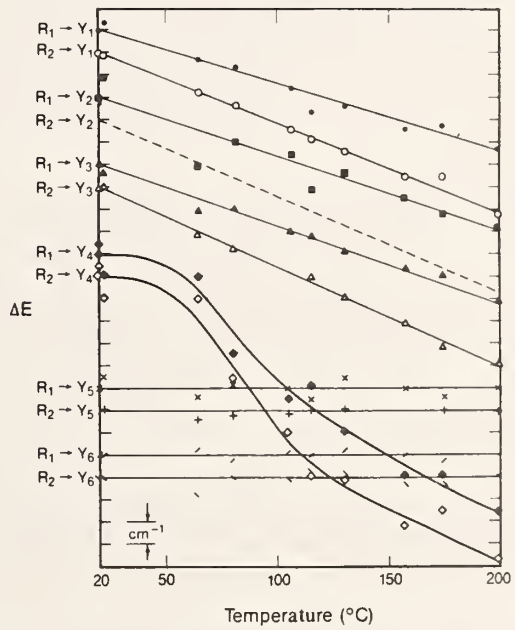

Fig. 3. Plot showing the variation in the wavelength for maximum laser power as a function of Nd:YAG crystal temperature for all 12 lines from the $^4F_{3/2}$ manifold to the $^4I_{11/2}$ manifold. The dotted line is the deduced temperature variation for the $R_2 \rightarrow Y_2$ transition at 1.0551 μm that did not oscillate.

μm, the shifts appear to vary linearly with temperature. The strongly nonlinear thermal movement of these two lines is due to the shift and broadening with temperature of the Y_4 Stark sublevel. In Table I we list the thermal shifts of all the transitions giving an endpoint-to-endpoint average shift for the R_1, $R_2 \rightarrow Y_4$ transitions. From our work there is fivefold redundancy in determining the relative thermal shift of the R_1 and R_2 levels (in principle, there would be sixfold redundancy but this is reduced by 1 since the $R_2 \rightarrow Y_2$ line did not oscillate). While our results are not inconsistent with a zero relative tempera-

TABLE I
THERMAL SHIFTS OF THE TRANSITIONS BETWEEN THE STARK ENERGY SUBLEVELS IN THE $^4F_{3/2}$ MANIFOLD AND IN THE $^4I_{11/2}$ MANIFOLD, AND THE RELATIVE THERMAL SHIFT OF THE R_1 AND R_2 STARK LEVELS SHIFT IN AN Nd:YAG LASER

		$^4I_{11/2}$					
		Y_1	Y_2	Y_3	Y_4	Y_5	Y_6
$^4F_{3/2}$ R_1	Wavelength(μm)	1.0615	1.0646	1.0738	1.0779	1.1161	1.1225
	Thermal shift (cm^{-1}/100°C)	-3.0	-3.3	-3.5	-6.1	0.0	0.0
R_2	Wavelength(μm)	1.052	1.0551	1.0641	1.0682	1.1055	1.1121
	Thermal shift (cm^{-1}/100°C)	-4.0	(-4.3)	-4.6	-7.0	0.0	0.0
Relative thermal shift between R_1 & R_2 (cm^{-1}/100°C)		-1.0	(-1.0)	-1.1	-0.9	0.0	0.0

ture shift between R_1 and R_2, there is an indication of a small linear separation of these levels with increasing temperature. This possibility was also noted in [3]. There is twofold redundancy in determining the relative thermal shift of any pair of Stark sublevels in the lower $^4I_{11/2}$ level. These redundancies provide a self-consistency check of the relative movement of the Stark sublevels in each manifold. Thus, we are able to predict the thermal shift of the weak $R_2 \rightarrow Y_2$ 1.0551 μm transition to be approximately -4.3 $cm^{-1}/100°C$. This is plotted as the dashed line in Fig. 2.

Fig. 3 shows that for those lines with shorter wavelength (and stronger intensity), the 1.052, 1.0615, 1.0641, and 1.0738 μm lines, the thermal shifts are roughly linear and the shift difference in each pair is consistent. The 1.052 μm line moves about -7.3 cm^{-1} from room temperature to 200°C or about -4.0 $cm^{-1}/100°C$. This is in agreement with the shift measured by Kushida [13]. The 1.0615 μm line moves about -3.0 cm^{-1} for a temperature change of 100°C. This compares to the -2.7 $cm^{-1}/100°C$ thermal variation measured by Marling [14] and to the -3.8 $cm^{-1}/100°C$ temperature shift measured by Kushida [13]. Thus the relative shift with temperatures of the R_1 and R_2 Stark levels is about -1 $cm^{-1}/100°C$ from this pair of transitions. Almost the same relative thermal shift is obtained for the pair consisting of the 1.0641 μm line (R_2–Y_3) and the 1.0738 μm line (R_1–Y_3). The 1.0641 μm transition moves about -4.6 $cm^{-1}/100°C$ and the 1.0738 μm transition moves about -3.5 $cm^{-1}/100°C$. Thus, this pair indicates a relative shift of about -1.1 $cm^{-1}/100°C$ between the R_1 and R_2 Stark levels.

From these two pairs of lines, it would appear that the R_2 sublevel in the $^4F_{3/2}$ manifold moves to a lower energy with increasing temperature about 1 $cm^{-1}/100°C$ faster than the R_1 level. However, for the lines at 1.1055 μm (R_2–Y_5), 1.1121 μm (R_2–Y_6), 1.1161 μm (R_1–Y_5) and 1.1225 μm (R_1–Y_6) we measured almost no shift for a change of nearly 200°C in temperature. Thus, these lines indicate that R_1 and R_2 shift with temperature at nearly the same rate.

The thermal shift of the 1.0682 μm line (R_2–Y_4) and of the 1.0779 μm line (R_1–Y_4) are strongly nonlinear in this temperature range. Thus it is difficult to determine the relative shift of R_1 and R_2 from this pair. As stated earlier, we did assign an endpoint-to-endpoint average shift for these two lines. This result and the thermal shifts for the remaining transitions are summarized in the table. By assigning equal weight to each of the measured shift differences, we could average our results to give a relative thermal shift of -0.6 ± 0.6 $cm^{-1}/100°C$ between Stark sublevels R_1 and R_2. The error of ± 0.6 $cm^{-1}/100°C$ includes both the statistical and the systematic uncertainties.

DISCUSSION

There are a number of reasons the various transitions in the $^4F_{3/2} \rightarrow {}^4I_{11/2}$ manifold have different measured thermal shifts. The crystalline field at the site of the impurity Nd ion is a function of the local strain. When this strain is dynamically produced by the lattice vibrations, the interaction between the Nd ion and the local crystalline field causes temperature-dependent broadenings and shifts of the energy levels of the ion. The thermal behaviors of linewidths and line positions are frequently dominated by this dynamic phonon–impurity interaction not only in the Nd:YAG crystal but in other impurity:crystalline hosts as well [13]. The crystalline field strength can also be changed by thermal expansion of the crystalline lattice, but this appears to be a minor contribution to the thermal shifts and broadenings in hard crystals such as Nd:YAG [13]. When the temperature of the crystal is increased, energy levels and hence, spectral lines, broaden as the higher phonon states are occupied. Usually, the phonon–impurity interaction lowers an energy level and usually the dependence with temperature of higher levels is larger than for lower levels because of smaller energy denominators. As a result, the spectral lines are generally expected to move to the longer wavelengths when the temperature is increased [13]. This general feature is confirmed by our experimental results.

We also observed that the longer the wavelength the wider the linewidth and the more complex the thermal shift. The shorter wavelength lines have relatively narrow and symmetrical lineprofiles ($\Delta\nu \sim 5$ cm^{-1}) that broaden only slightly with temperature. Therefore we can deduce that both of the upper Stark levels R_2 and R_1 and the lower Stark levels Y_1, Y_2, Y_3 remain spectrally narrow in the temperature range from 20–200°C. We also found the shift of these transitions to be simply linear in this temperature range. The intermediate-wavelength transitions have a wider and asymmetric line profile ($\Delta\nu \gtrsim 10$ cm^{-1}), and from the arguments above, that implies that the Y_4 Stark level is $\gtrsim 5$ cm^{-1} wider than Y_1, Y_2, and Y_3. The fact that the transitions that terminate on the Y_4 Stark level move in a nonlinear fashion with temperature in our measurement range might be explained by the asymmetrical thermal broadening of the Y_4 level. While some of the thermal broadening mechanisms give rise to a sym-

metrical line shape, other mechanisms, such as the direct, single-resonant-phonon interaction, cause asymmetric broadening [13]. If the line profile, first broadened asymmetrically to the red ($\sim 80°C$) because of the thermal behavior of the Y_4 level, then the measured line shift would appear to move strongly toward the red. If later ($\sim 150°C$) the broadening becomes more symmetric (or asymmetric to the blue) then the rate of the red shift would decrease.

The longest wavelength transitions have the widest linewidths ($\Delta\nu \gtrsim 13\ cm^{-1}$) among all the transitions between the $^4F_{3/2}$ and $^4I_{11/2}$ manifolds. Thus the Y_5 and Y_6 Stark sublevels are the broadest in the $^4I_{11/2}$ manifold. Hence the thermal shifts of these transitions are somewhat obscured by the thermal broadening over our relatively small change in temperature. Clearly these upper energy levels in the lower Stark manifold generally move with R_1 and R_2 with change in temperature. These results are in basic agreement with earlier work on the thermal shift of some of these transitions [13]–[18].

Acknowledgment

The authors wish to thank D. Nabors, R. Byer, and T. Baer for many helpful discussions.

References

[1] B. Zhou, T. J. Kane, G. J. Dixon, and R. L. Byer, "Efficient, frequency-stable laser-diode-pumped Nd:YAG laser," *Opt. Lett.*, vol. 10, pp. 62–64, Feb. 1985.

[2] T. M. Baer, "Frequency doubled, diode pumped Nd:YAG laser," *Proc. Soc. Photo-Opt. Instrum. Eng.*, vol. 610, pp. 45–47, Jan. 1986.

[3] R. J. Mears, L. Reekie, S. B. Poole, and D. N. Payne, "Neodymium-doped silica single-mode fibre lasers," *Electron. Lett.*, vol. 21, pp. 738–740, Aug. 15, 1985; I. P. Alcock, A. I. Ferguson, D. C. Hanna, and A. C. Tropper, "Tunable, continuous-wave neodymium-doped monomode-fiber laser operating at 0.900–0.945 and 1.070–1.135 μm," *Opt. Lett.*, vol. 11, pp. 709–711, Nov. 1986.

[4] T. J. Kane and R. L. Byer, "Monolithic, unidirectional single-mode Nd:YAG ring laser," *Opt. Lett.*, vol. 10, pp. 65–67, Jan. 1985.

[5] W. R. Trutna, Jr., D. K. Donald, and M. Nazarathy, "Unidirectional diode-laser-pumped Nd:YAG ring laser with a small magnetic field," *Opt. Lett.*, vol. 12, pp. 248–250, Apr. 1987.

[6] W. J. Kozlovsky, C. D. Nabors, and R. L. Byer, "Efficient second harmonic generation of a diode-laser-pumped CW Nd:YAG laser using monolithic MgO:$LiNbO_3$ external resonant cavities," *IEEE J. Quantum Electron.*, vol. 24, pp. 913–919, June 1988; R. L. Byer "Diode pumped solid state laser," *Science*, to be published; T. Y. Fan, G. J. Dixon, and R. L. Byer, "Efficient GaAlAs diode-laser-pumped operation of Nd:YLF at 1.047 μm with intracavity doubling to 523.6 nm," *Opt. Lett.*, vol. 11, pp. 204–206, Apr. 1986.

[7] See, for example, J. T. Lin and C. Chen, "Choosing a nonlinear crystal," *Laser Optron.*, vol. 6, pp. 59–63, Nov. 1987, and references therein.

[8] T. Baer, "Large-amplitude fluctuations due to longitudinal mode coupling in diode-pumped intracacity-doubled Nd:YAG lasers," *J. Opt. Soc. Amer. B*, vol. 3, pp. 1175–1180, Jan. 1986.

[9] J. C. Bergquist, W. M. Itano, and D. J. Wineland, "Recoilless optical absorption and Doppler sidebands in a single trapped ion," *Phys. Rev. A*, vol. 36, pp. 428–430, July 1, 1987.

[10] J. C. Bergquist, D. J. Wineland, W. M. Itano, H. Hemmati, H.-U. Daniel, and G. Leuchs, "Energy and radiative lifetime of the $5d^9 6s^2\ ^2D_{5/2}$ state in HgII by Doppler-free two-photon laser spectroscopy," *Phys. Rev. Lett.*, vol. 55, pp. 1567–1570, Oct. 7, 1985.

[11] W. M. Itano, J. C. Bergquist, R. G. Hulet, and D. J. Wineland, "Radiative decay rates in Hg+ from observations of quantum jumps in a single ion," *Phys. Rev. Lett.*, vol. 59, pp. 2732–2734, Dec. 14, 1987.

[12] D. J. Wineland, W. M. Itano, J. C. Bergquist and R. G. Hulet, "Laser cooling limits and single-ion spectroscopy," *Phys. Rev. A*, vol. 36, pp. 2220–2232, Sept. 1, 1987.

[13] T. Kushida, "Linewidths and thermal shifts of spectral lines in neodymium-doped yttrium aluminum garnet and calcium fluorophospate," *Phys. Rev.*, vol. 185, pp. 500–508, Sept. 10, 1969.

[14] J. Marling, "1.05–1.44 μm tunability and performance of the CW Nd^{3+}:YAG laser," *IEEE J. Quantum Electron.*, vol. QE-14, pp. 56–62, Jan. 1978.

[15] A. A. Kaminskii, "High-temperature spectroscopic investigation of stimulated emission from lasers based on crystals and glasses activated with Nd^{3+} ions," *Sov. Phys. JETP*, vol. 27, pp. 388–399, Sept. 1968.

[16] D. E. McCumber and M. D. Sturge, "Linewidths and temperature shift of the *R* lines in ruby," *J. Appl. Phys.*, vol. 34, pp. 1682–1684, June 1963.

[17] W. M. Yen, W. C. Scott, and A. L. Schawlow, "Phonon-induced relaxation in excited optical states of trivalent praseodymium in LaF_3," *Phys. Rev.*, vol. 136, pp. A271–A283, Oct. 5, 1964.

[18] T. Kushida and M. Kikuchi, "*R*, *R'* and *B* absorption linewidths and phonon-induced relaxations in ruby," *J. Phys. Soc. Japan*, vol. 23, pp. 1333–1348, Dec. 1967.

[19] M. Birnbaum and C. F. Klein, "Stimulated emission cross section at 1.061 μm in Nd:YAG," *J. Appl. Phys.*, vol. 44, pp. 2928–2930, June 1973.

[20] V. A. Buchenkov, I. B. Vitrishchak, V. G. Evdokimova, L. N. Soms, A. Stepanov, and V. K. Stupnikov, "Temperature dependence of giant pulse amplification in YAG:Nd^{3+}," *Sov. J. Quantum Electron.*, vol. 11, pp. 702–705, June 1981.

NBS-114A (REV. 2-80)

U.S. DEPT. OF COMM. BIBLIOGRAPHIC DATA SHEET (See instructions)	1. PUBLICATION OR REPORT NO. NIST/TN-1324	2. Performing Organ. Report No.	3. Publication Date October 1988

4. TITLE AND SUBTITLE

Trapped Ions and Laser Cooling II

5. AUTHOR(S)

D.J. Wineland, W.M. Itano, J.C. Bergquist, J.J. Bollinger

6. PERFORMING ORGANIZATION (If joint or other than NBS, see instructions)

National Institute of Standards and Technology
~~NATIONAL BUREAU OF STANDARDS~~
DEPARTMENT OF COMMERCE
WASHINGTON, D.C. 20234

7. Contract/Grant No.

8. Type of Report & Period Covered

9. SPONSORING ORGANIZATION NAME AND COMPLETE ADDRESS (Street, City, State, ZIP)

U.S. Office of Naval Research
800 North Quincy
Arlington, VA 2217

and

U.S. Air Force
Office of Scientific Research
Bolling Air Force Base, DC 20332

10. SUPPLEMENTARY NOTES

☐ Document describes a computer program; SF-185, FIPS Software Summary, is attached.

11. ABSTRACT (A 200-word or less factual summary of most significant information. If document includes a significant bibliography or literature survey, mention it here)

This Technical note is a collection of selected reprints of the Ion Storage Group for the period July 1985 to September 1988.

12. KEY WORDS (Six to twelve entries; alphabetical order; capitalize only proper names; and separate key words by semicolons)

atomic clocks; atomic spectroscopy; frequency standards; ion storage; laser cooling; laser spectroscopy; trapped ions

13. AVAILABILITY

☒ Unlimited

☐ For Official Distribution. Do Not Release to NTIS

☒ Order From Superintendent of Documents, U.S. Government Printing Office, Washington, D.C. 20402.

☐ Order From National Technical Information Service (NTIS), Springfield, VA. 22161

14. NO. OF PRINTED PAGES

200

15. Price

NATIONAL INSTITUTE OF STANDARDS AND TECHNOLOGY
(formerly NATIONAL BUREAU OF STANDARDS)
U.S. DEPARTMENT OF COMMERCE
GAITHERSBURG, MD 20899

Official Business
Penalty for Private Use $300